

A Thesis Submitted for the Degree of PhD at the University of Warwick

Permanent WRAP URL:

<http://wrap.warwick.ac.uk/98781/>

Copyright and reuse:

This thesis is made available online and is protected by original copyright.

Please scroll down to view the document itself.

Please refer to the repository record for this item for information to help you to cite it.

Our policy information is available from the repository home page.

For more information, please contact the WRAP Team at: wrap@warwick.ac.uk

An Investigation Into Glucagon Receptor Pharmacology

Kerry Barkan

Doctor of Philosophy

University of Warwick
School of Life Sciences

September 2017

Contents

Chapter 1. Introduction	1
1.1. Membrane proteins	1
1.1.1. The receptor concept	1
1.2. G protein-coupled receptors (GPCRs)	2
1.3. GPCRs classification	2
1.3.1. Class A (Rhodopsin-like) receptors	3
1.3.1.1. A _{2A} receptor; an archetype class A GPCR	4
1.3.2. Class B (Secretin-like) receptors	5
1.3.2.1. Receptor activity-modifying proteins (RAMPs)	5
1.5. G proteins	6
1.5.1. G protein cycle	7
1.5.1.1. G _s family	12
1.5.1.2. G _{i/o} family	12
1.5.1.3. G _q family	13
1.5.1.4. G _{12/13} family	13
1.5.2. $\beta\gamma$ -subunit signalling	14
1.6. Major effectors of G proteins	15
1.6.1. Adenylyl cyclases and the cAMP pathway	15
1.6.2. Phospholipase C (PLC)	17
1.7. β -arrestins	18
1.7.1. β -arrestins; desensitisation and internalisation	18
1.7.2. β -arrestins; an alternative signalling system	19
1.8. G protein and β -arrestin mediated ERK1/2 activation	20
1.9. Signalling bias: a relatively new field	22
1.10. Compounds and toxins as tools for deconvoluting GPCR signalling	23
1.11. GPCR dimerisation	24
1.11.1. Beyond class C GPCR	24
1.11.2. Dimerisation and receptor trafficking	25
1.11.3. Dimerisation and signal transduction	26
1.11.4. Dimerisation in class B GPCRs	27
1.12. GPCR structures	28
1.13. GPCR residue numbering	30
1.14. The glucagon receptor (GCGR)	31
1.15. GCGR structures	32
1.16. Insight into receptor activation; Comparison between active and inactive class B crystal structures	34
1.17. Inactive receptor state; conformation stabilisation	35
1.17.1. The E/DRY motif in class A GPCRs	35
1.17.2. HETX motif in class B GPCRs	36

1.17.3. TM2-6-7-Helix 8 network in class B GPCRs	37
1.18. Intracellular GPCR domains ICL1 and Helix 8	38
1.18.1. The importance of ICL1 in cell-surface expression and G protein-coupling	38
1.18.1.1. ICL1 cysteine and cell-surface expression	38
1.18.1.2. ICL1 and G protein-coupling	39
1.18.2. Helix 8 of GPCRs	40
1.19. Aims of this study	41
Chapter 2. Materials and Methods	43
2.1. Cell culture methodology	43
2.1.1. Cell lines	43
2.1.2. CRISPR knockout HEK 293 cell lines	44
2.1.3. GCGR stable expressing HEK 293 cell line generation	44
2.1.4. Long-term storage and recovery	45
2.2. Hepatocyte Isolation from C57BL/6 mouse	46
2.3. Cell viability assay	47
2.4. Transient transfection	47
2.5. Ligands and compounds	48
2.6. Constructs and molecular biology	49
2.6.1. RAMP constructs	49
2.6.2. GCGR constructs	50
2.6.3. GLP-1R construct	53
2.6.4. A _{2A} R constructs	54
2.7. RNA extraction, quality determination and cDNA synthesis	55
2.7.1. RNA extraction	55
2.7.2. RNA quality determination	56
2.7.3. cDNA synthesis	56
2.8. Pharmacological characterisation techniques	59
2.8.1. cAMP accumulation assay	59
2.8.2. Phospho-ERK assay	61
2.8.3. Intracellular Ca ²⁺ mobilisation assay	62
2.8.4. IP ₁ accumulation assay	63
2.9. Receptor cell-surface expression analysis	65
2.9.1. Enzyme-linked Immunosorbent Assay (ELISA)	65
2.9.2. Fluorescence-activated cell sorting (FACS) analysis of GCGR cell-surface expression	66
2.10. Molecular biology techniques	67
2.10.1. Molecular cloning reagents	67
2.10.2. Bacterial transformation	68
2.10.3. PCR amplification of DNA for cloning	68
2.10.4. PCR screening of plasmid DNA from bacterial colonies	68
2.10.5. Quality control and sequencing of DNA	69

2.11. Common media	69
2.11.1. Hanks balanced salt solution (HBS)	69
2.11.2. Phosphate buffer saline (PBS)	69
2.11.3. Bacterial growth medium	69
2.12. Data analysis	70
2.13. Modelling mutant GPCR structure	72
2.14. Live cell imaging in HEK 293 cells	73
Chapter 3. Establishing a robust assay system	74
3.1. Introduction	74
3.2. Optimisation of the cAMP assay	75
3.2.1. Cell number	75
3.2.2. Ligand stimulation time	77
3.2.2.1. To include or exclude the 'true basal' stimulation point?	77
3.2.2.2. Optimising stimulation time	80
3.2.3. DNA concentration and time post-transfection	85
3.3. Transfection reagent	90
3.4. Tools to investigate G protein bias	93
3.4.1. NF449; an antagonist of G _s	93
3.4.2. YM-254890; an inhibitor of G _q	96
3.5. Optimisation of the IPOne assay	102
3.6. Generation of a HEK 293 cell line stably expressing GCGR	105
3.7. Receptors expression in a hepatic cell line: Hep 3B	108
3.7.1. Investigating GPCR mRNA expression in Hep 3B cells	108
3.7.2. Optimisation of the cAMP assay in Hep 3B cells	110
3.8. Characterisation of CRISPR knockout HEK 293 cell lines	115
3.8.1. Growth rate and viability	115
3.8.2. Maximum cAMP response in CRISPR knockout HEK 293 cell lines	118
3.8.3. cAMP response in $\Delta G\alpha_s$ HEK 293 cells changes over time	120
3.8.4. Maximum PMA response in CRISPR knockout HEK 293 cell lines	122
3.8.5. Summary	123
3.9. Analysis of GCGR cell-surface expression using fluorescence-activated cell sorting (FACS)	125
3.9.1. FACS: Data collection and analysis	125
3.9.2. DNA concentration at transfection and detectable cell-surface expression	129
Chapter 4. Investigating GCGR pharmacology	132
4.1. Introduction	132
4.2. Investigating the cAMP response at the GCGR	133
4.2.1. GCG and oxyntomodulin stimulates a robust cAMP response	133
4.2.2. Variation in absolute potencies of GCG and oxyntomodulin at	137

GCGR	
4.2.3. Mammalian expression vectors: A comparison of cAMP signalling in GCGR transfected HEK 293	140
4.2.3.1. Measured potency varies between vectors	140
4.2.3.2. Significantly elevated basal for pcDNA3.1 and pVITRO1 when compared to pmCherry-N1 expressing GCGR	141
4.2.4. Summary	144
4.3. Investigating the intracellular Ca ²⁺ response at the GCGR	145
4.3.1 GCG and oxyntomodulin stimulates intracellular Ca ²⁺ response at GCGR	145
4.4. Investigating the ERK1/2 response at the GCGR	154
4.4.1. GCG stimulates a ERK1/2 response in three GCGR expressing cell lines	154
4.4.2. Measured potency of GCG and oxyntomodulin stimulated pERK1/2 response is cell line dependent	157
4.4.2.1. pERK1/2 response in GCGR transfected HEK 293T cells and GCGR stable CHO-K1 cells	157
4.4.2.2. pERK1/2 response in a generated GCGR stable HEK 293 cell line	160
4.4.3. PKA and cAMP play no role in the GCGR stimulated ERK1/2 response	163
4.4.4. The specific G $\beta\gamma$ subunits inhibitor, gallein, had no effect on the measured pERK1/2 response	167
4.4.5. The specific G _{q/11} inhibitor, YM-254890, reduced the potency of the pERK1/2 response following GCG stimulation	170
4.4.6. Investigating the importance of G proteins and β -arrestin1/2 in GCGR stimulated pERK1/2 response	173
4.4.7. Summary	176
4.5. Pharmacological characterisation of two potential GCGR antagonists	177
4.5.1. des-His ¹ ,[Glu ⁹]-glucagon amide is a partial agonist at the GCGR in transfected HEK 293T cells	177
4.5.2. L-168,049 is a competitive antagonist at the GCGR in HEK 293T cells	183
4.5.3. Summary	188
4.6. Investigating the action of a potential GCGR biased agonist; TH-GCG	188
4.6.1. TH-GCG induces a robust cAMP response in GCGR transfected HEK 293T cells	188
4.6.2. TH-GCG fails to induce an Ca ²⁺ i in GCGR transfected HEK 293T cells	192
4.6.3. TH-GCG fails to induce a detectable IP ₁ response in GCGR transfected HEK 293T cells	194
4.6.4. TH-GCG shows a distinctly different cAMP response in the hepatocyte cell line; Hep 3B	197
4.6.5. Investigation the cAMP response to TH-GCG in hepatocytes extracted from C57BL/6 mice	199
4.6.5.1. TH-GCG induces a robust cAMP response in C57BL/6 hepatocytes	199

4.6.6. TH-GCG stimulated a pERK1/2 response in GCGR transfected HEK 293 cells but fails to stimulate a response in stable CHO-K1 cells	203
4.6.7. Summary	206
4.7. Investigation the pharmacological consequences of RAMP2-GCGR interaction	208
4.7.1. Cell-surface expression of GCGR is not influenced by RAMP2 co-expression	208
4.7.2. RAMP2 potentiated the response of GCG at the GCGR	211
4.7.3. No RAMP2-dependent potentiation of GCG response in HEK 293T cells transfected with GCGR and RAMP2 dual expression vector	214
4.7.4. Summary	219
4.8. Pharmacology in a hepatic cell line: Hep 3B	220
4.8.1. GCG and oxyntomodulin stimulates a robust cAMP response in Hep 3B cells	220
4.8.2. Adrenomedullin stimulates a cAMP response in Hep 3B cells	223
4.8.3. GCG, oxyntomodulin and GLP-1(7-36)amide induce a pERK1/2 response in Hep 3B cells	227
4.8.4. Pharmacological characterisation of two potential GCGR antagonists in Hep 3B cells	231
4.8.4.1. des-His ¹ ,[Glu ⁹]-GCG appears to acts as non-competitive antagonist of the GCG stimulated cAMP response in Hep 3B cells	231
4.8.4.2. L-168,049 acts as a competitive antagonist of the GCG stimulated cAMP response	234
4.8.5. Summary	237
Chapter 5. Investigating pharmacological role of GCGR regions	
5.1. Introduction	240
5.2. Investigating pharmacological role of GCGR intracellular loop 1	241
5.2.1. Cell-surface expression of GCGR intracellular loop 1 mutants	241
5.2.2. cAMP response in GCGR ICL1 transfected HEK 293 cells	245
5.2.3. pERK1/2 response in GCGR ICL1 mutants transfected HEK 293 cells	248
5.2.4. Intracellular Ca ²⁺ response in GCGR ICL1 mutants transfected HEK 293 cells	251
5.2.5. Assessing the bias for each pathway at ICL1 mutants	255
5.2.6. Molecular modelling of ICL1 mutants in three GCGR structures	256
5.2.7. Summary	259
5.3. Investigating the role of A _{2A} R ICL1 in cAMP signalling	260
5.3.1. NECA stimulated CHO-K1 cells fail to show a cAMP response	260
5.3.2. NECA stimulated cAMP response in WT and mutant A _{2A} R	262
5.3.3. CGS 21680 stimulated cAMP response in WT and mutant A _{2A} R	266
5.3.4. Molecular modelling of ICL1 mutants in A _{2A} R structures	269
5.3.5. Summary	276
5.4. An investigation into conserved GPCR residues within GCGR	278

5.4.1. An investigation into the '[K/R]KLH' motif in GCGR	278
5.4.2. An investigation into the importance of R173 in GCGR signalling	284
5.4.2.1. Cell-surface expression of R173A and R173A, N174A mutants similar to WT GCGR	284
5.4.2.2. R173A ^{2,46} mutant shows severe reduction of GCG and oxyntomodulin-mediated cAMP accumulation	285
5.4.2.3. Molecular modelling of R173A mutants in three GCGR structures	289
5.4.2.4. Summary	292
5.4.3. Investigating the importance of two conserved residues within helix 8 of GCGR; E406 and E410	293
5.4.3.1. Cell-surface expression of E406A and E406A, E410A show reduced cell-surface expression	293
5.4.3.2. Elevated basal cAMP accumulation in E406A and E406A, E410A GCGR mutants	296
5.4.3.3. Molecular modelling of E406 and E410 mutants in three GCGR structures	300
5.4.3.4. Summary	303
5.5. Investigating pharmacological role of GCGR TM4	305
5.5.1. Cell-surface expression of GCGR TM4 mutants	305
5.5.2. cAMP response in GCGR TM4 mutants transfected HEK 293T cells	308
5.5.3. cAMP response in GCGR TM4 mutants transfected HEK 293 cells	311
5.5.4. pERK1/2 response in GCGR TM4 mutants transfected HEK 293T cells	314
5.5.5. Intracellular Ca ²⁺ response in GCGR TM4 mutants transfected HEK 293T cells	317
5.5.6. Molecular modelling of TM4 mutants in three GCGR structures	320
5.5.7. Summary	323
6. General Discussion and Further Work	325
6.1. General Discussion	325
6.2. Further Work	334
References	337

Acknowledgements

Firstly, I would like to offer my sincerest gratitude to my supervisor, Dr Graham Ladds, who has supported and guided me through my PhD journey from the very start. His guidance and knowledge has provided me with direction, motivated and drive through the most difficult times. I would also like to thank the entire Graham Ladds group, which has been growing in size over the past year. In particular, I would like to thank Ian Winfield whom I have worked alongside for the past three years. My thanks also go to Dr Matthew Harper, Dr Maja Wallberg whom I have been lucky enough to work with on a collaborative project, and Dr Cathryn Weston whom I have also published with at the start of my PhD. A big thank you is due to Professor Mark Wheatley at the University of Birmingham for his supervision during a three-month project and his PhD student Sian Bailey who went above and beyond in her support.

I would also like to thank my family, particularly my father and grandfather, for their continuous encouragement despite the distance.

Finally, I would like to thank The University of Warwick and the BBSRC for funding this PhD.

Declaration

This thesis is submitted to the University of Warwick in support of my application for the degree of Doctor of Philosophy. The work presented is my own with the exception of the ICL1 GCGR mutants (G165A-T172A) constructs, which were acquired through a collaborative project with Dr. Ali Jazayeri at Heptares Therapeutics. This thesis has not been submitted for a degree at another university.

Kerry Barkan

Abstract

The glucagon receptor (GCGR), a family B G protein-coupled receptor (GPCR), plays an important role in regulating blood glucose levels through its ability to bind the 29 amino acid peptide hormone, glucagon (GCG). Antagonising GCG action is a potential therapeutic option for reducing hepatic glucose production. However, GCG-based therapy is currently limited to acute emergency treatment of hypoglycemia in patients with type 1 diabetes (T1D) (Habegger *et al.*, 2010). Further insight into GCGR-mediated signalling pathways and mechanism of activation may provide the basis for therapeutic development.

We investigated the ligand stimulated GCGR signalling using multiple assays including those measuring cAMP accumulation, ERK1/2 phosphorylation and intracellular Ca^{2+} (Ca^{2+}_i) mobilisation. Through site directed mutagenesis and FACS analysis for the investigation of cell-surface expression, we identified several important residues. They included K168^{12.49}, L169^{12.50}, H170^{12.51} and T172^{2.45} of the ICL1 region (G165^{1.63}-T172^{2.45}) as potential determinant in signalling bias at the GCGR through $G_{q/11}$ -coupling, C171^{2.44} as a critical determinant of GCGR expression and R173^{2.46} as an essential residue for G protein-coupling. Helix 8 residue E406^{8.49} was implicated in maintaining GCGR in an inactive state. Finally, TM4 residues G271^{4.49}, L277^{4.55} and V280^{4.58} were found to play an important role in successful translation and/or trafficking of GCGR and (Ca^{2+}_i) mobilisation.

The GCGR-mediated pERK1/2 response was found to be both $G_{q/11}$ and β -arrestin1/2 mediated, whereas it was independent of PKA or $G\beta\gamma$ -subunits. The GCG analogue TH-GCG, contrary to previous reports (Wakelam *et al.*, 1986, Lenzen *et al.*, 1990), was characterised as a partial agonist at the GCGR, inducing a robust cAMP response but fails to induce a detectable Ca^{2+}_i or IP_1 response. We also identified a RAMP2-dependent potentiation of the GCG stimulated cAMP response at the GCGR.

The research described in this thesis has produced novel data that contributes to a clearer understanding of GCGR pharmacology.

Abbreviations

A _{2A} R	adenosine A _{2A} receptor
AC	adenylate cyclase
ADP	adenosine diphosphate
AKAP	A-kinase-anchoring proteins
AM	adrenomedullin
AMP	ampicillin
AMY	amylin
AP-1	activator protein 1
APC	allophycocyanin
ATP	adenosine triphosphate
BAPTA	1,2-Bis(2-aminophenoxy)ethane-N,N,N',N'-tetraacetic acid tetrakis(acetoxymethyl ester)
bp	base pair
BRET	bioluminescence resonance energy transfer
BSA	bovine serum albumin
C-terminus	carboxyl terminus
cAMP	cyclic adenosine 3',5'-monophosphate
cDNA	complementary DNA
CFP	cyan fluorescent protein
CGRP	calcitonin gene related peptide
CGS 21689	2-[p -(2-carboxyethyl)phenylethylamino]-50-ethylcarboxamidoadenosine
CHO	chinese hamster ovary
CLR	calcitonin receptor-like receptor
CRF	corticotropin-releasing factor
CRF	corticotropin-releasing factor
CRF ₁ R	corticotropin-releasing factor receptor 1
CRISPR	clustered regularly interspaced, short palindromic repeat
CT	calcitonin
DAG	diacylglycerol
DMEM	Dulbecco's modified Eagle's medium
DMSO	dimethyl sulphoxide
DNA	deoxyribose nucleic acid
E. coli	Escherichia coli
ECD	extracellular N-terminal domain
ECL	extra-cellular loop
EDTA	ethylenediaminetetraacetic acid
ELISA	enzyme-linked immunosorbent assay
Emax	maximum level of signal
ER	endoplasmic reticulum
ERK1/2	extracellular signal-regulated kinase 1/2

FACS	fluorescence activated cell sorting
FBS	fetal bovine serum
FFA4	free fatty acid 4 receptor
FRET	fluorescence resonance energy transfer
G protein	guanine nucleotide-binding proteins
GABA	glutamate, γ -aminobutyric acid
GAP	GTPase-activating protein
GbR	metabotropic γ -aminobutyric acid type b receptor
GCG	glucagon
GCGR	glucagon receptor
GDP	guanosine 5'-diphosphate
GEF	guanine nucleotide exchange factor
GFP	green fluorescence protein
GIP	gastric inhibitory polypeptide
GIPR	gastric inhibitory polypeptide receptor
GLP-1	glucagon-like peptide 1
GLP-1R	glucagon-like peptide 1 receptor
GNAS	$G\alpha_s$ -subunit encoding guanine nucleotide binding α -stimulating
GPCR	G protein-coupled receptor
GRAFS	Glutamate, Rhodopsin, Adhesion, Frizzled/Taste and Secretin
GRK2	GPCR kinase 2
GTP	guanosine 5'-triphosphate
HBSS	Hank's balanced salt solution
HEK	human embryonic kidney
HTRF	homogeneous time resolved fluorescence
IBMX	3-Isobutyl-1-methylxanthine
ICL	intracellular loop
IP ₁	inositol monophosphate
IP ₃	inositol 1,4,5 trisphosphate
IP ₃	inositol 1,4,5 trisphosphate
JNK	Jun N-terminal kinases
KAN	kanamycin
LANCE	Lanthanide Chelate Excite
MAP	mitogen activated protein
MAPK	mitogen activated protein kinase
MAPKK	mitogen activated protein kinase kinase
MAPKKK	mitogen activated protein kinase kinase kinase
MCS	multi-cloning site
	mitogen activated protein (MAP) extracellular signal-regulated kinases
MEK	ERK kinase
MEME	minimal essential medium Eagle
mGluR	metabotropic glutamate receptor
NAD	nicotinamide adenine dinucleotide

N-terminus	amino terminus
NAM	negative allosteric modulator
NECA	5'-N-Ethylcarboxamidoadenosine
NESP55	chromagranin-like neuroendocrine secretory protein
OPD	O-phenylenediamine dihydrochloride
OTR	oxytocin receptor
PAM	positive allosteric modulator
PAR2	proteinase activated receptor 2
PBS	phosphate buffered saline
PCR	polymerase chain reaction
	negative logarithm of concentration of agonist required to produce a
pEC ₅₀	half-maximal response
PH	pleckstrin-homology
PIP2	phosphatidylinositol 4,5-bisphosphate
PKA	protein kinase A
PKC	protein kinase C
PLC	phospholipase C
PLL	Poly-L-lysine
PMA	Phorbol 12-myristate 13-acetate
PTH	parathyroid hormone
PTHr	parathyroid hormone type 1 receptor
PTX	pertussis toxin
RAMP	receptor activity-modifying protein
RGS	regulators of G protein signalling
RhoGEF	rhoGTPase nucleotide exchange factor
RNA	ribonucleic acid
RTK	receptor tyrosine kinase
SEM	standard error of the mean
StaR	thermostabilised receptor
T4L	T4-lysozyme
TM	transmembrane
TSHR	thyrotropin receptor
V ₂ R	V2 vasopressin receptor
VPAC	vasoactive intestinal polypeptide receptor
WT	wild-type
β ₂ AR	β ₂ adrenergic receptor

List of Figures

Figure	Page
1.1 Heterotrimeric G protein activation cycle.	9
1.2 cAMP pathway and crosstalk with MAPK/ERK pathway	17
1.3 G protein and β -arrestin mediated ERK activation.	22
1.4 Full-length GCGR crystal structure	29
1.5 Schematic representation of proglucagon processing in the pancreatic α -cells and intestinal L-cells	32
2.1 G418 kill curve for HEK 293 cells	45
2.2 pVITRO1-neo-mcs vector map	50
2.3 Principles of the LANCE® cAMP assay kit	60
2.4 Principles of the LANCE® <i>Ultra</i> cAMP assay kit	61
2.5 Schematic of G_q -mediated signaling following GPCR activation and tools to measure the downstream signaling components.	65
3.1 Typical LANCE cAMP standard curve	76
3.2 Forskolin stimulated cAMP response in Flp-In HEK 293T cells plated at various densities	76
3.3 cAMP response in Flp-In HEK 293T cells stably expressing the GLP-1R or GCGR, with or without the true basal stimulation point	79
3.4 cAMP response in Flp-In CHO-K1 cells stably expressing the GLP-1R at various time points	82
3.5 cAMP dose-response in Flp-In CHO-K1 cells stably expressing the GLP-1R at various time points	83
3.6 8 minutes stimulation time at 1,000 and 2,000 cells/well is optimal in Flp-In HEK 293T cells stably expressing the GLP-1R	83
3.7 cAMP response in HEK 293T cells transfected with pcDNA3.1 containing GCGR	85
3.8 cAMP response in HEK 293T cells 24 or 48 hours post-transfection with pcDNA3.1 containing GCGR.	87
3.9 Influence of DNA concentration at transfection on measured cAMP response in HEK 293 cells	89
3.10 Influence of transfection reagent on cell viability in HEK 293	91
3.11 Comparison of transfection reagents on measured cAMP response	92
3.12 Schematic of NF449 activity at G_s and predicted dose-response data	94
3.13 Assessing NF449 as an inhibitor of G_s activity	95
3.14 YM-254890 treatment has no effect on measured cAMP response in HEK 293T cells	98
3.15 Effect of YM-254890 treatment on Ca^{2+} responses in HEK 293T cells	100
3.16 Cell number and stimulation time optimisation for IP1 accumulation assay	103
3.17 Cell-surface expression of mCherry-tagged GCGR in G418 selected HEK 293 cells	106
3.18 Comparison of cAMP response in transient and stable GCGR expressing HEK 293 cells	106

3.19	Expression profile of receptors in Hep 3B cells	109
3.20	Expression profile of G proteins in Hep 3B cells	110
3.21	cAMP response to forskolin in Hep 3B at various cell densities	112
3.22	cAMP response to GCG in Hep 3B at 10, 000 and 20, 000 cells/well	112
3.23	cAMP response to GCG in Hep 3B at 5, 000 cells/well as measured using the LANCE® Ultra cAMP assay kit	113
3.24	Comparison of cAMP response to GCG in Hep 3B and GCGR transfected HEK 293 cells	113
3.25	Cell number directly correlates with luminescent output for CellTiter-Glo® Luminescent Cell Viability Assay.	117
3.26	Measurement of cell viability in HEK 293 knockout cell lines	117
3.27	Comparison of cell growth profiles of WT and knockout HEK 293 cell lines	118
3.28	Maximal forskolin responses in HEK 293 knockout cell lines	119
3.29	cAMP response in ΔG_s HEK 293 cells changes over passage	121
3.30	Comparison of PMA responses in HEK 293 knockout cell lines	123
3.31	FACS data analysis: example manual gating of untransfected HEK 293 cells	127
3.32	FACS data analysis: example gating of single untransfected HEK 293 cells	127
3.33	Example histograms generated from flow cytometry of untransfected and vector only/GCGR transfected HEK 293 cells	128
3.34	Example histograms generated from flow cytometry of WT or mutant GCGR transfected HEK 293 cells	129
3.35	DNA concentration at transfection and detectable cell-surface expression of WT and mutant GCGR, as determined by FACS analysis	131
4.1	cAMP response in GCGR transfected HEK 293 cells	135
4.2	cAMP responses in GCGR transfected HEK 293T and HEK 293 cells	138
4.3	cAMP response in HEK 293 cells transfected with pcDNA3.1 or pVITRO1 expressing GCGR	142
4.4	Ca ²⁺ i mobilization in HEK 293T cells expressing GCGR +/- YM-254890 treatment.	148
4.5	Ca ²⁺ i mobilization dose-response in HEK 293T cells expressing GCGR +/- YM-254890 treatment	149
4.6	Ca ²⁺ i mobilization in GCGR stably expressing CHO-K1 cells +/- YM-254890 treatment	150
4.7	Ca ²⁺ i mobilization dose-response in GCGR stably expressing CHO-K1 cells +/- YM-254890 treatment	151
4.8	GCG stimulated pERK1/2 response in three alternative cell lines	155
4.9	GCG and Oxyntomodulin stimulated pERK1/2 response in GCGR transfected HEK 293T cells and CHO-K1 cells stably expressing GCGR	158
4.10	GCG and Oxyntomodulin stimulated pERK1/2 response in HEK 239 cells stably expressing GCGR	161
4.11	G protein mediated activation of extracellular signal-regulated kinase 1	163

	and 2 (ERK1/2) though both α and $\beta\gamma$ subunits	
4.12	pERK1/2 response in CHO-K1 cells stably expressing GCGR	164
4.13	pERK1/2 response in CHO-K1 cells stably expressing GCGR +/- PKA inhibitor	165
4.14	pERK1/2 response in CHO-K1 cells stably expressing GCGR +/- $G\beta\gamma$ inhibitor	168
4.15	pERK1/2 response in CHO-K1 cells stably expressing GCGR +/- $G_{q/11}$ inhibitor	171
4.16	GCG stimulated pERK1/2 response in WT and various knockout HEK 239 cells lines	174
4.17	GCG dose-response is within the dynamic range of the cAMP assay in HEK 293T cells	170
4.18	Activity of des-His ¹ ,Glu ⁹ -GCG in GCGR transfected HEK 293T cells	180
4.19	cAMP response to des-His ¹ ,Glu ⁹ -GCG in GCGR/vector only transfected HEK 293T cells	181
4.20	Activity of L-168,049 in GCGR transfected HEK 293T cells	185
4.21	cAMP response to L-168,049 in GCGR/vector only transfected HEK 293T cells	186
4.22	TH-GCG induces a concentration-dependent increase in cAMP accumulation in HEK 293T cells expressing GCGR	190
4.23	TH-GCG stimulated cAMP response is GCGR-dependent in HEK 293T cells	191
4.24	TH-GCG fails to induce a Ca^{2+} i response in HEK 293T cells expressing GCGR	193
4.25	TH-GCG fails to induce a measurable IP1 response in HEK 293T cells or CHO-K1 cells expressing GCGR	196
4.26	TH-GCG fails to induce a concentration-dependent increase in cAMP accumulation in Hep 3B cells	198
4.27	Forskolin induces a concentration-dependent increase in cAMP accumulation in C57BL/6 hepatocytes	200
4.28	TH-GCG and GCG induce a concentration-dependent increase cAMP accumulation in C57BL/6 hepatocytes	201
4.29	Investigating the TH-GCG stimulated pERK1/2 response in GCGR transfected HEK 293T cells and CHO-K1 cells stably expressing GCGR	204
4.30	RAMP2 does not influence the cell-surface expression of myc-tagged GCGR in transfected	209
4.31	GCGR does not influence the cell-surface expression of FLAG-tagged RAMP2 in transfected HEK 293T cells	210
4.32	RAMP2 potentiates the GCG response at the GCGR in transfected HEK 293T cells	212
4.33	RAMP2 fails to potentiate the cAMP response in HEK 293T cells transfected with the pVITRO vector expressing GCGR and RAMP2	216
4.34	FLAG-RAMP2 cell-surface expression was elevated in HEK 293T cells transfected with pVITRO1 expressing RAMP2 only when compared to	218

	pVITRO1 expressing RAMP2 and GCGR	
4.35	cAMP signaling profile in Hep 3B cells	221
4.36	The measured potency for GCG and oxyntomodulin varies across experimental repeats in Hep 3B cells	223
4.37	cAMP signaling profile in Hep 3B cells	225
4.38	The measured potency for AM varies across experimental repeats in Hep 3B cells	226
4.39	GCG, oxyntomodulin and GLP-1(7-36)amide stimulates a pERK1/2 response in 'young' Hep 3B cells	229
4.40	Activity of des-His ¹ ,Glu ⁹ -glucagon amide in Hep 3B	232
4.41	Activity of L-168,049 in Hep 3B	235
5.1	GCGR family structure-based alignment	242
5.2	Cell-surface expression of WT and GCGR ICL1 mutants	244
5.3	Effect of GCGR ICL1 mutants on cAMP response	246
5.4	Effect of GCGR ICL1 mutants on pERK1/2 response	249
5.5	Effect of GCGR ICL1 mutants on Ca ²⁺ _i response	253
5.6	Radar plot of antilog $\Delta\Delta(\text{Tau}/K_A)$.	255
5.7	ICL1 region within crystal structure of full-length GCGR	258
5.8	GCGR and A _{2A} R structure-based alignment	261
5.9	NECA induces a cAMP response in mock transfected HEK 293 cells	261
5.10	NECA failed to stimulate Ca ²⁺ _i mobilisation in CHO-K1 cells expressing A _{2A} R	263
5.11	Effect of A _{2A} R ICL1 mutants on NECA stimulated cAMP response	264
5.12	Effect of A _{2A} R ICL1 mutants on CGS21680 stimulated cAMP response	267
5.13	ICL1 region within crystal structure of A _{2A} R bound to ZM241385	273
5.14	Comparison of polar contacts within ZM241385 bound WT and alanine containing A _{2A} R crystal structure	274
5.15	[K/R]KLH motif and helix 8 conserved glutamate residues in crystal structure of full-length GCGR	280
5.16	Modelled S167R mutant within full-length GCGR crystal structure	281
5.17	WT and S167R GCGR show similar cell-surface expression in HEK 293 cells as determined by FACS analysis	282
5.18	cAMP response in WT and S167R GCGR mutants	282
5.19	Cell-surface expression of WT, R173A and R173A, N174A GCGR are similar in transfected HEK 293 cells, as determined by FACS analysis	285
5.20	GCG and oxyntomodulin induced cAMP response is attenuated in R173A transfected HEK 293	287
5.21	Comparison of polar contacts within WT and modelled R173A containing crystal structure of full-length GCGR at position 173	290
5.22	GCGR family structure-based alignment of helix 8	295
5.23	Cell-surface expression of WT and Helix 8 GCGR mutants, as determined by FACS analysis	295
5.24	cAMP response in WT and helix 8 GCGR mutant	297
5.25	E406A, E410A GCGR mutant showed a ligand-independent elevated	298

	basal cAMP level	
5.26	Comparison of polar contacts at position 406 within WT and modelled E406A mutant full-length crystal structure	302
5.27	GCGR family structure-based alignment of TM4 region	306
5.28	Cell-surface expression of WT and GCGR TM4 mutants	307
5.29	Effect of TM4 mutations on the GCGR stimulated cAMP response in HEK 293T cells.	309
5.3	Effect of TM4 mutations on the GCGR stimulated cAMP response is reproducible the in HEK 293 cells	312
5.31	Effect of GCGR TM4 mutants on pERK1/2 response	315
5.32	Effect of GCGR TM4 mutants on Ca ²⁺ i mobilization in transfected HEK 293T cells	318
6.1	GCGR-mediated ERK activation	328

List of Tables

Table	Page
1.1 α -subunits of heterotrimeric G proteins	10
2.1 Transfection components according to size of tissue culture plate for Fugene® HD and PEI	48
2.2 Oligonucleotides used to create GCGR mutants in ICL1, TM2, TM4 and helix 8	52
2.3 Reaction components for QuikChange (site or multi site-directed) mutagenesis kit	53
2.4 Cycle parameters for QuikChange (site or multi site-directed) mutagenesis kit	53
2.5 Oligonucleotides used to create A _{2A} R mutants in ICL1 region, TM1, ICL1 and TM2	54
2.6 Oligonucleotides used in RT-PCR of cDNA synthesized from RNA extracted from HEK 293T and Hep 3B cells	57
2.7 Gene specific oligonucleotides to human G α -subunits used in RT-PCR of cDNA synthesized from RNA extracted from Hep 3B cells	58
2.8 Cycling parameters for <i>Taq</i> DNA polymerase for 200 bp product	59
2.9 Components Ca ²⁺ containing and Ca ²⁺ -free of HBS	69
3.1 Forskolin stimulated cAMP response in Flp-In HEK 293T cells plated at various densities	77
3.2 cAMP response in Flp-In HEK 293T cells stably expressing the GLP-1R or GCGR, with or without the true basal stimulation point	80
3.2 Optimising ligand stimulation time for cAMP accumulation assay	84
3.3 cAMP response in HEK 293T cells 24 or 48 hours post-transfection with pcDNA3.1 containing GCGR.	88
3.4 Influence of DNA concentration at transfection on measured cAMP response in HEK 293 cells	89
3.5 Comparison of transfection reagents on measured cAMP response	92
3.6 Assessing NF449 as an inhibitor of G _S activity	96
3.7 YM-254890 treatment has no effect on measured cAMP response in HEK 293T cells	99
3.8 Effect of YM-254890 treatment on Ca ²⁺ i respons in HEK 293T cells	101
3.9 Cell number and stimulation time optimisation for IP ₁ accumulation assay	104
3.10 Comparison of cAMP response in transient and stable GCGR expressing HEK 293 cells	107
3.11 Optimisation of the cAMP assay in Hep 3B cells	114
3.12 Comparison of cAMP response to GCG in Hep 3B and GCGR transfected HEK 293 cells	115
3.13 cAMP response in Δ G _S HEK 293 cells changes over passage	121
4.1 cAMP response in GCGR transfected HEK 293 cells	136
4.2 cAMP responses in GCGR transfected HEK 293T and HEK 293 cells	139
4.3 Size, promoter and enhancers present in three mammalian expression	140

	vectors.	
4.4	cAMP response in HEK 293 cells transfected with pmCherry-N1, pcDNA3.1 or pVITRO1 expressing GCGR	143
4.5	Ca ²⁺ i mobilization dose-response in GCGR expressing cell lines +/- YM-254890 treatment	152
4.6	GCG stimulated pERK1/2 response in three alternative cell lines.	156
4.7	GCG and Oxyntomodulin stimulated pERK1/2 response in GCGR transfected HEK 293T cells and CHO-K1 cells stably expressing GCGR	159
4.8	GCG and Oxyntomodulin stimulated pERK1/2 response in HEK 239 cells stably expressing GCGR	162
4.9	pERK1/2 response in CHO-K1 cells stably expressing GCGR +/- PKA inhibitor	166
4.10	pERK1/2 response in CHO-K1 cells stably expressing GCGR +/- Gβγ inhibitor	169
4.11	pERK1/2 response in CHO-K1 cells stably expressing GCGR +/- G _{q/11} inhibitor	172
4.12	GCG stimulated pERK1/2 response in WT and various knockout HEK 239 cells lines	175
4.13	Activity of des-His ¹ ,Glu ⁹ -GCG in GCGR/Vector only transfected HEK 293T cells	182
4.14	Activity of L-168,049 in GCGR/vector only transfected HEK 293T cells	187
4.15	TH-GCG induces a concentration-dependent increase in cAMP accumulation in HEK 293T cells expressing GCGR	191
4.16	TH-GCG fails to induce a Ca ²⁺ i response in HEK 293T cells expressing GCGR	194
4.17	TH-GCG fails to induce a concentration-dependent increase in cAMP accumulation in Hep 3B cells	198
4.18	Forskolin induces a concentration-dependent increase in cAMP accumulation in C57BL/6 hepatocytes	201
4.19	TH-GCG and GCG induce a concentration-dependent increase cAMP accumulation in C57BL/6 hepatocytes	202
4.20	Investigating the TH-GCG stimulated pERK1/2 response in GCGR transfected HEK 293T cells and CHO-K1 cells stably expressing GCGR	203
4.21	RAMP2 potentiates the GCG response at the GCGR in transfected HEK 293T cells	213
4.22	RAMP2 fails to potentiate the cAMP response in HEK 293T cells transfected with the pVITRO vector expressing GCGR and RAMP2	217
4.23	cAMP signaling profile in Hep 3B cells	222
4.24	cAMP signaling profile in Hep 3B cells	225
4.25	Rank order of potency at the CLR with RAMP1-3.	226
4.26	Rank order of potency at the CALCR receptor with and without RAMP1-3	226
4.27	GCG, oxyntomodulin and GLP-1(7-36)amide stimulates a pERK1/2 response in 'young' Hep 3B cells	230

4.28	Activity of des-His ¹ ,Glu ⁹ -glucagon amide in Hep 3B.	233
4.29	Activity of L-168,049 in Hep 3B	236
5.1	Colour code key for structural-alignment	243
5.2	Effect of GCGR ICL1 mutants on cAMP response	247
5.3	Effect of GCGR ICL1 mutants on pERK1/2 response	250
5.4	Effect of GCGR ICL1 mutants on Ca ²⁺ _i response	254
5.5	Comparison of GCGR residue polar contacts within WT and modelled ICL1 mutant structures	257
5.6	Effect of A _{2A} R ICL1 mutants on NECA stimulated cAMP response	265
5.7	Effect of A _{2A} R ICL1 mutants on CGS21680 stimulated cAMP response	268
5.8	Comparison of A _{2A} R residue polar contacts within WT and modelled A _{2A} R mutant crystal structures	271
5.9	cAMP response in WT and S167R GCGR mutants	283
5.10	GCG and oxyntomodulin induced cAMP response is attenuated in R173A transfected HEK 293	288
5.11	Comparison of polar contacts at position 173 within WT GCGR and modelled R173A/ R173A, R174A mutant structures	291
5.12	cAMP response in WT and helix 8 GCGR mutant	299
5.13	Comparison of polar contacts at position 406 and 410 within WT GCGR and modelled E406A/E410A/E406A, E410A GCGR mutant structures	301
5.14	Effect of TM4 mutations on the GCGR stimulated cAMP response in HEK 293T cells	310
5.15	Effect of TM4 mutations on the GCGR stimulated cAMP response is reproducible the in HEK 293 cells	313
5.16	Effect of GCGR TM4 mutants on pERK1/2 response	316
5.17	Effect of GCGR TM4 mutants on Ca ²⁺ _i mobilization in transfected HEK 293T cells	319
5.18	Comparison of GCGR residue polar contacts within WT and modelled TM4 mutant structures	321

Chapter 1. Introduction

1.1. Membrane proteins

The cell is the basic structural and functional unit of life. Surrounded by a lipid bilayer known as a membrane, a cell contains the organelles responsible for performing the individual tasks of that particular cell-type (Alberts *et al.*, 2002, Lodish *et al.*, 2000). The membrane serves as a barrier, separating the cell's internal and external environment and selectively allows the influx and efflux of material (Alberts *et al.*, 2002, Lodish *et al.*, 2000). Associated with each membrane is a complement of membrane proteins, which can be classified into two categories; intrinsic proteins which have one or more segment embedded in the lipid bilayer or extrinsic proteins which either interact directly with the polar head groups of the lipid bilayer or indirectly with integral membrane proteins (Alberts *et al.*, 2002, Lodish *et al.*, 2000). The binding of a chemical signal molecule to either cell-surface or intracellular receptors generates a cascade of intracellular signals that control diverse biological functions within a cell.

1.1.1. The receptor concept

The receptor concept was the result of multiple complementary lines of evidence (reviewed in Triggle, 2000 and Rang, 2006) and provides the basic framework for the scientific discipline of pharmacology (Rang, 2006). In cellular signalling, chemical recognition is the function of receptors. Here, the receptor translates the information of the ligand interaction into a cellular response (Triggle, 2000). The linear sequence of amino acids and ultimately the three-dimensional representation of the sequence (receptor structure) provide the basis for receptor classification (Triggle 2000). Four principal families of chemically sensitive receptors have been described; ion channels,

enzyme associated, nuclear and G protein-coupled receptors (GPCRs) (Triggle 2000).

1.2. G protein-coupled receptors (GPCRs)

G protein-coupled receptors (GPCRs) constitute the largest and most diverse family of membrane receptors in eukaryotes with approximately 1000 members (Lefkowitz *et al.*, 2007). These seven-transmembrane (7TM) receptors, as their name implies, couple to heterotrimeric guanine nucleotide-binding proteins (G proteins) comprising of a single α -, β -, and γ -subunits, allowing the transduction of signals from extracellular molecules as diverse as hormones, neuropeptides, odours, photons and glycoproteins (Rosenbaum *et al.*, 2009).

GPCRs play an important role in a plethora of diverse physiological and pathological processes (Lefkowitz *et al.*, 2007). Unsurprisingly, therefore, they are one of the major targets of pharmaceutical drugs, with around 30 to 50% of currently available pharmaceutical drugs targeting only ~20% of the known GPCRs (Salon *et al.*, 2011). This discrepancy between total GPCRs members and currently targeted GPCRs does not infer that the majority of this receptor family is 'undruggable', but likely reflects the lengthy pharmaceutical pipeline and lack of complete GPCR knowledge (Salon *et al.*, 2011).

1.3. GPCRs classification

All GPCRs are integral membrane proteins, which share the same topology of a 7TM domain, an extracellular N-terminal domain (ECD) and a cytoplasmic C-terminus (Furness *et al.*, 2012). Despite this apparent structural similarity, GPCRs are in fact extremely diverse which makes the development of GPCR classification systems difficult (Davies *et al.*, 2007). The majority of GPCRs can be classified into three of the six families (A, B or C) of the A-F classification system (Kolakowski, 1994). According to the alternative GRAFS

(Glutamate, Rhodopsin, Adhesion, Frizzled/Taste and Secretin) classification system, based on phylogenetic studies, the majority of human GPCRs fall into five main families; Rhodopsin (Class A), Secretin (Class B), Glutamate (Class C), Adhesion and Frizzled/Taste (Fredriksson *et al.*, 2003, Schioth and Fredriksson, 2005).

Regardless of the classification system, most consist of three primary families based on sequence analysis and functional similarity (Rosenbaum *et al.*, 2009). The largest sub-family, class A rhodopsin-like, comprises receptors for a vast array of ligands including ions, lipids, steroids, glycoproteins, nucleotides, biogenic amines (muscarinic and dopaminergic ect) and small peptides (Müller *et al.*, 2012, Hiller *et al.*, 2013). The class B, secretin-like GPCRs, form a group of 15 receptors including receptors for several peptide hormones such as corticotropin-releasing factor (CRF) glucagon-like peptide 1 (GLP-1), glucagon (GCG) and calcitonin gene related peptide (CGRP) (Hollenstein *et al.*, 2014, Müller *et al.*, 2012). The class C metabotropic glutamate receptor (mGluR) comprise the receptors that bind glutamate, γ -aminobutyric acid (GABA), Ca^{2+} , amino acids and taste compounds (Nisweder and Jeffrey, 2010).

1.3.1. Class A (Rhodopsin-like) receptors

The class A rhodopsin-like receptors account for over 80% of all known GPCRs (Hiller *et al.*, 2013). The first insight into the structure of GPCRs was from the two-dimensional crystals of bovine rhodopsin (Schertler *et al.*, 1993). This GPCR can be found in the rod photoreceptor cells of the retina and converts photons into chemical signals allowing vertebrates to sense light (Zhou *et al.*, 2012). More recently, multiple research groups have obtained three-dimensional crystal structures of rhodopsin leading to significant progress in our understanding of the entire GPCRs superfamily (Palczewski *et al.*, 2000).

The most variable structure among the family of GPCRs is the N-terminus, with class A GPCRs having a relatively short sequence (10-50 amino acids) when compared to class B and C (~100-600) (Kobilka, 2007). A conserved feature among all class A GPCRs include the stretch of amino acid residues glutamic acid/aspartic acid-arginine-tyrosine (E^{3.49}/D^{3.49} R^{3.50} Y^{3.51} (E/DRY) motif) of TM3 and a negatively charged aspartic acid/glutamic acid (D/E^{6.30}) in TM6, involved in stabilising the inactive state conformation (Vogel *et al.*, 2008) (See 1.17.1). Another highly conserved motif is Asn-Pro-X-X-Tyr (NPXXY) (where X represents any amino acid) located in the cytoplasmic end of TM7 (Barak *et al.*, 1995) and conformational changes within this motif are associated with GPCR activation (Rosenbaum *et al.*, 2009).

1.3.1.1. A_{2A} receptor; an archetype class A GPCR

In the work presented in this thesis, the adenosine A_{2A} receptor (A_{2A}R) was chosen as an archetype class A G_s-coupled GPCR to investigate the importance of intracellular loop one (ICL1). This was due to the availability of multiple A_{2A}R crystal structures (Liu *et al.*, 2012, Lebon *et al.*, 2011, Lebon *et al.*, 2015 and Carpenter *et al.*, 2016, to name a few) and past laboratory experience investigating this receptor.

This receptor binds the purine nucleoside, adenosine, and is one of the four receptor subtypes which also include, A₁, A_{2B} and A₃, (A₁R, A_{2B}R and A₃R) (Sheth *et al.*, 2014). These receptors either inhibit cyclic adenosine 3',5'-monophosphate (cAMP) accumulation in the case of A₁R and A₃R through coupling to G_{i/o} or stimulate cAMP accumulation in the case of A_{2A}R and A_{2B}R via coupling to G_s (Sheth *et al.*, 2014). The A_{2A}R is an attractive therapeutic target due to its importance in mediating vasodilation, protecting tissues from inflammatory damage and supporting the synthesis of new blood vessels (de Lera Ruiz *et al.*, 2013).

Similarly to other GPCRs, the signalling pathway following A_{2A}R stimulation depends on the cell and tissue type, the signalling machinery that

particular cell possesses and the G protein to which it couples. In addition to elevated cAMP levels following A_{2A}R stimulation, there is also evidence to suggest activation of kinases including extracellular signal-regulated kinase 1/2 (ERK1/2) (Schulte and Fredholm, 2000, Orr *et al.*, 2015). On the other hand, A_{2A}R has been demonstrated not to induce an intracellular Ca²⁺ response following agonism (Orr *et al.*, 2015).

1.3.2. Class B (Secretin-like) receptors

There are fifteen known receptors that form class B, the second largest family of GPCRs (Hollenstein *et al.*, 2014). In comparison to the diverse ligands bound by class A GPCRs, class B GPCRs predominantly bind peptide hormones of around 30-40 amino acids including the glucagon subfamily (GCG, GLP-1, GLP-2, glucose dependent inulinotropic polypeptide (GIP)), secretin, calcitonin (CT), CGRP, amylin (AMY) and adrenomedullin (AM), to name a few (Pal *et al.*, 2012). The relatively large ECD (~100-160) containing three disulphide bonds is characteristic of class B GPCRs and, in combination with the 7TM domain, is known to be important for peptide binding (Hoare, 2005).

These receptors are important therapeutic targets for brain and metabolic diseases such as migraine, cardiovascular disease, cancer, obesity, diabetes, stress and anxiety, to name a few (Sexton and Wootten, 2013).

1.3.2.1. Receptor activity-modifying proteins (RAMPs)

Several class B GPCRs are known to form heterodimers with receptor activity-modifying proteins (RAMPs) (Conner *et al.*, 2004) and have been reported to modulate both cell-surface expression and pharmacology (Magalhaes *et al.*, 2012).

Mammalian cells express three RAMPs (RAMP1-3) (McLatchie *et al.*, 1998) which share approximately 31% identity in primary amino acid

sequence (Qi and Hay, 2010). Despite the low sequence identity, all three RAMPs have a common structure: an N-terminal signal peptide between 22 and 42 amino acids, a highly conserved single-TM domain spanning ~22 amino acids, a long extracellular N-terminal (~90 amino acids for RAMP1 and RAMP3, ~102 amino acids for RAMP2) a short intracellular C-terminal tail (~9 amino acids) and four conserved cysteine residues presumed to form disulphide bonds (Sexton *et al.*, 2006, Qi and Hay, 2010).

One of the best characterised interactions between RAMPs and a GPCR is that observed for the class B calcitonin receptor-like receptor (CLR) (Conner *et al.*, 2004). A stable heteromeric complex is formed between CLR and RAMPs in the ER, which is maintained through their life cycle (Sexton *et al.*, 2006). The expression of CLR alone in mammalian cells renders the receptor unable to interact with its endogenous ligands where it remains in the endoplasmic reticulum (ER) (Wootten *et al.*, 2013). The co-expression of CLR with RAMPs in HEK 293T cells allows the functional cell-surface expression of the receptor (McLatchie *et al.*, 1998). Similarly RAMPs, particularly RAMP1, are retained within the ER when not associated with a receptor partner (McLatchie *et al.*, 1998).

RAMPs have not only been shown to escort CLR to the cell surface (Flahaut *et al.*, 2002, Sexton *et al.*, 2006), but also to modify the biochemical properties of the receptor (Watkins *et al.*, 2014, Weston *et al.*, 2015 (Section 4.7)). For example, RAMPs have been shown to alter the ligand selectivity of CLR (McLatchie *et al.*, 1998). While independent heterodimerisation of CLR with RAMP1 forms a CGRP receptor, heterodimerisation with RAMP2 or RAMP3 forms an adrenomedullin (AM) receptor (McLatchie *et al.*, 1998).

Aside from class B GPCRs, RAMPs have also been reported to interact with the class C calcium-sensing receptor (CaSR) where RAMP 1 and RAMP3 enable its cell-surface expression (Desai *et al.*, 2014, Bouschet *et al.*, 2005). The ubiquitous and abundant expression of RAMPs in the majority of mammalian tissue suggests that they may play an important role in defining the functional properties of GPCRs (Christopoulos, 2003). Enhancing

our current knowledge of GPCRs and their interactions with RAMPs is of huge importance, both academically and for potential drug development.

1.5. G proteins

GPCRs, as their name implies, couple to G proteins comprising of α -, β -, and γ -subunits. The α -subunit is a 37-42 kDa protein containing the guanine nucleotide-binding pocket and has intrinsic GTPase activity (Goldsmith and Dhanasekaran, 2007). 17 α -subunits have been identified to date, with those showing more than 50% identity in the amino acid sequence grouped into one of four distinct classes; G_s , G_i , G_q and G_{12} (Simon *et al.*, 1991) (Table 1.1). The $\beta\gamma$ -subunit is formed through the tight association of the individual 35 kDa β -subunit and the 8-11 kDa γ -subunit, of which 5 and 12 have been identified respectively (Goldsmith and Dhanasekaran, 2007). Although any combinations of α -, β - and γ -subunits is possible, not all are observed (Goldsmith and Dhanasekaran, 2007). Efficient plasma membrane targeting of the G protein requires assembly of the $G\alpha$ and $G\beta\gamma$ -subunit and post-translational modifications on the $G\alpha$ -subunit (myristic and/or palmitic acid) and $G\gamma$ -subunit (farnesol or geranylgeraniol) (Vogler *et al.*, 2008).

1.5.1. G protein cycle

On agonist binding, the active GPCR conformation is stabilised promoting interaction with the G proteins. The release of guanosine 5'-diphosphate (GDP) from the 'inactive' state α -subunit allows guanosine 5'-triphosphate (GTP) binding and subsequent dissociation from the GPCR and the $\beta\gamma$ -subunit (Gilman 1987) (Figure 1.1). In turn, both the α -subunit and $\beta\gamma$ -subunit stimulate a number of distinct downstream effectors (Gilman 1987), ultimately leading to changes in intracellular secondary messenger levels and effectively connecting the external cellular environment to a plethora of internal cellular regulators (Hofmann *et al.*, 2009).

The hydrolysis of GTP back to GDP, triggered by the intrinsic GTPase activity of $G\alpha$ -subunit, leads to re-association of the individual G protein subunits, thereby completing the activation-inactivation GTPase cycle and allowing rebinding to the GPCR (Bourne *et al.*, 1991). The GTPase cycle is highly regulated by GTPase-activating proteins (GAPs) and guanine nucleotide exchange factors (GEFs). Despite the intrinsic GTPase activity of G proteins, GTP hydrolysis is very slow and requires GAPs to accelerate the cleavage (Bos *et al.*, 2007). These include regulators of G protein signalling (RGS) proteins which are specific for the $G\alpha$ -subunit, terminating the GPCR signalling cascade (Wettschureck and Offermanns, 2005).

GEFs induce the release of bound GDP through a reduction in nucleotide affinity and a subsequent increase in GTP-bound G protein due to approximately 10-fold higher cellular concentration of GTP compared to GDP (Bos *et al.*, 2007). The $\beta\gamma$ -subunit is thought to enhance efficiency of GTP/GDP exchange due to the preference of this subunit to bind $G\alpha$ -subunit-GDP over $G\alpha$ -subunit-GTP and the GPCR itself to bind G proteins more tightly than to either subunit alone. Through these preferences, the reaction is driven towards replacing GDP for GTP (Bourne *et al.*, 1991).

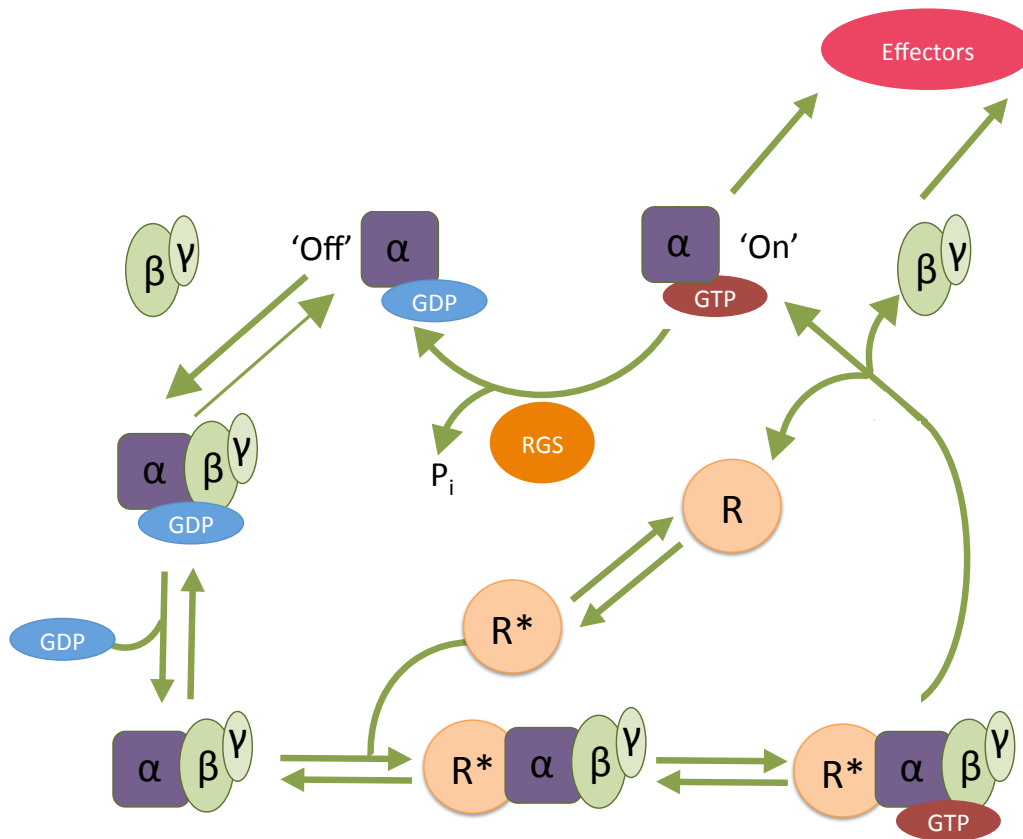


Figure 1.1 Heterotrimeric G protein activation cycle. In the absence of agonist, the G protein-GDP forms a tight inactive complex. G protein also exists in a nucleotide-free state and can stabilising receptor conformations that have high binding affinity for agonists (Yao *et al.*, 2009). On agonist binding to GPCR (R^*), the active GPCR conformation is stabilised. GTP binding to the G protein leads to dissociation from the GPCR and the $G\beta\gamma$ -subunit. In turn, both the $G\alpha$ -subunit and $G\beta\gamma$ -subunit stimulate a number of distinct downstream effectors. The activation cycle is terminated by the intrinsic GTPase activity of the $G\alpha$ -subunit, which allows GTP hydrolysis and reassociation with $G\beta\gamma$ -subunit. The GTPase cycle of G proteins is highly regulated by guanine nucleotide exchange factors (GEFs), which stimulate the exchange of GDP for GTP, and GTPase-activating proteins (GAPs), which antagonise GEFs and accelerate GTP hydrolysis back to GDP. Regulators of G protein signalling (RGS) proteins are specific for the $G\alpha$ -subunit. Image created using information from Gilman 1987 and Denis *et al.*, 2012.

Table 1.1. α -subunits of heterotrimeric G proteins. α -subunits are grouped into one of four distinct classes; G_s , G_i , G_q and G_{12} and examples of inhibitors. Adapted from Wetttschreck and Offermanns, 2005.

Family	Members	Gene	Tissue Expression	Reference for expression	Effectors (+) activates (-) inhibits	Inhibitor
G_s	$G\alpha_s$	GNAS	Ubiquitous	Kozasa <i>et al.</i> , 1988	All ACs Caveolin	NF449 (Hohenegger <i>et al.</i> , 1998)
	$G\alpha_{sXL}$	GNASXL	Neuroendocrine	Pasolli <i>et al.</i> , 2000	All ACs (+)	
	$G\alpha_{olf}$	GNAL	Olfactory neurons, epithelium, brain	Jones and Reed 1989 Zhuang <i>et al.</i> , 2000 Belluscio <i>et al.</i> , 1998	All ACs (+)	
	$G\alpha_{i1}$	GNAI1	Widely distributed		AC1, AC5 and AC6 (-)	PTX (Fong <i>et al.</i> , 1988)
$G_{i/o}$	$G\alpha_{i2}$	GNAI2	Ubiquitous		AC1, AC5 and AC6 (-)	PTX (Fong <i>et al.</i> , 1988)
	$G\alpha_{i3}$	GNAI2	Widely distributed		AC1, AC5 and AC6 (-)	PTX (Fong <i>et al.</i> , 1988)
	$G\alpha_o$	GNAO	Neuronal, neuroendocrine		AC1 (-)	PTX (Fong <i>et al.</i> , 1988)
	$G\alpha_z$	GNAZ	Neuronal, platelets and pancreatic islets	Fong <i>et al.</i> , 1988 Carlson <i>et al.</i> , 1989 Zigman <i>et al.</i> , 1994	AC1, AC5 and AC6 (-)	
	$G\alpha_{gust}$	GNAG	Taste cells, Brush cells	McLaughlin <i>et al.</i> , 1992 Höfer <i>et al.</i> , 1996	cAMP-specific Ca/CaM stimulated PDE1A (+)	PTX (Fong <i>et al.</i> , 1988)
	$G\alpha_{t1}$	GNAT1	Retinal rods, taste cells	Lerea <i>et al.</i> , 1986 McLaughlin <i>et al.</i> , 1993	PDE6 γ subunit	PTX (Fong <i>et al.</i> , 1988)

	$G\alpha_{12}$	GNAT2	Retinal cones	Lerea <i>et al.</i> , 1986	PDE6 γ subunit	PTX (Fong <i>et al.</i> , 1988)
G_q	$G\alpha_q$	GNAQ	Ubiquitous	Strathmann and Simon 1990 Wilkie <i>et al.</i> , 1991	Phospholipase C β 1- β 4 (+) Burtens tyrosine kinase (Btk) (+)	YM-254890 (Takasaki <i>et al.</i> , 2004)
	$G\alpha_{11}$	GNA11	Almost ubiquitous, not in T cells	Strathmann and Simon 1990 Wilkie <i>et al.</i> , 1991	Phospholipase C β 1- β 4 (+)	YM-254890 (Takasaki <i>et al.</i> , 2004).
	$G\alpha_{14}$	GNA14	Kidney, spleen, lung,	Wilkie <i>et al.</i> , 1991	Phospholipase C β 1- β 4 (+)	YM-254890 (Takasaki <i>et al.</i> , 2004).
	$G\alpha_{15}$	Gna15	Hematopoietic cells	Amatruda <i>et al.</i> , 1991	Phospholipase C β 1- β 4 (+)	None (Giannone <i>et al.</i> , 2010).
G_{12/13}	$G\alpha_{12}$	GNA12	Ubiquitous	Strathmann and Simon 1991	Tec kinase phosphorylated leukemia-associated RhoGEF (LARG) (+) Burtens tyrosine kinase (Btk) (+) Ras-GAP1 ^m (+)	
	$G\alpha_{13}$	GNA13	Ubiquitous	Strathmann and Simon 1991	p115-RhoGEF (+) PDZ-RhoGEF (+) Leukemia-associated RhoGEF (LARG) (+)	

1.5.1.1. G_s family

The nucleotide sequence encoding the α -subunit of the G_s protein is 20 kb; composed of 13 exons and 12 introns (Kozasa *et al.*, 1988). The G α_s -subunit encoding guanine nucleotide binding α -stimulating (GNAS) locus is complex, undergoing genomic imprinting and generating multiple gene products with the use of four alternative first exons that splice onto a common set of downstream exons (Liu *et al.*, 2000). In addition to coding for the G α_s -subunit itself, GNAS also encodes a chromogranin-like neuroendocrine secretory protein NESP55 and a larger variant of G α_s , G α_{sXL} (Plagge *et al.*, 2004). While G α_s expression is biallelic (Hayward *et al.*, 1998), NESP55 and G α_{sXL} are expressed from maternal and paternal alleles, respectively (Hayward *et al.*, 1998). G α_{sXL} -subunit is mostly identical to G α_s -subunit with the exception of a XL-specific N-terminus and is able to act as a fully functional G_s protein (Plagge *et al.*, 2008), activating adenylyl cyclases (ACs) resulting in elevated cAMP levels (Wettschureck and Offermanns, 2005).

1.5.1.2. G_{i/o} family

Of the G_{i/o} family members G_{i1}, G_{i2} and G_{i3} are structurally similar, widely expressed and are known to mediate receptor-dependent inhibition of ACs (Wettschureck and Offermanns, 2005). Interestingly and distinct from other G proteins, the effect of G_o appears to be primarily mediated by the G $\beta\gamma$ -subunit where the activity of the G α_o -subunit is unclear (Wettschureck and Offermanns, 2005). G_{gust}, G_{t1} and G_{t2} are members of this family that show more restricted expression and are involved in specific sensory function (Table 1.1). Pertussis toxin (PTX) from *Bordetella pertussis* (Aktories 2011) is a multisubunit toxin composed of an A protomer (also known as S1) and a B oligomer (a pentameric ring of subunits S2, S3, two S4 and S5) and can be used as a tool to study the function of G_{i/o} family members (Carbonetti, 2011). Once in the cytosol, the A subunit hydrolyses nicotinamide adenine

dinucleotide (NAD) and transfers adenosine diphosphate (ADP)-ribose to cysteine residing within the C-terminus of the α -subunit of inhibitory $G_{i/o}$ proteins (with the exception of G_{α_z} -subunit which lacks this cysteine (Fong *et al.*, 1988)), leading to the inhibition of $G_{i/o}$ protein-coupled pathways (Fields and Casey, 1997, Kozasa *et al.*, 1988).

1.5.1.3. G_q family

The α -subunits of each of the four G_q family members, G_{α_q} , $G_{\alpha_{11}}$, $G_{\alpha_{14}}$ and $G_{\alpha_{15}}$ are expressed from four individual genes (Offermanns *et al.*, 2003) (Table 1.1). These G proteins mediate regulation of phospholipase C (PLC) β -isoforms leading to hydrolysis of phosphatidylinositol 4,5-bisphosphate (PIP_2), generating inositol 1,4,5-trisphosphate (IP_3) and diacylglycerol (DAG), with a subsequent rise in intracellular calcium (Ca^{2+}_i) and activation of protein kinase C (PKC), respectively (Exton *et al.*, 1994). In addition to activation of PKC, GPCRs coupled to the $G_{q/11}$ such as the proteinase activated receptor 2 (PAR2) and the free fatty acid 4 receptor (FFA4) have also been implicated in activation of the ERK cascade (Déry *et al.*, 1998 and Young *et al.*, 2010 respectively).

$G_{\alpha_{15/16}}$ -subunits are considered promiscuous whereby they initiate a specific effector response (PLC β) following stimulation of receptors which are known to activate the G_q family of G proteins and receptors that normally couple to G_s and G_i proteins (Offermanns and Simon, 1995).

1.5.1.4. $G_{12/13}$ family

Although only studied in more detail relatively recently the $G_{12/13}$ family members, G_{12} and G_{13} , are being found to couple to a growing number of GPCRs and are amongst the most important in the context of cancer development (Rasheed *et al.*, 2015). The upregulated expression of $G_{12/13}$ has been consistently reported in aggressive cancers such as prostate cancer

and dominantly active forms have been reported to induce both invasion and metastatic behaviours in a number of cell types (Dorsam and Gutkind, 2007). These G proteins are known to activate RhoGTPase nucleotide exchange factors (RhoGEFs) which are key Rho regulators; both transduce signals to Rho and directly activate Rho GTPase by inducing GDP exchange for GTP (Chikumi *et al.*, 2004). Rho GTPase once activated, in turn regulates a number of downstream effectors including cytoskeletal proteins (Siebler, 2009).

1.5.2. $\beta\gamma$ -subunit signalling

One of five β -subunits irreversibly interacts with a single 12 γ -subunits to form the $G\beta\gamma$ -subunit, a signal mediator in its own right (Smrcka, 2008). Although extensive detail into the unique roles and effectors of $G\beta\gamma$ has not been described in this thesis, a number of reviews exist (Smrcka, 2008, Dupré, 2009 and Khan, 2013).

Ligand binding to GPCR and G protein activation is followed by the stimulation of a number of distinct downstream effectors both by the $G\alpha$ and $G\beta\gamma$ -subunit (Gilman 1987). Unlike the $G\alpha$ -subunit, $G\beta\gamma$ does not undergo significant conformational changes on GPCR activation and lacks a catalytic site (Smrcka 2008). It is suggested that G protein activation exposes $G\beta\gamma$ surface allowing binding and regulation of a growing list of molecules and effectors including inward rectifying K^+ channels, GPCR kinase 2 (GRK2), AC and PLC- β (Smrcka 2008). In one well-characterised example, free $G\beta\gamma$ is thought to bind the pleckstrin-homology (PH) domain in GRK2 thereby localising it to the membrane where it is able to interact and phosphorylate GPCRs (Pitcher *et al.*, 1995).

In addition to providing a mechanism of plasma membrane recruitment, $G\beta\gamma$ is also thought to directly activate some effectors through altering their enzymatic activity, such as binding the catalytic domain of PLC- β (Smrcka 2008). In many cases, the activation of a particular pathway such as

the mitogen-activated protein (MAP) kinase (MAPK) pathway is not one mechanism but a number of distinct mechanisms, which likely reflect cell-type, GPCR, and G protein of that pathway (Khan 2013). In the case of the MAPK pathway, three mechanisms have been described, namely the activation of an intracellular effector such as PLC- β , recruitment of GRK isoforms leading to phosphorylation of the GPCR and recruitment of β -arrestin which in turn acts as an adaptor for Src (a non-receptor tyrosine kinase) and finally, transactivation of a receptor tyrosine kinase (RTK) activating classic MAPK signalling pathway (Khan 2013).

1.6. Major effectors of G proteins

1.6.1. Adenylyl cyclases and the cAMP pathway

ACs, large transmembrane ATP-pyrophosphate lyases, represent the major effector of G_s -coupled GPCRs that generates cAMP and pyrophosphate (PPi) from ATP. A total of ten human AC isoforms have been identified, nine of which are membrane-bound designated AC1-9 and a tenth lacking a membrane span and resembling the cyanobacterial AC enzymes (Sadana and Dessauer, 2009). In addition to receiving stimulatory signals from G_s and inhibitory signals from G_i , they are also capable of responding to $G\beta\gamma$ -subunit (stimulatory or inhibitory depending on the AC isoform) (Tang and Gilman, 1991), Ca^{2+} , protein kinases including protein kinase A (PKA), protein kinase C (PKC) and calmodulin kinases (Ca^{2+} -CaM) (Birnbaumer, 2007).

Forskolin, a potent activator of AC (AC1-8 but not 9 or 10) is a useful tool in the investigation signalling cascades involving AC and cAMP (Seamon *et al.*, 1981). This compound binds to the catalytic core of AC, opposite the active site and promotes the assembly of the two domains (Zhang *et al.*, 1997) leading to activation and subsequent elevations in cAMP (Seamon *et al.*, 1981).

The intracellular levels of cAMP are regulated by the activity of both ACs and phosphodiesterases (PDEs). Eleven different PDE families exist, each consisting of several different isoforms and spliced variants (Bender and Beavo, 2006). Similarly to ACs, PDE isoforms differ in their expression patterns generating cell type specific responses (Sassone-Corsi, 2012). Elevations in cAMP activate three main effectors; PKA, exchange protein activated by cAMP (epac) which is a cAMP regulated GEF and cyclin-nucleotide-gated ion channels (Sassone-Corsi, 2012) (Figure 1.2).

Inactive PKA is composed of a regulatory subunit dimer and two reversibly associated catalytic subunits (Manni *et al.*, 2008). Cooperative binding of cAMP to the four binding sites on the regulatory subunit causes dissociation of the catalytic subunits thus activating PKA (Manni *et al.*, 2008). A-kinase-anchoring proteins (AKAPs) are known to bind various enzymes, including the regulatory subunit of PKA, sequestering them near to their specific effectors and substrates, effectively providing specificity in secondary messenger signal transduction (Wong and Scott, 2004). Activated PKA in turn phosphorylates many different substrates including other kinases, transcription factors and GPCRs, in addition to regulating other signalling pathways (Pierce *et al.*, 2002). One such pathway includes the activation and inhibition of the MAPK pathway through the regulation of Raf (Dumaz and Marais, 2003). In most cell types, PKA is suggested to downregulate the MAPK/ERK pathway by interfering with the Ras-mediated activation of Raf-1 (Dumaz and Marais, 2003). On the other hand, PKA is also implicated in activating ERK through inhibition of various phosphatases involved in the downregulation of MAPK signalling (Sassone-Corsi, 2012).

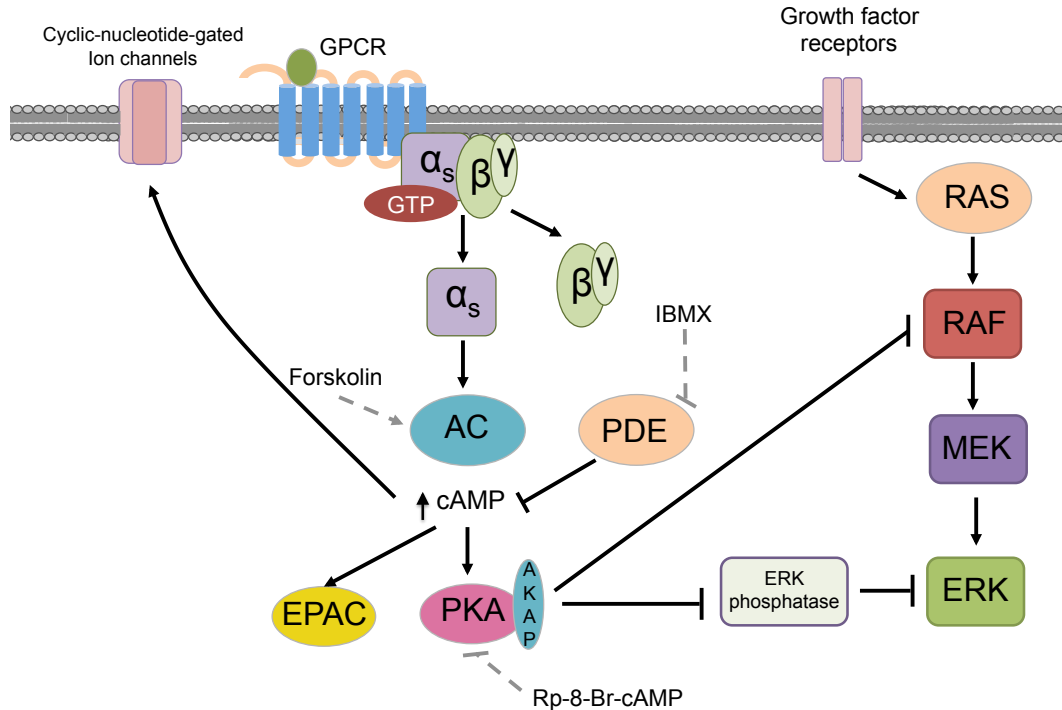


Figure 1.2. cAMP pathway and crosstalk with MAPK/ERK pathway.

ACs are activated by G α_s -coupled GPCRs through the binding of both the G α_s and G $\beta\gamma$ subunit (Tang and Gilman, 1991) resulting in elevated cAMP levels. The intracellular levels of cAMP are regulated by the balance of ACs and phosphodiesterases (PDEs) activity. ACs and PDEs can be activated and inhibited by the chemical compounds forskolin (Zhang *et al.*, 1997) and 3-Isobutyl-1-methylxanthine (IBMX) (Schmidt *et al.*, 2000), respectively. PKA can be inhibited by Rp-8-bromo-cAMP (Rp-8-Br-cAMP) (Schwede *et al.*, 2000). These chemicals provide invaluable tools for the investigation of cAMP signal transduction pathways. Elevations in cAMP activates three main effectors; the serine/threonine kinase, PKA, the guanine-nucleotide-exchange factor (GEF) EPAC and cyclin-nucleotide-gated ion channels (Sassone-Corsi, 2012). Activated PKA in turn phosphorylates many different substrates including other kinases, transcription factors, GPCRs, in addition to regulating signalling components of other pathways such as MAPK/ERK pathway (Dumaz and Marais, 2003).

1.6.2. Phospholipase C (PLC)

Activation of all four isoforms of PLC- β (PLC- β 1 through 4) is predominantly through GPCR coupled to the G α -subunit of the G q family. Activation of PLC- β can also occur through direct stimulation by G $\beta\gamma$ -subunits and increased Ca $^{2+}$ (Kadamur and Ross 2013). PLC catalyses the hydrolysis of PIP $_2$ generating two important secondary messengers; IP $_3$ and DAG (Exton *et al.*,

1994). Through binding to a conserved C1 domain, DAG in turn stimulates a number of enzymes including PKC (Colón-González and Kazanietz, 2006). In addition to the traditional role in PKC activation, DAG is also known to recruit a number of effector proteins such as protein kinase D (PKD) and DAG kinases (DGK) β and γ (Griner and Kazanietz, 2007). More recently, DAG has also been reported to mediate regulation of the two-pore domain potassium channels, TASK-1 and TASK-3 (Wilke *et al.*, 2014). The secondary messenger IP₃ acts at Ca²⁺ release channels, such as the IP₃ receptors located in the ER, allowing Ca²⁺ to diffuse down the electrochemical gradient into the cytoplasm (Foskett *et al.*, 2007). IP₃ is also the substrate for IP₁ synthesis, which in turn stimulates a number of protein kinases and transcription factors (Kadamur and Ross 2013).

1.7. β -arrestins

1.7.1. β -arrestins; desensitisation and internalisation

Since their discovery (Kuhn, 1984), our current understanding of arrestin structure and function has expanded hugely with binding to the majority of phosphorylated GPCRs now known to be a central mechanism in regulating signalling (Gurevich and Gurevich, 2006). There are four mammalian arrestin proteins and seven GRK genes that can undergo alternative splicing (Claing *et al.*, 2002). Arrestin 1 and GRK 1 regulate rhodopsin in the retinal rods whereas arrestin 4 and GRK 7 regulate colour opsins within the retinal cones (Lefkowitz and Shenoy 2005). The regulation of most GPCRs is through, the almost ubiquitously expressed arrestin 2 and arrestin 3 (from herein referred to as β -arrestin 1 and 2, respectively (β -arrestin1/2)) and GRKs 2, 3, 5 and 6 (Lefkowitz and Shenoy 2005). For the majority of agonist bound GPCRs, receptor phosphorylation by GRKs is followed by β -arrestins binding to the phosphorylated C-terminus and subsequent receptor desensitisation and internalisation (Moore *et al.*, 2007).

GPCR internalisation is achieved via the bound β -arrestin acting as a linker to components of the endocytic machinery including clathrin (Goodman 1996) and adaptor protein 2 (AP-2) (Laporte *et al.*, 2002), in addition to mediating receptor ubiquitination, thereby targeting them to the proteasome for degradation (Shenoy *et al.*, 2001). The process of endocytosis, not only plays a role in receptor desensitisation, internalisation and receptor degradation, but also in receptor resensitisation by dephosphorylation and recycling (Krueger *et al.*, 1997).

1.7.2. β -arrestins; an alternative signalling system

Binding of β -arrestin to the cytoplasmic surface of the receptor core has been suggested to result in steric hindrance of further G protein-coupling (Shukla *et al.*, 2014, Kumari *et al.*, 2016). However, this view that β -arrestins essentially 'arrest' GPCR signalling has been challenged by the observation that a number of GPCRs including the V2 vasopressin receptor (V₂R) (Feinstein *et al.*, 2013) and parathyroid hormone type 1 receptor (PTH1R) (Ferrandon *et al.*, 2009) are able to maintain G protein signalling after internalisation to endosomes (Irannejad *et al.*, 2013). More recent work has provided direct evidence for the formation of a super-complex composed of a single GPCR, G protein and β -arrestin (Thomsen *et al.*, 2016). In this super-complex, β -arrestin mediated receptor internalisation had no interference with G protein-coupling (Thomsen *et al.*, 2016) and may provide a physical basis for sustained G protein signalling within cellular compartments.

β -arrestins are now appreciated to serve as an alternative signalling system where they are able to recruit multiple enzymatic effectors (Luttrell and Gesty-Palmer, 2010) through serving as adaptor, scaffold proteins and/or signal transducers (Peirce *et al.*, 2002). Indeed, recent work has shown that β -arrestins remain active after GPCR dissociation allowing them to remain at the cell-surface, presumably signalling independently (Nuber *et al.*, 2016).

Although extensive detail into the growing list of endocytic and signalling proteins bound by β -arrestins is beyond the scope of this work, β -arrestins are known to bind a number of components involved in the MAPK pathway (Gesty-Palmer *et al.*, 2006, Lefkowitz *et al.*, 2006). Here, β -arrestins can form complexes with several signalling protein including Raf, MEK, ERK1/2 and JNK3, thereby stimulating the MAPK pathway (Luttrell *et al.*, 2001, McDonald *et al.*, 2000).

1.8. G protein and β -arrestin mediated ERK1/2 activation

One of the major cellular effectors activated by GPCRs are the MAPKs, which include ERK1/2 (Eishingdrelo and Kongsamut, 2013). ERK1/2 are downstream components of the MAPK pathway. This conserved cascade consisting of MAP kinase kinase kinases (MAPKKKs) (such as Raf isoforms and Ste11), MAP kinase kinases (MAPKKs) (such as MAP/ERK kinase 1 and 2 (MEK1/2)) and finally MAPKs themselves (such as ERK1/ERK2 and Jun N-terminal kinases (JNK1-3)) (Qi and Elion 2005). ERK1 and ERK2 (ERK1/2) have many known targets (including transcription factors such as activator protein 1 (AP-1), nuclear factor (NF)- κ B and Myc) and regulate a number of cellular processes including proliferation, differentiation and meiosis (Qi and Elion 2005).

ERK1/2 activation has been reported to occur via G protein and β -arrestin mediated pathways for a number of GPCRs (Gesty-Palmer *et al.*, 2006). For example, PTHR activation stimulates ERK1/2 phosphorylation is both G protein (involving PKA or PKC) and β -arrestins dependent (Gesty-Palmer *et al.*, 2006). As previously indicated, both $G\alpha$ and $G\beta\gamma$ -subunits of the G protein are able to activate signal transduction pathways leading to ERK1/2 phosphorylation and may be via a PKA mediated pathway (Figure 1.2). GPCRs are also reported to activate ERK1/2 through G_q -mediated (Eishingdrelo and Kongsamut, 2013) or β -arrestin-mediated signalling pathways (Wei *et al.*, 2003, Lefkowitz *et al.*, 2006) (Figure 1.3).

In order to distinguish between G_q protein or β -arrestin-mediated pathways, various PKC inhibitors such as GF109203X and small interfering (si) ribonucleic acid (RNA) (siRNA) targeted to β -arrestins have been employed (Gesty-Palmer, 2006). Whereas G protein mediated ERK activation is rapid, transient and blocked by PKC inhibitors, β -arrestin mediated activation is slower in onset and persists longer (Lefkowitz and Shenoy 2005). In addition, whereas ERK activated through G protein-dependent mechanisms tend to translocate to the nucleus leading to transcriptional regulation and cell proliferation, β -arrestin mediated activated ERK tends to remain in the endocytic vesicles within the cytosol (Lefkowitz and Shenoy 2005). As an example, GLP-1 activates ERK1/2 through either PKA or β -arrestin1 dependent mechanisms (Quoyer *et al.*, 2010). Whereas the PKA-dependent pathway leads to a rapid and transient ERK1/2 phosphorylation with translocation to the nucleus, β -arrestin1 mediated pathway produces a late ERK1/2 phosphorylation that is cytoplasm restricted (Quoyer *et al.*, 2010).

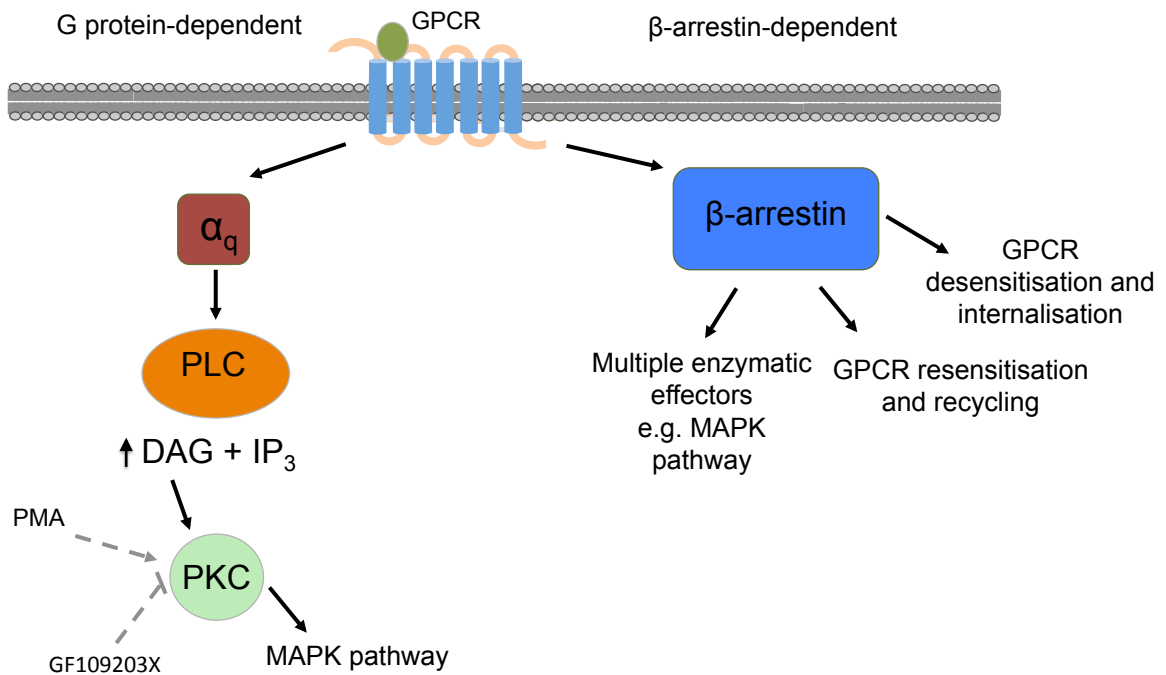


Figure 1.3. G protein and β -arrestin mediated ERK activation. GPCRs are able to activate ERK1/2 in a G protein-dependent or β -arrestin-mediated signalling pathways (Wei *et al.*, 2003). The G protein signal transduction pathways leading to ERK1/2 activation may be PKA (Figure 1.2) or PKC mediated (shown here) (Eishingdrelo and Kongsamut, 2013). Both PKC inhibitors (such as GF109203X) and activators (such as PMA) are useful tools for the investigation into ERK1/2 signalling. β -arrestins are able to recruit multiple enzymatic effectors including components of the MAPK cascade (Luttrell and Gesty-Palmer, 2010).

1.9. Signalling bias: a relatively new field

The classic view of GPCR activation is based on the idea that a receptor's conformation is induced or stabilised on agonist binding leading to an 'active' conformation. Signalling bias (biased agonism or agonist receptor-trafficking) is the phenomenon by which the activated signalling cascade of a single receptor is determined by the bound ligand resulting in different physiological outcomes (Wisler *et al.*, 2014, Bologna *et al.*, 2017). Although the functional coupling of a single GPCR to more than one G protein has been known for years, it is an increasingly recognised concept that ligands can determine a bias towards a particular G protein (Kenakin, 1995), β -arrestin (Lefkowitz and

Shenoy, 2005) or one of the G protein subunits ($G\alpha$ or $G\beta\gamma$) (Blättermann *et al.*, 2012).

Signalling bias can be determined, not only by the changes in second messenger levels or activated cascade components, but also receptor desensitisation, down regulation and degradation (Koole *et al.*, 2013). A number of mathematical methods are used to estimate relative bias towards G protein or β -arrestin mediated pathways. Bias quantification can be achieved through fitting concentration-response curves for each agonist and analysing them by nonlinear regression using the operational model of agonism to determine the τ/K_A ratio (where τ is a measure of coupling efficiency or efficacy and K_A denotes the dissociation constant) (Black and Leff, 1983, Evans *et al.*, 2010, Rajagopal *et al.*, 2011).

This field has seen recent growth due to its implications in drug design with work carried out on a number of receptors including the GLP-1 receptor (GLP-1R) (Wootten *et al.*, 2013b), μ -Opioid receptor (Thompson *et al.*, 2015) and free fatty acid receptor 1 (FFAR1) (Mancini *et al.*, 2015). Unsurprisingly, this has been coupled to an increasing list of identified biased ligands, including orthosteric ligands (bind at the endogenous ligand bindings site) and biased allosteric modulators, which bind to a site distinct from the orthosteric-binding site and modulate the efficacy/affinity of another ligand (Wisler *et al.*, 2014).

1.10. Compounds and toxins as tools for deconvoluting GPCR signalling

The investigation of G proteins and the role they play in GPCR signalling has been made possible by the availability of tools and technologies to dissociate their coupling to downstream signalling cascades. Among these tools are short interfering and short hairpin RNAs (Krumins *et al.*, 2006) and knockout cell lines (Alvarez-Curto *et al.*, 2016) generated using technology such as clustered regularly interspaced short palindromic repeat (CRISPR)/Cas-based RNA-guided DNA endonucleases (Ran *et al.*, 2013). Alternatively, chemical

inhibitors and toxins functionally inhibit, whilst allowing the protein to remain physically intact (Schrage *et al.*, 2015).

Through the utilisation of pharmacological tools with activity at a particular G protein, functional uncoupling of a receptor of interest to a downstream output measure (such as cAMP) can be used to indicate G protein-coupling. Despite the advances in our understanding of G proteins, specific inhibitors have only been described against the G_i and G_q family (Schmitz *et al.*, 2014) (Table 1.1). Signalling via the $G\beta\gamma$ -subunit of the G protein can also be investigated using the specific $G\beta\gamma$ small molecule inhibitor gallein (Lehmann *et al.*, 2008).

Members of the G_i family, with the exception of the $G\alpha_z$ -subunit (Fong *et al.*, 1988), are well-known targets of PTX, as previously described (Section 1.5.1.2) (Fields and Casey, 1997). Although not specific, the suramin analogue, NF449 is a selective inhibitor of the P2X1 receptor with reported inhibitory activity at G_s (Hohenegger *et al.*, 1998, Halls and Cooper, 2010).

YM-254890, a cyclic depsipeptide isolated from *Chromobacterium* sp. QS3666, is a G_q inhibitor (Takasaki *et al.*, 2004). This compound specifically inhibits the release of GDP from $G\alpha_q$, $G\alpha_{11}$ and $G\alpha_{14}$ subunit through binding to a hydrophobic cavity and stabilising the GDP-bound form (Nishimura *et al.*, 2010). A close structural analogue of YM-254890, FR900359 (also known as UBO-QIC), first isolated from the evergreen plant *Ardisa crenata* (Fujioka *et al.*, 2001), is also a selective inhibitor of $G\alpha_q$, $G\alpha_{11}$ and $G\alpha_{14}$ with extraordinary stability (Schrage *et al.*, 2015). Since the discovery of these compounds they have become an invaluable tool for the deconvolution of GPCR signalling and for the investigation of G_q -mediated cellular responses. The availability of YM-254890 and FR900359 to the scientific community has been described as restricted (Xiong *et al.*, 2016). However, YM-254890 can be acquired from Wako Pure Chemical Industries Ltd.

1.11. GPCR dimerisation

1.11.1. Beyond class C GPCR

The growing body of evidence indicating the existence of some GPCRs forming homodimers, heterodimers or as part of large oligomeric complexes has challenged the classic view of GPCRs existing as monomeric entities (Terrillion and Bouvier, 2004, Milligan, 2004).

Although the existence of dimerisation amongst GPCRs is largely accepted, particularly for the class C GPCRs where there is evidence of obligate dimerisation (Marshall *et al.*, 1999), their functional significance including G protein and β -arrestin coupling, downstream signalling and receptor internalisation remains unclear and even controversial (Terrillion *et al.*, 2004). In particular, the difficulty in analysing GPCR dimerisation in native cells has led to the suggestion that some experimental evidence could be attributed to receptor overexpression which often occurs in cellular models (Angers *et al.*, 2002). Answering these fundamental questions surrounding receptor dimerisation could be an important step towards the development of GPCR targeted therapeutics.

1.11.2. Dimerisation and receptor trafficking

There is a growing body of evidence that GPCR dimerisation plays an essential role in the entire GPCR lifecycle; from ER exit to internalisation as a dimeric complex (Milligan, 2009). A number of heterodimers have been reported to co-internalise following stimulation with only one of the receptors cognate ligand including the α_{1a}/α_{1b} adrenergic and A_{2A} adenosine/D2 dopamine receptors (Stanasila *et al.*, 2003 and Ginés *et al.*, 2002, respectively).

The requirement of dimerisation for cell-surface expression has been well established for a number of GPCRs (Terrillon and Bouvier, 2004). The exit from the ER requires complete and correct folding and masking of any ER retention signal or hydrophobic regions that would otherwise retain the

receptor, mostly through interaction(s) with chaperones (Reddy and Corley, 1998). A classic example of obligate dimerisation for successful ER exit is the metabotropic gamma-aminobutyric acid (GABA) type b receptor (GABA_B), a class C GPCR formed of two distinct gene products, GABA_B receptor 1 (GBR1) and GABA_B receptor 2 (GBR2) (Marshall *et al.*, 1999). Although GBR2 alone is able to reach the cell surface, it is non-functional and requires co-expression of GBR1 which itself is only able to exit the ER following masking of the carboxy-terminal ER retention motif by heterodimerisation with GBR2 (Margeta-Mitrovic *et al.*, 2000).

Studies looking at a number of class A GPCR truncated mutants including V₂R (Zhu and Wess, 1998) and dopamine D₃ receptor (Karpa *et al.*, 2000) co-expressed with their respective wild-type (WT) receptors revealed prevention of WT receptor cell surface expression (Milligan *et al.*, 2010). In other words, the mutant acts as a 'dominant-negative' preventing expression of the co-expressed WT GPCR (Milligan *et al.*, 2010).

1.11.3. Dimerisation and signal transduction

Studies on the GABA_B receptor provided the first convincing evidence that dimerisation has implications in signal transduction (Margeta-Mitrovic *et al.*, 2000). Despite GBR1 harbouring the binding site for the agonist GABA, co-expression of GBR2 is required for both cell-surface expression of GBR1 and formation of a functional receptor capable of coupling to the G protein (Margeta-Mitrovic *et al.*, 2000). Interestingly, selectivity for different G protein subfamilies by some GPCRs has been suggested to be influenced by heterodimerisation (Milligan, 2007). As an example, in contrast to the individually expressed δ- and μ- opioid receptors, known to couple to PTX sensitive G protein G_i, co-expression of these receptors caused a loss in G_i-coupling but its retained ability to inhibit AC following PTX treatment suggesting coupling to a PTX insensitive G protein, G_z (George *et al.*, 2000).

1.11.4. Dimerisation in class B GPCRs

Whilst the evidence surrounding GPCR dimerisation amongst class A and C continues to grow, research focused on the class B GPCRs remains sparse in comparison (Ng *et al.*, 2012). Despite this, there is considerable evidence for homodimerisation amongst some members of this class including secretin receptor (Ding *et al.*, 2002), vasoactive intestinal polypeptide receptors (VPAC1 and VPAC2) (Harikumar *et al.*, 2006) and GLP-1R (Harikumar *et al.*, 2012). In addition, there is also evidence for some heterodimers amongst class B GPCRs such as the secretin receptor with GLP-1R (Harikumar *et al.*, 2017) and the GLP-1R with GIPR (Schelshorn *et al.*, 2012), to name a few, although functional consequences have not been reported.

The structural basis for GPCR dimerisation remains elusive, but TM4 has been implicated to constitute the dimerisation interface (Harikumar *et al.*, 2007, Harikumar *et al.*, 2012, Xue *et al.*, 2015, Harikumar *et al.*, 2017). In a secretin receptor TM peptide competition experiment, only TM4 peptide segment disrupted the measure of dimerisation and resulted in reduced signalling implicating dimerisation in receptor functionality (Harikumar *et al.*, 2007). One study demonstrated that double and triple substitutions within the hydrophobic face of TM4 within GLP-1R (L256A^{4.49}, V259A^{4.55} or G252A^{4.49}, L256A^{4.55}, V259A^{4.58} (See Section 1.13 for details on numbering system)) had selective effect on signalling, suggested to be a consequence of a disturbed homodimerisation interface (Harikumar *et al.*, 2012). Here, stimulation with peptide ligands including GLP-1(7-36)amide and oxyntomodulin showed a completely abolished Ca²⁺_i mobilisation and attenuation (~10-fold) in potency for cAMP accumulation and ERK1/2 phosphorylation in the TM4 mutant when compared to WT GLP-1R (Harikumar *et al.*, 2012). In contrast, the allosteric agonist compound 2 showed a completely abolished cAMP accumulation response and a small reduction in the ERK1/2 phosphorylation (Harikumar *et al.*, 2012). These findings suggested that dimerisation of GLP-1R plays an important role in the control of signal bias via altering the coupling efficiency

of this receptor to a number of known GLP-1R effectors such as G_s , G_q and potentially to β -arrestins.

1.12. GPCR structures

The general structure of GPCRs can be divided into three regions including the extracellular regions consisting of the ECD and three extracellular loops (ECL1-3), the TM regions consisting of TM1-7 (Figure 1.4) and the intracellular region consisting of ICL1-3, the amphipathic helix 8 (not present in all GPCRs) and the C terminus (Venkatakrisnan *et al.*, 2013). Improving the structural information available on GPCR through solving the crystal structures allow an expansion on pharmacological data and provide a template for the rational design of structure-based drugs.

To date, of the approximately 1000 mammalian GPCRs (Lefkowitz *et al.*, 2007), the crystal structures of 40 inactive class A GPCRs and a handful of agonist bound class A GPCRs have been solved, including β_2 AR in complex with the heterotrimeric G_s protein (Rasmussen *et al.*, 2011). Of the 15 class B GPCRs, the crystal structures of four have been solved to date; GCGR (Siu *et al.*, 2013, Jazayeri *et al.*, 2016 and Zhang *et al.*, 2017), CRF₁R (Hollenstein *et al.*, 2013), CTR (Liang *et al.*, 2017) and GLP-1R (Song *et al.*, 2017, Jazayeri *et al.*, 2017, Zhang *et al.*, 2017b). However of these class B structures, two of the GCGR (Siu *et al.*, 2013 and Jazayeri *et al.*, 2016) and the CRF₁R (Hollenstein *et al.*, 2013) structures lack the ECD which, in combination with the 7TM domain, is known to be important for peptide binding (Hoare, 2005).

The ECD of class B GPCRs is stabilised by three disulphide bonds and contribute most of the binding affinity of the receptor for the peptide (Underwood *et al.*, 2010). Using X-ray crystallography or NMR, the structure of a number of ECDs in combination with peptide ligands including the GLP-1R (Runge *et al.*, 2008, Underwood *et al.*, 2010), GIPR (Parthier *et al.*, 2007) and GCGR (Koth *et al.*, 2012) have given insight into the mechanism of

peptide binding (Culhane *et al.*, 2015). Such structures, in combination with ligand binding studies, employing truncated and chimeric peptide ligands, provided the basis of the two-step, two-domain model of activation (as reviewed in Pal *et al.*, 2012). This model proposes that in the absence of a ligand, the ECD is mobile through flexibility in the linker connected to TM1 and the C-terminal of the peptide forms an initial complex with the ECD, which in turn allows the N-terminal of the peptide to interact with the 7TM domain and activate the GPCR (Pal *et al.*, 2012).

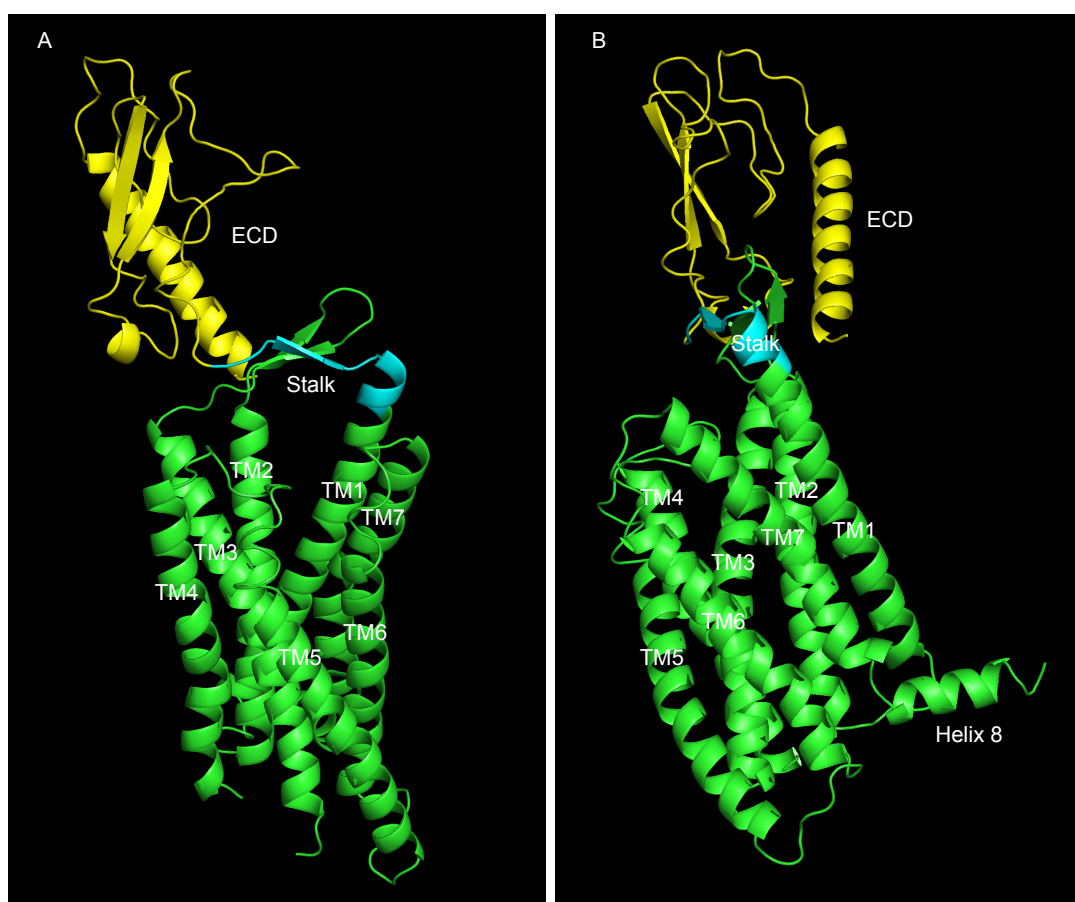


Figure 1.4. Full-length GCGR crystal structure: full-length GCGR in complex with the negative allosteric modulator (NAM) NNC0640 solved by Zhang *et al.*, 2017 at a resolution of 3 Å (PDB ID: 5XEZ) shown as **A**) cartoon representation in MacPyMOL. **B**) Figure A rotated (counterclockwise as viewed from the top) 270° along the y axis. The mAb1 and T4L (inserted into the ICL2 between A256 and E260) has been removed for clarity. The ECD (Q27-D124), stalk (G125-K136) and TMD (M137-W418) are coloured in yellow, cyan and green, respectively. Labelling of TMDs was in line with residues numbering indicated in GPCRdb.org; TM1 (Q131-L166), TM2 (C171-R201), TM3 (S217-L255), TM4 (S262-E290), TM5 (N300-A335), TM6 (Y343-F367), TM7 (Q374-L403), helix 8 (N404-N429).

1.13. GPCR residue numbering

There are a number of GPCR residue numbering schemes employed for the various classes of GPCRs. The class A Ballesteros-Weinstein number scheme (Ballesteros and Weinstein, 1995) consists of two numbers, the first of which is based on TM1-7 and the second on the position relative to the most conserved residue (defined as number 50) within that TM helix. As an example, 3.49 denote a residue located in TM3, one residue before the most conserved residue R3.50. A problem with this numbering system is that not all reference residues are conserved across all receptors within class A making the identification of residues not always straightforward (Isberg *et al.*, 2015).

The Wootten class B GPCR numbering system (Wootten *et al.*, 2013c), is similar to the Ballesteros-Weinstein number scheme and denotes the most conserved residue in each class B GPCR TM domain as .50, preceded by the TM number and the absolute residue number is shown in superscript. As an example, G393^{7.50} of GCGR denotes a glycine at position 393 within TM7 and is the most conserved in the secretin-like class B receptors (Siu *et al.*, 2013). In the case of amino acids falling between two TM regions such as ICL1, within this thesis, the first number indicates the TM immediately before and after (such as ICL1 S167^{12.48} within GCGR).

The class C GPCR Pin numbering system was used in the publication of the mGluR5 structure, whereas the class F Wang scheme was used in the publication of the Smoothed receptor structure (Pin *et al.*, 2003 and Wang *et al.*, 2014, respectively).

GPCRDB provides tools supporting alignment of all GPCR classes displaying the residue numbers from the various schemes; Ballesteros and Weinstein (A), Wootten (B), Pin (C) and Wang (F) (Isberg *et al.*, 2017). In this thesis, the Wootten class B and Ballesteros and Weinstein class A GPCR numbering system was employed for the GCGR and A_{2A}R, respectively.

1.14. The glucagon receptor (GCGR)

GCG is a 29-amino acid peptide hormone produced by the α -cells of the pancreatic islets through posttranscriptional processing of proglucagon peptide (Rouillé, 1997) (Figure 1.5). GCG binds the glucagon receptor (GCGR) leading to the stimulation of glycogenolysis (the enzymatic breakdown of glycogen) and gluconeogenesis (the synthesis of glucose from lactate and amino acids), effectively counteracting the consequences of excessive insulin and ultimately resulting in glucose release into the bloodstream (Quesada *et al.*, 2008). GCGR is also stimulated by the GCG related 37-amino acid peptide oxyntomodulin (Pocai, 2012, Weston *et al.*, 2015). This peptide is mainly produced in gut endocrine L-cells (Figure 1.5) and is able to modulate gastric acid secretion from gastric oxyntic glands (Pocai, 2014). It has been described as a full agonist of the GCGR-mediated cAMP accumulation while showing 100-fold reduced potency when compared to GCG (Pocai *et al.*, 2009, Weston *et al.*, 2015).

Although the GCGR is reported to mediate its effects through the activation of G_s , studies have highlighted the possibility of GCGR to activate alternative G proteins such as $G_{q/11}$, leading to a downstream increased intracellular DAG and IP_3 via Ca^{2+} activated $PLC\beta$ (Xu and Xie, 2009, Wakelam *et al.*, 1986). Interestingly, the GCG analogue (1-N- α -trinitrophenylhistidine,12-homoarginine)glucagon (TH-GCG) was previously reported in hepatocytes extracted from male Sprague-Dawley rats to neither activate AC or cause cAMP response, but was shown to fully stimulate glycogenolysis, gluconeogenesis and stimulates the production of inositol phosphates (Wakelam *et al.*, 1986). This was described as an alternative mechanism by which GCG activation may exert its effects independent of cAMP and that this may indicate the existence of two distinct receptors for GCG, one coupled to inositol phospholipid breakdown and another coupled to stimulate AC activity. Similar findings were reported in hepatocytes extracted from guinea pigs (Lenzen *et al.*, 1990). These early findings may be explained by signaling bias where the downstream signaling cascade initiated by TH-

GCG is predominantly through G_q-coupling. However, relatively little research has been performed to investigate alternative G protein-coupling within the GCGR and to confirm these early findings.

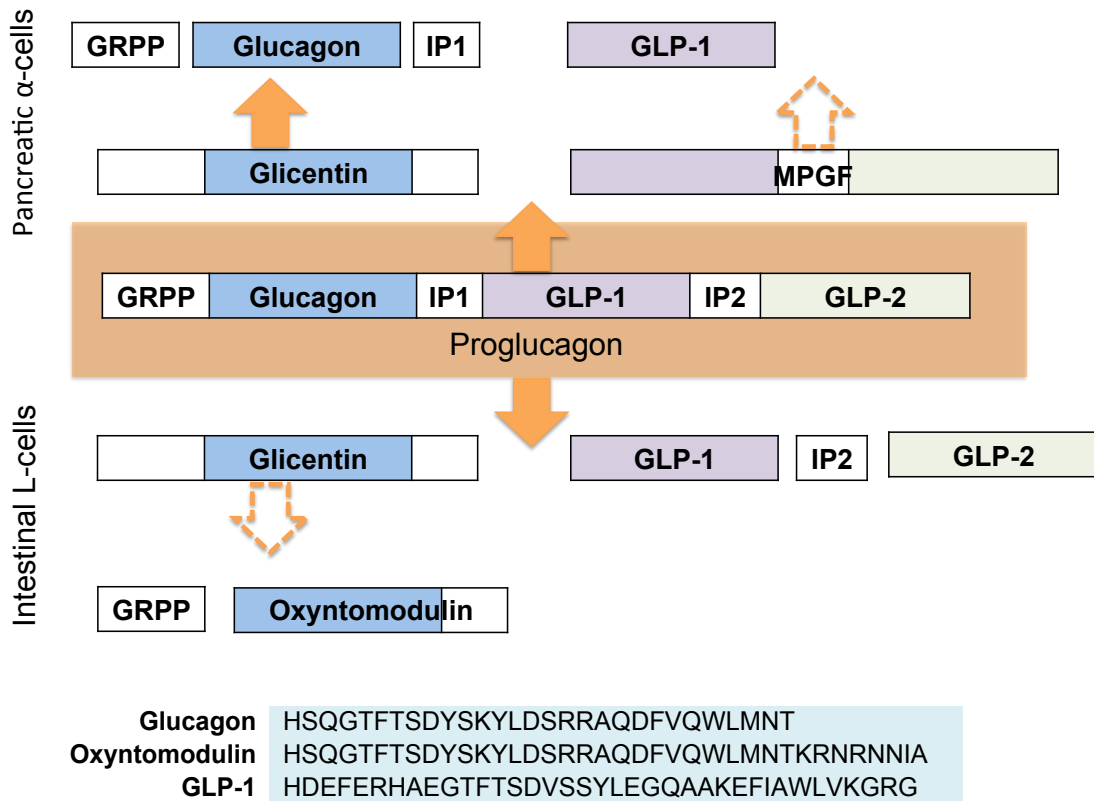


Figure 1.5. Schematic representation of proglucagon processing in the pancreatic α -cells and intestinal L-cells. Glicentrin, GLP-1, GLP-2, GCG, oxyntomodulin, glicentin-related pancreatic polypeptide (GRPP), major proglucagon fragment (MPGF), intervening peptide 1 and 2 (IP1 and IP2, respectively), are all processed from a single messenger RNA (mRNA) transcript expressing in the α -cells of the pancreatic islets, intestinal L-cells and central nervous system (CNS). This proglucaon mRNA is translated into a single 160 amino acid precursor protein which undergoes tissue-specific posttranslational processing. Partial processing is indicated by dashed arrows. Figure adapted from Janssen *et al.*, 2013 and Rouillé, 1997. The amino acid sequence of GCG, oxyntomodulin, GLP-1 and GLP-1(7-36) are also shown.

1.15. GCGR structures

The first crystal structure of the 7TM domain of GCGR bound to the negative allosteric modulator (NAM), NNC0640, was solved to a resolution of 3.4 Å (Sui *et al.*, 2013 PDB ID: 4L6R). Interestingly, a comparison between this structure and that of 15 known inactive class A GPCR structures revealed that both the position and orientation of the helices within the 7TM domain were conserved, but there are a number of distinct features (Sui *et al.*, 2013). Such features include the long N-terminal end of helix I (the stalk) extending three helical turns above the extracellular membrane boundary, the 16 residue ECL1 when compared to 4-6 residues in class A GPCRs and the positioning of the extracellular tips of the 7TM helices creating a wider and deeper cavity in the ligand-binding pocket (Sui *et al.*, 2013). With the CRF₁R structure also revealing a wider and deeper ligand-binding pocket when compared to class A GPCRs, this appears to be a conserved feature amongst class B GPCRs (Hollenstein *et al.*, 2013).

The second crystal structure of GCGR in complex with the antagonist MK-0893 was solved at a resolution of 2.5 Å (Jazayeri *et al.*, 2016 PDB ID: 5EE7). In order to facilitate crystallisation, the GCGR ECD was removed, the C-terminus truncated, 11 amino acid substitutions made to creating a thermostabilised receptor (StaR) (such as R173A) and T4-lysozyme (T4L) inserted into ICL2. The conformation of the 7TM domain was found to be similar to the first resolved GCGR structure with the conserved disulphide bond between C294^{45,50} in ECL2 and C224^{3,29} stabilising the 7TM fold (Jazayeri *et al.*, 2016). Within this structure, the N-terminus of TM5 unwinds by one helical turn allowing ECL2 to extend across the bundle forming a cap to the entrance of the orthosteric site and mediates interactions from TM3 across to TM6 and TM7 (Jazayeri *et al.*, 2016). MK-0893 was found to bind at an allosteric site in a position between TM6 and TM7, effectively straddling TM6 from within the lipid bilayer, and may restrict the outward movement of TM6 required for G protein-coupling (Jazayeri *et al.*, 2016).

Most recently, the crystal structure of the full-length inactive GCGR structure in complex with the NNC0640, and antigen-binding fragment (Fab) of an inhibitory antibody (mAb1) was solved to a resolution of 3.0 Å (Zhang *et al.*, 2017 PDB ID: 5XEZ). This full-length GCGR structure has a similar 7TM domain compared to the two previously solved structures (Siu *et al.*, 2013 and Jazayeri *et al.*, 2016) and a similar ECD comprising the common α - β - β - α fold as observed in the ECD structures of GCGR (Koth *et al.*, 2012) and GLP-1R (Underwood *et al.*, 2010). NNC0640 was found to bind to the extracellular surface of the 7TM domain in a cleft between TM6 and TM7, similar to the binding site of MK-0893 at GCGR (Jazayeri *et al.*, 2016) and the two NAMs (PF-06372222 and NNC0640) at GLP-1R (Song *et al.*, 2017). The identification of this novel allosteric binding site not only expands the current understanding of the mechanism of GCGR and indeed other class B GPCR activation, but also provided the opportunity for structure-based drug design for the class B GPCRs.

1.16. Insight into receptor activation; Comparison between active and inactive class B crystal structures

Recently, the X-ray structure of peptide agonist-bound GLP-1R (Jazayeri *et al.*, 2017) and cryo-EM structures of the class B salmon calcitonin (sCT) unmodified CTR (at a nominal resolution of 3.8 Å) and peptide-activated rabbit GLP-1R (nominal resolution of 3.9 Å) both in complex with heterotrimeric G_s were solved (Liang *et al.*, 2017 and Zhang *et al.*, 2017b, respectively). The comparison between these active structures and inactive GPCR structures, such as the CRF₁R and GCGR, provided some insight into conformational changes upon class B GPCR activation.

Relative to the inactive structures of GCGR (Jazayeri *et al.*, 2016) and CRF₁R (Hollenstein *et al.*, 2013), TM6 in CTR showed a large outward movement at the cytoplasmic and extracellular face (15 Å and 9-11 Å, respectively (measured from alpha carbon (C α) of X^{6.35})), with a 60° kink at the centre of TM6 formed around the highly conserved Pro^{6.47}-X-X-Gly^{6.50}

(PXXG) motif (CTR P384^{6.47}-X-X-G387^{6.50}) (Liang *et al.*, 2017). This movement at the cytoplasmic face was suggested to open the bundle to accommodate interactions with the α 5-helix of G_s (Liang *et al.*, 2017). This sharp kink in the PXXG motif was also reported in the active structure of GLP-1R and caused the intracellular half of TM6 to move outwards by 18 Å (measured from C α of K346^{6.35}) (Zhang *et al.*, 2017b). This movement was indicated to allow interactions between the N-terminus of GLP-1(7-36)amide and the binding pocket (Zhang *et al.*, 2017b). Given the similarities between both G_s bound GLP-1R and CTR structures, the outward movement of TM6 is likely to be a conserved mechanism of receptor activation for class B GPCRs.

1.17. Inactive receptor state; conformation stabilisation

1.17.1. The E/DRY motif in class A GPCRs

The highly conserved E/DRY (E^{3.49}/D^{3.49} R^{3.50} Y^{3.51}) motif in TM3, is one of the mostly highly conserved sequences motifs in GPCRs (Rovati *et al.*, 2007). The “ionic lock” (Vogel *et al.*, 2008) is proposed to stabilise the inactive receptor conformation and involves a salt bridge between the R^{3.50} within the E/DRY motif in TM3 and a negatively charged D/E^{6.30} in TM6 (Audet and Bouvier, 2012). This R^{3.50}-E^{6.30} ionic lock is consistently shown in the inactive rhodopsin receptor crystal structures and in a number of other class A GPCRs including the antagonist bound A_{2A}R (Doré *et al.*, 2011), D₃R (Chien *et al.*, 2010) and A₁R (Cheng *et al.*, 2017, Glukhova *et al.*, 2017) suggesting this mechanism may be a general feature of class A GPCR.

In some GPCRs where the ionic lock is absent, such as the β_2 AR, there are residues capable of forming strong interactions between TM3 and TM6 (Trzaskowski *et al.*, 2012). Disruption of this interaction has been shown to lead to TM6 movement away from the TM bundle creating a crevice in the cytoplasmic region of the receptor (Xiaojie *et al.*, 2006), providing a deep pocket for the G protein (Rasmussen *et al.*, 2011). This is highly similar to the

outward movement of TM6 reported for the class B GLP-1R and CTR active structures (Zhang *et al.*, 2017b and Liang *et al.*, 2017, respectively), previously described. Indeed, mutations the E/DRY motif have been shown to induce constitutive activity (agonist independent increase in basal activity) for a number of GPCRs including the β_2 AR, rhodopsin receptor and oxytocin receptor (OTR) (Rovati *et al.*, 2007).

In the A_{2A} R, R102^{3.50} of the E/DRY motif engages in two salt bridges, one with E228^{6.30} and another with the adjacent D101^{3.49} (Fanelli and Felling, 2011). Other residues implicated to be involved in the ionic lock of the A_{2A} R include Y112^{34.53} in the ICL2 and T41^{2.39} in TM2, where D101^{3.49} forms hydrogen bonds with both residues (Martínez-Archundia and Correa-Basurto, 2014). In the A_{2A} R, R102^{3.50} may act to strengthen the polar interactions between the motif, ICL2 and TM2 and may have direct implications on G protein activation (Jaakola *et al.*, 2008).

1.17.2. HETX motif in class B GPCRs

Similar to the functional role of the E/DRY motif in class A GPCRs, an extensive polar interaction network is formed between residues H^{2.50}, E^{3.50}, T^{6.42} and Y^{7.57} known as the HETX motif (or TM2-3-6-7 network) and is suggested to lock class B GPCRs in an inactive conformation (Liang *et al.*, 2017). Interestingly, T^{6.42} within TM6 of class B GPCRs is suggested to mimic the D/E^{6.30} in class A GPCRs and disruption of the restraint imposed by T^{6.42} facilitates the outward movement of TM6 and thus receptor activation (Cordomí *et al.*, 2015). Indeed, within the inactive structure of GCGR, the side chain of T351^{6.42} forms a hydrogen-bond interaction with Y400^{7.57} (Siu *et al.*, 2013). While the H^{2.50}-E^{3.50} interaction is maintained in two of the inactive GCGRs structures (Sui *et al.*, 2013 and Jazayeri *et al.*, 2016) and in the active CTR structure (Liang *et al.*, 2017), the polar interactions between T^{6.42} and Y^{7.57} are broken within the active CTR structure and form new hydrogen bonds with the TM6 backbone (Liang *et al.*, 2017). This lost interaction

supposedly releasing the constraint on TM6 and possibly allows transition of TM6 away from the TM bundle (Liang *et al.*, 2017). Indeed, this outward movement of TM6 and HETX motif disruption was also found in the active GLP-1R structure (Zhang *et al.*, 2017b) suggesting this conformational change may be conserved amongst class B GPCRs.

Similarly as has been reported from mutations within the E/DRY motif (Rovati *et al.*, 2007), mutations within the HETX motif have also been shown to result in constitutive receptor activity. For example mutation of T^{6.42} within GCGR to alanine led to an increased constitutive activity (Hjorth *et al.*, 1998), suggesting this motif may be implicated in maintaining the receptor in an inactive state.

1.17.3. TM2-6-7-Helix 8 network in class B GPCRs

The TM2-6-7-Helix 8 (R^{2.46}, R/K^{6.37}, N^{8.47} and E^{8.49}) network similarly to HETX motif, has been implicated to form part of the class A E/DRY motif equivalent in class B GPCRs (Vohra *et al.*, 2013). It should be noted that position N^{8.47} has also been denoted N^{7.61} in the literature (Liang *et al.*, 2017 and Zhang *et al.*, 2017), and is at the TM7-helix 8 junction.

Within GLP-1R, R176^{2.46}, R348^{6.37} and helix 8 N406^{8.47} and E408^{8.49} were implicated to be important for stabilising the inactive receptor (Wootten *et al.*, 2016) and outward movement of TM6 on receptor activation breaks these polar interactions (Zhang *et al.*, 2017b). The residues within this disrupted network may in turn form electrostatic interactions with the α 5-helix of G_s (Zhang *et al.*, 2017b). This outward opening of the cytoplasmic half of TM6 and the cytoplasmic end of TM5, TM2, TM3 and TM7 was shown to form the binding cavity for G_s and additional electrostatic interactions described between E412^{8.53} of helix 8 and H171 of ICL1 with G β of the G protein (Zhang *et al.*, 2017b).

A similar TM2-6-7-helix 8 network was also evident in the GCGR structure involving R173^{2.46}, R346^{6.37}, N404^{8.47} and E406^{8.49} (Siu *et al.*, 2013)

and within the CTR structure involving R180^{2.46}, K340^{6.37} N395^{8.47} and E397^{8.49} (Liang *et al.*, 2017). In both the GCGR inactive structure and a CTR homology model, R^{2.46} forms tight interactions with R/K^{6.37} and E^{8.49} (Sui *et al.*, 2013 and Liang *et al.*, 2017, respectively). Whilst the salt bridge between R^{2.46} and E^{8.49} was maintained in the active CTR-G_s structure, the one between K^{6.37} and E^{8.49} was broken with the residues shown to be 26 Å apart, thereby releasing constraints on TM6 (Liang *et al.*, 2017). These findings may implicate the importance of the helix 8 E^{8.49} for class B GPCR activity (Section 1.18.2).

1.18. Intracellular GPCR domains ICL1 and Helix 8

The intracellular region of GPCRs consists of ICL1-3, helix 8 and the C-terminus which are all capable of forming interactions with GPCR effectors including G proteins, kinases and β-arrestins (Venkatakrisnan *et al.*, 2013). A number of studies looking at class B GPCRs have proposed critical roles for residues within ICL1-3 including maintaining GPCR in an inactive state (Martínez-Archundia and Correa-Basurto, 2014), coupling to G proteins (Mathi *et al.*, 1997, Conner *et al.*, 2006 and Kleinau *et al.*, 2010), protein folding and correct transport (Thomas *et al.*, 2007). Here, we focus on previous research looking at the importance of ICL1 and helix 8 only.

1.18.1. The importance of ICL1 in cell-surface expression and G protein-coupling

1.18.1.1. ICL1 cysteine and cell-surface expression

The importance of ICL1 C^{2.44} has been studied in GPCRs including GLP-1R, PTHR1 and the CLR (Mathi *et al.*, 1997 and Underwood *et al.*, 2013, Thomas *et al.*, 2007 and Conner *et al.*, 2006, respectively). Mutation within CLR (C149A^{2.44}) had no influence on receptor cell-surface expression or cAMP response (Conner *et al.*, 2006), whereas the similar mutation in GLP-1R (C174A^{2.44}) resulted in reduced cell-surface expression and cAMP response

(Mathi *et al.*, 1997 and Underwood *et al.*, 2013). Similarly, C217^{2.44} of PTHR1 was implicated as a critical determinant of cell-surface translocation and function (Thomas *et al.*, 2007). Imaging of mutant PTHR1 showed fluorescence signal concentrated to the interior of the cell suggesting C217^{2.44} has a distinctive role in protein folding and correct transport (Thomas *et al.*, 2007).

1.18.1.2. ICL1 and G protein-coupling

Multiple studies have highlighted the importance of conserved R^{2.46} for G protein-coupling including the CGRP receptor model (R151^{2.46}) (Vohra *et al.*, 2013) and in the structure of the peptide-activated rabbit GLP-1R in complex with heterotrimeric G_s (R176^{2.46}) (Zhang *et al.*, 2017b). Within this latter structure, it was suggested that the lost interactions for R176^{2.46}, N406^{8.47} and E408^{8.39} in helix 8 on receptor activation may be stabilised through hydrogen bonds or electrostatic interactions with residues of the G_s α5-helix (Zhang *et al.*, 2017b).

Mutagenesis studies in combination with measurement of secondary messenger responses have provided additional evidence to support these structural findings. In one such study looking at alanine substitution mutants of all the conserved residues within the ICLs of the CGRP receptor, R151^{2.46} of the ICL1 region (K145-R151) was found to be crucial for G protein-coupling, as determined by the severe reduction of CGRP-mediated cAMP accumulation, but had no effect on cell-surface expression (Conner *et al.*, 2006). Similarly, a number of residues within the ICL1 region of GLP-1R and CLR were implicated as important for the cAMP response, suggesting a role for ICL1 in G_s-coupling (Mathi *et al.*, 1997 and Conner *et al.*, 2006, respectively). The cAMP response measured in C174A^{2.44}, R176A^{2.46} and N177A^{2.47} GLP-1R was significantly reduced when compared to WT, which was not necessarily correlated with reduced cell-surface expression (Mathi *et al.*, 1997). For example, R176A^{2.46} showed the lowest cAMP response with a

10-fold reduced GLP-1(7-36)amide potency but had no reduced cell-surface expression when compared to WT (Mathi *et al.*, 1997). In another study, mutation of GIPR R169^{2.46} to alanine resulted in a 7-fold reduction in cAMP potency with a small decrease in cell-surface expression (Cordomí *et al.*, 2015).

The importance of ICL1 has also been implicated in class A GPCRs. In one such study, the ICL1 and helix 8 amino acids of the class A GPCR thyrotropin receptor (TSHR) were systematically investigated using site-directed mutagenesis and cAMP and IP accumulation assays (Kleinau *et al.*, 2010). A number of ICL1 alanine mutants were found to reduce both cAMP and IP accumulation whereas some (and a single helix 8 mutant) were identified to impact IP but not cAMP accumulation (Kleinau *et al.*, 2010). This finding was interpreted as TSHR G_q-coupling requiring more selective interactions when compared to G_s-coupling and was speculated to be the case for other GPCRs (Kleinau *et al.*, 2010). This may implicate ICL1 as a mediator of G protein selectivity and therefore could be involved in signalling bias.

1.18.2. Helix 8 of GPCRs

Within GPCRs, the structure of the cytoplasmic C-terminus is the least well-defined domain and likely reflects the conformational plasticity (Sensoy and Weinstein, 2014). Within class A GPCRs, helix 8 is defined as an amphiphathic helix that is initiated just after the conserved NPXXY motif in TM7, usually oriented parallel to the membrane bilayer and perpendicular to the TM bundle (Gehret *et al.*, 2010). Despite very little or no sequence homology between class A and B GPCRs, there is suggested to be striking topological similarity of helix 8 (Conner *et al.*, 2008) (Figure 1.4). The CTR structure revealed a very long extended helix 8 (Liang *et al.*, 2017) similar to that in the GCGR structure detailing a 20-residue helix 8 (Sui *et al.*, 2013).

The conserved nature of helix 8 in both structures suggested that this might be a conserved feature of not only class A GPCRs but also class B GPCRs.

Helix 8 is implicated in a range of functions including cell-surface expression (Timossi *et al.*, 2004, Liang *et al.*, 2017) and G protein-coupling (Delos Santos *et al.*, 2006, Kleinau *et al.*, 2010). Interestingly, one helix 8 TSHR mutant was found to reduce IP but not the cAMP response, implicating this residue as sensitive to G_q but not G_s activation and may suggest a role for helix 8 in G protein-coupling specificity (Kleinau *et al.*, 2010).

Intramolecular links between helix 8 and the TM domains have been observed in a number of GPCRs structures and have been implicated to be important in receptor activation and deactivation for both class A (Huynh *et al.*, 2009) and class B GPCRs (Zhang *et al.*, 2017b). In particular, E^{8.49} is fully conserved in class B GPCRs and may play a role in GPCR activation (Kirkpatrick *et al.*, 2012) where it has been implicated in the TM2-6-7-helix 8 network (Section 1.17.3) and G protein-coupling (Liang *et al.*, 2017). For example, helix 8 residues within the structures of CTR (A407^{8.59}, W413^{8.65} and Q408^{8.60}) and GLP-1R (R419^{8.60} (and possible further electrostatic interaction with E412^{8.53} and ICL1 H171^{12.49})) were predicted to interact with Gβ (Liang *et al.*, 2017 and Zhang *et al.*, 2017b, respectively). It is possible helix 8 plays a crucial part of a functional activation switch. With this in mind, determining the interactions between helix 8 and other regions within the GPCR and how this might influence receptor signalling is of interest.

1.19. Aims of this study

In order to understand how GPCRs, through multiple conformational states, mediate signal transduction at the molecular level, we must begin to understand how agonist binding leads to receptor activation and subsequent stimulation of downstream signalling. We hypothesise that GCGR is able to activate multiple downstream signalling cascades.

Using mutagenesis, knockout cell lines and multiple assays measuring downstream signalling components (cAMP, pERK1/2 and Ca²⁺i mobilisation),

this work aims to explore this hypothesis and expand current knowledge on GCGR activity. We aim to characterise the action of two known GCGR agonists (GCG and oxyntomodulin) and two potential GCGR antagonists (des-His¹,[Glu⁹]-glucagon amide (des-His¹,[Glu⁹]-GCG) and L-168,049 (Unson *et al.*, 1989 and Cascieri *et al.*, 1999,. respectively)) both in transfected and hepatocyte cell lines. We also aim to investigate the activity of the GCG analogue TH-GCG, previously suggested to act at a receptor distinct from GCG (Wakelam *et al.*, 1986).

We aim to investigate the ICL1 region and several other residues within GCGR including the helix 8 residues E406^{8.49} (implicated in the TM2-6-7-helix 8 network (Section 1.17.3) and G protein-coupling (Liang *et al.*, 2017)) and three TM4 residues (G271^{4.49}, L277^{4.55}, V280^{4.58}) (suggested to form a homodimerisation interface in GLP-1R (Harikumar *et al.*, 2012)) to determine their importance for both GCGR cell-surface expression and signalling. The A_{2A}R, due to the availability of multiple crystal structures, was chosen as an archetype class A G_s-coupled receptor to further investigate the importance of ICL1 across GPCR classes.

Chapter 2. Materials and Methods

2.1. Cell culture methodology

2.1.1. Cell lines

Cell lines were maintained using standard subculturing routines as guided by the European Collection of Cell Culture (ECACC) and checked annually for mycoplasma infection using an EZ-PCR mycoplasma test kit from Biological Industries (Kibbutz Beit-Haemek, Israel). All procedures following were performed in a sterile tissue culture hood using aseptic technique and solutions used in the propagation of each cell line were sterile and pre-warmed to 37°C.

The Flp-In human embryonic kidney-293 (HEK 293) cells stably expressing the GLP-1R and the CRISPR/Cas9 genome-edited HEK 293 cells were kindly gifted to us by Dr Dan Donnelly (University of Leeds) and Dr Asuka Inoue (Tohoku University, Japan), respectively. All HEK 293 cell lines and HEK 293T cells were cultured in Dulbecco's modified Eagle's medium (DMEM) supplemented with 10 percent fetal bovine serum (FBS) purchased from Sigma-Aldrich Company Ltd (Sigma-Aldrich, F9665) (Dorset, UK) and placed in a humidified 5 percent CO₂ incubator at 37°C. Human black hepatocyte carcinoma (Hep 3B) cells were purchased from ATCC (Middlesex, UK) and cultured in minimal essential medium Eagle (MEME) (Sigma-Aldrich, M5650), supplemented with 10 percent FBS and 2 mM L-glutamine (Sigma-Aldrich). Chinese hamster ovary (CHO)-K1 cells, including the CHO-K1 cells stably expressing GCGR or GLP-1R (kindly gifted to us by Dr David Hornigold and Dr Jacqui Naylor at MedImmune Ltd, Cambridge UK) were cultured in F-12 Nutrient Mixture (Ham) GlutaMAX™ purchased from Thermo Fisher Scientific (31765035) (Wilmington, Massachusetts, US) supplemented with 10 percent FBS. All cell lines were harvested following washing with PBS using 0.05 percent Trypsin-ethylenediaminetetraacetic acid (EDTA) (Sigma-Aldrich, 59417C).

2.1.2. CRISPR knockout HEK 293 cell lines

The parental HEK 293 cell line and the various knockout HEK 293 cell lines generated through the use of CRISPR/Cas-based RNA-guided DNA endonucleases were kindly made and gifted to us by Dr Asuka Inoue (Alvarez-Curto *et al.*, 2016). Here, the genes encoding the various G proteins and β -arrestin1/2 were targeted by a CRISPR-Cas9 system (Ran *et al.*, 2013) with some modifications (Schrage *et al.*, 2015). Briefly, HEK 293 cells were transfected with G protein/ β -arrestin1/2 targeting sgRNA sequence containing vector(s) (pX330; Addgene plasmid 442230) and a pGreen Lantern vector encoding a GFP. GFP-positive cells were isolated using a cell sorter (SH800, Sony, Japan), and cultured in a 96-well plate for approximately 2 weeks until wells containing an apparent single colony were selected for passages. Successful introduction of the null mutation was confirmed through a polymerase chain reaction (PCR) and restriction enzyme digest or Sanger sequencing method (FASMAC, Japan), western blot analysis for protein expression and through functional assays. The absence of G protein or β -arrestin1/2 expression in each cell line, although confirmed by others (Schrag *et al.*, 2015, Alvarez-Curto *et al.*, 2016), was not re-confirmed by us.

2.1.3. GCGR stable expressing HEK 293 cell line generation

The aminoglycoside antibiotic Geneticin®, or G418 (Thermo Fisher Scientific) was used to select for HEK 293 cells expressing pmCherry-N1 vector (Clontech Laboratories, 632523) (California US) containing the *neo* gene (Davies and Jimenez, 1980) and GCGR (made by a previous postdoctoral research associate in the Dr Ladds laboratory group, Dr Cathryn Weston). The optimum concentration of G418 to select for transfected cells was determined through performing a kill curve (Figure 2.1). Here, HEK 293 cells were treated with several antibiotic concentrations ranging from 100-1000 $\mu\text{g/ml}$ in a 24-well tissue culture plate and the lowest concentration at which 100 percent death occurred over the 10 days determined as 800 $\mu\text{g/ml}$ G418.

HEK 293 cells were seeded at 25 percent confluency in the antibiotic containing media 48 hours post-transfection and the media changed every 3 days. Following selection and passage, cells were maintained in 800 µg/ml G418. Stably expressing HEK 293 cells were confirmed using a fluorescence microscope to assess cell-surface expression of the mCherry-tagged GCGR and measuring cAMP accumulation following stimulation with GCG using the LANCE® cAMP Detection Kit (PerkinElmer, Inc. (Waltham, Massachusetts, US) (Section 3.6).

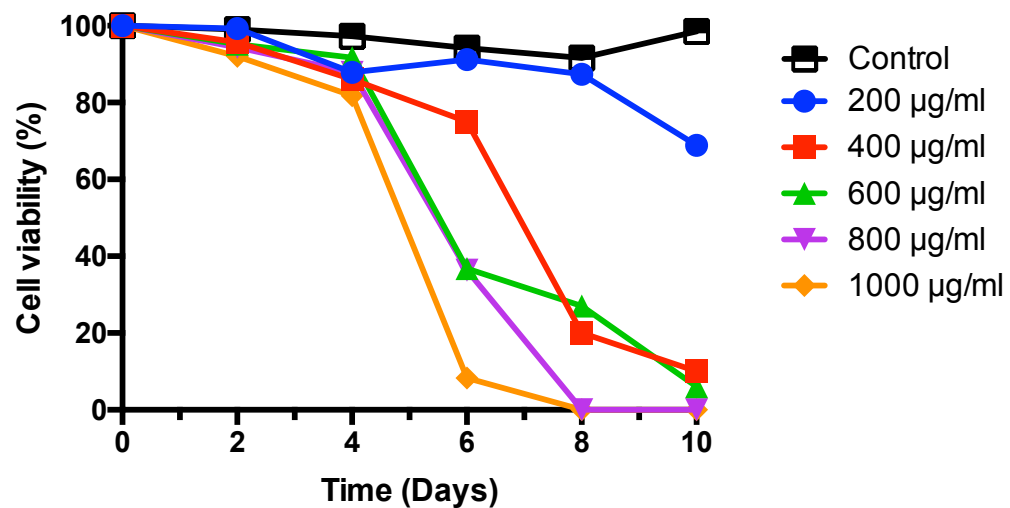


Figure 2.1. G418 kill curve for HEK 293 cells. A kill curve was performed for HEK 293 cells to determine the optimal concentration of G418. This was determined as the lowest concentration required in order to kill 100 percent of HEK 293 cells (800 µg/ml).

2.1.4. Long-term storage and recovery

Cells cultured in a 75 cm² flask at approximately 80 percent confluence were harvested, washed and suspended in 2 ml of freezing down media (90 percent FBS, 10 percent dimethyl sulfoxide (DMSO)) and divided equally into two cryogenic vials (Greiner Bio-One, Kremsmünster, Austria) prior to placement in a freezing container at -80 °C for 24 hours and subsequently being transferred to a liquid nitrogen vessel.

Recovery of cells from long term storage was achieved by thawing the cells in a 37°C water bath with constant agitation for 2 minutes and transferred to a 25 cm² flask containing 10 ml of pre-warmed growth media. Once healthy cells were completely adhered, the media was replaced and the cell lines maintained as previously described.

2.2. Hepatocyte Isolation from C57BL/6 mouse

Dr Maja Wallberg performed the following procedure for the extraction of intact hepatocyte from C57BL/6 mice within the small laboratory animal unit of the Department of Pathology (University of Cambridge) in accordance with the UK Animals Scientific Procedures Act (1986). The following protocol was adapted from Mederacke *et al.*, 2015 and Shen *et al.*, 2012. Rather than using anaesthetised live mice, these mice were euthanised and used for both islet isolation and hepatocytes isolation for same day experiments, thereby minimising waste. Mouse euthanasia was performed and abdomen entered through a midline incision. The inferior vena cava was exposed by carefully moving the viscera outside of the abdominal cavity. Using a 23-gauge syringe needle, 5 ml ice-cold collagenase P (Roche Diagnostics, 11213857001) solution (0.5 mg/ml) dissolved in HBSS (containing 1 mM CaCl₂ and 10 mM HEPES (Thermo Fisher Scientific)) was injected into the inferior vena cava.

Once the liver appeared pale in colour and inflated, the portal vein was cut and the remaining collagenase P injected. The liver was then cut out of the mouse and placed into ice cold HBSS, supplemented as above, on ice prior to transfer to a 37°C water bath for 20 minutes. The tissue was then transferred through a metal tea strainer into a falcon tube to release the hepatocytes before centrifuging for 2 minutes at 1000 RPM. The digested and mechanically separated liver was then transferred through a sterile nylon mesh into a 15 ml falcon tube and washed twice in unsupplemented DMEM with 2 minutes centrifugation at 1000 RPM. Hepatocytes were then counted using a hemocytometer and cell viability determined using trypan blue (Sigma-Aldrich) staining. Typically, hepatocytes showed a 1:1 ratio of live and

dead hepatocytes. Hepatocytes were delivered in DMEM culture medium (Thermo Fisher Scientific) to the Department of Pharmacology (University of Cambridge) within 15 minutes of completing the extraction for cAMP accumulation assay (LANCER® Ultra cAMP Detection Kit (PerkinElmer)).

2.3. Cell viability assay

The quantification of ATP as a measure of cell viability was conducted using the CellTiter-Glo® Luminescent Cell Viability Assay (Promega, Wisconsin, US). Since ATP amount is directly proportional to cell number (Section 3.8.1), cell number when comparing viability across cell lines was controlled for. Cells were harvested using 0.05 percent Trypsin-EDTA (Sigma-Aldrich) and washed before counting and plating in 25 µl of media (5000 cells/well) on a white 384-well Optiplates (PerkinElmer). 25 µl of the CellTiter-Glo® Reagent containing thermostable luciferase from the firefly *Photuris pennsylvanica* (Ultra-Glo™ Recombinant Luciferase) was added to each well containing the cells and incubated at room temperature on an orbital shaker for 2 minutes to induce cell lysis. The amount of ATP was determined using an ATP standard curve where a tenfold serial dilution of adenosine 5'-triphosphate disodium salt hydrate (Sigma-Aldrich) (10 µM to 0.01 nM; 25 µl contains 2.5×10^{-10} to 2.5×10^{-16} moles of ATP) was made immediately prior to addition of 25 µl reagent. Media without cells was used as a blank control, again with the addition of 25 µl of the CellTiter-Glo® Reagent. The plate was then incubated at room temperature for 10 minutes to allow signal stabilisation prior to reading the luminescence on a Mithras LB 940 (Berthold technology Ltd, Bad Wildbad, Germany).

2.4. Transient transfection

Transfections were conducted 24 or 48 hours prior to assay using either Fugene® HD (Roche Diagnostics) or more commonly polyethylenimine (PEI, linear, $M_w = 25,000$ g/mol) (Polysciences Inc) at a 1:3 DNA:Fugene ratio or

1:2 DNA:PEI ratio when cells were 60-80 percent confluent (Section 3.3). PEI was dissolved to a concentration of 1 mg/ml in accordance with the manufacturers instructions. Briefly, 100 mg of PEI was added to 90 mL of water (i.e. to a concentration of 1.11 mg/ml) and 12 M hydrochloric acid (HCl) was added to reach a pH less than 2.0. The solution was stirred continuous for approximately 3 hours until the solution became mostly clear prior to the addition of 10 M sodium hydroxide dropwise until a pH 7.0 was achieved. Aliquots of stock PEI were stored at -20°C. DNA concentration for transfection was determined for each individual cell line and expression vector but unless otherwise stated was conducted as shown in Table 2.1 and optimised in Section 3.2.3. For Fugene® HD, serum free media and Fugene® HD was allowed to complex for 5 minutes prior to addition of DNA and a further 15 minutes incubation before addition to plated cells dropwise. For transfection with PEI, serum free media, DNA and PEI were allowed to complex for 10 minutes prior to addition to plated cells dropwise.

Table 2.1. Transfection components according to size of tissue culture plate for Fugene® HD and PEI

Tissue culture plate	Total media volume	DNA amount	DNA (100ng/ul stock)	Serum free media to a total of	Fugene® HD	PEI (1mg/mL stock)
96-well	100 µl	100 ng	1 µl	10 µl	0.3 µl	0.2 µl
24-well plate	500 µl	250 ng	2.5 µl	25 µl	0.75 µl	0.5 µl
6-well plate	1000 µl	500 ng	5 µl	50 µl	1.5 µl	1 µl

2.5. Ligands and compounds

GCG, oxyntomodulin, 1-N- α -trinitrophenylhistidine,12-homoarginine)glucagon (TH-GCG) (made up in DMSO), GLP-1(7-36)amide and GLP-1(9-36)amide and oxytocin were synthesised by Alta Biosciences (University of Birmingham, UK). des-His¹,Glu⁹-glucagon amide was purchased from Bachem (Bubendorf, Switzerland) and L-168,049 purchased from Trocris Biosciences (Bristol, UK). The small molecular agonist of GLP-1R, BETP (4-

(3-benzyloxyphenyl)-2-ethylsulfinyl-6-(trifluoromethyl)pyrimidine) (Willard *et al.*, 2012), was purchased from Tocris Biosciences and made up in DMSO. The potent adenosine receptor agonist 5'-N-Ethylcarboxamidoadenosine (NECA) was purchased from Thermo Fisher Scientific and the selective A_{2A}R agonist, CGS 26180 (2-[p-(2-carboxyethyl)phenylethylamino]-50-ethylcarboxamidoadenosine) (Jarvis *et al.*, 1989) from Tocris Biosciences, both of which were made up in DMSO. Unless otherwise stated, all ligands were made up in deionised water, supplemented with 0.1 percent BSA (Sigma-Aldrich, A2153) in order to reduce adsorption to plastic or glass surfaces.

Forskolin, a potent activator of AC (AC1-8 but not 9 or 10) leading to elevations in cAMP (Seamon *et al.*, 1981) was purchased from Sigma-Aldrich and made up in DMSO. NF449, a suramin analogue, was purchased from Abcam (Cambridge, UK) and used to pretreat cells at 10 µM for 30 minutes prior to ligand stimulation as previously reported (Halls and Cooper, 2010). The availability of YM-254890, a specific G_{q/11} inhibitor (Takasaki *et al.*, 2004), has been described as restricted by the scientific community (Xiong *et al.*, 2016). However, this compound was readily available and purchased from Wako Pure Chemical Industries Ltd (Osaka, Japan) and used at 100 nM for 30 minutes prior to ligand stimulation. The specific Gβγ small molecule inhibitor gallein (Santa Cruz Biotechnology, Inc, Texas, USA) (Lehmann *et al.*, 2008) was used to pretreat cells at 0.1 µM, 1 µM and 10 µM for 30 minutes (Dubin *et al.*, 2012) prior to ligand stimulation. The cAMP analogue and PKA inhibitor Rp-8-bromo-cAMP (Rp-8-Br-cAMP) (Sigma-Aldrich) (Schwede *et al.*, 2000) was used to pre-treat cells at 10 µM for 15 minutes (Gjertsen *et al.*, 1995) prior to ligand stimulation. The inhibitory were all made up in DMSO and in experiemnts 'untreated' cells were treated with the equivalent amount of DMSO as a control.

2.6. Constructs and molecular biology

2.6.1. RAMP constructs

cDNA constructs of pcDNA3.1 expressing N-terminally FLAG-tagged RAMPs were kindly donated by Prof. Patrick Sexton (Monash University, Australia). The dual expression pVITRO1-neo-MCS vector (pVITRO) (Figure 2.2) was purchased from InvitroGen (Paisley, UK). Various pVITRO constructs were made using standard molecular cloning techniques including RAMP1 (as a none interacting control) or FLAG-tagged RAMP2 at multiple cloning site 1 (MCS1) with or without N-terminally myc-tagged GCGRmCherry at multiple cloning site 2 (MCS2).

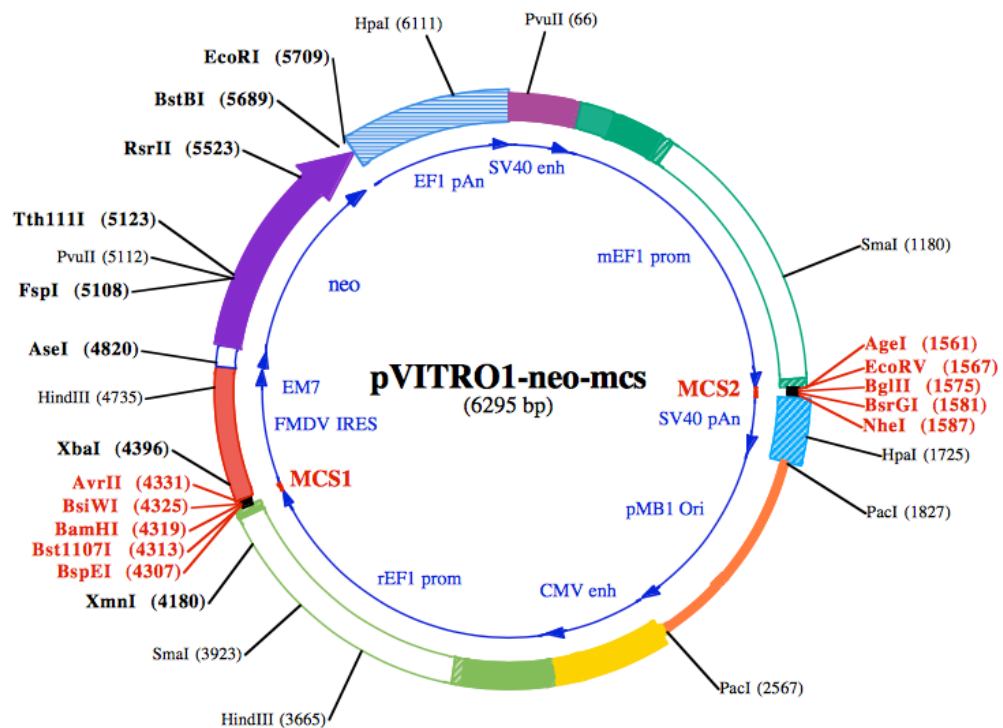


Figure 2.2. pVITRO1-neo-mcs vector map. The pVITRO1-neo-mcs plasmid, containing two multiple cloning sites (MCS), is selected with kanamycin in *E.coli* and G418 in mammalian cells. Taken from InvitroGen document containing information about the vector.

2.6.2. GCGR constructs

GCGR ICL1 alanine mutants (G165A, L166A, S167A, K168A, L169A, H170A, C171A and T172A) were kindly donated by Dr. Ali Jazayeri (Heptares Therapeutics). Dr Cathryn Weston, a past member of the Dr Ladds Laboratory group, previously cloned myc-GCGR into the vector pmCherry-N1 vector and pcDNA3.1 (Clontech Laboratories, 632523). The GCGR mutants (Table 2.2) were made using this pmCherry-N1 vector expressing myc-tagged GCGR.

All oligonucleotides used for mutagenesis were designed using the online Agilent Genomics 'QuikChange Primer Design' tool (Table 2.2). For multiple and single mutations, the QuikChange Lightning Multi Site-Directed Mutagenesis Kit (Agilent Technologies) or QuikChange Lightning Site-Directed Mutagenesis Kit (Agilent Technologies) was used in accordance with the manufacturers instructions, respectively. The reaction components and cycle parameters for each of the QuikChange Lightning kits are detailed in Table 2.3 and Table 2.4, respectively. The elongation cycle parameter of 186 seconds is based on 30 seconds/kb for the template size of 6203 bp (pmCherry-N1 vector (4722 bp) with the inserted GCGR (1431 bp)). All mutants in the pmCherry-N1 vector were sequenced using the CMV forward oligonucleotide (CGCAAATGGGCGGTAGGCGTG) and mCherry reverse oligonucleotide (CATGAACTCCTTGATGATGGC).

Table 2.2. Oligonucleotides used to create GCGR mutants in ICL1, TM2, TM4 and helix 8. WT GCGR was initially cloned into pmCherry-N1 vector and all oligonucleotides designed using the online Agilent Genomics 'QuikChange Primer Design' tool.

Target	Product	Oligonucleotide targeting sense strand of template	Oligonucleotide targeting antisense strand of template
ICL1	S167A, K168A	⁴⁸⁹ GGTGCAGTGCAGCgcGC TGAGGCCCCCC ⁵¹⁷	⁵¹⁷ GGGGGGCCTCAGCgcGCT GCACTGCACC ⁴⁸⁹
ICL1	S167R, K168R	⁴⁸⁸ GGTGCAGTGCAGCcTtCT GAGGCCCCCCA ⁵¹⁷	⁵¹⁷ TGGGGGGCCTCAGaAgGCT GCACTGCACC ⁴⁸⁸
TM2	R173A	⁵⁰³ CGTGGATGGCATTGgcG GTGCAGTGCAGCT ⁵³⁴	⁵³⁴ AGCTGCACTGCACCgcCAA TGCCATCCACG ⁵⁰³
TM2	R173A, N174A	⁵⁰⁰ GATTCGCGTGGATGGCA gcGgcGGTGCAGTGCAGCTT GC ⁵⁴⁰	⁵⁴⁰ GCAAGCTGCACTGCACCgc CgcTGCCATCCACGCGAATC ⁵⁰⁰
TM4	V280A	⁸²⁰ CTGCCCAGGGGcCGACG AACAGCATGGGGGCAC ⁸⁵²	⁸⁵² GTGCCCCCATGCTGTTTCGT CGcCCCCTGGGCAG ⁸²⁰
TM4	L277A, V280A	⁸²⁰ CTGCCCAGGGGcCGACG AACgcCATGGGGGCAC ⁸⁵²	⁸⁵² GTGCCCCCATGgcGTTTCGT CGcCCCCTGGGCAG ⁸²⁰
TM4 ¹	G271A, L277A, V280A	⁸²⁵ GGGCACCCAGgCGATG CCCAGG ⁸⁰³	⁸⁰³ CCTGGGCATCGcCTGGGG TGCC ⁸²⁵
Helix 8	E406A	¹²⁰⁵ GCTCCGACTGCACCgCC TTGTTGAGGAAG ¹²³³	¹²³³ CTTCCTCAACAAGGcGGT GCAGTCGGAGC ¹²⁰⁵
Helix 8	E410A	¹²²⁰ GCCGCCGCAGCgCCGA CTGCACC ¹²⁴²	¹²⁴² GGTGCAGTCGGcGCTGCG GCGGC ¹²²⁰
Helix 8 ²	E406A, E410A	¹²²⁰ GCCGCCGCAGCgCCGA CTGCACC ¹²⁴²	¹²⁴² GGTGCAGTCGGcGCTGCG GCGGC ¹²²⁰

¹Triple mutant made using double mutant as template

²Double helix 8 mutant made using E406A as template, therefore oligonucleotides used to make double mutant are the same as creating single E410A mutant

The start and end nucleotide position within the GCGR sequence bound by the oligonucleotide are indicated by superscript and point mutations are indicated by lower case.

Table 2.3. Reaction components for QuikChange (site or multi site-directed) mutagenesis kit.

Site-Directed Mutagenesis Kit		Multi Site-Directed Mutagenesis Kit	
10x reaction buffer	5µl	10x reaction buffer	2.5µl
dsDNA template	100 ng	dsDNA template	100 ng
Sense primer	125 ng	Sense primer	100 ng
Antisense primer	125 ng	Antisense primer	100 ng
dNTP mix	1µl	dNTP mix	1µl
QuikSolution reagent	1.5µl	QuikSolution reagent	0.75µl
ddH ₂ O	To a final volume of 50µl	ddH ₂ O	To a final volume of 25µl
QuikChange Lightning enzyme blend	1µl	QuikChange Lightning Multi enzyme blend	1µl

Table 2.4. Cycle parameters for QuikChange (site or multi site-directed) mutagenesis kit.

Site-Directed Mutagenesis Kit				Multi Site-Directed Mutagenesis Kit			
Step	Cycles	Temp	Time (s)	Step	Cycles	Temp	Time (s)
1	1	95°C	120	1	1	95°C	120
2	18	95°C	20	2	30	95°C	20
		60°C	10			55°C	30
		68°C	186			65°C	186
3	1	68°C	300	3	1	65°C	300
4	1	4°C	Paused	4	1	4°C	Paused

2.6.3. GLP-1R construct

The GLP-1R in pGFP-N1 vector was generously donated to us by Dr. Alessandro Bisello (Univeristy of Pittsburgh).

2.6.4. A_{2A}R constructs

The A_{2A}R receptor was first cloned into the pmCherry-N1 vector and the mutants subsequently made using the QuikChange Lightning Site-Directed Mutagenesis Kit (Agilent Technologies) in accordance with the manufacturers instructions and as detailed previously (Tables 2.3 and 2.4). The elongation cycle parameter of 179 seconds is based on 30 seconds/kb for the template size of 5952 bp (pmCherry-N1 vector (4722 bp) with the inserted A_{2A}R (1230 bp)). The oligonucleotides used for site-directed mutagenesis were designed using the online Agilent Genomics ‘QuikChange Primer Design’ tool (Table 2.6.8).

Table 2.5. Oligonucleotides used to create A_{2A}R mutants in ICL1 region, TM1, ICL1 and TM2. WT A_{2A}R was initially cloned into pmCherry-N1 vector and all oligonucleotides designed using the online ‘QuikChange Primer Design’ tool.

Product	Oligonucleotide targeting sense strand of template	Oligonucleotide targeting antisense strand of template
L33A	⁷⁴ GCAGGTTGCTGTTGgcCCACA CGGCCAGC ¹⁰³	¹⁰³ GCTGGGCCGTGTGGgcCAACA GCAACCTGC ⁷⁴
N34A	⁷⁷ TCTGCAGGTTGCTGgcGAGCC ACACGGCCC ¹⁰⁶	¹⁰⁶ GGGCCGTGTGGCTCgcCAGCA ACCTGCAGA ⁷⁷
S35A	⁷⁹ ACGTTCTGCAGGTTGgcGTTG AGCCACACGGC ¹¹⁰	¹¹⁰ GCCGTGTGGCTCAACgcCAAC CTGCAGAACGT ⁷⁹
N36A	⁸¹ GGTGACGTTCTGCAGGgcGCT GTTGAGCCACACG ¹¹⁴	¹¹⁴ CGTGTGGCTCAACAGCgcCCT GCAGAACGTCACC ⁸¹
L37A	⁸⁴ GTTGGTGACGTTCTGCgcGTT GCTGTTGAGCCAC ¹¹⁷	¹¹⁷ GTGGCTCAACAGCAACgcGCA GAACGTCACCAAC ⁸⁴
Q38A	⁸⁶ AGTAGTTGGTGACGTTcgcCA GGTTGCTGTTGAGCC ¹²¹	¹²¹ GGCTCAACAGCAACCTGgcGA ACGTCACCAACTACT ⁸⁶
N39A	⁸⁷ CACAAAGTAGTTGGTGACGgc CTGCAGGTTGCTGTTGAGC ¹²⁶	¹²⁶ GCTCAACAGCAACCTGCAGgc CGTCACCAACTACTTTGTG ⁸⁷
V40A	⁹³ CCACAAAGTAGTTGGTGgCGT TCTGCAGGTTGCTG ¹²⁷	¹²⁷ CAGCAACCTGCAGAACGcCAC CAACTACTTTGTGG ⁹³
T41A	⁹⁵ CACCACAAAGTAGTTGGcGAC GTTCTGCAGGTTGC ¹²⁹	¹²⁹ GCAACCTGCAGAACGTCgCCA ACTACTTTGTGGT ⁹⁵
N42A	⁹⁶ CAGTGACACCACAAAGTAGG CGGTGACGTTCTGCAGGTTG ¹³⁵	¹³⁵ CAACCTGCAGAACGTCACCgcC TACTTTGTGGTGTCACTG ⁹⁶

The start and end nucleotide position within the GCGR sequence bound by the oligonucleotide are indicated by superscript and point mutations are indicated by lower case

2.7. RNA extraction, quality determination and cDNA synthesis

2.7.1. RNA extraction

Where possible, all solutions and glassware were treated with 0.1 percent (v/v) diethyl pyrocarbonate (DEPC) for the inactivation of RNase prior to autoclaving. Gel electrophoresis tank for RNA integrity analysis was treated for 10 minutes with 3 percent hydrogen peroxide.

RNA was extracted from HEK 293T or Hep 3B cells cultured to ~80 percent confluence in a 6-well plate using an RNeasy Plus Mini Kit purchased from QIAGEN (Manchester, UK) in accordance with the manufacturers instructions. The principle of this kit involves homogenisation of cells in a buffer containing the strong protein denaturant guanidine-isothiocyanate, immediately inactivating RNase. The lysate was then passed through a spin column to eliminate genomic DNA (gDNA). Here, guanidine-isothiocyanate (being a strong chaotropic agent) also disrupting the structure of the nucleic acid and helps to drive gDNA binding to the column. Ethanol was then added to the flow through, providing binding conditions for RNA, and subsequently passed through a RNeasy spin column where the RNA binds to the membrane prior to elution in RNase free water.

Briefly, HEK 293T or Hep 3B cells in a 6-well plate was washed in PBS, trypsinated and FBS supplemented medium added. The suspended cells were then transfer to an RNase free polypropylene tube and centrifuged for 5 minutes at 300 x *g* in a microcentrifuge (RPM ~2000). The supernatant was aspirated and the pellet loosened by flicking the base of the tube prior to addition of 600 μ l of Buffer RLT Plus containing β -mercaptoethanol (β -ME) (10 μ l per 1 ml Buffer RLT Plus) to initiate cell lysis. β -ME addition to the buffer is essential and irreversibly denatures RNases released following the cell lysis through reducing disulphide bonds. The tube was then vortexed briefly and the homogenised lysate transferred to the gDNA elimination column placed in a 2 ml collection tube. Following ha centrifugation step at > 8000 x *g* (>10,000 RPM) for 30 seconds, 1 volume of 70 percent ethanol was

added to the flow through and transferred to an RNeasy spin column placed in a 2 ml collection tube. All the following centrifugation steps were performed at $> 8000 \times g$ ($>10,000$ RPM). This column was then centrifuged for 15 seconds, the flow through discarded prior a wash with 700 μ l of Buffer RW1 and additional 15 seconds centrifugation. The spin column then received two washes with 500 μ l of Buffer RPE twice and centrifuged for 15 seconds followed by 2 minutes. In the final step, the RNeasy spin column was transferred to a 1.5 ml collection tube and 50 μ l of RNase free water added prior to centrifugation for 1 minute.

2.7.2. RNA quality determination

RNA quality was determined using Nanodrop technology (NanoDrop Lite, Thermo Scientific, Wilmington, USA). Pure RNA was indicated with an A_{260}/A_{280} ratio of 1.9–2.1. This ratio is influenced by the solution the RNA is eluted in (i.e. water or Tris-HCl) (Okamoto and Okabe, 2000). As such, all samples including those with low ratios were further analysed by denaturing agarose gel electrophoresis with a ratio of 28s rRNA to 18s rRNA at approximately 2:1 indicative of good quality RNA. To make 1 L of running buffer, in a fume hood, 20 ml of 37 percent formaldehyde (Sigma-Aldrich) and 100 ml of 10X MOPS (3-(N-morpholino)propanesulfonic acid) buffer (0.4 M MOPS (pH 7.0), 0.1 M sodium acetate, 0.01 M EDTA) was added to 880 ml of water. For the gel, 1g of agarose in 72 ml of water was heated until dissolved and then cooled to 60°C prior to addition of 10 ml 10X MOPS buffer and 18 ml 37 percent formaldehyde (12.3 M). Prior to RNA loading, the samples were added to equal volumes of the ethidium bromide and formamide containing RNA loading dye (Thermo Fisher Scientific, R0641) and heated to 70°C for 10 minutes to denature.

2.7.3. cDNA synthesis

Following RNA extraction and quality determination, complementary DNA (cDNA) synthesis was carried out using a QuantiTect Reverse Transcription Kit (QIAGEN) according to the manufacturers instructions. Here, 1 µg of RNA was used for cDNA synthesis as the protocol was optimised for 10 pg to 1 µg of RNA. Following cDNA synthesis, the samples were placed on ice prior to amplification using PCR and *Taq* DNA polymerase (Thermo Fisher Scientific), in accordance with the manufacturers instructions (cycle parameters detailed in Tables 2.6 and 2.7)

All oligonucleotides for reverse transcription-PCR (RT-PCR) (Table 2.6) were ordered from Sigma-Aldrich and checked for off-targets using NCBI Primer-BLAST. All oligonucleotides were initially tested using vectors containing the receptor of interest as template DNA at both 50°C and 60°C. In order to determine the size of the PCR products, a 100 bp DNA ladder (New England BioLabs, N3231, Massachusetts, USA) was used.

Table 2.6. Oligonucleotides used in RT-PCR of cDNA synthesised from RNA extracted from Hep 3B cells. Reference for each oligonucleotide pair is indicated.

Gene	GenBank accession number	Sense oligonucleotide	Antisense oligonucleotide	Size	Anne-aling temp (°C)
GAPDH ¹	NM_002046	⁶⁴² TGCACCACCA ACTGCTTAGC ⁶⁶¹	⁷²⁸ GGCATGGACTG TGGTCATGAG ⁷⁰⁸	87	60
GCGR ²	NM_000160	⁴¹⁸ CCAGTGTCAC CACAACCTGA ⁴³⁷	⁴⁹⁴ AGGAATACTTGT CGAAGGTTCTGT ⁴⁷¹	77	60
GLP-1R ³	NM_002062	⁸⁶⁴ CTACGTGAGC ATAGGCTGGG ⁸⁸³	⁹⁹⁸ ATGGGCAGCCG GATAATGAG ⁹⁷⁹	135	60
GIPR ²	NM_000164	¹²³² CCAAGCTCGG CTTTGAGAT ¹²¹⁴	¹²⁷⁵ GTAGAGGACG CTGACCAGGA ¹²⁵⁶	62	60
CLR ⁴	NM_005795	¹¹⁵⁰ ACCAGGCCTT AGTAGCCACA ¹¹⁶⁹	¹⁴⁴⁵ ACAAATTGGGC CATGGATAA ¹⁴²⁶	296	60
RAMP1 ⁴	NM_005855	²¹⁰ CTGCCAGGAG GCTAACTACG ²²⁹	⁵⁰⁷ GACCACGATGA AGGGGTAGA ⁴⁸⁸	298	60
RAMP2 ⁴	NM_005854	²³² GGGGGACGGT GAAGAACTAT ²⁵¹	⁴⁵⁸ GTTGGCAAAGT GGATCTGGT ⁴³⁹	227	60
RAMP3 ⁴	NM_005856	⁹⁰ AACTTCTCCCG TTGCTGCT ¹⁰⁸	⁴⁴² GACGGGTATAA CGATCAGCG ⁴²³	353	60

¹ Stockinger *et al.*, 2004. ² Zwermann *et al.*, 2009. ³ Ge *et al.*, 2014. ⁴ Linscheid *et al.*, 2005. The start and end nucleotide position within the sequence bound by the oligonucleotide are indicated by superscript

Table 2.7. Gene specific oligonucleotides to human G α -subunits used in RT-PCR of cDNA synthesised from RNA extracted from Hep 3B cells. PrimerBank IDs (Spandidose *et al.*, 2010) are also provided. (See Table 1.1 for more information on G α -subunits).

Gene	GenBank accession number/Primer Bank ID	Sense oligonucleotide	Antisense oligonucleotide	Size	Annealing temp (°C)
GNAS	AJ224868/3297877a1	⁵¹ CGACGACACT CCCGTCAAC ⁶⁹	²²⁷ CCCGGAGA GGTACTTTTC CT ²⁰⁷	177	60
GNAI1	NM_002069/156071490c1	²⁵⁴ TTAGGGCTAT GGGGAGGTTGA ²⁷⁴	⁴³⁹ GGTACTCTC GGGATCTGTT GAAA ⁴¹⁷	186	60
GNAI2	NM_001166425/261878574c1	⁹⁴ TACCGGGCGG TTGTCTACA ¹¹²	¹⁸² GGGTCGGC AAAGTCGATCT G ¹⁶³	89	60
GNAI3	NM_006496/169646784c1	⁵⁵ ATCGACCGCA ACTTACGGG ⁷³	²⁸³ AGTCAATCT TTAGCCGTCC CA ²⁶³	229	60
GNAZ	NM_002073/45580725c1	⁴⁴ GGTCCCGGAG AATTGACCG ⁶²	²¹⁸ ATGAGGGG CTTGTACTCCT TG ¹⁹⁸	175	60
GNAO	NM_138736/162461737c1	⁴⁴ GGAGCAAGGC GATTGAGAAAA ⁶⁴	²¹² GGCTTGTAC TGTTTCACGTC T ¹⁹²	169	60
GNAQ	NM_002072/312176363c1	¹⁸⁹ TGGGTCAGGA TACTCTGATGAA G ²¹¹	³³² TGTGCATGA GCCTTATTGTG C ³¹²	144	60
GNA11	NM_002067/115511048c1	²²⁰ GGCTTCACCA AGCTCGTCTAC ²⁴⁰	³⁹¹ CACTGACGT ACTGATGCTC G ³⁷²	172	60
GNA12	NM_007353/42476110c1	²⁴⁶ CCGCGAGTTC GACCAGAAG ²⁶⁴	⁴⁹⁰ TGATGCCAG AATCCCTCCA GA ⁴⁷⁰	245	60
GNA13	NM_006572/215820623c1	⁷⁹ CAGCAACGCA AGTCCAAGGA ⁹⁸	²⁹⁸ CCAGCACCC TCATACCTTTG A ²⁷⁸	220	60
GNA14	NM_004297/222418795c1	²⁶³ GAGCGATGGA CACGCTAAGG ²⁸²	⁴³⁰ TCCTGTCGT AACACTCCTG GA ⁴¹⁰	168	60
GNA15	NM_002068/156104882c1	³⁵⁴ CCAGGACCCC TATAAAGTGACC AT ³⁷⁵	⁴⁷⁹ GCTGAATCG AGCAGGTGGA AT ⁴⁵⁹	126	60

The start and end nucleotide position within the sequence bound by the oligonucleotide are indicated by superscript

Table 2.8. Cycling parameters for *Taq* DNA polymerase for 200 bp product

Step	Cycles	Temperature	Time (s)
1	1	94°C	180
2	30	94°C	45
		60°C	30
		72°C	18
3	1	72°C	600
4	1	4°C	Paused

2.8. Pharmacological characterisation techniques

2.8.1. cAMP accumulation assay

1,000 HEK 293T or CHO-K1 cells/well were assayed 24 hours post-transfection and stimulated with appropriate ligand for 8 minutes prior to cAMP accumulation measured using LANCE® cAMP Detection Kit (PerkinElmer) (Figure 2.3) in accordance with the manufacturers instructions. In order to achieve a bigger signalling window for cAMP assays using CHO-K1 cells transfected with A_{2A}R, cells were assayed 48 hours post-transfection rather than 24 hours.

For hepatocytes from isolated C57BL/6 mice and Hep 3B cells, 5000 cells/well were stimulated for 30 minutes and cAMP accumulation measured using LANCE® Ultra cAMP Detection Kit (PerkinElmer) (Figure 2.4) in accordance with the manufacturers instructions.

Ligands were diluted in stimulation buffer (PBS supplemented with 0.1 percent BSA and 0.5mM of the non-specific inhibitor of cAMP and cGMP phosphodiesterases (PDEs) 3-Isobutyl-1-methylxanthine (IBMX) (Sigma-Aldrich) (Schmidt *et al.*, 2000)) to the appropriate concentration range to be assayed. Cells were harvested, counted using a haemocytometer, re-suspended in stimulation buffer and seeded at the appropriate concentration in a white 384-well Optiplates (PerkinElmer). The plate was sealed with a ThermalSeal® film (EXCEL Scientific, California, US) during incubation periods before detecting the time-resolved fluorescence resonance energy transfer (TR-FRET) signal using a Mithras LB 940 Ex. λ 340 nm and Em. λ

665 nm (Berthold technology). TR-FRET combines standard FRET technology with time-resolved measurement of fluorescence, allows the elimination of short-lived background fluorescence. Here, with the acceptor emitting long-lived fluorescence when engaged in FRET, a delay of around 50-150 μ seconds between excitation and measurement allows any non-specific short-lived emission to be eliminated. All results were normalised to responses seen to endogenous ligand or forskolin maximum (100 μ M) (Sigma-Aldrich).

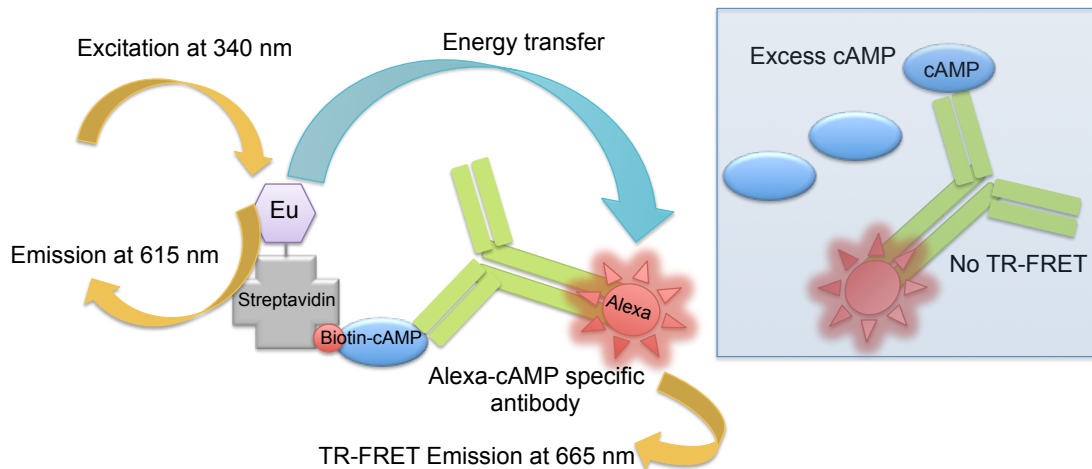


Figure 2.3. Principles of the LANCE® cAMP assay kit. The assay is based on competition for binding sites on the cAMP specific antibody between the europium labelled cAMP tracer (Streptavidin labelled with europium tightly bound to biotin labelled cAMP) and free cAMP produced by the stimulated cells (sample cAMP). Light pulse at 340 nm excited the europium of the cAMP tracer and the energy emitted is transferred to the Alexa Fluor® 647 labelled anti-cAMP antibodies, if bound to the tracer, generating a TR-I signal at 665 nm. The fluorescence intensity measured at 665 nm will decrease in the presence of excess cAMP giving a signal which is inversely proportional to the concentration of cAMP.

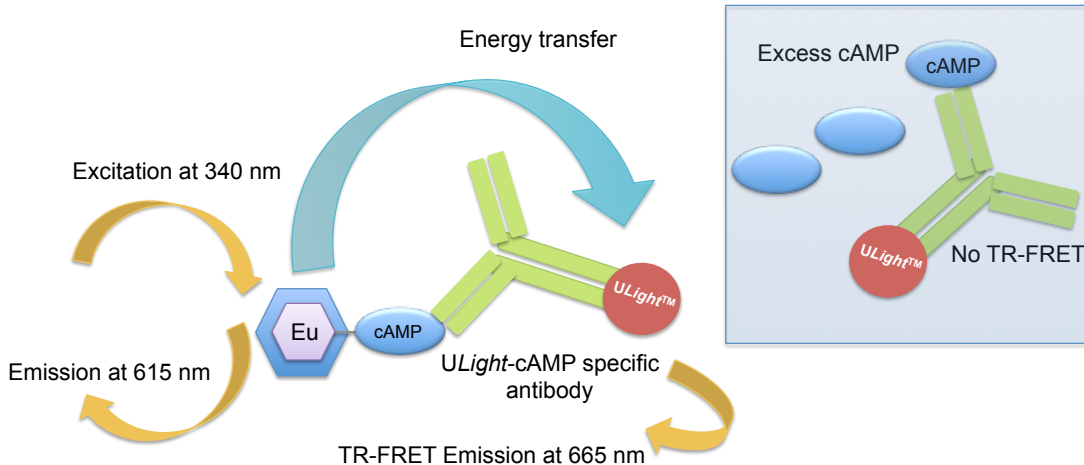


Figure 2.4. Principles of the LANCE® Ultra cAMP assay kit. The assay principle is similar to that of the LANCE® cAMP assay kit, where there is again competition between the europium labeled cAMP tracer and the sample cAMP for binding to the cAMP-specific monoclonal antibody. Here however, rather than labeled with Alexa Fluor® 647, the antibody is labeled with ULight™ dye.

2.8.2. Phospho-ERK assay

ERK1/2 phosphorylation was measured using the homogeneous time resolved fluorescence (HTRF)® Phospho-ERK (T202/Y204) Cellular Assay Kit (Cisbio Bioassays, Codolet, France) two-plate format in according with the manufacturers instructions. This kit is based on similar principles to the TR-FRET technology used in the LANCE® cAMP Detection Kit (PerkinElmer), combining standard FRET technology with time-resolved measurement of fluorescence. HEK 293T cells, 48 hours post-transfection and 24 hours serum starved, and Hep 3B cells, serum starved for 4 hours, were harvested using 0.05 percent Trypsin-EDTA and washed before plating in HBS (50,000 cells/well) on a white 384-well Optiplates (PerkinElmer). Following 5 minutes ligand stimulation at 37°C the cells were incubated at room temperature, on an orbital shaker, for 30 minutes with the provided total protein lysis buffer (Triton X100) and blocking reagent (sodium orthovanadate). Cells were then incubated for 2 hours at room temperature with premixed phospho-ERK1/2 Cryptate (donor)/d2 antibody (acceptor) (v/v) prepared in detection buffer. At

all incubation stages, the plate was sealed with a ThermalSeal® film (EXCEL Scientific). Plate reading was conducted using a Mithras LB 940 (Berthold technology). All results were normalised to 5 minutes stimulation with 1 µM Phorbol 12-myristate 13-acetate (PMA) (Sigma-Aldrich), a direct protein kinase C (PKC) activator (Jiang and Fleet, 2012)

2.8.3. Intracellular Ca²⁺ mobilisation assay

HEK 293T or CHO-K1 cells were transfected 24 hours following plating at 50,000 cells per well of a Poly-L-lysine (PLL) (Sigma-Aldrich) coated 96 well F-bottom µCLEAR® black CELLSTAR® microplates (Greiner Bio-One). 48 hours post-transfection, cell media was removed, washed once in HBS and incubated with 100 µl per well of Fluo-8, AM (21092-AT) (Strattech Scientific, Newmarket, UK) or CalciFluor™ Rhod-4, AM (Santa Cruz Biotechnology, Inc) dye solution (Ca²⁺ containing HBS with Pluronic® F-127 (Thermo Fisher Scientific), at a 1:1000 dilution) for 1 hour in the dark at room temperature. Such dyes allow the measurement of Ca²⁺_i mobilisation from the endoplasmic reticulum (ER), downstream from G_q-mediated signalling (Figure 2.5). Fluo-8, AM was used for all assays with the exception of those investigating receptors containing a GFP-tag. For GFP-tagged constructs, Rhod-4, AM was the dye of choice.

In order to achieve the optimal Ca²⁺_i mobilisation signal in assays using CHO-K1 cells, HBS was supplemented with probenecid (soluble at 1 M NaOH) (Alfa Aesar, Massachusetts, USA) to inhibit organic-anion transporters and thereby block efflux of intracellular dyes (Di Virgilio F *et al.*, 1990). In such experiments, probenecid (working concentration of 2.5 mM and the supplemented HBS subsequently buffered to pH 7.4) was used in all wash stages and dye loading, excluding the final step before ligand addition.

Following dye removal, cells were washed and treated with 100 µl of Ca²⁺ containing HBS for 30 minutes at room temperature in the dark to allow for de-esterification. In experiments using the specific G_{q/11} inhibitor YM-254890 (Takasaki *et al.*, 2004), the Ca²⁺ containing HBS was supplemented

with 100 nM YM-254890. The HBS was then replaced with nominally Ca^{2+} free HBS prior to ligand stimulation with 20 μl of each ligand at appropriate concentrations. Detection of Fluo-8, AM or CalciFluor Rhod-4, AM was then conducted on a FlexStation® Multi-Mode Microplate Reader (Molecular Devices, Sunnyvale, California US), using Ex. λ 490 nm and Em. λ 520 nm or Ex. 530 nm and Em. 555 nm, respectively. For each individual experiment, the minimum and maximum fluorescence values (F) of the indicator (F_{\min} and F_{\max}) when Ca^{2+} -free (addition of 20 μl nominally Ca^{2+} free HBS containing 0.1 percent triton and 10 mM BAPTA (selective chelator of Ca^{2+})) and Ca^{2+} -saturated (addition of 20 μl HBS containing 0.1 percent triton, 10 mM CaCl_2), together with the background fluorescence were determined. Once background fluorescence was subtracted from each reading, the cytosolic free Ca^{2+} concentration ($[\text{Ca}^{2+}]_i$) was calculated using the equation:

$$[\text{Ca}^{2+}]_i = \frac{K_d \times (F - F_{\min})}{(F_{\max} - F)}$$

where K_d for Fluo-8 AM is 390 nM and the K_d for Rhod-4 AM 525 nM. For data analysis, the original Ca^{2+}_i responses are plotted as change in intracellular Ca^{2+} ($\Delta[\text{Ca}^{2+}]_i$ nM) over time and the maximum response at each ligand concentration plotted against log concentration to generate concentration dose-response curves. Data were analysed using a three-parameter logistic equation to acquire pEC_{50} , E_{\max} , Basal and Span (refers to the range (E_{\max} – Basal)) values.

2.8.4. IP_1 accumulation assay

The accumulation of inositol monophosphate (IP_1), the downstream metabolite of inositol 1, 4, 5-triphosphate (IP_3) induced by the activation of phospholipase C (PLC), was measured using the IP-One HTRF® assay kit (Cisbio Bioassays) (Figure 2.5) in accordance with the manufacturers

instructions. This assay utilises lithium chloride (LiCl) which inhibits the activity of inositol monophosphatase preventing the breakdown of IP₁, thus resulting in accumulation of IP₁ which can be measurement as a substitute for IP₃ (Garbison *et al.*, 2004). Based on a competition or native IP₁ and IP₁ coupled to the dye d2 by the monoclonal antibody, the signal is inversely proportional to the concentration of IP₁ in the cell lysate.

HEK 293T cells were harvested, re-suspended in stimulation buffer and counted 48 hours post-transfection. Cells were plated at various densities in a 7 µl volume of stimulation buffer were plated on white 384-well Optiplates (PerkinElmer). Ligands were diluted in stimulation buffer containing LiCl (50 mM) to the appropriate concentration range to be assayed. Cells were subsequently stimulated with 7 µl of ligand, the plate sealed with a ThermalSeal® film (EXCEL Scientific) and then incubated for 2 hours at 37°C. Following the addition of the HTRF® reagents, IP₁ coupled to the dye d2 followed by the monoclonal antibody labeled with Lumi4™-Tb cryptate specific for IP₁ (3 µl of each), the plate was incubation for 2 hour at room temperature prior to HTRF® signal detection using a Mithras LB 940 (Berthold technology) Ex. λ 620 nm and Em. λ 665 nm. All results were calculated from the 665nm / 620nm ratio and expressed as a percentage of the response seen to carbacol.

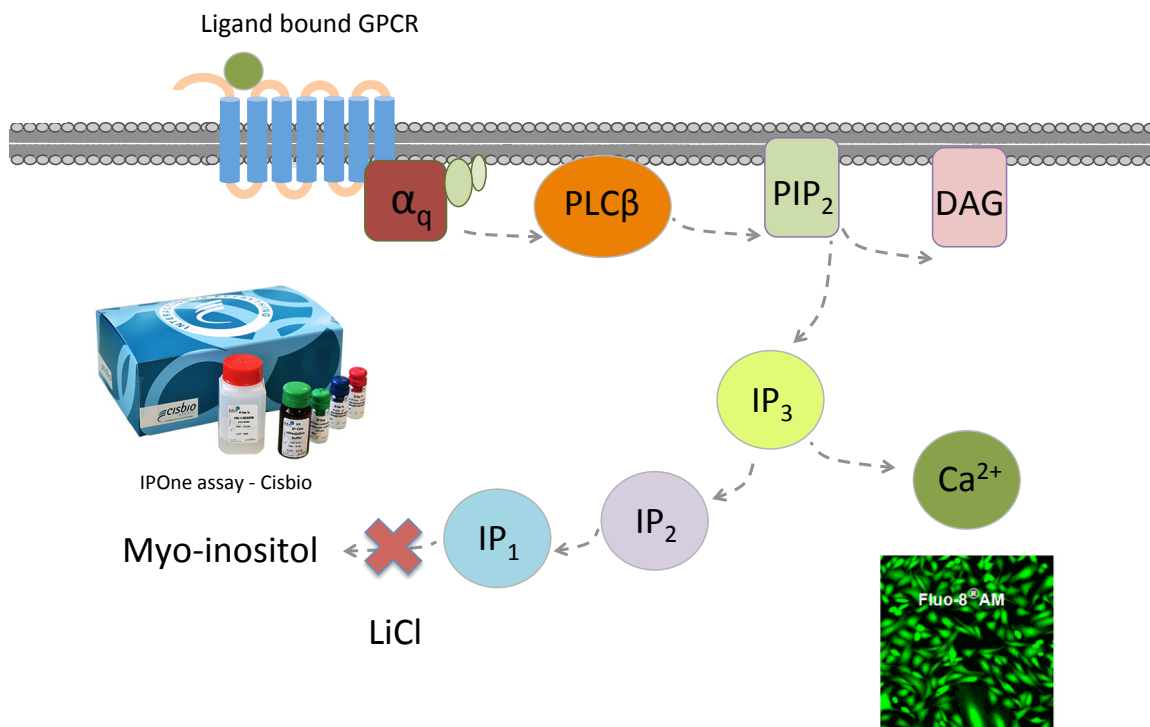


Figure 2.5 Schematic of G_q-mediated signalling following GPCR activation and tools to measure the downstream signalling components. Activation of phospholipase C (PLC) by G_q leads to increased intracellular diacylglycerol (DAG) and inositol 1,3-5-triphosphate (IP₃). Elevated intracellular levels of IP₃ in turn act on IP₃R on endoplasmic reticulum (ER), leading to mobilisation of Ca²⁺ from the ER (Mikoshiba, 2007) which can be measured using fluorescent Ca²⁺ binding dyes such as Fluo-8, AM (Startech Scientific) (image shows Ca²⁺ signalling HEK 293 cells) IP₁ can be measured using the IOne assay (Cisbio Bioassays) to infer intracellular levels of IP₃. This assay utilises lithium chloride (LiCl), which inhibits the breakdown of IP₁ resulting in accumulation in the cells (Garbison *et al.*, 2004).

2.9. Receptor cell-surface expression analysis

2.9.1. Enzyme-linked Immunosorbent Assay (ELISA)

HEK 293T cells were seeded onto PLL-coated 24-well plates and assayed 48 hours post-transfection. All incubation steps were conducted at room temperature on a orbital shaker unless stated otherwise. Cells were fixed with 250 μ l of formaldehyde (3.7 percent) for 15 minutes without shaking, washed three times with PBS and treated with 500 μ l of PBS supplemented with 1 percent BSA (Sigma-Aldrich, A2153) for 45 minutes. Cells were then

incubated for 1 hour with 250 µl of primary antibody (mouse anti-myc, (Fisher Scientific, Loughborough, UK) or mouse anti-FLAG M2 (Sigma-Aldrich) diluted 1:2000 in PBS with 1 percent BSA. Following a second wash stage and a second blocking stage for 15 minutes, cells were incubated for 1 hour with 250 µl of secondary antibody (anti-mouse horseradish peroxidase (HRP)-linked antibody (GE-Healthcare, Pittsburg, PA) in PBS) diluted 1:4000. Following a final wash stage, cells were treated with 250 µl of SigmaFast O-phenylenediamine dihydrochloride (OPD) (Sigma-Aldrich) in accordance with manufacturers instructions. The reaction was stopped with 1M sulphuric acid (H₂SO₄) and absorbance measured using a Mithras LB 940 microplate reader (Berthold technology) at 492 nm. Ideally, readings were normalised to co-transfected RAMP2/CLR as 100 percent and untagged RAMP1 as a non-interacting control as 0 percent, where appropriate.

2.9.2. Fluorescence-activated cell sorting (FACS) analysis of GCGR cell-surface expression

HEK 293T cells were harvested 48 hours post-transfection with GCGR constructs using a non-enzymatic cell dissociation solution (Sigma-Aldrich) and washed with PBS prior to counting. 1×10^6 cells were washed three times in FACS buffer (PBS supplemented with 1 percent BSA and 0.03 percent sodium azide) before re-suspending in 50 µl FACS buffer containing anti-GCGR (AGR-024 (Alomone Labs, Jerusalem, Israel)) at 1:50 dilution and incubated at room temperature for 1 hour. All samples were washed three times with FACS buffer and re-suspended in 50 µl FACS buffer containing Allophycocyanin (APC)-conjugated anti-Rabbit IgG (Thermo Fisher Scientific, 31984) at 1:150 dilution and incubated for 1 hour at room temperature in the dark. The cells received a final three washes and were re-suspended in 300 µl FACS buffer. Due to propidium iodide (PI) (Thermo Fisher Scientific) staining (10 µl per sample for 10 minutes) only showing less than 5 percent of

the population as dead and showing considerable spectral overlap with APC it was not used to eliminate dead cell from data analysis.

FACS analysis was conducted using a BD Accuri™ C6 Plus Flow Cytometer which is equipped with a blue (488 nm) and red (640 nm) laser, two light scatter detectors (FSC and SSC) and four fluorescence detectors (FL1 Em. λ 530/30 nm, FL2 Em. λ 585/40 nm, FL3 Em. λ 570 and FL4 Em. λ 675/25 nm). FL2 and FL4 optical filters were chosen for PI (Ex. λ 535 nm and Em. λ 617 nm) and APC (Ex. λ 633 nm and Em. λ 660 nm), respectively. Unstained cells and cells transfected with vector alone were used as controls for autofluorescence and unspecific antibody binding, respectively. All data is collected by the flow cytometer and analysis can be conducted at anytime using the BD Accuri™ C6 software (Section 3.9). As such, experimental set up and data collection was equivalent regardless of the fluorescent protein tagged to the GCGR (GFP- or mCherry-tagged). The images for figures were made in FlowJo® (V7.6.5), an analysis platform for single-cell flow cytometry analysis.

2.10. Molecular biology techniques

2.10.1. Molecular cloning reagents

All restriction endonucleases, T4 DNA ligase and Taq DNA polymerase were purchased from Life Technologies Ltd and used in accordance with the manufacturers instructions. Taq DNA polymerase was used for amplification of DNA products for the purpose of analysis. The high fidelity DNA polymerase Phusion® (New England BioLabs) was used for amplification of products to be used in cloning. Sigma-Aldrich synthesised all oligonucleotides. Standard methods of DNA preparation were utilised as previously described (Sambrook *et al*, 1989). Plasmid DNA was isolated and purified using a QIAprep Miniprep Kit (Qiagen) and recovered from agarose gels using QIAquick Gel Extraction Kit (Qiagen).

2.10.2. Bacterial transformation

Escherichia coli (*E. coli*) DH5 α competent cells (Stratagene, San Diego, California, US) were used for amplification of plasmids. An aliquot of DH5 α cells, stored at -80°C, was thawed on ice for 30 minutes prior to addition of 100 ng of high quality DNA, gentle mixing and a further 30 minutes incubation on ice. The competent cell and DNA mixture was then subject to heat shock at 42°C for 30 seconds and returned to ice for 2 minutes. 500 μ l of pre-warmed Lysogeny broth (LB) broth was added to the cells and incubated shaking (220 RPM) at 37°C for one hour. Following this step, an appropriate volume was plated on prewarmed agar plates containing the selective antibiotic, the plate inverted and incubated at 37°C for 16 hours overnight.

2.10.3. PCR amplification of DNA for cloning

The DNA polymerase Phusion® High-Fidelity DNA polymerase (New England BioLabs) was used in accordance with the manufacturers instructions for a total reaction volume of 50 μ l. This reaction contained Phusion HF buffer, 10 ng of template DNA, 200 μ M deoxyribonucleoside triphosphates (dNTPs) consisting of dATP, dCTP, dGTP and dTTP (purchased from Fermentas) and 0.5 μ M of both forward and reverse oligonucleotides (Synthesised by Sigma-Alrich Co Ltd). Post addition of 0.5 μ l of the polymerase enzyme itself thermocycling was conducted in a T3 Thermocycler (Biometra, Göttingen Germany).

2.10.4. PCR screening of plasmid DNA from bacterial colonies

Single bacterial colony was suspended in 100 μ l of sterile distilled H₂O and 1 μ l of this suspension used as a template in a 10 μ l PCR reaction. The PCR products and 1 kb DNA ladder (New England BioLabs, N3232) were ran on a 1-2 percent agarose gel stained with 0.5 μ g/ml ethidium bromide to determining the presence or absence of DNA insert.

2.10.5. Quality control and sequencing of DNA

Quality of DNA was checked through gel electrophoresis on 1-2 percent agarose gel stained with 0.5 µg/ml ethidium bromide and the 260/280 nm ratio (~1.8 accepted as pure) determined through measurement of nucleic acid concentration using a Nanodrop Lite (Thermo Fisher Scientific). Sequencing of constructs prior to use was completed by GATC (GATC Biotech, London, UK).

2.11. Common media

2.11.1. Hanks balanced salt solution (HBS)

HBS was made both Ca²⁺ containing and Ca²⁺-free (Table 2.9) and adjusted to pH 7.3 using NaOH. All protocols using HBS contain Ca²⁺ unless stated otherwise.

Table 2.9. Components Ca²⁺ containing and Ca²⁺-free of HBS

Component	Final Concentration	Amount per 1 L
NaCl	135mM	7.89g
KCl	5.9mM	0.44g
MgCl ₂ .6H ₂ O	1.2mM	0.245g
CaCl ₂ *	1.5mM	1.5ml of 1M stock
HEPES	11.6mM	2.75g
Glucose	11.5mM	2.05g

* Not added for Ca²⁺-free HBS

2.11.2. Phosphate buffer saline (PBS)

PBS was made using tablets (Sigma-Aldrich, P4417) dissolved in deionised water and autoclaved. Here a single tablet in 200 ml water gives a solution composed of 0.1 M phosphate buffer, 0.0027 M potassium chloride and 0.137 M sodium chloride solution at a pH of 7.4.

2.11.3. Bacterial growth medium

Lysogeny broth (LB broth) was made using LB broth powder (Sigma-Aldrich, L3022) and used for growth of *E. coli* bacteria. Here, 10 g of powder was

dissolved in 500 ml of deionised water prior to autoclaving for sterilisation. Addition of antibiotic (Ampicillin or kanamycin at a working concentration of 100 µg/mL or 50 µg/mL, respectively (both purchased from Sigma-Aldrich)), where appropriate, was performed after cooling. Similarly, LB broth agar plates were made using LB broth powder with the addition of agar (Sigma-Aldrich, 05040). Again, autoclaving was performed and antibiotic added as appropriate following cooling to 60°C in a water bath. Pouring of plates was performed next to a flame. Plates were allowed to solidify and dry at room temperature overnight before sealing in a bag and storing at 4°C.

2.12. Data analysis

All concentration response data were analysed using Prism 6 version 6.0h (GraphPad Software Inc., San Diego, California, US). $-\log EC_{50}$ (pEC_{50}) and E_{max} values were determined using the following three-parameter logistic equation as described previously (May *et al.*, 2007):

$$Y = Basal + \frac{(E_{max} - Basal)}{1 + 10^{(\log EC_{50} - \log [A])}}$$

where *Basal* represents the y value in the absence of ligand(s); E_{max} is the maximal system stimulation in the presence of ligand(s) (in other words the lower and upper plateaus of the concentration response curve); [A] is the ligand concentration, and $\log EC_{50}$ is the concentration of ligand which generates a half maximal response (E_{max}).

To determine efficacy in the system, data was fitted to the operational model of agonism (Black and Leff, 1983) using the following equation, which was manually inputted into Prism 6 by Dr Graham Ladds:

$$Y = Basal + \frac{E_m - Basal}{1 + ((10^{\log KA}) + (10^{\log [A]})) / (10^{(\log \tau + \log [A])})}$$

where *Basal* represents the y value in the absence of ligand; E_m is the maximal system stimulation; K_A is the dissociation constant of agonist-receptor in molar concentration; $[A]$ is the ligand concentration, and τ is the operational measure of efficacy which as previously mentioned incorporates both signalling efficacy and receptor density.

This model explicitly describes agonist function in terms of the ligand-receptor interaction and the subsequent receptor signal transduction cascade (Kenakin *et al.*, 2012). This allows the estimation of $\log K_A$, the agonist-receptor functional dissociation constant, and $\log \tau$, the operational measure of efficacy which incorporates signalling efficacy (the efficacy of the agonist to activate a particular pathway and the ability and the system to convert the receptor stimulus into a response) and receptor density (Kenakin *et al.*, 2003, Wootten *et al.*, 2016). The operational model of agonism is widely used but a number of limitations, which include the fact that the model does not consider dynamics and does not account for ligand-independent signaling (Stott *et al.*, 2016). In addition, the model cannot correct for examples in which other co-factors that affect signaling are differentially expressed, such as GRKs (Gundry *et al.*, 2017).

Where appropriate, the obtained values of efficacy, τ , and dissociation constant, K_A , were then used to quantify signalling bias as change in $\log(\tau/K_A)$ ($\Delta\log(\tau/K_A)$) relative to the reference ligand or wild-type receptor, as described previously (Kenakin *et al.*, 2012):

$$\Delta\text{Log}\left(\frac{\tau}{K_A}\right) = \text{Log}\left(\frac{\tau}{K_A}\right)_{\text{Test}} - \text{Log}\left(\frac{\tau}{K_A}\right)_{\text{Reference ligand}}$$

$$\Delta\text{Log}\left(\frac{\tau}{K_A}\right) = \text{Log}\left(\frac{\tau}{K_A}\right)_{\text{Mutant}} - \text{Log}\left(\frac{\tau}{K_A}\right)_{\text{Wild type}}$$

To determine the actual ligand bias ($\Delta\Delta\log(\tau/K_A)$) of an agonist for one pathway over another it is necessary to evaluate the differences between

$\Delta\log(\tau/K_A)$ values for a given agonist between pathways and is given by the equation:

$$\Delta\Delta\text{Log}\left(\frac{\tau}{K_A}\right) = \Delta\text{Log}\left(\frac{\tau}{K_A}\right)_{\text{Pathway 1}} - \Delta\text{Log}\left(\frac{\tau}{K_A}\right)_{\text{Pathway 2}}$$

pEC_{50} , basal, maximal responses, pK_A and $\log \tau$ obtained from fitting concentration response curves were compared by paired Student's t-test or one-way ANOVA followed by Dunnett's test for multiple comparisons. Cell-surface analysis data from ELISA or FACS analysis was compared by one-way ANOVA followed by Dunnett's test for multiple comparisons.

2.13. Modeling mutant GPCR structure

Modeller (version 9.18) can be used for homology and comparative modeling of protein 3D-structure (Eswar *et al.*, 2007) and allows us to mutate specific residues within a pre-existing protein structure where Protein Data Bank (PDB) files exist. The PDB format provides a standard representation for protein structures derived from X-ray and NMR studies. Here, Modeller was used for rapid comparative modeling for each substitution mutation made in both the GCGR and $A_{2A}R$ to provide predictions to help explain experimental data. The current available GCGR PDB files used in this work included 5XEZ (Zhang *et al.*, 2017), 5ee7 (Jazayeri *et al.*, 2016) and 4l6r (Siu *et al.*, 2013) and for $A_{2A}R$ includes 3EML (Jaakola *et al.*, 2008).

The Modeller command (`mod9.18 mutate_model.py seq1 165 ALA A > seq1A.log`) was run from the Mac OS X 'Terminal' application using Python 2.3. This command reads the PDB file (in the example this is seq1), changes the sequence as determined by the residue number and defined amino acid on the specified chain (in this example; 165, alanine (ALA) and A (only one chain in the chosen PDB files), respectively), build new coordinates for the other atoms and write the mutated file (seq1A.log). All PDB files were viewed in MacPyMol (version 1.7.4.5) and the WT (original PDB file) and mutated

receptor (PDB file created by running the command) compared visually to assess any predicted changes in amino acid interactions and structure.

2.14. Live cell imaging in HEK 293 cells

Transfected cells were seeded into an 8-well microscope slide (Thistle Scientific, Glasgow, UK) and placed in a humidified 5 percent CO₂ incubator at 37°C for 25 hours. Growth medium was replaced with HEPES buffer (Thermo Fisher Scientific) prewarmed to 37°C, as detailed previously (Weston *et al.*, 2015). Cells were viewed on a True Confocal Scanner Leica TCS SP5 microscope (Leica Microsystems Ltd, Milton Keynes, UK).

Chapter 3. Establishing a robust assay system

3.1. Introduction

In the work presented in this thesis, investigation of receptor pharmacology required utilisation of a number of assays for the measurement of downstream signalling components, receptor cell-surface expression analysis, pharmacological tools and cell lines. Having recently started to utilise cell lines for the investigation into receptor cell signalling, these methods were new to the Ladds' research group and required optimisation in order to establish robust assay systems. In this chapter, steps taken to achieve such optimisation for a number of variables for the measurement of cAMP and IP₁ accumulation are detailed. These variables included; cell number, ligand stimulation time, DNA concentration at transfection, time post-transfection and DNA transfection reagent. We also investigated the activity of two G protein inhibitors for the purpose of exploring G protein-coupling of GPCR.

We conducted characterisation of a number cell lines, utilised in chapters 4 and 5 to answer key research questions. These included the generated stably GCGR expressing HEK 293 cell line, various CRISPR G protein and β -arrestin1/2 knockout HEK 293 cell lines (gifted from Dr Asuka Ioune) and the immortalised human hepatocellular carcinoma cell line, Hep 3B.

Finally, we detailed steps in the analysis of data acquired from FACS, conducted using the BD Accuri™ C6 Plus Flow Cytometer, to quantify GCGR cell-surface expression. Using this method of receptor cell-surface analysis, we also investigated the possibility of manipulating cell-surface expression by altering DNA concentration. This was conducted with the aim of achieving equal WT and mutant receptor cell-surface expression in order to investigate the influence of such mutation on GCGR signalling, independent of cell-surface expression variability.

3.2. Optimisation of the cAMP assay

3.2.1. Cell number

In order to establish a robust assay system, optimisation of cell number for the cAMP accumulation assay (LANCER® cAMP Detection Kit or LANCER® Ultra cAMP Detection Kit) are essential. Flp-In HEK 293T cells stably expressing the GLP-1R (hereafter referred to as Flp-In GLP-1R HEK cells) and Flp-In CHO-K1 cells stably expressing the GLP-1R (hereafter referred to as Flp-In GLP-1R CHO-K1 cells) were acquired at the beginning of this work and, despite expressing GLP-1R rather than the predominant receptor of interest (GCGR), provide an initial starting point for establishing a robust assay system.

Flp-In GLP-1R HEK cells were plated at a range of cell numbers in a 384-well plate and stimulated for 30 minutes with forskolin prior to measuring cAMP accumulation. The cAMP standard curve (SC) was used to assess the dynamic range of the assay and to estimate the quantity of cAMP produced by a cell (Figure 3.1). The concentration dose-responses seen to forskolin at the various cell numbers were shown to reside within the cAMP SC (Figure 3.2). Unsurprisingly, the basal cAMP accumulation and forskolin maximum response were shown to be cell number dependent with both showing elevations on increasing cell number (Table 3.1). The signalling window at 4,000 and 5,000 cells per well was reduced (as indicated by the span) with an apparent increased forskolin potency (Table 3.1), indicating that we are at the upper end of the dynamic range of the LANCER® cAMP assay. These findings suggest that the optimal cell number was 1,000 or 2,000 where the forskolin concentration dose-response curve covers most of the linear region of the cAMP SC (marked by the dashed grey line in Figures 3.1 and 3.2) and show the largest signalling window (span). With these findings in mind, 1,000 cells per well was chosen as the optimal number for the experiments utilising the LANCER® cAMP assays described in chapters 4 and 5, unless otherwise stated.

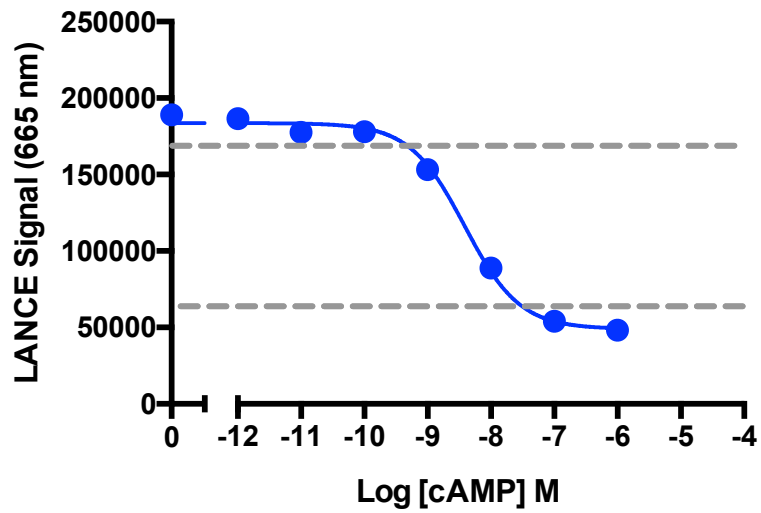


Figure 3.1. Typical LANCE cAMP standard curve. The representative curve contains 4 repeats conducted in duplicate. The grey dashed line marks the linear region of the cAMP standard curve. All values are mean \pm SEM expressed LANCE Signal at 665 nm detected using a Mithras LB 940 (Berthold technology) Ex. λ 340 nm and Em. λ 665 nm.

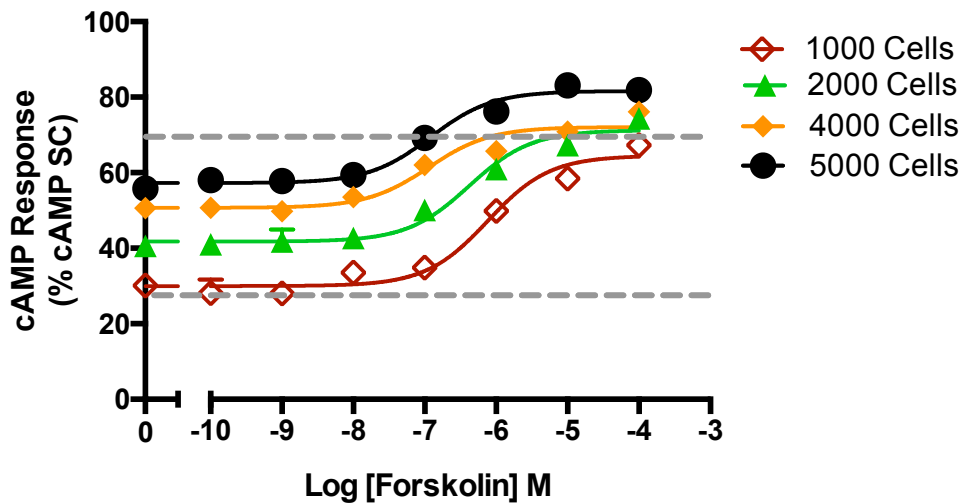


Figure 3.2. Forskolin stimulated cAMP response in Flp-In HEK 293T cells plated at various densities. Flp-In HEK 293T cells expressing GLP-1R were plated at various cell numbers on a 384-well plate, exposed to forskolin for 30 minutes and cAMP accumulation detected. The grey dashed line marks the linear region of the cAMP standard curve as shown in Figure 3.1. All values are mean \pm SEM expressed as percentage cAMP standard curve (SC) response where $n = 3$ independent experimental repeats, conducted in duplicate.

Table 3.1. Forskolin stimulated cAMP response in Flp-In HEK 293T cells plated at various densities. Potency (pEC₅₀), maximal response (E_{max}), basal and span for forskolin response measured in Flp-In HEK 293T cells stably expressing GLP-1R using a cAMP accumulation assay

Cell number	cAMP			
	pEC ₅₀ ^a	E _{max} ^b	Basal ^c	Span ^d
1,000	6.12 ±0.1	64.5 ±1.7	29.9 ±1.0	34.5 ±1.9
2,000	6.38 ±0.1	71.2 ±1.3*	41.8 ±0.9***	29.5 ±1.5
4,000	6.95 ±0.2**	72.1 ±1.2**	50.7 ±1.0***	21.4 ±1.5***
5,000	6.92 ±0.1**	81.6 ±0.9***	57.3 ±0.8***	24.4 ±1.2**

Flp-In HEK 293T cells stably expressing GLP-1R were stimulated with forskolin prior to measurement of cAMP accumulation to generate concentration response curves. To calculate pEC₅₀, E_{max}, Basal and Span values, data were analysed using a three-parameter logistic equation.

^a Negative logarithm of forskolin concentration required to produce a half-maximal response

^b Maximal response to forskolin as percentage cAMP standard curve (SC)

^c The low plateau of the fitted sigmoidal concentration dose-response curve

^d The difference between E_{max} and basal signalling

All values are mean ± SEM expressed percentage cAMP SC response where *n* = 3 independent experimental repeats, conducted in duplicate. Statistical significance (*, *p*<0.05;** , *p*<0.01;***, *p*<0.001) comparing forskolin response in 1,000 cells/well was determined by one-way ANOVA with Dunnett's post test.

3.2.2. Ligand stimulation time

3.2.2.1. To include or exclude the 'true basal' stimulation point?

Flp-In HEK 293T stably expressing GLP-1R showed a concentration-dependent increases in cAMP accumulation following forskolin stimulation for 30 minutes and the fitted concentration dose-response curve was found to reside within the dynamic range of the cAMP assay (Figure 3.1). However, the ideal stimulation time appeared to depend on the potency of the ligand investigated and the cellular model chosen. The fitted concentration dose-response curve to cAMP accumulation data acquired in Flp-In GLP-1R CHO-K1 cells or Flp-In CHO-K1 cells stably expressing GCGR (hereafter referred to as Flp-In GCGR CHO-K1 cells) were found to depend on the inclusion or

exclusion of the 'true basal' (stimulation with buffer only) data point (Figure 3.3).

In Flp-In GCGR CHO-K1 cells, a 30 minute stimulation with oxyntomodulin produced a concentration dose-response where the fitted curve at low concentrations of oxyntomodulin (0.01 pM to 10 pM) was in line with the 'true basal', irrespective of inclusion or exclusion of the 'true basal' stimulation data point (Figure 3.3 A). Here, the fitted oxyntomodulin concentration dose-response curves were identical, irrespective of the 'true basal' point. However, stimulation with GCG, known to be a more potent agonist at the GCGR when compared to oxyntomodulin (Weston *et al.*, 2015, Section 4.2.1), showed a significantly elevated cAMP accumulation (72.6 ± 1.9 percentage forskolin response) at only 0.1 pM of GCG (Figure 3.3 A).

A similar scenario was found in Flp-In GLP-1R CHO-K1 cells (Figure 3.3 B). A 30 minute stimulation of Flp-In GLP-1R CHO-K1 cells with the small molecule agonist of GLP-1R, BETP (Willard *et al.*, 2012), produces a concentration dose-response where the cAMP accumulation points at low concentrations of the compound (10 pM - 0.1 μ M) were in line with the 'true basal' stimulation point (shown as 10 pM on Figure 3.3 B). However, stimulation with 0.1 pM of GLP-1(7-36)amide showed a large cAMP accumulation (78.3 ± 1.1 percentage forskolin response).

The LANCE® cAMP assay utilises IBMX, a non-specific inhibitor of cAMP and cGMP PDEs (Schmidt *et al.*, 2000), therefore any cAMP produced in the cell will accumulate over the stimulation time period. As a result of this large cAMP accumulation between the 'true basal' stimulation point and the lowest ligand concentration of GCG or GLP-1(7-36)amide, a sigmoidal concentration dose-response curve for either ligand could not be determined (Table 3.2). These results are likely to be due to high receptor expression where potent agonists, even at very low concentrations, over the 30-minute stimulation period is sufficient to induce a large cAMP accumulation and a resulting decreased signalling window. Given this finding, further optimisation

into the stimulation time was required to circumvent this issue (Section 3.2.2.2).

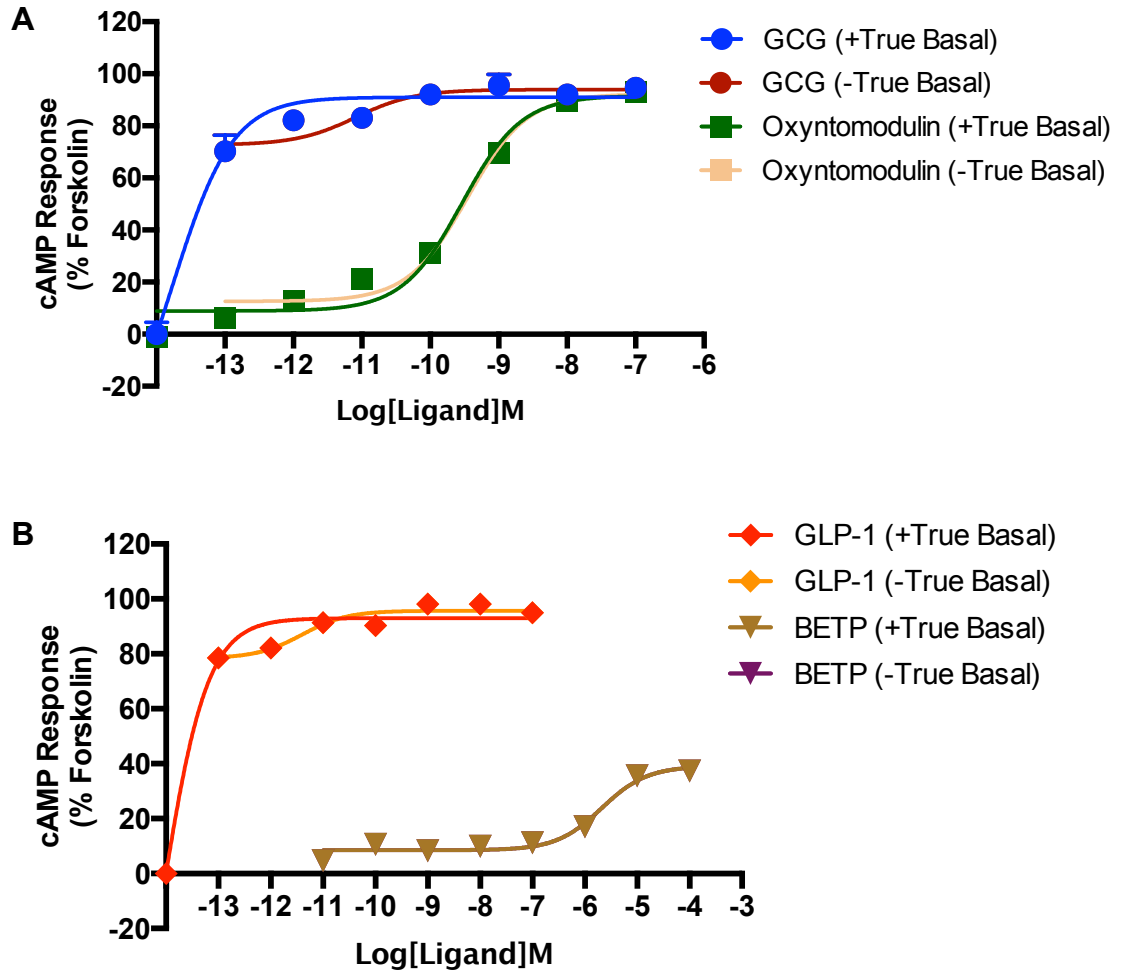


Figure 3.3. cAMP response in Flp-In HEK 293T cells stably expressing the GLP-1R or GCGR, with or without the true basal stimulation point. A) Flp-In HEK 293T cells stably expressing GCGR were stimulated with GCG or oxyntomodulin for 30 minutes and cAMP accumulation detected. **B)** Flp-In HEK 293T cells stably expressing A) GLP-1R were stimulated with GLP-1(7-36)amide or BETP for 30 minutes and cAMP accumulation detected. Cells were plated at 1,000 cells per well of a 384-well plate. The ‘true basal’ cAMP response is the point at which cells were ‘stimulation’ with buffer only in the absence of ligand. All values are mean \pm SEM expressed as percentage forskolin response where $n = 2$ independent experimental repeats, conducted in triplicate.

Table 3.2. cAMP response in Flp-In HEK 293T cells stably expressing the GLP-1R or GCGR, with or without the true basal stimulation point. Potency (pEC₅₀), maximal response (E_{max}), basal and span for forskolin response measured in Flp-In CHO-K1 cells stably expressing GLP-1R or GCGR using a cAMP accumulation assay

Flp-In GCGR CHO-K1 cells				
Ligand +/- True basal	pEC ₅₀ ^a	E _{max} ^b	Basal ^c	Span ^d
GCG +	N.D			
GCG -	11.09 ±0.2	72.6 ±1.9	72.6 ±3.2	21.3 ±3.6
Oxyntomodulin +	9.54 ±0.1	91.6 ±3.1	8.9 ±2.2	82.7 ±3.7
Oxyntomodulin -	9.46 ±0.1	92.3 ±2.2	12.6 ±1.7	79.7 ±2.7
Flp-In GLP-1R CHO-K1 cells				
Ligand +/- True basal	pEC ₅₀ ^a	E _{max} ^b	Basal ^c	Span ^d
GLP-1 +	N.D			
GLP-1 -	11.4 ±0.2	95.7 ±1.1	78.4 ±2.1	17.3 ±2.3
BETP +	5.68 ±0.1	39.1 ±1.9	8.5 ±1.9	30.6 ±2.0
BETP -	5.68 ±0.1	39.1 ±1.9	8.5 ±1.9	30.6 ±2.0

Flp-In CHO-K1 cells stably expressing GCGR or GLP-1R were stimulated with forskolin prior to measurement of cAMP accumulation to generate concentration response curves. To calculate pEC₅₀, E_{max}, Basal and Span values, data were analysed using a three-parameter logistic equation. +/- Indicates the inclusion (+) or exclusion (-) of the 'true basal' stimulation point where cells received stimulation with buffer only.

^a Negative logarithm of forskolin concentration required to produce a half-maximal response

^b Maximal response to forskolin as percentage forskolin response

^c The low plateau of the fitted sigmoidal concentration dose-response curve

^d The difference between E_{max} and basal signalling

All values are mean ± SEM expressed percentage forskolin response where *n* = 2 independent experimental repeats, conducted in duplicate. Statistical significance (*, *p* < 0.05; **, *p* < 0.01; ***, *p* < 0.001) comparing ligand responses with or without the 'true basal' stimulation point was determined by unpaired Student's t-test (two-tailed).

N.D denotes not determined, here a true concentration dose-response curve could not be fitted to the stimulation data

3.2.2.2. Optimising stimulation time

In order to address the issue surrounding elevated cAMP accumulation at very low ligand concentrations, a time course of GLP-1(7-36)amide stimulation at various concentrations was performed using Flp-In GLP-1R CHO-K1 cells. Here, Flp-In GLP-1R CHO-K1 cells were stimulated with forskolin (100 nM), GLP-1(7-36)amide (0.1 nM, 10 nM or 100 nM) or

stimulation buffer only for 2, 4, 8, 16 or 32 minutes prior to measurement of cAMP accumulation.

Importantly, there was no cAMP accumulation detected following stimulation with buffer only at any time point (Figure 3.4). As would be expected, the mean cAMP accumulation measured following forskolin or GLP-1(7-36)amide stimulation was shown to increase with increasing stimulation time (Table 3.2). No significant difference was found between the responses measured at 2 and 4-minute stimulation with GLP-1(7-36)amide or forskolin. Fitting a three-parameter logistics equation to the cAMP accumulation data acquired for each time point following GLP-1(7-36)amide stimulation at 0.1 nM, 10 nM and 100 nM produced clear concentration dose-response curves (Figure 3.5). These data show an enhanced signalling window with stimulation time greater than 4 minutes. It is assumed that a sigmoidal concentration dose-response curve for 32-minute stimulation would not be fitted if a cAMP accumulation point acquired from 0.1 pM GLP-1(7-36)amide stimulation was included, as previously indicated (Figure 3.3 B).

The ideal stimulation time would give a large signalling window and allow any potential differences in maximum response between ligands to be detected. When analysing the responses across GLP-1(7-36)amide concentrations and forskolin for each time point, with the exception of stimulation buffer only, there was found to be no significant difference in mean responses for 2 or 4 minutes stimulation when compared to 0.1 nM GLP-1(7-36)amide stimulation (Table 3.2).

At 32, 16 and 8 minute stimulation, there was a significantly different response detected between GLP-1(7-36)amide (0.1 nM) and forskolin stimulation. The stimulation time of 8 minutes was the only time which showed a significantly different cAMP accumulation between GLP-1(7-36)amide concentrations (0.1 nM versus 100 nM) (41.52 ± 0.96 and 52.39 ± 3.06 percentage forskolin response, respectively).

To assess if the stimulation time of 8 minutes is also appropriate for an alternative cell line, Flp-In GLP-1R HEK cells (1,000 and 2,000 cells per well)

were stimulated with GLP-1(7-36)amide for 8 minutes and cAMP accumulation detected (Figure 3.6). There was shown to be a robust cAMP response without an elevated basal for 1,000 cells per well whereas 2,000 cells still showed a slight elevated basal cAMP level (22.0 ± 2.9 percent forskolin response). The findings presented here suggest that 8 minutes stimulation time and the cell density of 1,000 cells appears to be ideal to avoid experimentally induced elevations in basal responses and to enable the detection of any potential differences in maximal responses between ligands. With these findings in mind, 8 minutes stimulation time and 1,000 cells per well were used in experiments utilising the cAMP assays described in chapters 4 and 5, unless otherwise stated.

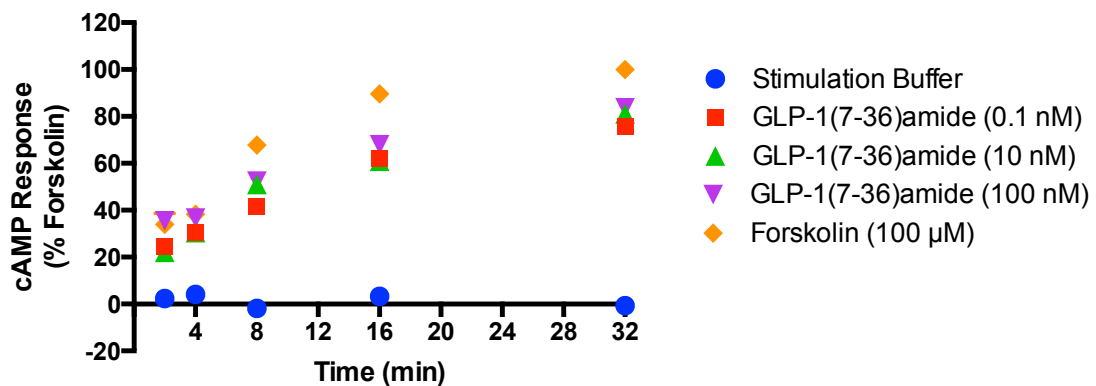


Figure 3.4. cAMP response in Flp-In CHO-K1 cells stably expressing the GLP-1R at various time points. Flp-In GLP-1R CHO-K1 cells (1000 cells per well of a 384-well plate) were stimulated with forskolin, GLP-1(7-36)amide or stimulation buffer only (no ligand) for various times and cAMP accumulation detected. All values are mean \pm SEM expressed as percentage forskolin response where $n = 3$ independent experimental repeats, conducted in duplicate.

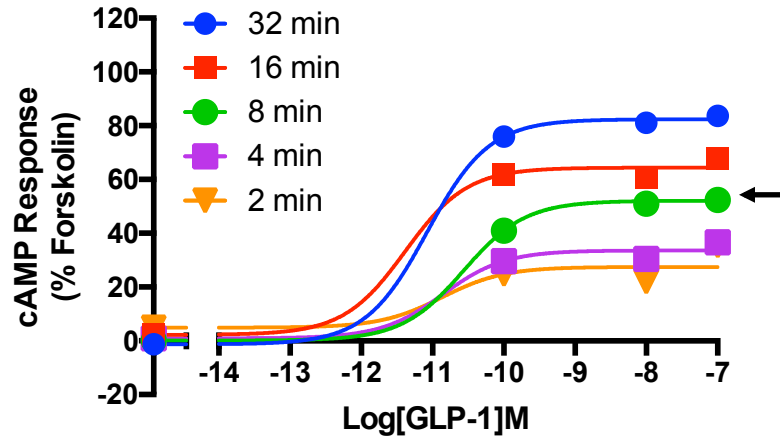


Figure 3.5. cAMP concentration dose-response in Flp-In CHO-K1 cells stably expressing the GLP-1R at various time points. Three-parameter logistics equation fitted to the time point data presented in figure 3.4. Flp-In GLP-1R CHO-K1 cells were stimulated with GLP-1(7-36)amide (GLP-1) for various times and cAMP accumulation detected. Arrow indicates the optimal stimulation time. All values are mean \pm SEM expressed as percentage forskolin response at 32 minutes where $n = 3$ independent experimental repeats, conducted in duplicate.

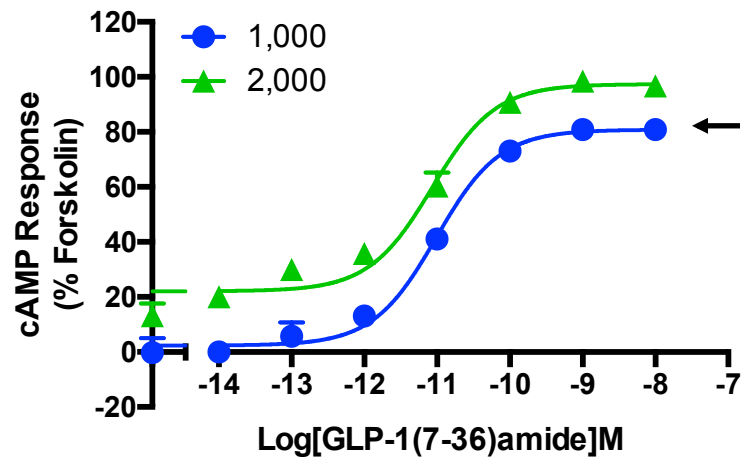


Figure 3.6. 8 minutes stimulation time at 1,000 and 2,000 cells/well is optimal in Flp-In HEK 293T cells stably expressing the GLP-1R. Flp-In HEK 293T cells expressing GLP-1R were plated at 1,000 or 2,000 cells/well of a 384-well plate, stimulated with GLP-1(7-36)amide for 8 minutes and cAMP accumulation detected. Arrow indicates the optimal cell density. All values are mean \pm SEM expressed as percentage forskolin response where $n = 3$ independent experimental repeats, conducted in duplicate.

Table 3.2. Optimising ligand stimulation time for cAMP accumulation assay. cAMP response to GLP-1(7-36)amide or forskolin stimulation in Flp-In HEK 293T cells stably expressing the GLP-1R at various time points

Statistical significance across time point					
Time (min)	Buffer only	GLP-1 0.1 nM	GLP-1 10 nM	GLP-1 100 nM	Forskolin 100 nM
32	-0.65 ±1.13	75.60 ±0.34***	81.04 ±3.45***	83.64 ±2.24***	100.00 ±1.25***
16	3.32 ±1.57	62.11 ±0.93***	60.88 ±1.44***	67.87 ±1.10***	89.65 ±3.70***
8	-1.87 ±1.08	41.52 ±0.96***	51.00 ±1.23***	52.39 ±3.06**	67.85 ±3.21***
4	4.12 ±1.75	30.41 ±0.76**	30.46 ±2.67***	36.69 ±1.16	38.30 ±4.84
2	2.36 ±1.33	24.45 ±0.43	22.07 ±2.13	35.44 ±3.91	33.98 ±6.66
Statistical significance across ligands/ligand concentrations					
Time (min)	Buffer only	GLP-1 0.1 nM	GLP-1 10 nM	GLP-1 100 nM	Forskolin 100 nM
32	-0.65 ±1.13***	75.60 ±0.34	81.04 ±3.45	83.64 ±2.24	100.00 ±1.25***
16	3.32 ±1.57***	62.11 ±0.93	60.88 ±1.44	67.87 ±1.10	89.65 ±3.70***
8	-1.87 ±1.08***	41.52 ±0.96	51.00 ±1.23	52.39 ±3.06*	67.85 ±3.21***
4	4.12 ±1.75***	30.41 ±0.76	30.46 ±2.67	36.69 ±1.16	38.30 ±4.84
2	2.36 ±1.33***	24.45 ±0.43	22.07 ±2.13	35.44 ±3.91	33.98 ±6.66

Flp-In CHO-K1 cells stably expressing GLP-1R were stimulated for various times with buffer only, GLP-1(7-36)amide at various concentrations or forskolin (100 nM) prior to measurement of cAMP accumulation.

^a Negative logarithm of forskolin concentration required to produce a half-maximal response

^b Maximal response to forskolin as percentage forskolin response

^c The low plateau of the fitted sigmoidal dose-response curve

^d The difference between E_{max} and basal signalling

All values are mean ± SEM expressed percentage forskolin response where $n = 3$ independent experimental repeats, conducted in duplicate. Statistical significance (*, $p < 0.05$; **, $p < 0.01$; ***, $p < 0.001$) was conducted either across time points comparing each response to 2 minute stimulation for each ligand concentration or across ligand concentrations comparing each response to GLP-1(7-36)amide 0.1 nM at each time point using one-way ANOVA with Dunnett's post test

3.2.3. DNA concentration and time post-transfection

Reducing the ligand stimulation time to 8 minutes was shown to be optimal for the measurement of cAMP accumulation in stably expressing Flp-In HEK 293T and CHO-K1 cells (Section 3.2.2.2). In cells transfected with high copy number constructs, such as the vectors pmCherry-N1 expressing GCGR and pcDNA3.1 expressing GFP-tagged GCGR, and stimulated for 8 minutes 48 hours post-transfection, these was found to be a high cAMP accumulation at very low concentrations of GCG (0.1 pM – 10 pM) resulting in an elevated 'basal' cAMP response (Figure 3.7). A sigmoidal concentration dose-response could not be determined with the inclusion of the 'true basal' stimulation point (Figure 3.7), as was previously described (Section 3.2.2.1, Figure 3.3). With the aim of reducing this elevated basal, an optimisation into DNA concentration and incubation time post-transfection (prior to experimental assay) was conducted.

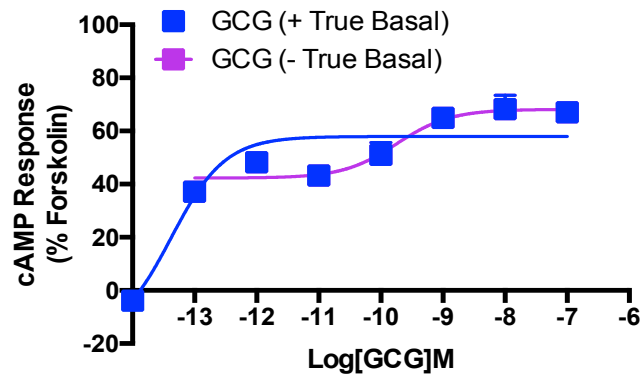


Figure 3.7. cAMP response in HEK 293T cells transfected with pcDNA3.1 containing GCGR: HEK 293T cells 48 hours post transfection with pcDNA3.1 containing GFP-tagged GCGR were stimulated with GCG for 8 minutes and cAMP accumulation detected. Cells were plated at 1000 cells per well of a 384-well plate. The 'true basal' cAMP response is the point at which cells were 'stimulation' with buffer only in the absence of ligand. All values are mean \pm SEM expressed as percentage forskolin response where $n = 2$ independent experimental repeats, conducted in duplicate.

Here, HEK 293T cells in a 24-well plate were transfected with various concentrations of pcmCherry-N1 expressing GCGR and assayed for ligand

stimulated cAMP accumulation 24 or 48 hours post-transfection (Figure 3.8). The responses seen to stimulation of cells transfected with 50 ng per well of GCGR containing vector or vector alone showed significantly reduced maximal response, basal and span at both 24 and 48 hours post-transfection when compared to 250 ng per well (Figure 3.8 and Table 3.3). In addition, these responses were not significantly different from each other, possibly indicating unsuccessful transfection at 50 ng per well. Although the measured response to GCG in vector only transfected cells could indicate a low level of endogenous GCGR expression, the determined potency showed large variability in the data (pEC_{50} 8.95 ± 0.9 and 9.75 ± 0.5 for 24 and 48 hours post-transfection, respectively) and consequently, low confidence in the determined response.

The cAMP response to GCG stimulation 24 and 48-hours post-transfection with GCGR concentrations of 150 and 200 ng per well showed no significant differences for potency, maximal response, basal or span values (Table 3.3) when compared to 250 ng per well. This indicates that, at least for this vector within HEK 293T cells, an increase in DNA concentrations above 150 ng per well does not translate into an enhanced cAMP response. A direct comparison between 24 and 48 hours post-transfection indicate a clear discrepancy between basal cAMP levels and the measured range of the response (Table 3.3). At 48 hours, there is an elevated basal cAMP accumulation and reduction in the signalling window as a consequence. This is likely to be an artefact of high receptor expression and as such, where transfection of receptor is required, cAMP assays were conducted 24 hours post-transfection with 250 ng of DNA (Figure 3.8). For experiments investigating weak responses, such as the in CHO-K1 cells transfected with $A_{2A}R$, 48 hours post-transfection was conducted.

To further investigate the influence of DNA concentration at 24 hours post-transfection on the measured cAMP accumulation, HEK 293 cells (gifted from Dr Asuka Ioune) were transfected with pmCherry-N1 containing GCGR at either 500 ng or 250 ng per well (24-well plate) and stimulated with GCG or

oxyntomodulin (Figure 3.9). Despite a small reduction in oxyntomodulin stimulated maximum response at 250 ng per well when compared to 500 ng per well (E_{max} 60.1 \pm 4.0 and 72.9 \pm 4.3 percentage forskolin response, respectively), there was shown to be no significance difference between each responses measured at the two DNA concentrations (Table 3.4). This finding confirmed that doubling the DNA concentration at transfection did not translate to a proportional increased in maximum cAMP accumulation.

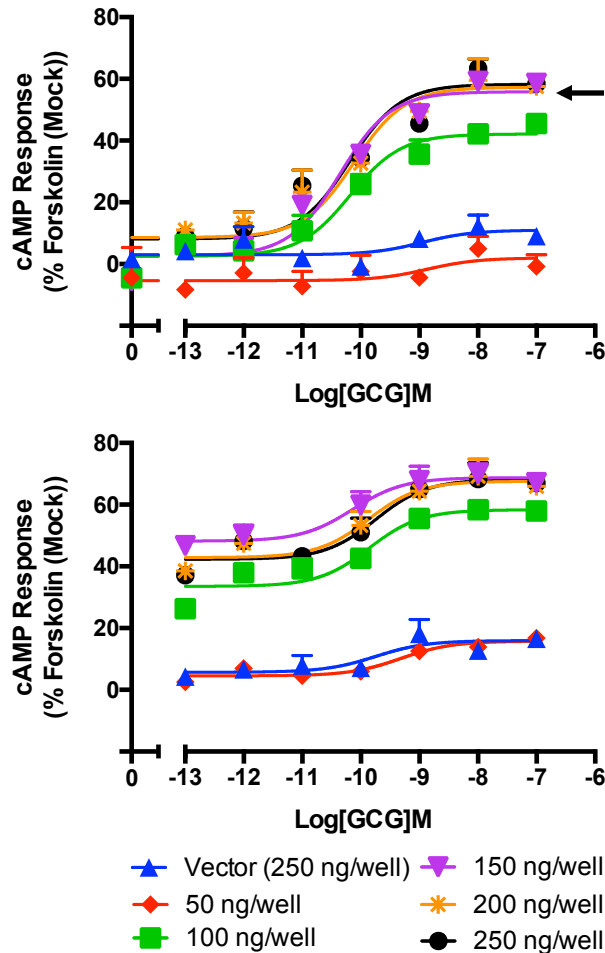


Figure 3.8. cAMP response in HEK 293T cells 24 or 48 hours post-transfection with pcDNA3.1 containing GCGR. HEK 293T cells **A)** 24 or **B)** 48 hours post-transfection with pcDNA3.1 containing GFP-tagged GCGR were stimulated with GCG for 8 minutes and cAMP accumulation detected. Cells were plated at 1,000 cells per well of a 384-well plate. The ‘true basal’ point (‘stimulation’ with buffer only) for data acquired from 48 hours post-transfected cells was excluded to allow fitting of the three-parameter concentration dose-response curve. Arrow indicates 250 ng at 24-hours post transfection as the chosen optimal conditions. All values are mean \pm SEM expressed as percentage forskolin response where $n = 2$ independent experimental repeats. conducted in duplicate.

Table 3.3. cAMP response in HEK 293T cells 24 or 48 hours post-transfection with pcDNA3.1 containing GCGR. Potency (pEC_{50}), maximal response (E_{max}), basal and span for GCG stimulated cAMP response measured in GCGR transfected HEK 293T cells 24 and 48 hours post-transfection, measured using cAMP assay

24 hours post-transfection				
DNA (ng/well)	pEC_{50} ^a	E_{max} ^b	Basal ^c	Span ^d
Vector only	8.95 ±0.9	11.0 ±2.5***	3.0 ±1.3	7.9 ±2.7***
50	8.87 ±1.2	1.9 ±3.9***	-5.4 ±2.1**	7.3 ±4.2***
100	10.18 ±0.2	42.1 ±2.3*	2.5 ±2.0	39.6 ±3.0*
150	10.36 ±0.1	55.8 ±2.4	2.6 ±2.2	53.2 ±3.1
200	10.12 ±0.2	58.3 ±4.0	8.6 ±3.2	57.3 ±5.0
250	10.19 ±0.2	58.3 ±3.8	8.1 ±3.2	58.3 ±4.9
48 hours post-transfection (-True basal)				
DNA (ng/well)	pEC_{50} ^a	E_{max} ^b	Basal ^c	Span ^d
Vector only	9.75 ±0.5	16.0 ±1.8***	5.7 ±1.6***	10.3 ±2.3**
50	9.32 ±0.3	15.8 ±1.2***	4.5 ±1.3***	11.2 ±1.7**
100	9.86 ±0.2	33.5 ±2.1***	33.5 ±1.9*	24.8 ±2.0
150	10.14 ±0.2	68.8 ±1.8	48.2 ±2.1	20.6 ±2.7
200	9.87 ±0.2	67.6 ±1.8	42.9 ±2.4	24.7 ±3.2
250	9.74 ±0.2	68.1 ±2.3	42.3 ±2.1	25.9 ±3.0

HEK 293T cells 24 or 48 hours post-transfection with pcDNA 3.1 containing GCGR were stimulated with GCG prior to measurement of cAMP accumulation.

^a Negative logarithm of GCG concentration required to produce a half-maximal response

^b Maximal response to GCG as percentage forskolin response

^c The low plateau of the fitted sigmoidal concentration dose-response curve

^d The difference between E_{max} and basal signalling

All values are mean ± SEM expressed percentage forskolin response in mock transfected (Vector only) where $n = 3$ independent experimental repeats, conducted in duplicate. Statistical significance (*, $p < 0.05$; **, $p < 0.01$; ***, $p < 0.001$) between responses when compared to **250 ng/well** of vector containing GCGR was determined by one-way ANOVA with Dunnett's post test.

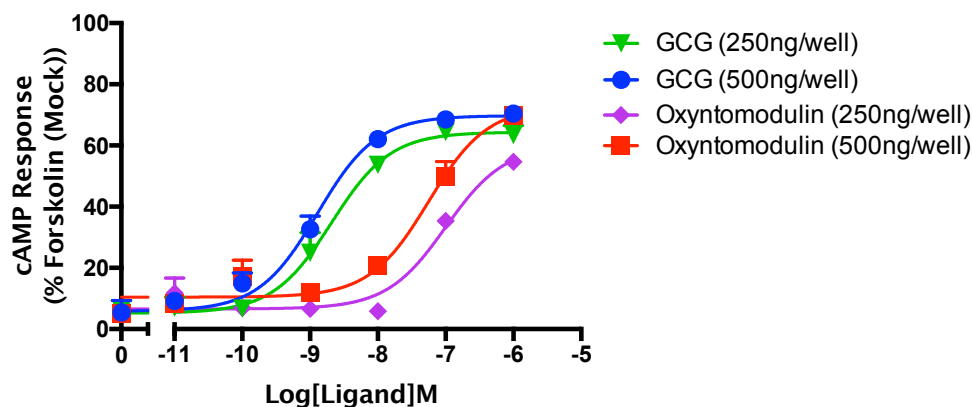


Figure 3.9. Influence of DNA concentration at transfection on measured cAMP response in HEK 293 cells. HEK 293 cells were transfected with 500 ng/well or 250 ng/well of pmCherry-N1 vector containing GCGR. HEK 293 cells (1,000 cells/well), 24 hours post-transfection, were exposed to GCG or oxyntomodulin for 8 minutes and cAMP accumulation detected. All values are mean \pm SEM expressed as percentage forskolin response (100 μ M) (mock transfected with vector only) were $n = 2$ independent experimental repeats, conducted in duplicate.

Table 3.4. Influence of DNA concentration at transfection on measured cAMP response in HEK 293 cells. Potency (pEC_{50}), maximal response (E_{max}), basal and span for GCG/oxyntomodulin stimulated cAMP response measured in GCGR transfected HEK 293 cells using cAMP assay

GCG				
DNA (ng/well)	pEC_{50} ^a	E_{max} ^b	Basal ^c	Span ^d
250	8.7 \pm 0.1	64.4 \pm 1.9	5.2 \pm 1.4	59.2 \pm 2.3
500	8.9 \pm 0.1	69.9 \pm 2.0	5.3 \pm 1.8	64.4 \pm 3.6
Oxyntomodulin				
DNA (ng/well)	pEC_{50} ^a	E_{max} ^b	Basal ^c	Span ^d
250	7.0 \pm 0.1	60.1 \pm 4.0	6.6 \pm 1.4	53.5 \pm 4.2
500	7.3 \pm 0.1	72.9 \pm 4.3	8.8 \pm 1.3	63.5 \pm 3.0

HEK 293 cells were transfected with pmCherry-N1 containing GCGR and stimulated 24 hours post-transfection with GCG/oxyntomodulin prior to cAMP accumulation measurement.

To calculate pEC_{50} , E_{max} , basal and span values, data were analysed using a three-parameter logistic equation.

^a Negative logarithm of GCG/Oxyntomodulin concentration required to produce a half-maximal response

^b Maximal response to GCG/Oxyntomodulin as percentage forskolin response (Mock transfected with Vector)

^c The low plateau of the fitted sigmoidal concentration dose-response curve

^d The difference between E_{max} and basal signalling

Statistical significance (*, $p < 0.05$; **, $p < 0.01$; ***, $p < 0.001$) comparing GCG/Oxyntomodulin response at the two DNA concentration was determined using unpaired t test.

3.3. Transfection reagent

There are many transfection reagents available to laboratories for the introduction of DNA or RNA into cell lines. In our laboratory, Fugene® HD transfection reagent was predominantly used for DNA transfection due to its apparent low toxicity to cells and ease of transfection of difficult-to-transfect cell lines, such as primary cell lines (Gresch and Altrogge *et al.*, 2012). Here, polyethylenimine (PEI), a high-charge cationic polymer that readily binds to negatively charged DNA, was investigated as an alternative due to its low cost (0.0095 pence per transfection with 500 ng of DNA versus 56 pence i.e. 5936 times cheaper).

Quantification of ATP as a measure of cell viability was performed in PEI or Fugene® HD transfected and untransfected cells using the CellTiter-Glo® Luminescent Cell Viability Assay (Figure 3.10) (See section 3.8.1 for optimisation of ATP assay). There was a significant lower ATP amount for both PEI and Fugene® HD transfected HEK 293 cells when compared to untransfected cells indicating reduced viability as a consequence of transfection. Importantly, there was no statistically significant difference between cells transfected with PEI or Fugene® HD suggesting these two reagents have equal effects on HEK 293 cell viability.

In order to measure any differences between transfections reagents at the secondary messenger level, the cAMP response to GCG and oxyntomodulin was measured in both PEI or Fugene® HD transfected HEK 293 cells (Figure 3.11 and Table 3.5). Importantly, the potency measured for either GCG or oxyntomodulin showed no significant difference between transfection reagents. There was however a significantly bigger maximum response for GCG and oxyntomodulin (E_{max} 69.8 \pm 2.0 and 72.9 \pm 4.3 percentage forskolin response, respectively) and signalling window, as determined by the span (63.9 \pm 2.5 and 63.5 \pm 3.0 percentage forskolin response, respectively), for Fugene® HD transfected cells when compared to PEI transfected cells (E_{max} 97.4 \pm 1.3 and 95.5 \pm 3.6, Span 86.9 \pm 1.7 and 83.9

±3.7 percentage forskolin response). This is likely to indicate a slightly superior transfection efficiency with Fugene® HD when compared to PEI.

Due to the levels of HEK 293 cell viability being equivalent irrespective of the transfection reagent used and PEI being significantly cheaper when compared to Fugene® HD, PEI was utilised for transfection of HEK 293 cells in routine experiments. For experiments where the maximal response is required or in the case where a small measured response needs to be maximised, Fugene® HD should be considered.

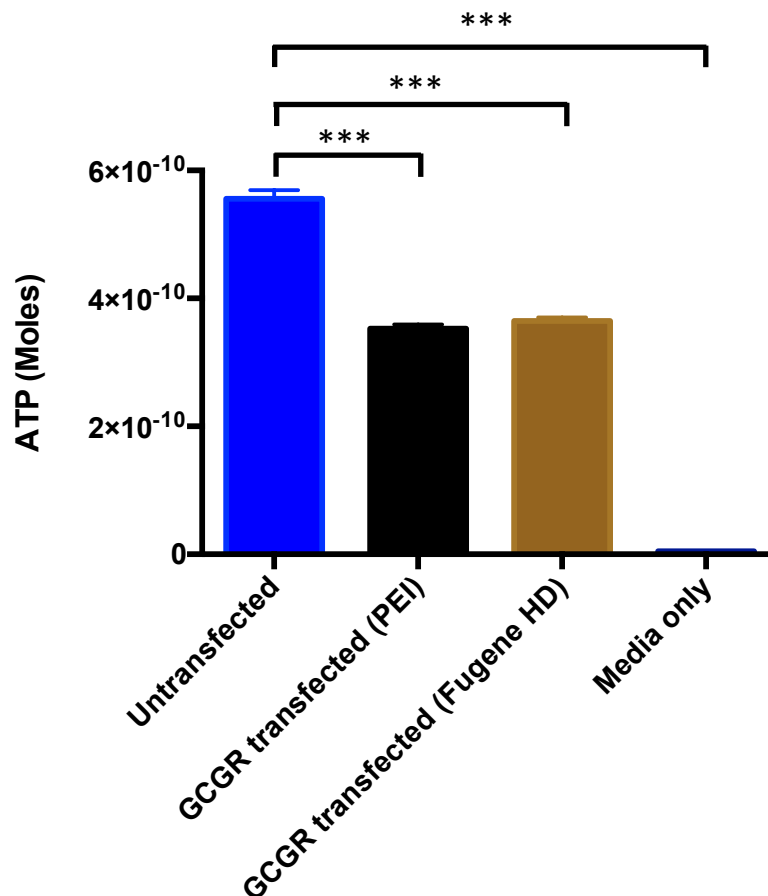


Figure 3.10. Influence of transfection reagent on cell viability in HEK 293. Quantification of ATP as a measure of cell viability was conducted using the CellTiter-Glo® Luminescent Cell Viability Assay (Promega) in a 384-well format with 5,000 cells/well. Comparison of ATP produced from untransfected WT HEK 293 cells and GCGR transfected WT HEK 293 cells with either PEI or Fugene HD (24 hours post transfection with 500 ng of DNA). Values are mean ± SEM expressed in Moles were $n \geq 4$ independent experimental repeats, conducted in quadruplicate. Statistical significance in comparison to WT and between transfection reagents was determined using one-way analysis of variance and Dunnett's post-test.

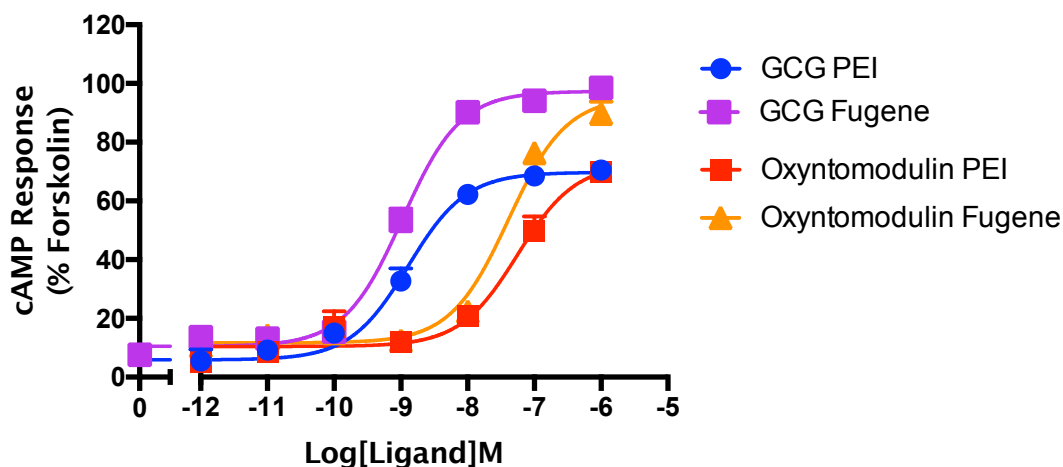


Figure 3.11. Comparison of transfection reagents on measured cAMP response. HEK 293 cells transfected with 500 ng/well of pmCherry-N1 vector containing GCGR were stimulated with GCG or oxyntomodulin for 8 minutes and cAMP accumulation detected. All values are mean \pm SEM expressed as percentage forskolin response (100 μ M) (mock transfected with vector only) were $n = 2$ independent experimental repeats, conducted in duplicate.).

Table 3.5. Comparison of transfection reagents on measured cAMP response. Potency (pEC_{50}), maximal response (E_{max}), basal and span for GCG/oxyntomodulin stimulated cAMP response measured in Fugene® HD or PEI GCGR transfected HEK 293 cells as measured using a cAMP assay

GCG				
Reagent	pEC_{50} ^a	E_{max} ^b	Basal ^c	Span ^d
PEI	8.9 \pm 0.1	69.8 \pm 2.0	5.3 \pm 1.8	63.9 \pm 2.5
Fugene	8.9 \pm 0.1	97.4 \pm 1.3***	10.5 \pm 1.1	86.9 \pm 1.7**
Oxyntomodulin				
Reagent	pEC_{50} ^a	E_{max} ^b	Basal ^c	Span ^d
PEI	7.3 \pm 0.1	72.9 \pm 4.3	8.8 \pm 1.3	63.5 \pm 3.0
Fugene	7.4 \pm 0.1	95.5 \pm 3.6***	11.7 \pm 1.6	83.9 \pm 3.7*

HEK 293 cells were transfected with pmCherry-N1 containing GCGR using Fugene® HD or PEI and stimulated 24 hours-post transfection with GCG/oxyntomodulin for 8 minutes prior to cAMP accumulation measurement.

^a Negative logarithm of GCG/oxyntomodulin concentration required to produce a half-maximal response

^b Maximal response to GCG/oxyntomodulin as percentage forskolin response (Mock transfected with Vector)

^c The low plateau of the fitted sigmoidal concentration dose-response curve

^d The difference between E_{max} and basal signalling

Statistical significance (*, $p < 0.05$; **, $p < 0.01$; ***, $p < 0.001$) comparing GCG/Oxyntomodulin response between the two transfection reagents was determined using unpaired t-test (two-tailed)

3.4. Tools to investigate G protein bias

3.4.1. NF449; an antagonist of G_s

Many GPCRs have been reported to couple and initiate pathways through multiple G proteins (Woehler and Ponimaskin, 2009). Some class B GPCRs have been suggested to couple to G_s as well as G_i, including GCGR (Xu and Xie, 2009). To determine if we could block G_s in order to study G_i-coupling (Figure 3.12), we investigated the activity of NF449, a selective inhibitor of the P2X1 receptor with reported inhibitory activity for G_s (Hohenegger *et al.*, 1998). Flp-In GCGR CHO-K1 cells received a 30-minute pre-treatment with NF449 or DMSO control prior to stimulated with forskolin, GCG, oxyntomodulin or CT (the cognate ligand to CTR, known to couple to G_s).

Importantly, NF449 treatment had no influence on the forskolin mediated cAMP response (Figure 3.13 A and Table 3.6) indicating that this compound has no influence on AC mediated cAMP accumulation. There was no difference in the measured cAMP responses to GCG or oxyntomodulin stimulated with or without NF449 treatment (Figure 3.13 B and Table 3.6) indicating the absence of detectable G_i-coupling at the GCGR. This is distinct from a report suggesting G_{i/o}-coupling of the GCGR (Xu and Xie, 2009). However, GCGR could be very efficiently coupled to G_s or there may be a high receptor reserve in this cell line making inhibition difficult to detect. With this in mind, we next sought to investigate the ability of NF449 to inhibit the G_s-stimulated cAMP response following stimulation of an endogenously expressing G_s-coupled receptor.

The concentration-dependent cAMP accumulation to CT indicated the endogenous expression of CTR in Flp-In GCGR CHO-K1 cells (Figure 3.13 C and Table 3.6). When comparing NF449 pre-treated cells stimulated with CT when to untreated cells, there was a significant rightward shift in potency (pEC₅₀ 9.01 ±0.2 and 10.18 ±0.2, respectively) as predicted (Figure 3.12), but no significant change in maximal response in. This finding suggests that CT is potentially G_i-coupled and NF449 is indeed capable of inhibiting G_s activity

but this inhibition is not complete, even for an endogenously expressed receptor such as CTR. Within this in mind, it is likely that in cell lines where receptor expression is high, the incomplete inhibition of G_s activity by NF449 allows the remaining G_s protein to efficiently activate AC leading to a full cAMP response. In order to assess G_i -coupling of GCGR, and indeed other receptors, it may be necessary to conduct G_s inhibition experiments in cell lines that endogenously express the receptor of interest. Alternatively, a G_s knockout cell line in combination with initial forskolin stimulation could be used whereby we look for an inhibition of the cAMP response with increasing ligand concentration.

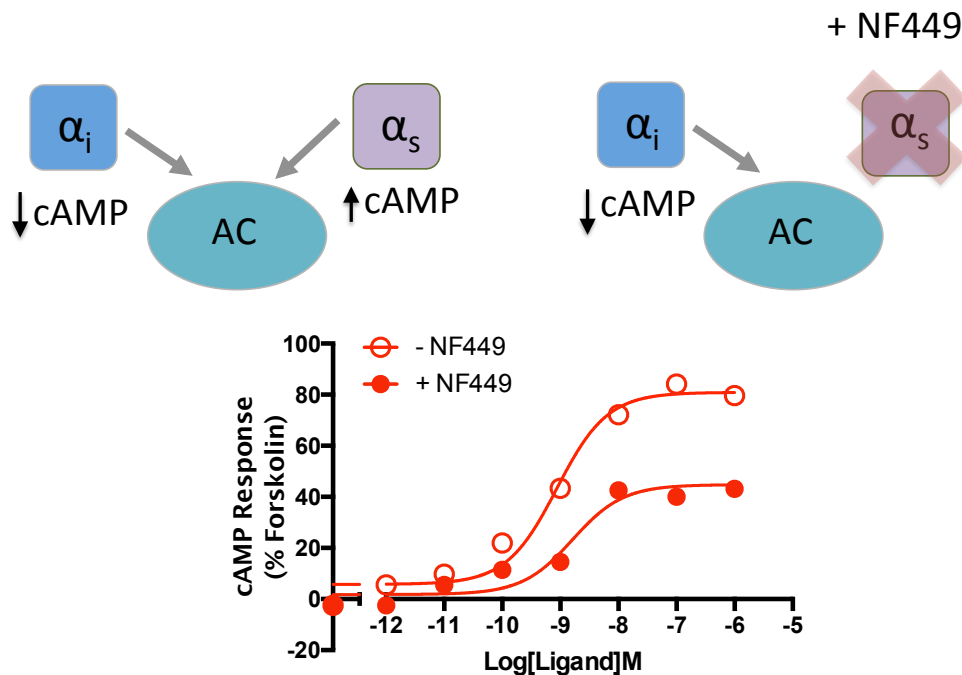


Figure 3.12. Schematic of NF449 activity at G_s and predicted concentration dose-response data. ACs receives stimulatory signals from G_s and inhibitory signals from G_i (Tang and Gilman, 1991). GPCRs known to couple to G_s -stimulate intracellular cAMP formation through AC whereas receptors which couple to G_i result in inhibition of cAMP formation by AC. NF449 is a selective inhibitor of the P2X1 receptor with reported inhibitory activity for G_s (Hohenegger *et al.*, 1998). If a GPCR is coupled to both G_s and G_i -mediated pathways, treatment with NF449 could be predicted to reduce the maximum cAMP response when compared to untreated (shown here) or reduce the potency of the ligand tested.

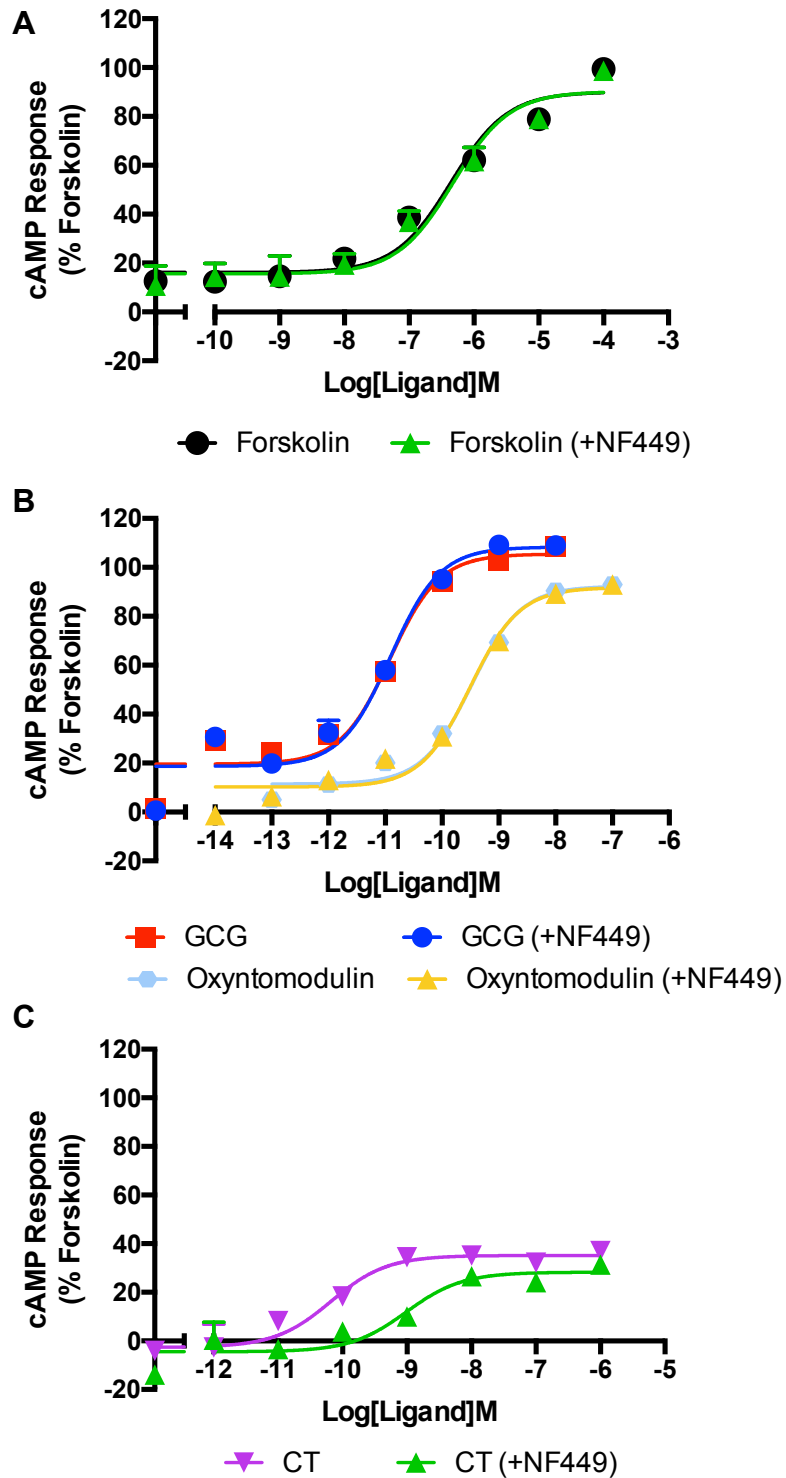


Figure 3.13. Assessing NF449 as an inhibitor of G_s activity. Flp-In GCGR CHO-K1 cells (1,000 cells/well) were pre-treated with NF449 10 μ M or DMSO control for 30 minutes prior to stimulated with **A**) forskolin, **B**) the GCGR agonists, GCG or oxyntomodulin or **C**) CT for 8 minutes and cAMP accumulation detection. All values are mean \pm SEM expressed as percentage forskolin response where $n = 3$ independent experimental repeats, conducted in duplicate.

Table 3.6. Assessing NF449 as an inhibitor of G_s activity. Potency (pEC₅₀), maximal response (E_{max}), affinity (pK_A) and coupling efficacy (logτ) for GCGR and CT agonists +/- NF449 measured Flp-In GCGR CHO-K1 cells using a cAMP accumulation assay

Ligand	cAMP			
	pEC ₅₀ ^a	E _{max} ^b	pK _A ^c	log τ ^d
Forskolin	6.32 ±0.2	90.2 ±4.6	5.68 ±0.2	0.57 ±0.12
Forskolin (+NF449)	6.35 ±0.2	90.0 ±4.6	5.64 ±0.2	0.58 ±0.13
GCG	10.91 ±0.1	105.5 ±3.0	10.08 ±0.2	0.77 ±0.12
GCG (+NF449)	10.92 ±0.1	108.3 ±2.5	9.97 ±0.2	0.88 ±0.21
Oxyntomodulin	9.48 ±0.1	110.5 ±4.0	8.89 ±0.2	0.46 ±0.07
Oxyntomodulin (+NF449)	9.51 ±0.1	91.8 ±2.4	8.92 ±0.1	0.46 ±0.04
CT	10.18 ±0.2	35.2 ±2.0	9.98 ±0.2	-0.23 ±0.05
CT (+NF449)	9.01 ±0.2**	28.1 ±2.6	8.95 ±0.2*	-0.32 ±0.04

Flp-In GCGR CHO-K1 cells (1,000 cells/well) were pre-treated with NF449 10μM or DMSO control for 30 minutes prior to stimulated with forskolin, GCG, oxyntomodulin or CT for 8 minutes and cAMP accumulation detected to generate concentration response curves. To calculate pEC₅₀ and E_{max}, data were analysed using a three-parameter logistic equation. Data was also analysed by an operational model of agonism (Black and Leff, 1983) to determine affinity (pK_A) and coupling efficacy (log τ).

^a Negative logarithm of ligand concentration required to produce a half-maximal response

^b Maximal response to ligand as percentage forskolin (-NF449)

^c The negative logarithm of the relative equilibrium disassociation constant for each ligand generated through use of the operational model for partial agonism relative to NF449 untreated ligand stimulation.

^d τ is the coupling efficiency parameter, generated by comparison to the NF449 untreated ligand using the operational model for partial agonism

Statistical significance (*, $p < 0.05$; **, $p < 0.01$; ***, $p < 0.001$) comparing NF449 treated to untreated for each of the ligands was determined unpaired Student's t-test (two-tailed).

3.4.4. YM-254890; an inhibitor of G_q

A number of GPCRs are reported to couple to the G_q family of G proteins including the oxytocin receptor (OTR) (Gimpl and Fahrenholz, 2001), leading to Ca²⁺i mobilisation and elevation in cellular IP₃ (Figure 2.5). The cyclic depsipeptide YM-254890 is described as a specific G_{q/11} inhibitor (Takasaki *et al.*, 2004) through blocking of GDP exchange for GTP (Nishimura *et al.*, 2010). In order to investigate G_{q/11}-coupling at a receptor of interest, cells were pre-treated with YM-254890 for 30 minutes prior to ligand stimulation

and measurement Ca^{2+}_i mobilisation using fluorescent Ca^{2+} binding dyes such as Fluo-8, AM as detailed in section 2.8.3. To assess potential off-target activity of YM-254890, specifically on G protein-dependent and G protein-independent (forskolin) mediated changes in cAMP levels, cAMP accumulation was measured in transfected HEK 293T cells stimulated with the appropriate ligand in the presence or absence of YM-254890 30 minute pre-treatment.

There was found to be no significant difference in cAMP accumulation in forskolin stimulated untransfected HEK 293T cells (Figure 3.14 A and Table 3.7) or to GCG and GLP-1(7-36)amide stimulated GCGR and GLP-1R transfected HEK 293T cells, respectively (Figure. 3.14 B/C and Table 3.7), with or without YM-254890 treatment. This finding suggests YM-254890 treatment has no influence on the ability of HEK 293T cells to produce a cAMP response through either G_s -dependent (GCGR and GLP-1R) or G_s -independent (forskolin) mechanism. In addition, given the similar response in YM-254890 treated and untreated HEK 293T cells, YM-254890 has no apparent toxicity to HEK 293T cells.

The Ca^{2+}_i response in HEK 293T cells stimulated with ionomycin, a Ca^{2+} ionophore, was unaffected by YM-254890 pretreatment (Figure 3.15 A and Table 3.8). This finding confirms that ionomycin causes a Ca^{2+}_i response independent of $G_{q/11}$ and YM-254890 has no apparently off-target activity. On the other hand, YM-254890 pre-treatment was shown to completely abolish the Ca^{2+}_i mobilisation in GCGR and GLP-1R transfected HEK 293T cells stimulated with GCG or GLP-1(7-36)amide, respectively (Figures 3.15 B/C and Table 3.8). The ability of YM-254890 to inhibit Ca^{2+}_i responses from GCGR (See Section 4.3.1 for further analysis of the Ca^{2+}_i response at the GCGR) and GLP-1R transfected cells stimulated with ligand, confirms these pathways are $G_{q/11}$ -mediated and not through downstream signalling via G_s -coupling or alternative G proteins.

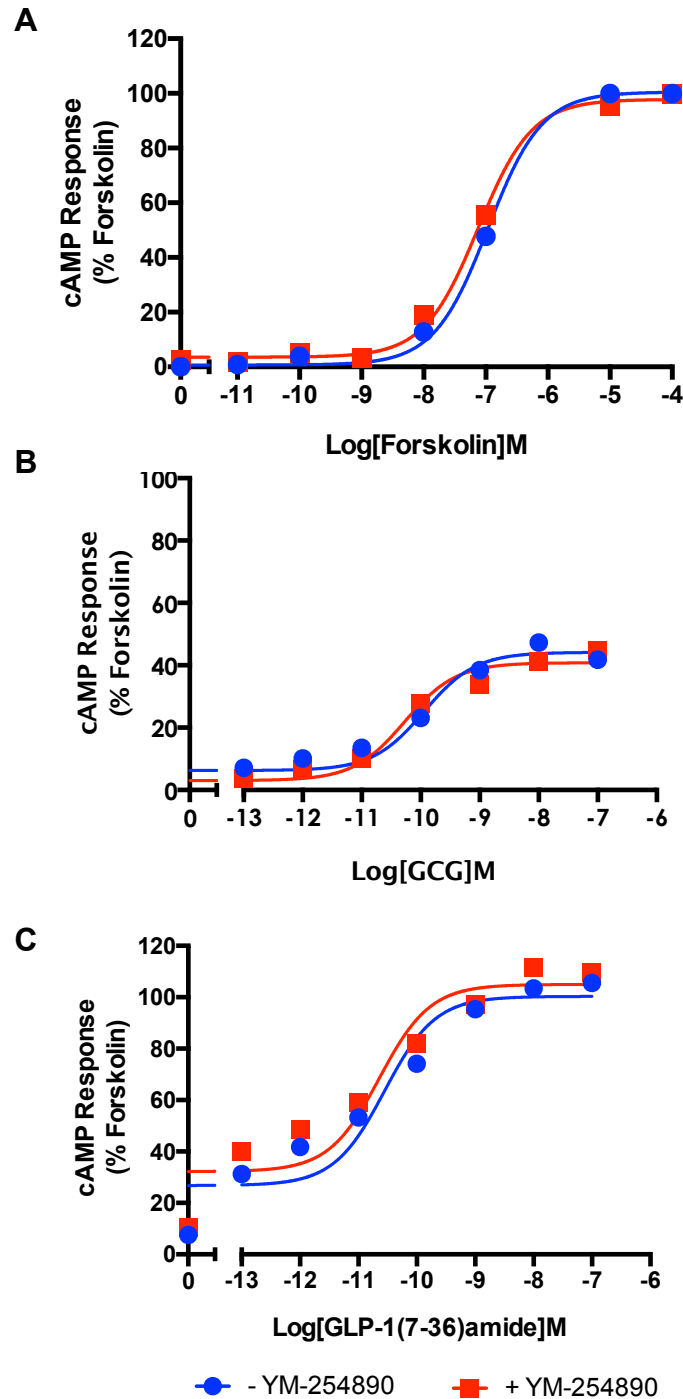


Figure 3.14. YM-254890 treatment has no effect on measured cAMP response in HEK 293T cells. HEK 293T cells received 30 minutes treatment with YM-254890 (100 nM) or DMSO control immediately prior to plating on a 384-well Optiplate. The cAMP response was detected following 8 minutes stimulation with **A)** forskolin in untransfected HEK 293T cells **B)** GCG in HEK 293T cells transfected with pcDNA3.1 expressing GCGR or **C)** GLP-1(7-36)amide in HEK 293T cells transfected with pcDNA3 expressing GLP-1R. All values are mean \pm SEM expressed as percentage forskolin response where $n \geq 3$ independent experimental repeats, conducted in duplicate.

Table 3.7. YM-254890 treatment has no effect on measured cAMP response in HEK 293T cells. Potency (pEC₅₀), maximal response (E_{max}), basal, span, affinity (pK_A) and coupling efficacy (log τ) for forskolin, GCG or GLP-1(7-36)amide stimulated cAMP accumulation measured in untransfected, GCGR or GLP-1R transfected HEK 293T cells +/- YM-254890 treatment

Ligand	cAMP			
	pEC ₅₀ ^a	E _{max} ^b	Basal ^c	Span ^d
Forskolin	6.97 ±0.05	100.5 ±2.0	0.7 ±1.3	99.8 ±2.3
Forskolin (+ YM-254890)	7.13 ±0.06	97.8 ±2.2	3.6 ±1.5	94.2 ±2.6
GCG	9.94 ±0.17	44.2 ±2.2	6.3 ±1.8	37.9 ±2.7
GCG (+ YM-254890)	10.27 ±0.17	40.8 ±1.9	3.1 ±1.7	37.8 ±2.5
GLP-1(7-36)amide	10.55 ±0.18	100.3 ±3.8	26.8 ±3.9	73.6 ±5.2
GLP-1(7-36)amide (+ YM-254890)	10.64 ±0.23	105.0 ±5.0	32.2 ±5.2	72.8 ±5.2

HEK 293T cells received 30 minutes treatment with YM-254890 (100 nM) or DMSO control immediately prior to stimulation with forskolin (untransfected cells), GCG (GCGR transfected cells) or GLP-1(7-36)amide (GLP-1R transfected cells) and measurement of Ca²⁺i response to generate concentration response curves. To calculate pEC₅₀, E_{max}, Basal and Span values, data were analysed using a three-parameter logistic equation. Data was also analysed by an operational model of agonism (Black and Leff, 1983) to determine affinity (pK_A) and coupling efficacy (log τ).

^a Negative logarithm of ligand concentration required to produce a half-maximal response

^b Maximal response to ligand as percentage forskolin response

^c The low plateau of the fitted sigmoidal dose-response curve

^d The difference between E_{max} and basal signalling

^e The negative logarithm of functional affinities that describes the affinity of the receptor when coupled to a given signaling pathway generated through use of the operational model for partial agonism

^f τ is the coupling efficiency parameter generated through use of the operational model for partial agonism. All values are mean ± SEM expressed percentage forskolin response where $n \geq 5$ independent experimental repeats, conducted in duplicate. Statistical significance (*, $p < 0.05$; **, $p < 0.01$; ***, $p < 0.001$) in the difference between responses +/- YM-254890 treatment was determined by one-way unpaired Student's t-test (two-tailed). N.R denotes no response

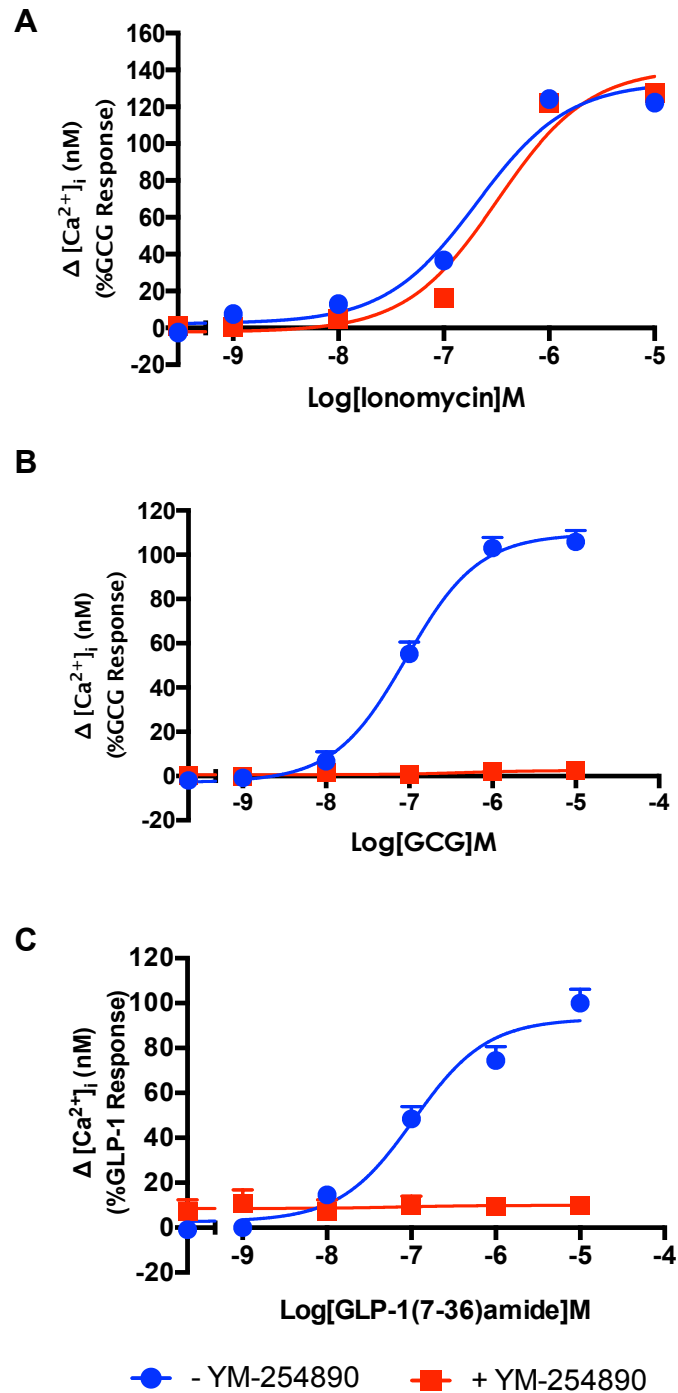


Figure 3.15. Effect of YM-254890 treatment on Ca^{2+}_i response in HEK 293T cells: HEK 293T cells received 30 minutes treatment with YM-254890 (100 nM) or DMSO control immediately prior ligand stimulation and Ca^{2+}_i mobilisation measured. **A)** Untransfected HEK 293T cells were stimulated with ionomycin **B)** HEK 293T cells transiently expressing pVITRO1 vector containing mCherry-tagged GCGR (48 hours post transfection) stimulated with GCG or **C)** HEK 293T cells transiently expressing pcDNA3.0 vector containing mCherry-tagged GLP-1R (48 hours post transfection) stimulated with GLP-1(7-36)amide. All values are mean \pm SEM expressed as percentage GCG response where $n \geq 3$ independent experimental repeats, conducted in duplicate.

Table 3.8. Effect of YM-254890 treatment on Ca²⁺i response in HEK 293T cells. Potency (pEC₅₀), maximal response (E_{max}), basal, span, affinity (pK_A) and coupling efficacy (log τ) for ionomycin, GCG or GLP-1(7-36)amide stimulated Ca²⁺i measured in GCGR or GLP-1R transfected HEK 293T cells +/- YM-254890 treatment

HEK 293T					
Ca ²⁺ i					
Ligand	pEC ₅₀ ^a	E _{max} ^b	Basal ^c	Span ^d	
Ionomycin	6.69 ±0.20	133.1 ±10.8	2.4 ±7.0	131.1 ±12.0	
Ionomycin (+ YM-254890)	6.49 ±0.23	141.0 ±14.9	-2.2 ±8.3	143.2 ±15.9	
GCG	7.01 ±0.13	103.6 ±5.7	-0.1 ±4.4	103.7 ±6.8	
GCG (+ YM-254890)		N.R	-1.1 ±2.4	N.R	
GLP-1(7-36)amide	6.97 ±0.12	93.1 ±4.4	2.7 ±4.1	90.5 ±5.6	
GLP-1(7-36)amide (+ YM-254890)		N.R	-1.2 ±1.1	N.R	

Transfected HEK 293T cells received 30 minutes treatment with YM-254890 (100 nM) or DMSO control immediately prior to stimulation with ionomycin or GCG (for GCGR transfected cells) or GLP-1(7-36)amide (for GLP-1R transfected cells) and measurement of Ca²⁺i response to generate concentration response curves. To calculate pEC₅₀, E_{max}, Basal and Span values, data were analysed using a three-parameter logistic equation. Data was also analysed by an operational model of agonism (Black and Leff, 1983) to determine affinity (pK_A) and coupling efficacy (log τ).

^a Negative logarithm of ligand concentration required to produce a half-maximal response

^b Maximal response to ligand as percentage GCG/GLP-1(7-36)amide response

^c The low plateau of the fitted sigmoidal dose-response curve

^d The difference between E_{max} and basal signalling

^e The negative logarithm of functional affinities that describes the affinity of the receptor when coupled to a given signaling pathway generated through use of the operational model for partial agonism

^f τ is the coupling efficiency parameter generated through use of the operational model for partial agonism

All values are mean ± SEM expressed percentage GCG/GLP-1(7-36)amide response where $n \geq 5$ independent experimental repeats, conducted in duplicate. Statistical significance (*, $p < 0.05$; **, $p < 0.01$; ***, $p < 0.001$) in the difference between ionomycin responses was determined by one-way unpaired Student's t-test (two-tailed).

N.R denotes no response

3.5. Optimisation of the IPOne assay

Ca²⁺i mobilisation is downstream of G_q-mediated activation of PLC-β (Figure 2.5). An alternative readout of the G_q-mediated signalling cascade is IP₁, the downstream metabolite of IP₃, which can be measured using the IP-One HTRF® assay kit (Cisbio Bioassays) (Section 2.8.4). This assay utilises LiCl, which inhibits the breakdown of IP₁ resulting in accumulation in the cells (Garbison *et al.*, 2004). In order to achieve the optimal signalling window for measuring IP₁ accumulation using this kit, both cell number and ligand stimulation time must be optimised.

For GCGR and GLP-1R described as predominantly G_s-coupled, the measured ligand potency for Ca²⁺i mobilisation was weaker when compared to cAMP accumulation (Tables 3.8 and 3.7, respectively). In order to investigate the maximum measurable signal and optimisation for this assay, the predominantly G_q-coupled oxytocin receptor (OTR) (Gimpl and Fahrenholz, 2001) was chosen. HEK 293 cells transfected with the OTR (48 hours post-transfection) were plated at a range of cell densities in a 384-well plate and stimulated for either 1 or 2 hours with oxytocin (OT) prior to measuring IP₁ accumulation.

The concentration responses seen to both 1 and 2-hour stimulation with OT at the various cell numbers were shown to reside within the SC (Figure 3.16 and Table 3.9). The measured potency for OT showed some variation between cell numbers, although this was not significant. Both the basal IP₁ level and the maximum response to OT stimulation was found to depend on the number of cells per well and showed an increase with increasing cell number. The difference between the maximum response and the basal response (span) was found to be largest for 20,000 cells per well at both stimulation times, but slightly bigger following 2 hours stimulation when compared to 1 hour (35.2 ±1.8 and 32.9 ±1.7 percentage SC, respectively). This finding indicated that 20,000 cells per well with a 2-hour stimulation time

were the optimal conditions to achieve the largest signalling window for the measurement of IP₁ accumulation.

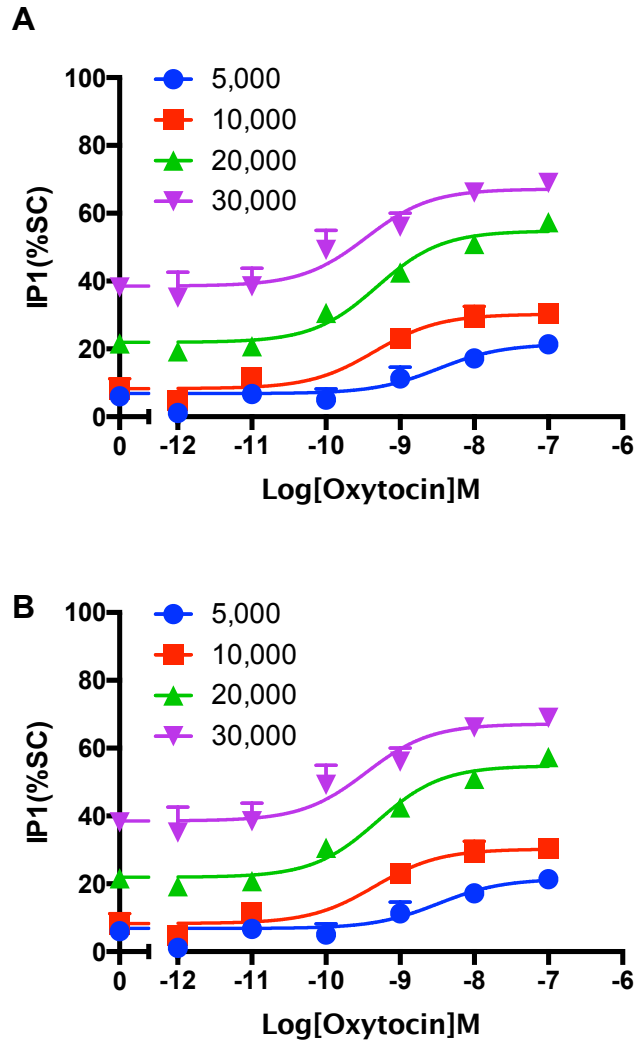


Figure 3.16. Cell number and stimulation time optimisation for IP₁ accumulation assay. HEK 293 cells transiently expressing the Oxytocin receptor (48 hours post transfection) were seeded at various densities (5,000, 10,000, 20,000 or 30,000 cells/well) exposed to Oxytocin for **A**) 1 hour or **B**) 2 hours and IP₁ accumulation detected using the IP-One HTRF® assay kit (Cisbio Bioassays). All values are mean ± SEM expressed as percentage IP₁ standard curve (SC) were *n* = 1, conducted in duplicate.

Table 3.9. Cell number and stimulation time optimisation for IP₁ accumulation assay Potency (pEC₅₀), maximal response (E_{max}), basal and span HEK 293 cells transfected with OTR measured using IP₁ accumulation assay

1 hour stimulation				
Cell number	pEC ₅₀ ^a	E _{max} ^b	Basal ^c	Span ^d
5,000	8.49 ±0.6	21.5 ±3.8	6.8 ±1.7	14.6 ±3.9
10,000	9.34 ±0.3	30.3 ±2.1	8.3 ±1.2	21.9 ±2.4
20,000	9.31 ±0.1	54.8 ±1.4	21.9 ±1.0	32.9 ±1.7
30,000	9.46 ±0.3	67.2 ±3.1	38.6 ±2.1	28.6 ±2.1
2 hour stimulation				
Cell number	pEC ₅₀ ^a	E _{max} ^b	Basal ^c	Span ^d
5,000	9.67 ±0.2	24.0 ±1.3	5.1 ±1.0	18.9 ±1.5
10,000	9.21 ±0.1	45.4 ±1.1	13.0 ±0.7	32.5 ±1.3
20,000	9.72 ±0.1	64.5 ±1.5	29.3 ±1.1	35.2 ±1.8
30,000	9.91 ±0.1	73.8 ±1.4	41.8 ±1.1	32.0 ±1.8

HEK 293 cells transiently expressing the OTR (48 hours post transfection) were seeded at various densities (5,000, 10,000, 20,000 or 30,000 cells/well) exposed to oxytocin for 1 hour or 2 hours and IP₁ accumulation detected. To calculate pEC₅₀ and E_{max}, data were analysed using a three-parameter logistic equation.

^a Negative logarithm of OT concentration required to produce a half-maximal response

^b Maximal response to OT given as the percentage standard IP₁ curve (SC)

^c The low plateau of the fitted sigmoidal concentration dose-response curve

^d The difference between E_{max} and basal signalling

Statistical significance (*, $p < 0.05$; **, $p < 0.01$; ***, $p < 0.001$) of the difference between responses when compared to that in 5,000 cells for each stimulation time was determined by one-way ANOVA with Dunnett's post test.

Bold text highlights the cell number that produced the largest signalling window

3.6. Generation of a HEK 293 cell line stably expressing GCGR

Transfection, the introduction of foreign nucleic acid into cells, can either be transient or stable (Kim and Eberwine, 2010). Here, we generate a HEK 293 cell line stably expressing GCGR to overcome issues associated with transfection variability across experiments and across the cell population, in addition to speeding up experiments once the cell line has been generated. HEK 293 cells were transfected with pmCherry-N1 vector expressing GCGR (generating a C-terminally mCherry-tagged GCGR) and selection of stable cells performed using the appropriate concentration of Geneticin® (G418) (800 µg/ml), as indicated by performing a kill curve of HEK 293 cells (Section 2.1.3).

Confocal fluorescence microscopic images of HEK 293 cells selected for using G418 showed the presence of mCherry-tagged GCGR localised both on the membrane surface and within what appear to be vesicles within the cytoplasm of the cell (Figure 3.17). These vesicles may contain mCherry only, or the fluorescently tagged receptor being trafficked to or away from the cell-surface. In order to check if this GCGR expression was functional, these HEK 293 cells and HEK 293 cells transiently transfected with the same vector (pmCherry-N1 expressing GCGR) were stimulated with GCG or oxyntomodulin and the cAMP response measured (Figure 3.18 and Table 3.10). Both the GCG and oxyntomodulin concentration-dependent cAMP responses showed no significant differences between the transient or stable cell lines for any of the measured parameters. This finding suggests similar GCGR signalling regardless of transient or stable transfection. These cells, presumably with a greater proportion expressing the receptor of interest, were used to investigate the GCGR-mediated ERK1/2 activation in an attempt to maximise the signalling window (Section 4.4.2.2).

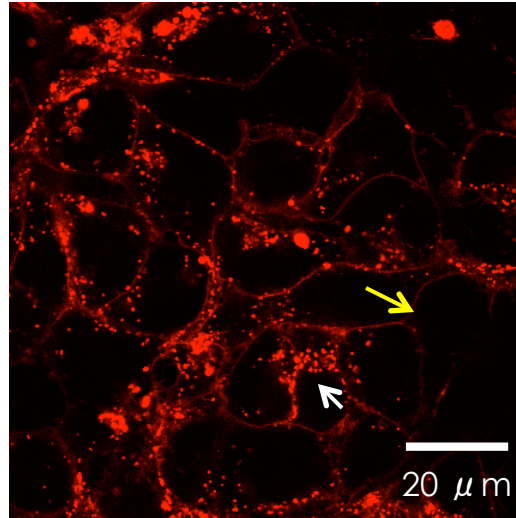


Figure 3.17. Cell-surface expression of mCherry-tagged GCGR in G418 selected HEK 293 cells. HEK 293 cells were transfected with pmCherry-N1 containing GCGR and stably transfected cells selected for using Geneticin® (G418) at a concentration of 800 μg/ml. The stable cell line was confirmed using confocal fluorescence microscopy. Yellow arrow indicates cell-surface localised receptor whereas possible vesicles containing the receptor are indicated by the white arrow.

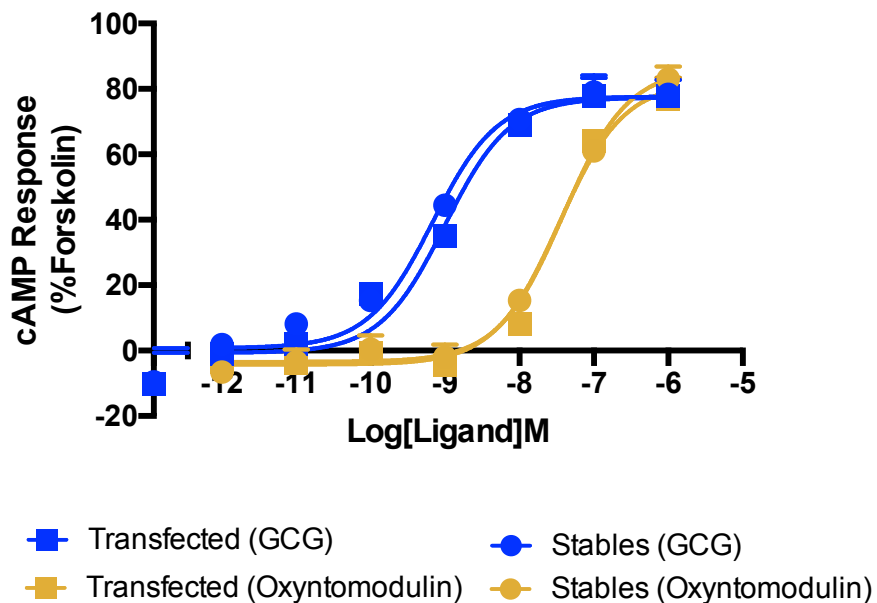


Figure 3.18. Comparison of cAMP response in transient and stable GCGR expressing HEK 293 cells. HEK 293 cells transiently (24 hours post transfection) or stably expressing mCherry-tagged GCGR were exposed to GCG or oxyntomodulin for 8 minutes and cAMP accumulation detected. All values are mean ± SEM expressed as percentage forskolin response where $n \geq 5$ independent experimental repeats, conducted in duplicate.

Table 3.10. Comparison of cAMP response in transient and stable GCGR expressing HEK 293 cells. Potency (pEC_{50}), maximal response (E_{max}), basal, span, affinity (pK_A) and coupling efficacy ($\log \tau$) for GCG and oxyntomodulin stimulated cAMP response HEK 293 cells transiently or stably transfected with GCGR

		GCG				
	pEC_{50}^a	E_{max}^b	Basal ^c	Span ^d	pK_A^e	$\log \tau^f$
Transfected	9.00 ±0.1	77.4 ±3.1	-0.7 ±2.6	78.1 ±3.9	8.35 ±0.1	0.54 ±0.08
Stables	9.17 ±0.1	77.7 ±2.4	-0.8 ±2.4	76.9 ±3.5	8.52 ±0.1	0.54 ±0.07
		Oxyntomodulin				
	pEC_{50}^a	E_{max}^b	Basal ^c	Span ^d	pK_A^e	$\log \tau^f$
Transfected	7.47 ±0.1	82.0 ±3.8	-4.2 ±1.8	86.3 ±4.0	6.70 ±0.2	0.68 ±0.11
Stables	7.41 ±0.1	86.3 ±3.5	-3.4 ±1.6	89.8 ±3.6	6.53 ±0.2	0.82 ±0.13

GCGR stable or transiently expressing HEK 293 cells were stimulated with GCG or oxyntomodulin prior to measurement of cAMP accumulation to generate concentration response curves for each construct. To calculate pEC_{50} , E_{max} , Basal and Span values, data were analysed using a three-parameter logistic equation. Data was also analysed by an operational model of agonism (Black and Leff, 1983) to determine affinity (pK_A) and coupling efficacy ($\log \tau$).

^a Negative logarithm of GCG/oxyntomodulin concentration required to produce a half-maximal response

^b Maximal response to GCG/oxyntomodulin as percentage forskolin response (Transfected/stables)

^c The low plateau of the fitted sigmoidal dose-response curve

^d The difference between E_{max} and basal signalling

^e The negative logarithm of functional affinities that describes the affinity of the receptor when coupled to a given signalling pathway generated though use of the operational model for partial agonism

^f τ is the coupling efficiency parameter generated though use of the operational model for partial agonism
Statistical significance (*, $p < 0.05$; **, $p < 0.01$; ***, $p < 0.001$) between responses in transfected and stable HEK 293 cells to GCG or oxyntomodulin was determined using unpaired Student's t-test (two-tailed)

3.7. Receptors expression in a hepatic cell line: Hep 3B

3.7.1. Investigating GPCR mRNA expression in Hep 3B cells

In the work presented in this thesis, both stable and transient transfected cell lines were used for the investigation of GCGR signalling. We sought to characterise the immortalised human hepatocellular carcinoma cell line, Hep 3B, with the aim of moving into a more physiologically relevant system and so removing the complication associated with overexpression of receptors. Despite the use of Hep 3B and similar cell lines in research, little is currently known about the GPCR expression and associated pharmacology. Through the use of RT-PCR we investigated the GPCR expression profile of the Hep 3B cell line with a particular focus on GCGR, known to be expressed in hepatocytes, RAMPs and G proteins.

The resulting RT-PCR products from samples extracted from Hep 3B cells were analysed by gel electrophoresis and densitometry. mRNA expression was detected for the housekeeping gene GAPDH, GCGR and RAMP2 and small levels detected for GIPR, CLR, RAMP1 and RAMP3 (Figure 3.19). Analysis of G protein mRNA expression revealed Hep 3B cells express $G\alpha_s$, $G\alpha_{i1-3}$, $G\alpha_q$, $G\alpha_{11}$ and $G\alpha_{12/13}$ -subunits (Figure 3.20).

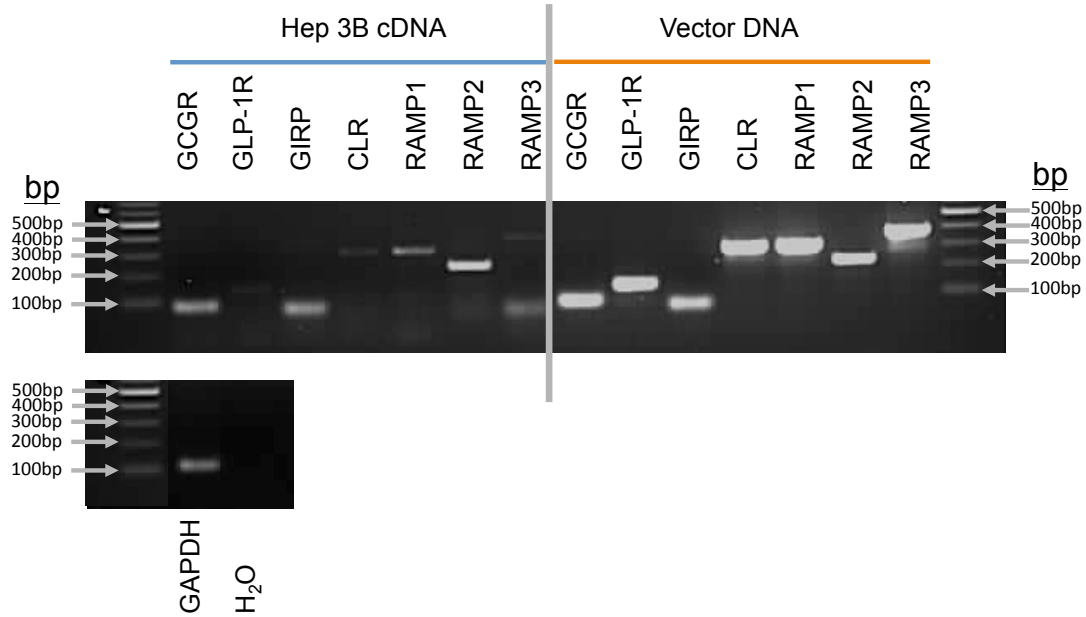


Figure 3.19. Expression profile of receptors in Hep 3B cells. RNA was extracted from Hep 3B, genomic DNA eliminated and then cDNA synthesised for the analysis of GCG, GLP-1R, GIRP, CLR and RAMP1-3 expression by RT-PCR using specific oligonucleotides (Table 2.6) (60°C). Representative image of products from PCR analysed by gel electrophoresis (2 percent agarose gel) with 100 bp ladder for size comparison. Vector DNA containing the receptor target was used as a positive control at (10 ng per reaction). A reaction containing GAPDH primers with water added rather than cDNA was used as a negative control. Hep 3B cells were at passage number 4 (1 passage after extraction from N₂ (stocks at P3)).

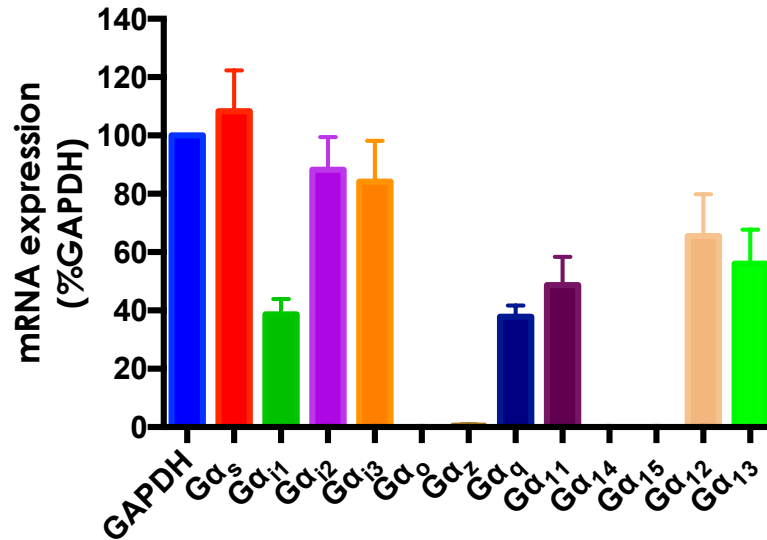


Figure 3.20. Expression profile of G proteins in Hep 3B cells. RNA was extracted from Hep 3B, genomic DNA eliminated and then cDNA synthesised for the analysis of G protein expression by RT-PCR using specific primers (Table 2.7) (60°C). Representative image of products from PCR analysed by gel electrophoresis (2 percent agarose gel with 100 bp ladder for size comparison). Bars represent combined results from PCR samples analysed using densitometry, where n = 4 independent experimental repeats. Note that Hep 3B cells used for this RT-PCR analysis were passage number 5, 6, 7 and 8 (N₂ stocks at P3).

3.7.2. Optimisation of the cAMP assay in Hep 3B cells

We next sought to determine the capacity of Hep 3B cells to signal via cAMP for the purpose of further pharmacological characterisation of endogenous receptor expression. As was conducted for cell lines transiently or stably expressing a receptor of interest (Section 3.2), it was necessary to determine the optimum cell density giving the highest signalling window, while staying within the assays dynamic range.

Here, the cAMP accumulation following forskolin or GCG stimulation was determined for Hep 3B cells at various cell densities using the LANCE® cAMP assay kit. Forskolin showed a concentration-dependent increase in cAMP accumulation in Hep 3B cells, with no significant difference between the four cell densities tested (Figure 3.21 and Table 3.11). The average basal

responses were approximately 63.0 percent of the cAMP SC. The maximum forskolin responses (100 μ M) approached 100 percent of the SC as the number of cells increased from 2,000 to 20,000 cells per well, with the largest span determined at 10,000 cells per well (41.2 \pm 1.5 percentage SC) (Table 3.11). These findings suggested that we were at the upper end of the cAMP assay kits dynamic range and increasing cell number further would reduce the forskolin signalling window. A concentration-dependent cAMP accumulation was also detected for GCG at 10,000 and 20,000 cells per well with a significantly reduced span (5.5 \pm 0.7 and 6.8 \pm 1.1 percentage SC, respectively) when compared to forskolin (41.2 \pm 1.5 and 33.3 \pm 2.0 percentage SC, respectively), whereas no response could be determined for 2,000 or 4,000 cells per well (Figure 3.22 and Table 3.11).

These initial tests indicated a small signalling window for GCG and the difficulty in acquiring a high cell count for Hep 3B cells indicated a need for a more sensitive cAMP assay. The more sensitive LANCE® Ultra cAMP assay kit gave a larger signalling window for 5,000 cells per well (Figure 3.23) when compared to 20,000 cells per well (18.6 \pm 1.2 and 6.8 \pm 1.1 percent SC, respectively) (Table 3.11).

Despite an improvement in the signalling window using the more sensitive assay (LANCE® Ultra cAMP assay kit), a direct comparison between the GCG response detected in Hep 3B cells when compared to HEK 293 cells transiently transfected with GCGR (5,000 rather than 1,000 cells per well, respectively), show a significant reduced amplitude and potency (Figure 3.24 and Table 3.12). This may reflect a relatively low level of GCGR expression when compared to that seen in a GCGR transfected cell line and/or reduced coupling to the cAMP signalling pathway. The signalling components and associated expression levels are likely to be different within Hep 3B and HEK 293 cells. It should also be noted that the reproducibility of these results using Hep 3B cells decrease as the age increases above passage 8 and as such, only young cells (passage < 8) should be used for experiments. To achieve the maximum signalling window in experiments

utilising Hep 3B cells to investigate ligand stimulated cAMP accumulation, the LANCE® Ultra cAMP assay kit was used with a 30 minute ligand stimulation of 5,000 cells per well.

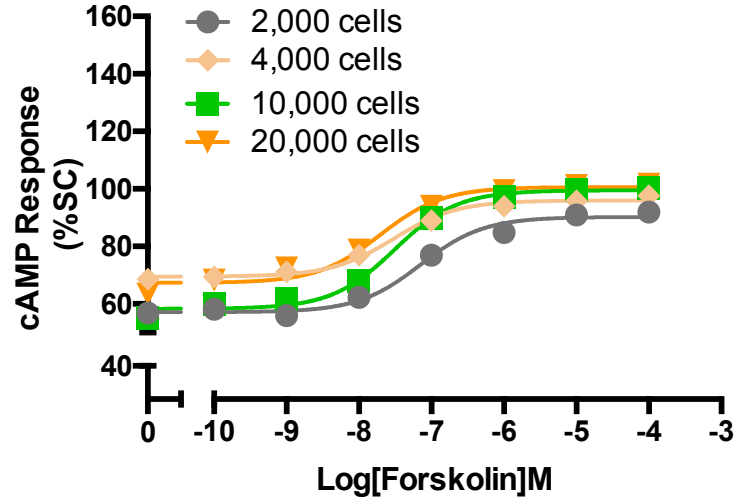


Figure 3.21. cAMP response to forskolin in Hep 3B at various cell densities. Hep 3B cells at various cell densities (2,000, 4,000, 10,000 or 20,000 cells/well) were exposed to forskolin for 30 minutes and cAMP accumulation detected using the LANCE cAMP kit. All values are mean \pm SEM expressed as percentage cAMP standard curve (SC) where $n = 2$ independent experimental repeats, conducted in duplicate.

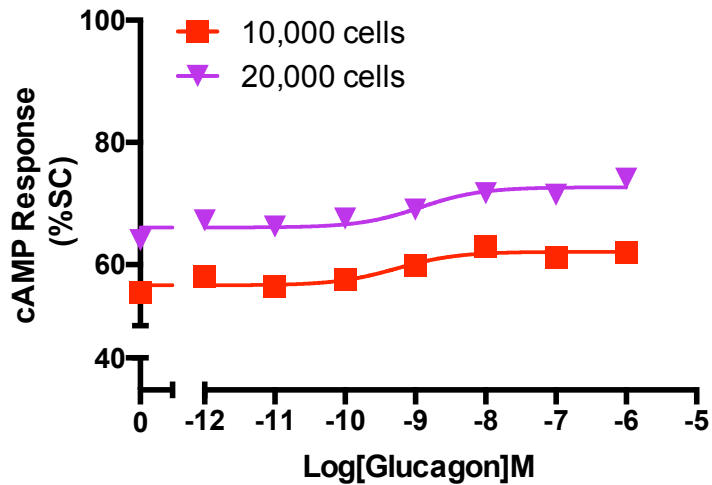


Figure 3.22. cAMP response to GCG in Hep 3B at 10,000 and 20,000 cells/well: Hep 3B cells at 10,000 or 20,000 cells/well were exposed to GCG for 30 minutes and cAMP accumulation detected using the LANCE cAMP kit. All values are mean \pm SEM expressed as percentage cAMP standard curve (SC) where $n = 2$ independent experimental repeats, conducted in duplicate.

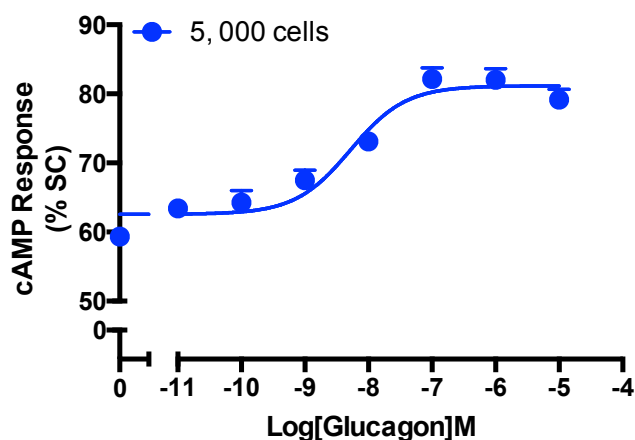


Figure 3.23. cAMP response to GCG in Hep 3B at 5,000 cells/well as measured using the LANCE® Ultra cAMP assay kit. Hep 3B cells at 5,000 cells/well were exposed to GCG for 30 minutes and cAMP accumulation detected using the more sensitive LANCE Ultra cAMP kit. All values are mean \pm SEM expressed as percentage forskolin response (100 μ M) where $n \geq 5$ independent experimental repeats, conducted in duplicate.

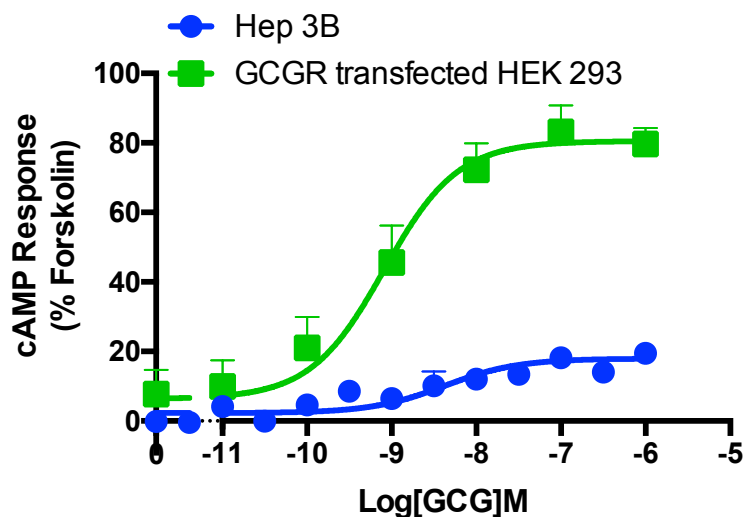


Figure 3.24. Comparison of cAMP response to GCG in Hep 3B and GCGR transfected HEK 293 cells. Hep 3B cells (5,000 cells/well) or GCGR transfected HEK 293 cells (1,000 cells/well) (Gifted from Dr Asuka Ioune) were stimulated with GCG for 30 or 8 minutes prior cAMP accumulation detection using the normal cAMP kit or a more sensitive cAMP kit, respectively. All values are mean \pm SEM expressed as percentage of individual forskolin response (100 μ M) (100%) and individual basal response (0%) where $n \geq 5$ independent experimental repeats, conducted in duplicate.

Table 3.11. Optimisation of the cAMP assay in Hep 3B cells. Potency (pEC₅₀), maximal response (E_{max}), basal and span for forskolin/GCG stimulated cAMP response measured Hep 3B cells using the LANCE/LANCE Ultra cAMP assay kit

Forskolin				
Cells/well	pEC ₅₀ ^a	E _{max} ^b	Basal ^c	Span ^d
2,000	7.15 ±0.1	90.2 ±0.7	57.1 ±0.7	33.1 ±1.0
4,000	7.52 ±0.1	96.0 ±0.6	69.5 ±0.6	26.4 ±0.8
10,000	7.51 ±0.1	99.5 ±1.1	58.3 ±1.1	41.2 ±1.5
20,000	7.71 ±0.2	100.6 ±1.4	67.3 ±1.5	33.3 ±2.0
<i>5,000*</i>	<i>7.25 ±0.1</i>	<i>94.6 ±2.0</i>	<i>66.2 ±1.7</i>	<i>28.4 ±1.5</i>
GCG				
Cells/well	pEC ₅₀ ^a	E _{max} ^b	Basal ^c	Span ^d
2,000		N.R	52.5 ±1.7	N.R
4,000		N.R	54.5 ±1.8	N.R
10,000	9.27 ±0.3	62.1 ±0.6	56.6 ±0.5	5.5 ±0.7
20,000	8.93 ±0.4	72.7 ±0.9	66.1 ±0.8	6.8 ±1.1
<i>5,000*</i>	<i>8.28 ±0.2</i>	<i>62.6 ±0.9</i>	<i>81.2 ±0.9</i>	<i>18.6 ±1.2</i>

Hep 3B cells were stimulated with forskolin or GCG prior to measurement of cAMP accumulation to generate concentration response curves. To calculate pEC₅₀, E_{max}, Basal and Span values, data were analysed using a three-parameter logistic equation.

^a Negative logarithm of forskolin/GCG concentration required to produce a half-maximal response

^b Maximal response to forskolin/GCG as percentage cAMP standard curve

^c The low plateau of the fitted sigmoidal concentration dose-response curve

^d The difference between E_{max} and basal signalling

All values are mean ± SEM expressed percentage cAMP standard curve where *n* = 2 independent experimental repeats, conducted in duplicate.

N.R denotes no response. In this case, a concentration dose-response could not be fitted with considerable accuracy due to variation between repeats.

* and *Italic* text represents result acquired using the more sensitive LANCE Ultra cAMP kit

Table 3.12. Comparison of cAMP response to GCG in Hep 3B and GCGR transfected HEK 293 cells. Potency (pEC₅₀), maximal response (E_{max}), basal and span for forskolin/GCG stimulated cAMP response measured Hep 3B or GCGR transfected HEK 293 cells using the LANCE/LANCE Ultra cAMP assay kit

Cell type	GCG			
	pEC ₅₀ ^a	E _{max} ^b	Basal ^c	Span ^d
HEK 293	9.09 ±0.1	80.5 ±1.6	6.4 ±1.1	74.2 ±1.8
<i>Hep 3B*</i>	<i>8.28 ±0.2***</i>	<i>2.3 ±1.0***</i>	<i>2.3 ±0.7</i>	<i>15.7 ±1.2***</i>

Hep 3B cells or HEK 293 cells transfected with pmCherry-N1 containing GCGR were stimulated with GCG prior to measurement of cAMP accumulation to generate concentration response curves. To calculate pEC₅₀, E_{max}, Basal and Span values, data were analysed using a three-parameter logistic equation.

^a Negative logarithm of GCG concentration required to produce a half-maximal response

^b Maximal response to GCG as percentage forskolin response

^c The low plateau of the fitted sigmoidal concentration dose-response curve

^d The difference between E_{max} and basal signalling

All values are mean ± SEM expressed percentage forskolin response where *n* ≥ 5 independent experimental repeats, conducted in duplicate.

* *and Italic* text represents result acquired using the more sensitive LANCE Ultra cAMP kit

3.8. Characterisation of CRISPR knockout HEK 293 cell lines

3.8.1. Growth rate and viability

The parental HEK 293 cell line and various CRISPR G protein and β-arrestin1/2 knockout HEK 293 cell lines (gifted to us by Dr Asuka Inoue) provide a potentially invaluable tool for the investigation of various GPCR signalling pathways. We first sought to conduct some basic characterisation experiments to assay any variation between the parental and knockout cell lines in terms of growth rate, viability and signalling capacity. Here we investigate if the knockout of each G protein or β-arrestin1/2 had an influence on growth rate and viability.

The quantification of ATP as a measure of cell viability was conducted using the CellTiter-Glo® Luminescent Cell Viability Assay (Recino *et al.*,

2017). As would be expected, cell number directly correlates with luminescent output ($R^2 = 0.98$) (Figure 3.25) and as such, cell number must be accounted for when investigating variability between cell lines. To further investigate any differences in viability across cell lines, repeats were conducted using 5,000 cells per well and luminescence (RLU) values were normalised to an ATP standard (Figure 3.8.1.2). There was found to be a significantly increase amount of ATP in $\Delta G\alpha_s$, $\Delta G\alpha_q$ and $\Delta G\alpha_{s/q/12}$ when compared to parental (WT) HEK 293 cells whereas the $\Delta\beta$ -arrestin1/2 cell line showed similar ATP levels. Although ATP amount is a measure of viability, and these findings may indicate an increased viability with $G\alpha_s$, $G\alpha_q$ and $G\alpha_{s/q/12}$ knockout, cells can also release ATP in response to mechanical stress or biological activation (Ostrom *et al.*, 2000). It could be possible that $\Delta G\alpha_s$, $\Delta G\alpha_q$ and $\Delta G\alpha_{s/q/12}$ cell lines are more susceptible to such mechanical stress or biological activation (as might be imposed by trypsinisation, for example) in comparison to WT and $\Delta\beta$ -arrestin1/2 cells.

The growth profiles of WT and G proteins or β -arrestin1/2 knockout HEK 293 cell lines were tested over various time points within a 72-hour period following plating at 100,000 cells per well of a 24-well tissue culture plate. There was found to be considerable variation in growth rate across the 72-hour period with the difference becoming more evident as the time post seeding increases (Figure 3.27). On day 3 (72 hours post seeding), WT and $\Delta G\alpha_q$ cells reached confluence and showed a faster growth when compared to the other cell lines.

Interestingly, cell viability does not appear to correlate with growth rate. For example, $\Delta\beta$ -arrestin1/2 cell line despite showing reduced growth when compared to WT at 48 and 72 hours had similar ATP levels (Figure 3.8.1.2). On the other hand the $\Delta G\alpha_q$ cell line, which showed a more similar growth rate to WT, had increased ATP levels. $\Delta G\alpha_s$ and $\Delta G\alpha_{s/q/12}$, which showed a reduced growth when compared to WT at 48 and 72 hours, again show an increase in ATP levels. It appears that an increase in ATP levels i.e. viability cannot account for a faster growth rate and other factors are in play. This

variability should be considered when interpreting experimental data acquired using these knockout cell lines.

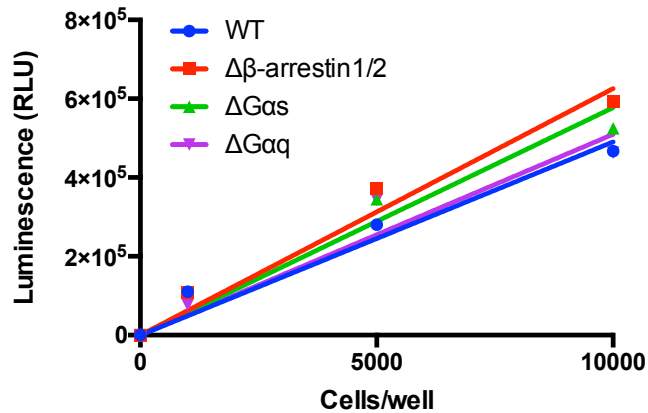


Figure 3.25. Cell number directly correlates with luminescent output for CellTiter-Glo® Luminescent Cell Viability Assay. Quantification of ATP, as a measure of cell viability, for 1,000, 5,000 and 10,000 cells shows a strong correlation between cell number luminescent output ($R^2 = 0.98$).

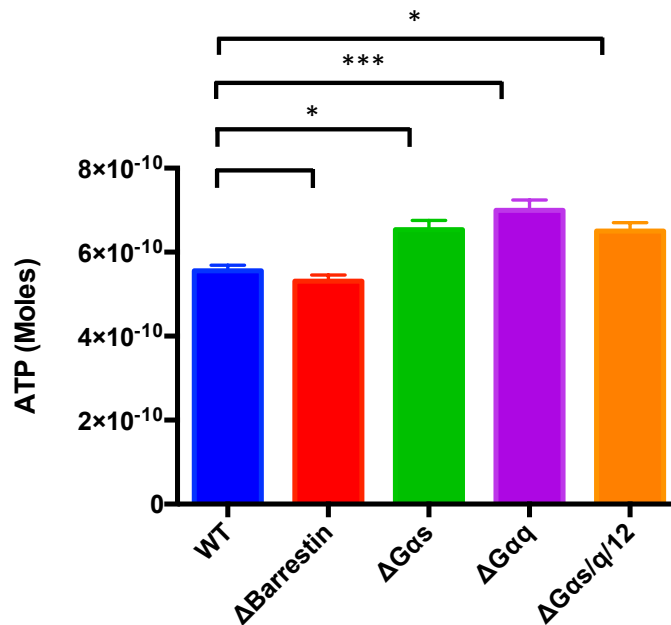


Figure 3.26. Measurement of cell viability in HEK 293 knockout cell lines. Quantification of ATP as a measure of cell viability was conducted using the CellTiter-Glo® Luminescent Cell Viability Assay (Promega) in a 384-well format. Comparison of ATP produced from WT HEK 293 cells and knockout cell lines at 5,000 cells/well. All values from individual experiments are interpolated to an ATP standard. Values are mean ± SEM expressed in Moles were $n \geq 4$ independent experimental repeats, conducted in quadruplicate. Statistical significance in comparison to WT was determined using one-way analysis of variance and Dunnett's post-test.

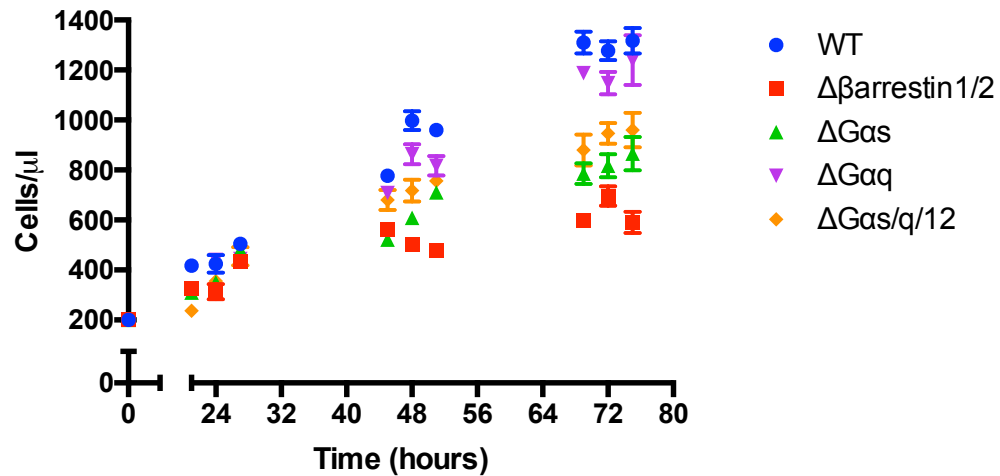


Figure 3.27. Comparison of cell growth profiles of WT and knockout HEK 293 cell lines. All lines were seeded at 100,000 cells per well of a 24-well tissue culture plate (200 cells/μl in a 500 μl volume of media) at time-point zero and density at various time points (21, 24, 27, 45, 48, 51, 69, 72 and 75 hours) determined using manual counting with a haemocytometer. On the third day following seeding (72 hours) WT and ΔGαq had reached confluence.

3.8.2. Maximum cAMP response in CRISPR knockout HEK 293 cell lines

In order to investigate GPCR signalling in the CRISPR knockout cell lines, it is necessary to initially compare the maximal signalling capacity of the downstream signalling component of interest. In the case of a cAMP accumulation assay, this would be the maximum cAMP response of the system. Here, each cell line was stimulated for 8 minutes with 100 μM of the potent AC activator, forskolin, and the cAMP accumulation measured.

The maximum forskolin response determined in Δβ-arrestin1/2 or ΔGαq was not significantly different to WT (Figure 3.28). There was however a significantly reduced cAMP accumulation in both ΔGαs and ΔGαs/q/12 when compared to WT (Figure 3.28) indicating a reduced capacity for cAMP production in these cell lines. Interestingly, there was found to be no significant difference between the cAMP responses determined in ΔGαs and ΔGαs/q/12 suggesting the reduction capacity for cAMP signalling is attributable to the absence of the Gαs-subunit. ACs receives stimulatory signals from Gs and inhibitory signals from Gi (Tang and Gilman, 1991). It could be

speculated that in the $\Delta G\alpha_s$ HEK 293 cell line, where basal stimulatory signals from G_s are presumably absent, G_i is able to bind and inhibit AC to a greater extent thereby leading to a reduced cellular cAMP level.

The interpretation of these data presumes the only difference between parental HEK 293 cells and the knockout cell lines is the absence of the G protein or β -arrestin1/2. However, it is possible that the reduction in cAMP capacity is independent of the targeted knockout. Indeed, the process of genome editing and subsequent growth in vitro imposes selective conditions on the cells that often adapt through mutation (Lin *et al.*, 2014). As such, the cell lines may have cellular variations in addition to the targeted deletion. The findings presented here suggest that cAMP data acquired from these cells should be normalised to the maximum forskolin response measured in each individual cell line thereby attempting to account for the variability in cAMP signalling capacity.

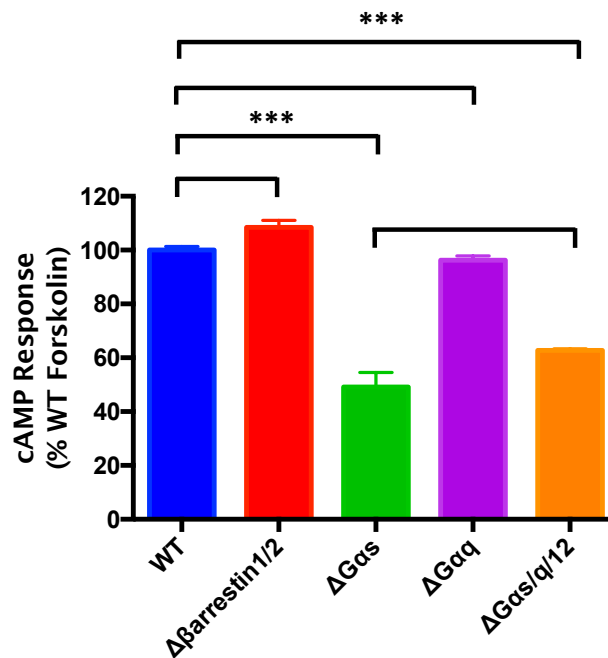


Figure 3.28. Maximal forskolin responses in HEK 293 knockout cell lines. WT and knockout HEK 293 cell lines transiently expressing pmCherry-N1 vector containing GCGR (24 hours post transfection) were exposed to 100 μ M forskolin for 8 minutes and cAMP accumulation detected. All values are mean \pm SEM expressed as percentage WT forskolin response were $n \geq 5$ independent experimental repeats, conducted in duplicate. Statistical significance in comparison to WT was determined using one-way analysis of variance and Dunnett's post-test.

3.8.3. cAMP response in $\Delta G\alpha_s$ HEK 293 cells changes over time

The $\Delta G\alpha_s$ HEK 293 cell line could be used for the investigation of G_i -coupling at a particular GPCR of interest. In theory, this was similar to using NF449 to inhibit G_s and looking for a reduction in cAMP accumulation (Figure 3.12). Here, $\Delta G\alpha_s$ HEK 293 cells transfected with a vector expressing the GPCR would need to receive an initial forskolin stimulation to cause an elevation in intracellular cAMP levels. We would then look for a reduction in the cAMP levels following stimulation with a ligand active at this GPCR as an indicator of G_i -coupling. We first sought to confirm an absence of G_s -mediated signalling through performing a cAMP accumulation assay in $\Delta G\alpha_s$ HEK 293 cells transfected with pmCherry-N1 expressing GCGR.

The cAMP accumulation following GCG stimulation of $\Delta G\alpha_s$ HEK 293 cells transfected with GCGR was shown to change over passage number (Figure 3.29 and Table 3.13). There was no detectable cAMP response from cells early from nitrogen storage (passage < 5). However, as passage number increased, there appeared to be a gain in cAMP response to GCG stimulation. This gained GCG response had a significantly reduced potency and maximal response when compared to WT HEK 293 cells (pEC_{50} 8.32 ± 0.3 and 9.13 ± 0.1 , E_{max} 57.3 ± 6.5 and 90.9 ± 2.2 , respectively). This finding may indicate the presence of a mixed population of cells, with $G\alpha_s$ -subunit expression presence or absent. A number of the CRISPR-Cas9-mediated biallelic knockout cell lines, including $\Delta G\alpha_s$ and $\Delta G\alpha_{s/q/12}$ HEK 293 cells, have been shown to have a slower growth rate when compared to the WT HEK 293 parental cell line (Figure 3.27). As a result of this growth disadvantage, if there were a small subclonal (contaminating) population within the culture with a faster growth rate, they would in time outgrow the mutant population. With this in mind, experiments should be conducted on cells with a low passage number (<5). However, without conducting western blot analysis and confirming the lack of each particular G protein and β -arrestin1/2 over time,

the data acquired from these gifted cell lines need to be interpreted with caution.

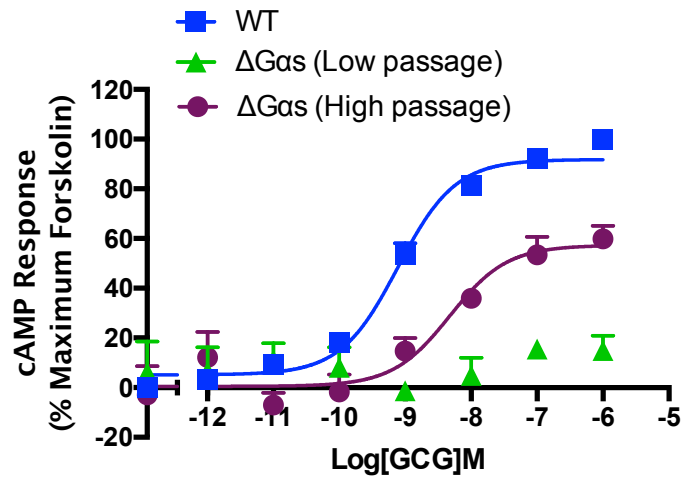


Figure 3.29. cAMP response in $\Delta G\alpha_s$ HEK 293 cells changes over passage. WT and $\Delta G\alpha_s$ HEK 293 cells transiently expressing pmCherry-N1 vector expressing GCGR (24 hours post transfection) were exposed to GCG for 8 minutes and cAMP accumulation detected. The $\Delta G\alpha_s$ HEK 293 cells were either low passage (< 5 out of nitrogen storage) or high passage (>5 out of nitrogen storage). All values are mean \pm SEM expressed percentage maximum forskolin response for each individual cell line were $n \geq 5$ independent experimental repeats, conducted in duplicate.

Table 3.13. cAMP response in $\Delta G\alpha_s$ HEK 293 cells changes over passage. Potency (pEC_{50}), maximal response (E_{max}), basal and span for GCG stimulated cAMP response in WT and $\Delta G\alpha_s$ HEK 293 cells transiently transfected with pmCherry-N1 expressing GCGR

	cAMP			
	pEC_{50} ^a	E_{max} ^b	Basal ^c	Span ^d
WT	9.13 \pm 0.1	90.9 \pm 2.2	5.1 \pm 1.7	85.8 \pm 2.7
$\Delta G\alpha_s$ low passage		N.R	0.2 \pm 1.2	N.R
$\Delta G\alpha_s$ high passage	8.32 \pm 0.3***	57.3 \pm 6.5***	0.5 \pm 3.6	56.8 \pm 7.1***

Parental WT HEK 293 cells or $\Delta G\alpha_s$ HEK 293 cells (either low passage (< 5 out of nitrogen storage) or high passage (>5 out of nitrogen storage)) were transiently transfected with GCGR and stimulated with GCG prior to measurement of cAMP accumulation to generate concentration response curves for each construct. To calculate pEC_{50} , E_{max} , Basal and Span values, data were analysed using a three-parameter logistic equation

^a Negative logarithm of GCG concentration required to produce a half-maximal response

^b Maximal response to GCG as percentage forskolin response (for each individual cell line)

^c The low plateau of the fitted sigmoidal concentration dose-response curve

^d The difference between E_{max} and basal signalling.

Statistical significance (*, $p < 0.05$; **, $p < 0.01$; ***, $p < 0.001$) comparing GCG response between the WT and high passage $\Delta G\alpha_s$ HEK 293 cells was determined using unpaired Student's t-test (two-tailed). N.R denotes no response

3.8.4. Maximum PMA response in CRISPR knockout HEK 293 cell lines

These CRISPR knockout cell lines may provide a useful tool in investigating the upstream components important in GCGR-mediated ERK signalling. Having shown a reduced capacity for forskolin mediated cAMP accumulation in $\Delta G\alpha_s$ and $\Delta G\alpha_{s/q/12}$, we next sought to investigate the maximum activation of ERK1/2 between the various cell lines. Here, each cell line was stimulated for 5 minutes with 1 μ M PMA, a direct protein kinase C (PKC) activator (Robinson *et al.*, 1992), and pERK1/2 measured using the homogeneous time resolved fluorescence (HTRF)[®] Phospho-ERK (Thr202/Tyr204) Cellular Assay Kit (Cisbio Bioassays).

There was found to be a significant elevation in PMA stimulated ERK1/2 phosphorylation, as indicated by the increased HTRF ratio, for all knockout cell lines when compared to WT HEK 293 cells (Figure 3.30). This finding indicates enhanced ERK1/2 signalling capacity within the knockout cell lines and may indicate higher PKC expression levels when compared to WT. In order to account for this variability in further analysis of ERK1/2 activation described in chapter 4, the ligand stimulated pERK1/2 responses were normalised to the response measured to PMA response each individual cell line.

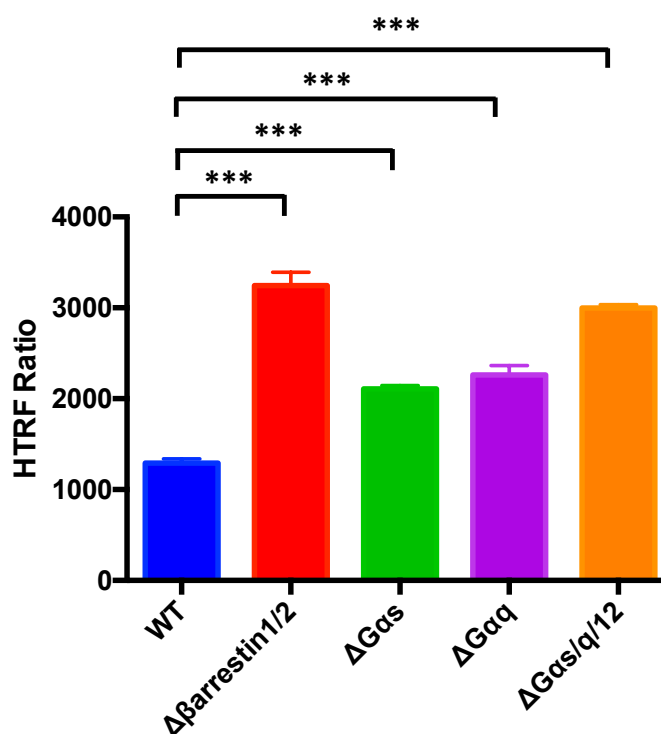


Figure 3.30. Comparison of PMA responses in HEK 293 knockout cell lines. WT and knockout HEK 293 cell lines transiently expressing pmCherry-N1 vector containing GCGR (48 hours post transfection) were exposed to 1 μ M PMA for 5 minutes and pERK1/2 detected. All values are mean \pm SEM expressed as the HTRF ratio were $n \geq 5$ independent experimental repeats, conducted in duplicate. Statistical significance in comparison to WT was determined using one-way analysis of variance and Dunnett's post-test.

3.8.5. Summary

Initial characterisation of the gifted parental and various CRISPR G protein and β -arrestin1/2 knockout HEK 293 cell lines indicated significant variability in terms of viability, growth rate and maximum cAMP accumulation/pERK activation. There were significantly increased ATP levels in $\Delta G\alpha_s$, $\Delta G\alpha_q$ and $\Delta G\alpha_{s/q12}$ when compared to WT, suggesting an increased viability. Another possible explanation may have been an increased susceptibility to mechanical stress or biological activation (as might be imposed by trypsinisation, for example) thereby resulting in increased ATP release. Interestingly, cell viability did not appear to correlate with growth rate and

whereas WT and $\Delta G\alpha_q$ cells reached confluence and showed a faster growth when compared to the other cell lines, they had similar ATP levels.

The maximum cAMP accumulation, as determined by forskolin stimulation at 100 μ M, was significantly reduced in both $\Delta G\alpha_s$ and $\Delta G\alpha_{s/q/12}$. This finding indicates a reduced capacity for cAMP production independent of G proteins. As may be expected $\Delta G\alpha_s$ transfected with pmCherry-N1 expressing GCGR showed no cAMP response following GCG stimulated. However, there was found to be a gain in cAMP response with increasing passage number. This latter finding indicated a mixed population of cells, presence or absence of $G\alpha_s$ -subunit expression and outgrowth of the mutant population.

There was found to be a significant elevation in PMA stimulated ERK1/2 phosphorylation, for all knockout cell lines when compared to WT. Despite showing a reduced capacity for cAMP signalling, $\Delta G\alpha_s$ and $\Delta G\alpha_{s/q/12}$ appear to show an enhanced ability for ERK1/2 activation thereby suggesting both enhanced and reduced expression/regulation of various signalling pathway components. This finding provides additional evidence to suggest these knockout cell lines have cellular differences other than the individual G protein or β -arrestin1/2 knockout, which may be due as a consequence of the knockout (compensatory) or independent. Indeed, the process of genome editing and passage may have induced selective conditions resulting in additional cellular variations other than the targeted deletion. Given the variability in viability, growth rate, cAMP and pERK1/2 maximum responses, data acquired using these knockout cell lines should be interpreted with caution. In addition, when analysing both cAMP and pERK1/2 response data acquired using these cells, the ligand stimulated responses should be initially normalised to the maximum response (forskolin or PMA) determined for each individual cell lines prior to further normalisation and comparison.

3.9. Analysis of GCGR cell-surface expression using fluorescence-activated cell sorting (FACS)

3.9.1. FACS: Data collection and analysis

Flow cytometry assesses the fluorescence of thousands of individual cells in seconds and allows a larger scale investigation of cells at a population level when compared to traditional fluorescence microscopy. In the work presented in this thesis, FACS was conducted using the BD Accuri™ C6 Plus Flow Cytometer to quantify receptor cell-surface expression in collaboration with Dr Matthew Harper (Department of Pharmacology, University of Cambridge). Specifically, this technique was used for the cell-surface expression analysis of WT and mutant GCGR.

The following figures show analysis of data acquired from untransfected and mCherry-tagged GCGR (WT and mutant) transfected HEK 293 cells as examples of data collection and analysis, which was performed on data presented in chapter 5. Here in order to quantify WT and mutant GCGR cell-surface expression in HEK 293 cells, transfected cells were incubated with anti-GCGR antibody followed by APC-conjugated anti-rabbit IgG secondary antibody. The fluorescence detector FL4 (Em. λ 675/25 n) was used to detect APC fluorescence and data subsequently analysed as described here.

Manual gating of untransfected HEK 293 cells was conducted in order to exclude debris and dead cells from analysis with 82.8 percent of events included (Figure 3.31). Gating for single cells was then conducted to exclude clumps of cells and accounted for 81.2 percent of the population (Figure 3.32). For non-transfected cells, stained with both primary and secondary antibodies, the histogram generated from debris removal and single cell gating reveals a single peak, as would be expected (Figure 3.33). To assess unspecific binding of APC-conjugated secondary antibody, HEK 293 cells were transfected with vector only (pmCherry-N1) and stained with both primary and secondary antibodies. A visible shift in FL4 fluorescence was

seen with the emergence of two peaks, indicating the occurrence of unspecific binding and two distinct populations of HEK 293 cells, respectively (Figure 3.33).

FACS sorted HEK 293 cells transfected with vector expressing mCherry-tagged WT GCGR showed a visible shift in FL4 fluorescence intensity which was greater than that observed for both untransfected and vector only transfected (Figure 3.33). This finding suggested that WT GCGR were indeed detected on the cell-surface of HEK 293 cells. The histograms generated from HEK 293 cells transfected with vector expressing TM4 mutant GCGR (L277A, V280A) showed a reduced shift in FL4 when compared to the histogram generated from HEK 293 cells transfected with vector expressing WT GCGR, suggesting a reduced cell-surface expression (Figure 3.34). Again, there is an emergence of two peaks for both WT and all mutant GCGR transfected HEK 293 cells indicating two distinct populations.

It should be noted that a test with propidium iodide (PI) to assess the proportion of dead cells accounted for less than 5 percent of the collected events and could not account for the additional peak. It appears transfections, regardless of receptor expression, was causing the emergence of two distinct populations. This finding is unexpected and cannot be explained with any certainty. However, transfection could be inducing a change in the regulation of HEK 293 cell size giving rise to two distinctly different sized populations.

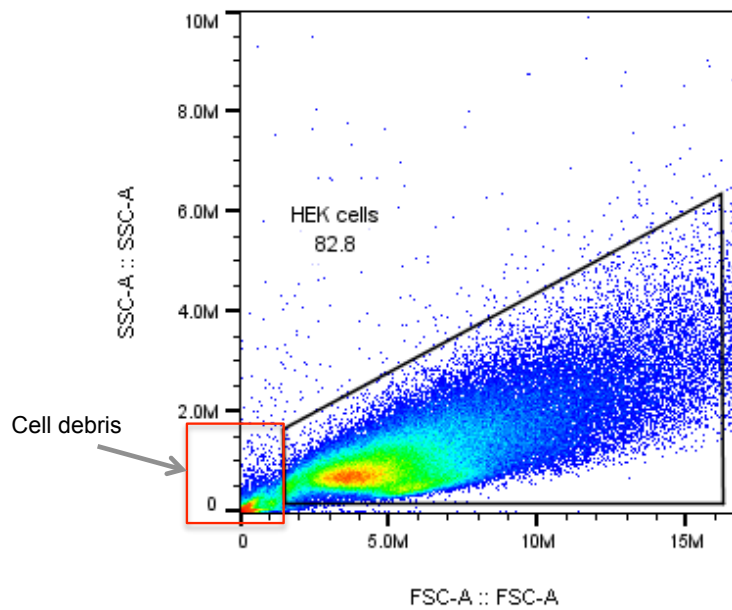


Figure 3.31. FACS data analysis: example manual gating of untransfected HEK 293 cells. HEK 293 cells were incubated with anti-GCGR antibody followed by APC-conjugated anti-rabbit IgG secondary antibody. Data was acquired on a BD Accuri C6 and analysed with BD Accuri™ C6 software with a total of 20,000 gated events captured. Here, cells are analysed using side scatter area (SSC-A) by forward scatter area (FSC-A). The drawn gate excludes events with low FSC and high SSC thereby excluding debris and dead cells from analysis.

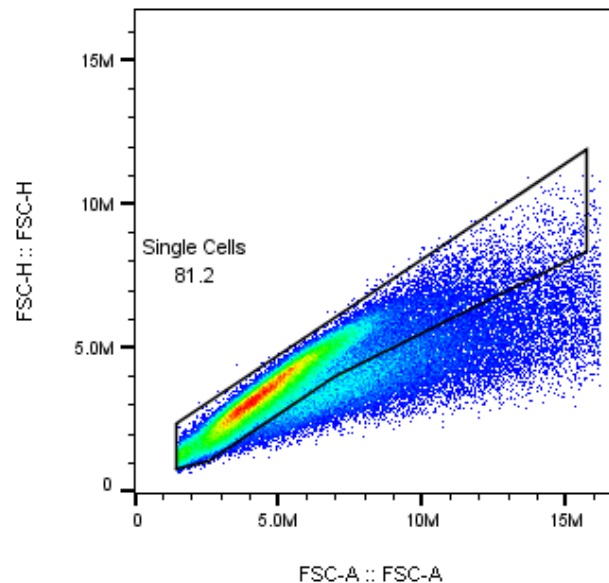


Figure 3.32. FACS data analysis: example gating of single untransfected HEK 293 cells. HEK 293 cells were incubated with anti-GCGR antibody followed by APC-conjugated anti-rabbit IgG secondary antibody. Data was acquired on a BD Accuri C6 and analysed with BD Accuri™ C6 software with a total of 20,000 gated events captured. Here, FSC-Height (FSC-H) by FSC-Area (FSC-A) is plotted. Cells along the diagonal are the single cells and are gated, as shown by the black box. The single cells account for 81.2% of the population. The cells off this diagonal are clumps of cells and are excluded from the data.

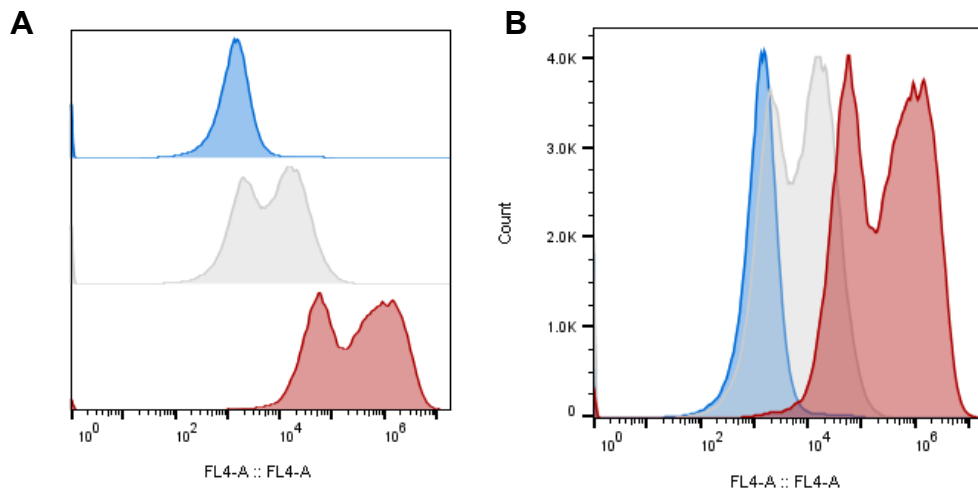


Figure 3.33. Example histograms generated from flow cytometry of untransfected and vector only/GCGR transfected HEK 293 cells. HEK 293 cells untransfected (blue), transfected with mCherry-N1 vector only (grey) and WT mCherry-tagged GCGR (red) were incubated with anti-GCGR antibody followed by APC-conjugated anti-rabbit IgG secondary antibody. Data were acquired on a BD Accuri C6 and analysed with BD Accuri™ C6 software. A total of 20,000 gated events captured. y-axis, cell count; x-axis, log scale of fluorescence intensity (FL4-A). The data is represented in two different ways; **A**) Stacked histograms and **B**) overlaid histograms. Right-shifted plot indicates more cell-surface expression.

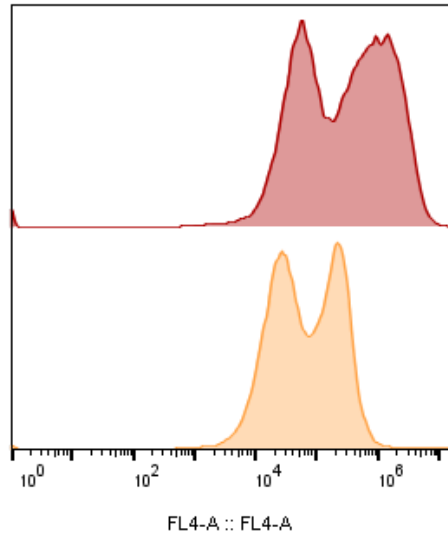


Figure 3.34. Example histograms generated from flow cytometry of WT or mutant GPCR transfected HEK 293 cells. HEK 293 cells transfected with WT mCherry-tagged GPCR (red) or the double GPCR TM4 mutant (L277A V280A) (orange) were incubated with anti-GPCR antibody followed by APC-conjugated anti-rabbit IgG secondary antibody.

3.9.2. DNA concentration at transfection and detectable cell-surface expression

As has been indicated by cAMP accumulation assays, receptor DNA concentration at transfection can influence the maximum cAMP response following ligand stimulation when below a given concentration (possibly 150 ng per well, as previously indicate (Section 3.2.3)). This finding could be interpreted in two ways. Firstly, DNA amount above a certain concentration does not increase the level of receptor cell-surface expression proportionately. Alternatively, despite a change in receptor cell-surface expression, the cAMP accumulation assay is able to detect similar maximal levels following ligand stimulation, presumably because there is more receptor than effectors in the system.

Achieving similar levels of cell-surface expression for WT and mutant GPCRs could be a valuable tool allowing the investigation into how the receptor mutation influences downstream signalling component levels

independent of receptor cell-surface expression. In order to investigate if DNA concentration at transfection influences receptor cell-surface expression, FACS was performed on HEK 293 cells transfected with varying amounts of WT and mutant GCGR DNA, and analysed as previously described (Section 3.9.1).

There was shown to be a reduction in cell-surface expression with decreasing concentration of DNA for WT and a number of GCGR mutants (Figure 3.35). However, this reduction in cell-surface expression was not proportional to the changes in DNA concentration. For example, when transfected with half the amount of DNA (125 ng of rather than 250 ng), the decrease in cell-surface expression was shown to be only 20.9 percent for WT GCGR and 17.6 percent for the helix 8 E406A GCGR mutant. This evidence suggests that although DNA amount at transfection can influence receptor cell-surface expression, controlling expression through altering DNA concentration is not a trivial task. It seems that an alternative system other than transient transfection where expression levels are suggested to not be as high, such as the Flp-In expression system (Wootten *et al.*, 2016), may be preferable to overcome issues associated with high expression.

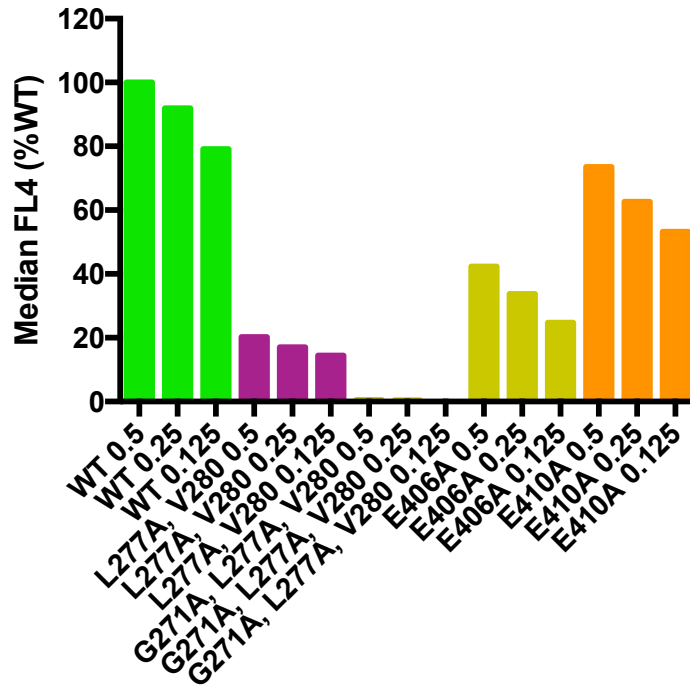


Figure 3.35. DNA concentration at transfection and detectable cell-surface expression of WT and mutant GCGR, as determined by FACS analysis. FACS analysis was conducted 48 hours post transfection of HEK 293 with 0.5 μ g, 0.25 μ g or 0.125 μ g (indicated by 0.5, 0.25 or 0.125 on the graph) WT or mutant GCGR containing pmCherry-N1 DNA per well of a 24-well plate. Cells were incubated with anti-GCGR antibody (1:50 dilution) followed by APC-conjugated anti-rabbit IgG secondary antibody (1:150 dilution). The values represent median FL4 with the data normalised to vector transfected (0%) and WT GCGR (100%), $n = 1$.

Chapter 4. Investigating GCGR pharmacology

4.1. Introduction

Having performed a number of assay optimisations and cell line characterisations (Chapter 3), I next sought to utilise these established assay systems to investigate the hypothesis that GCGR signals through multiple pathways. Studies have highlighted the possibility that GCGR couples to alternative G proteins other than the classical G_s-coupled GCGR pathway such G_{q/11} (Xu and Xie, 2009 and Wakelam *et al.*, 1986). In this chapter, GCGR signalling and G protein-coupling at the GCGR using assays measuring cAMP accumulation, pERK1/2 response or Ca²⁺_i mobilization is investigated. We also look to investigate the influence of RAMP2, known to interact with GCGR (Christopoulos *et al.*, 2003), on the classic G_s-coupled GCGR pathway.

In addition to characterising the activity of two known GCGR agonists (GCG and oxyntomodulin) and two potential GCGR antagonist (des-His¹,[Glu⁹]-glucagon amide (des-His¹,[Glu⁹]-GCG) and L-168,049), the activity of the GCG analogue, TH-GCG, was also investigated. TH-GCG was previously reported to stimulate production of inositol phosphates but not cAMP and this finding was proposed to indicate the existence of two distinct receptors for GCG (Wakelam *et al.*, 1986). We investigated the hypothesis that TH-GCG is acting at the classical GCGR and that these previous findings could be explained by signalling bias, where the downstream signalling cascade initiated by TH-GCG is predominantly through G_q-coupling.

GCG is known to cause a rapid, concentration-dependent phosphorylation and activation of MEK1/2 and ERK1/2 (Jiang *et al.*, 2001). However, extensive detail into the signalling pathways leading to this activation is lacking. It was reported that both a PKA (H-89) and MEK (PD98059) inhibitor completely abolished GCG induced ERK1/2 activation in β cells and HEK 293 cells (Dalle *et al.*, 2004 and Jiang *et al.*, 2001,

respectively), indicating that both cAMP-dependent PKA and MEK (upstream from ERK1/2) activity is necessary for ERK1/2 activation. Other research has also implicated the importance of the PLC/Ca²⁺i cascade for ERK1/2 phosphorylation (Li *et al.*, 2006). ERK activation is described to be downstream of both G protein (G_s, G_i, G_q and the G_{βγ} subunit) and β-arrestin mediated pathways (DeWire *et al.*, 2007). Although implicated in GCGR desensitisation and down regulation (Krilov *et al.*, 2011), relatively little research has been conducted on the role of β-arrestins in GCGR signalling. To expand on these findings, we conducted an investigation into the potential G protein and β-arrestins mediated pathways leading to ERK1/2 activation.

This work utilising multiple cell lines including HEK 293T, HEK 293, CHO-K1 and Hep 3B cells, in addition to hepatocytes extracted from C57BL/6 mice. Despite the use of Hep 3B cells and similar cell lines in research, little is currently known about the receptor expression and associated pharmacology. Having investigated the GPCR and RAMPs mRNA expression in Hep 3B cells and identified the likely expression of GCGR (Section 3.7), I next sought to investigate functional protein expression through the cAMP accumulation and a pERK1/2 response assay kits.

4.2. Investigating the cAMP response at the GCGR

4.2.1. GCG and oxyntomodulin stimulates a robust cAMP response

Although the role of glucagon (GCG) in blood glucose regulation is well studied, a far more complex picture emerged with this pancreatic hormone shown to also regulate lipid metabolism, stimulate energy expenditure and induce satiety, to name a few (Habegger *et al.*, 2010). In order to explore the full pharmacological potential of GCG, we sought to investigate the mechanism of action at the GCGR.

Using HEK 293 cells transfected with pmCherry-N1 expressing GCGR containing the C-terminal mCherry-tag, we first wanted to confirm previous reports that GCGR mediates its effects through G_s-coupling. The following

experiments were performed in line with optimisations presented in chapter 3 (Section 3.2). GCGR transfected HEK 293 cells, challenged with GCG or oxyntomodulin, induced a concentration-dependent increase in cAMP concentration (Figure 4.1 A and Table 4.1). There was also found to be a concentration-dependent increase in cAMP accumulation to GLP-1(7-36)amide (Figure 4.1 and Table 4.1). These responses were found to be GCGR specific with no cAMP accumulation detected in vector only transfected HEK 293 cells (Figure 4.1 C). Oxyntomodulin displayed significantly reduced in both potency and affinity when compared to GCG (Table 4.1) and confirms previous findings of reduced potency (Weston *et al.*, 2015). Similarly, GLP-1(7-36)amide also showed a significantly reduced potency and affinity when compared to GCG and also showed a reduced efficacy, as determined by fitting the operational model of agonism (Table 4.1).

The basal response to both oxyntomodulin and GLP-1(7-36)amide was also significantly lower than GCG. This elevated basal response for GCG is likely a reflection of the cAMP assay sensitivity rather than a true elevation. As was shown elsewhere (Section 3.2.2.1), very low concentrations of GCG ligand was shown to activate GCGR leading to perceived elevated basal cAMP level. Oxyntomodulin on the other hand, with reduced potency, did not show this elevation in basal cAMP (Section 3.2.2.1, Figure 3.3 A).

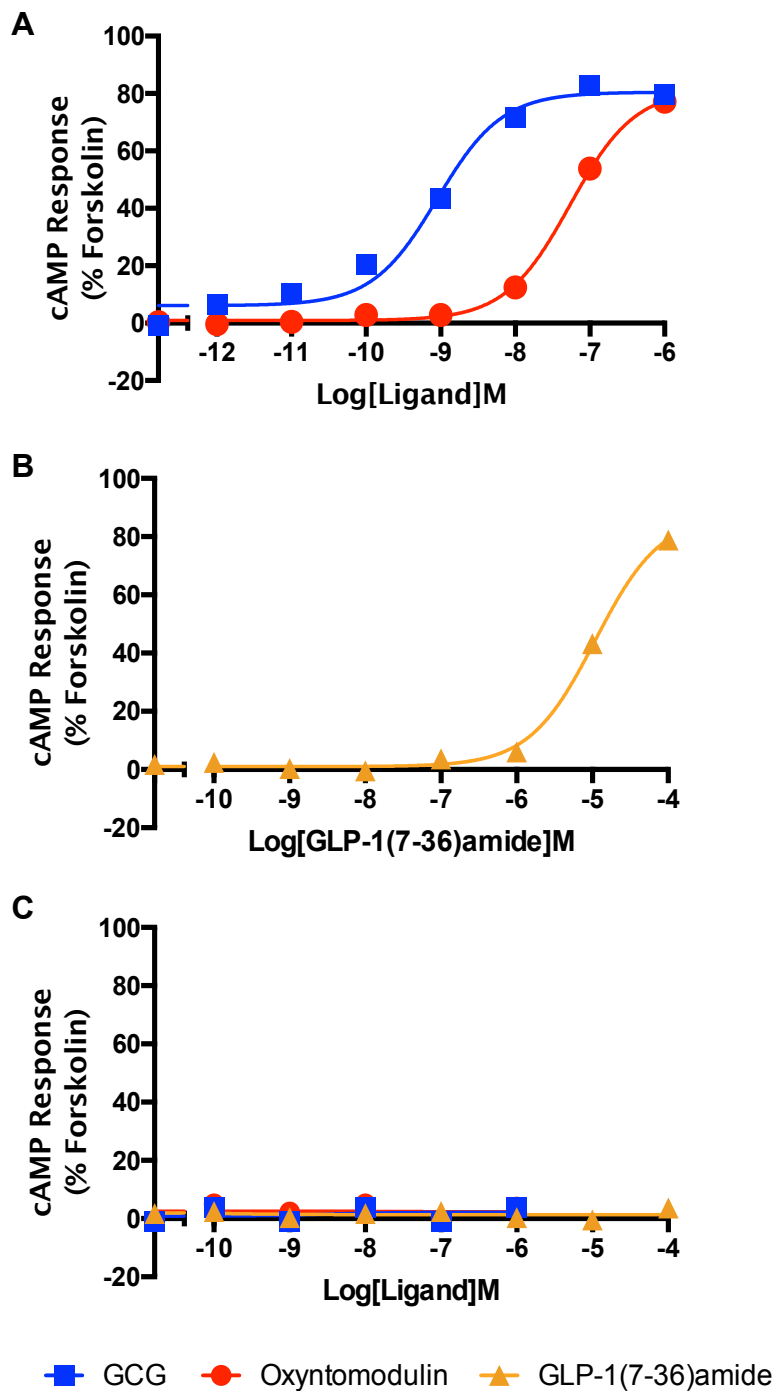


Figure 4.1. cAMP response in GPCR transfected HEK 293 cells: HEK 293 cells transiently expressing **A/B)** pmCherry-N1 vector containing GCGR or **C)** vector only were stimulated with GCG, oxyntomodulin or GLP-1(7-36)amide for 8 minutes and cAMP accumulation detected. All values are mean \pm SEM expressed as percentage forskolin response where $n \geq 5$ independent experimental repeats, conducted in duplicate.

Table 4.1. cAMP response in GCGR transfected HEK 293 cells. Potency (pEC_{50}), maximal response (E_{max}), basal, span, affinity (pK_A) and coupling efficacy ($\log\tau$) for GCG or oxyntomodulin measured in GCGR transfected HEK 293 cells using a cAMP assay

Ligand	cAMP					
	pEC_{50}^a	E_{max}^b	Basal ^c	Span ^d	pK_A^e	$\log\tau^f$
GCG	9.04 ±0.1	80.5 ±1.7	6.1 ±1.2	74.4 ±1.7	8.37 ±0.1	0.58 ±0.05
Oxyntomodulin	7.27±0.1***	81.5 ±2.1	0.9 ±1.0*	80.6 ±2.1	6.54 ±0.1***	0.64 ±0.06
GLP-1(7-36)amide	4.97±0.1***	85.5 ±2.5	1.0 ±0.4*	84.5 ±1.5	4.07 ±0.1***	0.84 ±0.08*

HEK 293 cells (1000 cells/well) transiently transfected with pmCherry-N1 containing GCGR were stimulated with GCG, oxyntomodulin or GLP-(7-36)amide for 8 minutes prior to measurement of cAMP accumulation to generate concentration response curves. To calculate pEC_{50} , E_{max} , Basal and Span values, data were analysed using a three-parameter logistic equation. Data was also analysed by an operational model of agonism (Black and Leff, 1983) to determine affinity (pK_A) and coupling efficacy ($\log\tau$).

^a Negative logarithm of GCG concentration required to produce a half-maximal response

^b Maximal response to GCG as percentage forskolin response

^c The low plateau of the fitted sigmoidal dose-response curve

^d The difference between E_{max} and basal signalling

^e The negative logarithm of functional affinities that describes the affinity of the receptor when coupled to a given signalling pathway generated though use of the operational model for partial agonism

^f τ is the coupling efficiency parameter generated though use of the operational model for partial agonism
All values are mean ± SEM expressed as percentage WT forskolin response where $n \geq 5$ independent experimental repeats, conducted in duplicate.

Statistical significance (*, $p < 0.05$; **, $p < 0.01$; ***, $p < 0.001$) compared to GCG response was determined by unpaired Student's t-test (two-tailed).

4.2.2. Variation in absolute potencies of GCG and oxyntomodulin at GCGR

When investigating the GCG and oxyntomodulin induced cAMP response, there were found to be clear differences between the responses measured in two cell lines; HEK 293T (gifted from Professor Colin Taylor in the Department of Pharmacology) and HEK 293 cells transiently transfected with pmCherry-N1 expressing GCGR (Figure 4.2). Here, when all variables were accounted for such as DNA concentration, DNA quality and cell confluency at transfection, the measured potencies (pEC_{50}) and maximum response (E_{max}) for each agonist were significantly different between cell lines (Table 4.2.2).

HEK 293T cells showed a reduced potency and maximal response when compared to HEK 293 cells, despite presumably expressing the temperature-sensitive allele of the SV40 T antigen. This T antigen enables the amplification of vectors containing the SV40 origin of replication and increases the expression level obtained by transfection (Lin *et al.*, 2014).

The differences between these two cell lines tested, and indeed other cell lines, is likely due to a number of cellular variables. One big variable is likely to be the cytosolic signalling molecules that interact with the agonist bound receptor either directly or indirectly ultimately leading to the cellular response. In other words, some cell lines will have the ability to amplify the response to a greater extent than another. It appears that these two cell lines differ in sensitivity to the agonist stimulation i.e. the ability to transduce the signal. HEK 293 may have an increased receptor density and stimulus-response efficiency when compared to HEK 293T leading to the increased maximal response and potency of the agonist. This is reflected by the smaller $\log \tau$ values in HEK 293T compared to HEK 293 cells (Table 4.2). These findings highlight what is often seen in science, where the reported potency for a ligand can be very different between laboratory groups and is likely to depend on the assay system and cell lines used. This particular HEK 293T cell lines were not used in further experiments, and others were acquired

which showed a greater GCGR stimulated cAMP response for experiments detailed later (Section 4.3 and 4.5).

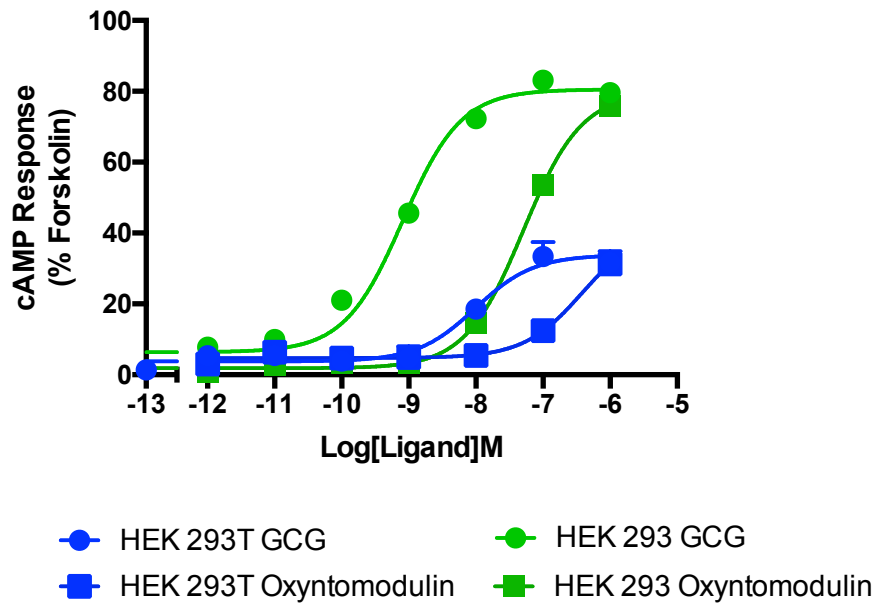


Figure 4.2. cAMP responses in GCGR transfected HEK 293T and HEK 293 cells. HEK 293T and HEK 293 (cells transiently expressing pmCherry-N1 vector containing GCGR (24 hours post transfection) were exposed to GCG or oxyntomodulin for 8 minutes and cAMP accumulation detected. All values are mean \pm SEM expressed as percentage forskolin response (for each individual cell line) where $n \geq 5$ independent experimental repeats, conducted in duplicate.

Table 4.2. cAMP responses in GCGR transfected HEK 293T and HEK 293 cells. Potency (pEC_{50}), maximal response (E_{max}), basal, span, affinity (pK_A) and coupling efficacy ($\log \tau$) for GCG or oxyntomodulin measured in GCGR transfected HEK 293 cells using a cAMP assay

GCG						
Cell line	pEC_{50}^a	E_{max}^b	Basal ^c	Span ^d	pK_A^e	$\log \tau^f$
HEK 293	9.04 ±0.1	80.5 ±1.7	6.1 ±1.2	74.4 ±1.7	8.37 ±0.1	0.58 ±0.05
HEK 293T	8.00 ±0.2***	33.8 ±2.1***	3.8 ±1.2	30.1 ±2.3***	7.84 ±0.2	-0.34 ±0.04***
Oxyntomodulin						
Cell line	pEC_{50}^a	E_{max}^b	Basal ^c	Span ^d	pK_A^e	$\log \tau^f$
HEK 293	7.27±0.1	81.5 ±2.1	0.9 ±1.0	80.6 ±2.1	6.54 ±0.1	0.64 ±0.06
HEK 293T	6.42 ±0.2***	41.4 ±8.3***	4.7 ±1.0	36.6 ±8.1***	6.21 ±0.2	-0.20 ±0.36***

HEK 293 cells or HEK 293T cells (1000 cells/well) transiently transfected with pmCherry-N1 containing GCGR were stimulated with GCG for 8 minutes prior to measurement of cAMP accumulation to generate concentration response curves. To calculate pEC_{50} , E_{max} , Basal and Span values, data were analysed using a three-parameter logistic equation. Data was also analysed by an operational model of agonism (Black and Leff, 1983) to determine affinity (pK_A) and coupling efficacy ($\log \tau$).

^a Negative logarithm of GCG concentration required to produce a half-maximal response

^b Maximal response to GCG as percentage forskolin response (to each individual cell line)

^c The low plateau of the fitted sigmoidal dose-response curve

^d The difference between E_{max} and basal signalling

^e The negative logarithm of functional affinities that describes the affinity of the receptor when coupled to a given signalling pathway generated through use of the operational model for partial agonism

^f τ is the coupling efficiency parameter generated through use of the operational model for partial agonism

All values are mean ± SEM expressed as % WT forskolin response where $n \geq 5$ independent experimental repeats, conducted in duplicate.

Statistical significance (*, $p < 0.05$; **, $p < 0.01$; ***, $p < 0.001$) compared to response in HEK 293 cells for each ligand was determined by unpaired Student's t-test (two-tailed).

4.2.3. Mammalian expression vectors: A comparison of cAMP signalling in GCGR transfected HEK 293

4.2.3.1. Measured potency varies between vectors

Transfection, the introduction of foreign nucleic acid into cells, was used extensively in this work for the characterisation of GCGR pharmacology. The gene of interest was cloned into an expression vector (plasmid), which directed the host cellular machinery to express the protein of interest. Here, we investigate the cAMP response in HEK 293 cells transfected with one of three different vectors expressing GCGR

HEK 293 cells were transfected with pmCherry-N1, pcDNA3.1 or pVITRO1 (Table 4.3) expressing GCGR and stimulated for 8 minutes with GCG or oxyntomodulin (24-hours post transfection) prior to measurement of cAMP accumulation. The GCG and oxyntomodulin responses measured in HEK 293 cells transfected with GCGR containing pmCherry-N1 vector showed significantly lower potency when compared to the potency determined in cells transfected with pcDNA3.1 or pVITRO1 expressing GCGR (Figure 4.3 and Table 4.4). This finding could indicate a receptor with reduced signalling capability, possibly as a consequence of the mCherry-tag. The maximal response for both GCG and oxyntomodulin were not significantly different between vectors. However, the measured affinity and coupling efficacy of both ligands were determined to be greater in pcDNA3.1 and pVITRO1 transfected cells when compared to pmCherry-N1.

Table 4.3. Size, promoter and enhancers present in three mammalian expression vectors.

Vector	Size (bp)	Promoter	Enhancer
pmCherry-N1	4722	CMV	CAG
pcDNA3.1	5428	CMV	CAG
pVITRO1	6295	rEF-1 α /mEF-1 α	CMV/SV40

Cytomegalovirus immediate-early promoter (CMV)
rat/mouse elongation factor 1 α promoter (rEF-1 α / mEF-1 α).
Simian virus 40 (SV40) enhancer

4.2.3.2. Significantly elevated basal for pcDNA3.1 and pVITRO1 when compared to pmCherry-N1 expressing GCGR

Despite cAMP assay optimisations including time-post transfection the assay was conducted, cell density and ligand stimulation time (Section 3.2), the basal response in HEK 293 cells transfected with either GCGR containing pcDNA3.1 or pVITRO1 was elevated at low concentration of GCG stimulation (0.01 pM to 1 pM), whereas at the 'true basal' stimulation point (no ligand), the response aligned with zero percentage forskolin response (Figure 4.3).

There was a significantly elevated basal response to GCG and reduced span, in pcDNA3.1 and pVITRO1 when compared to pmCherry-N1 (Table 4.4). This finding could indicate that GCGR expression is higher from pcDNA3.1 and pVITRO1 vectors leading to greater GCGR cell-surface expression and activation over the 8-minute stimulation period at very low ligand concentrations. The reduced span in the GCG stimulated cAMP response in pcDNA3.1 and pVITRO1 is most probably a consequence of this elevated basal response, leading to a smaller signalling window.

An elevated basal cAMP response was only seen for oxyntomodulin stimulation in HEK 293 cells transfected with pVITRO1 expressing GCGR; possibly suggesting that expression from pVITRO1 is superior to pcDNA3.1. In a mammalian expression vector, the promoter is used to drive the gene expression and vary in strength depending on the cellular context. Interestingly, pVITRO1 has a different promoter when compared to the other two vectors tested and may offer an explanation to a superior expression level. Indeed, a systematic comparison between various promoters in a number of cell types revealed elongation factor 1 α promoter (EF-1 α) (present in pVITRO1, Table 4.4) to show consistently strong expression in all cell types tested, including HEK 293T cells (Qin *et al.*, 2010). On the other hand, the CMV promoter showed variability in expression across cell types with very strong promotion shown in HEK 293T cells (Qin *et al.*, 2010).

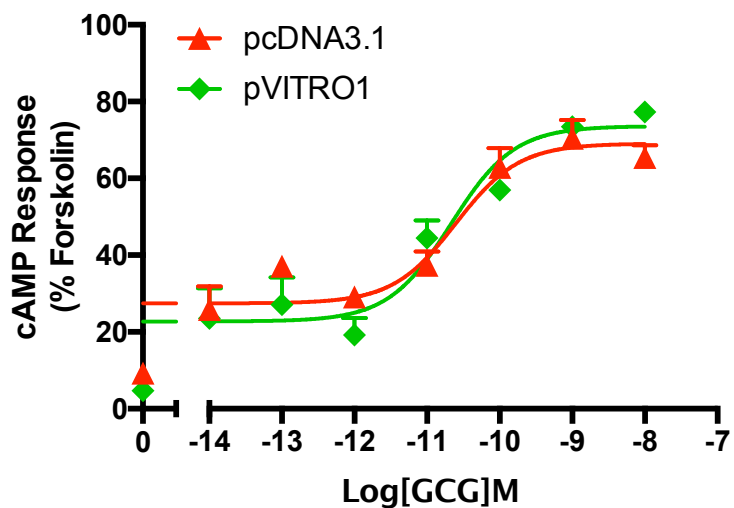


Figure 4.3. cAMP response in HEK 293 cells transfected with pcDNA3.1 or pVITRO1 expressing GCGR. HEK 293 cells transiently (24 hours post transfection) expressing GCGR containing pcDNA3.1 or pVITRO1 were exposed to GCG for 8 minutes and cAMP accumulation detected. All values are mean \pm SEM expressed as percentage forskolin response where $n \geq 5$ independent experimental repeats, conducted in duplicate.

Table 4.4. cAMP response in HEK 293 cells transfected with pmCherry-N1, pcDNA3.1 or pVITRO1 expressing GCGR. Potency (pEC_{50}), maximal response (E_{max}), basal, span, affinity (pK_A) and coupling efficacy ($\log\tau$) for GCG and oxyntomodulin measured in various GCGR containing vector transfected HEK 293 cells using a cAMP assay

GCG						
HEK 293						
Construct	pEC_{50}^a	E_{max}^b	Basal ^c	Span ^d	pK_A^e	$\log\tau^f$
pmCherry-N1	9.04 ± 0.1	80.5 ± 1.7	6.1 ± 1.2	74.4 ± 1.7	8.37 ± 0.1	0.58 ± 0.05
pcDNA3.1	10.59 ± 0.3**	69.0 ± 3.8	29.7 ± 3.6***	39.3 ± 5.0***	10.23 ± 0.3***	0.10 ± 0.10**
pVITRO1	10.59 ± 0.3**	73.9 ± 4.3	26.6 ± 4.3**	47.3 ± 5.1**	10.15 ± 0.3***	0.26 ± 0.11
Oxyntomodulin						
HEK 293						
Construct	pEC_{50}^a	E_{max}^b	Basal ^c	Span ^d	pK_A^e	$\log\tau^f$
pmCherry-N1	7.27 ± 0.1	69.3 ± 4.5	0.9 ± 1.0	66.7 ± 2.1	6.54 ± 0.1	0.64 ± 0.06
pcDNA3.1	8.98 ± 0.1***	61.1 ± 2.7	5.0 ± 2.8	56.1 ± 3.7	8.59 ± 0.2***	0.16 ± 0.05***
pVITRO1	8.82 ± 0.1***	72.5 ± 2.2	12.1 ± 2.1**	60.5 ± 3.0	8.32 ± 0.1***	0.34 ± 0.05**

^a Negative logarithm of GCG concentration required to produce a half-maximal response

^b Maximal response to GCG as percentage forskolin response

^c The low plateau of the fitted sigmoidal dose-response curve

^d The difference between E_{max} and basal signalling

^e The negative logarithm of functional affinities that describes the affinity of the receptor when coupled to a given signalling pathway generated through use of the operational model for partial agonism

^f τ is the coupling efficiency parameter generated through use of the operational model for partial agonism
All values are mean ± SEM expressed as % WT forskolin response where $n \geq 5$ independent experimental repeats, conducted in duplicate.

Statistical significance (*, $p < 0.05$; **, $p < 0.01$; ***, $p < 0.001$) compared to response in GCGR containing pmCherry-N1 vector transfected cells was determined by one-way ANOVA with Dunnett's post test

4.2.4. Summary

The results presented here confirm the concentration-dependent increase in cAMP concentration following both GCG or oxyntomodulin stimulation at the GCGR. As previously reported (Weston *et al.*, 2015), oxyntomodulin was confirmed to be significantly reduced in potency and affinity (as measured using the operational model of agonism (i.e. indirect)) when compared to GCG. There was also found to be a concentration-dependent increase in cAMP accumulation following GLP-1(7-36)amid stimulation but with a significantly reduced potency, affinity and efficacy. This latter finding confirms previous findings reporting the activity of GLP-1(7-36)amide at the GCGR (Weston *et al.*, 2015).

Interestingly, depending on the chosen cellular model, there was found to be variation in measured potency and maximal response with a lower potency response measured to both GCG and oxyntomodulin stimulation in HEK 293T cells when compared to HEK 293 cells. These measured differences between HEK 293 and HEK 293T cells, and indeed other cell lines, is likely due to a number of cellular variables. One big variable is likely to be the cytosolic signalling molecules that interact with the agonist bound receptor either directly or indirectly ultimately leading to the cellular response. In other words, some cell lines will have the ability to amplify the response to a greater extent than another. Indeed, the absolute potency of an agonist at GPCRs is not only dependent on the affinity and intrinsic efficacy operating at the level of that particular receptor, but also on the properties of the assay system (Kenakin *et al.*, 2012). The assay system is a complex combination of receptor density and factors that translate the receptor stimulus into cellular response (stimulus-response mechanisms) (Kenakin, 2003). These findings presented here highlight that the potency measured for a particular ligand is variable and is likely to depend on a number of factors including the cell line, receptor expression systems and chosen assay.

Similarly, the measured parameters were also dependent on the chosen vector with reduced potency, affinity and efficacy measured in cells transfected with GCGR containing pmCherry-N1 when compared to pcDNA3.1 or pVITRO1. The similar 260/280 nm ratio of all three DNA constructs indicating similar DNA quality, determined using a Nanodrop Lite (Thermo Fisher Scientific), and similar size of the plasmids (Table 4.3) suggests these variable cannot account for the differences in potency for GGC or oxyntomodulin measured between vectors. Similarly, differences in vector promoters cannot explain these findings given that both pcDNA3.1 and pmCherry-N1 have the same CMV promoter. Given the vectors are not identical, they are likely to be transcribed differently regardless of the type of promoter. The reduced potency, affinity and efficacy of GCG and oxyntomodulin at the mCherry-tagged GCGR suggest this C-terminal addition may be interfering with the signalling at the GCGR. However, the ability to visualise the receptor makes it an invaluable tool for the investigation of GCGR signalling.

4.3. Investigating the intracellular Ca^{2+} response at the GCGR

4.3.1 GCG and oxyntomodulin stimulates intracellular Ca^{2+} response at GCGR

In addition to the classical G_s -coupled GCGR pathway, studies have highlighted the possibility that GCGR couples to alternative G proteins such as $G_{q/11}$ (Xu and Xie, 2009, Wakelam *et al.*, 1986). Having demonstrated that GCG and oxyntomodulin stimulation at the GCGR induces a concentration-dependent increase in cAMP, we next sought to investigate if a number of peptide ligands acting at the GCGR (Section 4.2.1) result in intracellular Ca^{2+} (Ca^{2+i}) release from the endoplasmic reticulum (ER) and if this response was $G_{q/11}$ mediated.

HEK 293T cells transfected with pmCherry-N1 expressing GCGR and GCGR stably expressing CHO-K1 cells were stimulated with increasing concentrations of GCG, oxyntomodulin or GLP-1(7-36)amide and the Ca^{2+} i mobilisation measured using a FlexStation® Multi-Mode Microplate Reader. The results are presented as changes in Ca^{2+} i concentration over time to each ligand concentration in transfected HEK 293 and stable CHO-K1 cells (Figure 4.4 and 4.6, respectively) and as dose-response curves through fitting the highest response at each ligand concentration to a three-parameter logistics equation (Figure 4.5 and 4.7, respectively). A robust concentration-dependent increase in Ca^{2+} i response was detected following stimulation with GCG or oxyntomodulin in both cell lines (Table 4.5). Importantly, these Ca^{2+} i responses measured at the highest ligand concentration were abolished through a 30-minute pre-treatment with the specific $G_{q/11}$ inhibitor, YM-254890 (Takasaki *et al.*, 2004 and Section 3.4.4), thereby confirming the Ca^{2+} i response is $G_{q/11}$ mediated.

In both cell lines, oxyntomodulin was shown to have significantly reduced potency when compared to GCG. In HEK 293T cells, oxyntomodulin showed a similar maximum response when compared to GCG identifying it as a lower potency full agonist of the GCGR mediated Ca^{2+} i response. However, in CHO-K1 cells stably expressing GCGR, oxyntomodulin showed a reduced maximal response suggesting it is partial agonist of the Ca^{2+} i response rather than a full agonist.

Despite similar potencies for the measured Ca^{2+} i in each cell line for each ligand, in HEK 293T cells oxyntomodulin was demonstrated to have reduced affinity when compared to GCG whereas in CHO-K1 cells oxyntomodulin showed similar affinity yet reduced efficacy when compared to GCG. These findings reflect those previously reported for the cAMP response findings (Figure 4.2) suggesting differences in measured responses between cell lines. These differences are likely due to a number of cellular variables such as differences in cytosolic signalling molecules that interact with the

agonist bound receptor either directly or indirectly ultimately leading to variable cellular responses.

A Ca^{2+} response to GLP-1(7-36)amide was only determined at the highest tested concentration (100 μM) in HEK 293T cells and as such, a true dose-response curve could not be fitted due to insufficient data points. The response at 100 μM was abolished with a 30 minute pre-treatment with YM-254890 thereby indicating that this response was $G_{\alpha_q/11}$ mediated. These data suggest the activity of GLP-1(7-36)amide is very weak at inducing an Ca^{2+} response through GCGR. Alternatively such high concentration of ligand may force the receptor into an interaction/active state, which would otherwise not occur. When tested in GCGR stably expressing CHO-K1 cells, although a response at 100 μM GLP-1(7-36)amide was not tested, no response was detected at a concentration of 10 μM (Figure 4.6 C).

The findings presented here highlight that ligand activated GCGR is not only able to couple to G_s leading to concentration-dependent increases in cAMP, but can also induce a $G_{q/11}$ mediated Ca^{2+} response.

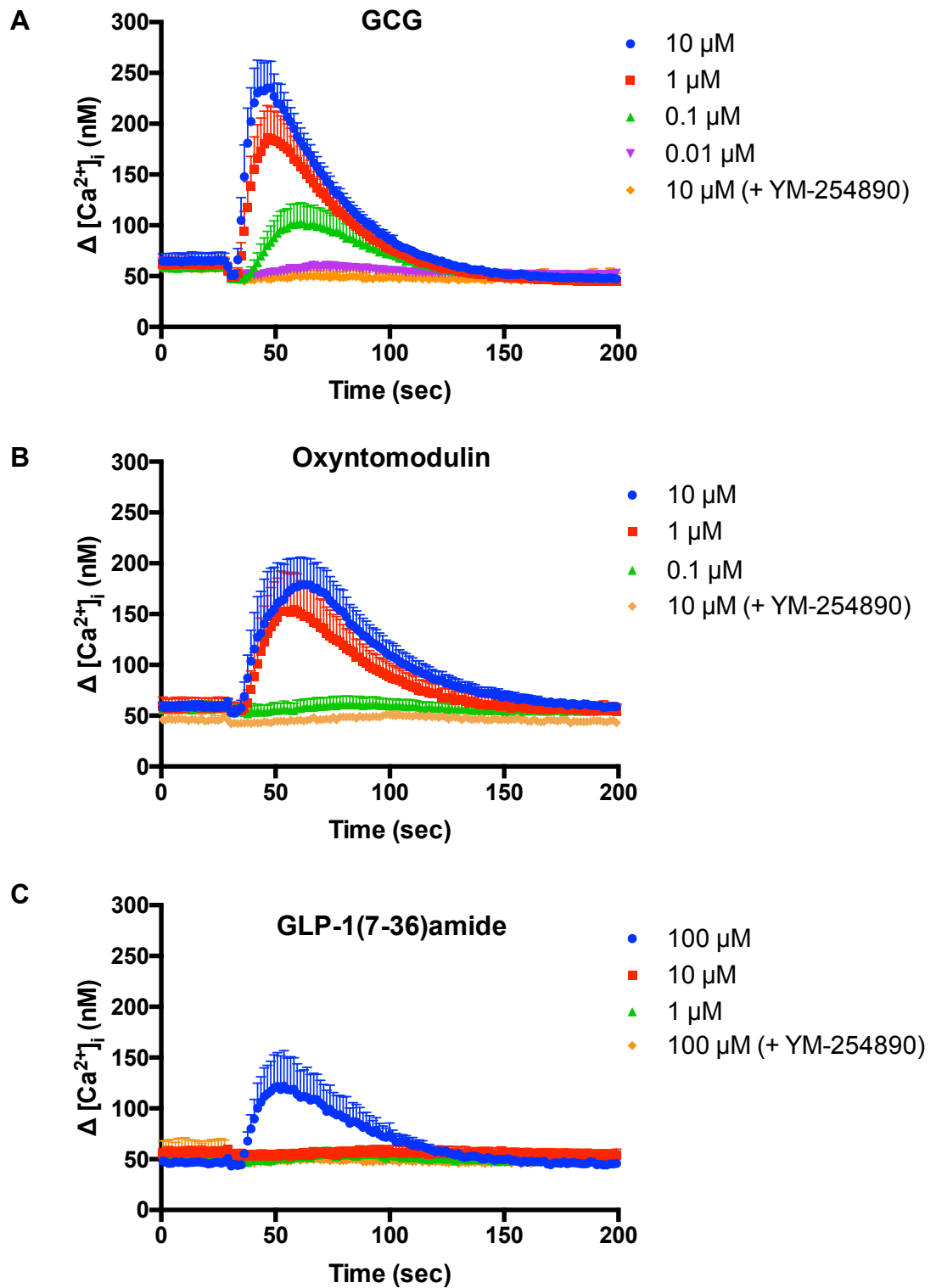


Figure 4.4 Ca^{2+}_i mobilisation in HEK 293T cells expressing GCGR +/- YM-254890 treatment. HEK 293T cells transiently expressing pVITRO1 vector containing mCherry-tagged GCGR (48 hours post transfection) received 30 minutes treatment with YM-254890 (100 nM) or DMSO control immediately prior to ligand stimulation with **A**) GCG, **B**) oxyntomodulin or **C**) GLP-1(7-36)amide and Ca^{2+}_i mobilisation measured. All values are mean \pm SEM expressed change in Ca^{2+}_i where $n \geq 3$ independent experimental repeats, conducted in duplicate.

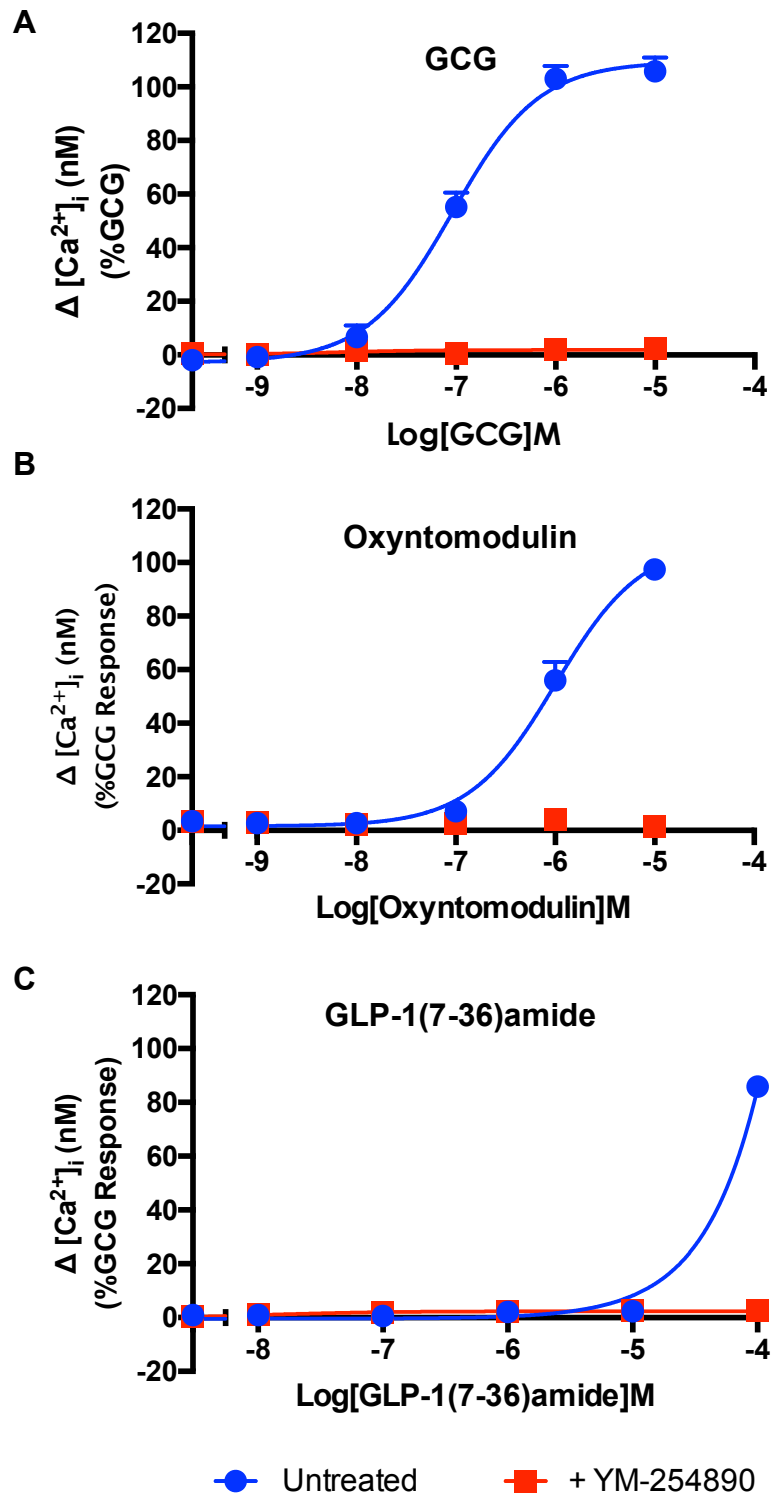


Figure 4.5. Ca^{2+}_i mobilisation dose-response in HEK 293T cells expressing GCGR +/- YM-254890 treatment. HEK 293T cells transiently expressing pVITRO1 vector containing mCherry-tagged GCGR (48 hours post transfection) received 30 minutes treatment with YM-254890 (100 nM) or DMSO control immediately prior to ligand stimulation with **A**) GCG, **B**) oxyntomodulin or **C**) GLP-1(7-36)amide and Ca^{2+}_i mobilisation measured. All values are mean \pm SEM expressed as percentage GCG response where $n \geq 3$ independent experimental repeats, conducted in duplicate.

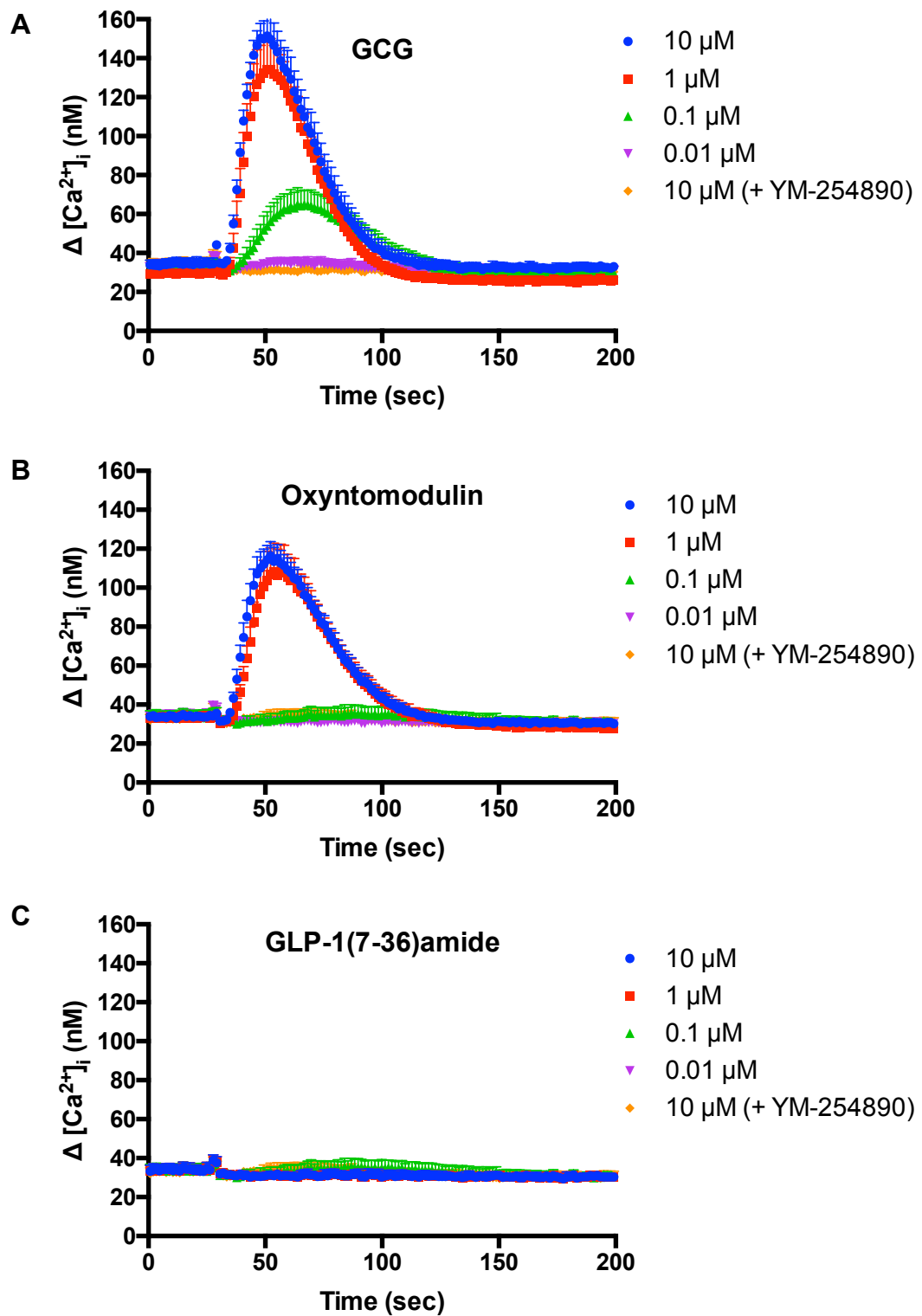


Figure 4.6. Ca^{2+}_i mobilisation in GCGR stably expressing CHO-K1 cells +/- YM-254890 treatment. CHO-K1 cells stably expressing GCGR stimulation with **A)** GCG, **B)** oxyntomodulin or **C)** GLP-1(7-36)amide at various concentrations and Ca^{2+}_i mobilisation measured. All values are mean \pm SEM expressed as change in intracellular Ca^{2+} (Ca^{2+}_i) where $n \geq 3$ independent experimental repeats, conducted in duplicate.

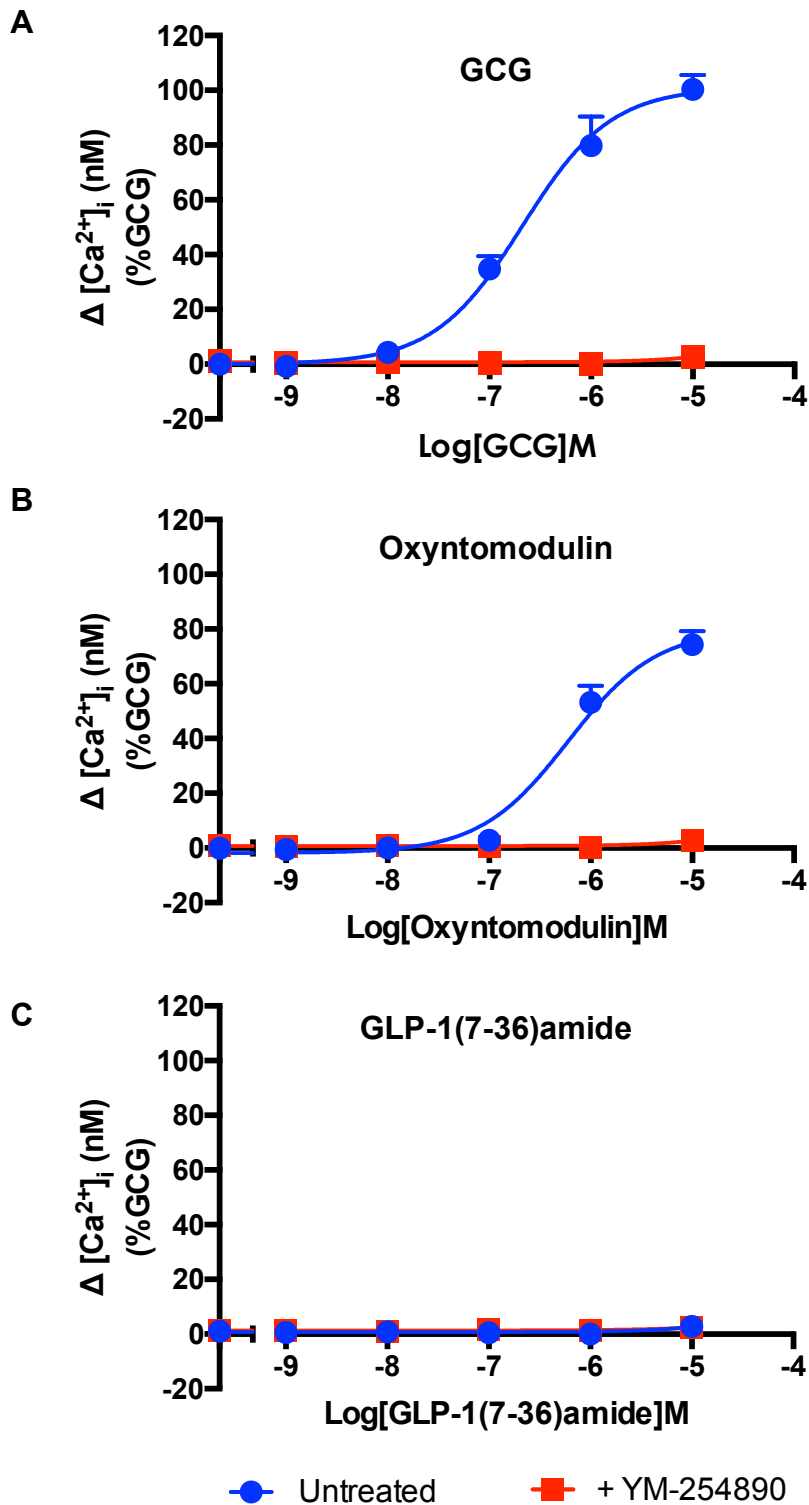


Figure 4.7. Ca^{2+}_i mobilisation dose-response in GCGR stably expressing CHO-K1 cells +/- YM-254890 treatment. CHO-K1 cells stably expressing GCGR received 30 minutes treatment with YM-254890 (100 nM) or DMSO control immediately prior to ligand stimulation with A) GCG, B) oxyntomodulin or C) GLP-1(7-36)amide and Ca^{2+}_i mobilisation measured. All values are mean \pm SEM expressed as percentage GCG response where $n \geq 3$ independent experimental repeats, conducted in duplicate.

Table 4.5. Ca²⁺i mobilisation dose-response in GCGR expressing cell lines +/- YM-254890 treatment Potency (pEC₅₀), maximal response (E_{max}), basal, span, affinity (pK_A) and coupling efficacy (log τ) for GCG, oxyntomodulin or GLP-1(7-36)amide stimulated Ca²⁺i measured in GCGR transfected HEK 293T cells or GCGR stably expressing CHO-K1 cells +/- YM-254890 treatment

HEK 293T						
Ca ²⁺ i						
Ligand	pEC ₅₀ ^a	E _{max} ^b	Basal ^c	Span ^d	pK _A ^e	log τ ^f
GCG	7.01 ±0.13	103.6 ±5.7	-0.1 ±4.4	103.7 ±6.8	6.12 ±0.15	0.86 ±0.11
GCG (+ YM-254890)		N.R	-1.1 ±2.4		N.R	
Oxyntomodulin	6.00 ±0.07***	107.9 ±6.1	1.5 ±1.7	106.4 ±6.1	5.14 ±0.21**	0.79 ±0.18
Oxyntomodulin (+ YM-254890)		N.R	0.4 ±1.6		N.R	
GLP-1		N.D#	1.0 ±1.3		N.D#	
GLP-1 (+ YM-254890)		N.R	-0.2 ±1.2		N.R	
CHO-K1						
Ca ²⁺ i						
Ligand	pEC ₅₀ ^a	E _{max} ^b	Basal ^c	Span ^d	pK _A ^e	log τ ^f
GCG	6.68 ±0.11	101.0 ±4.1	0.0 ±3.0	101.0 ±4.8	5.88 ±0.18	0.73 ±0.11
GCG (+ YM-254890)		N.R	0.2 ±1.0		N.R	
Oxyntomodulin	6.22 ±0.12*	79.9 ±4.1**	-1.9 ±2.3	81.7 ±4.4*	5.74 ±0.15	0.31 ±0.06*
Oxyntomodulin (+ YM-254890)		N.R	1.0 ±2.0		N.R	
GLP-1		N.R	0.3 ±1.5		N.R	
GLP-1 (+ YM-254890)		N.R	2.7 ±2.3		N.R	

GCGR transfected HEK 293T cells received 30 minutes treatment with YM-254890 (100 nM) or DMSO control immediately prior to stimulation with GCG, oxyntomodulin or GLP-1(7-36)amide and measurement of Ca^{2+} ; response to generate concentration response curves. To calculate pEC_{50} , E_{max} , Basal and Span values, data were analysed using a three-parameter logistic equation. Data was also analysed by an operational model of agonism (Black and Leff, 1983) to determine affinity (pK_A) and coupling efficacy ($\log \tau$).

^a Negative logarithm of ligand concentration required to produce a half-maximal response

^b Maximal response to ligand as percentage GCG response

^c The low plateau of the fitted sigmoidal dose-response curve

^d The difference between E_{max} and basal signalling

^e The negative logarithm of functional affinities that describes the affinity of the receptor when coupled to a given signalling pathway generated through use of the operational model for partial agonism

^f τ is the coupling efficiency parameter generated through use of the operational model for partial agonism

All values are mean \pm SEM expressed percentage GCG response where $n \geq 5$ independent experimental repeats, conducted in duplicate.

Statistical significance (*, $p < 0.05$; **, $p < 0.01$; ***, $p < 0.001$) in the difference between GCG and oxyntomodulin stimulated response was determined by one-way unpaired Student's t-test (two-tailed).

N.D# denotes a response were a true dose-response curve could not be generated due to insufficient data points

N.R denotes no response

4.4. Investigating the ERK1/2 response at the GCGR

4.4.1. GCG stimulates a ERK1/2 response in three GCGR expressing cell lines

ERK activation is described to be downstream of both G protein (G_s , G_i , G_q and the $G_{\beta\gamma}$ subunit) and β -arrestin mediated pathways, which are independent of each other (DeWire *et al.*, 2007). Here, I sought to investigate the signalling components important in the GCGR-mediated ERK1/2 activation.

Using three alternative GCGR expressing cell lines, either stable CHO-K1 (10,000 cells/well) or transfected HEK 293T or HEK 293 cells (50,000 cells/well) and the (HTRF)[®] Phospho-ERK (Thr202/Tyr204) Cellular Assay Kit, we initially tested the pERK1/2 response following a 5 minute stimulation with GCG. A pERK1/2 response was measured following GCG stimulation in all three cell lines tested, with no significant difference in potency. CHO-K1 cells stably expressing GCGR following stimulation with GCG showed a pERK1/2 response that was larger than the measured PMA response (E_{max} 191.9 \pm 11.3 percentage PMA response (1 μ M)). A pERK1/2 response was also measured following GCG stimulation in HEK 293T and HEK 293 cells transfected with pmCherry-N1 expressing GCGR, although the maximal response was reduced in comparison to that seen in CHO-K1 cells (Figure 4.8 and Table 4.6). This discrepancy in maximal response between HEK 293T/HEK 293 cells and CHO-K1 cells was despite the facts 1/5 of the number of cells were used (10,000 cells per well when compared to 50,000 cells per well). There are two potential interpretations as to why a significant difference in the maximum pERK1/2 response occurred, which may or may not be independent. Firstly, CHO-K1 cells may contain a greater level of the signalling components involved in the ERK1/2 response downstream of the receptor itself or there may be greater level of coupling to pathways leading to pERK1/2. Interestingly, Cisbio Bioassays provide a kit to measure total ERK1/2 (Total ERK1/2 Cellular Assay Kit) and validation experiments

performed by the company measuring the total ERK1/2 in various cell lines showed a similar but slightly greater level of total ERK1/2 in HEK 293 cells when compared to CHO-K1 cells. This suggests that difference in total ERK1/2 was unlikely to account for this increased pERK1/2 response seen in CHO-K1 cells, although differences in other signalling components may indeed provide an explanation.

Alternatively, the difference in response may be a consequence of receptor expression levels. In the stable CHO-K1 cells, where GCGR expression is expressed across the population this response is likely to be amplified providing a bigger signalling window. In GCGR transfected cells the levels of receptor expression may be lower in comparison to these CHO-K1 cells and as a result, we may be at the lower end of the assays dynamic range.

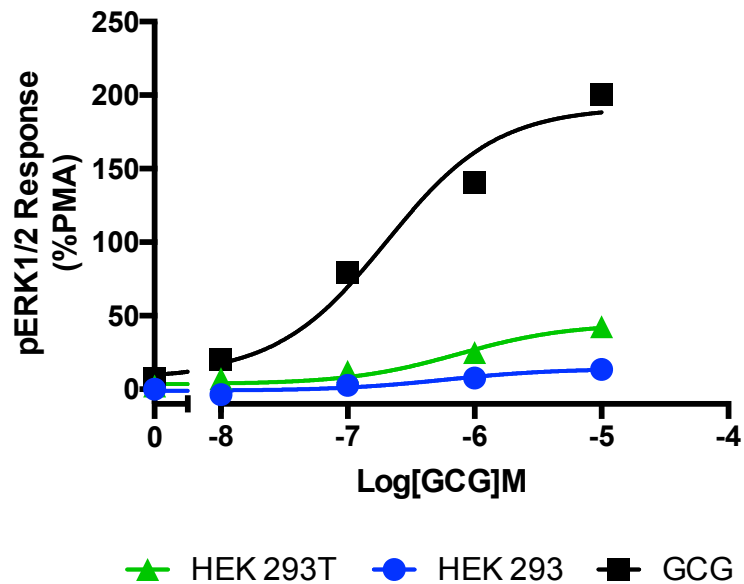


Figure 4.8. GCG stimulated pERK1/2 response in three alternative cell lines. HEK 293T or HEK 293 cells transiently expressing pmCherry-N1 vector containing GCGR (48 hours post transfection) or CHO-K1 cells stably expressing GCGR were serum starved for 24 hours and exposed to GCG for 5 minutes before measuring pERK1/2. CHO-K1 cells were plated at 10,000 cells per well in a 384-well plate whereas for HEK 293T and HEK 293 cells 50,000 cells per well were plated. All values are mean \pm SEM expressed as percentage PMA response (1 μ M) where $n \geq 5$ independent experimental repeats, conducted in duplicate.

Table 4.6. GCG stimulated pERK1/2 response in three alternative cell lines. Potency (pEC_{50}), maximal response (E_{max}), basal, span, affinity (pK_A) and coupling efficacy ($\log \tau$) for GCG in three cell lines expressing GCGR measured using a pERK1/2 assay

Construct	GCG					
	pEC_{50}^a	E_{max}^b	Basal ^c	Span ^d	pK_A^e	$\log \tau^f$
HEK 293T	6.12 \pm 0.19	44.7 \pm 4.3	3.5 \pm 1.8	41.2 \pm 4.5	6.02 \pm 0.2	-0.58 \pm 0.06
HEK 293	6.23 \pm 0.35	14.0 \pm 2.6*	1.0 \pm 1.4	15.0 \pm 2.8	6.20 \pm 0.4	-1.09 \pm 0.09*
GCGR CHO-K1	6.89 \pm 0.20	191.9 \pm 11.3***	5.8 \pm 9.3	182.8 \pm 13.0***	6.26 \pm 0.3	0.51 \pm 0.15***

CHO-K1 cells stably expressing GCGR and HEK 293T or HEK 293 cells transiently expressing GCGR were stimulated with GCG prior to measurement of pERK1/2 to generate concentration response curves for each construct. To calculate pEC_{50} , E_{max} , Basal and Span values, data were analysed using a three-parameter logistic equation. Data was also analysed by an operational model of agonism (Black and Leff, 1983) to determine affinity (pK_A) and coupling efficacy ($\log \tau$).

^a Negative logarithm of GCG concentration required to produce a half-maximal response

^b Maximal response to GCG as percentage PMA response (normalised to individual maximum PMA response at 1 μ M PMA)

^c The low plateau of the fitted sigmoidal dose-response curve

^d The difference between E_{max} and basal signalling

^e The negative logarithm of functional affinities that describes the affinity of the receptor when coupled to a given signalling pathway generated through use of the operational model for partial agonism

^f τ is the coupling efficiency parameter generated through use of the operational model for partial agonism
 Statistical significance (*, $p < 0.05$; **, $p < 0.01$; ***, $p < 0.001$) compared to HEK 293T cells transfected with GCGR (pmCherry-N1 vector) was determined by one-way ANOVA with Dunnett's post test

4.4.2. Measured potency of GCG and oxyntomodulin stimulated pERK1/2 response is cell line dependent

4.4.2.1. pERK1/2 response in GCGR transfected HEK 293T cells and GCGR stable CHO-K1 cells

Having established GCG induces a pERK1/2 response in various GCGR expressing cell lines, we next wanted to investigate if the GCG related peptide, oxyntomodulin, is also able to induce a pERK1/2 response in HEK 293T cells transfected with pmCherry-N1 expressing GCGR and CHO-K1 cells stably expressing GCGR.

Similar to GCG, oxyntomodulin induced a concentration-dependent increase in pERK1/2 in both GCGR expressing CHO-K1 and HEK 293T cells (Figure 4.9). The pERK1/2 response to GCG and oxyntomodulin in transfected HEK 293T cells showed no significant difference between measured potency, maximal response, affinity and efficacy (Figure 4.9 A and Table 4.7). In CHO-K1 cells stably expressing GCGR, again a similar maximum response was measured for GCG and oxyntomodulin, but oxyntomodulin showed a significant reduced potency (pEC_{50} 6.89 ± 0.2 and 5.85 ± 0.1 , respectively) and affinity (Figure 4.9 B and Table 4.7). A reduced potency was also found for the oxyntomodulin stimulated cAMP response measured in GCGR expressing cell lines (Section 4.2.1). This finding suggests oxyntomodulin has a reduced potency when compared to GCG at inducing pathways leading to both cAMP and pERK1/2 elevation.

It may be that the indistinguishable responses for GCG and oxyntomodulin in transfected HEK 293T cells is due to an experimental limitations rather than true cellular differences between HEK 293T and CHO-K1 cells. If this is the case, caution is required when interpreting such data particularly in the case where cell lines are used with particularly small pERK1/2 responses (E_{max}) such as that seen in transfected HEK 293 (Figure 4.8). Increasing the cell number above 50,000 per well is not recommended by the pERK1/2 assay kit supplier (Cisbio Bioassays), therefore in order to

maximise the signalling window for the measurable pERK1/2 response within HEK 293 cells it may be necessary to create stable cell lines to ensure a greater proportion of cells express the receptor of interest.

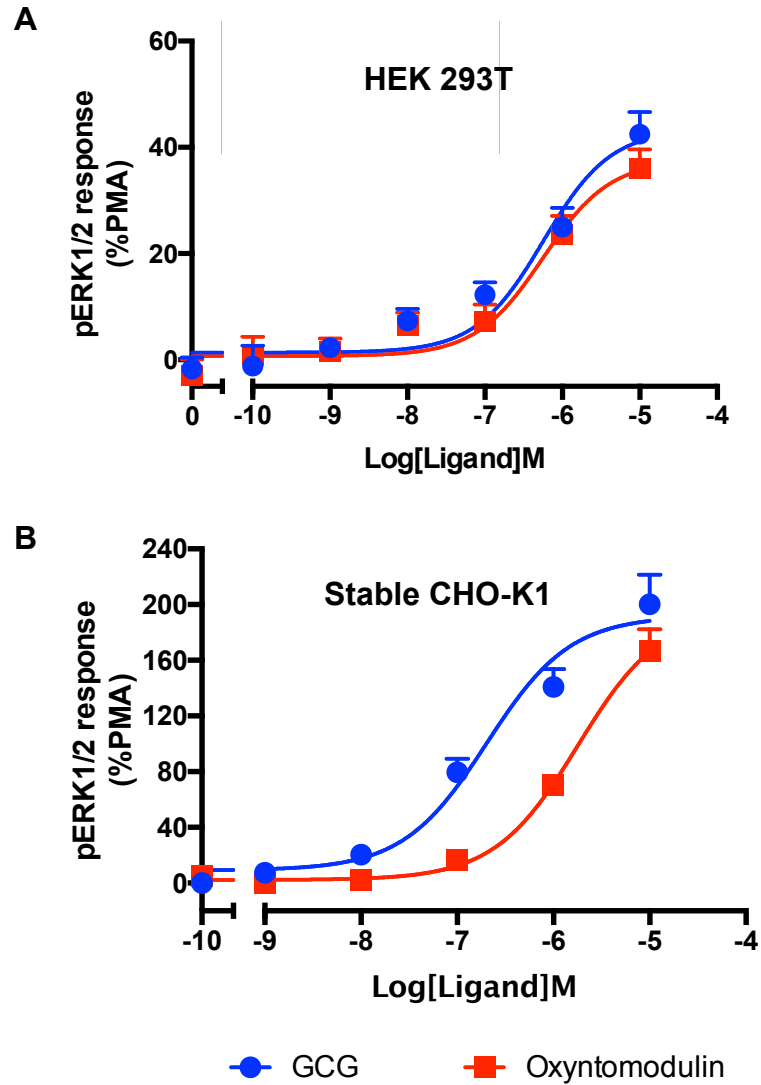


Figure 4.9. GCG and oxyntomodulin stimulated pERK1/2 response in GCGR transfected HEK 293T cells and CHO-K1 cells stably expressing GCGR. **A)** HEK 293T transiently expressing pmCherry-N1 vector containing GCGR (48 hours post transfection) or **B)** CHO-K1 cells stably expressing GCGR were serum starved for 24 hours and exposed to GCG or oxyntomodulin for 5 minutes before measuring pERK1/2. CHO-K1 cells were plated at 10,000 cells per well and HEK 293T cells at 50,000 cells per well in a 384-well plate. All values are mean \pm SEM expressed as percentage PMA (1 μ M) response where $n \geq 5$ independent experimental repeats, conducted in duplicate.

Table 4.7. GCG and Oxntomodulin stimulated pERK1/2 response in GCGR transfected HEK 293T cells and CHO-K1 cells stably expressing GCGR. Potency (pEC_{50}), maximal response (E_{max}), basal, span, affinity (pK_A) and coupling efficacy ($\log \tau$) for GCG in HEK 293T or CHO-K1 expressing GCGR measured using a pERK1/2 assay

HEK 293T						
Ligand	pEC_{50}^a	E_{max}^b	Basal ^c	Span ^d	pK_A^e	$\log \tau^f$
GCG	6.12 ±0.19	44.7 ±4.3	3.5 ±1.8	41.2 ±4.5	6.02 ±0.2	-0.58 ±0.06
Oxntomodulin	6.25 ±0.22	37.6 ±4.0	0.7 ±1.4	36.9 ±4.1	6.05 ±0.2	-0.23 ±0.08
GCGR CHO-K1						
Ligand	pEC_{50}^a	E_{max}^b	Basal ^c	Span ^d	pK_A^e	$\log \tau^f$
GCG	6.89 ±0.20	191.9 ±11.3	5.8 ±9.3	182.8 ±13.0	6.26 ±0.3	0.51 ±0.15
Oxntomodulin	5.85 ±0.13**	195.7 ±13.7	7.3 ±4.3	193.4 ±13.6	5.14 ±0.3*	0.62 ±0.18

CHO-K1 cells stably expressing GCGR or HEK 293T transiently expressing GCGR were stimulated with GCG or oxntomodulin prior to measurement of pERK1/2 to generate concentration response. To calculate pEC_{50} , E_{max} , Basal and Span values, data were analysed using a three-parameter logistic equation. Data was also analysed by an operational model of agonism (Black and Leff, 1983) to determine affinity (pK_A) and coupling efficacy ($\log \tau$).

^a Negative logarithm of ligand concentration required to produce a half-maximal response

^b Maximal response to ligand as percentage PMA response (normalised to maximum PMA response at 1 μ M PMA for each cell line)

^c The low plateau of the fitted sigmoidal dose-response curve

^d The difference between E_{max} and basal signalling

^e The negative logarithm of functional affinities that describes the affinity of the receptor when coupled to a given signalling pathway generated through use of the operational model for partial agonism

^f τ is the coupling efficiency parameter generated through use of the operational model for partial agonism. Statistical significance (*, $p < 0.05$; **, $p < 0.01$; ***, $p < 0.001$) compared to GCG response in HEK 293T or CHO-K1 cell line was determined by unpaired Student's t-test (two-tailed).

4.4.2.2. pERK1/2 response in a generated GCGR stable HEK 293 cell line

In an attempt to maximise the signalling window for the measurable pERK1/2 response within HEK 293 cells, a stable cell line was made to ensure a greater proportion of cells express the receptor of interest (Section 3.6.).

GCG stimulation in GCGR stably expressing HEK 293 cells induced a pERK1/2 response (Figure 4.10 and Table 4.8), which was comparable in potency (pEC_{50} 6.04 \pm 0.20) to the response in GCGR transfected HEK 293 cells and HEK 293T cells (pEC_{50} 6.23 \pm 0.35 and 6.12 \pm 0.19, respectively) (Figure 4.8 and Table 4.6). There was found to be an elevation in maximal response for this stable cell line in comparison to GCGR transiently transfected HEK 293 cells (14.0 \pm 2.6 and 30.7 \pm 3.5 percentage PMA response, respectively). This finding suggests that stable expression of GCGR does indeed increase the signalling window for pERK1/2 response analysis at the GCGR. It may be interesting to expand on these findings further by investigating the difference in GCGR cell-surface expression between stable and transiently transfected cells.

The measured potency of oxyntomodulin was not significantly different when compared to GCG (pEC_{50} 5.38 \pm 0.34 and 6.04 \pm 0.20, respectively). This finding is likely an experimental limitation where we are at the lower end of the assay dynamic range, as was suggested to be the case in transfected HEK 293T cells. Despite an increase in the signalling window with this GCGR stable HEK 293 cell line and a small difference in potency between GCG and oxyntomodulin, it could be suggested that GCGR stable CHO-K1 cells appear to be a more valuable cellular model for further investigation into pERK1/2 responses. In addition, the enhanced pERK1/2 signalling window for this stable GCGR expressing HEK 293 cell line was not considered great enough to justify repeating GCGR signalling analysis which was already done in HEK 293 cells transfected with GCGR (Section 4.2.1 and 4.3.1).

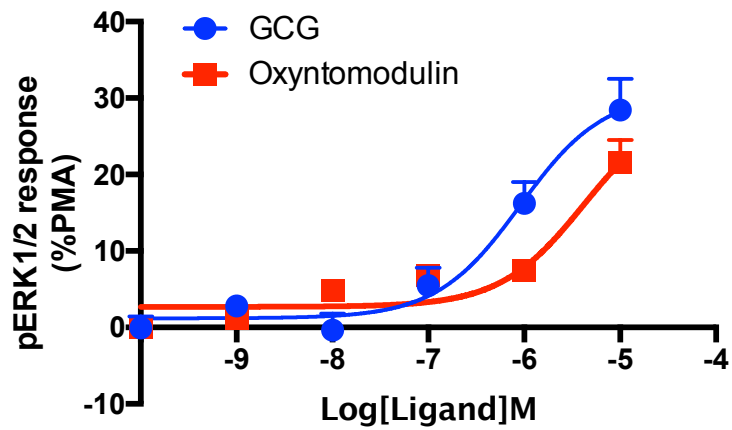


Figure 4.10. GCG and Oxyntomodulin stimulated pERK1/2 response in HEK 239 cells stably expressing GCGR. HEK 293 cells stably expressing GCGR were stimulated with GCG or oxyntomodulin for 5 minutes before measuring pERK1/2. Cells were plated at 50,000 cells per well in a 384-well plate. All values are mean \pm SEM expressed as percentage PMA response (1 μ M) where $n \geq 5$ independent experimental repeats, conducted in duplicate.

Table 4.8. GCG and Oxyntomodulin stimulated pERK1/2 response in HEK 239 cells stably expressing GCGR. Potency (pEC₅₀), maximal response (E_{max}), basal, span, affinity (pK_A) and coupling efficacy (log τ) for GCG in a GCGR stable generated HEK 293 cell line measured using a pERK1/2 assay

GCGR stable HEK 293						
Ligand	pEC ₅₀ ^a	E _{max} ^b	Basal ^c	Span ^d	pK _A ^e	log τ ^f
GCG	6.04 ±0.20	30.7 ±3.5	1.2 ±1.4	29.5 ±3.6	5.89 ±0.2	-0.37 ±0.07
Oxyntomodulin	5.38 ±0.34	29.3 ±7.1	2.7 ±1.0	26.6 ±6.8	5.24 ±0.4	-0.42 ±0.15

HEK 293 cells stably expressing GCGR were stimulated with GCG or oxyntomodulin prior to measurement of pERK1/2 to generate concentration response curves for each construct. To calculate pEC₅₀, E_{max}, Basal and Span values, data were analysed using a three-parameter logistic equation. Data was also analysed by an operational model of agonism (Black and Leff, 1983) to determine affinity (pK_A) and coupling efficacy (log τ).

^a Negative logarithm of ligand concentration required to produce a half-maximal response

^b Maximal response to ligand as percentage PMA response (normalised to maximum PMA response at 1 μ M PMA for each cell line)

^c The low plateau of the fitted sigmoidal dose-response curve

^d The difference between E_{max} and basal signalling

^e The negative logarithm of functional affinities that describes the affinity of the receptor when coupled to a given signalling pathway generated through use of the operational model for partial agonism

^f τ is the coupling efficiency parameter generated through use of the operational model for partial agonism

Statistical significance (*, $p < 0.05$; **, $p < 0.01$; ***, $p < 0.001$) compared to GCG response was determined by unpaired Student's t-test (two-tailed).

4.4.3. PKA and cAMP play no role in the GCGR stimulated ERK1/2 response

Protein kinase A (PKA) is known to be an important component of ERK1/2 activation (Dumaz and Marais, 2003) (Figure 4.11) and a number of studies have utilised PKA inhibitors to indicate the importance of this signalling component in GPCR stimulated ERK1/2 activation (Gesty-Palmer *et al.*, 2006). In this work, one such inhibitor, the cAMP analogue Rp-8-bromo-cAMP (Rp-8-Br-cAMP) was used to determine the role of PKA in GCGR mediated ERK1/2 activation.

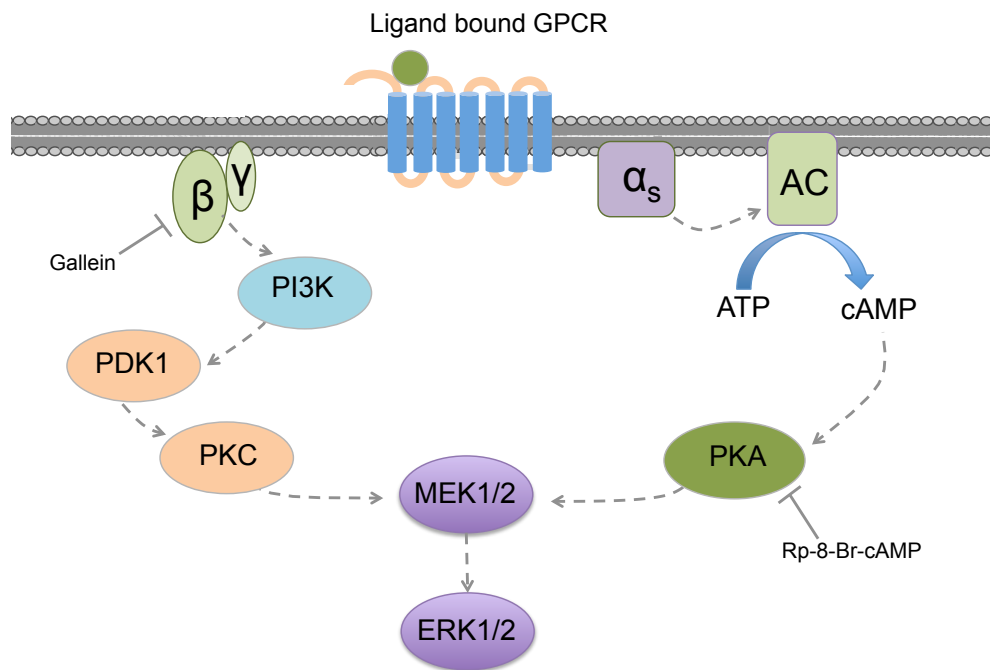


Figure 4.11. G protein mediated activation of extracellular signal-regulated kinase 1 and 2 (ERK1/2) through both α and $\beta\gamma$ subunits. Chen *et al.*, 2014 demonstrated that the G $\beta\gamma$ subunit, phosphoinositide 3-kinase (PI3K), and protein kinase C (PKC) were involved in the gland hormone melatonin 1 (MT1)-mediated activation of ERK1/2 through the GPCR, MT1 receptor. Gallein, a specific G $\beta\gamma$ small molecule inhibitor (Lehmann *et al.*, 2008), can be used to investigate the role of G $\beta\gamma$ subunit in GCGR stimulated ERK1/2 phosphorylation. GPCRs known to couple to G s stimulate intracellular cAMP formation through adenylyl cyclase (AC) which acts on protein kinase A (PKA). PKA is known to be an important component of ERK1/2 activation (Dumaz and Marais, 2003). The cAMP analogue Rp-8-bromo-cAMP (Rp-8-Br-cAMP) is a known antagonist of PKA (Schwede *et al.*, 2000) and can be used as a tool to investigate the role of PKA and upstream signalling components in GCGR mediated ERK activation.

Here, CHO-K1 cells stably expressing GCGR were pre-incubated with Rp-8-Br-cAMP (10 μ M) for 15 minutes prior to ligand stimulation and pERK1/2 measurement. CHO-K1 cells stably expressing GCGR showed a concentration-dependent pERK1/2 response to both GCG and oxyntomodulin (Figure 4.12). The potency of oxyntomodulin is lower than that detected for GCG (pEC₅₀ 6.89 \pm 0.20 and 5.85 \pm 0.13, respectively), as previously indicated (Figure 4.5). This is also the case for the cAMP response measured in these CHO-K1 cells stably expressing GCGR and suggests that oxyntomodulin has a reduced potency at the GCGR to elicit a cAMP and a pERK1/2 response when compared to GCG. Importantly, there was no induced pERK1/2 response detected following stimulation with forskolin (Figure 4.12), indicating that cAMP elevation alone could not induce a pERK1/2 response

Pre-incubation of CHO-K1 cells with the PKA inhibitor, Rp-8-bromo-cAMP, had no effect on the measured pERK1/2 response to either GCG or oxyntomodulin stimulation (Figure 4.13 and Table 4.9). The lack of significant difference between the two responses suggests that both GCG and oxyntomodulin stimulated pERK1/2 response is independent of PKA. These data, in combination with the lack of pERK1/2 response following forskolin stimulation suggests that elevated levels of cAMP cannot account for the measured pERK1/2 response in these cells.

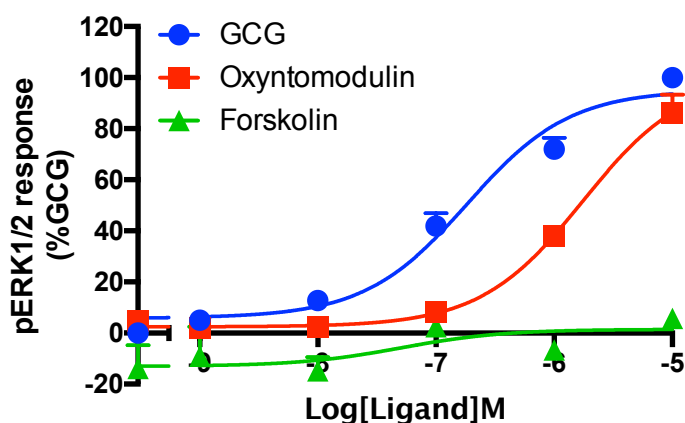


Figure 4.12. pERK1/2 response in CHO-K1 cells stably expressing GCGR: CHO-K1 cells stably expressing GCGR were serum starved for 24 hours and exposed to GCG, oxyntomodulin or forskolin for 5 minutes before measuring pERK1/2. CHO-K1 cells were plated at 10,000 cells per well in a 384-well plate. All values are mean \pm SEM expressed as percentage GCG response where $n \geq 5$ independent experimental repeats, conducted in duplicate.

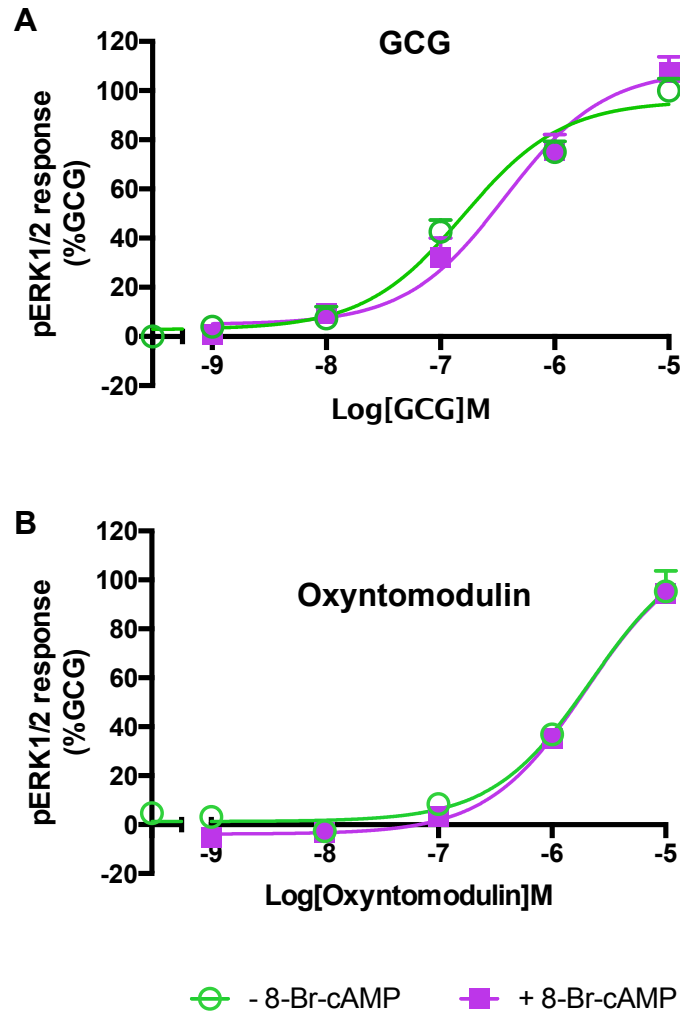


Figure 4.13. pERK1/2 response in CHO-K1 cells stably expressing GCGR +/- PKA inhibitor: CHO-K1 cells stably expressing GCGR were serum starved for 24 hours and pretreated for 15 minutes with the cAMP analogue Rp-8-bromo-cAMP (Rp-8-Br-cAMP) or DMSO control prior to stimulation with **A**) GCG or **B**) oxyntomodulin for 5 minutes before measuring pERK1/2. CHO-K1 cells were plated at 10,000 cells per well in a 384-well plate. All values are mean \pm SEM expressed as percentage GCG response in Rp-8-Br-cAMP untreated cells where $n \geq 5$ independent experimental repeats, conducted in duplicate.

Table 4.9. pERK1/2 response in CHO-K1 cells stably expressing GCGR +/- PKA inhibitor. Potency (pEC₅₀), maximal response (E_{max}), basal, span, affinity (pK_A) and coupling efficacy (logτ) for GCG in CHO-K1 cells stably expressing GCGR +/- 8-Br-cAMP measured using a pERK1/2 assay

+ DMSO (untreated)						
Ligand	pEC ₅₀ ^a	E _{max} ^b	Basal ^c	Span ^d	pK _A ^e	log τ ^f
GCG	6.80 ±0.11	95.9 ±4.0	2.8 ±3.2	93.0 ±4.8	6.36 ±0.1	0.24 ±0.05
Oxyntomodulin	5.66 ±0.12	115.9 ±9.3	1.3 ±2.7	155.2 ±13.0	5.02 ±0.2	0.53 ±0.15
+ 8-Br-cAMP						
Ligand	pEC ₅₀ ^a	E _{max} ^b	Basal ^c	Span ^d	pK _A ^e	log τ ^f
GCG	6.43 ±0.14	108.5 ±6.4	4.9 ±4.2	103.6 ±7.0	5.89 ±0.2	0.40 ±0.09
Oxyntomodulin	5.70 ±0.05	114.1 ±3.7	3.9 ±1.2	117.9 ±3.7	5.07 ±0.1	0.52 ±0.06

CHO-K1 cells stably expressing GCGR were stimulated with GCG or oxyntomodulin and the pERK1/2 to response measured in order to generate concentration response curves. To calculate pEC₅₀, E_{max}, Basal and Span values, data were analysed using a three-parameter logistic equation. Data was also analysed by an operational model of agonism (Black and Leff, 1983) to determine affinity (pK_A) and coupling efficacy (log τ).

^a Negative logarithm of ligand concentration required to produce a half-maximal response

^b Maximal response to ligand as percentage GCG response

^c The low plateau of the fitted sigmoidal dose-response curve

^d The difference between E_{max} and basal signalling

^e The negative logarithm of functional affinities that describes the affinity of the receptor when coupled to a given signalling pathway generated through use of the operational model for partial agonism

^f τ is the coupling efficiency parameter generated through use of the operational model for partial agonism
Statistical significance (*, $p < 0.05$; **, $p < 0.01$; ***, $p < 0.001$; ****, $p < 0.0001$) compared to GCG response in untreated CHO-K1 cells was determined by unpaired Student's t-test (two-tailed)

4.4.4. The specific G $\beta\gamma$ subunits inhibitor, gallein, had no effect on the measured pERK1/2 response

In the case of G protein mediated ERK1/2 activation, both α and $\beta\gamma$ subunits are able to activate the ERK cascades (Eishingdrelo and Kongsamut, 2013) (Figure 4.11). To define the role of G $\beta\gamma$ subunit in GCGR stimulation ERK1/2 phosphorylation, CHO-K1 cells stably expressing GCGR were pre-incubated for 30 minutes with gallein (10, 1 or 0.1 μM), a specific G $\beta\gamma$ small molecule inhibitor (Lehmann *et al.*, 2008), or DMSO control prior to GCG or oxyntomodulin stimulation and subsequent pERK1/2 measurement.

As previously shown (Figure 4.12), CHO-K1 cells stably expressing GCGR showed a concentration-dependent pERK1/2 response to both GCG or oxyntomodulin stimulation (Figure 4.14). Pretreatment with gallein, had no effect on the measured pERK1/2 response to either GCG or oxyntomodulin at any of the tested inhibitor concentration in terms of potency or maximal response (Figure 4.14 and Table 4.10). This finding suggests that signalling via the G $\beta\gamma$ -subunit cannot account for the GCGR-mediated pERK1/2 response.

The basal level of pERK1/2 showed an elevation with 10 μM gallein pretreatment. Whereas the true basal (stimulation with HBS only) response aligned at zero (percentage GCG), there appears to be an elevation in the basal pERK1/2 level at very low concentrations of GCG or oxyntomodulin. This finding suggests that G $\beta\gamma$ inhibition alone, in absence of any ligand, has no effect on the basal pERK1/2 response. However, at low concentrations of ligand (0.1 nM – 10 nM), it appears G $\beta\gamma$ inhibition causes an elevation in pERK1/2. One speculation into the cause of this elevation could be the inability of the G α -subunit to re-bind the G $\beta\gamma$ and complete the G protein cycle, thereby remaining active and stimulating a single or multiple pathways leading to elevated basal pERK1/2.

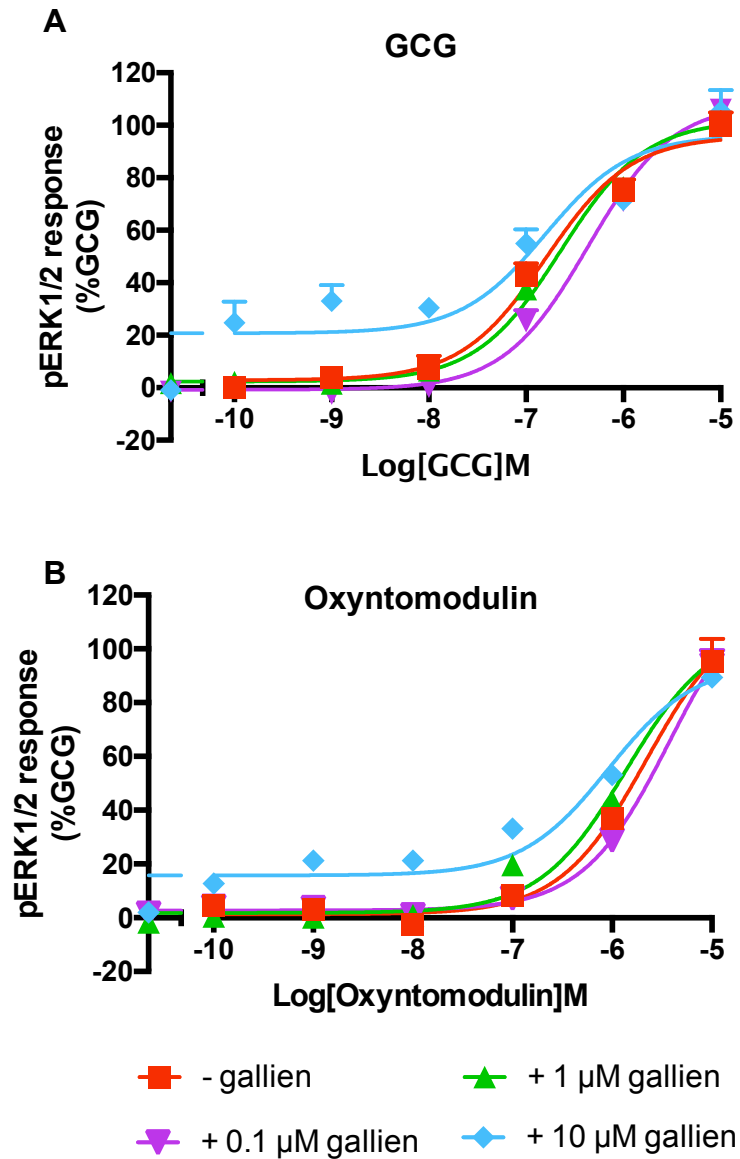


Figure 4.14. pERK1/2 response in CHO-K1 cells stably expressing GPCR +/- Gβγ inhibitor. CHO-K1 cells stably expressing GPCR were serum starved for 24 hours and pretreated for 30 minutes with the specific Gβγ small molecule inhibitor, gallein, at various concentrations (10, 1 or 0.1 μM) or DMSO control prior to stimulation with **A)** GCG or **B)** oxyntomodulin for 5 minutes and measuring pERK1/2. CHO-K1 cells were plated at 10,000 cells per well in a 384-well plate. All values are mean ± SEM expressed as percentage GCG response in gallein untreated cells where $n \geq 5$ independent experimental repeats, conducted in duplicate.

Table 4.10. pERK1/2 response in CHO-K1 cells stably expressing GCGR +/- Gβγ inhibitor. Potency (pEC₅₀), maximal response (E_{max}), basal, span, affinity (pK_A) and coupling efficacy (log τ) for GCG in CHO-K1 cells stably expressing GCGR -/+ gallein measured using a pERK1/2 assay

+ DMSO (untreated)						
Ligand	pEC ₅₀ ^a	E _{max} ^b	Basal ^c	Span ^d	pK _A ^e	log τ ^f
GCG	6.80 ±0.11	95.9 ±4.0	2.8 ±3.2	93.0 ±4.8	6.36 ±0.1	0.24 ±0.05
Oxyntomodulin	5.66 ±0.12	115.9 ±9.3	1.3 ±2.7	114.7 ±9.2	5.02 ±0.2	0.53 ±0.15
+ 10 μ M gallein						
Ligand	pEC ₅₀ ^a	E _{max} ^b	Basal ^c	Span ^d	pK _A ^e	log τ ^f
GCG	6.80 ±0.29	96.2 ±9.4	20.8 ±5.5**	75.5 ±10.4**	6.42 ±0.3	0.15 ±0.13
Oxyntomodulin	6.04 ±0.29	94.7 ±12.9	15.7 ±4.5**	79.0 ±13.2**	5.66 ±0.4	0.16 ±0.17

CHO-K1 cells stably expressing GCGR were stimulated with GCG or oxyntomodulin and the pERK1/2 to response measured in order to generate concentration response curves. To calculate pEC₅₀, E_{max}, Basal and Span values, data were analysed using a three-parameter logistic equation. Data was also analysed by an operational model of agonism (Black and Leff, 1983) to determine affinity (pK_A) and coupling efficacy (log τ).

^a Negative logarithm of ligand concentration required to produce a half-maximal response

^b Maximal response to ligand as percentage GCG response

^c The low plateau of the fitted sigmoidal dose-response curve

^d The difference between E_{max} and basal signalling

^e The negative logarithm of functional affinities that describes the affinity of the receptor when coupled to a given signalling pathway generated through use of the operational model for partial agonism

^f τ is the coupling efficiency parameter generated through use of the operational model for partial agonism
Statistical significance (*, $p < 0.05$; **, $p < 0.01$; ***, $p < 0.001$) compared to GCG/oxyntomodulin response in untreated CHO-K1 cells was determined by unpaired Student's t-test (two-tailed)

4.4.5. The specific $G_{q/11}$ inhibitor, YM-254890, reduced the potency of the pERK1/2 response following GCG stimulation

All the G_q family members (G_q , G_{11} , G_{14} and $G_{15/16}$) have been shown to activate ERK1/2 via the stimulation of PLC β (Goldsmith and Dhanasekaran, 2007). Here, an investigation was made into the role of the G_q -mediated pathway in the GCGR mediated pERK1/2 response using the specific $G_{q/11}$ inhibitor, YM-254890.

Having initially used YM-254890 to confirm the Ca^{2+} response to GCG stimulation in GCGR transfected HEK 293 cells and CHO-K1 cells stably expressing GCGR was $G_{q/11}$ mediated (Section 4.3), we sought to investigate if $G_{q/11}$ was also important in the GCG stimulated pERK1/2 response. Here, CHO-K1 cells stably expressing GCGR received a 30-minute pre-incubation with YM-254890 prior to stimulation with GCG and measurement of pERK1/2 (Figure 4.15 and Table 4.1). The potency and affinity of the GCG stimulated pERK1/2 response was significantly reduced in YM-254890 treated cells when compared to untreated DMSO control (pEC₅₀ 6.09 \pm 0.17 and 6.80 \pm 0.11, pK_A 5.44 \pm 0.3 and 6.36 \pm 0.1, respectively) (Table 4.1). This finding suggests that $G_{q/11}$ plays a role in the GCG stimulated pERK1/2 response in CHO-K1 cells stably expressing GCGR. However, given the maximal response to GCG was not significantly different in treated and untreated cells, it appears other cellular components and pathways, such as the β -arrestin mediated pathway, are also responsible for the measured pERK1/2 response.

Of note, the $G\beta\gamma$ subunit released from G_q -coupled GPCRs has also been shown to activate PLC β and therefore can also lead to activation of ERK1/2 via PLC-DAG-PKC as well as PLC-IP₃- Ca^{2+} pathways (Goldsmith and Dhanasekaran, 2007). Given that there was no difference in pERK1/2 response in $G\beta\gamma$ inhibitor treated and untreated GCGR expressing CHO-K1 cells, this result may infer that only the $G\alpha$ -subunit of $G_{q/11}$ and not the $G\beta\gamma$ is responsible for this reduced potency.

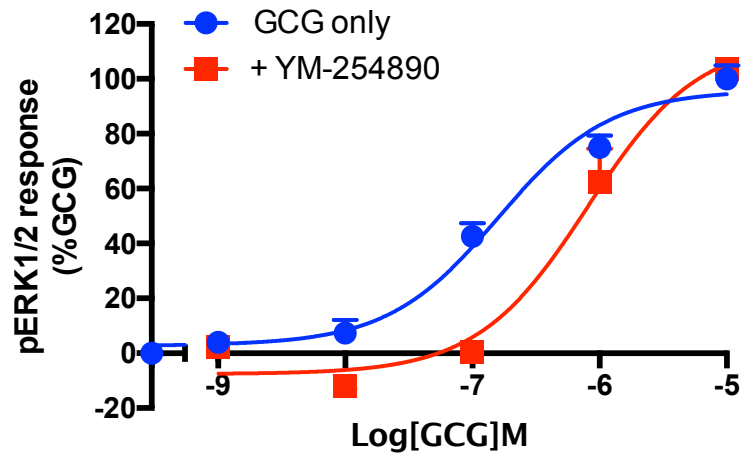


Figure 4.15. pERK1/2 response in CHO-K1 cells stably expressing GCGR +/- $G_{q/11}$ inhibitor. CHO-K1 cells stably expressing GCGR were serum starved for 24 hours and pretreated for 30 minutes with the specific $G_{q/11}$ inhibitor, YM-254890, at various concentrations (100 nM) or DMSO control prior to stimulation with GCG for 5 minutes and measuring pERK1/2. CHO-K1 cells were plated at 10,000 cells per well in a 384-well plate. All values are mean \pm SEM expressed as percentage GCG response in DMSO control treated cells where $n \geq 5$ independent experimental repeats, conducted in duplicate.

Table 4.11. pERK1/2 response in CHO-K1 cells stably expressing GCGR +/- G_{q/11} inhibitor. Potency (pEC₅₀), maximal response (E_{max}), basal, span, affinity (pK_A) and coupling efficacy (log τ) for GCG in CHO-K1 cells stably expressing GCGR +/- YM-254890 measured using a pERK1/2 assay

	pERK1/2					
	pEC ₅₀ ^a	E _{max} ^b	Basal ^c	Span ^d	pK _A ^e	log τ ^f
GCG only	6.80 ±0.11	95.9 ±4.0	2.8 ±3.2	93.0 ±4.8	6.36 ±0.1	0.24 ±0.05
+ YM-254890	6.09 ±0.17**	114.5 ±13.6	-7.6 ±5.0	122.1 ±13.7	5.44 ±0.3*	0.54 ±0.21

CHO-K1 cells stably expressing GCGR +/- pretreatment with the specific G_{q/11} inhibitor, YM-254890, were stimulated with GCG and the pERK1/2 response to GCG measured in order to generate concentration response curves. To calculate pEC₅₀, E_{max}, Basal and Span values, data were analysed using a three-parameter logistic equation. Data was also analysed by an operational model of agonism (Black and Leff, 1983) to determine affinity (pK_A) and coupling efficacy (log τ).

^a Negative logarithm of ligand concentration required to produce a half-maximal response

^b Maximal response to ligand as percentage GCG response

^c The low plateau of the fitted sigmoidal dose-response curve

^d The difference between E_{max} and basal signalling

^e The negative logarithm of functional affinities that describes the affinity of the receptor when coupled to a given signalling pathway generated through use of the operational model for partial agonism

^f τ is the coupling efficiency parameter generated through use of the operational model for partial agonism

Statistical significance (*, $p < 0.05$; **, $p < 0.01$; ***, $p < 0.001$) compared to GCG response in untreated CHO-K1 cells was determined by unpaired Student's t-test (two-tailed)

4.4.6. Investigating the importance of G proteins and β -arrestin1/2 in GCGR stimulated pERK1/2 response

To further investigate the potentially important upstream signalling component in the pERK1/2 response following GCGR stimulation, the parental (WT) and various CRISPR G protein and β -arrestin1/2 knockout HEK 293 cell lines (gifted to us by Dr Asuka Inoue), previously characterised in Section 3.8, were utilised.

A concentration-dependent increase in pERK1/2 was measured following GCG stimulation in WT and CRISPR G protein and β -arrestin1/2 knockout HEK 293 transfected with pmCherry-N1 expressing GCGR (Figure 4.16). This pERK1/2 response measured to GCG stimulation in the knockout cell was not significantly different in any of the measured parameters (pEC_{50} , E_{max} , Basal, Span values, affinity (pK_A) and coupling efficacy ($\log \tau$)) when compared to WT. Of note, the signalling window was small in this HEK 293 cell line ($15.0 \pm 2.8\%$ PMA response ($1 \mu M$)) as was shown earlier (Figure 4.16 and Table 4.12). As such, there was high variability in the data resulting in uncertainty in the fitted dose-response curves. With this in mind, drawing conclusions from these data is difficult. Despite this uncertainty, the pERK1/2 response in $G\alpha_q$ ($\Delta G\alpha_q$ and $\Delta G\alpha_{s/q/12}$) and β -arrestin1/2 knockout cell lines showed a reduction in maximum pERK response to GCG (E_{max} 79.1 ± 13.7 , 62.9 ± 13.0 and 61.0 ± 14.8 , respectively, expressed as a percentage of WT response) when compared to WT (E_{max} 103.6 ± 19.4). This finding could indicate the GCGR-mediated ERK1/2 activation is through a combination of $G\alpha_q$ and β -arrestin1/2 mediated pathways.

It appears in order to draw useful conclusions from these cell lines, an enhancement in the GCG signalling window would be required. However, the maximum cell number of 50,000 per well (as recommended by the pERK1/2 assay kit supplier (Cisbio Bioassays)) was used, and the only other alternative to enhance the possible window would be to increase GCGR expression via stable cell line generation. However, the generation of GCGR

stable WT HEK 293 cells was shown to only enhance the GCG stimulated pERK1/2 response by approximately 2-fold when compared to transfected WT HEK 293 cells (30.7 ± 3.5 and 14.0 ± 2.6 expressed as a percentage PMA response ($1 \mu\text{M}$), respectively). This small enhancement and additional cell line manipulation is likely to not be sufficient to justify the generation of the additional GCGR stable cell lines.

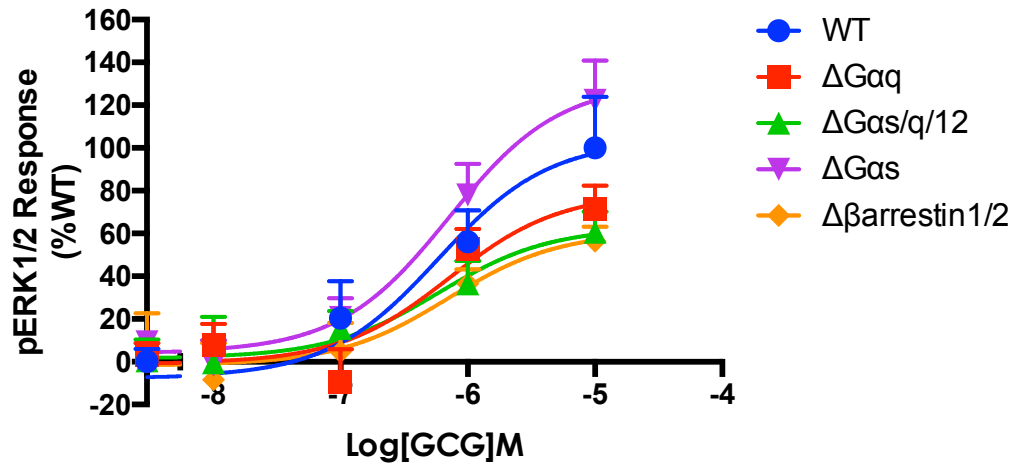


Figure 4.16. GCG stimulated pERK1/2 response in WT and various knockout HEK 239 cells lines. WT and various G protein or β -arrestin1/2 knockout HEK 293 cell lines were transfected with GCGR and stimulated with GCG for 5 minutes before measuring pERK1/2. Cells were plated at 50,000 cells per well in a 384-well plate. All values are mean \pm SEM expressed as percentage GCG response in WT cells where $n \geq 5$ independent experimental repeats, conducted in duplicate.

Table 4.12. GCG stimulated pERK1/2 response in WT and various knockout HEK 293 cells lines. Potency (pEC_{50}), maximal response (E_{max}), basal, span, affinity (pK_A) and coupling efficacy ($\log \tau$) for GCG in WT and various G protein or β -arrestin1/2 knockout HEK 293 cell lines transfected with GCGR measured using a pERK1/2 assay

	pERK1/2					
	pEC_{50}^a	E_{max}^b	Basal ^c	Span ^d	pK_A^e	$\log \tau$
WT	6.23 \pm 0.35	103.6 \pm 19.4	-7.3 \pm 10.7	110.9 \pm 20.5	5.70 \pm 0.5	0.38 \pm 0.25
ΔGq	6.15 \pm 0.33	79.1 \pm 13.7	-0.8 \pm 7.5	79.9 \pm 14.6	5.82 \pm 0.4	0.05 \pm 0.16
$\Delta Gs/q/12$	6.23 \pm 0.40	62.9 \pm 13.0	1.8 \pm 8.1	61.2 \pm 14.0	6.00 \pm 0.5	-0.15 \pm 0.16
ΔGs	6.15 \pm 0.24	130.6 \pm 15.7	4.3 \pm 8.7	126.3 \pm 16.8	5.27 \pm 0.4	0.81 \pm 0.40
$\Delta \beta$ arrestin1/2	6.16 \pm 0.46	61.0 \pm 14.8	-1.6 \pm 8.2	62.6 \pm 15.7	5.92 \pm 0.5	-0.15 \pm 0.17

WT and various G protein or β -arrestin1/2 knockout HEK 293 cell lines were transfected with GCGR and stimulated with GCG and pERK1/2 response measured in order to generate concentration response curves. To calculate pEC_{50} , E_{max} , Basal and Span values, data were analysed using a three-parameter logistic equation. Data was also analysed by an operational model of agonism (Black and Leff, 1983) to determine affinity (pK_A) and coupling efficacy ($\log \tau$).

^a Negative logarithm of ligand concentration required to produce a half-maximal response

^b Maximal response to ligand as % WT response

^c The low plateau of the fitted sigmoidal dose-response curve

^d The difference between E_{max} and basal signalling

^e The negative logarithm of functional affinities that describes the affinity of the receptor when coupled to a given signalling pathway generated through use of the operational model for partial agonism

τ is the coupling efficiency parameter generated through use of the operational model for partial agonism
Statistical significance (*, $p < 0.05$; **, $p < 0.01$; ***, $p < 0.001$) compared to GCG response in WT HEK 293 cells was determined by one-way ANOVA with Dunnett's post test

4.4.7. Summary

ERK1/2 activation is described to be downstream of both the $G\alpha$ and $G\beta\gamma$ subunits of G protein including G_s , G_i , and G_q (DeWire *et al.*, 2007). The results presented here have utilised a number of inhibitors including Rp-8-bromo-cAMP, gallein and YM-254890 targeted at inhibiting PKA, $G\beta\gamma$ and $G_{q/11}$, respectively. Whereas treatment with PKA and $G\beta\gamma$ specific inhibitors showed no effect on the measured pERK1/2 response to GCG or oxyntomodulin, inhibition of $G_{q/11}$ showed a reduction in potency of GCG.

The inability of PKA inhibition by Rp-8-bromo-cAMP or the genetic knockout of $G\alpha_s$ to influence the pERK1/2 response measured to GCG stimulation suggested that GCGR mediated pERK1/2 activation is independent of G_s stimulated pathway. Interestingly, the GCG and oxyntomodulin response following $G\beta\gamma$ inhibition through gallein treatment at 10 μ M showed an elevated basal pERK1/2 response at very low concentrations of ligand. One may speculate that the initial activation of GCGR at these very low ligand concentrations initiates the pERK1/2 cascade at a low level and that $G\beta\gamma$ is prevented from re-grouping with the $G\alpha$ -subunit which in turn can continuously activate the pathway leading to ERK1/2 activation.

The potency of the GCG stimulated pERK1/2 response was reduced following $G_{q/11}$ inhibition using YM-254890, suggesting that $G_{q/11}$ plays a role in the GCG stimulated pERK1/2 response at the GCGR. Consistent with these findings, chelation of Ca^{2+}_i was found to reduce GCG-mediated ERK1/2 activation, suggesting an increase in Ca^{2+}_i is required for maximal ERK activation (Jiang *et al.*, 2001).

The pERK1/2 data acquired in the knockout cell lines should be interpreted with caution due to the lack of statistical significance between responses and small signalling window. With this in mind, the pERK1/2 response in $G\alpha_q$ ($\Delta G\alpha_q$ and $\Delta G\alpha_{s/q/12}$) and β -arrestin1/2 knockout cell lines showed a reduction in maximum response. This finding may suggest that the

pERK1/2 response is produced by a combination of $G_{q/11}$ and β -arrestin1/2 mediated pathways.

Given the inability to fully inhibit the pERK1/2 response to ligand stimulation of GCGR with any of the tested inhibitors or knockout cell lines, it appears that the pERK1/2 response is a combination of a number of cellular components/pathways. It should also be noted that the knockout cell lines might display functional compensation, providing an explanation as to why we may not have seen full knockdown of GCGR-mediated ERK1/2 activation. An important follow up experiment would be to investigate the pERK1/2 response in $\Delta\beta$ -arrestin1/2 knockout HEK 293 cells transfected with GCGR, in the presence and absence of YM-254890 treatment. These data would provide additional evidence to support the hypothesis ERK1/2 phosphorylation in response to GCG stimulation at the GCGR is through a combination of both G_q and β -arrestin1/2 mediated pathways.

4.5. Pharmacological characterisation of two potential GCGR antagonists

4.5.1. des-His¹,[Glu⁹]-glucagon amide is a partial agonist at the GCGR in transfected HEK 293T cells

Receptor antagonists are useful tools for investigating the mechanism of action for cognate ligands. The GCG peptide analogue, des-His¹,[Glu⁹]-glucagon amide (des-His¹,[Glu⁹]-GCG), has been reported to act as an antagonist of GCG in several systems (Unson *et al.*, 1989) although the exact mechanisms of action in terms of binding and affect on downstream signaling at GCGR is not known. Here, we investigate the activity of des-His¹,[Glu⁹]-GCG in HEK 293T cells transfected with pcDNA3.1 expressing GCGR using the cAMP accumulation assay.

As previously shown, GCG stimulation of HEK 293T cells transfected with GCGR induced a concentration-dependent increase in cAMP (pEC_{50} of

10.03 \pm 0.1 and E_{\max} of 98.4 \pm 3.6 (percentage GCG response)) (Figure 4.17). It should be noted that the HEK 293T cells used for GCGR transfection in this assay were different to those previously used which showed reduced cAMP signalling to both GCG and oxyntomodulin (Figure 4.2). Importantly, the maximal response measured for GCG was reduced when compared to the maximum forskolin response (E_{\max} of 147.8 \pm 4.8) (Figure 4.17) and as such, the GCG response is within this maximum range allowing any enhancement in cAMP signal to be measureable (i.e. within the dynamic range of the assay).

Co-stimulation of HEK 293T cells with GCG and des-His¹,[Glu⁹]-GCG at a concentration of 1 μ M and 10 μ M, respectively, showed a rightward shift in measured GCG potency whereas there was no significant change in maximal response (Figure 4.18 A). Although this reduction in GCG potency only reached statistical significance at 10 μ M of des-His¹,[Glu⁹]-GCG (Table 4.13), this result suggests antagonism at the GCGR. In comparison to GCG stimulation only, the basal cAMP level is significantly elevated following co-stimulation with 1 or 10 μ M des-His¹,[Glu⁹]-GCG and very low GCG concentrations (\leq 10 pM). In addition, there was a significantly reduces span at 10 μ M des-His¹,[Glu⁹]-GCG co-stimulation. This finding suggests that des-His¹,[Glu⁹]-GCG has some agonistic activity at the GCGR.

Indeed, stimulation with only des-His¹,[Glu⁹]-GCG produced a robust cAMP response and when compared to GCG showed a reduced potency (pEC_{50} 10.03 \pm 0.1 and 7.64 \pm 0.2, respectively) and maximal response (E_{\max} 98.4 \pm 3.6 and 63.6 \pm 2.9, respectively) (Figure 4.18 B). The response to des-His¹,[Glu⁹]-GCG stimulation in vector only transfected HEK 293T cells showed a significantly reduced maximal response and basal response when compared to that seen in GCGR transfected HEK 293T cells (Figure 4.19 and Table 4.13). These findings suggests that the cAMP response following des-His¹,[Glu⁹]-GCG stimulation is indeed through the GCGR and it appears to be acting as a partial agonist. The small dose-response curve fitted to data from des-His¹,[Glu⁹]-GCG stimulation in vector only transfection HEK 293T cells

showed variability in potency (pEC_{50} 8.08 ± 0.5) and may indicate noise in the cAMP assay or a low level of GCGR expression.

Cells stimulated with 1 nM of GCG with increasing concentrations of des-His¹,[Glu⁹]-GCG remained at a plateau between des-His¹,[Glu⁹]-GCG concentrations of 0.01 nM – 10 nM, and although not significant, showed a small inhibition of the measured cAMP response at concentrations of 0.1 μ M – 10 μ M with a measured half maximal inhibitory concentration (pIC_{50}) of 6.01 ± 1.3 (Figure 4.18 B).

The findings presented here suggests des-His¹,[Glu⁹]-GCG to be a partial agonist at the GCGR in transfected HEK 293T cells. It should be noted that any partial agonist also acts as a competitive antagonist and provides an explanation for the reduced cAMP response following 1 nM GCG treatment at high concentrations of des-His¹[Glu⁹]-GCG (1 and 10 μ M).

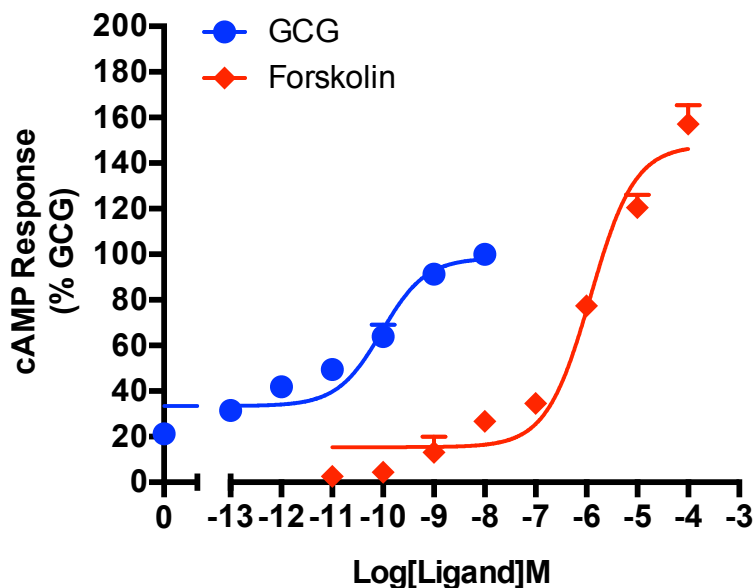


Figure 4.17. GCG dose-response is within the dynamic range of the cAMP assay in HEK 293T cells. HEK 293T cells transiently transfected with GCGR (1,000 cells/well) were exposed to GCG or forskolin for 8 minutes and cAMP accumulation detected using the LANCE cAMP kit. All values are mean \pm SEM expressed as percentage GCG response where $n \geq 5$ independent experimental repeats, conducted in duplicate. Here, the true basal for GCG (stimulation buffer without ligand) aligned with zero percentage GCG response but was excluded to allow better fit of the three-parameter logistic equation.

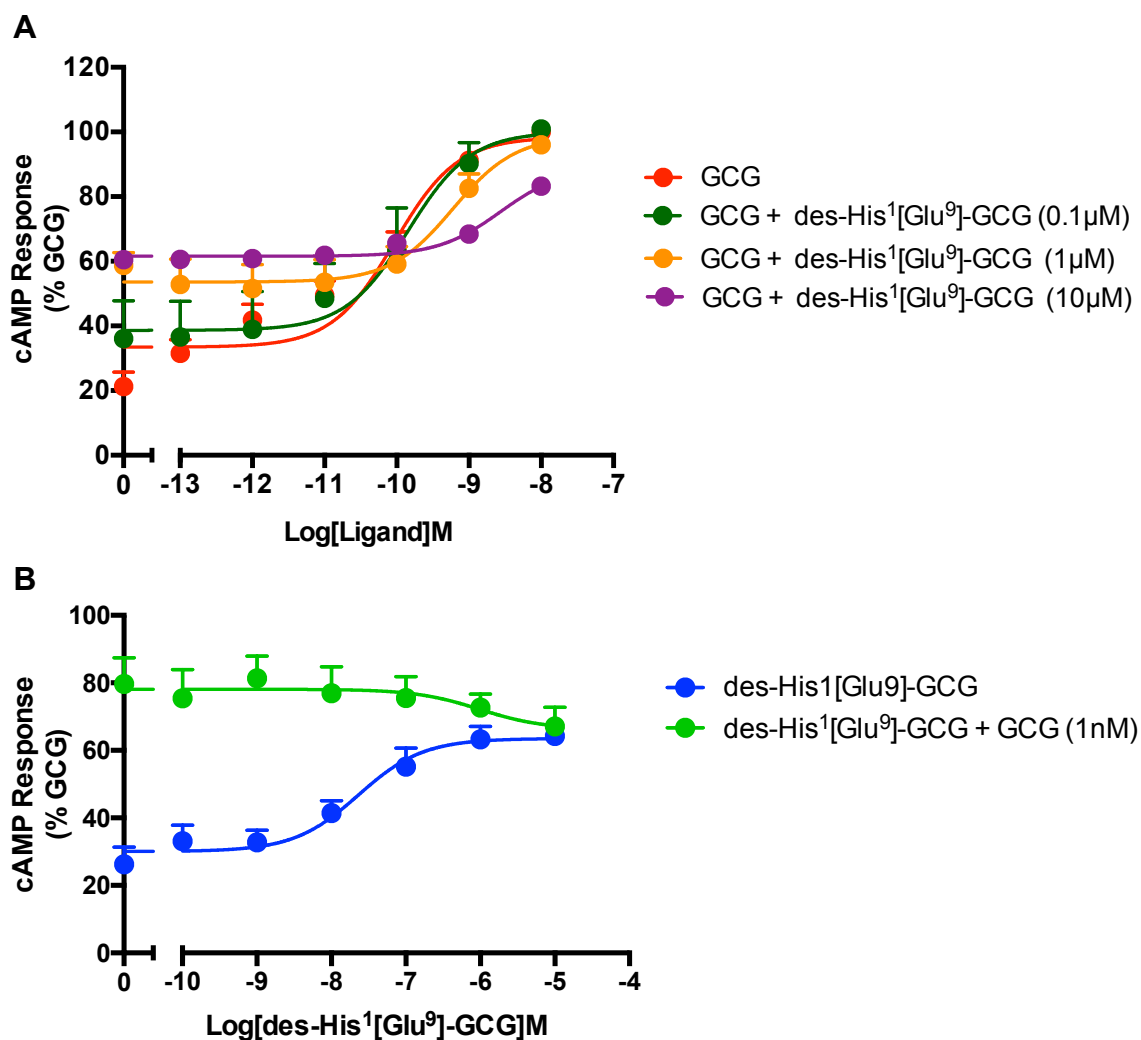


Figure 4.18. Activity of des-His¹,Glu⁹-GCG in GCGR transfected HEK 293T cells. HEK 293T cells transiently transfected with GCGR (1,000 cells/well) were exposed to **A**) GCG with or without various concentration of des-His¹,Glu⁹-GCG, or **B**) des-His¹,Glu⁹-GCG alone or in combination with 1nM GCG for 8 minutes and cAMP accumulation detected using the LANCE cAMP kit. All values are mean \pm SEM expressed as percentage GCG response where $n \geq 5$ independent experimental repeats, conducted in duplicate. Here, the true basal (stimulation buffer without ligand) aligned with zero percentage GCG response but was excluded to allow better fit of the three-parameter logistic equation.

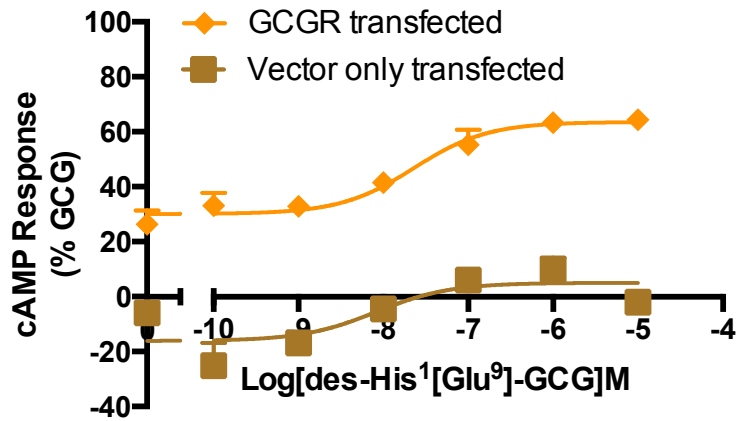


Figure 4.19. cAMP response to des-His¹,Glu⁹-GCG in GCGR/vector only transfected HEK 293T cells. HEK 293T cells transiently transfected with GCGR or vector alone (1,000 cells/well) were exposed to des-His¹,Glu⁹-GCG for 8 minutes and cAMP accumulation detected using the LANCE cAMP kit. All values are mean \pm SEM expressed as percentage GCG response where $n \geq 5$ independent experimental repeats, conducted in duplicate.

Table 4.13. Activity of des-His¹,Glu⁹-GCG in GCGR/Vector only transfected HEK 293T cells. Potency (pEC₅₀), maximal response (E_{max}), basal, span, affinity (pK_A) and coupling efficacy (log τ) for GCG/des-His¹,[Glu⁹]-GCG stimulation only with or co-stimulation of GCGR or vector only transfected HEK 293T cells using a cAMP assay

	des-His ¹ ,[Glu ⁹]-GCG only					
	pEC ₅₀ ^a	E _{max} ^b	Basal ^c	Span ^d	pK _A ^e	log τ ^f
GCGR transfected	7.64 ±0.2	63.6 ±2.9	30.1 ±2.6	33.5 ±3.7	7.44 ±0.3	-0.23 ±0.07
Vector only	8.08 ±0.5	5.03 ±2.6***	-16.1 ±5.1***	21.1 ±5.7	8.01 ±0.6	-0.74 ±0.12***
	GCG + des-His ¹ ,[Glu ⁹]-GCG					
	pEC ₅₀ ^a	E _{max} ^b	Basal ^c	Span ^d	pK _A ^e	log τ ^f
GCG only	10.03 ±0.1	98.4 ±3.6	33.4 ±2.4	64.9 ±4.1		
+ 0.1 μ M	9.85 ±0.3	100.0 ±8.4	38.6 ±5.1	61.4 ±9.4		
+ 1 μ M	9.22 ±0.3	98.9 ±6.8	53.6 ±2.8**	45.3 ±7.1		
+ 10 μ M	9.22 ±0.3	98.9 ±6.8	53.6 ±2.8**	45.3 ±7.1		
des-His ¹ ,Glu ⁹ -GCG only	7.64 ±0.2***	63.6 ±2.9**	30.1 ±2.6	33.5 ±3.7**		

HEK 293T cells transfected with GCGR were stimulated with GCG or des-His¹,[Glu⁹]-GCG alone or GCG in combination with various concentrations of des-His¹,[Glu⁹]-GCG prior to measurement of cAMP accumulation to generate concentration response curves for each construct. To calculate pEC₅₀, E_{max}, Basal and Span values, data were analysed using a three-parameter logistic equation. Data was also analysed by an operational model of agonism (Black and Leff, 1983) to determine affinity (pK_A) and coupling efficacy (log τ).

^a Negative logarithm of GCG concentration required to produce a half-maximal response

^b Maximal response to GCG as percentage GCG only response

^c The low plateau of the fitted sigmoidal dose-response curve

^d The difference between E_{max} and basal signalling

^e The negative logarithm of functional affinities that describes the affinity of the receptor when coupled to a given signalling pathway generated through use of the operational model for partial agonism

^f τ is the coupling efficiency parameter generated through use of the operational model for partial agonism

All values are mean \pm SEM expressed as percentage GCG only (+DMSO added as control) response where $n = 3$ independent experimental repeats, conducted in duplicate.

Statistical significance (*, $p < 0.05$; **, $p < 0.01$; ***, $p < 0.001$) compared to GCG only response was determined by one-way ANOVA with Dunnett's post test

4.5.2. L-168,049 is a competitive antagonist at the GCGR in HEK 293T cells

L-168,049, a small molecule non-peptide, has previously been reported to be a non-competitive antagonist of GCGR in several systems (Cascieri *et al.*, 1999). Given des-His¹,[Glu⁹]-GCG was found to be a partial agonist in GCGR transfected HEK 293T cells, we looked to investigate the activity of L-168,049 as a potential GCGR antagonist.

Here, HEK 293T cells transfected with pcDNA3.1 expressing GCGR, were stimulated with GCG only or in combination with varying concentration of L-168,049 (Figure 4.20 A). Co-stimulation with GCG and increasing concentrations of L-168,049 showed a progressive parallel rightward shift of the dose-response for GCG towards higher concentrations (Table 4.14). This shift in potency, although evident from as little as 0.01 μ M L-168,049, only reached statistical significance at 1 μ M and 10 μ M with a two-log shift (Figure 4.20 A). There was found to be no significant changes in maximal (E_{max}) or basal response with L-168,049 co-stimulation at any of the tested concentration. Given that co-stimulation of GCGR transfected HEK 293T cells with GCG and increasing concentrations of L-168,049 produced a progressive rightward shift in the GCG dose-response and the maximal response remained unchanged, L-168,049 could be classified as a competitive antagonist at the GCGR. However, it is likely that there is a high receptor reserve in the transfected cells where stimulation of only a fraction of this GCGR population produces a maximal response. As such, inhibition of the GCG response by L-168,049 could not occur unless this reserve was depleted or higher concentrations of antagonists were tested. With this in mind, in our hands and under these test conditions L-168,049 could be classified as a competitive antagonist at the GCGR, rather than a non-competitive antagonist, as was previously described (Cascieri *et al.*, 1999).

Cells co-stimulated with GCG at a concentration of 1 nM and increasing concentration of L-168,049 showed a half maximal inhibitory

concentration (pIC_{50}) of 7.08 ± 0.3 (Figure 4.20). Simulation with L-168,049 alone produced a cAMP response but showed reduced potency and maximal response when compared to GCG (pEC_{50} 10.03 ± 0.1 and 8.76 ± 0.2 , E_{max} 98.4 ± 3.6 and 46.6 ± 1.2 , respectively) (Figure 4.20 B). This finding is similar to that seen for des-His¹,[Glu⁹]-GCG, although L-168,049 shows increased potency in comparison (pEC_{50} 7.64 ± 0.2 and 8.76 ± 0.2 , respectively). This finding suggests that L-168,049 may have agonistic activity at the GCGR. However, control experiments in HEK 293T cells expressing vector alone showed no significant difference between the L-168,049 induced cAMP response in GCGR or vector only expressing HEK 293T cells (Figure 4.21 and Table 4.14). This finding suggests the apparent agonistic response is not GCGR specific and L-168,049, being yellow in colour, may have fluorescent properties causing an apparent dose-response curve with increasing concentrations. Further experiments may need to include a “no cells” control in order to subtract the baseline signal and categorically identify that L-168,049 is not acting at another receptor other than GCGR to cause an apparent dose-response.

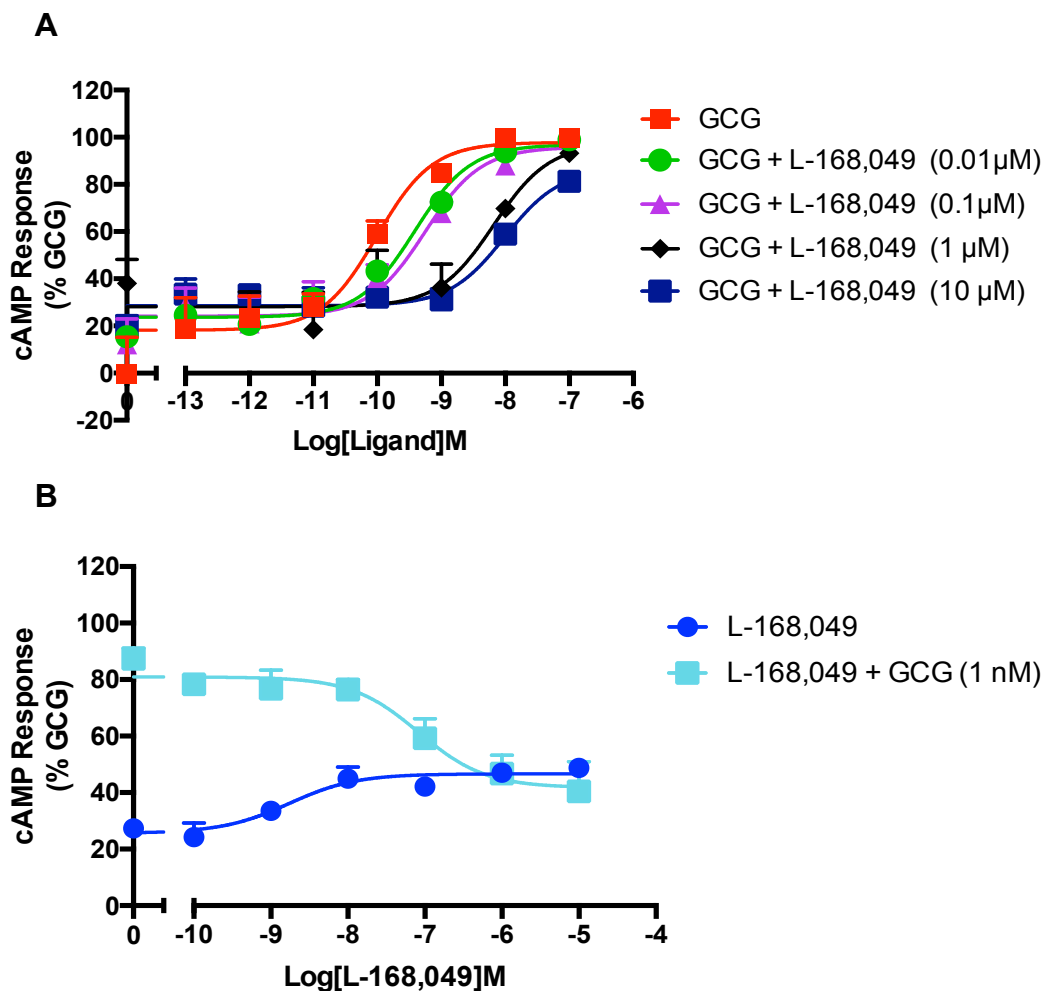


Figure 4.20. Activity of L-168,049 in GCGR transfected HEK 293T cells. HEK 293T cells transiently transfected with GCGR (1,000 cells/well) were exposed to **A**) GCG with or without various concentration L-168,049 or **B**) L-168,049 alone or in combination with 1nM GCG for 8 minutes and cAMP accumulation detected using the LANCE cAMP kit. The dashed grey arrow represents the expected reduction in maximal response on stimulation with higher L-168,049 concentrations if receptor reserve was depletion. All values are mean \pm SEM expressed as percentage GCG response where $n \geq 5$ independent experimental repeats, conducted in duplicate. Here, the true basal (stimulation buffer without ligand) aligned with 0 percentage GCG response but was excluded to allow better fit of the three-parameter logistic equation.

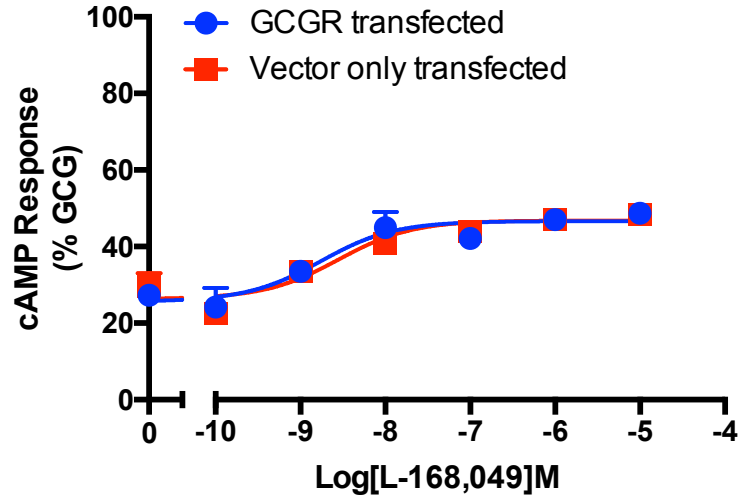


Figure 4.21. cAMP response to L-168,049 in GCGR/vector only transfected HEK 293T cells: HEK 293T cells transiently transfected with GCGR or vector alone (1,000 cells/well) were exposed to L-168,049 for 8 minutes and cAMP accumulation detected using the LANCE cAMP kit. All values are mean \pm SEM expressed as percentage GCG response where $n \geq 5$ independent experimental repeats, conducted in duplicate.

Table 4.14. Activity of L-168,049 in GCGR/vector only transfected HEK 293T cells. Potency (pEC_{50}), maximal response (E_{max}), basal, affinity (pK_A) and coupling efficacy ($\log \tau$) for GCG/L-168,049 stimulation only or GCG with L-168,049 co-stimulation of GCGR or vector only transfected HEK 293T cells using a cAMP assay

L-168,049 only						
	pEC_{50}^a	E_{max}^b	Basal ^c	Span ^d	pK_A^e	$\log \tau^f$
GCGR transfected	8.76 ±0.2	46.6 ±1.2	25.7 ±1.7	20.9 ±2.1	8.65 ±0.2	-0.54 ±0.05
Vector only	8.55 ±0.2	46.8 ±1.5	26.4 ±1.8	20.5 ±2.2	8.45 ±0.1	-0.55 ±0.05
GCG + L-168,049						
	pEC_{50}^a	E_{max}^b	Basal ^c	Span ^d	pK_A^e	$\log \tau^f$
GCG only	10.01 ±0.2	97.8 ±4.0	18.2 ±4.0	79.7 ±5.4		
+ 0.01 μ M	9.41 ±0.1	96.9 ±3.6	23.7 ±2.7	73.3 ±4.3		
+ 0.1 μ M	9.25 ±0.2	95.8 ±5.3	24.2 ±3.6	71.6 ±6.1		
+ 1 μ M	8.18 ±0.4***	97.4 ±12.8	28.2 ±5.2	69.2 ±13.3		
+ 10 μ M	8.01 ±0.2***	86.8 ±6.1	28.6 ±2.0	58.2 ±6.3		
L-168,049 only	8.76 ±0.2**	46.6 ±1.2***	25.7 ±1.7	20.9 ±2.1***		

HEK 293T cells transfected with GCGR were stimulated with GCG or L-168,049 alone or GCG in combination with various concentrations of L-168,049 prior to measurement of cAMP accumulation to generate concentration response curves for each construct. To calculate pEC_{50} , E_{max} , Basal and Span values, data were analysed using a three-parameter logistic equation. Data was also analysed by an operational model of agonism (Black and Leff, 1983) to determine affinity (pK_A) and coupling efficacy ($\log \tau$).^a Negative logarithm of GCG concentration required to produce a half-maximal response

^b Maximal response to GCG as percentage GCG only response

^c The low plateau of the fitted sigmoidal dose-response curve

^d The difference between E_{max} and basal signalling

^e The negative logarithm of functional affinities that describes the affinity of the receptor when coupled to a given signalling pathway generated through use of the operational model for partial agonism

^f τ is the coupling efficiency parameter generated through use of the operational model for partial agonism

All values are mean ± SEM expressed as percentage GCG only (+DMSO added as control) response where $n = 3$ independent experimental repeats, conducted in duplicate. Statistical significance (*, $p < 0.05$; **, $p < 0.01$; ***, $p < 0.001$) compared to GCG only response was determined by one-way ANOVA with Dunnett's post test

4.5.3. Summary

The findings presented here in HEK 293T cells transfected with pcDNA3.1 expressing GCGR characterise the GCG peptide analogue des-His¹,[Glu⁹]-GCG, previously reported to act as an antagonist of GCG in several systems (Unson *et al.*, 1989), as a partial agonist at the GCGR. On the other hand, L-168,049 was characterised as a competitive antagonist at the GCGR.

Stimulation of GCGR transfected HEK 293T cells with des-His¹,[Glu⁹]-GCG or L-168,049 was shown to stimulate cAMP accumulation. It could be argued that receptor expression may be higher in this transfected system when compared to an endogenously expressing cell lines and therefore we may be amplifying a small agonistic response. Whereas the des-His¹,[Glu⁹]-GCG stimulated cAMP response was shown to be GCGR specific, the L-168,049 induced cAMP response was not. With these findings in mind, it appears that neither des-His¹,[Glu⁹]-GCG or L-168,049 can be used as antagonists to investigate specific GCGR signalling. If L-168,049 is used, controls for autofluorescence need to be considered.

4.6. Investigating the action of a potential GCGR biased agonist; TH-GCG

4.6.1. TH-GCG induces a robust cAMP response in GCGR transfected HEK 293T cells

The GCG analogue TH-GCG was previously reported in hepatocytes to neither activate AC nor cause cAMP response, but was shown to fully stimulate glycogenolysis, gluconeogenesis and stimulates the production of inositol phosphates (Wakelam *et al.*, 1986). This was described as an alternative mechanism by which GCG activation may exert its effects independent of cAMP and that this may indicate the existence of two distinct receptors for GCG, one coupled to inositol phospholipid breakdown and

another coupled to stimulate AC activity. Here, we investigate the hypothesis that TH-GCG is acting at the classical GCGR and that these early findings can be explained by signalling bias where the downstream signalling cascade initiated by TH-GCG is predominantly through G_q -coupling.

We first sought to confirm that TH-GCG was unable to stimulate cAMP production using our assay system of HEK 293T cells transfected with GCGR expressed from the CMV promoter using pmCherry-N1. A robust cAMP response was determined in these HEK 293T cells following GCG or TH-GCG stimulation (Figure 4.22). TH-GCG showed a significantly reduced potency when compared to GCG (pEC_{50} 7.05 ± 0.14 and 9.52 ± 0.12 , respectively), with non-significant reduced maximal response (E_{max} 87.8 ± 4.8 and 101.5 ± 4.6 , respectively) (Table 4.15). These data suggest TH-GCG to be a lower potency agonist at the GCGR in HEK 293T cells transfected GCGR. Notably, HEK 293T cells transfected with vector alone showed a very weak response to TH-GCG, with large error for all the output parameters acquired from fitted data with a three-parameter logistic equation (Figure 4.23, Table 4.15). This result suggests the cAMP response seen to TH-GCG stimulation is GCGR specific.

Given the similar maximal response but reduced potency of TH-GCG at the GCGR, it appears TH-GCG is a lower potency full agonist at the GCGR in HEK 293T cells, most probably through the classical G_s -coupled pathway. This finding is distinct from previous reports in hepatocytes indicating TH-GCG does not cause an increase in cAMP (Wakelam *et al.*, 1986, Lenzen *et al.*, 1990). This unexpected finding may be as a result of receptor expression in the transfected HEK 293T cells when compared to primary hepatocytes. Alternatively, or in combination with receptor expression, the GCGR may be strongly coupled to the cAMP signalling components within HEK 293T cells, which may not be the case in hepatocytes. In order to test this theory, cells endogenously expressing GCGR, such as the hepatocyte cell line, Hep 3B, were tested for a TH-GCG stimulated cAMP response (Section 4.6.4).

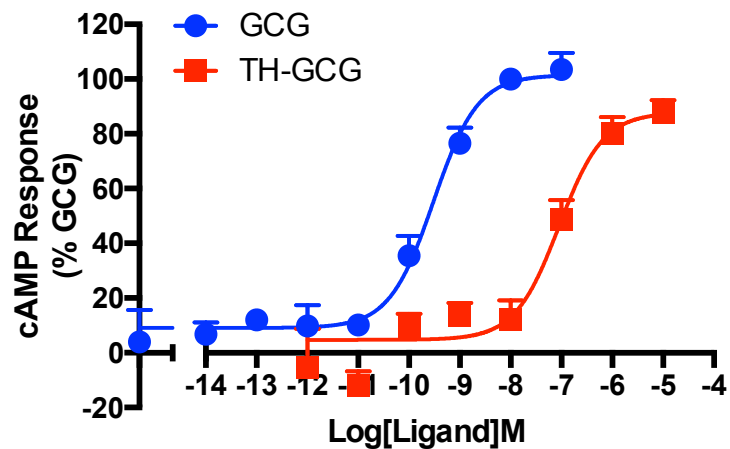


Figure 4.22. TH-GCG induces a concentration-dependent increase in cAMP accumulation in HEK 293T cells expressing GCGR. HEK 293T cells transiently (24 hours post transfection) expressing mCherry-tagged GCGR were exposed to GCG or TH-GCG for 8 minutes and cAMP accumulation detected. All values are mean \pm SEM expressed as percentage GCG response where $n \geq 5$ independent experimental repeats, conducted in duplicate.

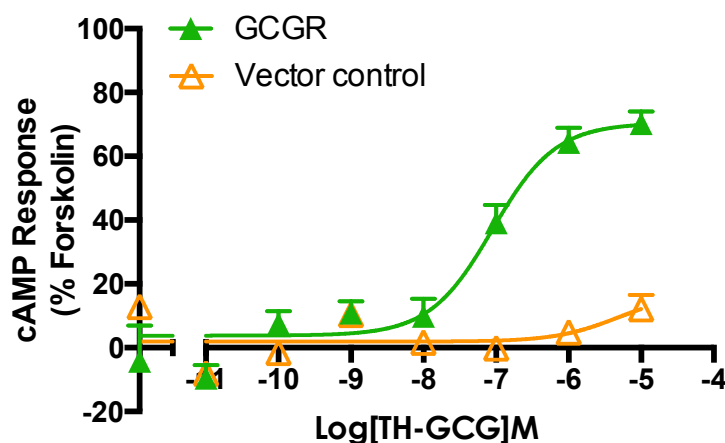


Figure 4.23. TH-GCG stimulated cAMP response is GCGR-dependent in HEK 293T cells. HEK 293T cells transiently (24 hours post transfection) expressing mCherry-tagged GCGR or vector only were exposed to GCG or TH-GCG for 8 minutes and cAMP accumulation detected. All values are mean \pm SEM expressed as percentage forskolin response where $n \geq 5$ independent experimental repeats, conducted in duplicate.

Table 4.15. TH-GCG induces a concentration-dependent increase in cAMP accumulation in HEK 293T cells expressing GCGR. Potency (pEC_{50}), maximal response (E_{max}), basal and span for GCG and TH-GCG stimulated cAMP response measured in GCGR/vector only transfected HEK 293T cells

HEK 293T				
cAMP				
Ligand	pEC_{50} ^a	E_{max} ^b	Basal ^c	Span ^d
GCG	9.52 \pm 0.12	101.5 \pm 4.6	9.1 \pm 2.7	92.4 \pm 5.1
TH-GCG	7.05 \pm 0.14***	87.8 \pm 4.8	4.7 \pm 3.6	83.0 \pm 5.7
TH-GCG (Vector control)		N.R	6.7 \pm 3.6	N.R

GCGR transfected (or vector only transfected) HEK 293T cells were stimulated with GCG or TH-GCG prior to measurement of cAMP accumulation to generate concentration response curves. To calculate pEC_{50} , E_{max} , Basal and Span values, data were analysed using a three-parameter logistic equation.

^a Negative logarithm of GCG/TH-GCG concentration required to produce a half-maximal response

^b Maximal response to GCG/TH-GCG as percentage GCG response

^c The low plateau of the fitted sigmoidal dose-response curve

^d The difference between E_{max} and basal signalling

All values are mean \pm SEM expressed percentage GCG response where $n \geq 5$ independent experimental repeats, conducted in duplicate. Statistical significance (*, $p < 0.05$; **, $p < 0.01$; ***, $p < 0.001$) in the difference between the cAMP responses to TH-GCG and GCG was determined by unpaired Student's t-test (two-tailed).

N.R denotes no response or where a true dose-response curve could not be generated

4.6.2. TH-GCG fails to induce an Ca^{2+} i in GCGR transfected HEK 293T cells

Having demonstrated a clear ability of TH-GCG to stimulate cAMP production in HEK 293T cells transfected with pmCherry-N1 expressing GCGR, we next wanted to determine if TH-GCG displayed a more potent activation of Ca^{2+} i release from the endoplasmic reticulum (ER).

HEK 293T cells were seeded in a 96-well plate, transfected with GCGR and stimulated with increasing concentrations of GCG or TH-GCG with the Ca^{2+} i mobilisation measured using a FlexStation® Multi-Mode Microplate Reader. In line with previous findings (Section 4.3.1), a robust GCG stimulated Ca^{2+} i response was detected in GCGR transfected HEK 293T cells, which was abolished by a 30 minute pre-treatment with the specific $G_{q/11}$ inhibitor, YM-254890 (Figure 4.24 A and Table 4.16), thereby confirming the Ca^{2+} i mobilisation was $G_{q/11}$ -mediated.

TH-GCG showed no detectable Ca^{2+} i response with or without YM-254890 pre-treatment (Figure 4.24 B and Table 4.16). This finding was unexpected given that previous findings have suggested TH-GCG stimulation in hepatocytes induces an inositol phosphate response (Wakelam *et al.*, 1986, Lenzen *et al.*, 1990) and inositol phosphate production is downstream of the $G_{q/11}$ -mediated Ca^{2+} i response (Goldsmith and Dhanasekaran, 2007). This lack of detectably Ca^{2+} i mobilisation may simply reflect the differences in cellular components between HEK 293T cells and hepatocytes. Alternatively, this hepatocyte cell line may not have been capable of inducing a measurable Ca^{2+} i mobilisation due to a reduced amplification when compared to HEK 293T cells transiently transfected with GCGR.

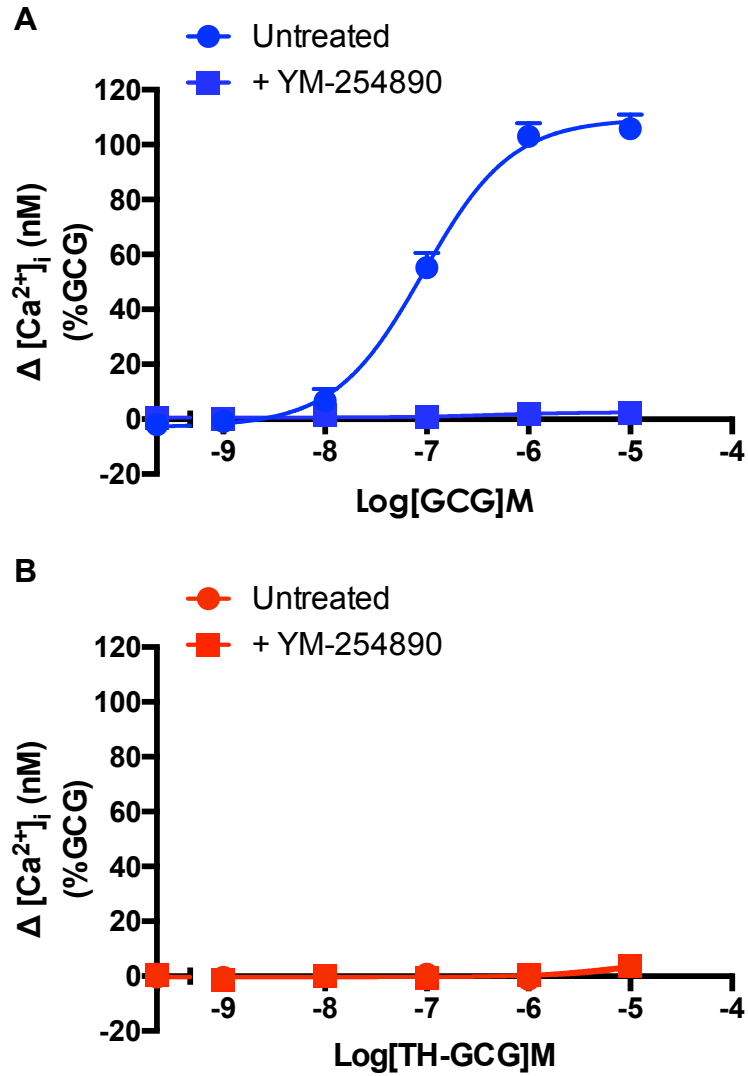


Figure 4.24. TH-GCG fails to induce a Ca^{2+}_i response in HEK 293T cells expressing GCGR. HEK 293T cells transiently expressing GCGR (48 hours post transfection) were exposed to **A**) GCG, **B**) TH-GCG and Ca^{2+}_i mobilisation measured +/- 30 minutes treatment with YM-254890 (100 nM) or DMSO control. All values are mean \pm SEM expressed as percentage GCG response where $n \geq 3$ independent experimental repeats, conducted in duplicate.

Table 4.16. TH-GCG fails to induce a Ca²⁺_i response in HEK 293T cells expressing GCGR Potency (pEC₅₀), maximal response (E_{max}), basal and span for GCG and TH-GCG stimulated Ca²⁺_i mobilisation measured in GCGR transfected HEK 293T cells

HEK 293T				
Ca ²⁺ _i				
Ligand	pEC ₅₀ ^a	E _{max} ^b	Basal ^c	Span ^d
GCG	7.01 ±0.13	103.6 ±5.7	-0.1 ±4.4	103.7 ±6.8
GCG (+ YM-254890)	N.R			
TH-GCG	N.R			
TH-GCG (+ YM-254890)	N.R			

GCGR transfected (or vector only transfected) HEK 293T cells were stimulated with GCG or TH-GCG prior to measurement of Ca²⁺_i response or IP₁ response to generate concentration response curves. CHO-K1 cells stably expressing GCGR were stimulated with GCG or TH-GCG and the IP₁ response measured. To calculate pEC₅₀, E_{max}, Basal and Span values, data were analysed using a three-parameter logistic equation.

^a Negative logarithm of GCG/TH-GCG concentration required to produce a half-maximal response

^b Maximal response to GCG/TH-GCG as percentage GCG response

^c The low plateau of the fitted sigmoidal dose-response curve

^d The difference between E_{max} and basal signalling

All values are mean ± SEM expressed percentage GCG response where *n* ≥ 5 independent experimental repeats, conducted in duplicate.

N.R denotes no response or where a true dose-response curve could not be generated.

4.6.3. TH-GCG fails to induce a detectable IP₁ response in GCGR transfected HEK 293T cells

The mobilisation of Ca²⁺_i can occur through a number of different signal transduction cascades. One such mechanism is the production of inositol triphosphate (IP₃) through classical G_q-coupling to PLCβ leading to activation of IP₃ receptors expressed on the ER and subsequent release of Ca²⁺ (Goldsmith and Dhanasekaran, 2007). TH-GCG has been reported to stimulate the production of inositol phosphates (Wakelam *et al.*, 1986). IP₃ is rapidly broken down to inositol monophosphate (IP₁), which is then further degraded to *myo*-inositol. With the addition of LiCl, IP₁ degradation is

inhibited and accumulates, thereby allowing measurement (as a substitute for IP₃) using the IP-One HTRF® assay kit (Cisbio Bioassays) previously optimised for OTR (Section 3.5).

Here, we sought to quantify IP₁ accumulation in HEK 293T cells expressing GCGR. Unfortunately, and despite optimisation of the IPOne assay used to measure IP₁ accumulation (Section 3.5), the measurement of IP₁ accumulation in GCGR transfected HEK 293T cells showed no response to GCG or TH-GCG (Figure 4.25 A). In order to increase any potential IP₁ signal, CHO-K1 cells stably expressing GCGR were also tested which showed uniform GCGR expression. Only a very weak response to GCG was measured at the highest GCG concentration (10 µM) in these CHO-K1 cells and a full dose-response curve could not be fitted due to insufficient data points (Figure 4.25 B). Again, TH-GCG showed no detectable IP₁ response. Given this finding and the small signalling window for the IP₁ response detected in oxytocin receptor transfected HEK 293T cells following oxytocin stimulation (Figure 3.5 and Table 3.5), a predominantly G_q-coupled receptor (Gimpl and Fahrenholz, 2001), this assay appears to lack sufficient sensitivity. Given the TH-GCG stimulated cAMP response was reduced in potency when compared to GCG, and GCG gave a very weak IP₁ response, the lack of IP₁ response following TH-GCG was expected. Although this finding reflects the lack of Ca²⁺_i mobilisation and is likely to hold true, we cannot exclude the possibility that a more sensitive assay may detect an IP₁ response to TH-GCG and indeed, a more robust IP₁ response following GCG stimulation.

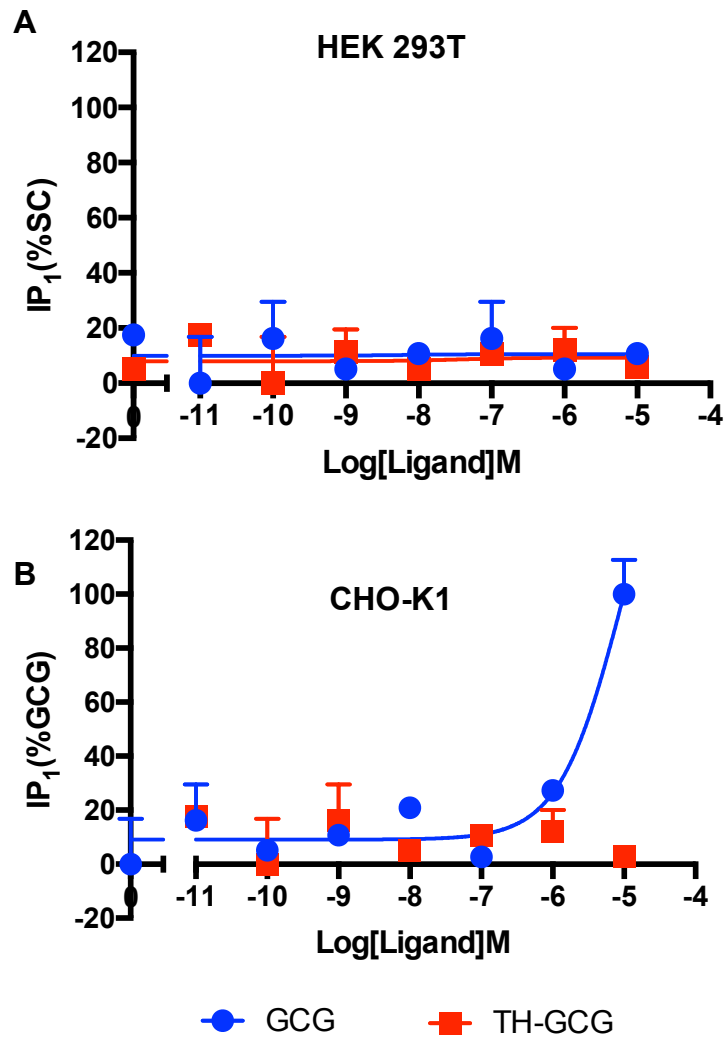


Figure 4.25. TH-GCG fails to induce a measurable IP₁ response in HEK 293T cells or CHO-K1 cells expressing GCGR. HEK 293T cells transfected with GCGR or CHO-K1 cells stably expressing GCGR (20,000 cells/well) were stimulated with GCG or TH-GCG for 2 hours and IP₁ accumulation detected using the IP-One HTRF® assay kit (Cisbio Bioassays). All values are mean \pm SEM expressed as percentage GCG response $n = 2$, conducted in duplicate.

4.6.4. TH-GCG shows a distinctly different cAMP response in the hepatocyte cell line; Hep 3B

Previous studies indicating TH-GCG stimulates an inositol phosphates response in the absence of a cAMP response was conducted in hepatocytes extracted from male Sprague-Dawley rats (Wakelam *et al.*, 1986) or guinea pigs (Lenzen *et al.*, 1990). In order to further investigate the activity of TH-GCG in a cellular context more closely matches that of these early experiments (Wakelam *et al.*, 1986, Lenzen *et al.*, 1990), the cAMP response was measured in the hepatocellular cell line, Hep 3B, endogenously expressing GCGR (Section 3.7).

Using the more sensitive LANCE® Ultra cAMP detection kit (Section 2.8.1, Figure 2.4), we sought to measure any potential cAMP response following GCG or TH-GCG stimulation in Hep 3B cells. This cAMP accumulation assay required a 30 minute ligand stimulation of 5,000 cells/well in line with optimisation experiments in chapter 3 (Section 3.7.2). As expected, Hep 3B cells showed a robust cAMP response following GCG stimulation (pEC_{50} 9.08 ± 0.16) (Figure 4.26 and Table 4.17). This finding and further characterisation of Hep 3B cells, which is presented later (Section 4.8), strongly suggests the endogenous expression of GCGR. The dose-response curve acquired from fitting a three-parameter logistics equation to the TH-GCG stimulated cAMP data was less robust with apparent fluctuating levels of cAMP at the basal response. There was a small reduction in the cAMP levels below the fitted basal response at high concentrations of TH-GCG (0.1 μ M, 1 μ M and 10 μ M) with a measured pIC_{50} of 6.96 ± 0.72 . Despite large variability in this TH-GCG stimulated cAMP response data, the results are distinctly different to those measured in transfected HEK 293T cells that characterised TH-GCG as a partial agonist at the GCGR. Although the cAMP response in Hep 3B cells more closely reflects the previously reported findings for this GCG analogue in hepatocytes (Wakelam *et al.*, 1986, Lenzen

et al., 1990), caution needs to be taken when interpreting these data due to the high variability in the TH-GCG stimulated cAMP data.

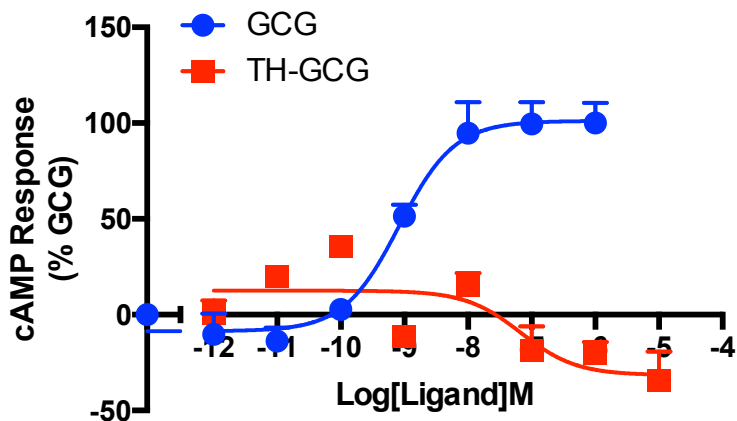


Figure 4.26. TH-GCG fails to induce a concentration-dependent increase in cAMP accumulation in Hep 3B cells. Hep 3B cells (5,000 cells/well) were exposed to GCG or TH-GCG for 30 minutes and cAMP accumulation detected using a LANCE Ultra cAMP kit. All values are mean \pm SEM expressed as percentage GCG response where $n \geq 3$ independent experimental repeats, conducted in duplicate.

Table 4.17. TH-GCG fails to induce a concentration-dependent increase in cAMP accumulation in Hep 3B cells Potency (pEC_{50}), maximal response (E_{max}), basal and span for GCG and TH-GCG stimulated cAMP response in Hep 3B cells

Ligand	cAMP			
	pEC_{50} ^a	E_{max} ^b	Basal ^c	Span ^d
GCG	9.08 \pm 0.16	101.2 \pm 5.0	-8.6 \pm 5.8	109.8 \pm 7.4
TH-GCG	N.R			

Hep 3B cells were stimulated with GCG or TH-GCG prior to measurement of cAMP accumulation to generate concentration response curves. To calculate pEC_{50} , E_{max} , Basal and Span values, data were analysed using a three-parameter logistic equation.

^a pEC_{50} : Negative logarithm of GCG concentration required to produce a half-maximal response

^b Maximal response to GCG/TH-GCG as percentage GCG response

^c The low plateau of the fitted sigmoidal dose-response curve

^d The difference between E_{max} and basal signalling

All values are mean \pm SEM expressed percentage GCG response where $n \geq 5$ independent experimental repeats, conducted in duplicate. Statistical significance (*, $p < 0.05$; **, $p < 0.01$; ***, $p < 0.001$) in response between GCG and TH-GCG was determined by one-way unpaired Student's t-test (two-tailed)

4.6.5. Investigation the cAMP response to TH-GCG in hepatocytes extracted from C57BL/6 mice

4.6.5.1. TH-GCG induces a robust cAMP response in C57BL/6 hepatocytes

The experiments utilising Hep 3B to investigate cAMP accumulation in response to TH-GCG provided a more physiologically relevant cell line, closer to the cellular model used in early experiments (Wakelam *et al.*, 1986 and Lenzen *et al.*, 1990), when compared to HEK 293T cells to investigate the activity of TH-GCG. The opportunity arose to allow acquisition of freshly isolated hepatocytes from C57BL/6 mice culled for the purpose of pancreatic islet isolation for a separate collaborative project with Dr Maja Wallberg in the Department of Pathology (University of Cambridge). These mouse hepatocytes were stimulated with GCG or TH-GCG for 30-minutes prior to cAMP accumulation detected using the LANCE® *Ultra* cAMP Detection Kit.

Initially, the capacity for these cells to signal was tested through forskolin stimulation at two cell densities. Stimulation of C57BL/6 hepatocytes plated at both 5,000 and 10,000 cells/well induced a dose dependent cAMP response to forskolin, indicated the capability to produce a cAMP signal via AC (Figure 4.27 and Table 4.18). There was no significant difference between potency and maximal response between the two cell numbers. However, the basal response in 10,000 cells/well was elevated relative to 5,000 cells/well producing a smaller span (Table 4.18) and as such, 5,000 cells per well was chosen to conduct further experiments.

Stimulation of C57BL/6 hepatocytes induced a robust cAMP response in a dose-dependent manner to both GCG and TH-GCG (Figure 4.28). The response to TH-GCG was significantly reduced in potency and affinity when compared to GCG (Table 4.19). Given the known expression of GCGR in the liver, the cAMP response measured following GCG stimulation was expected. The cAMP response to TH-GCG however, was an unexpected result due to findings reported here in Hep 3B cells and earlier studies in hepatocytes

suggesting a lack of cAMP response (Wakelam *et al.*, 1986, Lenzen *et al.*, 1990). Given the lack of cAMP response to TH-GCG in vector only transfected HEK 293T cells, the activity of TH-GCG in these hepatocytes is also likely through GCGR stimulation rather than an alternative receptor. If TH-GCG is indeed acting through GCGR as expected, it appears to be a lower potency agonist when compared to GCG.

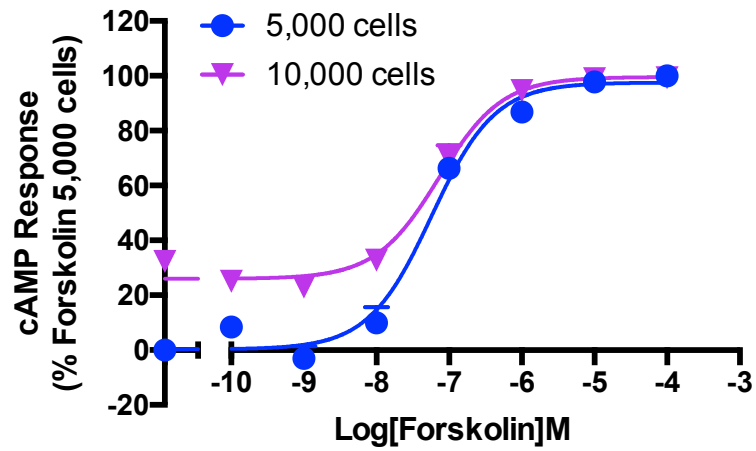


Figure 4.27. Forskolin induces a concentration-dependent increase in cAMP accumulation in C57BL/6 hepatocytes. Hepatocytes were isolated from the liver of C57BL/6 mice and plated at either 5,000 or 10,000 cells per well in a 384-well plate prior to stimulated with forskolin for 30 minutes and detections of cAMP accumulation. All values are mean \pm SEM expressed as percentage forskolin response in 5,000 cells/well where $n = 2$ independent experimental repeats, conducted in duplicate.

Table 4.18. Forskolin induces a concentration-dependent increase in cAMP accumulation in C57BL/6 hepatocytes. Potency (pEC_{50}), maximal response (E_{max}), basal and span for forskolin response measured in C57BL/6 hepatocytes using a cAMP accumulation assay

cAMP				
Cells/well	pEC_{50} ^a	E_{max} ^b	Basal ^c	Span ^d
5,000	7.24 ± 0.09	97.6 ± 2.6	0.3 ± 2.4	97.3 ± 3.4
10,000	7.14 ± 0.07	99.6 ± 1.7	26.0 ± 1.5***	73.6 ± 2.2*

C57BL/6 hepatocytes (5,000 or 10,000 cells/well) were stimulated with forskolin prior to measurement of cAMP accumulation to generate concentration response curves. To calculate pEC_{50} , E_{max} , Basal and Span values, data were analysed using a three-parameter logistic equation.

^a Negative logarithm of GCG/TH-GCG concentration required to produce a half-maximal response

^b Maximal response to GCG/TH-GCG as percentage GCG response

^c The low plateau of the fitted sigmoidal dose-response curve

^d The difference between E_{max} and basal signalling

All values are mean ± SEM expressed percentage GCG response where $n = 3$ independent experimental repeats, conducted in duplicate. Statistical significance (*, $p < 0.05$; **, $p < 0.01$; ***, $p < 0.001$) in the difference in response between 5,000 and 10,000 cells was determined by unpaired Student's t-test (two-tailed).

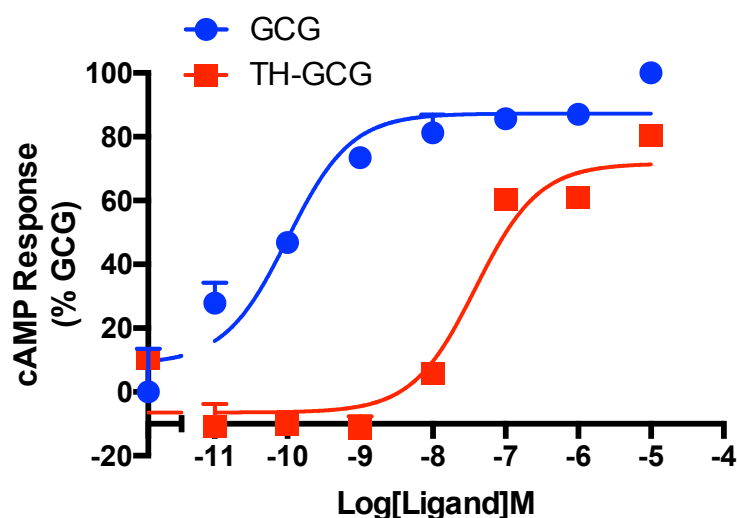


Figure 4.28. TH-GCG and GCG induce a concentration-dependent increase cAMP accumulation in C57BL/6 hepatocytes. Hepatocytes were isolated from the liver of C57BL/6 mice and stimulated with varying concentrations of glucagon (GCG) or TH-GCG for 30 minutes prior to cAMP accumulation detection. All values are mean ± SEM expressed as percentage GCG where $n = 3$ independent experimental repeats, conducted in duplicate.

Table 4.19. TH-GCG and GCG induce a concentration-dependent increase cAMP accumulation in C57BL/6 hepatocytes. Potency (pEC_{50}), maximal response (E_{max}), basal, span, affinity (pK_A) and coupling efficacy ($\log \tau$) for GCG and TH-GCG measured in C57BL/6 hepatocytes using a cAMP accumulation assay

Ligand	cAMP					
	pEC_{50}^a	E_{max}^b	Basal ^c	Span ^d	pK_A^e	$\log \tau^f$
GCG	10.0 ± 0.19	87.3 ± 3.6	8.9 ± 6.3	78.4 ± 7.0	9.34 ± 0.21	0.54 ± 0.09
TH-GCG	7.41 ± 0.23***	71.6 ± 6.6	-6.4 ± 3.8	78.1 ± 7.3	6.93 ± 0.27***	0.31 ± 0.11

C57BL/6 hepatocytes were stimulated with GCG or TH-GCG prior to measurement of cAMP accumulation to generate concentration response curves. To calculate pEC_{50} , E_{max} , Basal and Span values, data were analysed using a three-parameter logistic equation. Data was also analysed by an operational model of agonism (Black and Leff, 1983) to determine affinity (pK_A) and coupling efficacy ($\log \tau$).

^a Negative logarithm of GCG/TH-GCG concentration required to produce a half-maximal response

^b Maximal response to GCG/TH-GCG as percentage GCG response

^c The low plateau of the fitted sigmoidal dose-response curve

^d The difference between E_{max} and basal signalling

^e The negative logarithm of functional affinities that describes the affinity of the receptor when coupled to a given signalling pathway generated through use of the operational model for partial agonism

^f τ is the coupling efficiency parameter generated through use of the operational model for partial agonism

All values are mean ± SEM expressed percentage GCG response where $n = 3$ independent experimental repeats, conducted in duplicate. Statistical significance for the difference between GCG and TH-GCG responses was determined by unpaired Student's t-test (two-tailed).

4.6.6. TH-GCG stimulated a pERK1/2 response in GCGR transfected HEK 293 cells but fails to stimulate a response in stable CHO-K1 cells

The ability of TH-GCG to induce a pERK1/2 response has not been previously investigated. Here, we investigate the pERK1/2 response following TH-GCG stimulation in two GCGR expressing cell lines; transfected HEK 293T cells and stable CHO-K1 cells.

The pERK1/2 response to GCG and TH-GCG in transfected HEK 293T cells showed no significant difference between measured potency, maximal response, affinity and efficacy (Figure 4.29 A and Table 4.20). These data suggests TH-GCG acts as a full agonist of the pERK1/2 response following GCGR activation. In CHO-K1 cells stably expressing GCGR, whereas GCG induced a concentration-dependent increase in pERK1/2, TH-GCG failed to induce a response (Figure 4.29 B and Table 4.20).

These findings suggest the pERK1/2 response to TH-GCG is cell line dependent and may reflect differences in cellular components of the pERK1/2 pathway between the cell lines. However, caution should be exercised when interpreting the data in GCGR transfected HEK 293T cells due to the relatively low signalling window when compared to CHO-K1 cells. Similarly to what was previously suggested for the similar pERK1/2 responses following GCG and oxyntomodulin stimulation in GCGR transfected HEK 293T cells (Section 4.4.2), it may be that the indistinguishable responses between GCG and TH-GCG is due to an experimental limitation where we are at the lower end of the dynamic range of the assay. Given the GCGR stable CHO-K1 cells appear to be a more robust system for the analysis of pERK1/2 responses (Section 4.4.2.1), it seems reasonable to conclude that, at least in this cell line, TH-GCG fails to induce a pERK1/2 response.

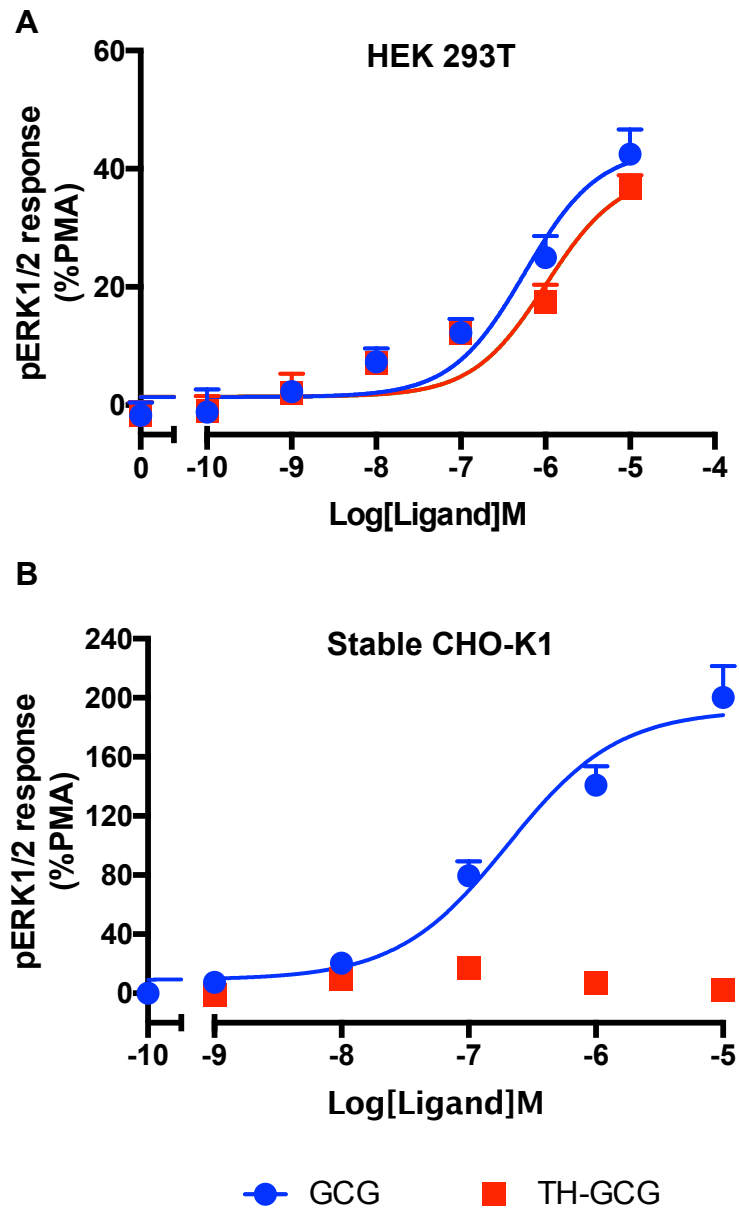


Figure 4.29. Investigating the TH-GCG stimulated pERK1/2 response in GCGR transfected HEK 293T cells and CHO-K1 cells stably expressing GCGR. **A)** HEK 293T transiently expressing pmCherry-N1 vector containing GCGR (48 hours post transfection) or **B)** CHO-K1 cells stably expressing GCGR were serum starved for 24 hours and exposed to GCG or TH-GCG for 5 minutes before measuring pERK1/2. CHO-K1 cells were plated at 10,000 cells per well and HEK 293T cells at 50,000 cells per well in a 384-well plate. All values are mean \pm SEM expressed as percentage PMA response (1 μ M) where $n \geq 5$ independent experimental repeats, conducted in duplicate.

Table 4.20. Investigating the TH-GCG stimulated pERK1/2 response in GCGR transfected HEK 293T cells and CHO-K1 cells stably expressing GCGR. Potency (pEC_{50}), maximal response (E_{max}), basal, span, affinity (pK_A) and coupling efficacy ($\log T$) for GCG in HEK 293T or CHO-K1 expressing GCGR measured using a pERK1/2 assay

HEK 293T						
Ligand	pEC_{50} ^a	E_{max} ^b	Basal ^c	Span ^d	pK_A ^e	$\log T$ ^f
GCG	6.12 ±0.19	44.7 ±4.3	3.5 ±1.8	41.2 ±4.5	6.02 ±0.2	-0.58 ±0.06
TH-GCG	6.00 ±0.21	39.4 ±4.6	1.4 ±1.4	37.9 ±4.7	5.78 ±0.2	-0.20 ±0.09
GCGR CHO-K1						
Ligand	pEC_{50} ^a	E_{max} ^b	Basal ^c	Span ^d	pK_A ^e	$\log T$ ^f
GCG	6.89 ±0.20	154.2 ±12.2	5.8 ±9.3	148.4 ±14.5	6.26 ±0.3	0.51 ±0.15
TH-GCG	N.R					

CHO-K1 cells stably expressing GCGR or HEK 293T transiently expressing GCGR were stimulated with GCG or TH-GCG prior to measurement of pERK1/2 to generate concentration response curves. To calculate pEC_{50} , E_{max} , Basal and Span values, data were analysed using a three-parameter logistic equation. Data was also analysed by an operational model of agonism (Black and Leff, 1983) to determine affinity (pK_A) and coupling efficacy ($\log T$).

^a Negative logarithm of ligand concentration required to produce a half-maximal response

^b Maximal response to ligand as percentage PMA response (normalised to maximum PMA response at 1 μ M PMA for each cell line)

^c The low plateau of the fitted sigmoidal dose-response curve

^d The difference between E_{max} and basal signalling

^e The negative logarithm of functional affinities that describes the affinity of the receptor when coupled to a given signalling pathway generated through use of the operational model for partial agonism

^f T is the coupling efficiency parameter generated through use of the operational model for partial agonism. Statistical significance (*, $p < 0.05$; **, $p < 0.01$; ***, $p < 0.001$; ****, $p < 0.0001$) compared to GCG response in HEK 293T or CHO-K1 cell line was determined by unpaired Student's t-test (two-tailed).

N.R denotes no response

4.6.7. Summary

The findings in GCGR transfected HEK 293T cells are distinct from those previously reporting the activity of TH-GCG (Wakelam *et al.*, 1986, Lenzen *et al.*, 1990) and suggest TH-GCG acts as a partial agonist at the GCGR leading to activation of cAMP accumulation, most probably through the classical G_s-dependent pathway. The lack of a detectable Ca²⁺_i and IP₁ response to TH-GCG stimulation in GCGR transfected HEK 293T cells appears to contradict the suggestion that this agonist acts through an alternative coupled pathway leading to inositol phospholipid breakdown. In comparison to the findings in GCGR transfected HEK 293T cells, the lack of detectable cAMP response in Hep 3B cells more closely reflects the previously reported findings for this GCG analogue in hepatocytes (Wakelam *et al.*, 1986, Lenzen *et al.*, 1990). However, caution needs to be taken when interpreting these data due to the high variability in the TH-GCG stimulated cAMP data in Hep 3B cells.

TH-GCG stimulation of C57BL/6 hepatocytes induced a robust cAMP response in a dose-dependent manner and was identified as a partial agonist when compared to GCG. Previous studies looking at cAMP production in response to TH-GCG were measured in hepatocytes extracted from male Sprague-Dawley rats (Wakelam *et al.*, 1986) or guinea pigs (Lenzen *et al.*, 1990). Although it could be argued that the hepatocytes from C57BL/6 mice may respond differently to TH-GCG stimulation when compared to those from rats or guinea pig, a more rational explanation is the differences between the methods used for cAMP measurement and the relative sensitivities. Indeed, a direct comparison between the methods used here and in previous research (Wakelam *et al.*, 1986) highlighted two completely different methods. Here, the cAMP response was measured after a 30 minute challenge with GCG or TH-GCG at a range of concentrations (10 µM – 0.01 nM) in the presence of IBMX (0.5 mM) using the highly sensitive LANCE® *Ultra* cAMP Detection Kit (PerkinElmer). On the other hand, despite using IBMX (1 mM), Wakelam *et al.*, 1986 measured intracellular cAMP after a 5 minute challenge of

hepatocytes at a single concentration (10 nM) using a binding assay utilising a protein from bovine muscle with high specificity for cAMP as described previously (Brown *et al.*, 1971). Aside from the fact a cAMP response may have been detected in rat hepatocytes if a higher concentration of TH-GCG was used, it is likely that the LANCE® *Ultra* cAMP detection kit has superior sensitivity. We can only assume the TH-GCG which was synthesised by Alta Biosciences (University of Birmingham, UK) was correct, but the possibility remains that we have an analogue which is variable to the TH-GCG used in these early studies.

In conclusion, using a sensitive cAMP accumulation assay, this work characterises TH-GCG as a partial agonist in both GCGR transfected HEK 293T cells and in C57BL/6 mice hepatocytes. Although GCG was shown to also stimulate a Ca^{2+} response in GCGR transfected HEK 293T cell in a $G_{q/11}$ -dependent manner, this was not the case for TH-GCG. With this in mind and contradictory to early findings, it appears TH-GCG is not a biased agonist at the GCGR and is acting through the classical G_s -coupled pathway leading to cAMP production.

Finally, this work also reports for the first time an investigation into the TH-GCG stimulated pERK1/2 response. The findings suggest a cell line dependent TH-GCG stimulated pERK1/2 response at the GCGR where a concentration-dependent increase in pERK1/2 was only reported in GCGR transfected HEK 293T cells and not stable CHO-K1 cells. On the other hand, with the conclusion that GCGR stable CHO-K1 cells appear to be a more robust system for the analysis of pERK1/2 responses (Section 4.4.2.1), it may be argued that TH-GCG stimulation at the GCGR does not induce a pERK1/2 response. As a side note, given the GCG stimulated pERK1/2 response was shown to be partially $G_{q/11}$ -dependent (Section 4.4.5), future experiments could include an investigation into the measured pERK1/2 response to TH-GCG stimulation in HEK 293T cells transfected with GCGR with and without the $G_{q/11}$ inhibitor, YM-254890. Such findings would indicate if the potential pERK1/2 response to TH-GCG stimulation at the GCGR is $G_{q/11}$ -mediated.

4.7. Investigation the pharmacological consequences of RAMP2-GCGR interaction

4.7.1. Cell-surface expression of GCGR is not influenced by RAMP2 co-expression

GCGR is known to interact with RAMP2 (Christopoulos *et al.*, 2003), although the pharmacological role of this RAMP2-GCGR interaction remains unknown. We first looked to investigate if the cell-surface expression of GCGR is influenced by co-expression of RAMP2 using ELISA. Here, HEK 293T cells were transfected with pcDNA3.1 vector expressing myc-tagged GCGR only (0.25 µg per well in a 24-well plate) or in combination with varying concentrations of pcDNA3.1 expressing FLAG-tagged RAMP2 (FLAG-RAMP2). pcDNA3.1 expressing RAMP1, was used to maintain the total DNA concentration at transfection to 0.50 µg per well in a 24-well plate. The choice to use RAMP1 rather than vector only was based on the attempt to put the same pressure on the cell in terms of transcription and translation.

Consistent with previous finding (Weston *et al.*, 2015), the cell-surface expression of GCGR was not influenced by co-expression with FLAG-RAMP2 at any of the tested FLAG-RAMP2 DNA concentrations (Figure 4.30). However, increasing the amount of RAMP2 relative to GCGR resulted in elevated levels of FLAG-tagged RAMP2 at the plasma membrane (Figure 4.31). Here, the cell-surface expression of FLAG-RAMP2 is concentration-dependent with increasing amount of FLAG-RAMP2 DNA at transfection correlating with increased cell-surface expression up until a GCGR:RAMP2 ratio of 0.8:1. At this point, the RAMP2 expression appears to have reached a plateau where increasing the RAMP2 concentration further does not translate to increased cell-surface expression. As would be expected, this finding confirms that increasing the level of DNA at transfection translates to increased protein expression to a certain point, after which saturation is effectively reached. Notably, there was no significant difference in cell-surface expression of FLAG-RAMP2 with or without co-expression of GCGR (Figure

4.31 ratio 1:1 vs 1:0). This confirms that cell-surface expression of RAMP2 is not influenced by GCGR.

RAMPs transport poorly to the cell-surface when expressed alone (Wootten *et al.*, 2013). Interestingly, FLAG-RAMP2 was detected on the cell-surface in the absence of GPCR co-transfection. This finding suggests the endogenous expression of another RAMP interacting receptor by HEK 293T cells such as CLR, which requires RAMP expression to reach the cell-surface, or CT receptor.

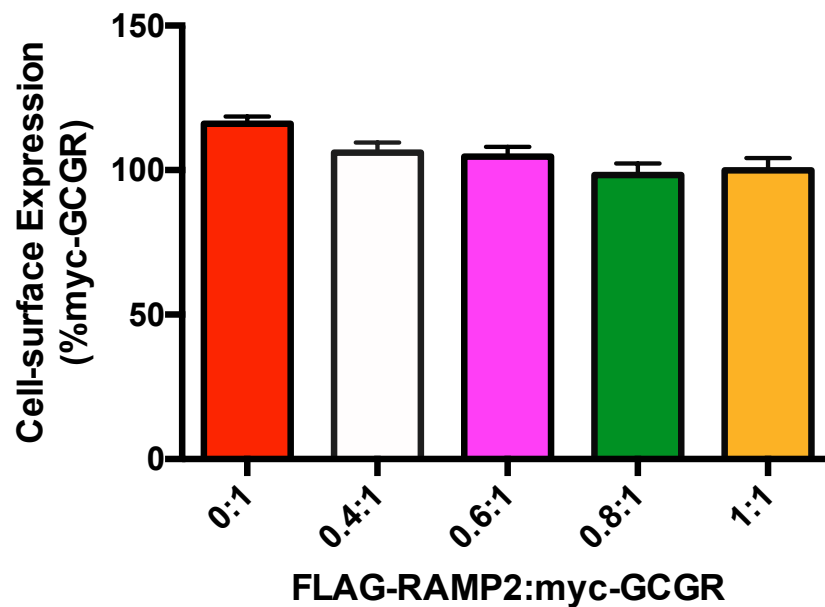


Figure 4.30. RAMP2 does not influence the cell-surface expression of myc-tagged GCGR in transfected HEK 293T cells. HEK 293T cells were transfected with myc-tagged GCGR (0.25 $\mu\text{g}/\text{well}$ of a 24-well plate) and varying amounts of FLAG-tagged RAMP2. In order to keep the total amount of DNA at transfection constant (0.50 $\mu\text{g}/\text{well}$ of a 24-well plate), RAMP1 DNA was used as a non-interacting control. ELISA was conducted 48-hours post transfection using primary antibody mouse anti-myc at a 1:2000 dilution followed by anti-mouse HRP-linked secondary antibody at a 1:4000 dilution. Values are mean \pm SEM expressed as percentage 1:1 FLAG-RAMP2:myc-GCGR ratio response where $n \geq 5$ independent experimental repeats, conducted in duplicate. Statistical significance (*, $p < 0.05$; **, $p < 0.01$; ***, $p < 0.001$) in the difference in cell-surface expression when compared to myc-GCGR only (0:1) was determined by one-way ANOVA with Dunnett's post test.

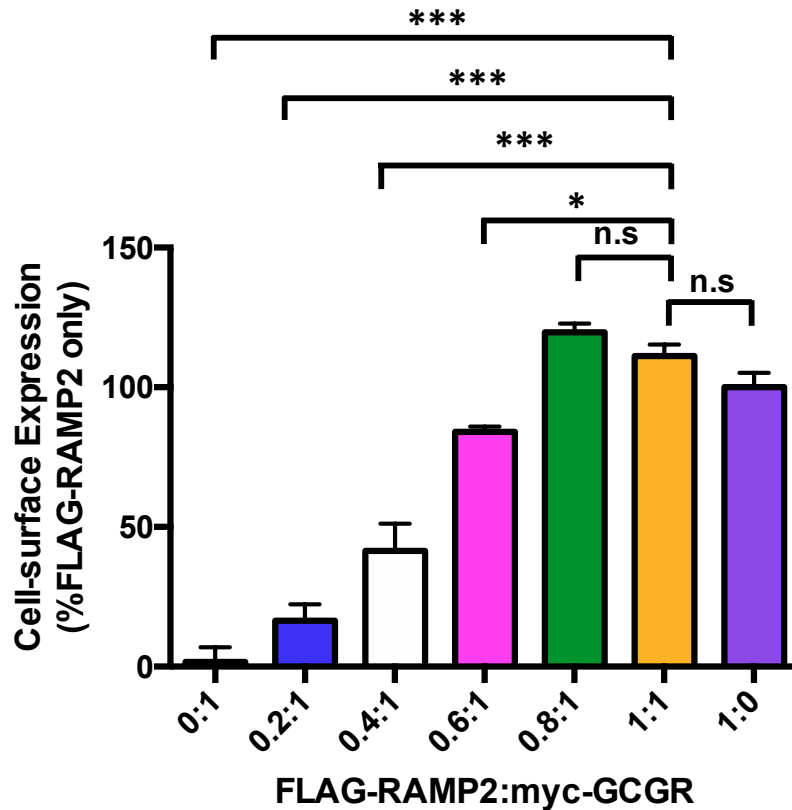


Figure 4.31. GCGR does not influence the cell-surface expression of FLAG-tagged RAMP2 in transfected HEK 293T cells. HEK 293T cells were transfected with myc-tagged GCGR (0.25 $\mu\text{g}/\text{well}$ of a 24-well plate) and varying amounts of FLAG-tagged RAMP2. In order to keep the total amount of DNA at transfection constant (0.50 $\mu\text{g}/\text{well}$ of a 24-well plate), RAMP1 DNA was used as a non-interacting control. ELISA was conducted 48-hours post transfection using primary antibody mouse anti-FLAG at a 1:2000 dilution followed by anti-mouse HRP-linked secondary antibody at a 1:4000 dilution. Values are mean \pm SEM expressed as percentage 1:0 FLAG-RAMP2:myc-GCGR ratio response (100%) and GCGR only transfected control (0%) where $n \geq 5$ independent experimental repeats, conducted in duplicate. Statistical significance (*, $p < 0.05$; **, $p < 0.01$; ***, $p < 0.001$) in the difference in cell-surface expression when compared to RAMP2:GCGR ratio of 1:1 was determined by one-way ANOVA with Dunnett's post test.

4.7.2. RAMP2 potentiated the response of GCG at the GCGR

Having shown the cell-surface expression of GCGR was not influenced by co-expression of RAMP2 in transfected HEK 293T cells, we next sought to investigate any pharmacological consequence of this potential RAMP2-GCGR interaction.

As previously conducted for cell-surface expression analysis, HEK 293T cells were transfected with GCGR and varying concentrations of RAMP2 and the none-interacting control RAMP1 to maintain the DNA concentration at transfection to 0.50 $\mu\text{g}/\text{well}$ of a 24-well plate. These cells were stimulated with GCG and the cAMP accumulation detected. As expected, GCG stimulated a robust cAMP response in HEK 293T cells transfected with pcDNA3.1 expressing GCGR (pEC_{50} 10.75 \pm 0.18, E_{max} 101.3 \pm 5.6 GCGR only response) (Figure 4.31 and Table 4.21). There was found to be no significant difference in the measured potency with RAMP2 co-transfection. On the other hand, there was a RAMP2-dependent increase in maximal response and span (Table 4.21). Here, increasing the RAMP2 level relative to GCGR resulted in a concentration-dependent increase in maximal cAMP response, which reached nearly a 5-fold increase in at a 1:1 ratio (E_{max} 463.5 \pm 47.5 percentage GCGR only response). The significant increase in relative efficacy ($\log\tau$) suggests that RAMP2 increases the ability of GCGR to transduce the signal following GCG stimulation (Figure 4.31). At a RAMP2:GCGR ratio of 0.8:1 and 1:1, there was also found to be a significant increase in affinity suggesting that RAMP2 expression increases the affinity of GCG for the GCGR. This is distinct from previous findings used ligand binding which reported no change in receptor affinity for GCG with RAMP2 co-expression (Weston *et al.*, 2015).

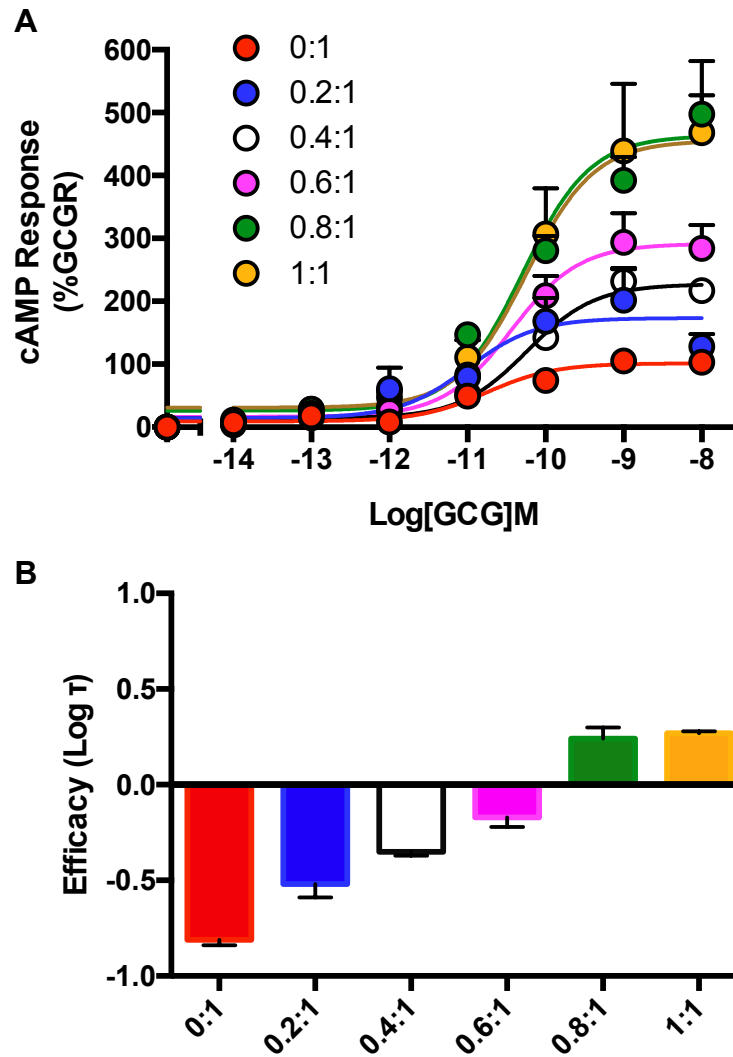


Figure 4.32. RAMP2 potentiates the GCG response at the GCGR in transfected HEK 293T cells. HEK 293T cells were transfected with GCGR (0.25 $\mu\text{g}/\text{well}$ of a 24-well plate) and increasing amounts of RAMP2. RAMP1 was used to maintain the total DNA concentration at transfection to 0.50 $\mu\text{g}/\text{well}$ as a non-interacting control (Christopoulos et al., 2003). **A**) cAMP response was detected in HEK 293T cells (1,000 cells/well) following a 8 minutes stimulation with GCG. **B**) Coupling efficacy ($\log \tau$) for GCG at each of the GCGR:RAMP2 ratios, determined using the operational model of agonism (Black and Leff, 1983). All cAMP accumulation values are mean \pm SEM expressed as percentage 0:1 RAMP2:GCGR ratio response where $n \geq 5$ independent experimental repeats, conducted in duplicate.

Table 4.21. RAMP2 potentiates the GCG response at the GCGR in transfected HEK 293T cells. Potency (pEC_{50}), maximal response (E_{max}), basal, span, affinity (pK_A) and coupling efficacy ($\log \tau$) for GCG in HEK 293T cells expressing GCGR and increasing amounts of RAMP2 (RAMP2:GCGR ratio), measured using a cAMP assay

Ratio	cAMP					
	pEC_{50}^a	E_{max}^b	Basal ^c	Span ^d	pK_A^e	$\log \tau^f$
0:1	10.75 ±0.18	101.3 ±5.6	9.0 ±4.8	92.3 ±7.1	10.69 ±0.2	-0.81 ±0.03
0.2:1	11.00 ±0.23	173.4 ±18.5**	14.3 ±14.7	159.0 ±22.8	10.88 ±0.3	-0.52 ±0.07***
0.4:1	10.24 ±0.10	227.3 ±8.6***	14.0 ±6.1	213.3 ±10.0*	10.08 ±0.1	-0.35 ±0.02***
0.6:1	10.44 ±0.19	275.2 ±18.2***	16.3 ±13.4	275.2 ±13.4***	10.22 ±0.2	-0.17 ±0.05***
0.8:1	10.25 ±0.13	455.4 ±20.8***	30.8 ±13.6	424.5 ±23.8***	9.81 ±0.1*	0.24 ±0.06***
1:1	10.29 ±0.23	463.5 ±47.5***	26.0 ±33.1	437.5 ±55.3***	9.84 ±0.3*	0.27 ±0.01***

HEK 293T cells transfected with the GCGR only or co-transfected with increasing concentrations of RAMP2 were stimulated with GCG and the cAMP response measured in order to generate concentration response curves. To calculate pEC_{50} , E_{max} , Basal and Span values, data were analysed using a three-parameter logistic equation. Data was also analysed by an operational model of agonism (Black and Leff, 1983) to determine affinity (pK_A) and coupling efficacy ($\log \tau$).

^a Negative logarithm of ligand concentration required to produce a half-maximal response

^b Maximal response to ligand as percentage GCGR only response (RAMP2:GCGR ratio 0:1)

^c The low plateau of the fitted sigmoidal dose-response curve

^d The difference between E_{max} and basal signalling

^e The negative logarithm of functional affinities that describes the affinity of the receptor when coupled to a given signalling pathway generated through use of the operational model for partial agonism

^f τ is the coupling efficiency parameter generated through use of the operational model for partial agonism
 Statistical significance (*, $p < 0.05$; **, $p < 0.01$; ***, $p < 0.001$) in the differences between GCG responses in the absence of RAMP2 co-transfection and with different RAMP2 levels was determined by one-way ANOVA with Dunnett's post test.

4.7.3. No RAMP2-dependent potentiation of GCG response in HEK 293T cells transfected with GCGR and RAMP2 dual expression vector

When co-transfecting cells with two or more different DNA constructs, the question of transfection efficiency, in terms of equal cellular uptake and expression arises. Such differences in the population of assayed cells would make the dissection of a signalling pathway difficult. With this in mind, a dual expression vector (pVITRO1) containing both constructs of interest was made; myc-GCGR at multiple cloning site 1 (MCS1) and FLAG-RAMP2 at multiple cloning site 2 (MCS2) (henceforward known as R2-GCGR). Control vectors containing myc-GCGR only at MCS1 and one also containing FLAG-RAMP3 (as a none interacting RAMP control) at multiple cloning site 2 (MCS2) (henceforward known as GCGR and R3-GCGR, respectively) was also made.

HEK 293T cells transfected with these pVITRO1 constructs were stimulated with GCG and cAMP accumulation detected. GCG stimulated a robust cAMP response in HEK 293T cells transfected with GCGR only expressing pVITRO1 (pEC_{50} 11.3 \pm 0.1, E_{max} 105.5 \pm 3.4 expressed as percentage GCGR only expressing vector) (Figure 4.33 and Table 4.22). Transfection of HEK 293T with the R2-GCGR dual expression vector showed no significant potentiation in GCG stimulated cAMP response when compared to either GCGR only expressing vector or R3-GCGR. This was unexpected; given the previous findings showing a RAMP2-dependent increase in maximal response to GCG (Figure 4.31 A). The two experiments used different vectors (pcDNA3.1 and pVITRO1) and may provide an explanation if transfection efficiency and expression is variable. Another concern is the possibility that despite the presence of a single copy of RAMP2 and GCGR on the dual expression vector, this does not necessarily translate to 1:1 protein expression.

ELISA was used to investigate if the cell-surface expression of FLAG-tagged RAMP2 was similar in HEK 293T cells transfected with pVITRO1

expressing FLAG-RAMP2 only or FLAG-RAMP2 and GCGR (R2-GCGR). FLAG-RAMP2 and CLR co-transfection was used as a positive control for a known RAMP2 interaction that has been reported to increase cell-surface expression of RAMP2 (Weston *et al.*, 2015). As expected, co-expression of FLAG-RAMP2 only expressing pVITRO1 with CLR resulted in a significant increase in cell-surface expression of FLAG-RAMP2 (Figure 4.34) confirming that RAMP2:CLR interaction increases trafficking to the cell-surface.

Interestingly, FLAG-RAMP2 cell-surface expression was found to be significantly higher when expressed from multiple cloning site 2 (MCS2) in the absence of GCGR at multiple cloning site 1 (MCS1) (Figure 4.34). In other words, it was noted that FLAG-RAMP2 cell-surface expression when cells were transfected with FLAG-RAMP2 only (ratio 1:0) was significantly more when compared to cells transfected with equal amounts of R2-GCGR (ratio 0:1) (Figure 4.34). This finding was unexpected given the only difference between these vectors is the presence or absence of GCGR at MCS1 and previous findings confirmed that neither the cell-surface expression of GCGR nor RAMP2 was influenced by co-expression (Figure 4.30 and 4.31, respectively). This may suggest that the transcription of RAMP2 is limited by the transcription of GCGR at MCS2 or that RAMP2 is being sequestered by GCGR somewhere in the receptor life-cycle. These data highlight that although in theory a 1:1 DNA ratio of GCGR to RAMP2 exists in dual expression vectors, this may not necessarily translate to a 1:1 protein expression ratio. An alternative explanation may be that RAMP1 actually influenced the previous reported results (section 4.7.2). However, given that previous findings have reported that GCGR does not interact with RAMP1 (Christopoulos *et al.*, 2003, Weston *et al.*, 2015), this is unlikely to be the case.

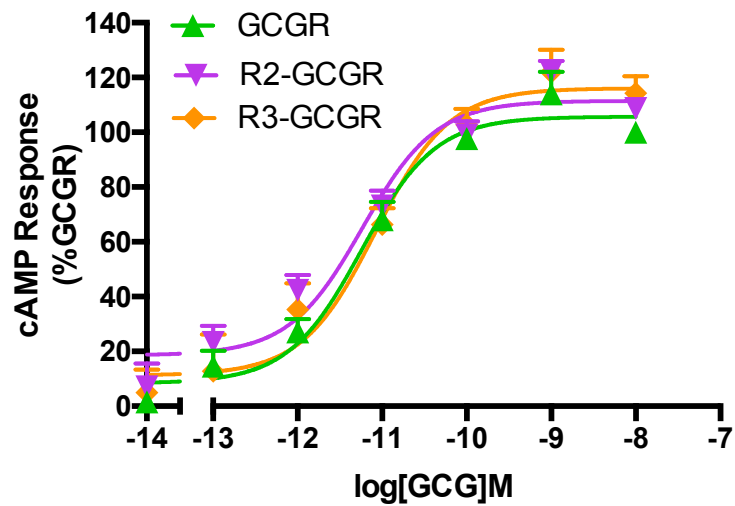


Figure 4.33. RAMP2 fails to potentiate the cAMP response in HEK 293T cells transfected with the pVITRO vector expressing GCGR and RAMP2. HEK 293T cells were transfected with the pVITRO1 dual expression vector containing myc-GCGR at multiple cloning site 1 (MCS1), with either no additional receptor in MCS2, FLAG-RAMP2 (MCS2) (R2-GCGR) or RAMP3 (R3-GCGR) (as a non-interacting RAMP control). 48-hours post transfection, HEK 293T cells (1,000 cells/well) were stimulated for with GCG for 8 minutes and cAMP accumulation measured. All values are mean \pm SEM expressed as percentage GCGR only expressing pVITRO1 response where $n \geq 5$ independent experimental repeats, conducted in duplicate.

Table 4.22. RAMP2 fails to potentiate the cAMP response in HEK 293T cells transfected with the pVITRO vector expressing GCGR and RAMP2. Potency (pEC_{50}), maximal response (E_{max}), basal, span, affinity (pK_A) and coupling efficacy ($\log \tau$) for GCG in HEK 293T cells expressing various pVITRO1 constructs measured using a cAMP assay

Construct	cAMP Response					
	pEC_{50}^a	E_{max}^b	Basal ^c	Span ^d	pK_A^e	$\log \tau^f$
GCGR	11.27 ±0.11	105.5 ±3.4	8.5 ±3.4	98.7 ±4.6	10.54 ±0.2	0.60 ±0.08
R2-GCGR	11.19 ±0.12	111.8 ±3.7	18.7 ±3.8	91.1 ±5.0	10.45 ±0.2	0.70 ±0.10
R3-GCGR	11.04 ±0.15	116.3 ±5.2	11.3 ±5.3	102.4 ±7.0	10.15 ±0.3	0.88 ±0.18

HEK 293T cells transfected with the pVITRO1 dual expression vector containing myc-GCGR at multiple cloning site 1 (MCS1), with either no additional receptor in MCS2 (GCGR), FLAG-RAMP2 (MCS2) (R2-GCGR) or RAMP3 (R3-GCGR) (as a non-interacting RAMP control) were stimulated with GCG and the cAMP response measured in order to generate concentration response curves. To calculate pEC_{50} , E_{max} , Basal and Span values, data were analysed using a three-parameter logistic equation. Data was also analysed by an operational model of agonism (Black and Leff, 1983) to determine affinity (pK_A) and coupling efficacy ($\log \tau$).

^a Negative logarithm of ligand concentration required to produce a half-maximal response

^b Maximal response to ligand as percentage GCGR response

^c The low plateau of the fitted sigmoidal dose-response curve

^d The difference between E_{max} and basal signalling

^e The negative logarithm of functional affinities that describes the affinity of the receptor when coupled to a given signalling pathway generated through use of the operational model for partial agonism

^f τ is the coupling efficiency parameter generated through use of the operational model for partial agonism

Statistical significance (*, $p < 0.05$; **, $p < 0.01$; ***, $p < 0.001$) in the differences between GCG responses when compared to GCGR only expressing pVITRO1 was determined by one-way ANOVA with Dunnett's post test

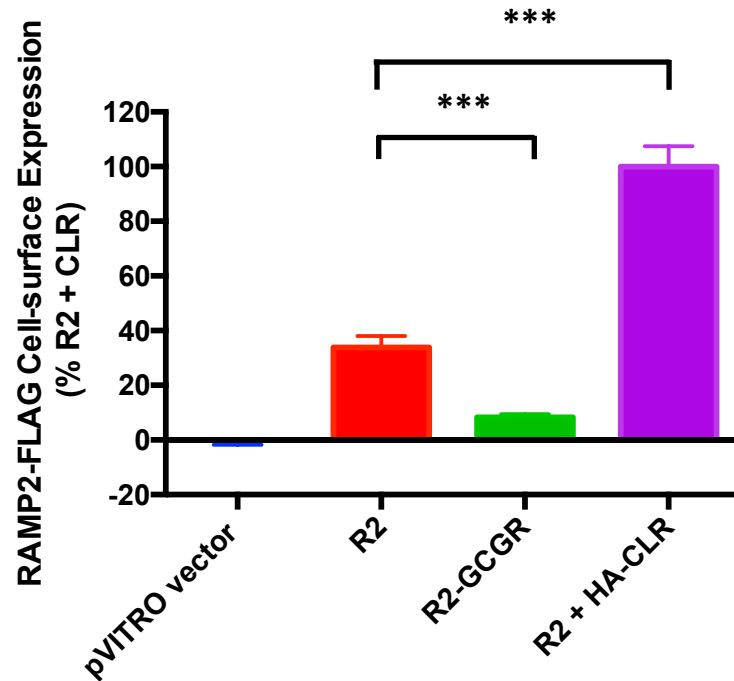


Figure 4.34. FLAG-RAMP2 cell-surface expression was elevated in HEK 293T cells transfected with pVITRO1 expressing RAMP2 only when compared to pVITRO1 expressing RAMP2 and GCGR. Cell-surface expression of RAMP2-FLAG, in HEK 293T cells transfected (0.25 μ g/well of a 24-well plate) with the dual expression vector (pVITRO1) containing FLAG-RAMP2 at multiple cloning site 2 (MCS2) only (R2) or FLAG-RAMP2 with GCGR at multiple cloning site 1 (MCS1) (R2-GCGR). ELISA was conducted 48-hours post transfection using primary mouse anti-FLAG at a 1:2000 dilution followed by anti-mouse HRP-linked secondary antibody at a 1:4000 dilution. Values are mean \pm SEM expressed as % R2 + CLR (100%) and vector only transfected control (0%) where $n \geq 5$ independent experimental repeats, conducted in duplicate. Statistical significance (*, $p < 0.05$; **, $p < 0.01$; ***, $p < 0.001$) in the differences in cell-surface expression between R2 only and R2-GCGR expressing vector was determined by unpaired Student's t-test (two-tailed).

4.7.4. Summary

RAMPs are known to interact with a number of GPCR leading to changes in cell-surface expression and ligand preferences (Christopoulos *et al.*, 2003). Although an interaction between GCGR and RAMP2 has previously been reported (Christopoulos *et al.*, 2003), the pharmacological consequence of this was not investigated. The results presented here identify a pharmacological consequence of RAMP2 and GCGR interaction, which is independent of cell-surface expression. There was found to be a RAMP2-dependent change in cAMP response to GCG with a RAMP2 concentration-dependent increase in maximal response. Interestingly, this finding could not be reproduced using a dual expression vector expressing both GCGR and RAMP2. Although this was unexpected, investigation into the RAMP2 cell-surface expression suggested that RAMP2 expression from MCS2 of the vector was reduced when GCGR was at MCS1. A change in RAMP2 expression relative to GCGR from the pVITRO1 vector may provide an explanation as to why a potentiation in GCG stimulated cAMP response was not seen. Speculation as to the cause of this reduced RAMP2 cell-surface expression includes the possibility that RAMP2 transcription is limited by the transcription of GCGR or that GCGR is somehow sequestering RAMP2.

These data highlight that although in theory a 1:1 DNA ratio of GCGR to RAMP2 exists in the dual expression vector, this does not appear to translate to a 1:1 protein expression ratio. This not only makes the investigation of RAMP2-GCGR interaction and pharmacology difficult, but also suggests the need for vector optimisation and investigation of expression levels in transfection experiments. Indeed, this raises further challenging questions such as the required number of RAMP2 to a single GCGR in order to lead to a potentiated cAMP response, as has been reported here.

4.8. Pharmacology in a hepatic cell line: Hep 3B

4.8.1. GCG and oxyntomodulin stimulates a robust cAMP response in Hep 3B cells

We previously investigated the GPCR and RAMPs mRNA expression in Hep 3B cells and, in combination with initial cAMP assays, suggested the likely expression of GCGR (Section 3.7). We wanted to expand on these initial experiments and give an indication of mRNA translation and functional protein expression in Hep 3B cells.

Hep 3B cells (5,000 cells/well) were stimulated with various ligands and cAMP accumulation detected using the LANCE cAMP *Ultra* detection kit (Section 2.8.1, Figure 2.8.1.2). A robust cAMP response was detected for GCG and oxyntomodulin in Hep 3B cells with similar passage number (Figure 4.35). No response was detected for GLP-1(7-36)amide, GIP(1-42) or (GIP). In addition, stimulation with the breakdown products of GLP-1(7-36)amide and GIP (GLP-1(9-36)amide and GIP(3-42), respectively) showed no detectable cAMP accumulation.

Oxyntomodulin is reported to be both an agonist of the GLP-1R and GCGR, despite showing a 10-fold or 100-fold reduction in potency when compared to the endogenous ligands GLP-1(7-36)amide or GCG, respectively (Pocai *et al.*, 2009). In accordance with this, and what was previously shown in transfected HEK 293 (Section 4.2.1), the potency of oxyntomodulin is approximately 100-fold lower than that seen to GCG (Table 4.23) suggesting that oxyntomodulin is acting at the GCGR. Studies have highlighted that GCGR ligands including GCG and oxyntomodulin can activate the GLP-1R, whereas GLP-1(7-36)amide has been suggested not to act at the GCGR (Runge *et al.*, 2003). In accordance with this, the lack of GLP-1(7-36)amide response suggests both the absence of GLP-1R expression itself and confirms the lack of GLP-1(7-36)amide activity at the GCGR in Hep 3B cells.

When looking at individual dose-responses to GCG and oxyntomodulin acquired from experiments using both early (<8) and late (>8) passage, there is considerable variation in pEC₅₀ values (mean pEC₅₀ 8.82 ± 0.74 and 7.15 ± 0.84, respectively) (Figure 4.36). This variability may be explained by a lack of stability in terms of receptor expression and the apparent loss of GCGR expression from as early as passage 8 supports this argument.

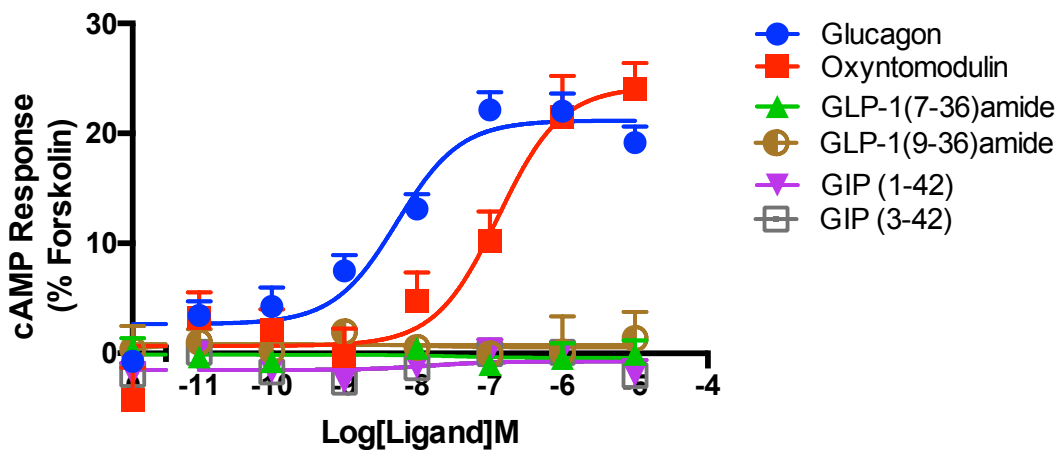


Figure 4.35. cAMP signalling profile in Hep 3B cells. Hep 3B cells (5,000 cells/well) with similar passage number (> 4 from N₂ but less than 8), were exposed to various ligands for 30 minutes and cAMP accumulation detected using a LANCE cAMP Ultra kit. All values are mean ± SEM expressed as percentage forskolin response (100 μM) where *n* ≥ 5 independent experimental repeats, conducted in duplicate.

Table 4.23. cAMP signalling profile in Hep 3B cells. Potency (pEC_{50}), maximal response (E_{max}), basal, span, affinity (pK_A) and coupling efficacy ($\log\tau$) for various ligand measured in Hep 3B cells using a cAMP accumulation assay

cAMP						
Construct	pEC_{50} ^a	E_{max} ^b	Basal ^c	Span ^d	pK_A ^e	$\log\tau$ ^f
Glucagon	8.28 ±0.16	21.17 ±0.9	2.66 ±0.9	18.52 ±1.2	8.19 ±0.2	-0.63 ±0.03
Oxyntomodulin	6.88 ±0.24***	24.23 ±2.4	0.68 ±1.3	23.55 ±2.6	6.76 ±0.2**	-0.51 ±0.06
GLP-1(7-36)amide	N.R	N.R	1.82 ±1.2		N.R	
GLP-1(9-36)amide	N.R	N.R	0.85 ±2.7		N.R	
GIP(1-42)	N.R	N.R	1.01 ±1.2		N.R	
GIP(3-42)	N.R	N.R	1.50 ±2.3		N.R	

Hep 3B cells were stimulated with various ligands prior to measurement of cAMP accumulation to generate concentration response curves for each construct. To calculate pEC_{50} , E_{max} , Basal and Span values, data were analysed using a three-parameter logistic equation. Data was also analysed by an operational model of agonism (Black and Leff, 1983) to determine affinity (pK_A) and coupling efficacy ($\log\tau$).

^a Negative logarithm of ligand concentration required to produce a half-maximal response

^b Maximal response to ligand as percentage forskolin response

^c The low plateau of the fitted sigmoidal dose-response curve

^d The difference between E_{max} and basal signalling

^e The negative logarithm of functional affinities that describes the affinity of the receptor when coupled to a given signalling pathway generated through use of the operational model for partial agonism

^f τ is the coupling efficiency parameter generated through use of the operational model for partial agonism

All values are mean ± SEM expressed as percentage forskolin response where $n \geq 5$ independent experimental repeats, conducted in duplicate.

Statistical significance (*, $p < 0.05$; **, $p < 0.01$; ***, $p < 0.001$) of oxyntomodulin response in comparison to GCG response was determined by unpaired Student's t-test (two-tailed).

N.R denotes no response

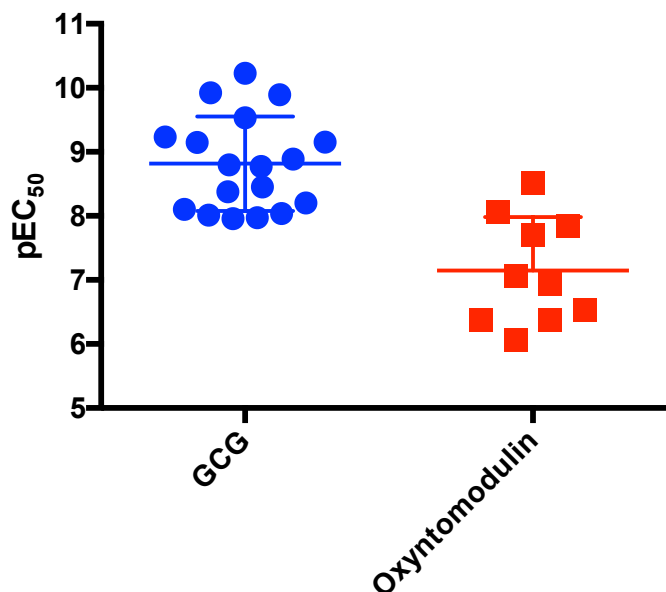


Figure 4.36. The measured potency for GCG and oxyntomodulin varies across experimental repeats in Hep 3B cells. Hep 3B cells (5,000 cells/well) were exposed to GCG or oxyntomodulin for 30 minutes and cAMP accumulation detected using a LANCE cAMP Ultra kit. The scatter plot shows single pEC₅₀ value acquired through fitting each repeat data to a three-parameter logistic equation. All values are mean ± SD where $n \geq 9$ independent experimental repeats.

4.8.2. Adrenomedullin stimulates a cAMP response in Hep 3B cells

In order to give a pharmacological indication of RAMP1-3 protein expressed, peptides known to be active at the CLR only when in combination with RAMPs (CGRP, AM and adrenomedullin 2 (AM2)) were utilised. A concentration-dependent cAMP response was detected for AM in Hep 3B cells with similar passage number, whereas there was no response detected to AM2 or CGRP stimulation (Figure 4.37 and Table 4.24). Similarly to the GCG and oxyntomodulin response data, when looking at individual dose-responses to AM acquired from experiments using various Hep 3B passages, there was considerable variation in potency values (mean pEC₅₀ 8.00 ± 1.32) (Figure 4.38). Again, this variability may be explained by a lack of stability in terms of receptor expression.

The specificity of CGRP, AM and AM₂ for CLR is conferred by RAMPs where expression of both is essential for the formation of functional receptors (Choksi *et al.*, 2002). RT-PCR results indicated significant mRNA expression of RAMP2 with a small level of CLR, RAMP1 and RAMP3 (Section 3.7.1). It has been suggested in a number of transfection studies that CLR functions as a CGRP preferring receptor when co-expressed with RAMP1 whereas it forms an AM and AM₂ preferring receptor when co-expressed with RAMP2 or RAMP3, respectively (Choksi *et al.*, 2002). According to the rank order of potency at the various CLR and RAMP combinations (Table 4.25), the response to AM stimulation in Hep 3B cells, in addition to the RT-PCR results (Figure 3.7.1), suggests the endogenous expression of a functional AM receptor (CLR and RAMP2).

To add an additional layer of complexity, AM is also known to act at the CTR and the amylin receptor (CTR expressed in combination with RAMPs) (Christopoulos *et al.*, 1999). An alternative explanation to the AM induced cAMP response aside from the stimulation of a functional AM receptor may be the expression and stimulation of the CTR or amylin receptor. In order to exclude this possibility and identify the receptor responsible for the measured AM response, Hep 3B cells need to be stimulated with CT and amylin. However, if Hep 3B cells do indeed express CTR or amylin receptor, and the various agonists exhibit the rank order of potency as previously indicated (Table 4.26), CGRP stimulation should give a greater response than AM at the CTR, AMY1 and AMY3 receptor. With this in mind, the lack of detectable CGRP response could indicate that AM is likely to be acting at the AM receptor.

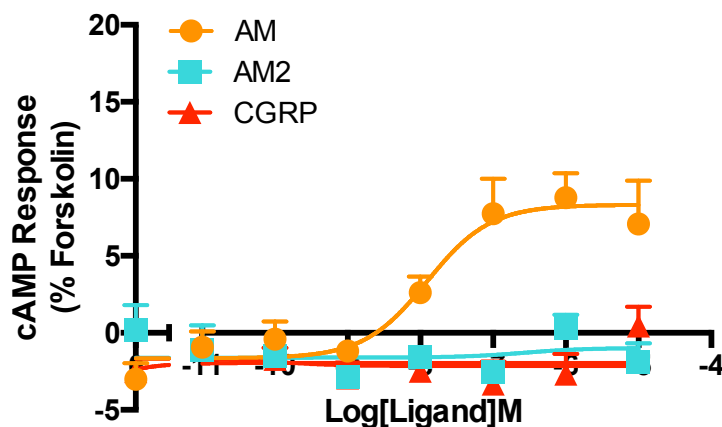


Figure 4.37. cAMP signalling profile in Hep 3B cells. Hep 3B cells (5,000 cells/well) with similar passage number (> 4 from N₂ but less than 8), were exposed to various ligands for 30 minutes and cAMP accumulation detected using a LANCE cAMP Ultra kit. All values are mean \pm SEM expressed as percentage forskolin response (100 μ M) where $n \geq 5$ independent experimental repeats, conducted in duplicate.

Table 4.24. cAMP signalling profile in Hep 3B cells. Potency (pEC_{50}), maximal response (E_{max}), basal, span, affinity (pK_A) and coupling efficacy ($\log \tau$) for various ligand measured in Hep 3B cells using a cAMP accumulation assay

Ligand	cAMP					
	pEC_{50} ^a	E_{max} ^b	Basal ^c	Span ^d	pK_A ^e	$\log \tau$ ^f
AM	7.91 ± 0.27	8.32 ± 1.03	-1.65 ± 0.8	9.97 ± 1.2	7.86 ± 0.3	-0.96 ± 0.06
AM2		N.R	-2.21 ± 0.8		N.R	
CGRP		N.R	-0.01 ± 0.9		N.R	

Hep 3B cells were stimulated with adrenomedullin (AM), adrenomedullin 2 (AM2) or calcitonin gene related peptide (CGRP) prior to measurement of cAMP accumulation to generate concentration response curves for each construct. To calculate pEC_{50} , E_{max} , Basal and Span values, data were analysed using a three-parameter logistic equation. Data was also analysed by an operational model of agonism (Black and Leff, 1983) to determine affinity (pK_A) and coupling efficacy ($\log \tau$).

^a Negative logarithm of ligand concentration required to produce a half-maximal response

^b Maximal response to ligand as percentage forskolin response

^c The low plateau of the fitted sigmoidal dose-response curve

^d The difference between E_{max} and basal signalling

^e The negative logarithm of functional affinities that describes the affinity of the receptor when coupled to a given signalling pathway generated through use of the operational model for partial agonism

^f τ is the coupling efficiency parameter generated through use of the operational model for partial agonism

All values are mean \pm SEM expressed as percentage forskolin response where $n \geq 5$ independent experimental repeats, conducted in duplicate.

N.R. denotes no response

Table 4.25. Rank order of potency at the CLR with RAMP1-3. Adapted from Moore and Salvatore *et al.*, 2012

	CT	AMY1	AMY2	AMY3
Composition	CT	CT + RAMP1	CT + RAMP2	CT + RAMP3
Rank order of potency	CT \geq AMY,CGRP >AM,AM2	AMY \geq CGRP \geq AM2>CT>AM	Poorly defined	AMY>CGRP> AM2>CT>AM

Table 4.24. Rank order of potency at the CALCR receptor with and without RAMP1-3. Adapted from Moore and Salvatore *et al.*, 2012

	CGRP	AM	AM2
Composition	CLR + RAMP1	CLR + RAMP2	CLR + RAMP3
Rank order of potency	CGRP \geq AM>AM2> AMY	AM>>CGRP,AM2 >AMY	AM \geq CGRP, AM2>AMY

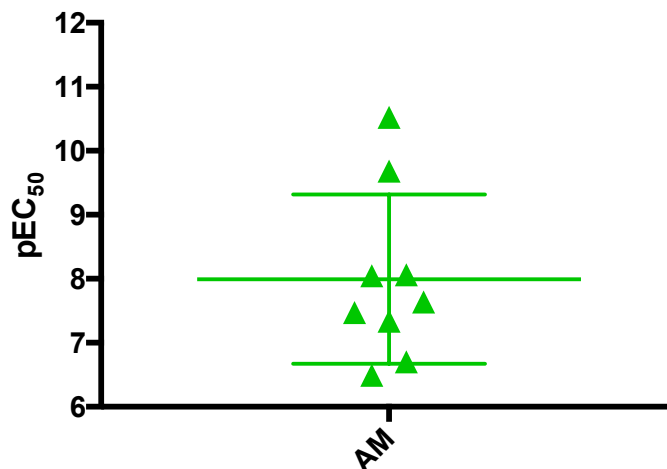


Figure 4.38. The measured potency for AM varies across experimental repeats in Hep 3B cells. Hep 3B cells (5,000 cells/well) were exposed to AM for 30 minutes and cAMP accumulation detected using a LANCE cAMP Ultra kit. The scatter plot shows single pEC₅₀ value acquired though fitting each repeat data to a three-parameter logistic equation. All values are mean \pm SD where $n \geq 9$ independent experimental repeats.

4.8.3. GCG, oxyntomodulin and GLP-1(7-36)amide induce a pERK1/2 response in Hep 3B cells

Given the probable expression of GCGR in Hep 3B cells (Section 3.7) and having demonstrated that GCG or oxyntomodulin stimulation of HEK 293T cells transfected with GCGR and CHO-K1 cells stably expressing GCGR induces a concentration-dependent increase in pERK1/2 (Section 4.4.2.1), we looked to investigate if a pERK1/2 response could also be measured in Hep 3B cells. In addition to investigation the pERK1/2 response to GCG and oxyntomodulin stimulation, we also test the response to GLP-1(7-36)amide. The latter was included due to the previous finding showing a lack of cAMP induced response to GLP-1(7-36)amide in Hep 3B cells.

A pERK1/2 response was detected following GCG, oxyntomodulin and GLP-1(7-36)amide stimulation in Hep 3B cells (Figure 4.39 A). The potency of the measured response to both oxyntomodulin and GLP-1(7-36)amide was lower when compared to GCG, although this was only significant for GLP-1(7-36)amide (Table 4.27). Notably, oxyntomodulin had a higher maximum response and basal level of pERK1/2 when compared to GCG. If this pERK1/2 response is through stimulation of GCGR, this would indicate that although showing reduced potency similar to what is seen for oxyntomodulin stimulated cAMP accumulation in Hep 3B cells, oxyntomodulin is able to induce a greater level of pERK1/2 when compared to GCG. Although a three-parameter does-response was fitted to these data, the points acquired for GCG and oxyntomodulin stimulation could also be fitted with linear regression suggesting more repeats may be needed for a better fit.

Surprisingly, the potency of the pERK1/2 response to GCG or oxyntomodulin stimulation was lower in GCGR transfected HEK 293T cells (pEC_{50} 6.12 \pm 0.19 and 6.25 \pm 0.22, respectively) and CHO-K1 cells (pEC_{50} 6.89 \pm 0.20 and 5.85 \pm 0.13, respectively) expressing stably GCGR (Section 4.4.2.1) when compared to that measured in Hep 3B cells (pEC_{50} 9.13 \pm 0.32 and 8.20 \pm 0.37). This finding may indicate a greater coupling of GCGR to the

pERK1/2 pathway within Hep 3B cells (at early passage) when compared to these alternative cell lines.

The GLP-1(7-36)amide concentration-dependent increase in pERK1/2 response was unexpected given the previous finding indicating a lack of cAMP response to GLP-1(7-36)amide stimulation in Hep 3B cells. Given the cAMP response indicated the absence of GLP-1R expression, it may be speculated that this pERK1/2 response detected here is GCGR-mediated. However, a more likely explanation for this finding is the variable loss of receptor expression in Hep 3B cells over passage number. Speculatively, it may be that Hep 3B cells used in the experiments characterising the cAMP responses to GLP-1(7-37)amide had lost the GLP-1R, whereas the Hep 3B cells used in the analysis of ERK1/2 activation expressed GLP-1R. If this was indeed the case, the elevated oxyntomodulin pERK1/2 response when compared to GCG and GLP-1(7-36)amide could be as a consequence of stimulation of both GCGR and GLP-1R.

The ability to measure a pERK1/2 response was shown to depend on the cell passage number, with experiments using as early as passage 8 failing to induce a response (Figure 4.39 B). Similarly to what was seen for ligand stimulated cAMP responses in Hep 3B cells, there was high variability in the measured potency for the ligand stimulated pERK1/2 responses (Table 4.27). Again, this variability may be explained by a lack of stability in terms of receptor expression and the apparent loss of a measurable pERK1/2 response at early passage supports this argument.

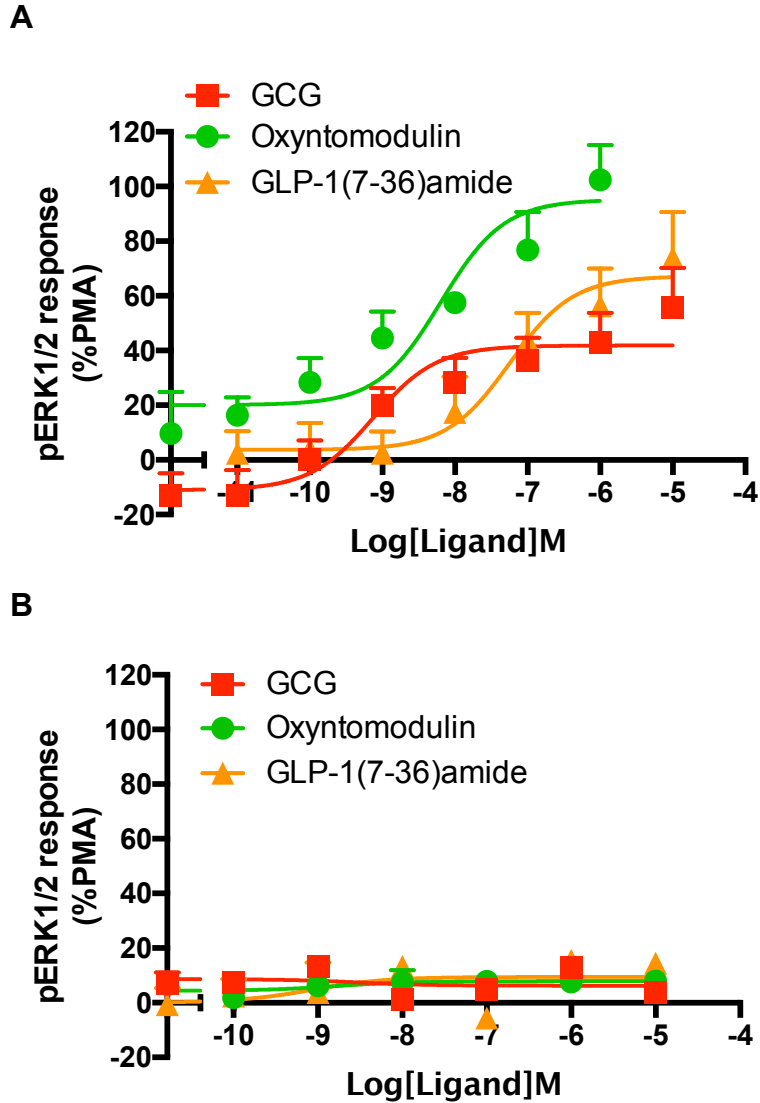


Figure 4.39. GCG, oxyntomodulin and GLP-1(7-36)amide stimulates a pERK1/2 response in ‘young’ Hep 3B cells. Hep 3B cells were serum starved for 4 hours and stimulated with GCG, oxyntomodulin or GLP-1(7-36)amide for 5 minutes before measuring pERK1/2. Cells were plated at 50,000 cells per well (maximum cell number suggested by kit supplier) of a 384-well plate. All values are mean \pm SEM expressed as percentage PMA response (1 μ M) where $n = 3$ independent experimental repeats including cells from passage 3, 4 and 5 (**A**) and $n = 2$ at 8 (**B**), conducted in duplicate.

Table 4.27. GCG, oxyntomodulin and GLP-1(7-36)amide stimulates a pERK1/2 response in 'young' Hep 3B cells. Potency (pEC₅₀), maximal response (E_{max}), basal, span, affinity (pK_A) and coupling efficacy (log τ) for various ligand measured in Hep 3B cells using a pERK1/2 assay

pERK1/2						
Ligand	pEC ₅₀ ^a	E _{max} ^b	Basal ^c	Span ^d	pK _A ^e	log τ ^f
GCG	9.13 ±0.32	41.9 ±4.9	-11.1 ±6.3	52.9 ±7.7	8.90 ±0.3	-0.17 ±0.08
Oxyntomodulin	8.20 ±0.37	95.2 ±9.5**	20.1 ±6.1*	75.1 ±10.9	7.59 ±0.5	0.48 ±0.22*
GLP-1(7-36)amide	7.25 ±0.37*	67.2 ±8.8	3.7 ±6.5	63.5 ±10.4	6.90 ±0.4*	0.08 ±0.14

Hep 3B cells (50,000 cells/well) were stimulated with GCG, oxyntomodulin or GLP-1(7-36)amide prior to measurement of pERK1/2 to generate concentration response curves. To calculate pEC₅₀, E_{max}, Basal and Span values, data were analysed using a three-parameter logistic equation. Data was also analysed by an operational model of agonism (Black and Leff, 1983) to determine affinity (pK_A) and coupling efficacy (log τ).

^a Negative logarithm of ligand concentration required to produce a half-maximal response

^b Maximal response to ligand as percentage PMA response (1 μ M)

^c The low plateau of the fitted sigmoidal dose-response curve

^d The difference between E_{max} and basal signalling

^e The negative logarithm of functional affinities that describes the affinity of the receptor when coupled to a given signalling pathway generated through use of the operational model for partial agonism

^f τ is the coupling efficiency parameter generated through use of the operational model for partial agonism. All values are mean \pm SEM expressed as percentage PMA response (1 μ M) where $n = 3$ independent experimental repeats including cells from passage 3, 4 and 5 (A) and $n = 2$ at passage 7 and 8 (B), conducted in duplicate. Statistical significance in comparison to GCG response was determined by one-way ANOVA with Dunnett's post test

4.8.4. Pharmacological characterisation of two potential GCGR antagonists in Hep 3B cells

4.8.4.1. des-His¹,[Glu⁹]-GCG appears to act as non-competitive antagonist of the GCG stimulated cAMP response in Hep 3B cells

We previously characterised des-His¹,[Glu⁹]-GCG as a partial agonist at the GCGR in HEK 293T cells transfected with pcDNA3.1 expressing GCGR. Here, we investigated its activity in Hep 3B cells endogenously express GCGR.

Using the more sensitive cAMP assay (LANCE cAMP *Ultra* detection kit), the cAMP response in Hep 3B cells was measured following stimulation with GCG alone or in combination with varying concentration of des-His¹,[Glu⁹]-GCG (Figure 4.40 and Table 4.28). Co-stimulation of Hep 3B cells with GCG and 1 μ M or 0.1 μ M of des-His¹,[Glu⁹]-GCG showed a reduction in maximum cAMP response which only reached statistical significance at 1 μ M. There was found to be no significant rightward shift in potency when co-stimulated with 1 μ M of des-His¹,[Glu⁹]-GCG. Although this data may suggest des-His¹,[Glu⁹]-GCG acts as a non-competitive antagonist in Hep 3B cells, caution should be exercised when interpreting these data given the large variability in response.

A dose-response curve was fitted to data acquired from stimulation with des-His¹,[Glu⁹]-GCG alone with an apparent reduced basal cAMP response at 10 μ M of des-His¹,[Glu⁹]-GCG. However, this stimulation data was variable resulting in large error and is unlike to be a true response. This is distinct from the agonistic activity of des-His¹,[Glu⁹]-GCG characterised in GCGR transfected HEK 293T cells.

When comparing the cAMP response to GCG stimulation in Hep 3B cells between experiments looking at either L-168,049 or des-His¹,[Glu⁹]-GCG, there is significantly different potencies (pEC₅₀ 8.14 \pm 0.2 and 9.43 \pm 0.2, respectively). Whereas experiments investigating des-His¹,[Glu⁹]-GCG conducted using very early passage (<4) Hep 3B cells gave a higher pEC₅₀

(9.43 ± 0.2), GCG responses determined from later passage (>4 but <8) looking at the activity of L-168,049 and ligand screening showed lower potency (pEC_{50} 8.14 ± 0.2 and 8.28 ± 0.16 , respectively). As previously indicated, there was considerable variability in measured potency values acquired from fitting a three-parameter logistics equation to individual repeats of GCG, oxytomodulin or AM stimulated cAMP data from various experimental repeats (Figure 4.36 and 4.38). Again, these data indicates poor reproducibility when using Hep 3B cells and is most likely due to loss of receptor with increasing passage.

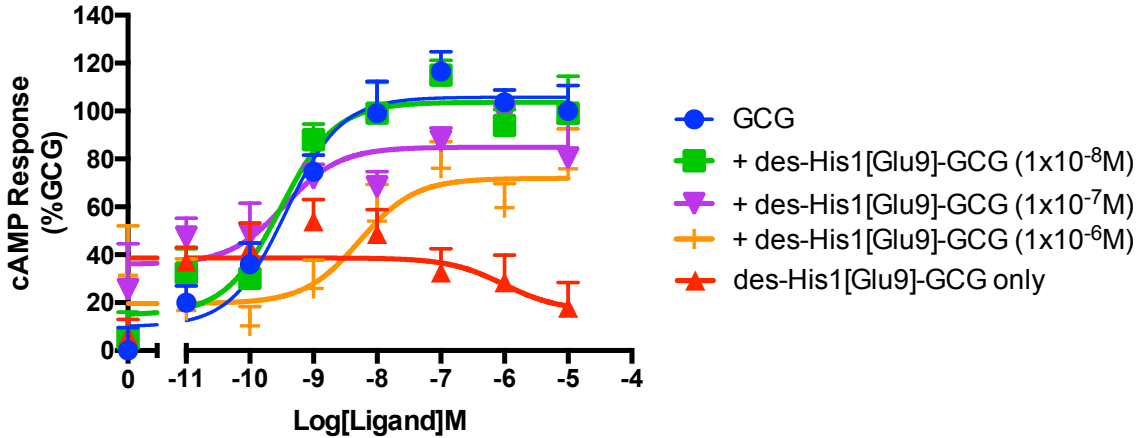


Figure 4.40. Activity of des-His¹,Glu⁹-glucagon amide in Hep 3B. Hep 3B cells (5,000 cells/well) were exposed to GCG with or without various concentration of des-His¹,Glu⁹-glucagon amide (des-His¹,Glu⁹-GCG), or des-His¹,Glu⁹-GCG alone for 30 minutes and cAMP accumulation detected using the LANCE *Ultra* cAMP kit. All values are mean \pm SEM expressed as percentage GCG response where $n = 3$ independent experimental repeats, conducted in duplicate.

Table 4.28. Activity of des-His¹,Glu⁹-glucagon amide in Hep 3B. Potency (pEC₅₀), maximal response (E_{max}), basal, span, affinity (pK_A) and coupling efficacy (log τ) for GCG, L-168,049 or des-His¹,[Glu⁹]-GCG only or GCG in combination with various concentrations of des-His¹,[Glu⁹]-GCG measured in Hep 3B cells using a cAMP accumulation assay

Construct	des-His ¹ ,Glu ⁹ -GCG					
	pEC ₅₀ ^a	E _{max} ^b	Basal ^c	Span ^d	pK _A ^e	log τ ^f
GCG only	9.43 ±0.2	105.8 ±4.8	10.0 ±6.3	95.8 ±7.5		
+ 1x10 ⁻⁸ M	9.52 ±0.2	103.6 ±6.0	14.9 ±7.6	88.7 ±9.2		
+ 1x10 ⁻⁷ M	9.46 ±0.4	84.9 ±5.7	36.0 ±7.4	48.9 ±8.8**		
+ 1x10 ⁻⁶ M	8.30 ±0.6	71.9 ±8.7**	19.6 ±8.5	52.3 ±11.6**		

Hep 3B cells were stimulated with GCG or des-His¹,[Glu⁹]-GCG only or GCG in combination with various concentrations of des-His¹,[Glu⁹]-GCG prior to measurement of cAMP accumulation to generate concentration response curves for each construct. To calculate pEC₅₀, E_{max}, Basal and Span values, data were analysed using a three-parameter logistic equation. Data was also analysed by an operational model of agonism (Black and Leff, 1983) to determine affinity (pK_A) and coupling efficacy (log τ).

^a Negative logarithm of GCG concentration required to produce a half-maximal response

^b Maximal response to GCG as percentage GCG only response

^c The low plateau of the fitted sigmoidal dose-response curve

^d The difference between E_{max} and basal signalling

^e The negative logarithm of functional affinities that describes the affinity of the receptor when coupled to a given signalling pathway generated through use of the operational model for partial agonism

^f τ is the coupling efficiency parameter generated through use of the operational model for partial agonism

All values are mean ± SEM expressed as percentage GCG only (+DMSO added as control) response where $n = 3$ independent experimental repeats, conducted in duplicate.

Statistical significance (*, $p < 0.05$; **, $p < 0.01$; ***, $p < 0.001$) compared to GCG only response was determined by one-way ANOVA with Dunnett's post test

N.R denotes no response

4.8.4.2. L-168,049 acts as a competitive antagonist of the GCG stimulated cAMP response

We previously characterised L-168,049 as a non-competitive antagonist at the GCGR in HEK 293T cells transfected with pcDNA3.1 expressing GCGR. Here, an investigation was made into the activity of this compound in Hep 3B cells endogenously express GCGR. Using the more sensitive cAMP assay (LANCE cAMP *Ultra* detection kit), the cAMP response in Hep 3B cells was measured following stimulated with GCG alone or in combination with varying concentration of L-168,049 (Figure 4.41 and Table 4.29).

Stimulated with GCG in combination with increasing concentrations of L-168,049, showed a rightward shift in GCG potency with statistical significance reached at the antagonist concentration of 1 μ M and above (Figure 4.41 and Table 4.29). L-168,049 stimulation alone showed no cAMP response in Hep 3B cells and suggests this compound has no agonistic activity. Interestingly however, there was a significant increase in basal response and a small but non significant increase in maximal response to GCG with increasing concentrations of L-168,049. This finding may indicate some agonistic activity of the compound or, more likely, fluorescent property leading to an apparent elevation with increasing concentrations (as was previously indicated in HEK 293T cells transfected with GCGR (Section 4.5.2)).

Ligand stimulation in combination with a non-competitive antagonist is expected to reduce the maximal response when compared to ligand stimulation alone. With this in mind, the results suggested L-168,049 to be a competitive antagonist and were unexpected given that this compound was found to be a non-competitive antagonist elsewhere (Section 4.5.2 and Cascieri *et al.*, 1999). However, an attempt to conduct Schild analysis of the data gave a slope of 0.2 rather than 1 and does not support the conclusion that this is a competitive antagonist. Again, due to variability of data acquired using Hep 3B cells, caution needs to be taken when interpreting the data.

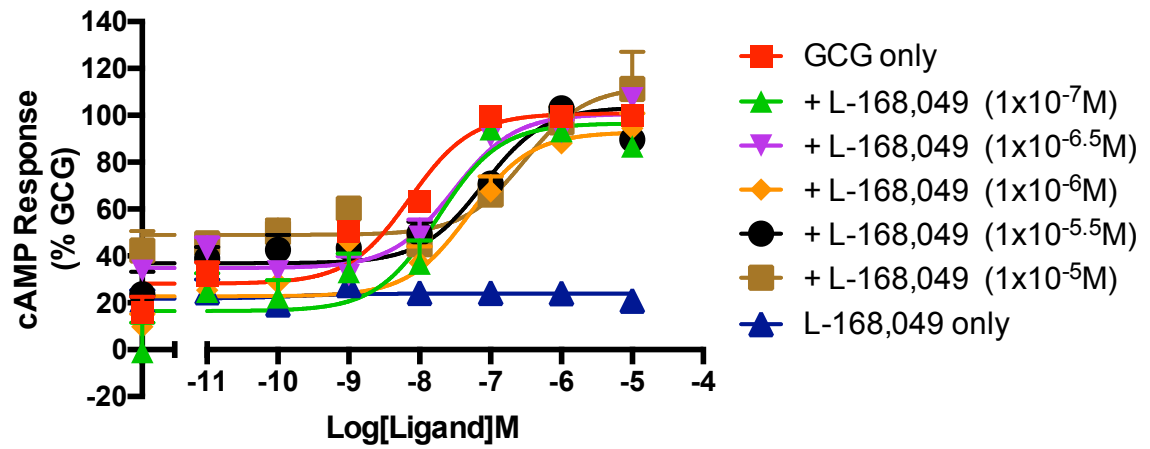


Figure 4.41. Activity of L-168,049 in Hep 3B. Hep 3B cells (5,000 cells/well) were exposed to GCG with or without various concentration of L-168,049, or L-168,049 alone for 30 minutes and cAMP accumulation detected using the LANCE Ultra cAMP kit. All values are mean \pm SEM expressed as percentage GCG response where $n = 3$ independent experimental repeats, conducted in duplicate.

Table 4.29. Activity of L-168,049 in Hep 3B. Potency (pEC₅₀), maximal response (E_{max}), basal, span, affinity (pK_A) and coupling efficacy (log τ) for GCG or L-168,049 only or GCG in combination with various concentrations of L-168,049 measured in Hep 3B cells using a cAMP accumulation assay

L-168,049						
	pEC ₅₀ ^a	E _{max} ^b	Basal ^c	Span ^d	pK _A ^e	log τ ^f
GCG only	8.14 ±0.2	100.8 ±3.9	28.1 ±3.7	72.7 ±5.1	7.46 ±0.2	0.58 ±0.11
+ 1x10 ⁻⁷ M	7.74 ±0.2	96.6 ±7.8	16.5 ±5.0	80.1 ±8.0	7.10 ±0.3	0.53 ±0.16
+ 1x10 ^{-6.5} M	7.53 ±0.2	100.6 ±5.1	34.8 ±3.5	65.8 ±5.8	6.88 ±0.3	0.53 ±0.15
+ 1x10 ⁻⁶ M	7.30 ±0.2*	92.8 ±5.2	22.8 ±4.1	70.1 ±6.5	6.75 ±0.3	0.41 ±0.12
+ 1x10 ^{-5.5} M	7.11 ±0.2*	103.5 ±6.7	36.9 ±3.1	66.6 ±6.1	6.41 ±0.3	0.61 ±0.22
+ 1x10 ⁻⁵ M	6.52 ±0.2***	112.3 ±7.7	49.0 ±2.6**	63.3 ±7.8	5.56 ±0.6**	0.92 ±0.49
L-168,049 only		N.R	23.9 ±1.7			N.R

Hep 3B cells were stimulated with GCG or L-168,049 only or GCG in combination with various concentrations of L-168,049 prior to measurement of cAMP accumulation to generate concentration response curves for each construct. To calculate pEC₅₀, E_{max}, Basal and Span values, data were analysed using a three-parameter logistic equation. Data was also analysed by an operational model of agonism (Black and Leff, 1983) to determine affinity (pK_A) and coupling efficacy (log τ).

^a Negative logarithm of GCG concentration required to produce a half-maximal response

^b Maximal response to GCG as percentage GCG only response

^c The low plateau of the fitted sigmoidal dose-response curve

^d The difference between E_{max} and basal signalling

^e The negative logarithm of functional affinities that describes the affinity of the receptor when coupled to a given signalling pathway generated through use of the operational model for partial agonism

^f τ is the coupling efficiency parameter generated through use of the operational model for partial agonism

All values are mean ± SEM expressed as percentage GCG only (+DMSO added as control) response where $n = 3$ independent experimental repeats, conducted in duplicate.

Statistical significance (*, $p < 0.05$; **, $p < 0.01$; ***, $p < 0.001$) compared to GCG only response was determined by one-way ANOVA with Dunnett's post test

N.R denotes no response

4.8.5. Summary

Primary human hepatocytes are considered to be the gold standard for the study of metabolism in the liver but their phenotypic instability and restricted accessibility has made way for alternative such as the immortalised human hepatocellular carcinoma cell line, Hep 3B. Despite the use of this and similar cell lines in research, little is currently known about the receptor expression and associated pharmacology. Here, Hep 3B cells were found to express mRNA for various G proteins (G_s , G_{i1-3} , G_q , G_{11} and $G_{12/13}$), GCGR, RAMP2, small levels of GIPR, CLR, RAMP1 and RAMP3.

The combined GCGR mRNA detection and robust response to GCG and oxyntomodulin strongly suggests the endogenous expression of GCGR, as would be expected for a hepatocyte cell line (Taborsky, 2010). Studies have highlighted that GCGR ligands including GCG and oxyntomodulin can activate the GLP-1R, whereas GLP-1(7-36)amide has been suggested not to act at the GCGR (Runge *et al.*, 2003). In accordance with this, the lack of GLP-1(7-36)amide response suggests both the absence of GLP-1R expression itself and confirms the lack of cAMP response to GLP-1(7-36)amide stimulation at the GCGR in Hep 3B cells. However, this finding is contradictory to the concentration-dependent increase in cAMP accumulation found in GLP-1(7-36)amide stimulated HEK 293 cells transfected with GCGR (Section 4.2.1) and may be due to a lack of RAMP2 expression (Weston *et al.*, 2015)

Previous work has identified cross-reactivity of GLP-1R ligands, including GLP-1(7-36)amide and liraglutide at the GCGR, which was abolished by a RAMP2 interaction (Weston *et al.*, 2014, Weston *et al.*, 2015). Such a previously unidentified role for GLP-1(7-36)amide ligands could be explained by the wide tissue expression of RAMPs. The background of a cell type, including the RAMP expression profile, and variation between cell batches can contribute greatly to the experimental observations (Tilakaratne *et al.*, 2000). Indeed, the observation that GLP-1(7-36)amide can act on

GCGR (Section 4.2.1, Weston *et al.*, 2014, Weston *et al.*, 2015) may depend on the absence of expression of RAMP2 in the particular tissue or cell type investigated. Alternatively, this apparent activity of GLP-1(7-36)amide ligands at the GCGR in transfected cell lines may be as a consequence of high receptor expression when compared to an endogenously expressing cell line. Here, in the case of Hep 3B cells, the lack of GLP-1(7-36)amide stimulated cAMP response may be a consequence of RAMP2 expression and interaction thereby abolishing the response.

Given the lack of cAMP response to GLP-1(7-36)amide, the GLP-1(7-36)amide concentration-dependent pERK1/2 response measured in Hep 3B is surprising and complicates the interpretation of the data. These findings may be explained by a variability in the loss of receptor expression over passage number. Speculatively, it may be that the experiments investigating the cAMP responses to GLP-1(7-36)amide stimulation had lost expression of GLP-1R and therefore failed to induce a detectable level of cAMP, whereas experiments looking at pERK1/2 response had a given level of GLP-1R expression in the Hep 3B cells used.

Given the rank order of potency at the various CLR/CT and RAMP combinations (Tables 4.25 and 4.26), the cAMP response detected following stimulation with AM but not AM2 or CGRP was interpreted as the expression of a functional AM receptor through the expression of CLR in combination with RAMP2. This robust response may not have been expected given the low level of detectably CLR expression when compared to GAPDH. However, the correlation between mRNA and protein expression is notoriously poor with most reports finding only a weak correlation between the two (Maier *et al.*, 2009). Even if the RT-PCR results do indeed reflect protein expression levels within Hep 3B, GPCR expression levels may not need to be high in order to produce a response as a result of signal amplification

In this work, the activity of two potential GCGR antagonists, des-His¹,[Glu⁹]-GCG and L-168,049, were investigated in Hep 3B cells and the findings were distinct from those determined in HEK 293T cells. L-168,049

was characterised as a competitive antagonist in HEK 293T cells and Hep 3B cells rather than a non-competitive antagonist as previously reported (Cascieri *et al.*, 1999). des-His¹,[Glu⁹]-GCG was characterised as a partial agonist in GCGR transfected HEK 293T cells but a non-competitive antagonist in Hep 3B cells.

There was considerable variability in data acquired using Hep 3B cells for both cAMP and pERK1/2 assays with an apparent loss in response using cells at passage 8 or higher. This indicates poor reproducibility when using Hep 3B cells and is most likely due to loss of receptor with increasing passage. In light of these data variability and time constraint on ligand stimulated responsiveness in Hep 3B cells, it appears that these cells are somewhat less valuable as a hepatocyte cell model to investigate GCGR signalling.

Chapter 5. Investigating pharmacological role of GCGR regions

5.1. Introduction

A number of studies looking at class B GPCRs have proposed critical roles for residues within ICL1-3 including maintaining GPCR in an inactive state (Martínez-Archundia and Correa-Basurto, 2014), coupling to G proteins (Mathi *et al.*, 1997, Conner *et al.*, 2006 and Kleinau *et al.*, 2010), protein folding and correct transport (Thomas *et al.*, 2007). In the work presented in this thesis, an investigation into the importance of GCGR regions and conserved residues for cell-surface expression and downstream signaling components (cAMP, pERK1/2 and Ca²⁺i mobilisation) was performed in line with optimisations presented in chapter 3. These included the GCGR ICL1 region (G165^{1.63}-T172^{2.45}), TM2 residue R173^{2.46}, helix 8 residues E406^{8.49} and E410^{8.53} and three TM4 residues (G271^{4.49}, L277^{4.55}, V280^{4.58}).

Despite significant differences between class A and B GPCRs, all share a common molecular architecture and bind the same G proteins suggesting a similar mechanism of receptor activation and G protein binding (Cordomí *et al.*, 2015). Until relatively recently, the available crystal structures were limited to class A GPCRs. Multiple crystal structures (both active and inactive) exist for the class A A_{2A}R including the A_{2A}R bound to the agonists NECA and adenosine (Lebon *et al.*, 2011), CGS 21689 (Lebon *et al.*, 2015), UK-432097 (Xu *et al.*, 2011) and the antagonist ZM241385 (Liu *et al.*, 2012, Doré *et al.*, 2013, Jaakola *et al.*, 2008,). In this thesis, due to the availability of these multiple crystal structures, the A_{2A}R was chosen as a class A G_s-coupled receptor to investigate the importance of ICL1.

To aid in interpretation of the experimental results, Modeller (version 9.18) was used to mutate specific residues within the currently available GCGR/A_{2A}R structures. All structures were viewed in MacPyMol (version 1.7.4.5) and the WT (original PDB file) and mutated receptor (PDB file

created by running the command) compared visually to assess any predicted changes in amino acid interactions and structure.

5.2. Investigating pharmacological role of GCGR intracellular loop 1

5.2.1. Cell-surface expression of GCGR intracellular loop 1 mutants

Mutations in the ICL1 region (Figure 5.1 A and Table 5.1) of a number of GPCRs, including the GLP-1R, have been implicated to result in both reduced cell-surface expression and secondary messenger responses (Mathi *et al.*, 1997 and Underwood *et al.*, 2013). In this work, using ICL1 region GCGR mutants (G165A-T172A), kindly donated by Dr. Ali Jazayeri (Heptares Therapeutics), and a number of assays measuring downstream responses we investigated the importance of this region (residues G165-T172) for receptor cell-surface expressing and signalling.

We first sought to investigate the cell-surface expression of both WT and mutant GCGR. Here, HEK 293 cells were transiently transfected with pcDNA3.1 containing the GFP-tagged GCGR and cell-surface expression determined using FACS analysis as previously described (Section 3.10.1). Confocal fluorescence microscopy images of HEK 293 cells expressing GFP-tagged WT GCGR showed localisation on the membrane surface (Figure 5.2 A). Seven of the eight ICL1 mutants tested showed similar cell-surface fluorescent levels and only C171A failed to show any cell-surface expression (Figure 5.2 A). The images for C171A showed complete absence of protein expression with no detectable GFP, suggesting a complete lack of expression and/or premature degradation. Through FACS analysis, the cell-surface expression of all but three mutants, L166A, H170A and T172A, were significantly reduced when compared to WT GCGR (70.2 ± 12.2 , 59.4 ± 18.2 , 75.3 ± 9.8 percentage WT, respectively) (Figure 5.2 B). These findings suggest that a number of amino acids within the ICL1 region of GCGR, appear to be important in trafficking to the cell-surface.

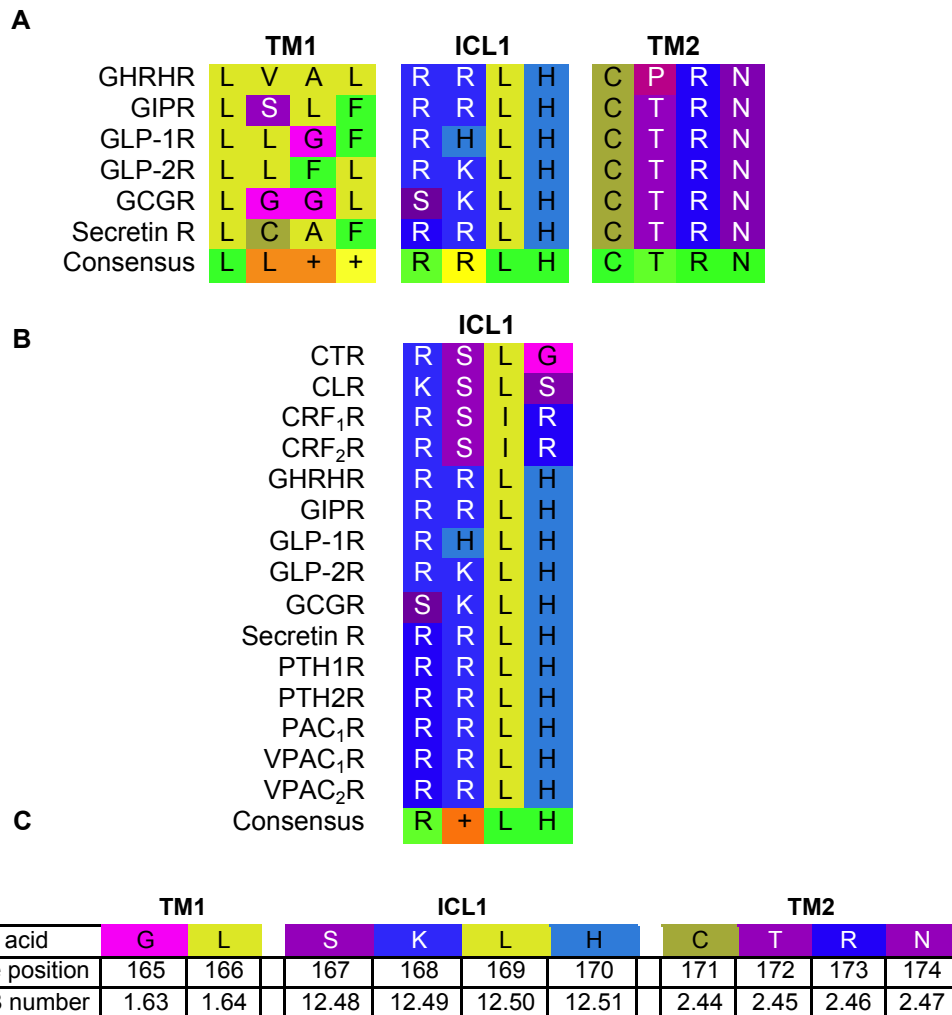




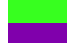






Figure 5.1. GCGR family structure-based alignment. **A)** GPCRdb.org structure-based alignment of part of TM1, ICL1 and part of TM2 within the GCGR family receptors; growth-hormone-releasing hormone (GHRH) receptor, GIPR, GLP-1R, GLP-2R, GCGR and the secretin receptor. **B)** Alignment of the class B GPCR ICL1 region, described as the K/RK₁LH motif (Vohra *et al.*, 2013) **C)** The residue position within TM1, ICL1 and TM2 of GCGR are given in both absolute and Class B (Wootten *et al.*, 2013c) numbers. Here, only the specific targeted regions for alanine substitution mutation within GCGR are shown. Amino acid residues are given as the single amino acid code and colours illustrate residue physico-chemical properties (Table 5.1).

A

	Alanine (Ala, A) Valine (Val, V), Leucine (Leu, L), Isoleucine (Ile, I), Methionine (Met, M)
	Glycine (Gly, G)
	Proline (Pro, P)
	Cysteine (Cys, C)
	Tyrosine (Tyr, Y), Phenylalanine (Phe, F), Tryptophan (Trp, W)
	Threonine (Thr, T), Serine (Ser, S), Asparagine (Asn, N), Glutamine (Gln, Q)
	Lysine (Lys, K), Arginine (Arg, R)
	Histidine (His, H)
	Glutamate (Glu, E), Aspartate (Asp D)

B






	17% consensus
	33% consensus
	50% consensus
	67% consensus
	100% consensus

Table 5.1. Colour code key for structural-alignment. A) amino acid colour code and **B)** percentage consensus (approximate) colour code acquired from GPCRdb.org

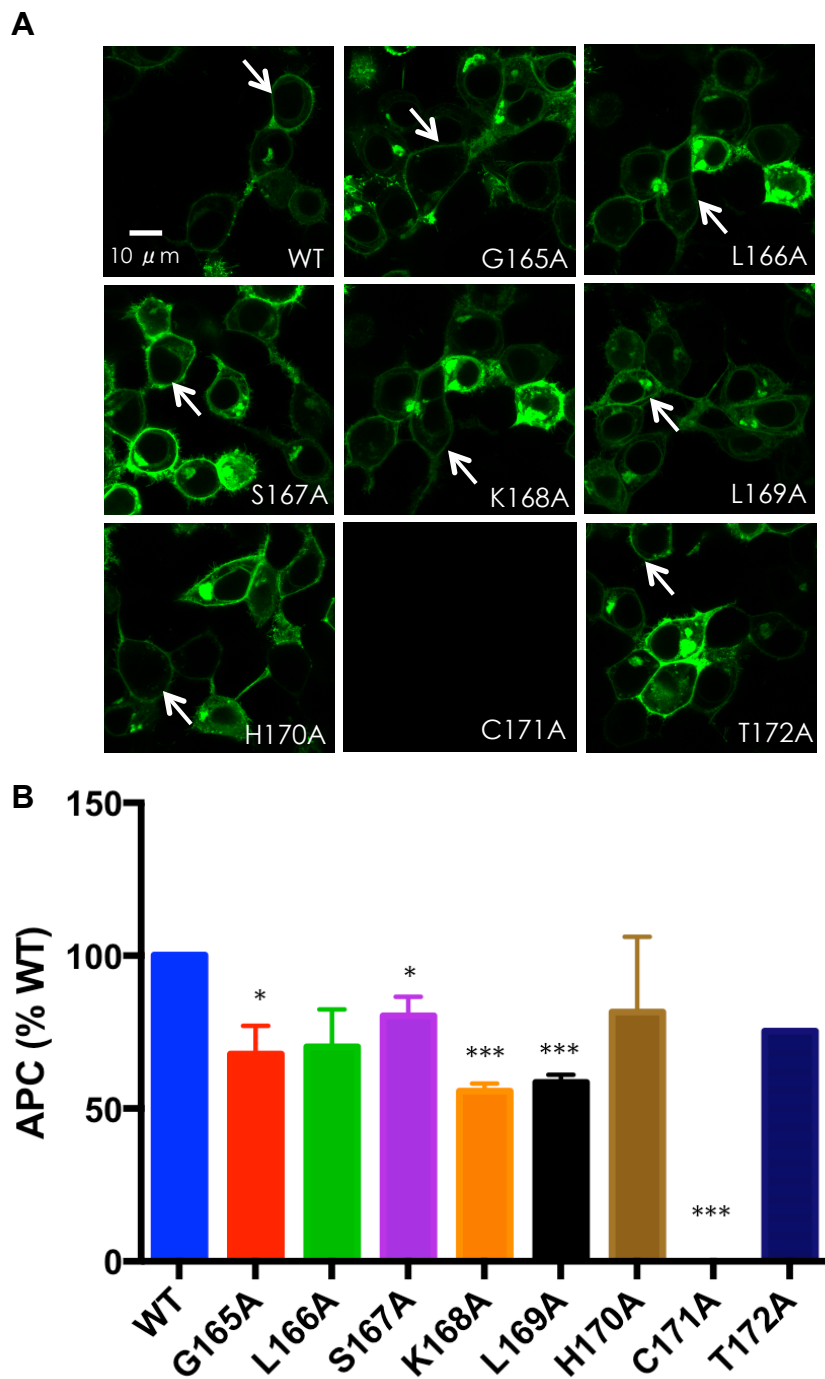


Figure 5.2. Cell-surface expression of WT and GCGR ICL1 mutants. HEK 293 cells were transfected with WT or mutant GCGR and cell-surface expression determined by **A**) confocal fluorescence microscopy (24 hours post transfection) representative image for each mutant and **B**) FACS analysis (48 hours post transfection); anti-GCGR primary antibody at a 1:50 dilution, APC-conjugated IgG secondary antibody at a 1:150 dilution. All values are mean \pm SEM expressed as percentage WT GCGR (100%) and vector only transfected control (0%) where $n = 3$ independent experimental repeats, conducted in duplicate. Arrow indicates cell-surface localised receptor. Statistical significance (*, $p < 0.05$; **, $p < 0.01$; ***, $p < 0.001$) compared to WT was determined by one-way ANOVA with Dunnett's post test.

5.2.2. cAMP response in GCGR ICL1 transfected HEK 293 cells

Having showed various ICL1 GCGR mutants had reduced cell-surface expression, we next sought to investigate the pharmacological consequences of these mutants. Here, HEK 293 cells transiently transfected with pcDNA3.1 expressing WT or the mutant GCGR were stimulated with GCG and the cAMP accumulation detected using the LANCE® cAMP detection kit.

With the exception of C171A, which showed no detectable cAMP response, there was found to be no significant difference in potency, basal response, span, affinity or efficacy for the measured cAMP response to GCG stimulation of WT and mutant GCGR (Figure 5.3 and Table 5.2). This lack of cAMP response in C171A transfected HEK 293 cells reflects the lack of detectable cell-surface expression, as was previously shown (Figure 5.3).

There was found to be a significantly reduced maximal response in G165A when compared to WT GCGR (E_{\max} 73.4 \pm 3.7 and 102.9 \pm 4.2, respectively) that suggests that glycine at position 165 is important in the GCGR mediated cAMP response to GCG. Although there was found to be a reduced cell-surface expression for G165A (Figure 5.3), given the similar or lower cell-surface expression detected for other ICL1 mutants with similar cAMP responses to WT GCGR, this is unlikely to account for the reduced cAMP response. It may be speculated that this amino acid is important in the coupling to G_s .

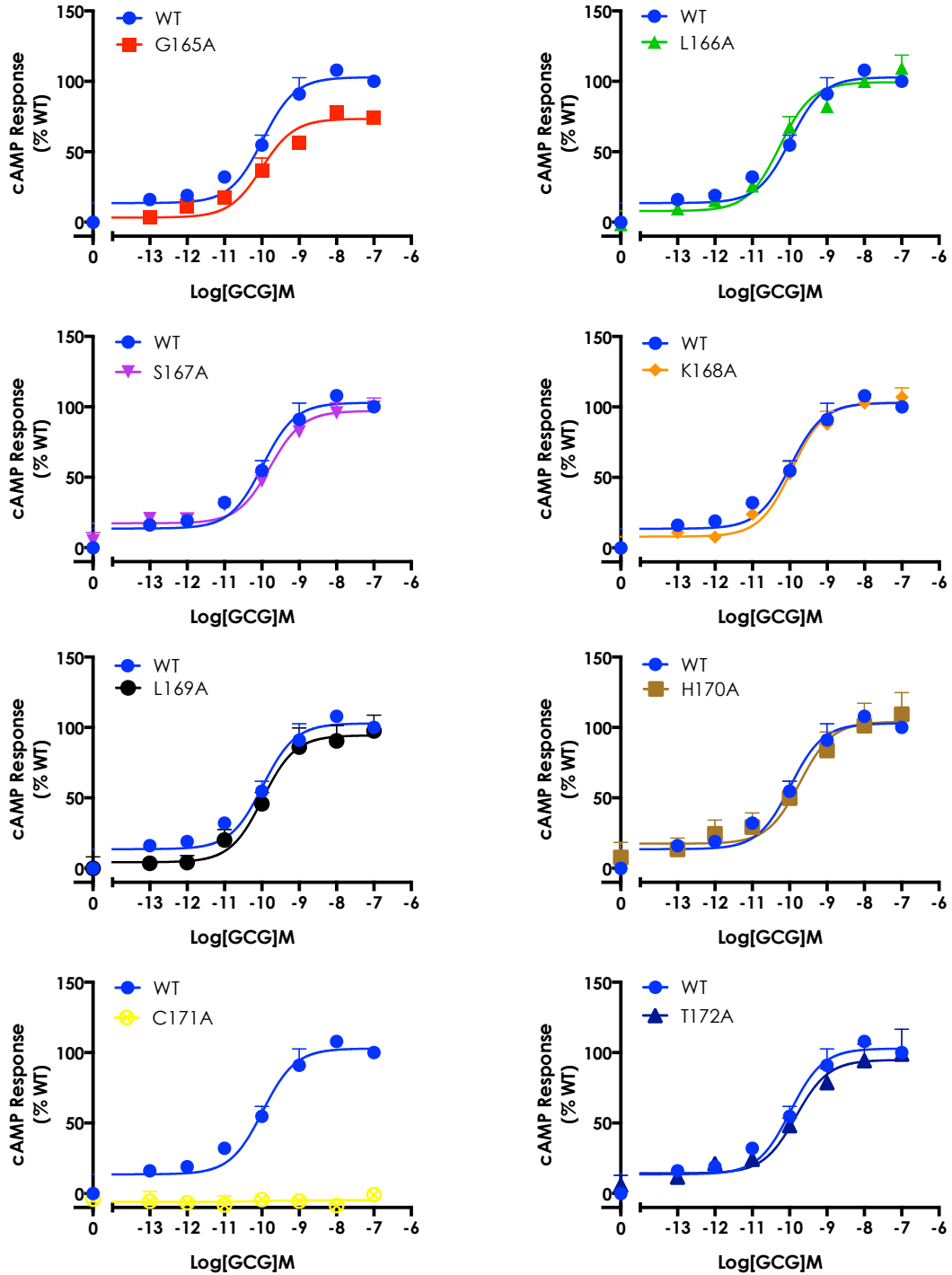


Figure 5.3. Effect of GPCR ICL1 mutants on cAMP response. HEK 293 cells transiently expressing pcDNA3.1 vector containing WT or alanine GPCR ICL1 mutants (24 hours post transfection) were exposed to GCG for 8 minutes and cAMP accumulation detected. All values are mean \pm SEM expressed as percentage WT forskolin response where $n \geq 5$ independent experimental repeats, conducted in duplicate. Arrow indicated significant change (Table 5.2) between WT and mutant response.

Table 5.2. Effect of GCGR ICL1 mutants on cAMP response. Potency (pEC₅₀), maximal response (E_{max}), basal, span, affinity (pK_A) and coupling efficacy (log τ) values for cAMP response to GCG stimulation in WT/mutant GCGR transfected HEK 293 cells

Construct	cAMP					
	pEC ₅₀ ^a	E _{max} ^b	Basal ^c	Span ^d	pK _A ^e	log τ ^f
WT	9.98±0.1	102.9 ±4.2	13.6 ±3.5	89.3 ±5.3	9.72±0.2	-0.17 ±0.05
G165A	10.00 ±0.2	73.4 ±3.7**	3.3 ±3.0	70.1 ±4.7	9.93±0.2	-0.34 ±0.05
L166A	10.27 ±0.2	99.4 ±4.0	7.9 ±3.7	91.5 ±5.3	10.06 ±0.2	-0.20 ±0.04
S167A	9.78 ±0.1	97.1±3.9	17.3 ±3.0	79.8 ±4.8	9.57 ±0.2	-0.23 ±0.04
K168A	9.95 ±0.1	103.2 ±4.1	8.0 ±3.6	95.3 ±5.3	9.68 ±0.2	-0.12 ±0.05
L169A	9.98 ±0.2	94.4 ±5.5	4.3 ±4.7	90.1 ±7.0	9.74 ±0.3	-0.13 ±0.09
H170A	9.73 ±0.3	104.0 ±8.0	17.5 ±6.1	86.6 ±9.7	9.59 ±0.2	-0.15 ±0.05
C171A		N.R	-5.9 ±2.0			N.R
T172A	9.83 ±0.2	94.8 ±0.2	14.3 ±4.3	80.5 ±6.8	9.57 ±0.2	-0.20 ±0.05

WT or mutant GCGR were transiently expressed in HEK 293 cells and stimulated with GCG prior to measurement of cAMP accumulation to generate concentration response curves for each construct. To calculate pEC₅₀, E_{max}, Basal and Span values, data were analysed using a three-parameter logistic equation. Data was also analysed by an operational model of agonism (Black and Leff, 1983) to determine affinity (pK_A) and coupling efficacy (log τ).

^a Negative logarithm of GCG concentration required to produce a half-maximal response

^b Maximal response to GCG as percentage forskolin response (Mock transfected with Vector), then normalized to the WT response

^c The low plateau of the fitted sigmoidal dose-response curve

^d The difference between E_{max} and basal signalling

^e The negative logarithm of functional affinities that describes the affinity of the receptor when coupled to a given signalling pathway generated through use of the operational model for partial agonism

^f τ is the coupling efficiency parameter generated through use of the operational model for partial agonism

All values are mean ± SEM expressed as percentage WT forskolin response where $n \geq 5$ independent experimental repeats, conducted in duplicate. Statistical significance (*, $p < 0.05$; **, $p < 0.01$; ***, $p < 0.001$) compared to WT GCGR was determined by one-way ANOVA with Dunnett's post test

5.2.3. pERK1/2 response in GCGR ICL1 mutants transfected HEK 293 cells

We next looked to investigate if the amino acids in ICL1 were important in the pERK1/2 response. Here, HEK 293 cells transiently transfected with pcDNA3.1 expressing WT or the mutant GCGR were stimulated with GCG and the pERK1/2 response determined.

As previously reported (Section 4.4), GCG stimulated a concentration-dependent increase in pERK1/2 in HEK 293 cells transfected with WT GCGR (Figure 5.4)

Similarly to what was reported for the cAMP response in GCGR ICL1 mutants, with the exception of C171A, there was found to be negligible differences in ERK1/2 phosphorylation following GCG stimulation in ICL1 GCGR mutants when compared to WT GCGR (Figure 5.4 and Table 5.3). It should be noted that the measured pERK1/2 responses showed variability between repeats and resulted in large error for the measured parameters. Nevertheless, these results suggest that the ICL1 plays a minimal, if any, role in the pERK1/2 signalling.

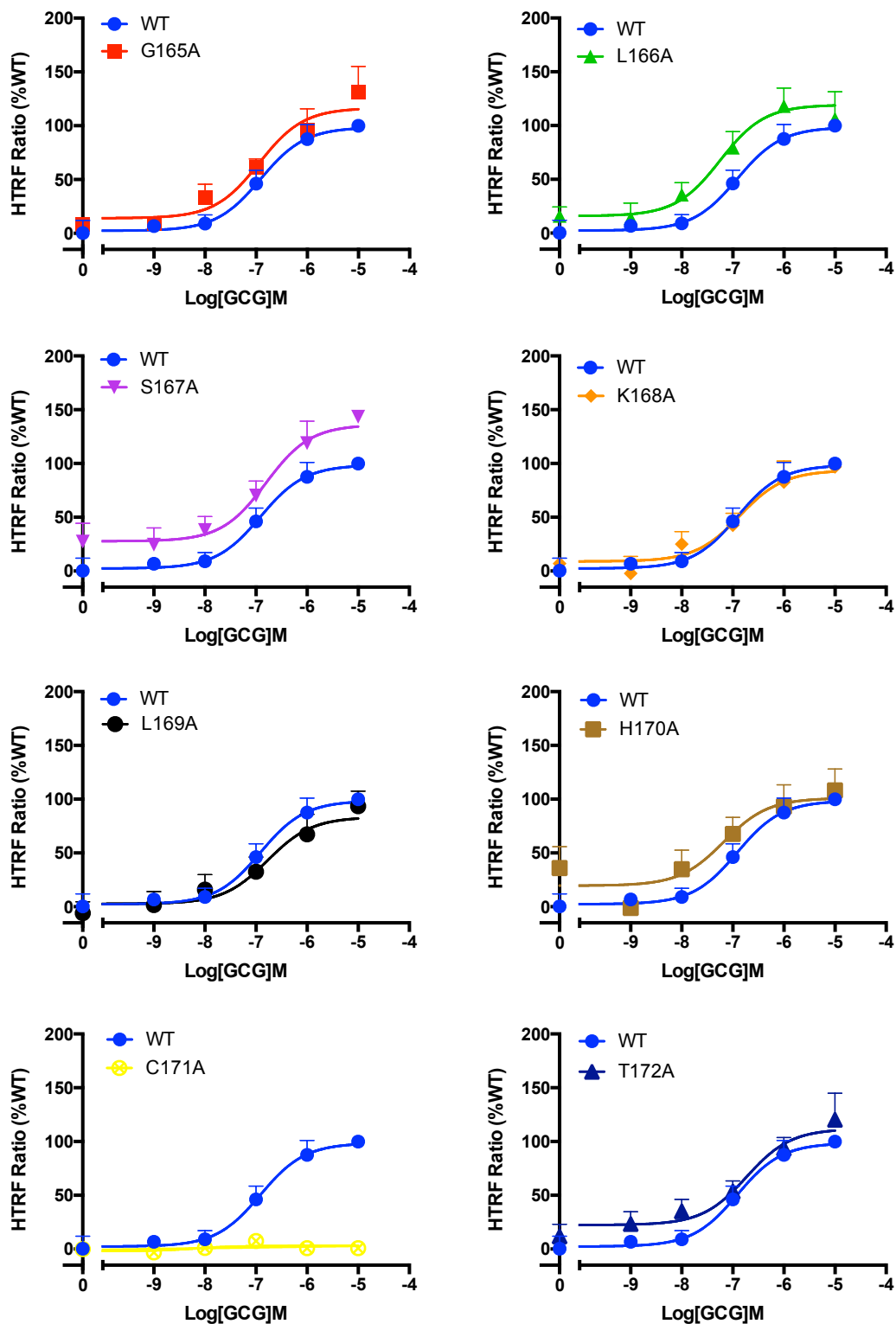


Figure 5.4. Effect of GPCR ICL1 mutants on pERK1/2 response. HEK 293 cells transiently expressing pcDNA3.1 vector containing WT or alanine GPCR ICL1 mutants (48 hours post transfection and 24 hours serum starved) were exposed to GCG for 5 minutes and pERK1/2 measured. All values are mean \pm SEM expressed as percentage WT GPCR response where $n \geq 5$ independent experimental repeats, conducted in duplicate. Arrow indicated significant change (Table 5.3) between WT and mutant response.

Table 5.3. Effect of GCGR ICL1 mutants on pERK1/2 response. Potency (pEC_{50}), maximal response (E_{max}), basal, span, affinity (pK_A) and coupling efficacy ($\log \tau$) values for a pERK1/2 response to GCG stimulation in WT/mutant GCGR transfected HEK 293 cells

Construct	pERK1/2					
	pEC_{50} ^a	E_{max} ^b	Basal ^c	Span ^d	pK_A ^e	$\log \tau$ ^f
WT	6.91±0.3	98.6 ±12.7	2.4 ±7.5	96.2 ±13.6	6.62 ±0.3	-0.02 ±0.11
G165A	6.94 ±0.2	116.5 ±13.1	14.0 ±7.4	102.4 ±14.2	6.60 ±0.3	0.09 ±0.12
L166A	7.2±0.3	123.4 ±13.7	16.3 ±10.3	107.1 ±15.9	6.81 ±0.3	0.15 ±0.13
S167A	7.24 ±0.3	114.5 ±13.9	11.3 ±10.8	103.3 ±16.0	6.38 ±0.5	0.23 ±0.21
K168A	6.87 ±0.4	93.6 ±16.7	8.9 ±9.7	84.7 ±17.9	6.61 ±0.4	-0.10 ±0.15
L169A	6.77 ±0.4	83.4 ±18.1	2.7 ±9.0	80.7 ±19.9	6.55 ±0.5	-0.16 ±0.16
H170A	7.18 ±0.5	101 ±16.4	19.6 ±12.5	81.5 ±19.1	6.92 ±0.5	-0.08 ±0.16
C171A		NR	-2.0 ±3.4		NR	
T172A	6.73 ±0.3	111.8 ±14.1	22.4 ±14.6	89.4 ±14.6	6.43 ±0.3	0.00 ±0.14

WT or mutant GCGR were transiently expressed in HEK 293T cells and stimulated with GCG prior to measurement of pERK1/2 to generate concentration response curves for each construct. To calculate pEC_{50} , E_{max} , Basal and Span values, data were analysed using a three-parameter logistic equation. Data was also analysed by an operational model of agonism (Black and Leff, 1983) to determine affinity (pK_A) and coupling efficacy ($\log \tau$).

^a Negative logarithm of GCG concentration required to produce a half-maximal response

^b Maximal response to GCG as percentage WT GCGR response

^c The low plateau of the fitted sigmoidal dose-response curve

^d The difference between E_{max} and basal signalling

^e The negative logarithm of functional affinity that describes the affinity of the receptor when coupled to a given signalling pathway generated through use of the operational model for partial agonism

^f τ is the coupling efficiency parameter generated through use of the operational model for partial agonism

All values are mean ± SEM expressed as percentage WT GCGR response where $n \geq 5$ independent experimental repeats, conducted in duplicate.

Statistical significance (*, $p < 0.05$; **, $p < 0.01$; ***, $p < 0.001$) compared to WT GCGR was determined by one-way ANOVA with Dunnett's post test

N.R denotes no response

5.2.4. Intracellular Ca²⁺ response in GCGR ICL1 mutants transfected HEK 293 cells

The findings presented elsewhere highlight that ligand activated GCGR is not only able to couple to G_s leading to concentration-dependent increases in cAMP accumulation, but can also induce a G_{q/11}-mediated Ca²⁺_i response (Section 4.3). Here we investigated if mutation of the ICL1 region of GCGR influences the GCG stimulated Ca²⁺_i mobilisation.

HEK 293 cells (transfected with GFP-tagged WT or mutant GCGR post plating) were loaded with CalciFluor™ Rhod-4, AM dye, stimulated with increasing concentrations of GCG and the Ca²⁺_i mobilisation measured using a FlexStation® Multi-Mode Microplate Reader. A 30-minute pre-treatment with the specific G_{q/11} inhibitor YM-254890 (Takasaki *et al.*, 2004) was used to confirm if the measured Ca²⁺_i responses were G_{q/11}-mediated. GCG stimulation of HEK 293 cells transfected with WT GCGR and ICL1 mutant GCGRs, with the exception of C171A which showed no detectable Ca²⁺_i response, showed a concentration-dependent increase in Ca²⁺_i mobilisation with no significant difference in potency (Figure 5.5 and Table 5.4). These responses were abolished with YM-254890 treatment confirming the responses were indeed G_{q/11}-mediated.

K168A, L169A, H170A and T172A showed a reduction in Ca²⁺_i when compared to WT GCGR (E_{max} 65.2 ±5.5, 54.4 ±4.8, 50.9 ±4.9, 70.0 ±5.3 and 111.5 ±4.5 respectively). In addition, K168A, L169A, H170A and T172A also showed a significant reduction in efficacy when compared to WT GCGR (log τ 0.10 ±0.07, -0.08 ±0.06, -0.12 ±0.06, 0.28 ±0.08 and 1.12 ±0.20, respectively). The reduced cell-surface expression (Figure 5.2) does not seem to correlate with reductions in maximal Ca²⁺_i response for all mutants, and therefore is unlikely to account for these results. It should be noted that logτ values were not correction for cell-surface expression as with transient transfection where expression levels are high we can lose some receptor expression without losing efficacy, presumably because there is more

receptor than effector. As such, correction for cell-surface expression is only suitable for systems where receptor expression is not as high compared to transient transfection. For example, whereas we see a significantly reduced cell-surface expression of G165A, the maximal Ca^{2+}_i response is not significantly different to WT GCGR. The findings suggest that the amino acids K168, L169, H170 and T172 of ICL1 may play a role in $G_{q/11}$ -mediated signalling, possibly through interactions with $G_{q/11}$ itself, whereas they appears to play less of a role in G_s -mediated signalling. It could be suggested that these residues play a role in signalling bias at the GCGR.

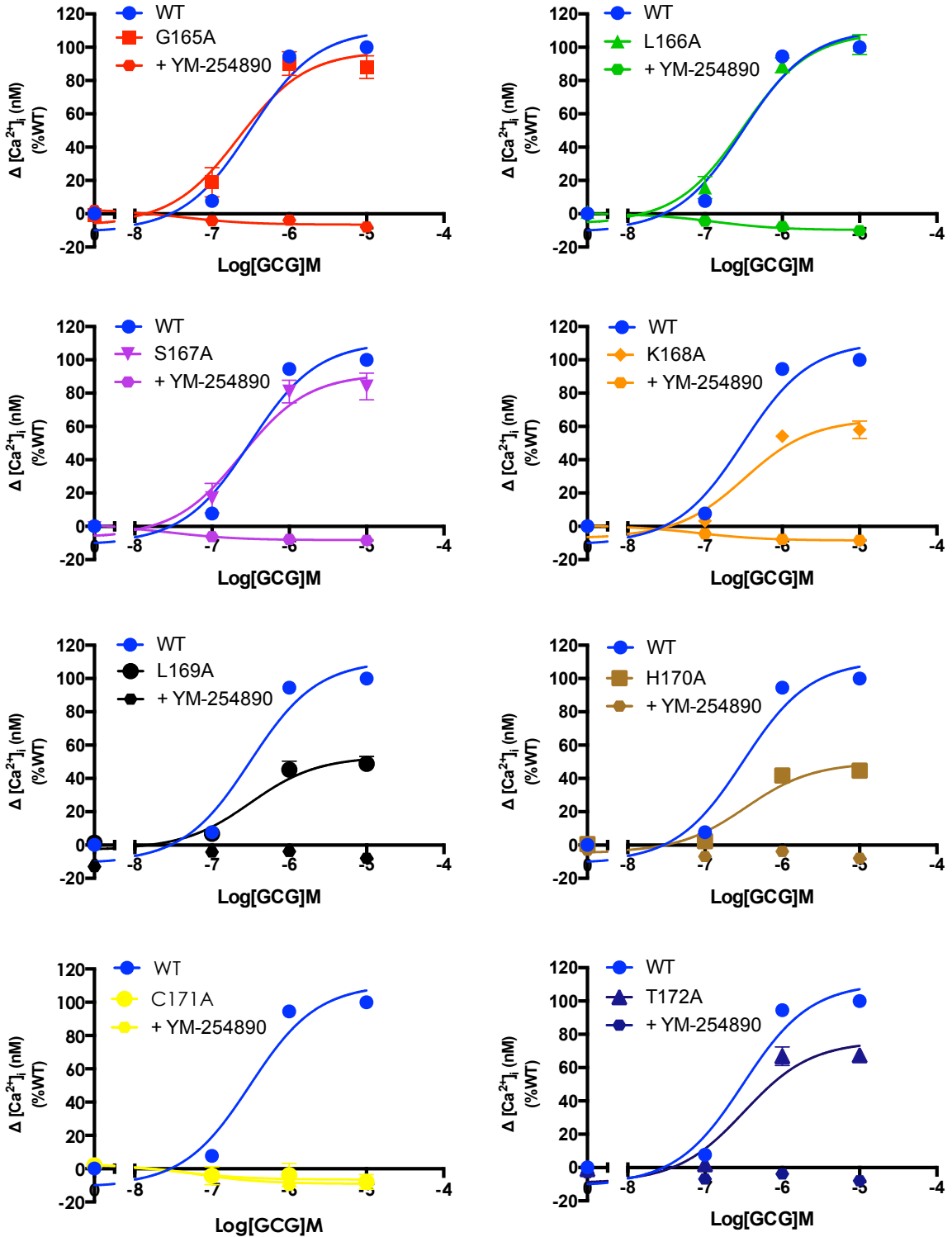


Figure 5.5. Effect of GPCR ICL1 mutants on Ca^{2+}_i response. HEK 293 cells transiently transfected with pcDNA3.1 vector expressing WT or alanine GPCR ICL1 mutants (48 hours post transfection) were exposed to GCG and Ca^{2+}_i mobilisation measured. All values are mean \pm SEM expressed as percentage WT GPCR response where $n \geq 5$ independent experimental repeats, conducted in duplicate. Arrow indicates significant change (Table 5.4) between WT and mutant response.

Table 5.4. Effect of GCGR ICL1 mutants on Ca²⁺i response. Potency (pEC₅₀), maximal response (E_{max}), basal, span, affinity (pK_A) and coupling efficacy (log τ) values for Ca²⁺i response to GCG stimulation in WT/mutant GCGR transfected HEK 293 cells +/- YM-254890 treatment

Construct	Ca ²⁺ i						
	pEC ₅₀ ^a	E _{max} ^b	Basal ^c	Span ^d	pK _A ^e	log τ ^f	+ YM-254890
WT	6.48 ±0.1	111.5 ±4.5	-10.3 ±4.6	121.0 ±5.4	5.36 ±0.2	1.12 ±0.20	N.R
G165A	6.58 ±0.2	100.7 ±9.2	-6.0 ±9.5	102.6 ±10.9	5.90 ±0.3	0.67 ±0.17	N.R
L166A	6.50 ±0.2	112.2 ±6.9	-5.3 ±7.2	114.1 ±8.4	5.44 ±0.3	1.02 ±0.27	N.R
S167A	6.65 ±0.2	95.5 ±7.9	-6.0 ±9.8	97.4 ±11.2	5.98 ±0.3	0.53 ±0.15	N.R
K168A	6.46 ±0.2	65.2 ±5.5**	-6.6 ±5.4	70.9 ±6.3***	6.13 ±0.2	0.10 ±0.07***	N.R
L169A	6.50 ±0.2	54.4 ±4.8***	-2.5 ±4.8	55.6 ±5.6***	6.24 ±0.2	-0.08 ±0.06***	N.R
H170A	6.46 ±0.2	50.9 ±4.9***	-4.5 ±4.3	54.0 ±5.2***	6.23 ±0.2	-0.12 ±0.06***	N.R
C171A	NR						N.R
T172A	6.44 ±0.2	70.0 ±5.3**	-8.9 ±6.1	84.6 ±7.3**	6.03 ±0.2	0.28 ±0.08**	N.R

WT or mutant GCGR were transiently expressed in HEK 293 cells and stimulated with GCG prior (+/- YM-254890 30-minute pre-treatment) to measurement of Ca²⁺i to generate concentration response curves for each construct. To calculate pEC₅₀, E_{max}, Basal and Span values, data were analysed using a three-parameter logistic equation. Data was also analysed by an operational model of agonism (Black and Leff, 1983) to determine affinity (pK_A) and coupling efficacy (log τ).^a Negative logarithm of GCG concentration required to produce a half-maximal response

^b Maximal response to GCG as percentage WT GCGR response

^c The low plateau of the fitted sigmoidal dose-response curve

^d The difference between E_{max} and basal signalling

^e The negative logarithm of functional affinity that describes the affinity of the receptor when coupled to a given signalling pathway generated through use of the operational model for partial agonism

^f τ is the coupling efficiency parameter generated through use of the operational model for partial agonism

All values are mean ± SEM expressed as percentage WT GCGR response where $n \geq 5$ independent experimental repeats, conducted in duplicate. Statistical significance (*, $p < 0.05$; **, $p < 0.01$; ***, $p < 0.001$) compared to WT GCGR was determined by one-way ANOVA with Dunnett's post test

5.2.5. Assessing the bias for each pathway at ICL1 mutants

The values of efficacy, τ , and dissociation constant, K_A , obtained from fitting the operational model of agonism (Black and Leff, 1983) for the cAMP, pERK1/2 and Ca^{2+} responses were used to quantify signalling bias as change in $\log(\tau/K_A)$ ($\Delta\log(\tau/K_A)$) relative to the WT receptor, as described previously (Section 2.10.7). The difference between these $\Delta\log(\tau/K_A)$ values was then calculated for Ca^{2+} mobilisation and cAMP response for the ICL1 mutant GCGRs, with the pERK1/2 response set as the reference pathway. Here, the antilog values are graphically represented in a radar plot (Figure 5.6).

The radar plot shows the mutants K168A, L169A and H170A (relative to WT and when pERK1/2 is set as the reference pathway) is biased away from Ca^{2+} . This was also found to be the case for L166A. Interestingly, L169A and K168A appear to have biased towards cAMP accumulation relative to pERK1/2 whereas most of the other mutants with the exception of T172A are biased away from cAMP accumulation.

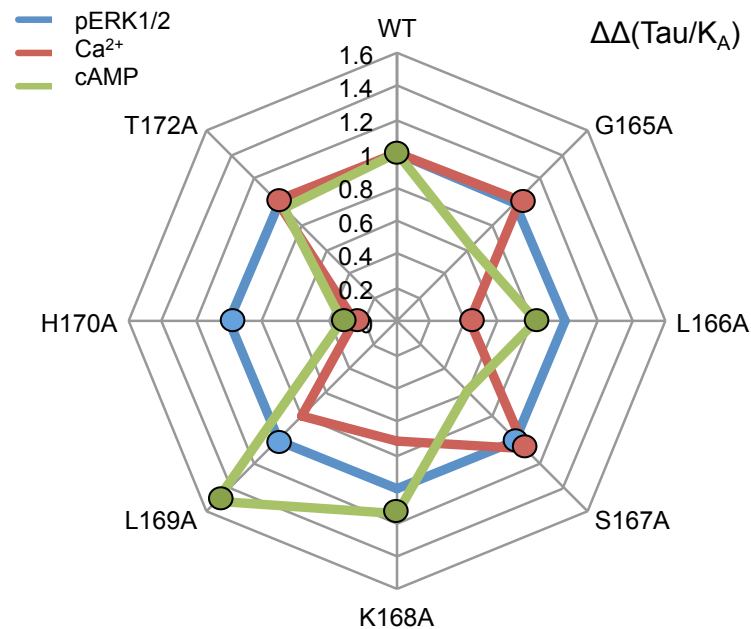


Figure 5.6. Radar plot of antilog $\Delta\Delta(\tau/K_A)$. The plot shows antilog $\Delta\Delta(\tau/K_A)$ values for Ca^{2+} mobilisation and cAMP accumulation for the ICL1 mutant GCGR relative to WT GCGR with the pERK1/2 response set as the reference pathway.

5.2.6. Molecular modelling of ICL1 mutants in three GCGR structures

Modeller (version 9.18) was used to mutate the various ICL1 residues (residues G165-T172) to alanine within the three available protein structures of inactive GCGR for which PDB files exist; 5XEZ (Zhang *et al.*, 2017), 4L6R (Siu *et al.*, 2013) and 5EE7 (Jazayeri *et al.*, 2016). The resulting PDB files were viewed in MacPyMol (version 1.7.4.5) and the WT and mutated receptor compared visually to assess any predicted changes in amino acid interactions and structure (Table 5.5). For illustrative purposes, the ICL1 region targeted for alanine substitution (G165-T172), in addition to R173 and N174 that are investigated later (Section 5.4.2) are shown within the NNC0640 bound full length GCGR structure (Zhang *et al.*, 2017) (Figure 5.7). Images acquired in MacPyMol comparing WT and modelled ICL1 alanine mutants, as can be seen later for the A_{2A}R (Figure 5.14), are not shown for these GCGR ICL1 mutants (G165A-T172A) as polar interactions are largely identical between the ICL1 residues regardless of alanine mutation.

There was found to be considerable variability in the interactions between the three different structures for the ICL1 region. For example, T172 of the NNC0640 bound full length GCGR (Zhang *et al.*, 2017) showed no polar interactions whereas T172 in the NNC0640 bound 7TM domain of GCGR (Siu *et al.*, 2013) showed a polar interaction with I176. Mutation to alanine had no effect on the interactions within the receptor structures for most residues. In addition, the lack of consistency between lost or gained interactions between structures on mutation make predictions as to the cause of changes in measured responses difficult.

There were no obvious and consistent changes in interactions for G165, K168A, L169A, H170A and T172A. This finding may lend further evidence to indicate that the reduced cAMP response measured for G165 and reduced Ca²⁺_i response measured for K168A, L169A, H170A and T172 was as a consequence of reduced coupling to G_s or G_{q/11}, respectively.

Table 5.5. Comparison of GCGR residue polar contacts within WT and modelled ICL1 mutant structures

NNC0640 bound full length GCGR 3 Å (5XEZ)			
G165	None	G165A	None
L166	None	L166A	None
S167	None	S167A	None
K168	Cys171	K168A	Cys171
L169	None	L169A	Leu166
H170	Arg261	H170A	Arg261
C171	Lys168 Ala175	C171A	Lys168
T172	None	T172A	Ala175
NNC0640 bound GCGR 3.4 Å (4L6R)			
G165	None	G165A	None
L166	None	L166A	None
S167	None	S167A	His170
K168	Cys171 Asn174	K168A	Cys171
L169	None	L169A	None
H170	None	H170A	None
C171	Lys168	C171A	Lys168
T172	Ile176	T172A	None
MK-0893 bound GCGR 2.5 Å (5EE7)			
G165	Ala161	G165A	Ala161 Ser167
L166	Ile162 Leu169	L166A	Ile162 Leu169
S167	His170	S167A	His170
K168	None	K168A	None
L169	Leu166 Cys171 Asn174	L169A	Leu166 Cys171 Asn174
H170	Leu163 Gly164 Ser167	H170A	Ser167
C171	Leu169 Asn174 Ala175	C171A	Leu169 Asn174 Ala175
T172	Ala175 Ile176 Asp1157	T172A	Ile176 Asp1157

Mutant models of the GCGR were made using Modeller and the resulting PDB structures compared with WT in PyMOL for any loss/gain of polar interactions. Alanine mutants were modelled for NNC0640 bound full length GCGR solved to a resolution of 3 Å ((PDB ID: 5XEZ) (Zhang *et al.*, 2017), NNC0640 bound GCGR solved to a resolution of 3.4 Å ((PDB ID: 4L6R) (Siu *et al.*, 2013) and MK-0893 bound GCGR solved to a resolution of 2.5 Å.

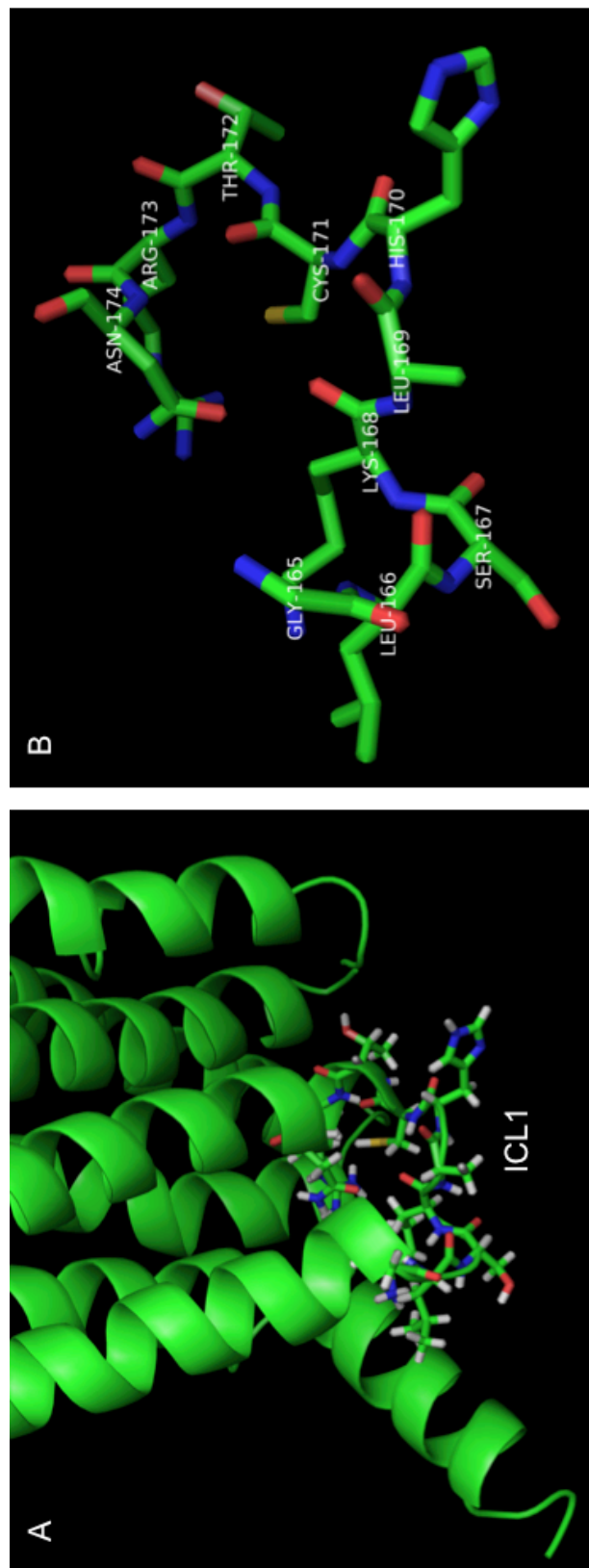


Figure 5.7. ICL1 region within crystal structure of full-length GCGR. Full-length GCGR in complex with the negative allosteric modulator (NAM) NNC0640 and antigen-binding fragment of an inhibitory antibody (mA1b) solved by Zhang *et al.*, 2017 at a resolution of 3 Å (PDB ID: 5XEZ) was imaged in MacPyMOL. **A)** Cartoon image of the 5XEZ structure with the residues correspond to the regions within the GCGR targeted for alanine substitution depicted as sticks. **B)** Zoomed in image of A, with cartoon and hydrogen atoms removed for clarity. The atom type within each residue is coloured red for oxygen, blue for nitrogen and white for hydrogen. Note, T4L inserted into the ICL2 of GCGR between A256 and E260 has been removed for clarity.

5.2.7. Summary

Using FACS for cell-surface expression analysis and assays for the measurement of downstream signaling components, we investigate the importance of the ICL1 region (residues G165-T172) in the GCGR expression and signalling. Cell-surface expression analysis of the ICL1 GCGR mutants revealed complete absence of C171A expression and a significant reduced expression of G165A, S167A, K168A and L169A GCGR mutants. These data indicates an importance of these amino acids for successful translation and/or trafficking to the cell-surface.

In particular, the complete lack of GFP in the confocal image of C171A indicated absence of receptor expression or premature degradation. Similarly, C217 in the ICL1 of human PTHR1 was implicated as a critical determinant of cell-surface translocation and function with the mutant receptor found to localise to the interior of the cell (Thomas *et al.*, 2007). It may be that a mutation in C171 leads to receptor misfolding and recognition by the cellular machinery for degradation. As might be expected given the lack of C171A cell-surface expression, there was no cAMP, pERK1/2 or Ca²⁺_i response following GCG stimulation.

There was negligible difference in cAMP production between any of the ICL1 GCGR mutants that demonstrated cell-surface expression with the exception of G165A, which showed a reduced maximal response when compared to WT GCGR (E_{max} 73.4 ±3.7 and 102.9 ±4.2 percentage WT response, respectively). This finding suggests that G165 is important in the GCGR mediated cAMP response to GCG, possibly through interaction with G_s. Similarly, there was no significant difference between the pERK1/2 responses between mutants and WT GCGR. Interestingly however, K168A, L169A, H170A and T172A showed a reduction in maximal Ca²⁺_i response to GCG (E_{max} expressed as percentage WT GCGR: 65.2 ±5.5, 54.4 ±4.8, 50.9 ±4.9 and 70.0 ±5.3, respectively) which through the use of a specific inhibitor, YM-254890, was confirmed to be G_{q/11}-mediated. This finding suggests that

the amino acids K168, L169, H170 and T172 of GCGR ICL1 (i.e. the residues towards TM2) may play a role in $G_{q/11}$ -mediated signalling, possibly through interactions with $G_{q/11}$. It could be suggested that these residues play a role in signalling bias at the GCGR, although the mechanism remains unclear. These findings are in line with work conducted by Ian Winfield (Dr Ladds Group) investigating the importance of ICL1 in G protein-coupling at the CLR. Due to the highly conserved nature of ICL1 within GPCRs both in terms of length and amino acid sequence, these results might also be important for other GPCRs. We aimed to further expand on this work by investigating potential interaction sites between ICL1 region and helix 8 (Section 5.4.3).

5.3. Investigating the role of $A_{2A}R$ ICL1 in cAMP signalling

5.3.1. NECA stimulated CHO-K1 cells fail to show a cAMP response

We have demonstrated the importance of a number of amino acids within the ICL1 region of the GCGR (residues G165-T172) for cAMP and Ca^{2+} signalling. Given the highly conserved nature of ICL1 within GPCRs both in terms of length and amino acid sequence, we sought to investigate if this region was also important in a class A G_s -coupled GPCR, the $A_{2A}R$. An alignment for this ICL1 region within GCGR and $A_{2A}R$ is shown in Figure 5.8.

Initial cAMP accumulation assays to NECA stimulation in untransfected HEK 293 and CHO-K1 cells demonstrated a robust response to NECA in HEK 293 cells but not CHO-K1 cells (Figure 5.9). This finding suggests the endogenous expression of one or a number of the adenosine receptors (A_1R , $A_{2A}R$, $A_{2B}R$ or A_3R) in HEK 293 cells. Given the absence of a cAMP response in CHO-K1 cells, these were chosen as the cellular model to test the various ICL1 $A_{2A}R$ mutants.

	TM1		ICL1			TM2						
	Amino acid		G	L	S	K	L	H	C	T	R	N
GCGR	Absolute position	165	166	167	168	169	170	171	172	173	174	
	Class B number	1.63	1.64	12.48	12.49	12.50	12.51	2.44	2.45	2.46	2.47	
A _{2A} R	Amino acid	L	N	S	N	L	Q	N	V	T	N	
	Absolute position	33	34	35	36	37	38	39	40	41	42	
	Class A number	1.59	1.60	12.48	12.49	12.50	12.51	2.37	2.38	2.39	2.40	

Figure 5.8. GCGR and A_{2A}R structure-based alignment. GPCRdb.org structure-based alignment of part of TM1, ICL1 and part of TM2 within GCGR and A_{2A}R. The residue position within TM1, ICL1 and TM2 are given in both absolute and Class B (Wootten *et al.*, 2013) numbers for GCGR or Class A (Ballesteros and Weinstein, 1995).for A_{2A}R. Here, only the specific targeted regions for alanine substitution mutation within the GCGR and A_{2A}R are shown. Amino acid residues are given as the single amino acid code and colours illustrate residue physico-chemical properties (Table 5.1).

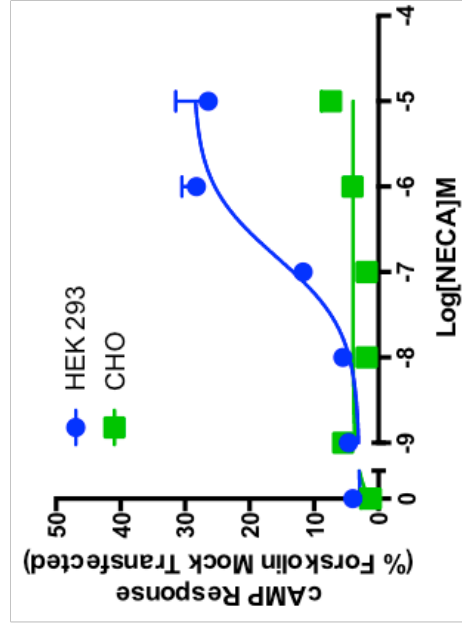


Figure 5.9. NECA induces a cAMP response in mock transfected HEK 293 cells. HEK 293 or CHO cells transiently transfected with vector only (48 hours post transfection) were exposed to NECA for 8 minutes and cAMP accumulation detected. All values are mean \pm SEM expressed as percentage mock forskolin response where $n = 3$ independent experimental repeats, conducted in duplicate.

5.3.2. NECA stimulated cAMP response in WT and mutant A_{2A}R

Stimulation of CHO-K1 cells transfected with A_{2A}R failed to induce a Ca²⁺_i response (Figure 5.10), as has been previously reported (Orr *et al.*, 2015). With this in mind, we looked to solely investigate the importance of ICL1 on cAMP responses following stimulation with the adenosine receptor agonist, NECA.

The A_{2A}R receptor was first cloned into the pmCherry-N1 vector, the ICL1 region (L33-N42) alanine mutants made using site-directed mutagenesis and confirmed by sequencing. CHO-K1 cells transfected with pmCherry-N1 expressing WT or mutants A_{2A}R demonstrated a concentration-dependent cAMP accumulation to NECA stimulation (Figure 5.11 and 5.6 respectively). Here, all responses are normalised to maximum forskolin response in mock-transfected CHO-K1 cells (vector only) to allow comparison between maximum responses to NECA.

Of the ten ICL1 A_{2A}R mutants tested, the potency of NECA was significantly reduced for N34A and L37A (pEC₅₀ 5.77 ±0.1 and 5.16 ±0.2) when compared to WT A_{2A}R (pEC₅₀ 6.23 ±0.1). These two mutants also showed reduced affinity, although this was only significant for L37A when compared to WT (pK_A 4.77 ±0.2 and 5.77 ±0.1 respectively) (Table 5.6). Given the reduced potency of NECA in N34A and L37A, these amino acids appear to be important in the receptors signalling capabilities. The reduced affinity suggests these amino acids may be important in binding of NECA. However, without performing a ligand-binding assay, the mechanism underlying the decrease in NECA potency for the mutant N34A and L37A cannot be determined.

The maximum response was reduced for N34A, Q38A and N42A (E_{max} 61.3 ±2.0, 60.6 ±2.7 and 56.3 ±3.1 percentage mock forskolin response, respectively) when compared to WT A_{2A}R (E_{max} 69.5 ±1.7). There was a significantly reduced basal cAMP response in N34A, L37A, Q38A and N42A (4.3 ±1.0, 0.3 ±1.8, 0.2 ±1.5 and 3.7 ±1.9 percentage mock forskolin) when

compared to WT $A_{2A}R$ (11.5 ± 1.0 percentage mock forskolin). These data suggest that the $A_{2A}R$ has a low level of basal activity in the absence of ligand, and these amino acids may play a role in maintaining this basal activity. On the other hand, T41A showed a significantly elevated basal cAMP response (26.5 ± 1.1). The elevated basal of T41A translated to a significantly reduced signalling window, as indicated by the reduced span (44.3 ± 1.8 percentage mock forskolin). This finding suggest T41A, independent of ligand, is in an active conformation resulting in an elevated basal cAMP level, possibly via G_s -coupling.

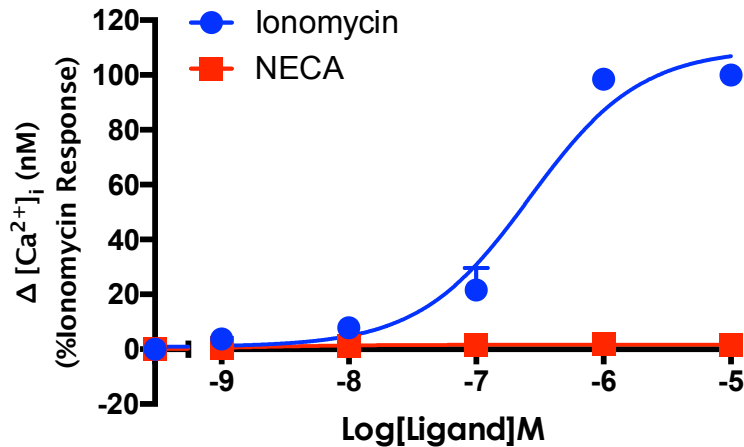


Figure 5.10. NECA failed to stimulate Ca^{2+}_i mobilisation in CHO-K1 cells expressing $A_{2A}R$. CHO-K1 cells transiently transfected with pmCherry-N1 vector expressing $A_{2A}R$ (48 hours post transfection) were exposed to ionomycin (control) and NECA and Ca^{2+}_i mobilisation measured. All values are mean \pm SEM expressed as percentage Ionomycin response where $n = 2$ independent experimental repeats, conducted in duplicate.

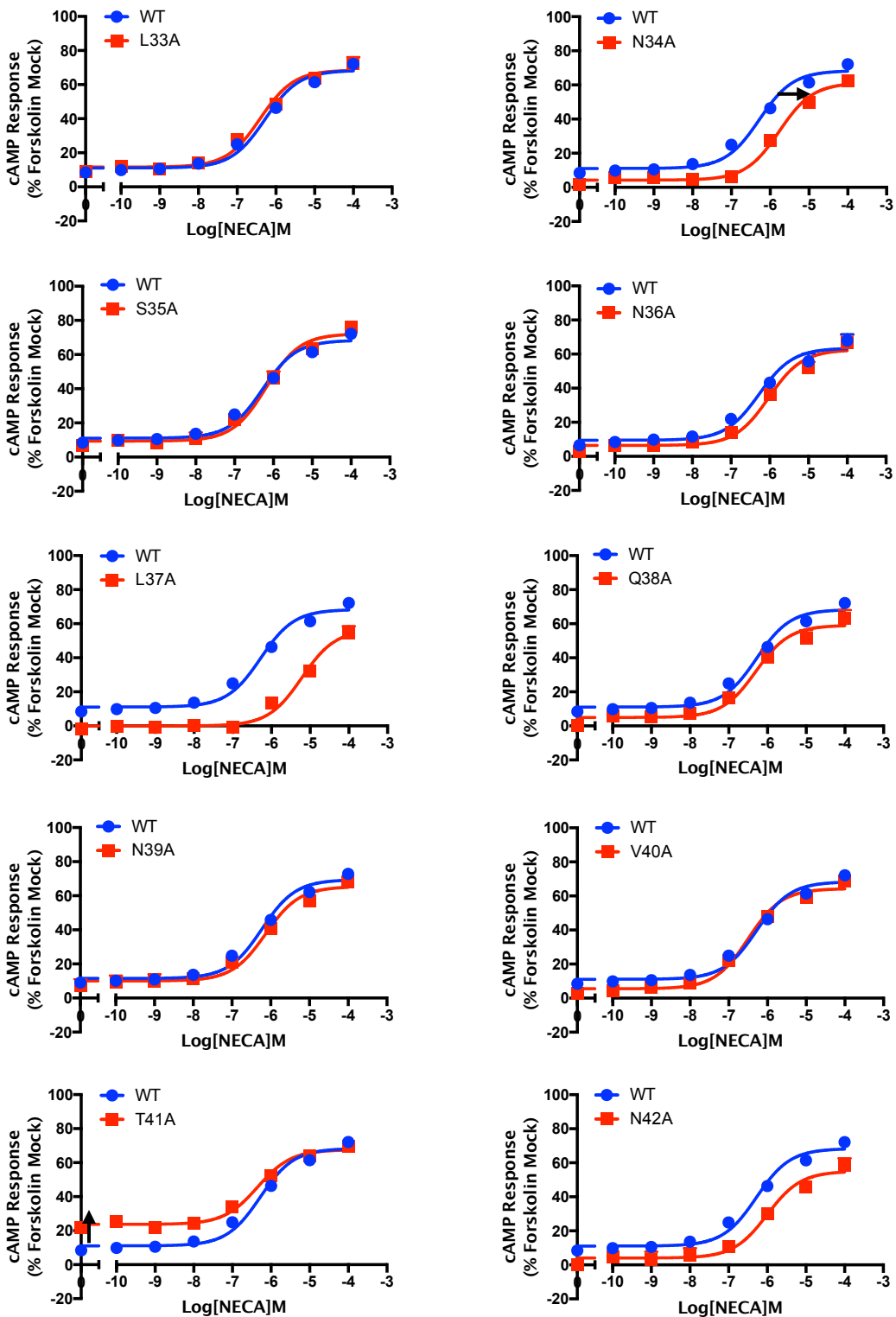


Figure 5.11. Effect of A_{2A}R ICL1 mutants on NECA stimulated cAMP response. CHO-K1 cells transiently expressing WT or alanine containing A_{2A}R ICL1 mutants (48 hours post transfection, 1000 cells/well) were exposed to NECA for 8 minutes and cAMP accumulation detected. All values are mean \pm SEM expressed as percentage forskolin mock response (mock transfected with vector only) where $n \geq 5$ independent experimental repeats, conducted in duplicate. Arrow indicates significant change in pEC₅₀ or elevated basal cAMP levels (Table 5.6) between WT and mutant.

Table 5.6. Effect of A_{2A}R ICL1 mutants on NECA stimulated cAMP response. Potency (pEC₅₀), maximal response (E_{max}), basal, span, affinity (pK_A) and coupling efficacy (log τ) values for cAMP response to NECA stimulation in WT/mutant A_{2A}R transfected CHO-K1 cells

Construct	NECA					
	pEC ₅₀ ^a	E _{max} ^b	Basal ^c	Span ^d	pK _A ^e	log τ ^f
WT	6.23 ±0.1	69.5 ±1.7	11.5 ±1.0	57.9 ±1.9	5.77 ±0.1	0.28 ±0.04
L33A	6.41 ±0.1	68.5 ±2.2	11.6 ±1.5	57.0 ±2.5	5.96 ±0.1	0.26 ±0.05
N34A	5.77 ±0.1*	61.3 ±2.0*	4.3 ±1.0**	57.0 ±2.2	5.38 ±0.1	0.17 ±0.04
S35A	6.19 ±0.1	72.2 ±2.4	9.4 ±1.5	62.8 ±2.7	5.67 ±0.1	0.35 ±0.05
N36A	6.01 ±0.1	66.3 ±2.7	7.2 ±1.5	59.1 ±3.0	5.56 ±0.1	0.24 ±0.05
L37A	5.16 ±0.2**	59.7 ±5.2	0.3 ±1.8**	59.4 ±5.4	4.77 ±0.2***	0.17 ±0.09
Q38A	6.12 ±0.1	60.6 ±2.7*	0.2 ±1.5***	58.3 ±3.1	5.59 ±0.1	0.25 ±0.05
N39A	6.27 ±0.1	63.6 ±3.1	6.9 ±1.8	56.8 ±3.5	5.86 ±0.2	0.19 ±0.06
V40A	6.37 ±0.2	67.9 ±4.0	15.4 ±2.6	52.5 ±4.5	5.95 ±0.2	0.21 ±0.09
T41A	6.42 ±0.1	70.8 ±1.5	26.5 ±1.1***	44.3 ±1.8**	6.02 ±0.1	0.18 ±0.04
N42A	6.00 ±0.1	56.3 ±3.1**	3.7 ±1.9*	52.6 ±3.5	5.66 ±0.2	0.08 ±0.06

WT or mutant A_{2A}R were transiently expressed in CHO-K1 cells and stimulated with NECA prior to measurement of cAMP accumulation to generate concentration response curves for each construct. To calculate pEC₅₀, E_{max}, Basal and Span values, data were analysed using a three-parameter logistic equation. Data was also analysed by an operational model of agonism (Black and Leff, 1983) to determine affinity (pK_A) and coupling efficacy (log τ).

^a Negative logarithm of NECA concentration required to produce a half-maximal response

^b Maximal response to NECA as percentage forskolin response (Mock transfected with pcDNA3.1 Vector)

^c The low plateau of the fitted sigmoidal dose-response curve

^d The difference between E_{max} and basal signalling

^e The negative logarithm of functional affinities that describes the affinity of the receptor when coupled to a given signalling pathway generated through use of the operational model for partial agonism

^f τ is the coupling efficiency parameter generated through use of the operational model for partial agonism

All values are mean ± SEM expressed as percentage mock forskolin response where $n \geq 5$ independent experimental repeats, conducted in duplicate. Statistical significance (*, $p < 0.05$; **, $p < 0.01$; ***, $p < 0.001$) compared to WT A_{2A}R was determined by one-way ANOVA with Dunnett's post test

5.3.3. CGS 21680 stimulated cAMP response in WT and mutant A_{2A}R

With a number of mutants showing distantly different NECA stimulated cAMP response when compared to WT A_{2A}R, we next wanted to identify if these amino acids were also important for the cAMP response following stimulation with another A_{2A}R active compound, the A_{2A}R selective CGS 21680 (Jarvis *et al.*, 1989), or if the mutants showed ligand specific differences.

CHO-K1 cells transfected with A_{2A}R showed a concentration-dependent increase in cAMP accumulation when stimulated with CGS 21680 (Figure 5.12 and Table 5.7). Of the ten ICL1 A_{2A}R mutants tested, the potency and maximum response was significantly reduced for N34A (pEC₅₀ 5.50 ±0.1, E_{max} 48.9 ±3.4) when compared to WT (pEC₅₀ 6.00 ±0.2, E_{max} 61.5 ±4.0). The other nine mutants showed no significant difference in measured potency or maximum response to CGS 21680. However, L37A and N42A also showed a reduced maximum response but we only see a significantly reduced span when compared to WT for L37A (59.6 ±4.5 and 43.7 ±3.7, respectively). There was also a reduced maximal response in N39A, which translated to a significant reduced span when compared to WT (44.2 ±2.7 and 59.6 ±4.5, respectively). N39A also showed a significantly reduced coupling efficacy (log τ -0.51 ±0.05).

As was previously shown (Figure 5.11 and Table 5.6), there was found to be a ligand-independent elevation in basal cAMP accumulation in CHO-K1 cells transfected with T41A when compared to WT A_{2A}R (19.8 ±2.2 and 1.9 ±2.4, respectively). Again, this elevated basal cAMP accumulation translated to a significantly reduced signalling window when compared to WT, as indicated by the reduced span (38.7 ±4.3 and 59.6 ±4.5, respectively). This finding suggest mutation of T41 to alanine, increases the level of constitutively active at the A_{2A}R.

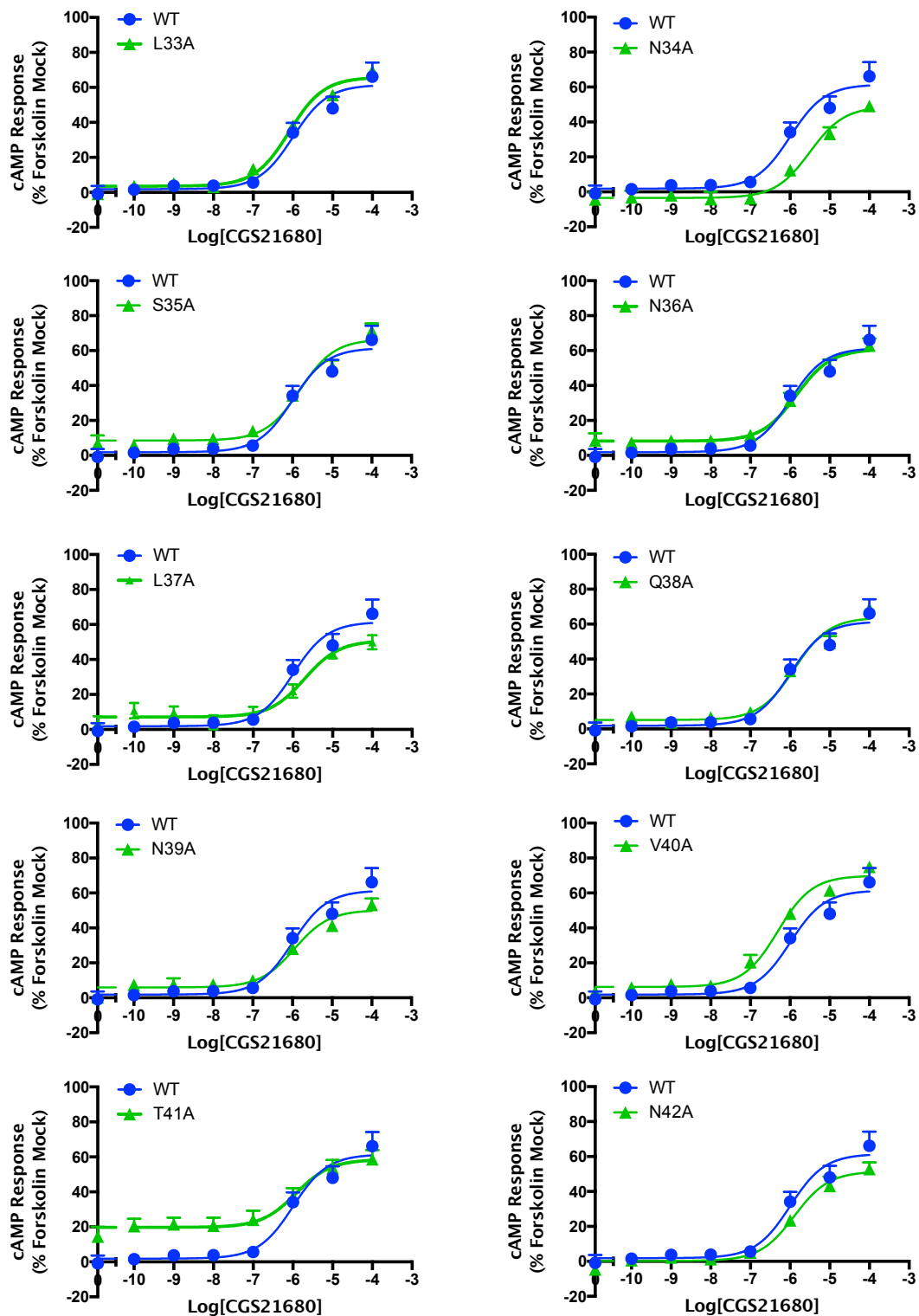


Figure 5.12. Effect of A_{2A}R ICL1 mutants on CGS21680 stimulated cAMP response. CHO-K1 cells transiently expressing WT or alanine containing A_{2A}R ICL1 mutants (48 hours post transfection, 1000 cells/well) were exposed to NECA for 8 minutes and cAMP accumulation detected. All values are mean \pm SEM expressed as percentage forskolin mock response (mock transfected with vector only) where $n \geq 5$ independent experimental repeats, conducted in duplicate. Arrow indicates significant change in pEC₅₀ or elevated basal cAMP levels (Table 5.7) between WT and mutant.

Table 5.7. Effect of A_{2A}R ICL1 mutants on CGS21680 stimulated cAMP response. Potency (pEC₅₀), maximal response (E_{max}), basal, span, affinity (pK_A) and coupling efficacy (log τ) values for cAMP response to CGS 21680 stimulation in WT/mutant A_{2A}R transfected CHO-K1 cells

CGS 21680						
Construct	pEC ₅₀ ^a	E _{max} ^b	Basal ^c	Span ^d	pK _A ^e	log τ
WT	6.00 ±0.2	61.5 ±4.0	1.9 ±2.4	59.6 ±4.5	5.59 ±0.2	0.19 ±0.08
L33A	6.09 ±0.1	65.8 ±2.1	3.6 ±2.1	62.3 ±2.4	5.64 ±0.1	0.26 ±0.04
N34A	5.50 ±0.1*	48.9 ±3.4*	-3.5 ±1.5	52.3 ±3.5	5.20 ±0.2	0.01 ±0.06
S35A	5.81 ±0.1	66.5 ±3.2	8.6 ±1.7	57.9 ±3.5	5.38 ±0.2	0.24 ±0.07
N36A	5.84 ±0.1	60.8 ±3.0	8.2 ±1.7	52.6 ±3.3	5.47 ±0.2	0.13 ±0.06
L37A	5.70 ±0.2	50.8 ±3.5	7.2 ±1.7	43.7 ±3.7*	5.43 ±0.2	-0.05 ±0.07
Q38A	5.89 ±0.1	63.8 ±2.9	5.2 ±1.5	58.6 ±3.2	5.47 ±0.1	0.21 ±0.06
N39A	5.94 ±0.1	50.2 ±2.5	6.0 ±1.4	44.2 ±2.7*	5.67 ±0.1	-0.51 ±0.05***
V40A	6.31 ±0.1	69.9 ±2.5	6.2 ±1.6	63.7 ±2.8	5.82 ±0.1	0.33 ±0.05
T41A	5.92 ±0.2	58.5 ±3.9	19.8 ±2.2***	38.7 ±4.3**	5.64 ±0.2	-0.03 ±0.08
N42A	5.90 ±0.1	51.5 ±2.6	0.3 ±1.4	51.2 ±2.8	5.58 ±0.1	0.02 ±0.05

WT or mutant A_{2A}R were transiently expressed in CHO-K1 cells and stimulated with CGS 21680 prior to measurement of cAMP accumulation to generate concentration response curves for each construct. To calculate pEC₅₀, E_{max}, Basal and Span values, data were analysed using a three-parameter logistic equation. Data was also analysed by an operational model of agonism (Black and Leff, 1983) to determine affinity (pK_A) and coupling efficacy (log τ).

^a Negative logarithm of NECA concentration required to produce a half-maximal response

^b Maximal response to NECA as percentage forskolin response (Mock transfected with pcDNA3.1 Vector)

^c The low plateau of the fitted sigmoidal dose-response curve. ^d The difference between E_{max} and basal signalling

^e The negative logarithm of functional affinities that describes the affinity of the receptor when coupled to a given signalling pathway generated through use of the operational model for partial agonism

^f τ is the coupling efficiency parameter generated through use of the operational model for partial agonism

All values are mean ± SEM expressed as percentage mock forskolin response where $n \geq 5$ independent experimental repeats, conducted in duplicate. Statistical significance (*, $p < 0.05$; **, $p < 0.01$; ***, $p < 0.001$) compared to WT A_{2A}R was determined by one-way ANOVA with Dunnett's post test

5.3.4. Molecular modelling of ICL1 mutants in A_{2A}R structures

Modeller (version 9.18) was used to mutate a number of ICL1 residues to alanine within four available protein structures of A_{2A}R for which PDB files exist; 4EIY (Liu *et al.*, 2012), 2YDV (Lebon *et al.*, 2011), 4UHR (Lebon *et al.*, 2015) and 5G53 (Carpenter *et al.*, 2016). These included N34, L37, Q38, T41 and N42, which showed a NECA or CGS 21680 stimulated cAMP accumulation significantly different to WT (Table 5.6 and 5.7, respectively). The resulting PDB files were viewed in MacPyMol (version 1.7.4.5) and the WT and mutated receptor compared visually to assess any predicted changes in amino acid interactions and structure (Table 5.8). As an example and to aid in illustration of polar interactions within WT and modelled mutated structure of A_{2A}R, images generated in MacPyMol for antagonist (ZM241385) bound A_{2A}R (Liu *et al.*, 2012) are shown (Figure 5.13 and 5.14).

Although the polar interactions for each residue showed variability between the four structures, there were a number of conserved interactions and lost interactions within the modelled mutated A_{2A}R structures irrespective of agonist/antagonist/G protein bound.

The modelled A_{2A}R containing alanine at position 34 showed a number of lost interactions and may account for the significantly reduced potency and maximum response to both NECA and CGS 21680. The lost interactions included helix 8 residues T298^{8.53} and E294^{8.49}, which were found to make a polar interaction with N34 in the majority of the A_{2A}R structures investigated (Table 5.8). Another potentially important interaction lost on mutation to alanine included N36.

Within all four A_{2A}R structures, L37 was shown to form polar interactions with N39 and N42 and were maintained within the modelled L37A structures. Interestingly, within the NECA-bound and G protein-bound A_{2A}R structures, mutation of L37 to alanine resulted in a gained interaction with N34. However, this gained polar contact had no effect on the interactions of N34 (with T298^{8.53} and E294^{8.49}) and the modelled structure does not appear

to offer an explanation for the reduced potency and maximum response to both NECA and CGS 21680.

Depending on the structure analysed, Q38 was shown to interact with V31, W32, N34 and S35. Whereas the interaction with V31 was found in all four of the A_{2A}R structures, the interaction with N34, W32 or S35 was found in three of the four investigated. On mutation to alanine, all of these interactions, with the exception of S35, were lost and may provide an indication as to the significantly reduced maximum response to NECA.

Viewing the crystal structure of the active-like conformation bound CGS 21680 A_{2A}R revealed that T41 interacts with D101 and R102 of the E/DRY motif and Y112 in ICL2. Although these interactions were only found in one of the three structures analysed here, T41 was shown to interact with D101 within two other A_{2A}R structures (Xu *et al.*, 2011 and Dore *et al.*, 2011). The E/DRY motif in TM3, is one of the mostly highly conserved sequences motifs in GPCRs (Rovati *et al.*, 2007) and is proposed to form part of the “ionic lock” stabilise the inactive receptor conformation (Vogel *et al.*, 2008). These interactions were lost in the modelled CGS 21680 bound T41A mutant A_{2A}R (4UHR) structure and may provide an explanation for the constitutive activity found for this mutated A_{2A}R. In other words, on mutation the “ionic lock” is broken resulting in a constitutively active A_{2A}R. Interestingly, the equivalent position for T41^{2.39} within GCGR is R173^{2.46} and was investigated further (Section 5.4.2).

N42 was found to interact with L37, N39 and V46 in all four A_{2A}R structures. Whereas the interactions between N42 with N39 and V46 were maintained on mutation to alanine, the interaction with L37 was lost. There was also found to be a gained interaction for this position with V45 in three of the four structures used to modelled mutant A_{2A}R. These interaction changes may provide an explanation for the reduced maximum response.

Table 5.8. Comparison of A_{2A}R residue polar contacts within WT and modelled A_{2A}R mutant crystal structures

ZM241385 bound (4EIY)			
N34	Leu37 Glu294 Thr298*	N34A	Leu37
L37	Asn34 Asn39* Asn42*	L37A	Asn34 Asn39* Asn42*
Q38	H bond Val31* Trp32	Q38A	None
T41	H ₂ O H bond(x2) Phe44 Val45	T41A	Phe44 Val45
N42	H ₂ O H bond(x2) Leu37* Asn39*(x2) Val46*	N42A	Asn39* Val46*
NECA bound (2YDV)			
N34	Ala30 Asn36 Glu294 Thr298*	N34A	Ala30
L37	Asn39* Asn42*	L37A	<u>Asn34</u> Asn39* Asn42*
Q38	Val31* Trp32 Ser35	Q38A	Ser35
T41	None	T41A	<u>Phe44</u>
N42	Leu37* Asn39*(x2) Val46*	N42A	Asn39*(x1) <u>Val45</u> Val46*
CGS21680 bound (4UHR)			
N34	Ala30 Asn36 Leu37 Gln38 Glu294 Thr298*	N34A	Ala30 Gln38
L37	Asn34 Asn39* Asn42*	L37A	Asn39* Asn42*
Q38	Val31* Asn34 Ser35	Q38A	Ser35
T41	Phe44 Asn39 Val45 Asp101 Arg102 Tyr112	T41A	Phe44
N42	Leu37* Asn39* Val46*	N42A	Asn39* <u>Val45</u> Val46*
Engineered G protein bound (5G53)			
N34	Ala30 Asn36 Gln38 Thr298*	N34A	Ala30 Gln38
L37	Asn39* Asn42*	L37A	<u>Asn34</u> Asn39* Asn42*
Q38	Val31* Trp32 Asn34 Ser35	Q38A	Ser35
T41	None	T41A	<u>Phe44</u> <u>Val45</u>
N42	Leu37* Asn39*(x3) Val46*	N42A	Asn39*(x2) Val46*

Mutant models of the A_{2A}R were made using Modeller and the resulting PDB structures compared with WT in PyMOL for any loss/gain of polar interactions. Alanine mutants (with a cAMP accumulation significantly different to WT (Table 5.6)) were modelled for A) antagonist (ZM241385) bound A_{2A}R solved by Liu *et al.*, 2012 at a resolution of 1.8 Å (PDB ID: 4EIY), B) agonist (NECA) bound A_{2A}R solved by Lebon *et al.*, 2011 at a resolution of 2.6 Å (PDB ID: 2YDV), C) agonist (CGS21680) bound A_{2A}R solved by Lebon *et al.*, 2015 at a resolution of 2.6 Å (PDB ID: 4UHR) and D) engineered G_s-protein bound at a resolution of 3.5 Å by Carpenter *et al.*, 2016 (PDB ID: 5G53).

Conserved interactions irrespective of agonist/antagonist/G protein bound are indicated by *

Underlined residues (e.g. Val45) indicate gain of polar interaction.

A residue with more than one polar interaction with another residue is indicated by (xn), where n gives the number of interactions.

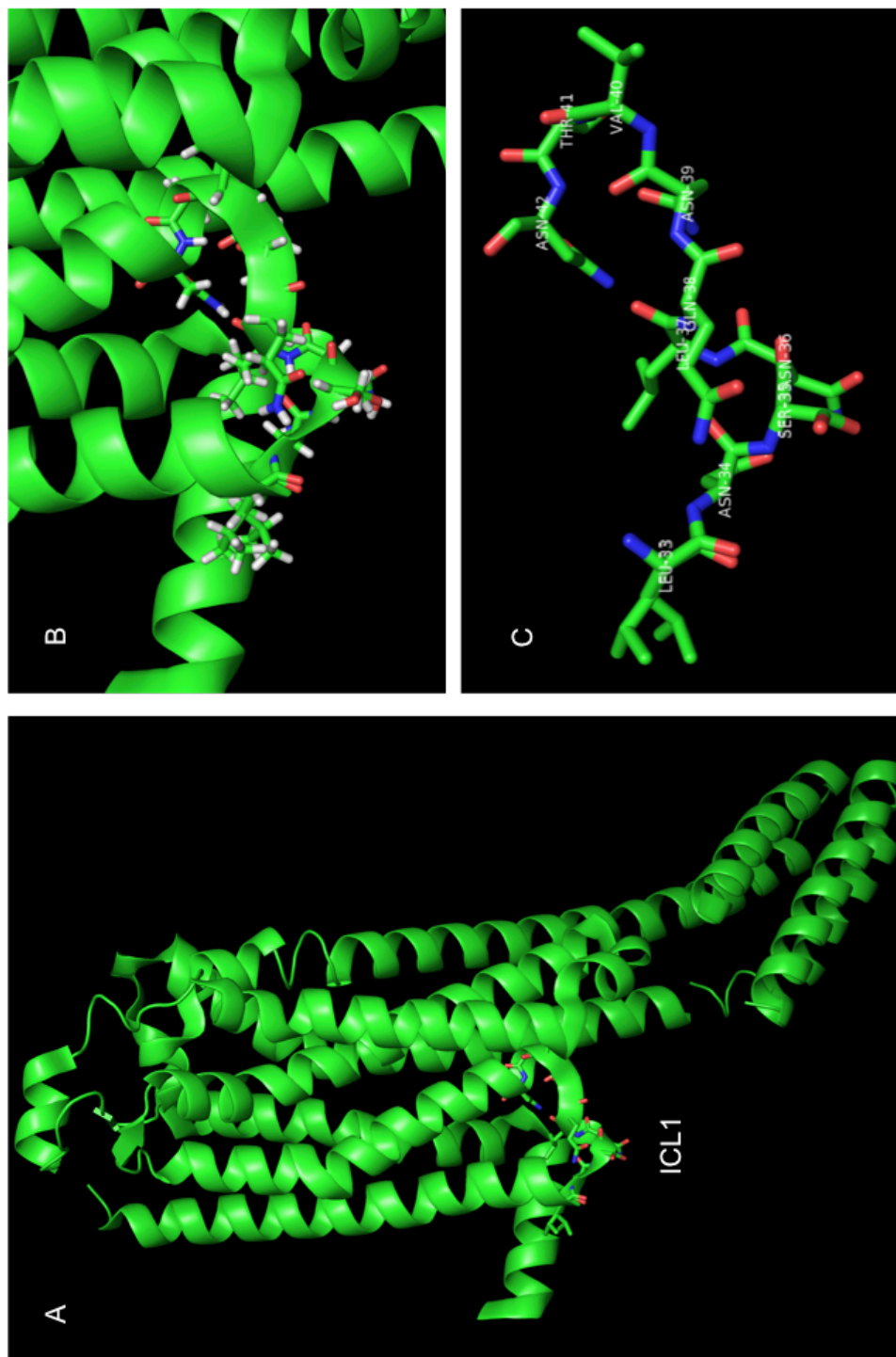
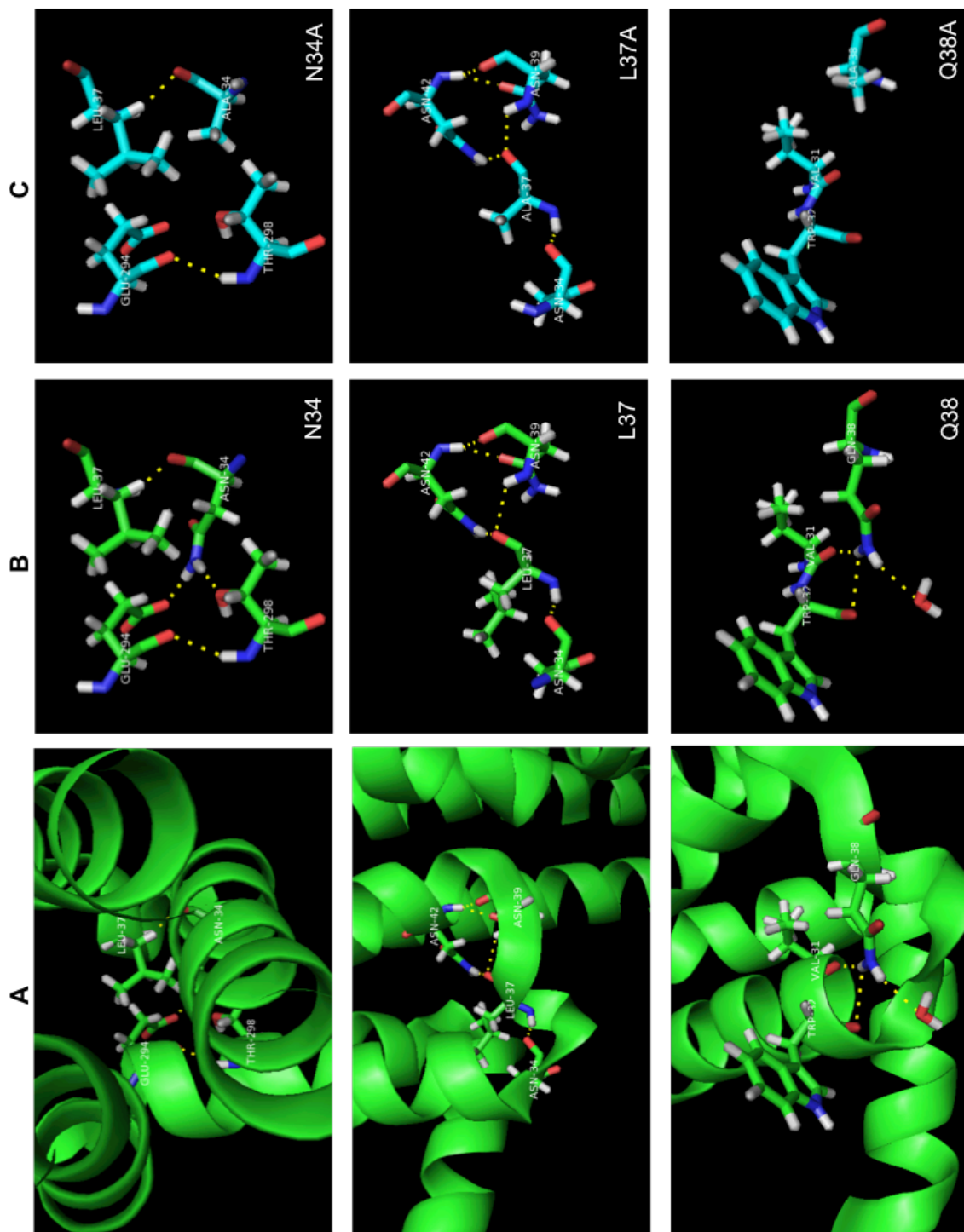


Figure 5.13. ICL1 region within crystal structure of $A_{2A}R$ bound to ZM241385. Antagonist (ZM241385) bound $A_{2A}R$ solved by Liu *et al.*, 2012 at a resolution of 1.8 Å (PDB ID: 4E1Y) was imaged in PyMOL. **A**) Cartoon image of 4E1Y with the residues correspond to the regions within the $A_{2A}R$ targeted for alanine substitution depicted as sticks. **B**) Zoomed in image of A, with hydrogen atoms added to the stick represented residues targeted for alanine substitution. **C**) Cartoon and hydrogen atoms removed for clarity. The atom type within each residue is coloured red for oxygen, blue for nitrogen and white for hydrogen.



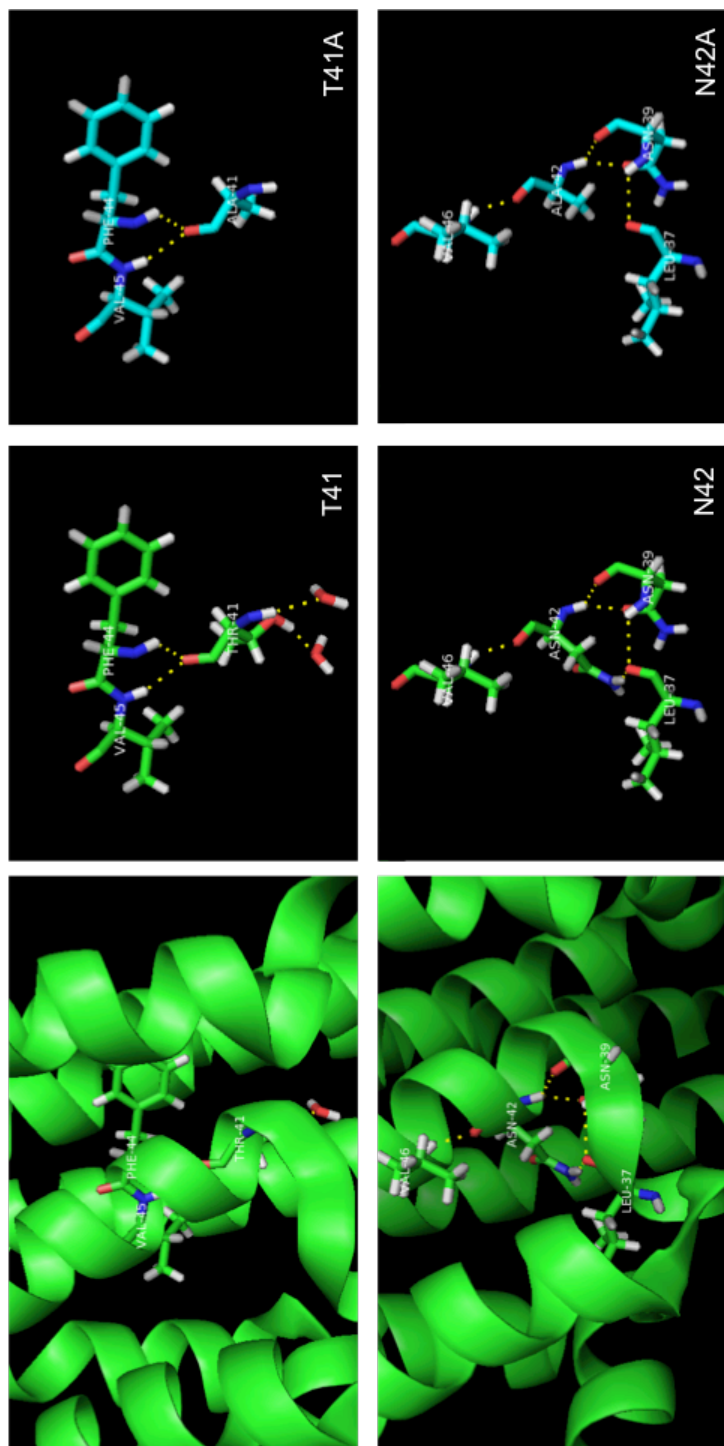


Figure 5.14. Comparison of polar contacts within ZM241385 bound WT and alanine containing A_{2A}R crystal structure. Antagonist (ZM241385) bound A_{2A}R solved by Liu *et al.*, 2012 at a resolution of 1.8 Å (PDB ID: 4E1Y) was viewed in PyMOL and alanine substitution mutants (with a cAMP response significantly different to WT (Table 5.6)) modeled using Modeller. The resulting PDB structures were compared with WT in PyMOL for any loss/gain of polar interactions. **A)** WT A_{2A}R with overlaying cartoon representation indicating the targeted residue position within the receptor and any polar interactions. **B)** Polar interactions within WT A_{2A}R without cartoon overlay for clarity **C)** Polar interactions within alanine containing A_{2A}R mutant without cartoon overlay for clarity. Residues are labeled in using the three-letter amino acid code (Table 5.1). The atom type within each residue is coloured red for oxygen, blue for nitrogen and white for hydrogen. A yellow dashed line indicates polar interactions.

5.3.5. Summary

In this work, the A_{2A}R was chosen as a class A G_s-coupled receptor to investigate the importance of the ICL1 region in receptor signalling as was conducted for the class B GPCR, GCGR. The potency (pEC₅₀), maximal response (E_{max}), basal, span, affinity (pK_A) and coupling efficacy (log τ) values for the cAMP response to NECA or CGS 21680 stimulation showed no significant differences between that measured in WT A_{2A}R and the A_{2A}R mutants L33A, S35A, N36A, V40A. These data suggest that these amino acids are unlikely to play an important role in the A_{2A}R mediated cAMP response to either agonist.

Mutation of asparagine at position 34 of A_{2A}R to alanine resulted in a significantly reduced potency and maximum response to both NECA and CGS 21680. This finding suggests that N34 is important in the activity of A_{2A}R to both agonists which may or may not be dependent on cell-surface expression. Interestingly, N34 was found to interact with the conserved helix 8 residue T298^{8.53} and E294^{8.49} within all four and three of the A_{2A}R structures investigated, respectively (Table 5.4). These interactions were lost within the modelled N34A structures and may indicate the importance of ICL1 and helix 8 interactions within A_{2A}R for activation and/or signal transduction following ligand stimulation (NECA and CGS 21680). Interestingly, the equivalent positions for E294^{8.49} and T298^{8.53} within GCGR are E406^{8.49} and E410^{8.53}, respectively, and were investigated further (Section 5.4.3).

Alanine substitution of L37 in A_{2A}R resulted in a reduced potency and maximum response to both NECA and CGS 21680 suggesting L37 is important in the A_{2A}R mediated cAMP response. However, there was only found to be a significantly reduced potency and affinity of NECA. Given that L37 appears to play a more significant role in the NECA stimulated cAMP response when compared to the CGS 21680, this finding may indicate a role for L37 in signalling bias at the A_{2A}R.

Given the basal cAMP level is independent of ligand stimulation, the finding that a number of A_{2A}R mutants showed significantly reduced basal cAMP levels in NECA stimulated cells but not for CGS 21680 suggests some variation that is independent of receptor mutation and ligand stimulation. With the exception of the measured elevated basal cAMP level in T41A, it appears that any significant differences in basal response may be due to experimental variable rather than a true biological effect.

Mutation of threonine at position 41 within the TM2 region (T41^{2.39}) of A_{2A}R to alanine resulted in agonist independent increase in basal activity within CHO-K1 cells. T41 was found to interact with D101 and R102 of the E/DRY motif and Y112 in the ICL2 in three A_{2A}R structures (Xu *et al.*, 2011, Dore *et al.*, 2011 Lebon *et al.*, 2015). These residues are implicated to be involved in the ionic lock of the A_{2A}R and proposed to stabilise the inactive receptor conformation (Martínez-Archundia and Correa-Basurto, 2014). Interestingly, mutations within the E/DRY motif have been shown to induce constitutive activity for a number of GPCRs including the β₂AR, rhodopsin receptor and oxytocin receptor (OTR) (Rovati *et al.*, 2007). Similarly, it appears that mutation of T41 of the A_{2A}R increases the level of constitutive activity at the A_{2A}R, possibly due to the loss of hydrogen bonds with residues involved in the ionic lock.

N42A showed reduced maximum response to both NECA and CGS 21680, although this was only significantly reduced for NECA. When comparing the cAMP responses between NECA and CGS 21680 in the Q38A and N39A A_{2A}R mutants, there were some clear differences. Whereas Q38A showed a significantly reduced maximum response to NECA when compared to WT, there was no such reduced maximal response to CGS 21680. On the other hand, whereas N39A showed a reduced CGS 21680 maximal response and efficacy, there was no such reduction following NECA stimulation. These findings may indicate the importance of ICL1 residues in signalling bias at the A_{2A}R and warrants further investigation.

The findings presented here suggest the ICL1 region of A_{2A}R plays a bigger role in the cAMP response when compared to the ICL1 region of the GCGR, where there was significantly reduced signalling for only one mutant (G165A). In order to further expand on these findings, analysis of the cell-surface expression of each A_{2A}R mutant needs to be conducted. This will give an indication as to whether the reduced signalling of some mutants could be explained by changes in receptor cell-surface expression. In addition, it may be interesting to investigate the effect of these mutants on the pERK1/2 response given that A_{2A}R has been reported to activate ERK1/2 signalling (Schulte and Fredholm, 2000, Orr *et al.*, 2015).

5.4. An investigation into conserved GPCR residues within GCGR

5.4.1. An investigation into the '[K/R]KLH' motif in GCGR

The [K/R]KLH motif occurs in the ICL1 of both class A and B GPCR families (Vohra *et al.*, 2013). Within the class B GPCR family, the consensus sequence is R^{12.48}[+]LH with 9 of the 15 members having the sequence RRLH or RKLH (Figure 5.1). Rather than K/R, GCGR has a serine at this position (S167^{12.48}) giving the sequence SKLH (Figure 5.15). In a model of the CLR in complex with G protein, K167^{12.48} within the sequence K167^{12.48}SLS was suggested to interact with the Gβ and possibly with the helix 8 residue (E^{8.49}) (Vohra *et al.*, 2013). However, within the cryo-EM structures of GLP-1R and CTR in complex with heterotrimeric G_s (Liang *et al.*, 2017 and Zhang *et al.*, 2017b, respectively), R^{12.48} was shown not to interact with Gβ or helix 8 residue (E^{8.49}).

We previously investigated the cAMP accumulation in HEK 293 cells transfected with a number of alanine substitution mutations within ICL1 of GCGR including S167A and K168A, which showed no significant effects on cAMP accumulation (Figure 5.4). Here, we investigate the consequences of

converting the serine to a positive charged arginine, effectively making the ICL1 sequence within GCGR closer to the consensus '[K/R]KLH' motif and possibly creating an interaction between S167R^{12.48} and a glutamate residue within helix 8 such as E406^{8.49} or E410^{8.53}. Molecular modelling of the S167R^{12.48} mutant within the full-length structure of GCGR suggests the gain of a polar interaction with E410^{8.53} rather than E406^{8.49} (Figure 5.16). S167^{12.48} was shown to interact with E410^{8.53} in the NNC0640 bound GCGR structure (Siu *et al.*, 2013) but not the full-length structure (Zhang *et al.*, 2017) (Table 3.3.3), possibly indicating differing interactions between the inactive conformational state.

Using FACS analysis, similar levels of cell-surface expression were found for WT and S167R (100.9 ±6.3 percentage WT response) (Figure 5.17). The effect of this mutation on the GCG and oxyntomodulin stimulated cAMP response was investigated. The responses between WT and S167R appeared similar for both GCG or oxyntomodulin stimulation (Figure 5.18 and Table 5.9) suggesting this residue is not critical for cAMP response.

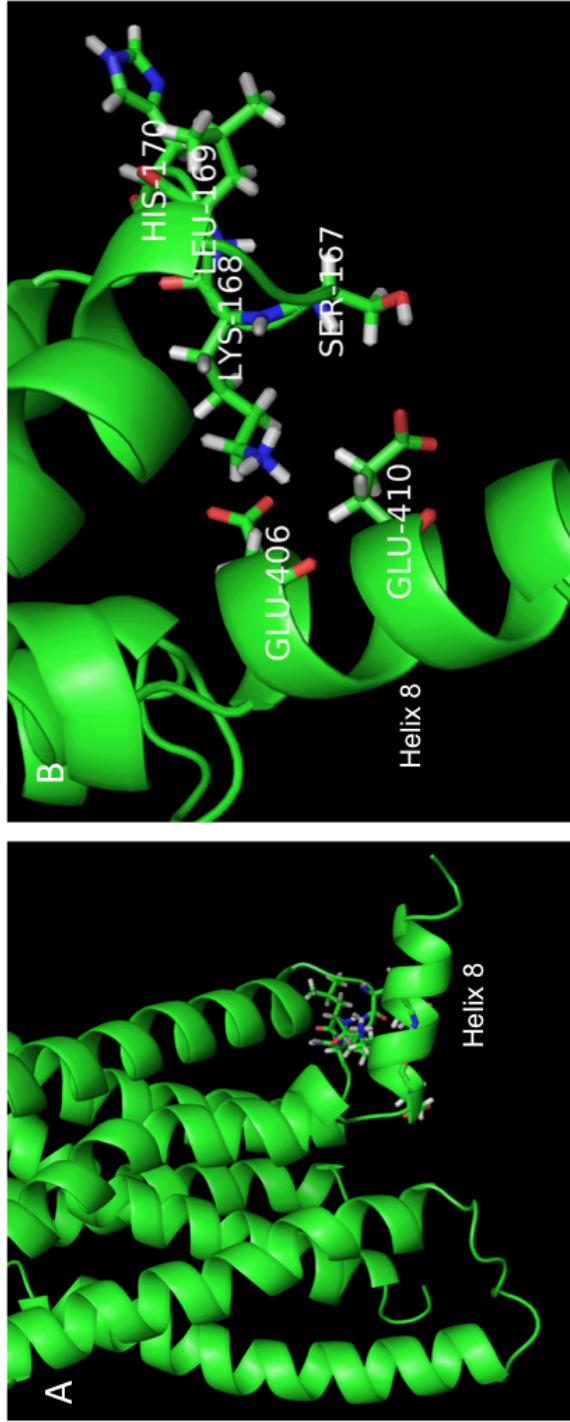


Figure 5.15. [K/R]K[LH] motif and helix 8 conserved glutamate residues in crystal structure of full-length GCGR. full length GCGR in complex with the negative allosteric modulator (NAM) NNC0640 solved by Zhang *et al.*, 2017 at a resolution of 3 Å (PDB ID: 5XEZ) was imaged in MacPyMOL. **A)** Cartoon image of the 5XEZ structure with the [K/R]K[LH] motif (SKLH) and conserved E406 and E410 in helix 8 depicted as sticks. **B)** Zoomed in image of A, rotated 90° and tilted downwards. Residues are labeled using the three-letter amino acid code (Table 5.1). The atom type within each residue is coloured red for oxygen, blue for nitrogen and white for hydrogen. A yellow dashed line indicates polar interactions. T4L inserted into the ICL2 of GCGR between A256 and E260 has been removed for clarity.

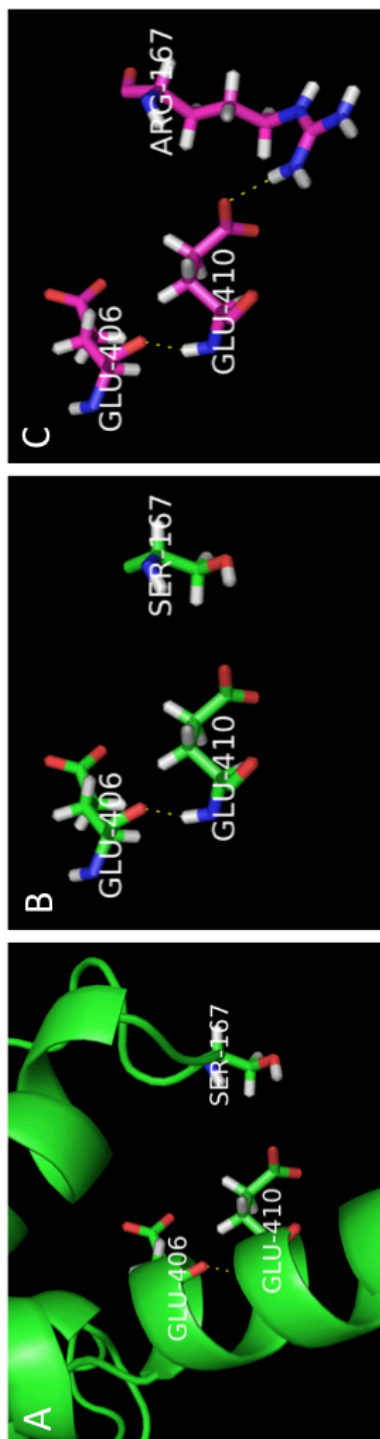


Figure 5.16. Modeled S167R mutant within full-length GCGR crystal structure. Full-length GCGR in complex with the negative allosteric modulator (NAM) NNC0640 solved by Zhang *et al.*, 2017 at a resolution of 3 Å (PDB ID: 5XEZ) was imaged in MacPyMOL. **A)** WT GCGR with S167, E406 and E410 depicted as sticks with overlaying cartoon **B)** A2, without cartoon overlay for clarity **C)** modeled arginine containing GCGR mutant (S167R) forms a polar contact with E410. Residues are labeled using the three-letter amino acid code (Table 5.1). The atom type within each residue is coloured red for oxygen, blue for nitrogen and white for hydrogen. A yellow dashed line indicates polar interactions. T4L inserted into the ICL2 of GCGR between A256 and E260 has been removed for clarity.

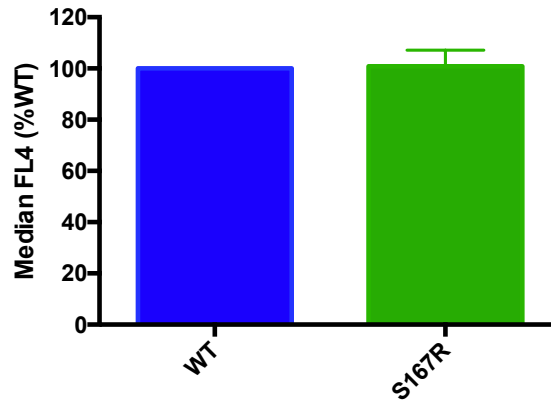


Figure 5.17. WT and S167R GCGR show similar cell-surface expression in HEK 293 cells as determined by FACS analysis. FACS analysis was conducted 48 hours post transfection of HEK 293 with WT or mutant GCGR containing pmCherry-N1. Anti-GCGR primary antibody at a 1:50 dilution, APC-conjugated IgG secondary antibody at a 1:150 dilution. Normalised to vector transfected (0%) and WT (100%), $n = 3$ independent experimental repeats. Statistical significance compared to WT was determined by unpaired Student's t-test (two-tailed).

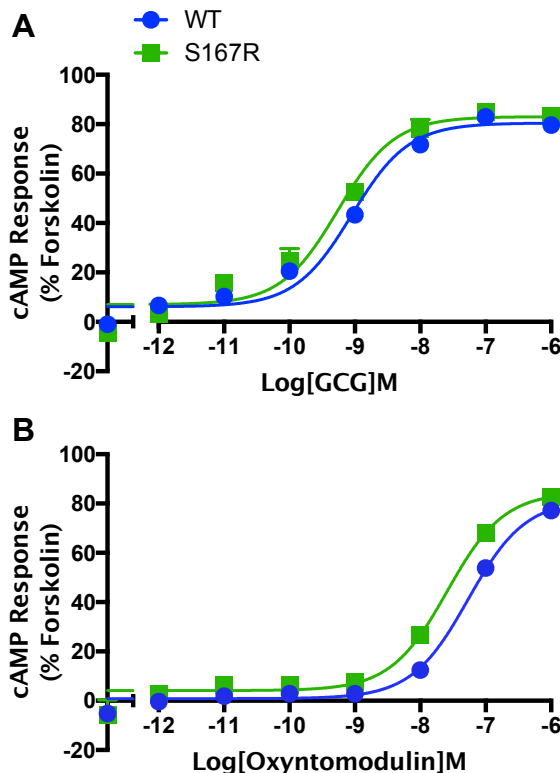


Figure 5.18. cAMP response in WT and S167R GCGR mutants. HEK 293 cells transiently expressing pmCherry-N1 vector containing WT or S167R GCGR (24 hours post transfection) were exposed to **A**) GCG or **B**) oxyntomodulin for 8 minutes and cAMP accumulation detected. All values are mean \pm SEM expressed as percentage forskolin response (mock transfected with vector only) where $n \geq 5$ independent experimental repeats, conducted in duplicate. Arrow indicated change between WT and mutant response.

Table 5.9. cAMP response in WT and S167R GCGR mutants. Potency (pEC₅₀), maximal response (E_{max}), basal, span, affinity (pK_A) and coupling efficacy (log τ) values for cAMP response to GCG/oxyntomodulin stimulation in WT/mutant GCGR transfected HEK 293 cells

GCG						
Construct	pEC ₅₀ ^a	E _{max} ^b	Basal ^c	Span ^d	pK _A ^e	log τ ^f
WT	9.09 ±0.1	81.5 ±1.5	7.6 ±1.1	74.0 ±1.8	8.38 ±0.1	0.60 ±0.04
S167R	9.26 ±0.1	83.1 ±2.8	7.0 ±2.5	76.1 ±3.6	8.52 ±0.2	0.65 ±0.09
Oxyntomodulin						
Construct	pEC ₅₀ ^a	E _{max} ^b	Basal ^c	Span ^d	pK _A ^e	log τ ^f
WT	7.27 ±0.1	81.5 ±2.2	0.9 ±1.0	80.7 ±2.3	6.54 ±0.1	0.64 ±0.06
S167R	7.59 ±0.1	84.7 ±2.1	4.1 ±1.1	80.6 ±2.3	6.79 ±0.1	0.72 ±0.07

WT or mutant GCGR were transiently expressed in HEK 293 cells and stimulated with GCG or oxyntomodulin prior to measurement of cAMP accumulation to generate concentration response curves for each construct. To calculate pEC₅₀, E_{max}, Basal and Span values, data were analysed using a three-parameter logistic equation. Data was also analysed by an operational model of agonism (Black and Leff, 1983) to determine affinity (pK_A) and coupling efficacy (log τ).

^a Negative logarithm of GCG concentration required to produce a half-maximal response

^b Maximal response to GCG as percentage forskolin response (Mock transfected with vector)

^c The low plateau of the fitted sigmoidal dose-response curve

^d The difference between E_{max} and basal signalling

^e The negative logarithm of functional affinities that describes the affinity of the receptor when coupled to a given signalling pathway generated through use of the operational model for partial agonism

^f τ is the coupling efficiency parameter generated through use of the operational model for partial agonism
All values are mean ± SEM expressed as percentage forskolin response (Mock transfected with vector) where $n \geq 5$ independent experimental repeats, conducted in duplicate.

Statistical significance (*, $p < 0.05$; **, $p < 0.01$; ***, $p < 0.001$) compared to WT GCGR was determined by unpaired Student's t-test (two-tailed)

5.4.2. An investigation into the importance of R173 in GCGR signalling

5.4.2.1. Cell-surface expression of R173A and R173A N174A mutants similar to WT GCGR

We previously investigated the importance of 8 residues within the ICL1 region of GCGR (residues G165-T172) and 10 residues of the class A A_{2A}R ICL1 region (L33-N42) (see Figure 5.8 for alignment) through alanine substitution and cAMP accumulation assays. Although there was little effect on the measured cAMP response in the GCGR alanine substitution mutants following GCG stimulation, there were a number of interesting findings for the A_{2A}R mutants including an enhanced constitutive activity for T41A. The equivalent position for T41^{2.39} within GCGR is 2.46 and contains the highly conserved positively charged residue at the bottom of TM2, R173^{2.46}.

Here, we expanded on the initial investigation by investigating the importance of R173^{2.46} for cell-surface expression and signalling of GCGR. We also created an alanine substitution mutation at position N174^{2.47} as a 'safeguard', to eliminate the polar amino acid that may contribute or substitute the interactions of R173A mutant. Having created this single and double alanine substitutions within GCGR, we first wanted to investigate the cell-surface expression of these mutants using FACS analysis. There was found to be no significant difference in cell-surface expression of R173A or R173A N174A when compared to WT GCGR (Figure 5.19).

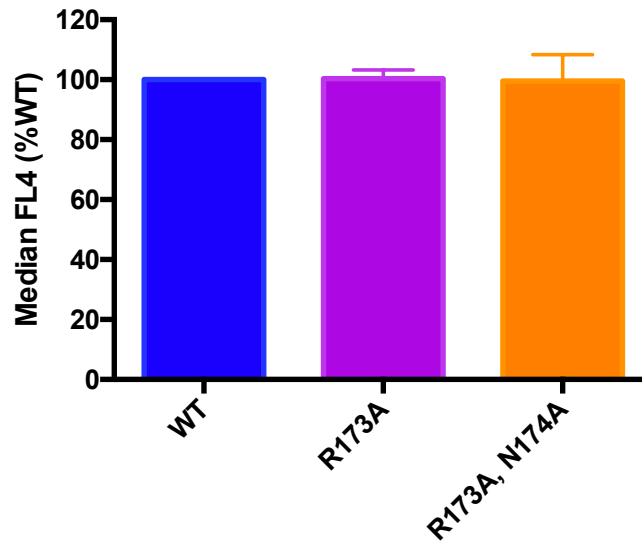


Figure 5.19. Cell-surface expression of WT, R173A and R173A N174A GPCR are similar in transfected HEK 293 cells, as determined by FACS analysis. FACS analysis was conducted 48 hours post transfection of HEK 293 with WT or mutant GPCR containing pmCherry-N1. Anti-GPCR primary antibody at a 1:50 dilution, APC-conjugated IgG secondary antibody at a 1:150 dilution. Normalised to vector transfected (0%) and WT (100%), $n = 3$ independent experimental repeats. Statistical significance compared to WT was determined by one-way ANOVA with Dunnett's post test.

5.4.2.2. R173A^{2.46} mutant shows severe reduction of GCG and oxyntomodulin-mediated cAMP accumulation

Multiple studies have highlighted the importance of the conserved GPCR R173^{2.46} equivalent for G protein-coupling in a number of class B GPCRs including CGRP receptor (Conner *et al.*, 2006) GIPR (Cordomí *et al.*, 2015) and GLP-1R (Mathi *et al.*, 1997). Having shown equivalent cell-surface expression of WT, single (R173A), and double (R173A N174A) TM2 mutant GPCR, we investigated the importance of the conserved R173^{2.46} residue for the GPCR-mediated cAMP accumulation.

HEK 293 cells transfected with pmCherry-N1 expressing WT or mutant GPCR were stimulated with GCG or oxyntomodulin prior to measurement of cAMP accumulation. The potency of GCG was severely attenuated (~100-

fold) in HEK 293 cells transfected with R173A when compared to WT (pEC_{50} 7.14 ± 0.1 and 9.09 ± 0.1 , respectively) (Figure 5.20 A and Table 5.10), whereas the maximum response was unaffected. The reduced potency may reflect a reduced affinity to GCG, as indicated by fitting the operational model of agonism.

The cAMP accumulation following oxyntomodulin stimulation was also attenuated. However, a full dose-response curve was not determined given the insufficient data points (Figure 5.20 B and Table 5.10) and a maximum response (50.3 ± 8.3 percentage forskolin response) and a pEC_{50} (6.23 ± 0.2) were predicted from the fit. We may have seen an oxyntomodulin maximum response equivalent to that seen in WT if we had stimulated at higher concentrations. Importantly, the measured responses to GCG or oxyntomodulin at the single and double TM2 mutants were equivalent (Figure 5.20 A/B and Table 5.10), suggesting R173 is the amino acid responsible for the attenuated cAMP accumulation. With this in mind, the single mutant N174A was not made and only the R173A mutant was investigated further.

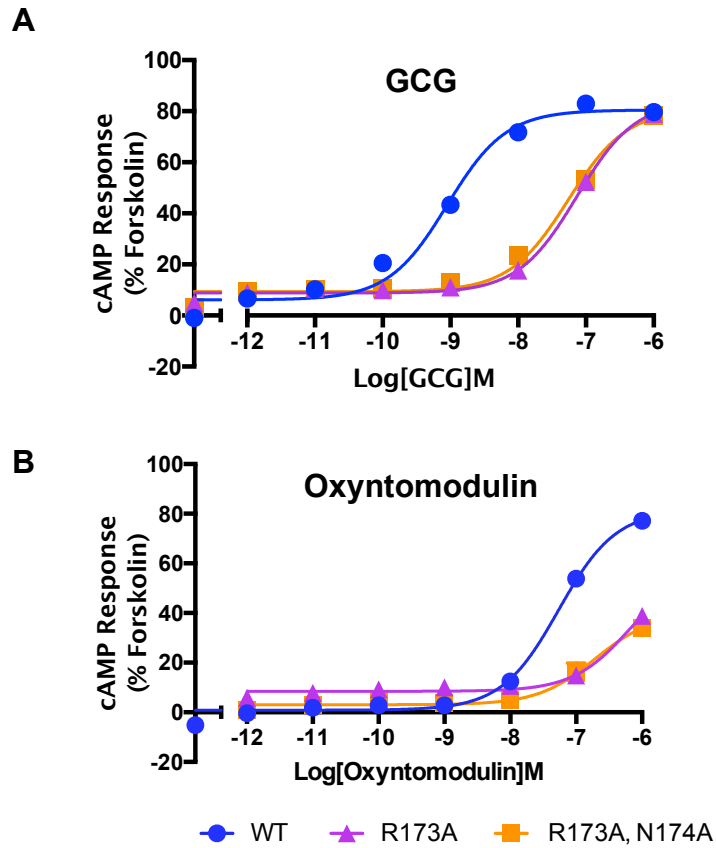


Figure 5.20. GCG and oxyntomodulin induced cAMP response is attenuated in R173A transfected HEK 293. HEK 293 cells transiently expressing pmCherry-N1 vector containing WT, R173A or R173A N174A GCGR (24 hours post transfection) were exposed to **A)** GCG or **B)** oxyntomodulin for 8 minutes and cAMP accumulation detected. All values are mean \pm SEM expressed as percentage forskolin response (mock transfected with vector only) where $n \geq 5$ independent experimental repeats, conducted in duplicate. Arrow indicated significant change (Table 5.10) between WT and mutant response.

Table 5.10. GCG and oxyntomodulin induced cAMP response is attenuated in R173A transfected HEK 293. Potency (pEC_{50}), maximal response (E_{max}), basal, span, affinity (pK_A) and coupling efficacy ($\log \tau$) values for cAMP response to GCG/oxyntomodulin stimulation in WT/mutant GCGR transfected HEK 293 cells

GCG						
Construct	pEC_{50} ^a	E_{max} ^b	Basal ^c	Span ^d	pK_A ^e	$\log \tau$ ^f
WT	9.09 ±0.1	81.5 ±1.5	7.6 ±1.1	74.0 ±1.8	8.38 ±0.1	0.60 ±0.04
R173A	7.14 ±0.1***	88.1 ±2.4*	9.6 ±0.7	78.5 ±2.5	6.37 ±0.1***	0.68 ±0.08
R173A, N174A	7.28 ±0.1***	82.2 ±3.4	11.7 ±1.1**	70.5 ±3.5	6.59 ±0.2***	0.57 ±0.10
Oxyntomodulin						
Construct	pEC_{50} ^a	E_{max} ^b	Basal ^c	Span ^d	pK_A ^e	$\log \tau$ ^f
WT	7.27 ±0.1	81.5 ±2.2	0.9 ±1.0	80.7 ±2.3	6.54 ±0.1	0.64 ±0.06
R173A	6.23 ±0.2	50.3 ±8.3	8.5 ±0.7	41.8 ±8.1	6.01 ±0.3	-0.08 ±0.26
R173A, N174A	6.60 ±0.2	55.2 ±5.8	11.0 ±1.2	44.2 ±5.7	6.51 ±0.2	-0.21 ±0.08

WT or mutant GCGR were transiently expressed in HEK 293 cells and stimulated with GCG or oxyntomodulin prior to measurement of cAMP accumulation to generate concentration response curves for each construct. To calculate pEC_{50} , E_{max} , Basal and Span values, data were analysed using a three-parameter logistic equation. Data was also analysed by an operational model of agonism (Black and Leff, 1983) to determine affinity (pK_A) and coupling efficacy ($\log \tau$).

^a Negative logarithm of GCG concentration required to produce a half-maximal response

^b Maximal response to GCG as percentage forskolin response (Mock transfected with vector)

^c The low plateau of the fitted sigmoidal dose-response curve

^d The difference between E_{max} and basal signalling

^e The negative logarithm of functional affinities that describes the affinity of the receptor when coupled to a given signalling pathway generated through use of the operational model for partial agonism

^f τ is the coupling efficiency parameter generated through use of the operational model for partial agonism

All values are mean ± SEM expressed as percentage forskolin response (Mock transfected with vector) where $n \geq 5$ independent experimental repeats, conducted in duplicate.

Statistical significance (*, $p < 0.05$; **, $p < 0.01$; ***, $p < 0.001$) compared to WT GCGR was determined by one-way ANOVA with Dunnett's post test

Italic text represent predicted fits due to insufficient data point and therefore statistics were not performed

5.4.2.3. Molecular modelling of R173A mutants in three GCGR structures

Modeller (version 9.18) was used to mutate specific residues within two of the three available protein structures of inactive GCGR for which PDB files exist; 5XEZ (Zhang *et al.*, 2017) and 4L6R (Siu *et al.*, 2013). The GCGR residue within the thermostabilised (StaR) MK-0893-bound GCGR receptor (5ee7 (Jazayeri *et al.*, 2016)), R173 was mutated to alanine and therefore this structure was not used. The resulting PDB files were viewed in MacPyMol (version 1.7.4.5) and the WT (original PDB file) and modelled mutated receptor compared visually to assess any predicted changes in amino acid interactions and structure. To aid in illustration of the lost polar interactions within R173A when compared to WT GCGR, images generated in MacPyMol for full length GCGR (Zhang *et al.*, 2017) are shown (Figure 5.21).

The overall structure when comparing the modelled mutant to WT showed no differences. Although the interactions made by R173 differ between the two inactive GCGR structures, consistently R173 interacts with E406 within helix 8 (Table 5.11). This consistency indicates the importance of the interaction, possibly through stabilisation of the inactive GCGR structure. In both modelled structures, mutation of R173 results in lost interaction with E406. Importantly, there were no gained or lost interactions for R173A within the modelled R173A N174A when compared to R173A (Table 5.11). This further supports the conclusion that R173 is the residue responsible for the attenuated cAMP response to both GCG and oxyntomodulin.

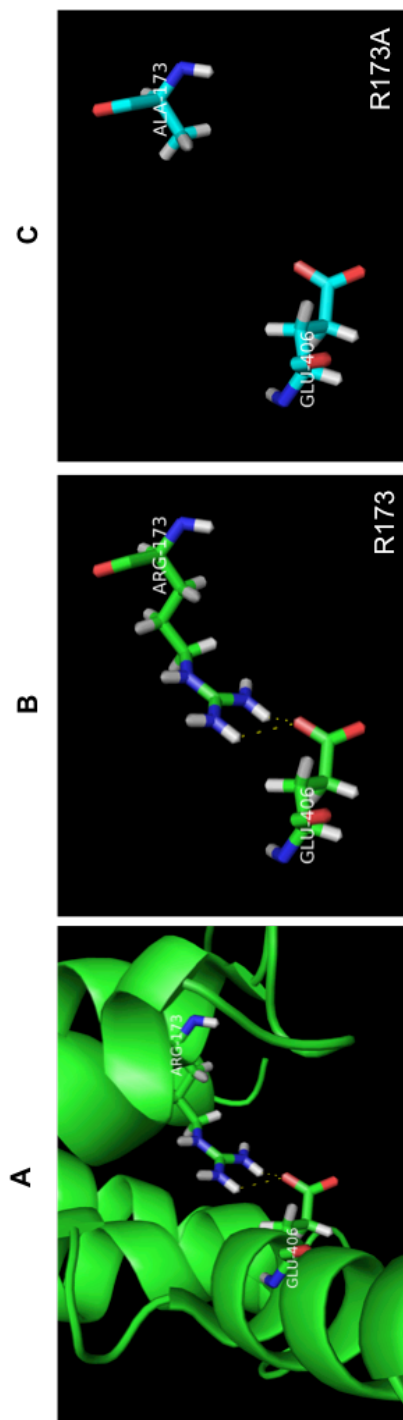


Figure 5.21. Comparison of polar contacts within WT and modeled R173A containing crystal structure of full-length GCGR at position 173. full length GCGR in complex with the negative allosteric modulator (NAM) NNC0640 and antigen-binding fragment of an inhibitory antibody (mA1b) solved by Zhang *et al.*, 2017 at a resolution of 3 Å (PDB ID: 5XEZ) was imaged in PyMOL. **A)** WT GCGR with overlaying cartoon representation indicating the targeted R173 residue and its polar interaction with helix 8. **B)** Polar interactions within WT GCGR without cartoon overlay for clarity **C)** Polar interactions for R173A GCGR mutant without cartoon overlay for clarity. Residues are labeled using the three-letter amino acid code (Table 5.1). The atom type within each residue is coloured red for oxygen, blue for nitrogen and white for hydrogen. A yellow dashed line indicates polar interactions.

Table 5.11 Comparison of polar contacts at position 173 within WT GCGR and modeled R173A/ R173A, R174A mutant structures

NNC0640 bound full length GCGR 3 Å (5XEZ)		
R173	Glu406(x2)	R173A None
R173 in R173 N174	Glu406(x2)	R173A in R173A N174A None
NNC0640 bound GCGR 3.4 Å (4I6R)		
R173	Ile176 His177 Glu406	R173A Ile176 His177
R173 in R173 N174	Ile176 His177 Glu406	R173A in R173A N174A Ile176 His177

Mutant models of the GCGR were made using Modeller and the resulting PDB structures compared with WT in PyMOL for any loss/gain of polar interactions. Alanine mutants were modeled for NNC0640 bound full length GCGR solved to a resolution of 3 Å (PDB ID: 5XEZ) (Zhang *et al.*, 2017) and NNC0640 bound GCGR solved to a resolution of 3.4 Å (PDB ID: 4I6R) (Siu *et al.*, 2013). A residue with more than one polar interaction with another residue is indicated by (xn), where n gives the number of interactions

5.4.2.4. Summary

R^{2.46} is highly conserved across class B GPCRs and is implicated to form part of the class A E/DRY motif equivalent, maintaining the receptor in the ground state (Vohra *et al.*, 2013). Within the CLR it was proposed that the class B E/DRY equivalent is formed by the glutamate in TM3 (E233^{3.50}) interacting with R173^{2.46} and a histidine in TM2 (H177^{2.50}) (Vohra *et al.*, 2013). Interestingly, no such interactions were found within the active or inactive structures of GLP-1R (Zhang *et al.*, 2017b and Song *et al.*, 2017, respectively) suggesting this may not be the case for other class B GPCRs. Mutations of the glutamic acid/aspartic acid within the E/DRY motif frequently induce constitutive activity and indicated that these residues maintain the receptor in the ground state (Rovati *et al.*, 2007). However, in some receptors mutation of these residues do not result in constitutive activity and the E/DRY motif is suggested to be directly involved in the receptor conformation and G protein-coupling (Rovati *et al.*, 2007).

The findings presented here suggests that R173, although not required for successful GCGR trafficking, is important for the GCGR-mediated cAMP response, as demonstrated by the attenuated response to both GCG and oxyntomodulin in HEK 293 transfected with R173A. This finding is similar to what was previously reported for the R176A^{2.46} GLP-1R mutant, which showed a reduction in cAMP accumulation whilst maintaining WT cell-surface expression levels (Mathi *et al.*, 1997).

Modelling of the R173A and R173A, N174A GCGR mutants within two of the three available protein structures of inactive GCGR (Zhang *et al.*, 2017 and Siu *et al.*, 2013) revealed the potentially important interaction between R173 and the helix 8 residue E406, which was lost within R173A (Section 5.4.2.2). It may be that this interaction is critical for GCGR stabilisation. Alternatively, or in addition to, R173 may be essential for G protein-coupling. This latter explanation seems highly plausible given that the residue at this position has been demonstrated to contact the G protein within a CGRP

receptor model (R173^{2.46}) (Vohra *et al.*, 2013) and in the structure of the class A GPCR β_2 -adrenergic receptor (AR)-Gs complex (Thr68^{2.39}) (Rasmussen *et al.*, 2011, PDB 3SN6). To add further weight to this explanation, within the solved peptide-activated rabbit GLP-1R in complex with heterotrimeric G_s, it was suggested that the lost interactions for R176^{2.46} in TM2, N406^{8.47} and E408^{8.49} in helix 8 caused by the outwards movement of TM6 on activation may be stabilised through hydrogen bonds or electrostatic interactions with residues of the G α_s α 5-helix (Zhang *et al.*, 2017b). Indeed, visualisation of the GLP-1R cryo-EM structure showed interactions between R176^{2.46} with T175^{2.45}, H180^{2.43} and Q390 of G α_s α 5-helix (Zhang *et al.*, 2017b). Modelling of R176A^{2.46} GLP-1R showed lost interactions with T175^{2.45} and Q390 of G α_s α 5-helix. It may be that a similar interaction of R173^{2.46} and G α_s α 5-helix within GCGR is a requirement for effective G protein activation, which is thus attenuated on mutation to alanine.

Interestingly, the residue present in the equivalent position of the A_{2A}R (T41^{2.39}) was shown to interact with D101^{3.49} and R102^{3.50} of the E/DRY motif and mutation to alanine resulted in constitutive activity. Given the absence of an elevated basal cAMP accumulation for R173A in GCGR, it appears this residue is involved in GCGR activation and/or G protein-coupling rather than maintaining the receptor in an inactive conformation.

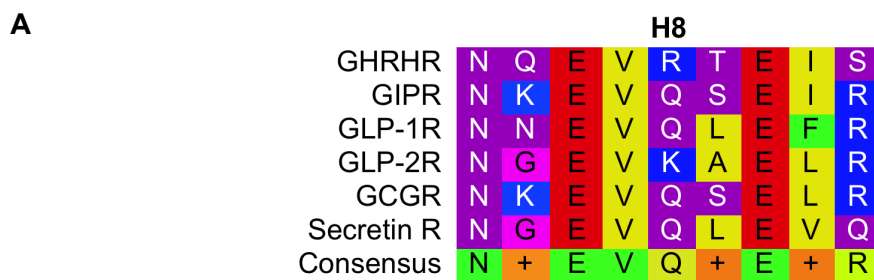
5.4.3. Investigating the importance of two conserved residues within helix 8 of GCGR; E406 and E410

5.4.3.1. Cell-surface expression of E406A and E406A E410A show reduced cell-surface expression

We previously showed the importance of R173^{2.46} within GCGR for the ligand stimulated cAMP accumulation (Section 5.4.2.2), which may have been a consequence of lost contact with G protein-coupling or recognition. Within the inactive structures of the GCGR, R173^{2.46} was demonstrated to form tight

interactions with E406^{8.49} (Siu *et al.*, 2013 and Zhang *et al.*, 2017). E406^{8.49} is fully conserved in all class B GPCRs and may play a role in GPGR activation (Kirkpatrick *et al.*, 2012) (Figure 5.22). Modelling of R173A in both structures demonstrated the lost interaction with E406^{8.49}, which may result in a GCGR confirmation unfavorable to receptor activation or G protein-coupling. In order to investigate the importance of this interaction, we create a single alanine substitution mutation at position E406^{8.49}. We also created an alanine substitution mutation at position E410^{8.53} as a 'safeguard', to eliminate the negative charge that may contribute or substitute the negative charge/interaction eliminated in the E406A mutant.

Having created this single and double alanine substitutions within GCGR, we first investigated the cell-surface expression of these mutants using FACS analysis (Figure 5.23). There was found to be a significantly reduced cell-surface expression for E406A and E406A E410A (53.8 ±5.8 and 21.5 ±1.3 percentage WT cell-surface expression, respectively), whereas there was no significant reduction in the cell-surface expression of E410A (91.4 ±9.1 percentage WT cell-surface expression). This suggesting that E406 is more crucial than E410 for the successful cell-surface expression of GCGR. Interestingly, when comparing the cell-surface expression of E406A and E406A E410A, the latter showed a significantly reduced expression. Although E410A alone has little effect on the measured GCGR cell-surface expression, mutation of both glutamate residues to alanine appears to impair the cell-surface expression of GCGR, possibly through premature degradation.



B

H8

Amino acid	N	K	E	V	Q	S	E	L	R
Absolute Position	404	405	406	407	408	409	410	411	412
Class B number	8.47	8.48	8.49	8.50	8.51	8.52	8.53	8.53	8.55

Figure 5.22. GCGR family structure-based alignment of helix 8. **A)** GPCRdb.org structure-based alignment of helix 8 within the GCGR family receptors; GHRH receptor, GIPR, GLP-1R, GLP-2R, GCGR and the secretin receptor. **B)** The residue position within helix 8 of GCGR are given in both absolute and Class B (Wootten *et al.*, 2013) numbers. Here, the two conserved glutamate residues targeted for alanine substitution are shown. Amino acid residues are given as the single amino acid code and colours illustrate residue physico-chemical properties (Table 5.1).

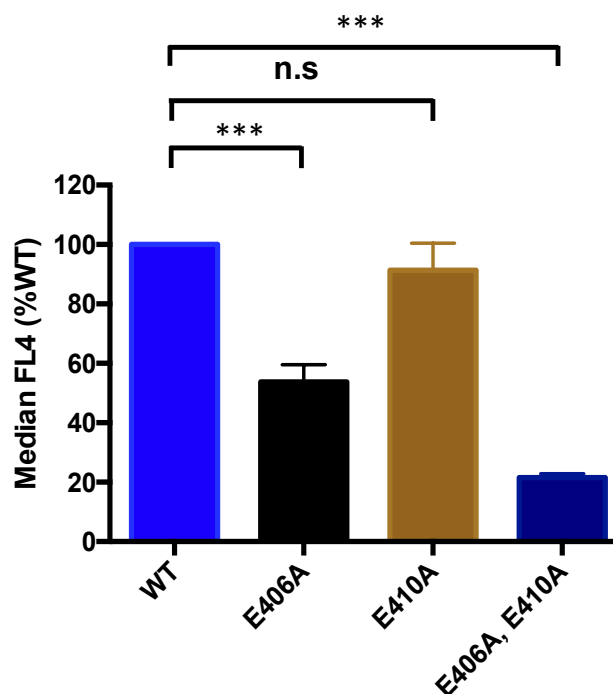


Figure 5.23. Cell-surface expression of WT and Helix 8 GCGR mutants, as determined by FACS analysis. FACS analysis was conducted 48 hours post transfection of HEK 293 with WT or mutant GCGR containing pmCherry-N1. Anti-GCGR primary antibody at a 1:50 dilution, APC-conjugated IgG secondary antibody at a 1:150 dilution. Normalised to vector transfected (0%) and WT (100%), $n = 3$ independent experimental repeats. Statistical significance (*, $p < 0.1$; **, $p < 0.01$; ***, $p < 0.001$) compared to WT was determined by one-way ANOVA with Dunnett's post test.

5.4.3.2. Elevated basal cAMP accumulation in E406A and E406A E410A GCGR mutants

Having shown a reduced cell-surface expression of E406A and E406A E410A, we investigate the consequence of these mutants on the ligand stimulated cAMP accumulation. HEK 293 cells transfected with pmCherry-N1 expressing WT or mutant GCGR were stimulated with GCG or oxyntomodulin prior to measurement of cAMP accumulation.

Consistent with previous findings in rat GCGR (Strudwick *et al.*, 2004), mutation of E406 resulted enhanced basal activity to both GCG and oxyntomodulin stimulation when compared to WT (Figure 5.24 1A/1B and Table 5.12). The cAMP response in E410A showed subtle differences when compared to WT and with the exception of a small elevation in basal, showed no significant differences between any of the measured parameters (Figure 5.24 2A/2B and Table 5.12). There was also found to be enhanced potency and basal cAMP response for the double helix 8 mutant (E406A E410A), but again only reached statistical significance for the enhanced constitutive activity (Figure 5.25 and Table 5.12).

These findings suggest that E406 when mutated alone appears to result in a level of constitutive activity, which is enhanced further by the additional substitution of E410 to alanine. This finding may be interpreted as an ability of E410 within E406A to substitute or contribute to the lost interaction with R173^{2,46} or other amino acids, effectively maintaining the receptor in a relatively inactive state when compared to the double mutant. As we mutate both residues, this interaction may be completely lost resulting in enhanced constitutive activity. In line with this, the double helix 8 mutant also showed a significantly elevated maximum response and efficacy for GCG, suggesting an enhanced ability for G protein-coupling.

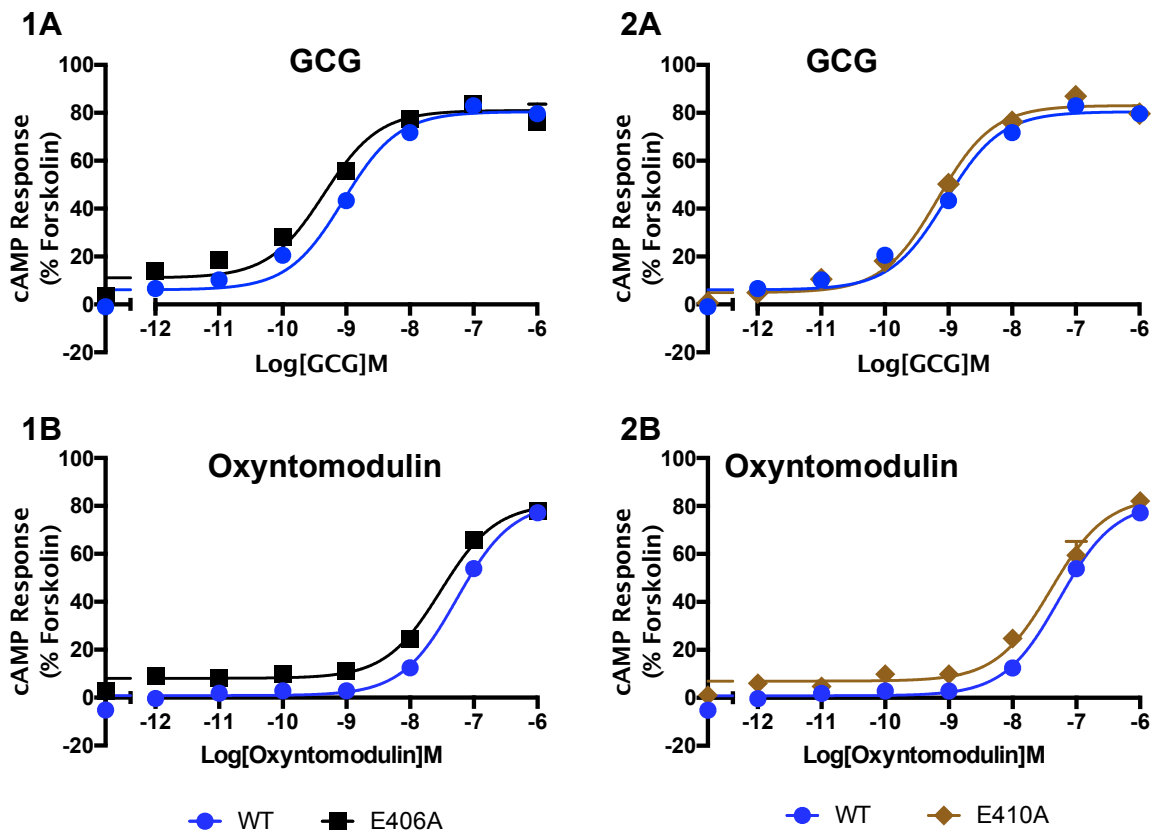


Figure 5.24. cAMP response in WT and helix 8 GPCR mutant. HEK 293 cells transiently expressing pmCherry-N1 vector containing 1) WT or E406A, 2) WT or E410A GPCR (24 hours post transfection) were exposed to **A**) GCG or **B**) oxyntomodulin for 8 minutes and cAMP accumulation detected. All values are mean \pm SEM expressed as percentage forskolin response (mock transfected with vector only) where $n \geq 5$ independent experimental repeats, conducted in duplicate. Arrow indicates small shift in pEC_{50} for E406A mutant

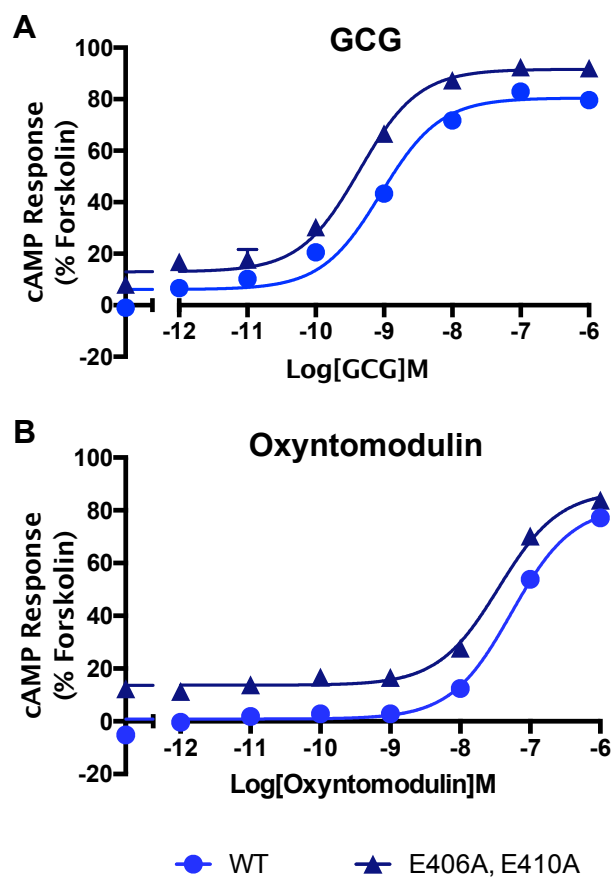


Figure 5.25. E406A E410A GCGR mutant showed a ligand-independent elevated basal cAMP level. HEK 293 cells transiently expressing pmCherry-N1 vector containing WT or E406A E410A GCGR (24 hours post transfection) were exposed to **A**) GCG or **B**) oxyntomodulin for 8 minutes and cAMP accumulation detected. All values are mean \pm SEM expressed as percentage forskolin response (mock transfected with vector only) where $n \geq 5$ independent experimental repeats, conducted in duplicate. Arrow indicate significant shift in pEC₅₀ and basal cAMP accumulation (Table 5.12) for E406A E410A mutant when compared to WT.

Table 5.12. cAMP response in WT and helix 8 GCGR mutant. Potency (pEC_{50}), maximal response (E_{max}), basal, span, affinity (pK_A) and coupling efficacy ($\log \tau$) values for cAMP response to GCG/oxyntomodulin stimulation in WT/mutant GCGR transfected HEK 293 cells

GCG						
Construct	pEC_{50} ^a	E_{max} ^b	Basal ^c	Span ^d	pK_A ^e	$\log \tau$ ^f
WT	9.09 ± 0.1	81.5 ± 1.5	7.6 ± 1.1	74.0 ± 1.8	8.38 ± 0.1	0.60 ± 0.04
E406A	9.35 ± 0.1	81.0 ± 1.9	11.1 ± 1.5*	69.9 ± 2.3	8.68 ± 0.1	0.57 ± 0.06
E410A	9.14 ± 0.1	84.6 ± 2.1	5.1 ± 1.4	79.5 ± 2.4	8.35 ± 0.1	0.71 ± 0.07
E406A, E410A	9.27 ± 0.1	92.1 ± 1.6**	19.6 ± 1.4***	72.5 ± 2.1	8.26 ± 0.1	0.96 ± 0.10**

Oxyntomodulin						
Construct	pEC_{50} ^a	E_{max} ^b	Basal ^c	Span ^d	pK_A ^e	$\log \tau$ ^f
WT	7.27 ± 0.1	81.5 ± 2.2	0.9 ± 1.0	80.7 ± 2.3	6.54 ± 0.1	0.64 ± 0.06
E406A	7.52 ± 0.1	81.0 ± 2.2	8.1 ± 1.0**	73.0 ± 2.3	6.84 ± 0.1	0.59 ± 0.06
E410A	7.40 ± 0.1	83.8 ± 3.4	7.0 ± 1.6*	76.8 ± 3.5	6.63 ± 0.2	0.68 ± 0.12
E406A, E410A	7.49 ± 0.1	88.3 ± 2.3	15.6 ± 2.3***	72.7 ± 2.4	6.63 ± 0.1	0.79 ± 0.10

WT or mutant GCGR were transiently expressed in HEK 293 cells and stimulated with GCG or oxyntomodulin prior to measurement of cAMP accumulation to generate concentration response curves for each construct. To calculate pEC_{50} , E_{max} , Basal and Span values, data were analysed using a three-parameter logistic equation. Data was also analysed by an operational model of agonism (Black and Leff, 1983) to determine affinity (pK_A) and coupling efficacy ($\log \tau$).

^a Negative logarithm of GCG concentration required to produce a half-maximal response

^b Maximal response to GCG as percentage forskolin response (Mock transfected with vector)

^c The low plateau of the fitted sigmoidal dose-response curve

^d The difference between E_{max} and basal signalling

^e The negative logarithm of functional affinities that describes the affinity of the receptor when coupled to a given signalling pathway generated through use of the operational model for partial agonism

^f τ is the coupling efficiency parameter generated through use of the operational model for partial agonism

All values are mean ± SEM expressed as percentage forskolin response (Mock transfected with vector) where $n \geq 5$ independent experimental repeats, conducted in duplicate.

Statistical significance (*, $p < 0.05$; **, $p < 0.01$; ***, $p < 0.001$) compared to WT GCGR was determined by one-way ANOVA with Dunnett's post test. Italic represent predicted fits due to insufficient data point and therefore statistics were not performed

5.4.3.3. Molecular modelling of E406 and E410 mutants in three GCGR structures

Modeller (version 9.18) was used to mutate E406 and E410 to alanine within the three available protein structures of inactive GCGR for which PDB files exist; 5XEZ (Zhang *et al.*, 2017), 4L6R (Siu *et al.*, 2013) and 5EE7 (Jazayeri *et al.*, 2016). The resulting PDB files were viewed in MacPyMol (version 1.7.4.5) and the WT and mutated receptor compared visually to assess any predicted changes in amino acid interactions and structure (Table 5.13). To aid in illustration of the lost polar interactions within the modelled E406A and E410A mutants when compared to WT GCGR, images generated in MacPyMol for full length GCGR (Zhang *et al.*, 2017) are shown (Figure 5.14).

There are differing interactions for E406 and E410 within the three WT GCGR structures. Notably however, E406 interacts with E410 in all three structures and R173 in both structures containing R173 (one structure lacks residue R173 (Jazayeri *et al.*, 2016)). In the modelled structures of E406A, whereas the interaction to E410 was maintained in all structures and did not depend on the presence of glutamate, the R173 interaction was lost (illustrated in Figure 5.14 C). This lost interaction with R173 may offer an explanation for the elevated basal cAMP response determined in E406A and E406A E410A (Table 5.12). It could be speculated that R173, now released from helix 8, is free to interact with the G protein in the absence of ligand leading to this small elevated cAMP levels.

Table 5.13. Comparison of polar contacts at position 406 and 410 within WT GCGR and modeled E406A/E410A/E406A, E410A GCGR mutant structures

NNC0640 bound full length GCGR 3 Å (5XEZ)			
E406	Arg173(x2) Asn404 Ser409 Glu410	E406A	Asn404 Ser409 Glu410
E410	Glu406 Val407 Ser409 Arg414	E410A	Glu406 Val407 Arg414
E406 in E406 E410	Arg173(x2) Asn404 Ser409 Glu410	E406 in E406A E410A	Asn404 Ser409 Ala410
E410 in E406 E410	Val407 Glu406 Ser409 Arg414	E410 in E406A E410A	Val407 Ala406 Arg414
NNC0640 bound GCGR 3.4 Å (4L6R)			
E406	Arg173 Ser409 Glu410	E406A	Ser409 Glu410
E410	Ser167 Glu406 Ser409 Arg413(x2) Arg414(x2)	E410A	Glu406 Ser409 Arg414
E406 in E406 E410	Arg173 Ser409 Glu410	E406 in E406A E410A	Ser409 Ala410
E410 in E406 E410	Ser167 Glu406 Ser409 Arg413(x2) Arg414(x2)	E410 in E406A E410A	Ala406 Ser409 6 Arg414
MK-0893 bound GCGR 2.5 Å (5EE7)			
E406	H2O H bond Arg346(x2) Asn404(x2) Glu410	E406A	Asn404 Glu410
E410	Glu406 Val407 Arg413(x2) Arg414	E410A	Glu406 Val407 Arg414
E406 in E406 E410	H2O H bond Arg346(x2) Asn404(x2) Glu410	E406A in E406A E410A	Asn404 Ala410
E410 in E406 E410	Glu406 Val407 Arg413(x2) Arg414	E410A in E406A E410A	Ala406 Val407 Arg414

Mutant models of the GCGR were made using Modeller and the resulting PDB structures compared with WT in PyMOL for any loss/gain of polar interactions. Alanine mutants were modeled for NNC0640 bound full length GCGR solved to a resolution of 3 Å (PDB ID: 5XEZ) (Zhang *et al.*, 2017), NNC0640 bound GCGR solved to a resolution of 3.4 Å (PDB ID: 4I6R) (Siu *et al.*, 2013) and MK-0893 bound GCGR solved to a resolution of 2.5 Å. A residue with more than one polar interaction with another residue is indicated by (xn), where n gives the number of interactions.

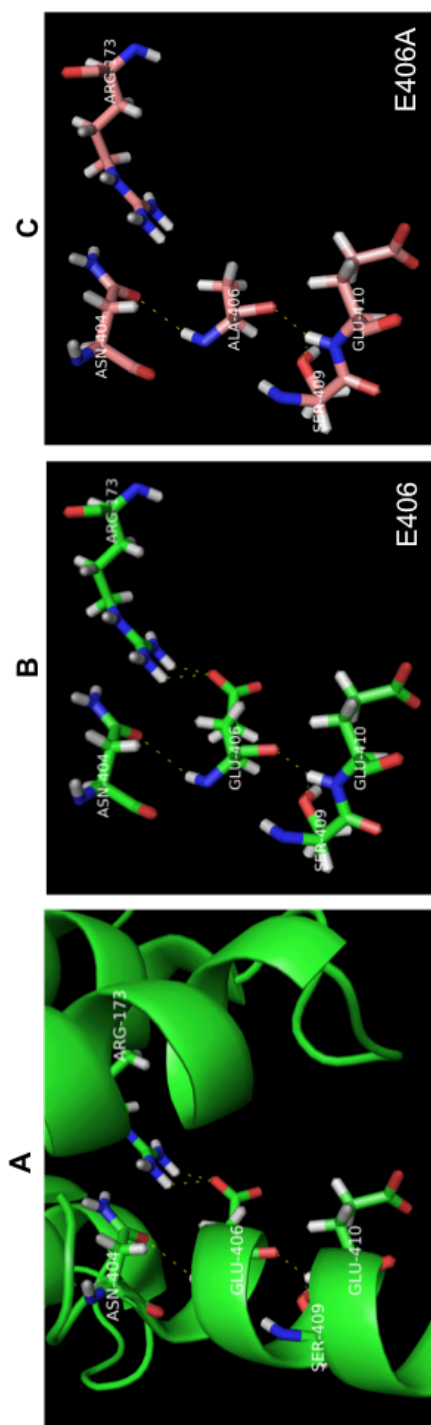


Figure 5.26. Comparison of polar contacts at position 406 within WT and modeled E406A mutant full-length crystal structure. Full-length GCGR (Zhang *et al.*, 2017, PDB ID: 5XEZ) was imaged in PyMOL. **A)** WT GCGR with overlaying cartoon representation indicating the helix 8 residue E406 or E410 and its polar interactions. **B)** Polar interactions for E406 or E410 within WT GCGR without cartoon overlay for clarity **C)** Polar interactions for E406A or E410A without cartoon overlay for clarity. Residues are labeled using the three-letter amino acid code (Table 5.1). The atom type within each residue is coloured red for oxygen, blue for nitrogen and white for hydrogen. A yellow dashed line indicates polar interactions.

5.4.3.4. Summary

Molecular modelling of the GLP-1R revealed an extensive hydrogen bond network in the ground state that is disrupted in the active state involving R176^{2.46}, R348^{6.37} and helix 8 N406^{8.47} and E408^{8.49} (TM2-6-7-helix 8 network) (Wootten *et al.*, 2016), which was also evident in the GCGR structure (Siu *et al.*, 2013). More recently, the solved peptide-activated rabbit GLP-1R in complex with heterotrimeric G_s (Zhang *et al.*, 2017) revealed receptor activation and outward movement of TM6 breaks these polar interactions within the TM2-6-7-helix 8 network and the HETX motif resulting in loss of the inactive state (Zhang *et al.*, 2017).

Mutation of R176^{2.46} and E408^{8.49} within GLP-1R were shown to reduce cell-surface expression to a similar extent (57-66% WT) and was suggested to support the role of these residues in a combined network (Wootten *et al.*, 2016). The results from analysis of GCGR cell-surface expression reported here are distinct from this finding and showed a significantly reduced expression for E406A^{8.49} but not R173A^{2.46} GCGR. The cell-surface expression of the double helix 8 mutant (E406A, E410A) was reduced to levels below that of the single helix 8 mutant (E406A), possibly as a result of significant conformational change and premature degradation.

In addition to reducing cell-surface expression of GLP-1R, mutation of E408^{8.49} within GLP-1R was shown to reduce cAMP signalling for a number of peptides including GLP-1(7-36)amide suggesting the residue selectively couples the GLP-1R to cAMP signalling (Wootten *et al.*, 2016). Here, despite the reduced cell-surface expression of E406A GCGR, there was a significantly elevated basal, indicating constitutive activity in E406A which was enhanced further by the additional substitution of E410 to alanine. This is consistent with previous reports in rat GCGR reporting E406A as having enhanced constitutive activity (Strudwick *et al.*, 2004). These data suggest that E406, may be involved in maintaining the receptor in an inactive conformation. There was shown to be a lost interacting between E406A and

R173 within the modelled E406A GCGR structures (Table 5.13) and may result in a lost inactive state or the ability of R173 to interact with the G protein more freely in the absence of ligand, thereby providing an explanation for elevated basal cAMP level.

Similarly, within the modelled R173A, the interaction with E406 was lost (Table 5.11). The finding of an attenuated cAMP response in R173A may suggest that the interaction with E406 is critical for GCGR ligand stimulated cAMP response. However, given that the E406A mutant showed little difference in cAMP response when compared to that of the WT, apart from an elevated basal cAMP level, it is more likely a reduced coupling to the G protein is a more plausible explanation for the attenuated cAMP response in R173A. Interestingly, within the solved peptide-activated rabbit GLP-1R in complex with heterotrimeric G_s, it was suggested that the lost interactions for R176^{2.46} in TM2, N406^{8.47} and E408^{8.39} in helix 8 caused by the outwards movement of TM6 on activation may be stabilised through hydrogen bonds or electrostatic interactions with residues of the G_s α5-helix (Zhang *et al.*, 2017). Indeed, visualisation of the activated rabbit GLP-1R reveals helix 8 residue E408^{8.49} to interact with Q390 of Gα_s α5-helix and two residues with the GLP-1R itself (N406^{8.47} and E412^{8.53}) with no apparent interaction with R176^{2.46} (Zhang *et al.*, 2017b). Interestingly, modelling of E408A^{8.49} within the GLP-1R structure reveals a lost interaction with Q390 of Gα_s α5-helix and N406^{8.47} whilst the interaction with E412^{8.53} was maintaining.

The findings presented here for GCGR and those previously reported for GLP-1R (Wootten *et al.*, 2016) suggest that E^{8.39} within helix 8 may play distinctly different roles between receptors within the class B GPCRs either through inactive state stabilisation (as seen for GCGR) or selectively coupling to cAMP signalling (as reported for GLP-1R (Wootten *et al.*, 2016)). Nevertheless, this residue may play a similar role in both receptors but the mechanism is more complex than can be dissected here.

5.5. Investigating pharmacological role of GCGR TM4

5.5.1. Cell-surface expression of GCGR TM4 mutants

Harikumar *et al.*, 2012 demonstrated that mutations of the hydrophobic face of TM4 (L256A^{4.55}, V259A^{4.58} or G252A^{4.49}, L256A^{4.55}, V259A^{4.58}) had selective effect on GLP-1R signalling, suggested to be as a result of the disturbed homodimerisation interface. In this work, using secondary messenger signalling assays, we investigated similar mutants in GCGR (L277A^{4.55}, V280A^{4.58} or G271A^{4.49}, L277A^{4.55}, V280A^{4.58}) (Figure 5.27).

We first sought to investigate the cell-surface expression of the L277A, V280A (double) and G271A, L277A, V280A (triple) GCGR mutant. Here, HEK 293T cells were transiently transfected with pmCherry-N1 expressing WT or mutant GCGR and cell-surface expression determined using FACS analysis. Confocal fluorescence microscopy images of HEK 293T cells expressing the mCherry-tagged WT GCGR showed localisation on the membrane surface (Figure 5.28 A). The localisation of mCherry-tagged double and triple mutant on the cell-surface appeared to be reduced in comparison to WT. This finding was confirmed by FACS analysis where the cell-surface expression of the double and triple mutant was significantly reduced (27.5 ± 6.5 and 6.1 ± 6.3 percentage WT cell-surface expressing, respectively) (Figure 5.27 B).

A

TM4

GHRHR	A	G	W	G	L	P	V	L	F	T	G	T	W
GIPR	L	G	W	G	A	P	A	L	F	V	I	P	W
GLP-1R	I	G	W	G	V	P	L	L	F	V	V	P	W
GLP-2R	L	G	W	A	F	P	V	L	F	V	V	P	W
GCGR	I	G	W	G	A	P	M	L	F	V	V	P	W
Secretin R	F	G	W	G	S	P	A	I	F	V	A	L	W
Consensus	+	G	W	G	A	P	+	L	F	V	V	P	W

B

TM4

Amino acid	I	G	W	G	A	P	M	L	F	V	V	P	W
Absolute position	270	271	272	273	274	275	276	277	278	279	280	281	282
Class B number	4.48	4.49	4.50	4.51	4.52	4.53	4.54	4.55	4.56	4.57	4.58	4.59	4.60

Figure 5.27. GCGR family structure-based alignment of TM4 region. A) GPCRdb.org structure-based alignment of TM4 within the GCGR family receptors; GHRH receptor, GIPR, GLP-1R, GLP-2R, GCGR and the secretin receptor. **B)** The residue position within TM4 of GCGR are given in both absolute and Class B (Wootten *et al.*, 2013) numbers. . Here, only the specific targeted region for alanine substitution mutation within the TM4 of GCGR are shown. Amino acid residues are given as the single amino acid code and colours illustrate residue physico-chemical properties (Table 5.1).

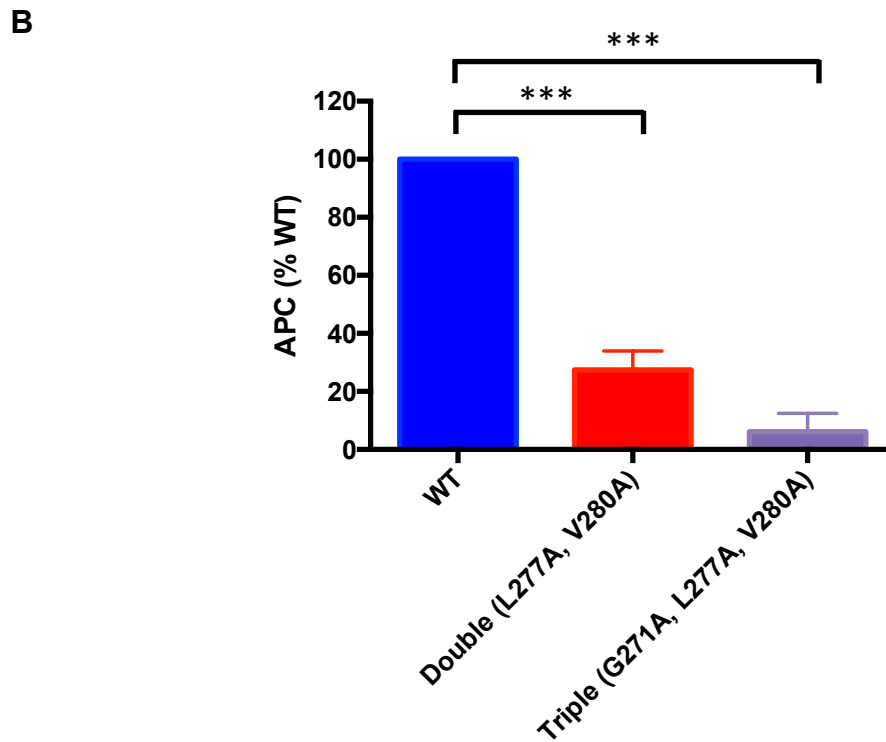
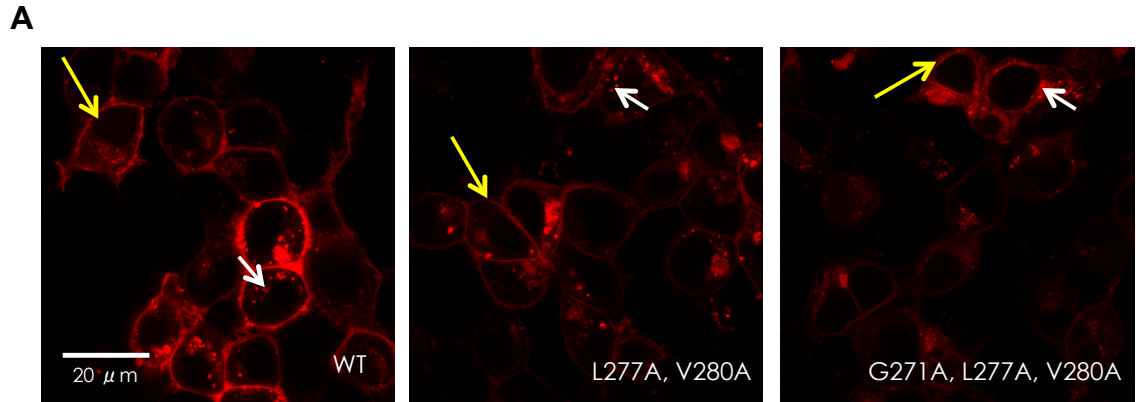


Figure 5.28. Cell-surface expression of WT and GCGR TM4 mutants. HEK 293 cells were transfected with WT or mutant GCGR containing pmCherry-N1 and cell surface expression determined by **A**) confocal fluorescence microscope (24 hours post transfection) and **B**) FACS analysis (48 hours post transfection); Anti-GCGR primary antibody at a 1:50 dilution, APC-conjugated IgG secondary antibody at a 1:150 dilution. Normalised to vector transfected (0%) and WT GCGR (100%), $n = 3$ independent experimental repeats. Yellow arrow indicates cell-surface localised receptor whereas white arrow indicate possible vesicles containing the receptor.

5.5.2. cAMP response in GCGR TM4 mutants transfected HEK 293T cells

Having shown reduced cell-surface expression of the L277A, V280A (double) and G271A, L277A, V280A (triple) GCGR mutants, we next sought to investigate the pharmacological consequence of these mutations on the cAMP response. Here, HEK 293T cells transiently transfected with pmCherry-N1 expressing WT or the mutant GCGR were stimulated with GCG or oxyntomodulin and the cAMP accumulation detected.

The potency and affinity of GCG was significantly reduced in HEK 293T cells transfected with pmCherry-N1 expressing the TM4 triple mutant (pEC_{50} 8.2 ± 0.1 and pK_A 7.58 ± 0.1) but not the double mutant (pEC_{50} 8.8 ± 0.1 and pK_A 8.26 ± 0.1) when compared to WT GCGR (pEC_{50} 8.7 ± 0.1 and pK_A 8.29 ± 0.1) (Figure 5.29 and Table 5.14). Similarly, the potency and affinity of oxyntomodulin was significantly reduced for the triple mutant (pEC_{50} 6.54 ± 0.1 and pK_A 5.74 ± 0.3) but not the double mutant (pEC_{50} 6.99 ± 0.1 and pK_A 6.09 ± 0.2) when compared to WT (pEC_{50} 6.97 ± 0.1 and pK_A 6.48 ± 0.1). These findings are in line with those previously reported for the similar TM4 GLP-1R mutants demonstrating attenuation (<10-fold) in potency for cAMP accumulation (Harikumar *et al.*, 2012). Given the only difference between the double and triple mutant is the G271A mutation, these data suggest that mutation of G271 is responsible for the reduced potency and affinity to both GCG and oxyntomodulin stimulation.

The maximal response to GCG and oxyntomodulin for both mutants was increase when compared to WT. This finding is unexpected given the significantly reduced cell-surface expression of the mutants and suggests that the cAMP accumulation assay is able to detect similar maximal levels following GCGR stimulation despite reduced receptor cell-surface expression, presumably because at this level there is more receptor than effectors in the system.

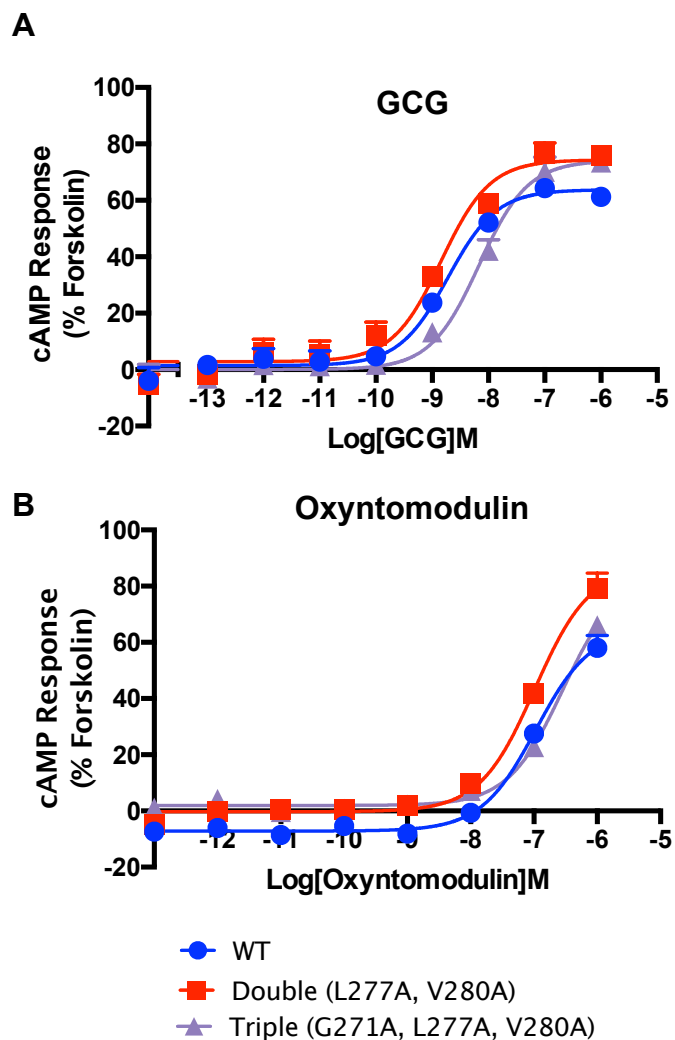


Figure 5.29. Effect of TM4 mutations on the GCGR stimulated cAMP response in HEK 293T cells. HEK 293T cells (1,000 cells/well) transiently expressing pmCherry-N1 vector containing WT or alanine containing GCGR TM4 mutants (24 hours post transfection) were exposed to **A)** GCG or **B)** oxyntomodulin for 8 minutes and cAMP accumulation detected. All values are mean \pm SEM expressed as percentage forskolin response (mock transfected with vector only) where $n \geq 5$ independent experimental repeats, conducted in duplicate.

Table 5.14. Effect of TM4 mutations on the GCGR stimulated cAMP response in HEK 293T cells. Potency (pEC_{50}), maximal response (E_{max}), basal, affinity (pK_A) and coupling efficacy ($\log \tau$) values for cAMP response to GCG/oxyntomodulin stimulation in WT/mutant GCGR transfected HEK 293T cells

HEK 293T						
GCG						
Construct	pEC_{50} ^a	E_{max} ^b	Basal ^c	Span ^d	pK_A ^e	$\log \tau$ ^f
WT	8.7 ± 0.1	63.8 ± 2.6	1.4 ± 1.4	62.3 ± 2.9	8.29 ± 0.1	0.24 ± 0.05
L277A, V280A	8.8 ± 0.1	74.4 ± 3.1*	2.8 ± 1.8	71.5 ± 3.5	8.26 ± 0.1	0.25 ± 0.07
G271A, L277A, V280A	8.2 ± 0.1**	74.1 ± 3.6*	0.1 ± 1.6	74.0 ± 3.8*	7.58 ± 0.1*	0.46 ± 0.08
Oxyntomodulin						
Construct	pEC_{50} ^a	E_{max} ^b	Basal ^c	Span ^d	pK_A ^e	$\log \tau$ ^f
WT	6.97 ± 0.1	65.0 ± 3.7	7.1 ± 1.1	72.1 ± 3.7	6.48 ± 0.1	0.31 ± 0.07
L277A, V280A	6.99 ± 0.1	87.0 ± 4.4*	-0.3 ± 1.3	87.3 ± 4.5	6.09 ± 0.2	0.83 ± 0.17*
G271A, L277A, V280A	6.54 ± 0.1*	84.4 ± 5.8*	2.0 ± 1.0	82.4 ± 5.7	5.74 ± 0.3*	0.72 ± 0.19

WT or mutant GCGR were transiently expressed in HEK 293T cells and stimulated with GCG or oxyntomodulin prior to measurement of cAMP accumulation to generate concentration response curves for each construct. To calculate pEC_{50} , E_{max} , Basal and Span values, data were analysed using a three-parameter logistic equation. Data was also analysed by an operational model of agonism (Black and Leff, 1983) to determine affinity (pK_A) and coupling efficacy ($\log \tau$).

^a Negative logarithm of GCG concentration required to produce a half-maximal response

^b Maximal response to GCG as percentage forskolin response (Mock transfected with vector)

^c The low plateau of the fitted sigmoidal dose-response curve

^d The difference between E_{max} and basal signalling

^e The negative logarithm of functional affinities that describes the affinity of the receptor when coupled to a given signalling pathway generated through use of the operational model for partial agonism

^f τ is the coupling efficiency parameter generated through use of the operational model for partial agonism

All values are mean ± SEM expressed as percentage forskolin response (Mock transfected with vector) where $n \geq 5$ independent experimental repeats, conducted in duplicate.

Statistical significance (*, $p < 0.05$; **, $p < 0.01$; ***, $p < 0.001$) compared to WT GCGR was determined by one-way ANOVA with Dunnett's post test

5.5.3. cAMP response in GCGR TM4 mutants transfected HEK 293 cells

For the purpose of experimental replication and to assess reproducibility of the results presented earlier (Section 5.5.2) in an alternative cell line, these experiments investigating the ligand stimulated cAMP accumulation for TM4 GCGR mutant were also performed in HEK 293 cell. Similarly to what was previously demonstrated in HEK 293T cells, HEK 293 cells transiently transfected with pmCherry-N1 expressing WT or the mutant GCGR were stimulated with GCG or oxyntomodulin and the cAMP accumulation detected.

Again, the potency of GCG was significantly reduced in the triple mutant when compared to WT (pEC_{50} 8.05 ± 0.1 and 9.09 ± 0.1), but there was also a significantly reduced potency for the double mutant (pEC_{50} 8.67 ± 0.1) (Figure 5.30 1A and Table 5.15). This was also found to be the case for oxyntomodulin where the potency was significantly reduced for the triple mutant when compared to WT (pEC_{50} 6.63 ± 0.1 and 7.27 ± 0.1) but the weaker potency in the double mutant (pEC_{50} 7.04 ± 0.1) was not significant (Figure 5.30 1B and Table 5.15). This reduction in potency, although greater, is in line with those previously reported for the similar TM4 GLP-1R mutants demonstrating attenuation (<10-fold) in potency for cAMP accumulation (Harikumar *et al.*, 2012).

The similar potency measured between the WT and double mutant for both GCG and oxyntomodulin responses in transfected HEK 293T (Table 5.14) suggested that G271 was the amino acid responsible for the reduced potency in the triple mutant. However, the data acquired in HEK 293 cells suggests L277 or V280 may also be important in the GCGR mediated cAMP response. In order to confirm which amino acid is responsible for the reduced potency in the double mutant, the single V280A mutant was made and the cAMP response detected following GCG or oxyntomodulin stimulation (Figure 5.30 2A/2B and Table 5.15). The potency of both GCG and oxyntomodulin was not significantly different to WT indicating that this mutation alone cannot account for the reduced potency measured in HEK 293 cells. Of course,

without making single mutants for all the amino acids within the triple mutant, we cannot exclude the possibility that it is the combination of mutations rather than one single amino acid causing the reduction in potency.

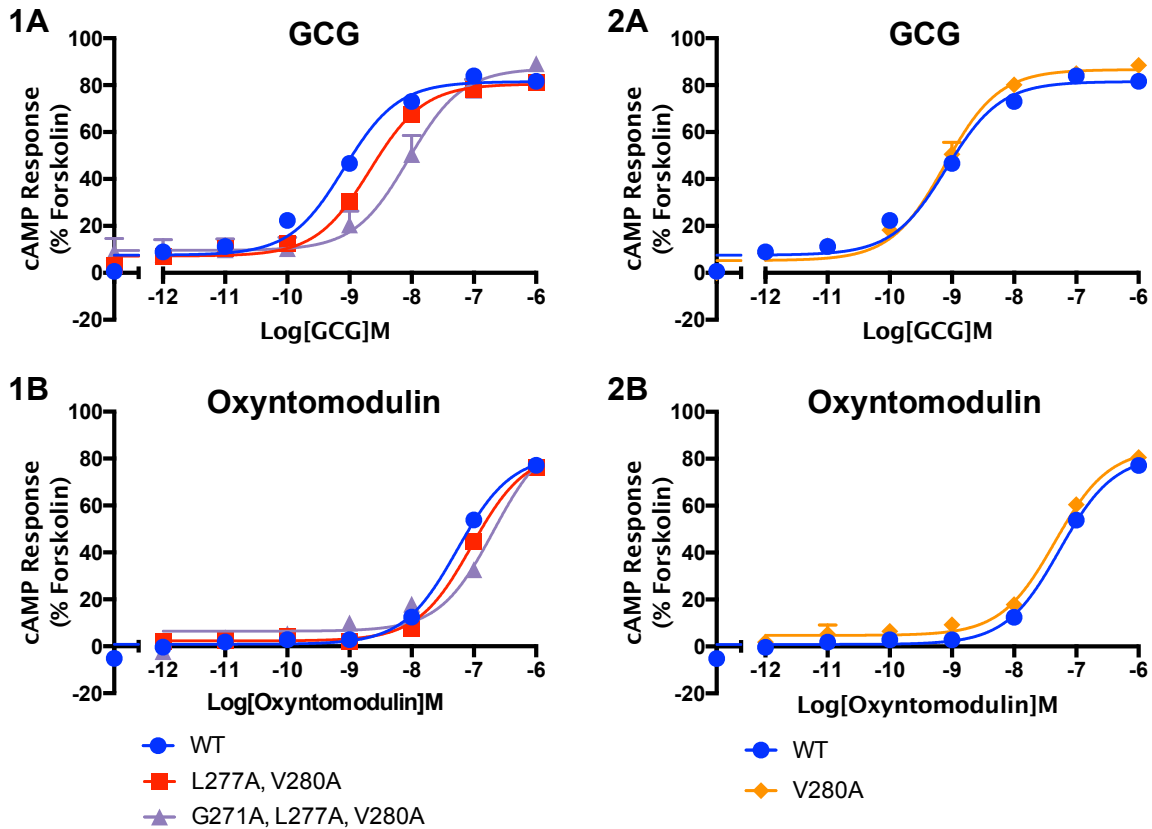


Figure 5.30. Effect of TM4 mutations on the GCGR stimulated cAMP response is reproducible the in HEK 293 cells. HEK 293 cells (1000 cells/well) transiently expressing pmCherry-N1 vector containing WT or alanine containing GCGR TM4 mutants (24 hours post transfection) were exposed to **A**) GCG or **B**) oxyntomodulin for 8 min and cAMP accumulation detected. All values are mean \pm SEM expressed as percentage forskolin response (100 μ M) (mock transfected with vector only) where $n \geq 5$ independent experimental repeats, conducted in duplicate.

Table 5.15. Effect of TM4 mutations on the GCGR stimulated cAMP response is reproducible in HEK 293 cells. Potency (pEC₅₀), maximal response (E_{max}), basal, span, affinity (pK_A) and coupling efficacy (log τ) values for cAMP response to GCG/oxyntomodulin stimulation in WT/mutant GCGR transfected HEK 293 cells

HEK 293						
GCGR						
Construct	pEC ₅₀ ^a	E _{max} ^b	Basal ^c	Span ^d	pK _A ^e	log τ ^f
WT	9.09 ±0.1	81.5 ±1.5	7.6 ±1.1	74.0 ±1.8	8.38 ±0.1	0.60 ±0.04
V280A	9.11 ±0.1	86.6 ±1.8	5.2 ±2.0	81.4 ±2.6	8.26 ±0.1	0.78 ±0.06
L277A, V280A	8.67 ±0.1*	80.5 ±1.9	7.2 ±1.3	73.3 ±2.1	7.99 ±0.1*	0.58 ±0.05
G271A, L277A, V280A	8.05 ±0.1***	87.2 ±4.2	9.6 ±2.5	77.6 ±4.7	7.20 ±0.2***	0.78 ±0.17

Oxyntomodulin

Construct	pEC ₅₀ ^a	E _{max} ^b	Basal ^c	Span ^d	pK _A ^e	log τ ^f
WT	7.27 ±0.1	81.5 ±2.2	0.9 ±1.0	80.7 ±2.3	6.54 ±0.1	0.64 ±0.06
V280A	7.34 ±0.1	84.4 ±2.1	4.7 ±2.1	72.9 ±2.5	6.56 ±0.1	0.70 ±0.07
L277A, V280A	7.04 ±0.1	83.1 ±2.3	2.3 ±2.3	80.8 ±2.5	6.28 ±0.1	0.68 ±0.07
G271A, L277A, V280A	6.45 ±0.1***	91.5 ±5.8	6.5 ±1.0	91.4 ±5.7	5.65 ±0.4*	1.00 ±0.32

WT or mutant GCGR were transiently expressed in HEK 293 cells and stimulated with GCG or oxyntomodulin prior to measurement of cAMP accumulation to generate concentration response curves for each construct. To calculate pEC₅₀, E_{max}, Basal and Span values, data were analysed using a three-parameter logistic equation. Data was also analysed by an operational model of agonism (Black and Leff, 1983) to determine affinity (pK_A) and coupling efficacy (log τ).

^a Negative logarithm of GCG concentration required to produce a half-maximal response

^b Maximal response to GCG as percentage forskolin response (Mock transfected with vector)

^c The low plateau of the fitted sigmoidal dose-response curve

^d The difference between E_{max} and basal signalling

^e The negative logarithm of functional affinities that describes the affinity of the receptor when coupled to a given signalling pathway generated through use of the operational model for partial agonism

^f τ is the coupling efficiency parameter generated through use of the operational model for partial agonism

All values are mean ± SEM expressed as percentage forskolin response (Mock transfected with vector) where $n \geq 5$ independent experimental repeats, conducted in duplicate.

Statistical significance (*, $p < 0.05$, **, $p < 0.01$, ***, $p < 0.001$) compared to WT GCGR was determined by one-way ANOVA with Dunnett's post test

5.5.4. pERK1/2 response in GCGR TM4 mutants transfected HEK 293T cells

Having shown a 10-fold reduced potency in the GCG and oxyntomodulin stimulated cAMP response for the triple (G271A, L277A, V280A) GCGR mutant in HEK 293T cells, we next looked to investigate the effect of both the double (L277A, V280A) and triple mutants on the pERK1/2 response. Here, HEK 293 cells transiently transfected with pmCherry-N1 expressing WT or mutant GCGR were stimulated with GCG or oxyntomodulin and the pERK1/2 response determined.

There was found to be negligible differences in the GCG or oxyntomodulin stimulated pERK1/2 response between HEK 293T cells transfected with WT or mutant GCGR for most of the measured parameters (Figure 5.31 and Table 5.16). There was however a reduced maximum response to GCG for both TM4 mutants which only reached significance for the double mutant when compared to WT GCGR (E_{max} 14.2 \pm 2.6 and 30.3 \pm 2.8, respectively). This was associated with a reduced coupling efficacy, which was only significant for the double mutant when compared to WT GCGR (log τ -0.72 \pm 0.08 and -0.35 \pm 0.05, respectively). Interestingly, the maximum pERK1/2 responses following oxyntomodulin stimulation of HEK 293T cells transfected with either TM4 mutant appeared identical to WT GCGR. This finding could suggest that TM4 mutants have a reduced ability to transduce the GCG signal to pERK1/2 when compared to oxyntomodulin.

It should be noted that the measured pERK1/2 responses showed variability between repeats and resulted in large error for the measured parameters. In addition, when comparing these responses to those also measured in HEK 293T cells (which used a higher cell count) (Section 4.4.2.1) there was a reduced potency and maximum response, suggesting some variability across experiments. In addition, we may be experiencing some experimental limitation where we are at the lower end of the assays dynamic range. Nevertheless, these data suggest that these TM4 amino

acids, within this experimental set up, appear not to play a significant role in the GCGR mediated pERK1/2 response.

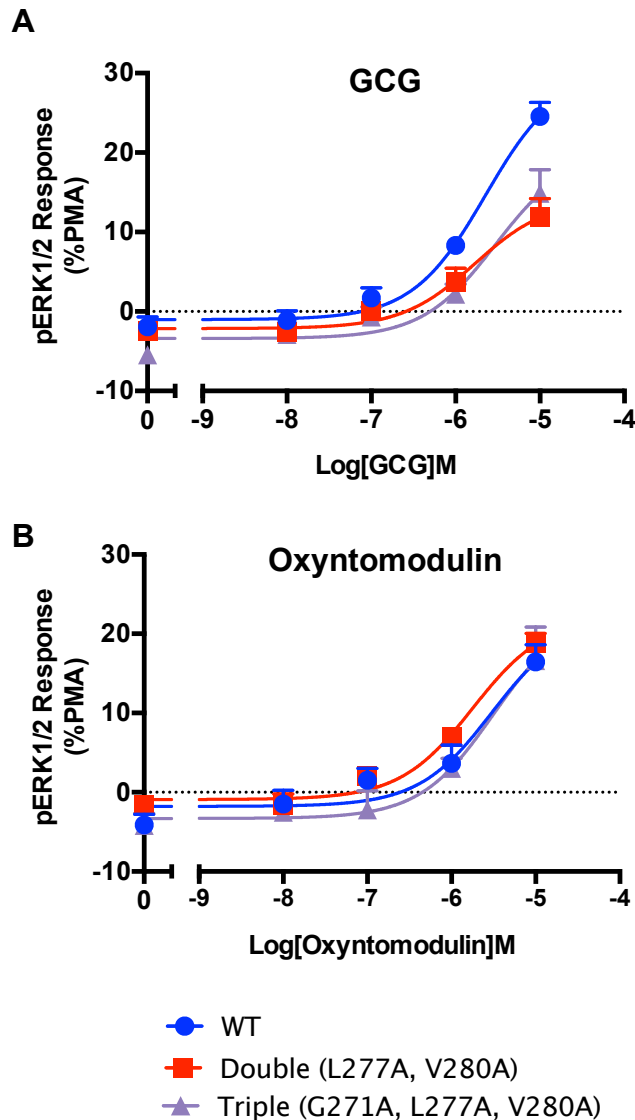


Figure 5.31. Effect of GCGR TM4 mutants on pERK1/2 response. HEK 293T cells (20,000 cells/well) transiently expressing pmCherry-N1 vector containing WT or alanine containing GCGR TM4 mutants (48 hours post transfection) were exposed to GCG or oxyntomodulin for 5 min and pERK1/2 detected. All values are mean \pm SEM expressed as percentage PMA response (1 μ M) where $n \geq 5$ independent experimental repeats, conducted in duplicate.

Table 5.16. Effect of GCGR TM4 mutants on pERK1/2 response. Potency (pEC_{50}), maximal response (E_{max}), basal, span, affinity (pK_A) and coupling efficacy ($\log \tau$) values for pERK1/2 response to GCG/oxyntomodulin stimulation in WT/mutant GCGR transfected HEK 293T cells

pERK1/2						
GCG						
Construct	pEC_{50} ^a	E_{max} ^b	Basal ^c	Span ^d	pK_A ^e	$\log \tau$ ^f
WT	5.65 ± 0.1	30.3 ± 2.8	-1.0 ± 0.8	31.3 ± 2.7	5.49 ± 0.2	-0.35 ± 0.05
L277A, V280A	5.77 ± 0.3	14.2 ± 2.6*	-2.1 ± 0.9	16.3 ± 2.6*	5.70 ± 0.3	-0.72 ± 0.08*
G271A, L277A, V280A	5.53 ± 0.3	20.3 ± 4.3	-3.4 ± 1.0	23.7 ± 4.1	5.41 ± 0.3	-0.53 ± 0.10
Oxyntomodulin						
Construct	pEC_{50} ^a	E_{max} ^b	Basal ^c	Span ^d	pK_A ^e	$\log \tau$ ^f
WT	5.52 ± 0.3	21.9 ± 5.2	-1.8 ± 1.2	23.7 ± 5.0	5.41 ± 0.3	-0.52 ± 0.12
L277A, V280A	5.75 ± 0.1	22.1 ± 2.5	-0.9 ± 1.0	23.1 ± 2.5	5.63 ± 0.2	-0.53 ± 0.06
G271A, L277A, V280A	5.51 ± 0.3	22.8 ± 6.1	-3.3 ± 1.4	26.1 ± 5.8	5.38 ± 0.4	-0.47 ± 0.13

WT or mutant GCGR were transiently expressed in HEK 293T cells and stimulated with GCG or oxyntomodulin prior to measurement of pERK1/2 to generate concentration response curves for each construct. To calculate pEC_{50} , E_{max} , Basal and Span values, data were analysed using a three-parameter logistic equation. Data was also analysed by an operational model of agonism (Black and Leff, 1983) to determine affinity (pK_A) and coupling efficacy ($\log \tau$).

^a Negative logarithm of GCG/oxyntomodulin concentration required to produce a half-maximal response

^b Maximal response to GCG/oxyntomodulin as percentage PMA response (1 μ M)

^c The low plateau of the fitted sigmoidal dose-response curve

^d The difference between E_{max} and basal signalling

^e The negative logarithm of functional affinities that describes the affinity of the receptor when coupled to a given signalling pathway generated through use of the operational model for partial agonism

^f τ is the coupling efficiency parameter generated through use of the operational model for partial agonism
Statistical significance (*, $p < 0.05$; **, $p < 0.01$; ***, $p < 0.001$) compared to WT was determined by one-way ANOVA with Dunnett's post test

5.5.5. Intracellular Ca²⁺ response in GCGR TM4 mutants transfected HEK 293T cells

Previous work demonstrated that mutations of the hydrophobic face of TM4 GLP-1R resulted in complete abrogation of the Ca²⁺_i mobilisation response to GLP-1(7-36)amide (Harikumar *et al.*, 2012). Here, we investigate the effect of similar mutants within GCGR on the Ca²⁺_i response.

HEK 293 cells (transfected with mCherry-tagged WT or mutant GCGR post plating) were loaded with Fluo-8, AM dye, stimulated with increasing concentrations of GCG or oxyntomodulin and the Ca²⁺_i measured using a FlexStation® Multi-Mode Microplate Reader. There was no significant difference in the potency of GCG stimulated Ca²⁺_i response in HEK 293 cells transfected with WT GCGR or double mutant (pEC₅₀ 5.92 ±0.2 and 5.96 ±0.3) whereas there was a significantly reduced maximum response (E_{max} 112.5 ±12.2 and 66.3 ±11.4 percentage WT response) (Figure 5.32 A and Table 5.17). Notably, there was a complete abolition of the measured Ca²⁺_i in the triple mutant. A Ca²⁺_i response to oxyntomodulin was only measured at the highest concentration (10 µM) in HEK 293T cells transfected with WT or double mutant and a full dose-response curve could not be fitted due to insufficient data points (Figure 5.32 B and Table 5.17). Nevertheless, this response was absent in the triple mutant.

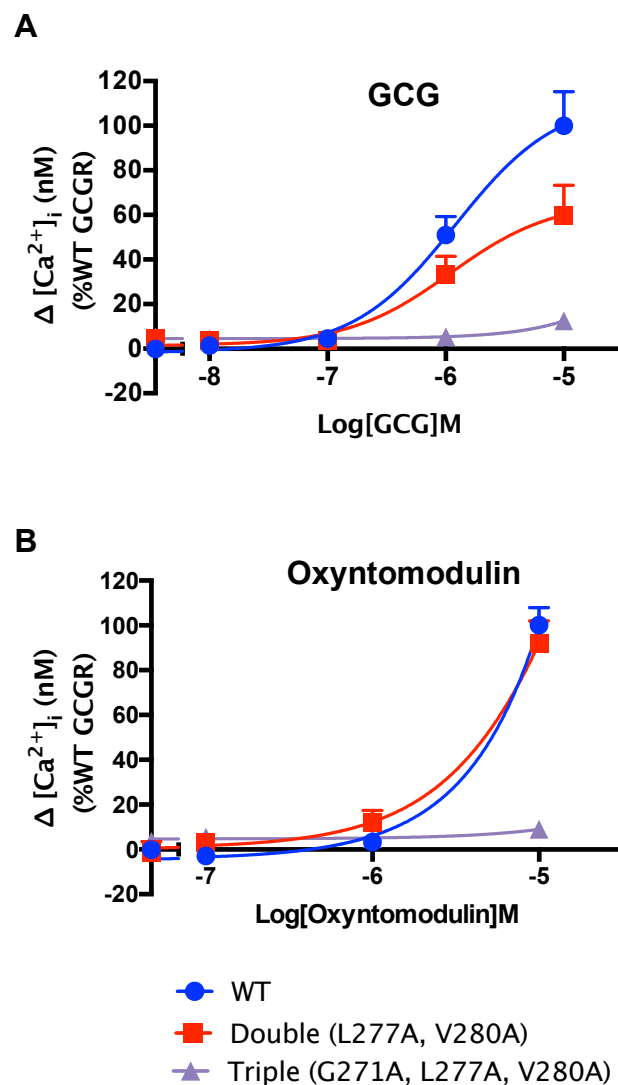


Figure 5.32. Effect of GCGR TM4 mutants on Ca^{2+}_i mobilisation in transfected HEK 293T cells. HEK 293T cells transiently expressing pmCherry-N1 vector containing WT GCGR or alanine containing mutants (48 hours post transfection) were exposed to GCG or oxyntomodulin and Ca^{2+}_i mobilisation detected. All values are mean \pm SEM expressed as change in Ca^{2+}_i (% WT GCGR response) $n \geq 5$ independent experimental repeats, conducted in duplicate.

Table 5.17. Effect of GCGR TM4 mutants on Ca²⁺i mobilization in transfected HEK 293T cells. Potency (pEC₅₀), maximal response (E_{max}), basal, span, affinity (pK_A) and coupling efficacy (log τ) values for Ca²⁺i response to GCG/oxyntomodulin stimulation in WT/mutant GCGR transfected HEK 293T cells

Ca ²⁺ i						
GCG						
Construct	pEC ₅₀ ^a	E _{max} ^b	Basal ^c	Span ^d	pK _A ^e	log τ ^f
WT	5.92 ±0.2	112.5 ±12.2	-1.5 ±6.2	114.0 ±12.7	4.71 ±0.8	1.18 ±0.75
L277A, V280A	5.96 ±0.3	66.3 ±11.4*	1.5 ±6.5	64.9 ±12.0*	5.61 ±0.4	0.08 ±0.17
G271A, L277A, V280A		N.R	3.2 ±4.1			N.R
Oxyntomodulin						
Construct	pEC ₅₀ ^a	E _{max} ^b	Basal ^c	Span ^d	pK _A ^e	log τ ^f
WT		N.D#	-1.2 ±2.1			N.D#
L277A, V280A		N.D#	-2.4 ±1.6			N.D#
G271A, L277A, V280A		N.R	-3.9 ±1.2			N.R

WT or mutant GCGR were transiently expressed in HEK 293T cells and stimulated with GCG or oxyntomodulin prior to measurement of Ca²⁺i to generate concentration response curves for each construct. To calculate pEC₅₀, E_{max}, Basal and Span values, data were analysed using a three-parameter logistic equation. Data was also analysed by an operational model of agonism (Black and Leff, 1983) to determine affinity (pK_A) and coupling efficacy (log τ).

^a Negative logarithm of GCG/Oxyntomodulin concentration required to produce a half-maximal response

^b Maximal response to GCG/Oxyntomodulin as percentage WT response

^c The low plateau of the fitted sigmoidal dose-response curve

^d The difference between E_{max} and basal signalling

^e The negative logarithm of functional affinities that describes the affinity of the receptor when coupled to a given signalling pathway generated through use of the operational model for partial agonism

^f τ is the coupling efficiency parameter generated through use of the operational model for partial agonism
Statistical significance (*, $p < 0.1$; **, $p < 0.01$; ***, $p < 0.001$) compared to WT was determined by unpaired Student's t-test (two-tailed)

N.R denotes no response. N.D# denotes not determined due to insufficient data points

5.5.6. Molecular modelling of TM4 mutants in three GCGR structures

Modeller (version 9.18) was used to model the TM4 mutants within the three available protein structures of inactive GCGR for which PDB files exist; 5XEZ (Zhang *et al.*, 2017), 4L6R (Siu *et al.*, 2013) and 5EE7 (Jazayeri *et al.*, 2016). The resulting PDB files were viewed in MacPyMol (version 1.7.4.5) and the WT and mutated receptor compared visually to assess any predicted changes in amino acid interactions and structure (Table 5.18).

The triple mutant (G271A, L277A, V280A) and WT structures completely overlaid indicating the overall structure is unaltered by these GCGR mutations. There were found to be some variations in interactions between the TM4 residues within the three structures. Interestingly, the modelled mutant receptors largely showed similar interactions when compared to WT structure with only small changes noted (Table 5.18). With this in mind; images of the models are not shown, as they would not be an informative visual aid.

Within the full length GCGR (5XEZ), G271A showed a lost interaction with L268 and V280A showed a gained interaction with A283. Within the NNC0640 bound GCGR structure (4L6R), with the exception of G271A, which again showed a lost interaction with L268, there was found to be no lost or gained interactions for any of the other residues. Finally, MK-0893 bound GCGR showed no interaction changes within the modelled mutants when compared to the WT structure. The lost interaction between G271A and L268 may provide an explanation for the reduced potency of the cAMP response and the abolished Ca^{2+}_i response in the triple GCGR mutant. However, given that there was shown to be small changes in the interactions within the modelled mutants for all three GCGR structures, it may be speculated that the triple mutant has altered interactions outside of the receptor itself, such as a reduced ability to form a dimeric interface with another GCGR.

Table 5.18. Comparison of GCGR residue polar contacts within WT and modeled TM4 mutant structures

NNC0640 bound full length GCGR 3 A (5XEZ)		
G271	Tyr267 Leu268	G271A Tyr267
L277	Gly273	L277A Gly273
V280	Met276 Val284	V280A Met276 Ala283 Val284
L277 in L277 V280	Gly273	L277A in L277A V280A Gly273
V280 in L277 V280	Met276 Val284	V280A in L277A V280A Met276 Ala283 Val284
G271 in G271 L277	Tyr267 Leu268	G271A in G271A Tyr267
V280		L277A V280A
L277 in G271 L277	Gly273	L277A in G271A Gly273
V280		L277A V280A
V280 in G271 L277	Met276 Val284	V280A in G271A Met276 Ala283 Val284
V280		L277A V280A
NNC0640 bound GCGR 3.4 A (4L6R)		
G271	Tyr267 Leu268 Ala274	G271A Leu268 Ala274
L277	Gly273	L277A Gly273
V280	Met276 Ala283 Val284	V280A Met276 Ala283 Val284
L277 in L277 V280	Gly273	L277A in L277A V280A Gly273
V280 in L277 V280	Met276 Ala283 Val284	V280A in L277A V280A Met276 Ala283 Val284
G271 in G271 L277	Tyr267 Leu268 Ala274	G271A in G271A Leu268 Ala274
V280		L277A V280A
L277 in G271 L277	Gly273	L277A in G271A Gly273
V280		L277A V280A
V280 in G271 L277	Met276 Ala283 Val284	V280A in G271A Met276 Ala283 Val284
V280		L277A V280A

MK-0893 bound GCGR 2.5 Å (5EE7)			
G271	Tyr267	G271A	Tyr267
L277	Gly273 Ala274	L277A	Gly273 Ala274
V280	Ala276 Ala283 Val284	V280A	Ala276 Ala283 Val284
L277 in L277 V280	Gly273 Ala274	L277A in L277A V280A	Gly273 Ala274
V280 in L277 V280	Ala276 Ala283 Val284	V280A in L277A V280A	Ala276 Ala283 Val284
G271 in G271 L277	Tyr267	G271A in G271A	Tyr267
V280	Gly273 Ala274	L277A V280A	Gly273 Ala274
L277 in G271 L277		L277A in G271A	
V280	Ala276 Ala283 Val284	L277A V280A	Ala276 Ala283 Val284
V280 in G271 L277		V280A in G271A	
V280		L277A V280A	

Mutant models of the GCGR were made using Modeller and the resulting PDB structures compared with WT in PyMOL for any loss/gain of polar interactions. Alanine mutants were modeled for NNC0640 bound full length GCGR solved to a resolution of 3 Å (PDB ID: 5XEZ) (Zhang *et al.*, 2017), NNC0640 bound GCGR solved to a resolution of 3.4 Å (PDB ID: 4I6R) (Siu *et al.*, 2013) and MK-0893 bound GCGR solved to a resolution of 2.5 Å.

5.5.7. Summary

Harikumar *et al.*, 2012, demonstrated that mutations of the hydrophobic face of TM4 (L256A^{4.55}, V259A^{4.58} or G252A^{4.49}, L256A^{4.55}, V259A^{4.58}) within GLP-1R resulted in <10-fold decrease in potency in the cAMP and pERK1/2 response but a complete loss of Ca²⁺i response to GLP-1(7-36)amide stimulation. It was suggested that this TM4 region forms the primary dimerisation interface for GLP-1R, and mutation of these residues effectively disturbed the interface (Harikumar *et al.*, 2012). Here, we report findings that three similar substitutions (G271A^{4.49}, L277A^{4.55}, V280A^{4.58}) within the TM4 region of GCGR showed complete abolishment of the Ca²⁺i response whereas there was only a small effect on cAMP accumulation and no measurable effect on the pERK1/2 response.

The reduced potency of the cAMP response and the abolished Ca²⁺i response in the triple GCGR mutant could be explained by the reduced cell-surface expression. Achieving similar levels of cell-surface expression to WT GCGR could allow the investigation into how the mutation influences secondary messengers levels independent of surface expression. However, previously tests looking at bringing the level of WT GCGR expression down to similar levels of the mutant GCGR through reducing DNA concentration at transfection was unsuccessful (Section 3.10.2). Here, DNA concentration was shown not to be proportional to the cell-surface expression.

The findings presented here suggest that these TM4 amino acids, particularly G271, appear to be important for the Ca²⁺i response whereas they are less crucial for the cAMP and pERK1/2 response. However, it should be noted that these findings could reflect the sensitivity of the assays. For example, in the case of the cAMP response, we may have more receptor than effectors in the transfected HEK 293T system resulting in only a small reduction in potency and no effect on maximal response for the triple mutant when compared to WT GCGR. It could be speculated that, similar to what was reported for the GLP-1R, these amino acids within TM4 may be

important in forming a dimeric interface. However, in order to test this hypothesis further experiments investigating dimerisation between WT GCGR and the TM4 mutant GCGR would need to be conducted.

Interestingly, despite the complete abolishment of the GCG stimulated Ca^{2+} mobilisation in HEK 293T cells transfected with the triple mutant, there was a pERK1/2 response detected for this mutant (Figure 5.31). Through the used of a $G_{q/11}$ specific inhibition (YM-254890), it was previously shown that the GCG stimulated Ca^{2+} mobilisation was $G_{q/11}$ -mediated (Section 4.3) and $G_{q/11}$ plays a role in the GCG stimulated pERK1/2 response in CHO-K1 cells stably expressing GCGR (Section 4.4.5). In combination with experiments using knockout cell lines, it was concluded that the GCG stimulated pERK1/2 response is via a combination of $G_{q/11}$ and β -arrestin1/2 mediated pathways (Section 4.4.6). The findings presented here for the TM4 mutant may be in line with this conclusion where the pERK1/2 response determined for the TM4 triple mutant may be attributed to a β -arrestin1/2 mediated pathway. An interesting follow up experiment would be to investigate the pERK1/2 response in the $\Delta\beta$ -arrestin1/2 knockout cell transfected with the TM4 mutant.

Chapter 6. General Discussion and Further Work

6.1. General Discussion

The GCGR is abundantly expressed in the liver, the major site of GCG action (Taborsky, 2010), the kidneys and to a lesser extent in other organs such as the heart, endocrine pancreas (predominantly β -cells), spleen, gastrointestinal tract and brain (Habegger *et al.*, 2010). Given this wide tissue distribution, it is not surprising GCG has a number of physiological effects beyond that of glucose homeostasis. Interestingly, a far more complex picture of the role GCG plays has emerged with this pancreatic hormone shown to also regulate lipid metabolism, stimulate energy expenditure and induce satiety, to name a few (Jones *et al.*, 2012, Habegger *et al.*, 2010, Day *et al.*, 2012).

In the work presented here, we investigated GCGR signalling using multiple assays including those measuring cAMP accumulation, Ca^{2+} mobilisation and ERK1/2 activation. In addition, we identify several residues within various regions of GCGR required for signalling and receptor cell-surface expression. These included the GCGR ICL1 region (G165^{1.63}-T172^{2.45}), TM2 residue R173^{2.46}, helix 8 residues E406^{8.49} and E410^{8.53} and three TM4 residues (G271^{4.49}, L277^{4.55}, V280^{4.58}, previously suggested to form a homodimerisation interface in GLP-1R (Harikumar *et al.*, 2012)).

Consistent with previous reports (Weston *et al.*, 2015), GCGR activation by GCG and oxyntomodulin resulted in increased cAMP levels in a number of cell lines (HEK 293, HEK 293T, CHO-K1 and Hep 3B cells). Interestingly, the potency of the measured response was shown to vary and depended on both cell type and chosen expression vector. This finding confirms that the absolute potency of an agonist at GPCRs is not only dependent on the affinity and intrinsic efficacy operating at the level of that particular receptor, but also on the properties of the assay system (Kenakin *et al.*, 2012). With this in mind, variables including the chosen cell line, receptor

expression systems and assay sensitivity should be considered when interpreting such experimental data.

An investigation into two potential GCGR antagonists in transfected HEK 293T cells revealed des-His¹,[Glu⁹]-glucagon amide (des-His¹,[Glu⁹]-GCG), previously reported to act as an antagonist (Unson *et al.*, 1989) was a partial agonist at the GCGR. In contrast to previous findings (Cascieri *et al.*, 1999), L-168,049 was characterised as a potential competitive antagonist in transfected HEK 293T cells, although its yellow colour and possible autofluorescence may limit its use in assays such as those based on TR-FRET. The characterisation of these potential GCGR antagonists was different when utilising Hep 3B cells, a model hepatocyte cell line, where GCGR was endogenously expressed. Here, des-His¹,[Glu⁹]-GCG was characterised as a non-competitive antagonist and L-168,049 as a competitive antagonist. This discrepancy again highlights that conclusions are often dependent on the experimental system. In order to draw sound scientific conclusions, characterisation of novel ligands must be tested in multiple diverse systems.

TH-GCG; a partial agonist of the GCGR-mediated cAMP response.

Studies have highlighted the possibility that GCGR couples to alternative G proteins such as G_{q/11} (Xu and Xie, 2009 and Wakelam *et al.*, 1986). In line with these early reports, in addition to the classic G_s-coupled pathway, both GCG and oxyntomodulin were found to stimulate a G_{q/11}-mediated Ca²⁺ response at the GCGR. We also investigated the hypothesis that the GCG analogue TH-GCG, previously suggested to act at a receptor distinct from GCG and stimulating the production of inositol phosphates but not cAMP (Wakelam *et al.*, 1986), may act as a biased agonist at the GCGR through G_q-coupling. Contrary to previous findings (Wakelam *et al.*, 1986, Lenzen *et al.*, 1990), TH-GCG was found to act as a partial agonist inducing a robust cAMP response, which was reduced in potency and maximal response when compared to GCG, in both HEK 293T cells transfected with GCGR and in hepatocytes freshly extracted from C57BL/6 mice. The LANCE® *Ultra* cAMP detection kit used in this study was likely to have superior sensitivity when

compared to the methods used for cAMP measurement in these early studies, offering an explanation for this discrepancy. TH-GCG failed to induce a detectable Ca^{2+} or IP_1 response in GCGR expressing HEK 293T further contradicting the previous findings suggestion TH-GCG stimulation leads to inositol phospholipid breakdown (Wakelam *et al.*, 1986, Lenzen *et al.*, 1990). Assuming the correct synthesis of TH-GCG by Alta Biosciences, TH-GCG appears not to be a biased GCGR agonist and acts at the classical G_s -coupled pathway.

GCGR-mediated ERK1/2 activation. Although GCG is known to cause a rapid, concentration-dependent phosphorylation and activation of ERK1/2 (Jiang *et al.*, 2001), extensive detail into the signalling pathways leading to this activation is lacking. This study provides an in-depth analysis of GCGR stimulated pERK1/2 activation through G protein and β -arrestin1/2 mediated pathways (Figure 6.1). Contrary to previous findings suggesting a role for PKA in GCG induced ERK1/2 activation in β cells and HEK 293 cells (Dalle *et al.*, 2004 and Jiang *et al.*, 2001, respectively), treatment with the PKA specific inhibitor Rp-8-bromo-cAMP showed no effect on the measured pERK1/2 response to GCG or oxyntomodulin in GCGR stably expressing CHO-K1 cells. This finding suggested that the GCGR-mediated ERK1/2 activation is independent of G_s stimulated pathway. Using the $G_{q/11}$ inhibition YM-254890 (Takasaki *et al.*, 2004), the potency of the GCG stimulated pERK1/2 response was reduced and indicating a role for $G_{q/11}$ and thereby presumably Ca^{2+} , in the GCGR-mediated pERK1/2 response. Interestingly, the pERK1/2 response in GCGR transfected $G\alpha_q$ ($\Delta G\alpha_q$ and $\Delta G\alpha_{s/q/12}$) knockout HEK 293 cells showed a reduction in maximum response and further supports this conclusion. These findings are consistent with reports that chelation of Ca^{2+} was found to reduce GCG-mediated ERK1/2 activation, suggesting an increase in Ca^{2+} is required for maximal ERK activation (Jiang *et al.*, 2001, Li *et al.*, 2006). The finding that the maximum pERK1/2 response to GCG was also reduced in β -arrestin1/2 knockout cells suggest that the GCGR-mediated pERK1/2 response is produced by a combination of G_q and

β -arrestin1/2 mediated pathways. Through the use of the specific G $\beta\gamma$ small molecule inhibitor gallein (Lehmann *et al.*, 2008), this G protein-dependent pERK1/2 response was suggested to be independent of G $\beta\gamma$ -subunit. Interestingly however, at low concentrations of ligand (0.1 nM – 10 nM), it appears G $\beta\gamma$ inhibition causes an elevation in the basal pERK1/2 response. One speculation into the cause of this elevation could be the inability of the α -subunit to re-bind the G $\beta\gamma$ and complete the G protein cycle, thereby remaining active and stimulating a single or multiple pathways leading to elevated basal pERK1/2.

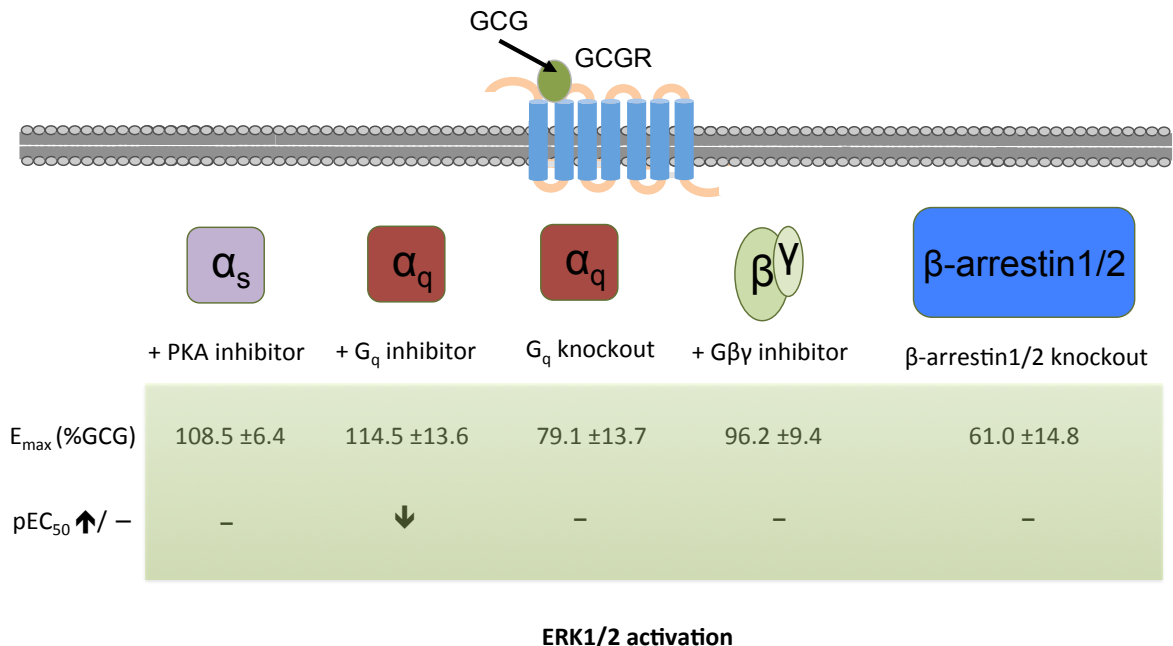


Figure 6.1. GCGR-mediated ERK1/2 activation. The work presented in this thesis suggest that the GCGR-mediated ERK1/2 activation following GCG stimulation is produced by a combination of G_q and β -arrestin1/2 mediated pathways. Treatment with the PKA inhibitor Rp-8-Br-cAMP or G $\beta\gamma$ inhibitor gallein showed no significant differences in ERK1/2 activation both in terms of maximum response (E_{max} expressed as a percentage GCG response) and pEC₅₀ (-). Inhibition of G_{q/11} through YM-254890 treatment showed a reduced GCG potency. Finally, utilising G_{q/11} or β -arrestin1/2 knockout cell lines transiently transfected with GCGR showed a reduced GCG stimulated maximal response when compared to WT.

A pharmacological consequence of RAMP2-GCGR interaction.

Similarly to other class B GPCRs, GCGR is reported to interact with RAMP2

(Christopoulos *et al.*, 2003). We investigated the consequence of this potential RAMP2-GCGR interaction in HEK 293T cells and identified a RAMP2-dependent potentiation of the GCG stimulated cAMP response, which was independent of cell-surface expression. This finding was suggested to be as a result of RAMP2 increasing the ability of GCGR to transduce the signal following GCG stimulation, as determined by an increase in relative efficacy ($\log\tau$). This finding suggests that the RAMP2 expression profile, which is likely to vary between cell types and across time, may alter the activity of GCGR active ligands. Indeed, previous work has identified cross-reactivity of GLP-1R ligands, including GLP-1(7-36)amide and liraglutide at the GCGR, which was abolished by a RAMP2 interaction (Weston *et al.*, 2014, Weston *et al.*, 2015). This finding may have important implications in the design of GCGR targeted therapeutics. In addition, to gain a true picture of GCGR receptor signalling, and other class B GPCRs, it may be necessary to investigate the RAMP expression profile in the chosen cellular system. Interestingly, this finding could not be reproduced using a dual expression vector expressing both GCGR and RAMP2. However, investigation into the RAMP2 cell-surface expression suggested that RAMP2 expression from MCS2 was reduced when GCGR was at MCS1. This latter finding highlighted that although in theory a 1:1 DNA ratio exists in a dual expression vector, this does not necessarily translate to a 1:1 protein expression ratio and caution should be exercised when interpreting experimental data acquired from using such dual expression vectors.

The importance of the ICL1 region in GPCR signalling. A number of studies looking at class B GPCRs have proposed critical roles for residues within ICL1 including G proteins-coupling (Mathi *et al.*, 1997, Conner *et al.*, 2006 and Kleinau *et al.*, 2010), protein folding and correct transport (Thomas *et al.*, 2007). In this study, we investigated the importance of the ICL1 region (G165^{1.63}-T172^{2.45}) for both GCGR cell-surface expression and signalling. Cell-surface expression analysis indicated the importance of a number of ICL1 amino acids for successful translation and/or trafficking of GCGR

including G165A^{1.63}, S167A^{12.48}, K168A^{12.49} and L169A^{12.50}, which all showed reduced cell-surface expression when compared to WT. C171^{2.44} was implicated as a critical determinant of GCGR expression given the complete lack of cell-surface expression and detectable GFP. This finding was in line with the previous report implicating this conserved residue as a critical determinant of cell-surface translocation and function of the PTH1R (Thomas *et al.*, 2007). An investigation into GCGR-mediated accumulation/activation of downstream signalling components following GCG stimulation showed negligible difference between WT and mutant GCGR for cAMP or pERK1/2 responses, with the exception of C171A, which showed no detectable response, and G165A^{1.63}, which showed a reduced maximal cAMP response. The latter finding may implicate a role for G165^{1.63} in the GCGR-mediated cAMP response, possibly through interaction with G_s protein. The mutants K168A^{12.49}, L169A^{12.50}, H170A^{12.51} and T172A^{2.45} (i.e. the residues towards TM2) showed a reduction in maximal Ca²⁺i response to GCG and, although the mechanism remains unclear, suggest these residues may play a role in signalling bias at the GCGR through G_{q/11}-coupling.

The highly conserved nature of ICL1 within GPCRs, both in terms of length and amino acid sequence, and the availability of multiple crystal structures for the class A GPCR A_{2A}R led to a similar investigation into the importance of ICL1 region (L33^{1.59}-N42^{2.40}) for cAMP signalling. Interestingly, a number of residues were identified to play a critical role in the measured cAMP accumulation. The ICL1 region of A_{2A}R was found to play a bigger role in the cAMP response when compared to that of GCGR, highlighting a potential difference between GPCR classes A and B. The potency of both NECA and CGS 21680 was reduced in N34A^{1.60}. Although this finding may be a consequence of reduced cell-surface expression, modelling of the mutant showed lost interactions with conserved helix 8 residues T298^{8.53} and E294^{8.49}. This may suggest the importance of ICL1 and helix 8 interactions within A_{2A}R, and potentially other GPCRs, for activation and/or signal transduction. Alanine substitution of L37^{12.50} resulted in a significantly reduced

potency to NECA but not CGS 21680, possibly indicating a role for L37^{12.50} in signalling bias at the A_{2A}R. Alanine substitution of T41^{2.39} increases the level of constitutive activity at the A_{2A}R, possibly due to the loss of hydrogen bonds with residues implicated in the ionic lock of the A_{2A}R including D101^{3.49} and R102^{3.50} of the E/DRY motif and Y112^{34.53} in ICL2 (Martínez-Archundia and Correa-Basurto, 2014). This latter finding is consistent with a number of reports showing an induced constitutive activity following mutations within the E/DRY motif of number of GPCRs including β₂AR, rhodopsin receptor and oxytocin receptor (OTR) (Rovati *et al.*, 2007).

The equivalent position for A_{2A}R T41^{2.39} within GCGR is R173^{2.46}, a highly conserved arginine across class B GPCRs. In line with a previous finding reported for the GLP-1R (Mathi *et al.*, 1997), mutation of R173^{2.46} to alanine was found to have no influence on cell-surface expression whereas there was severely attenuated ligand stimulated cAMP accumulation. Modelling of this mutant revealed a lost interaction between R173A^{2.46} and helix 8 residues E406^{8.49} and may implicate this interaction as critical for GCGR stabilisation. Alternatively, or in addition, R173^{2.46} may be essential for G protein-coupling. This latter explanation seems highly feasible given this residue has been suggested to contact G protein in a number of GPCR structures (Rasmussen *et al.*, 2011 and Zhang *et al.*, 2017b) and within the modelled CGRP receptor (Vohra *et al.*, 2013). To add further weight to this conclusion, modelling of R176A^{2.46} within the cryo-EM structure of activated rabbit GLP-1R in complex with heterotrimeric G_s reveals a lost interaction between and Q390 of Gα_s α5-helix (Zhang *et al.*, 2017b) and is likely to be the case for GCGR.

Within GCGR this residue appears to be involved in activation and/or G protein-coupling rather than maintaining the receptor in an inactive conformation as was reported for the A_{2A}R. In conclusion, the findings presented here suggest that the ICL1 region of GCGR or A_{2A}R play very different role in receptor activity.

The importance of conserved helix 8 residues for GPCR function.

There is suggested to be striking topological similarity between class A and B GPCRs helix 8 (Conner *et al.*, 2008) and this region has been implicated in a range of functions including cell-surface expression (Timossi *et al.*, 2004, Liang *et al.*, 2017) and G protein-coupling (Delos Santos *et al.*, 2006, Kleinau *et al.*, 2010). In this study, a number of residues implicated to be important in receptor activity were found to interact with helix 8, particularly the fully conserved residue E^{8.49} which has been implicated in the TM2-6-7-helix 8 network (involved in maintaining an inactive conformation) and G protein-coupling (Liang *et al.*, 2017). These residues included R173^{2.46}, shown to interact with helix 8 residues E406^{8.49} (Siu *et al.*, 2013 and Zhang *et al.*, 2017), and N34^{1.60} of A_{2A}R, shown to interact with helix 8 residue E294^{8.49} (Liu *et al.*, 2012, Lebon *et al.*, 2011, Lebon *et al.*, 2015 Carpenter *et al.*, 2016). Mutation of either of these residues within GCGR (R173^{2.46}) or A_{2A}R (N34^{1.60}) resulted in an attenuated ligand-dependent cAMP response.

Interestingly, the equivalent positions for the helix 8 A_{2A}R residues T298^{8.53} and E294^{8.49} are E406^{8.49} and E410^{8.53} within GCGR and may highlight a conserved interaction between helix 8 and the ICL1 region across GPCR classes. Consistent with previous findings in rat GCGR (Strudwick *et al.*, 2004), and despite a reduced cell-surface expression, mutation of E406^{8.49} to alanine resulted in enhanced potency to both GCG and oxyntomodulin stimulation and a statistically significant constitutive activity, which was further enhanced by mutation of E410. It may be speculated that mutation of both E406^{8.49} and E410^{8.53} (which may substitute or contribute to the lost interaction with R173^{2.46} in E406A^{8.49}) releases R173^{2.46}, which in turn interact with the G protein independent of ligand. This finding is distinct from previous reports in GLP-1R suggesting mutation of the equivalent residue (E408^{8.49}) reduce cAMP signalling (Wootten *et al.*, 2016). Visualisation of the cryo-EM structure of activated rabbit GLP-1R in complex with heterotrimeric G_s reveals helix 8 residue E408^{8.49} to interact with Q390 of Gα_s α5-helix with no apparent interaction with R176^{2.46} (Zhang *et al.*, 2017b). Interestingly,

modelling of E408A^{8.49} within the GLP-1R structure reveals a lost interaction with Q390 of Gα_s α5-helix. Therefore, whereas E^{8.49} within GLP-1R may be involved in selective coupling to cAMP signalling through G protein coupling, GCGR appears to be involved in maintaining the receptor in an inactive conformation.

We investigated the consequence of converting the S167^{12.46} within GCGR to arginine, effectively making the ICL1 sequence (SKLH) closer to the consensus [K/R]KLH motif (Vohra *et al.*, 2013). In a model of the CLR, the equivalent residue (K167^{12.48}) was suggested to interact with the Gβ and possibly with the E^{8.49} (Vohra *et al.*, 2013). Interestingly, within the modelled S167R^{12.46} GCGR mutant, there was a gained interaction with E410^{8.53} rather than E406^{8.49}. Given the previous presented findings, a gained interaction between helix 8 and ICL1 would be predicted to move the receptor to a more inactive conformation. However, contradictory to this prediction, there appeared to be enhanced GCGR activity with a lost interaction with helix 8 (as shown in E406A^{8.49} and E406A^{8.49}, E410A^{8.53}) and a small none significant increase in potency for both GCG and oxytomodulin.

GCGR TM4 residues; critical for cell-surface expression and Ca²⁺i response. Consistent with previous findings reported in GLP-1R (Harikumar *et al.*, 2012), three substitution mutations within the TM4 region of GCGR (G271^{4.49}, L277^{4.55}, V280^{4.58}) were found to selectively influence signalling whereby there was a complete abolishment of the Ca²⁺i response with only a small effect on cAMP accumulation and no measurable effect on the pERK1/2 response. Whereas these mutants were reported to have no influence on GLP-1R cell-surface expression (Harikumar *et al.*, 2012), we reported a significant reduced expression for the TM4 GCGR mutants. These findings suggested that this TM4 region plays an important role in successful translation and/or trafficking of GCGR and potentially the control of signal bias via altering the coupling efficiency of this receptor to a number of GCGR-mediated pathways. Given that the lipid face of TM4 has been implicated to be the predominant determinant for dimerisation in a number of GPCRs

(Harikumar *et al.*, 2007, Harikumar *et al.*, 2012, Xue *et al.*, 2015, Harikumar *et al.*, 2017), it may be speculated that the abolished Ca^{2+}_i mobilisation is a consequence of a lost ability for GCGR to form dimers. However, in order to investigate this hypothesis, dimerisation experiments would need to be conducted.

Hep 3B cells; a troublesome model hepatocyte cell line. In this study, a number of cell lines were used which stably or transiently expressing the receptor of interest. As has been highlighted, the background of a cell type and variation between cell batches can contribute greatly to the experimental observations (Tilakaratne *et al.*, 2000). With the intention to move into a more physiologically relevant cell line to investigation GCGR signalling, Hep 3B cells were characterised. These cells were demonstrated to endogenously express GCGR, however, the lost GCGR expression over passage, data variability and time constraint on ligand stimulated responsiveness indicated that these cells may not be the best model to investigate GCGR signalling.

Concluding remarks. In this thesis, an in-depth analysis of GCGR signalling was conducted contributing knowledge to how this receptor functions in terms signalling cascades and at a structural level where a number of residues were implicated as important in receptor function and cell-surface expression. The primary aim of this thesis was to expand on the current available knowledge on GCGR at a mechanistic, rather than physiological level. Evidence has suggested that GCG administration at low concentrations may play a role in normalising obesity-associated glucose intolerance, insulin resistance and dyslipidemia (Day *et al.*, 2012, Pocai *et al.*, 2009). However, the risk of hyperglycemia imposed by GCG administration has prevented further studies in humans (Day *et al.*, 2012) and current GCG-based therapy is limited to acute emergency treatment of hypoglycemia in patients with type 1 diabetes (T1D) (Habegger *et al.*, 2010). Alternatively, antagonism of GCG action may also provide a therapeutic approach to normalise blood glucose levels (Lotfy *et al.*, 2014). A novel approach was

recently reported using a fully human antibody fused to GCG, blocking ligand binding, and was found to normalise blood glucose without causing hypoglycaemia (Okamoto *et al.*, 2015). This study and others offering new insight into GCGR signalling provide the basis for advances in such therapeutic development.

6.2. Further Work

In order to investigate if the abolished Ca^{2+}_i response in the GCGR TM4 mutant is indeed a consequence of a disrupted dimerisation interface, as previously suggested (Harikumar *et al.*, 2012), dimerisation experiments would need to be conducted. A variety of approaches exist for the exploration of dimerisation, including fluorescent-based methods such as FRET and bioluminescence resonance energy transfer (BRET) (Goddard and Watts, 2012), co-immunoprecipitation and functional complementation assays (Guo *et al.*, 2017, Milligan and Bouvier, 2005). Although each approach has limitations that make the interpretation inconclusive (Guo *et al.*, 2017), a combination of multiple approaches may provide a more convincing body of evidence in support of a potential dimerisation of GCGR and the importance of TM4.

This study provides an in-depth analysis of the GCGR-mediated pERK1/2 response and suggests a role for both G_q and β -arrestin1/2-mediated pathways. Interestingly, the finding that TM4 mutant GCGR showed a similar pERK1/2 response to WT GCGR despite an abolished Ca^{2+}_i response further supports this conclusion and suggests that a β -arrestin1/2-mediated pathway may compensate for the loss of the G_q -mediated pathways. In order to test this hypothesis, an interesting follow up experiment would be to investigate the pERK1/2 response in the $\Delta\beta$ -arrestin1/2 knockout cell transfected with the TM4 mutant GCGR. In addition, it would be interesting to investigate if the measured pERK1/2 response in $\Delta\beta$ -arrestin1/2

HEK 293T cells transfected with GCGR could be abolished or further reduced by the treatment of YM-254890, thereby confirming the G_q-mediated pERK1/2 response.

Although not the primary aim of this work, a number of residues within the ICL1 region of A_{2A}R were found to play a significant role in the NECA or CGS 21680 simulated cAMP response (including N34A^{1.60} and 37A^{12.50}, which showed a reduced potency) and constitutive activity of A_{2A}R (T41A^{2.39}). This was distinct from the ICL1 region of GCGR where only one substitution showed a reduced cAMP accumulation following GCG stimulation (G165^{1.63}). However, as was conducted for the ICL1 mutant GCGRs, an analysis of WT and mutant A_{2A}R cell-surface expression must be conducted in order to confirm these findings are not a consequence of reduced cell-surface expression. Given that L37^{12.50} appears to play a more significant role in the NECA stimulated cAMP response when compared to the CGS 21680, this finding may indicate a role for L37^{12.50} in signalling bias at the A_{2A}R. To further investigate this, alternative agonists for the A_{2A}R, such as UK-432097 and adenosine, could be tested. In addition, given that A_{2A}R has been reported to activate ERK1/2 signalling (Schulte and Fredholm, 2000, Orr *et al.*, 2015), further analysis could include an investigation into the effect of these mutants on the pERK1/2 response to determine if this region is important in selective signalling.

To expand on the findings investigating the importance of various GCGR residues, radioligand binding experiments should be conducted. For the GCGR ICL1 region, the oxyntomodulin stimulated cAMP, pERK1/2 and Ca²⁺_i response could also be measured to determine if there are ligand-dependent differences between the responses. In addition, the influence of helix 8 mutants on alternative signalling such as pERK1/2 and Ca²⁺_i could also be investigated to indicate if this region is involved in signalling specificity.

References

- Aktories, K., 2011.** Bacterial protein toxins that modify host regulatory GTPases. *Nature reviews. Microbiology*, 9(7), pp.487–498.
- Alberts, B., Johnson, A., Lewis, J., Raff, M., Roberts, K., and Walter, P., 2002.** *Molecular Biology of the Cell*, 4th Edition.
- Alvarez-Curto, E., Inoue, A., Jenkins, L., Raihan, S.Z., Prihandoko, R., Tobin, A.B. and Milligan, G., 2016.** Targeted Elimination of G proteins and Arrestins Defines their Specific Contributions to both Intensity and Duration of G protein-Coupled Receptor Signalling. *J Biol Chem*, 30;291(53), pp 27147-27159
- Amatruda, T.T., Steele, D.A., Slepak, V.Z. and Simon, M.I., 1991.** G-Alpha-16, a G-Protein Alpha Subunit Specifically Expressed in Hematopoietic-Cells. *Proc Natl Acad Sci U S A*, 88(13), pp.5587–5591.
- Angers, S., Salahpour, A. and Bouvier, M., 2002.** Dimerization: an emerging concept for G protein-coupled receptor ontogeny and function. *Annu Rev Pharmacol Toxicol*, 42(1), pp.409–435.
- Audet, M. and Bouvier, M., 2012.** Restructuring G-protein- coupled receptor activation. *Cell*, 151(1), pp.14–23.
- Ballesteros, J.A. and Weinstein, H., 1995.** Integrated methods for the construction of three-dimensional models and computational probing of structure-function relations in G protein-coupled receptors. *Receptor Molecular Biology*, 25 pp.366–428.
- Barak, L.S., Ménard, L., Ferguson, S.S., Colapietro, A.M. and Caron, M.G., 1995.** The conserved seven-transmembrane sequence NP(X)₂Y of the G-protein-coupled receptor superfamily regulates multiple properties of the beta 2-adrenergic receptor. *Biochemistry*, 34(47), pp.15407–15414.
- Belluscio, L., Gold, G.H., Nemes, A. and Axel, R., 1998.** Mice deficient in G(olf) are anosmic. *Neuron*, 20(1), pp.69–81.
- Bender, A.T. and Beavo, J.A., 2006.** Cyclic nucleotide phosphodiesterases: molecular regulation to clinical use. *Pharmacol Rev*, 58(3), pp.488–520.
- Birnbaumer, L., 2007.** Expansion of signal transduction by G proteins. The second 15 years or so: from 3 to 16 alpha subunits plus betagamma dimers. *Biochim Biophys Acta*, 1768(4), pp.772–793.
- Black, J.W. and Leff, P., 1983.** Operational models of pharmacological agonism. *Proc R Soc Lond B Biol Sci*, 220(1219), pp.141–162.
- Blättermann, S., Peters, L., Ottersbach, P.A., Bock, A., Konya, V., Weaver, C.D., Gonzalez, A., Schröder, R., Tyagi, R., Luschnig, P., Gäb, J., Hennen, S., Ulven, T., Pardo, L., Mohr, K., Gütschow, M., Heinemann, A. and Kostenis, E., 2012.** A biased ligand for OXE-R uncouples G α and G $\beta\gamma$ signaling within a heterotrimer. *Nat Chem Biol*, 8(7), pp.631–638.
- Bologna, Z., Teoh, J.-P., Bayoumi, A.S., Tang, Y. and Kim, I.-M., 2017.** Biased G Protein-Coupled Receptor Signaling: New Player in Modulating Physiology and Pathology. *Biomol Ther*, 25(1), pp.12–25.
- Bos, J.L., Rehmann, H. and Wittinghofer, A., 2007.** GEFs and GAPs: critical elements in the control of small G proteins. *Cell*, 129(5), pp.865–877.
- Bourne, H.R., Sanders, D.A. and McCormick, F., 1991.** The Gtpase Superfamily - Conserved Structure and Molecular Mechanism. *Nature*, 349(6305), pp.117–127.
- Bouschet, T., Martin, S. and Henley, J.M., 2005.** Receptor-activity-modifying proteins are required for forward trafficking of the calcium-sensing receptor to the plasma membrane. *Journal of cell science*, 118(Pt 20), pp.4709–4720.

Brown, B.L., Albano, J.D., Ekins, R.P. and Sgherzi, A.M., 1971. A simple and sensitive saturation assay method for the measurement of adenosine 3':5'-cyclic monophosphate. *Biochem J*, 121(3), pp.561–562.

Carbonetti, N.H., 2010. Pertussis toxin and adenylate cyclase toxin: key virulence factors of *Bordetella pertussis* and cell biology tools. *Future microbiology*, 5(3), pp.455–469.

Carlson, K.E., Brass, L.F. and Manning, D.R., 1989. Thrombin and phorbol esters cause the selective phosphorylation of a G protein other than Gi in human platelets. *J Biol Chem*, 264(22), pp.13298–13305.

Carpenter, B., Nehmé, R., Warne, T., Leslie, A.G.W. and Tate, C.G., 2016. Structure of the adenosine A(2A) receptor bound to an engineered G protein. *Nature*, 536(7614), pp.104–107.

Cascieri, M.A., Koch, G.E., Ber, E., Sadowski, S.J., Louzides, D., de Laszlo, S.E., Hacker, C., Hagmann, W.K., MacCoss, M., Chicchi, G.G. and Vicario, P.P., 1999. Characterization of a novel, non-peptidyl antagonist of the human glucagon receptor. *J Biol Chem*, 274(13), pp.8694–8697.

Chen, L., He, X., Zhang, Y., Chen, X., Lai, X., Shao, J., Shi, Y. and Zhou, N., 2014. Melatonin receptor type 1 signals to extracellular signal-regulated kinase 1 and 2 via Gi and Gs dually coupled pathways in HEK-293 cells. *Biochemistry*, 53(17), pp.2827–2839.

Chikumi, H., Barac, A., Behbahani, B., Gao, Y., Teramoto, H., Zheng, Y. and Gutkind, J.S., 2004. Homo- and hetero-oligomerization of PDZ-RhoGEF, LARG and p115RhoGEF by their C-terminal region regulates their in vivo Rho GEF activity and transforming potential. *Oncogene*, 23(1), pp.233–240.

Cheng, R.K.Y., Segala, E., Robertson, N., Deflorian, F., Dore, A.S., Errey, J.C., Fiez-Vandal, C., Marshall, F.H. and Cooke, R.M., 2017. Structures of Human A1 and A2A Adenosine Receptors with Xanthines Reveal Determinants of Selectivity. *Structure*, 25(8), pp.1275–1285.e4.

Choksi, T., Hay, D.L., Legon, S., Poyner, D.R., Hagner, S., Bloom, S.R. and Smith, D.M., 2002. Comparison of the expression of calcitonin receptor-like receptor (CRLR) and receptor activity modifying proteins (RAMPs) with CGRP and adrenomedullin binding in cell lines. *Br J Pharmacol*, 136(5), pp.784–792.

Christopoulos, A., Christopoulos, G., Morfis, M., Udawela, M., Laburthe, M., Couvineau, A., Kuwasako, K., Tilakaratne, N. and Sexton, P.M., 2003. Novel receptor partners and function of receptor activity-modifying proteins. *J Biol Chem*, 278(5), pp.3293–3297.

Christopoulos, G., Perry, K.J., Morfis, M., Tilakaratne, N., Gao, Y., Fraser, N.J., Main, M.J., Foord, S.M. and Sexton, P.M., 1999. Multiple amylin receptors arise from receptor activity-modifying protein interaction with the calcitonin receptor gene product. *Mol Pharmacol*, 56(1), pp.235–242.

Claing, A., Laporte, S.A., Caron, M.G. and Lefkowitz, R.J., 2002. Endocytosis of G protein-coupled receptors: roles of G protein-coupled receptor kinases and beta-arrestin proteins. *Progress in Neurobiology*, 66(2), pp.61–79.

Colón-González, F. and Kazanietz, M.G., 2006. C1 domains exposed: from diacylglycerol binding to protein-protein interactions. *Biochim Biophys Acta*, 1761(8), pp.827–837.

Conner, A.C., Simms, J., Conner, M.T., Wootten, D.L., Wheatley, M. and Poyner, D.R., 2006. Diverse functional motifs within the three intracellular loops of the CGRP1 receptor. *Biochemistry*, 45(43), pp.12976–12985.

Conner, A.C., Simms, J., Hay, D.L., Mahmoud, K., Howitt, S.G., Wheatley, M. and Poyner, D.R., 2004. Heterodimers and family-B GPCRs: RAMPs, CGRP and

adrenomedullin. *Biochem Soc Trans*, 32(Pt 5), pp.843–846.

Conner, M., Hicks, M.R., Dafforn, T., Knowles, T.J., Ludwig, C., Staddon, S., Overduin, M., Günther, U.L., Thome, J., Wheatley, M., Poyner, D.R. and Conner, A.C., 2008. Functional and biophysical analysis of the C-terminus of the CGRP-receptor; a family B GPCR. *Biochemistry*, 47(32), pp.8434–8444.

Cordomi, A., Ismail, S., Matsoukas, M.-T., Escrieut, C., Gherardi, M.-J., Pardo, L. and Fourmy, D., 2015. Functional elements of the gastric inhibitory polypeptide receptor: Comparison between secretin- and rhodopsin-like G protein-coupled receptors. *Biochem Pharmacol*, 96(3), pp.237–246.

Culhane, K.J., Liu, Y., Cai, Y. and Yan, E.C.Y., 2015. Transmembrane signal transduction by peptide hormones via family B G protein-coupled receptors. *Frontiers in pharmacology*, 6(196).

Dalle, S., Longuet, C., Costes, S., Broca, C., Faruque, O., Fontés, G., Hani, E.H. and Bataille, D., 2004. Glucagon promotes cAMP-response element-binding protein phosphorylation via activation of ERK1/2 in MIN6 cell line and isolated islets of Langerhans. *J Biol Chem*, 279(19), pp.20345–20355.

Desai, A.J., Roberts, D.J., Richards, G.O. and Skerry, T.M., 2014. Role of receptor activity modifying protein 1 in function of the calcium sensing receptor in the human TT thyroid carcinoma cell line. *PLoS ONE*, 9(1), p.e85237.

Davies, J. and Jimenez, A., 1980. A new selective agent for eukaryotic cloning vectors. *Am J Trop Med Hyg*, 29(5 Suppl), pp.1089–1092.

Davies, M.N., Secker, A., Freitas, A.A., Mendao, M., Timmis, J. and Flower, D.R., 2007. On the hierarchical classification of G protein-coupled receptors. *Bioinformatics*, 23(23), pp.3113–3118.

Day, J.W., Gelfanov, V., Smiley, D., Carrington, P.E., Eiermann, G., Chicchi, G., Erion, M.D., Gidda, J., Thornberry, N.A., Tschöp, M.H., Marsh, D.J., SinhaRoy, R., DiMarchi, R. and Poci, A., 2012. Optimization of co-agonism at GLP-1 and glucagon receptors to safely maximize weight reduction in DIO-rodents. *Biopolymers*, 98(5), pp.443–450.

de Lera Ruiz, M., Lim, Y.-H. and Zheng, J., 2014. Adenosine A2A receptor as a drug discovery target. *Journal of medicinal chemistry*, 57(9), pp.3623–3650.

Delos Santos, N.M., Gardner, L.A., White, S.W. and Bahouth, S.W., 2006. Characterization of the residues in helix 8 of the human beta1-adrenergic receptor that are involved in coupling the receptor to G proteins. *J Biol Chem*, 281(18), pp.12896–12907.

Denis, C., Saulière, A., Galandrin, S., Sénard, J.-M. and Gales, C., 2012. Probing heterotrimeric G protein activation: applications to biased ligands. *Curr Pharm Des*, 18(2), pp.128–144.

Dewire, S.M., Ahn, S., Lefkowitz, R.J. and Shenoy, S.K., 2007. Beta-arrestins and cell signaling. *Ann Rev Physiol*, 69(1), pp.483–510.

Déry, O., Corvera, C.U., Steinhoff, M. and Bunnett, N.W., 1998. Proteinase-activated receptors: novel mechanisms of signaling by serine proteases. *Am J Physiol*, 274(6 Pt 1), pp.C1429–52.

Ding, W.-Q., Cheng, Z.-J., McElhiney, J., Kuntz, S.M. and Miller, L.J., 2002. Silencing of secretin receptor function by dimerization with a misspliced variant secretin receptor in ductal pancreatic adenocarcinoma. *Cancer research*, 62(18), pp.5223–5229.

Dore, A.S., Robertson, N., Errey, J.C., Ng, I., Hollenstein, K., Tehan, B., Hurrell, E., Bennett, K., Congreve, M., Magnani, F., Tate, C.G., Weir, M. and Marshall, F.H., 2011. Structure of the adenosine A(2A) receptor in complex with ZM241385 and the xanthines XAC and caffeine. *Structure*, 19(9), pp.1283–1293.

Dorsam, R.T. and Gutkind, J.S., 2007. G-protein-coupled receptors and cancer. *Nat Rev Cancer*, 7(2), pp.79–94.

Dubin, A.E., Schmidt, M., Mathur, J., Petrus, M.J., Xiao, B., Coste, B. and Patapoutian, A., 2012. Inflammatory signals enhance piezo2-mediated mechanosensitive currents. *Cell reports*, 2(3), pp.511–517.

Dumaz, N. and Marais, R., 2003. Protein kinase A blocks Raf-1 activity by stimulating 14-3-3 binding and blocking Raf-1 interaction with Ras. *J Biol Chem*, 278(32), pp.29819–29823.

Dupré, D.J., Robitaille, M., Rebois, R.V. and Hébert, T.E., 2009. The role of Gbetagamma subunits in the organization, assembly, and function of GPCR signaling complexes. *Annu Rev Pharmacol Toxicol*, 49(1), pp.31–56.

Eishingdrelo, H. and Kongsamut, S., 2013. Minireview: Targeting GPCR Activated ERK Pathways for Drug Discovery. *Curr Chem Genom Transl Med*, 7(1), pp.9–15.

Eswar, N., Webb, B., Marti-Renom, M.A., Madhusudhan, M.S., Eramian, D., Shen, M.-Y., Pieper, U. and Sali, A., 2007. Comparative protein structure modeling using MODELLER. *Curr Protoc Protein Sci*, Chapter 2, pp.Unit 2.9–2.9.31.

Evans, B.A., Broxton, N., Merlin, J., Sato, M., Hutchinson, D.S., Christopoulos, A. and Summers, R.J., 2011. Quantification of functional selectivity at the human $\alpha(1A)$ -adrenoceptor. *Mol Pharmacol*, 79(2), pp.298–307.

Exton, J.H., 1994. Phosphatidylcholine breakdown and signal transduction. *Biochim Biophys Acta*, 1212(1), pp.26–42.

Fanelli, F. and Felling, A., 2011. Dimerization and ligand binding affect the structure network of A(2A) adenosine receptor. *Biochim Biophys Acta*, 1808(5), pp.1256–1266.

Feinstein, T.N., Yui, N., Webber, M.J., Wehbi, V.L., Stevenson, H.P., King, J.D., Hallows, K.R., Brown, D., Bouley, R. and Vilardaga, J.-P., 2013. Noncanonical control of vasopressin receptor type 2 signaling by retromer and arrestin. *J Biol Chem*, 288(39), pp.27849–27860.

Ferrandon, S., Feinstein, T.N., Castro, M., Wang, B., Bouley, R., Potts, J.T., Gardella, T.J. and Vilardaga, J.-P., 2009. Sustained cyclic AMP production by parathyroid hormone receptor endocytosis. *Nat Chem Biol*, 5(10), pp.734–742.

Fields, T.A. and Casey, P.J., 1997. Signalling functions and biochemical properties of pertussis toxin-resistant G-proteins. *Biochem J*, 321 (Pt 3)(Pt 3), pp.561–571.

Gjertsen, B.T., Mellgren, G., Otten, A., Maronde, E., Genieser, H.G., Jastorff, B., Vintermyr, O.K., McKnight, G.S. and Døskeland, S.O., 1995. Novel (Rp)-cAMPS analogs as tools for inhibition of cAMP-kinase in cell culture. Basal cAMP-kinase activity modulates interleukin-1 beta action. *The Journal of biological chemistry*, 270(35), pp.20599–20607.

Glukhova, A., Thal, D.M., Nguyen, A.T., Vecchio, E.A., Jörg, M., Scammells, P.J., May, L.T., Sexton, P.M. and Christopoulos, A., 2017. Structure of the Adenosine A1 Receptor Reveals the Basis for Subtype Selectivity. *Cell*, 168(5), pp.867–877.e13.

Gundry, J., Glenn, R., Alagesan, P. and Rajagopal, S., 2017. A Practical Guide to Approaching Biased Agonism at G Protein Coupled Receptors. *Frontiers in neuroscience*, 11, p.17.

Flahaut, M., Rossier, B.C. and D, F., 2002. Respective roles of calcitonin receptor-like receptor (CRLR) and receptor activity-modifying proteins (RAMP) in cell surface expression of CRLR/RAMP heterodimeric receptors. *J Biol Chem*, 277(17), pp.14731–14737.

Fong, H.K., Yoshimoto, K.K., Eversole-Cire, P. and Simon, M.I., 1988. Identification of a GTP-binding protein alpha subunit that lacks an apparent ADP-

ribosylation site for pertussis toxin. *Proc Natl Acad Sci U S A*, 85(9), pp.3066–3070.

Foskett, J.K., White, C., Cheung, K.-H. and Mak, D.-O.D., 2007. Inositol trisphosphate receptor Ca²⁺ release channels. *Physiol Rev*, 87(2), pp.593–658.

Fredriksson, R., Lagerström, M.C., Lundin, L.-G. and Schiöth, H.B., 2003. The G-protein-coupled receptors in the human genome form five main families. Phylogenetic analysis, paralogon groups, and fingerprints. *Mol Pharmacol*, 63(6), pp.1256–1272.

Fujioka, M., Koda, S., Morimoto, Y. and Biemann, K., 2001. Structure of FR900359, a cyclic depsipeptide from *Ardisia crenata* Sims. pp.1–6.

Furness, S.G.B., Wooten, D., Christopoulos, A. and Sexton, P.M., 2012. Consequences of splice variation on Secretin family G protein-coupled receptor function. *Br J Pharmacol*, 166(1), pp.98–109.

Garbison, K.E., Heinz, B.A. and Lajiness, M.E., 2004. IP-3/IP-1 Assays. Assay Guidance Manual. Eli Lilly & Company and the National Center for Advancing Translational Sciences. Bookshelf ID: NBK92004.

Ge, Y., Yang, D., Dai, A., Zhou, C., Zhu, Y. and Wang, M.-W., 2014. The putative signal peptide of glucagon-like peptide-1 receptor is not required for receptor synthesis but promotes receptor expression. *Bioscience reports*, 34(6), pp.e00152–727.

Gehret, A.U., Jones, B.W., Tran, P.N., Cook, L.B., Greuber, E.K. and Hinkle, P.M., 2010. Role of helix 8 of the thyrotropin-releasing hormone receptor in phosphorylation by G protein-coupled receptor kinase. *Mol Pharmacol*, 77(2), pp.288–297.

George, S.R., Fan, T., Xie, Z., Tse, R., Tam, V., Varghese, G. and O'Dowd, B.F., 2000. Oligomerization of mu- and delta-opioid receptors. Generation of novel functional properties. *J Biol Chem*, 275(34), pp.26128–26135.

Gesty-Palmer, D., Chen, M., Reiter, E., Ahn, S., Nelson, C.D., Wang, S., Eckhardt, A.E., Cowan, C.L., Spurney, R.F., Luttrell, L.M. and Lefkowitz, R.J., 2006. Distinct beta-arrestin- and G protein-dependent pathways for parathyroid hormone receptor-stimulated ERK1/2 activation. *J Biol Chem*, 281(16), pp.10856–10864.

Giannone, F., Malpeli, G., Lisi, V., Grasso, S., Shukla, P., Ramarli, D., Sartoris, S., Monsurró, V., Krampera, M., Amato, E., Tridente, G., Colombatti, M., Parenti, M. and Innamorati, G., 2010. The puzzling uniqueness of the heterotrimeric G15 protein and its potential beyond hematopoiesis. *J Mol Endocrinol*, 44(5), pp.259–269.

Gilman, A.G., 1987. G proteins: transducers of receptor-generated signals. *Ann Rev Biochem*, 56(1), pp.615–649.

Gimpl, G. and Fahrenholz, F., 2001. The oxytocin receptor system: structure, function, and regulation. *Physiol Rev*, 81(2), pp.629–683.

Ginés, S., Hillion, J., Torvinen, M., Le Crom, S., Casadó, V., Canela, E.I., Rondin, S., Lew, J.Y., Watson, S., Zoli, M., Agnati, L.F., Verniera, P., Lluís, C., Ferré, S., Fuxe, K. and Franco, R., 2000. Dopamine D1 and adenosine A1 receptors form functionally interacting heteromeric complexes. *Proc Natl Acad Sci U S A*, 97(15), pp.8606–8611.

Goddard, A.D. and Watts, A., 2012. Contributions of fluorescence techniques to understanding G protein-coupled receptor dimerisation. *Biophysical reviews*, 4(4), pp.291–298.

Goldsmith, Z.G. and Dhanasekaran, D.N., 2007. G protein regulation of MAPK networks. *Oncogene*, 26(22), pp.3122–3142.

Goodman, O.B., Krupnick, J.G., Santini, F., Gurevich, V.V., Penn, R.B., Gagnon, A.W., Keen, J.H. and Benovic, J.L., 1996. Beta-arrestin acts as a clathrin adaptor

in endocytosis of the beta2-adrenergic receptor. *Nature*, 383(6599), pp.447–450.

Gresch, O. and Altrogge, L., 2012. Transfection of difficult-to-transfect primary mammalian cells. *Methods Mol Biol*, 801(Chapter 5), pp.65–74.

Griner, E.M. and Kazanietz, M.G., 2007. Protein kinase C and other diacylglycerol effectors in cancer. *Nat Rev Cancer*, 7(4), pp.281–294.

Guo, H., An, S., Ward, R., Yang, Y., Liu, Y., Guo, X.-X., Hao, Q. and Xu, T.-R., 2017. Methods used to study the oligomeric structure of G-protein-coupled receptors. *Bioscience reports*, 37(2), p.BSR20160547.

Gurevich, V.V. and Gurevich, E.V., 2006. The structural basis of arrestin-mediated regulation of G-protein-coupled receptors. *Pharmacol Ther*, 110(3), pp.465–502.

Habegger, K.M., Heppner, K.M., Geary, N., Bartness, T.J., DiMarchi, R. and Tschöp, M.H., 2010. The metabolic actions of glucagon revisited. *Nature reviews. Endocrinology*, 6(12), pp.689–697.

Halls, M.L. and Cooper, D.M.F., 2010. Sub-picomolar relaxin signalling by a pre-assembled RXFP1, AKAP79, AC2, beta-arrestin 2, PDE4D3 complex. *The EMBO journal*, 29(16), pp.2772–2787.

Harikumar, K.G., Lau, S., Sexton, P.M., Wootten, D. and Miller, L.J., 2017. Coexpressed Class B G Protein-Coupled Secretin and GLP-1 Receptors Self- and Cross-Associate: Impact on Pancreatic Islets. *Endocrinology*, 158(6), pp.1685–1700.

Harikumar, K.G., Morfis, M.M., Lisenbee, C.S., Sexton, P.M. and Miller, L.J., 2006. Constitutive formation of oligomeric complexes between family B G protein-coupled vasoactive intestinal polypeptide and secretin receptors. *Mol Pharmacol*, 69(1), pp.363–373.

Harikumar, K.G., Pinon, D.I. and Miller, L.J., 2007. Transmembrane segment IV contributes a functionally important interface for oligomerization of the Class II G protein-coupled secretin receptor. *J Biol Chem*, 282(42), pp.30363–30372.

Harikumar, K.G., Wootten, D., Pinon, D.I., Koole, C., Ball, A.M., Furness, S.G.B., Graham, B., Dong, M., Christopoulos, A., Miller, L.J. and Sexton, P.M., 2012. Glucagon-like peptide-1 receptor dimerization differentially regulates agonist signaling but does not affect small molecule allosterity. *Proc Natl Acad Sci U S A*, 109(45), pp.18607–18612.

Hayward, B.E., Kamiya, M., Strain, L., Moran, V., Campbell, R., Hayashizaki, Y. and Bonthron, D.T., 1998. The human GNAS1 gene is imprinted and encodes distinct paternally and biallelically expressed G proteins. *Proc Natl Acad Sci U S A*, 95(17), pp.10038–10043.

Hiller, C., Kühhorn, J. and Gmeiner, P., 2013. Class A G-protein-coupled receptor (GPCR) dimers and bivalent ligands. *J Med Chem*, 56(17), pp.6542–6559.

Hjorth, S.A., Orskov, C. and Schwartz, T.W., 1998. Constitutive activity of glucagon receptor mutants. *Mol Endocrinol (Baltimore, Md.)*, 12(1), pp.78–86.

Hoare, S.R.J., 2005. Mechanisms of peptide and nonpeptide ligand binding to Class B G-protein-coupled receptors. *Drug discovery today*, 10(6), pp.417–427.

Hofer, D., Puschel, B. and Drenckhahn, D., 1996. Taste receptor-like cells in the rat gut identified by expression of alpha-gustducin. *Proc Natl Acad Sci U S A*, 93(13), pp.6631–6634.

Hofmann, K.P., Scheerer, P., Hildebrand, P.W., Choe, H.-W., Park, J.H., Heck, M. and Ernst, O.P., 2009. A G protein-coupled receptor at work: the rhodopsin model. *Trends in biochemical sciences*, 34(11), pp.540–552.

Hohenegger, M., Waldhoer, M., Beindl, W., Böing, B., Kreimeyer, A., Nickel, P., Nanoff, C. and Freissmuth, M., 1998. Galpha-selective G protein antagonists. *Proc Natl Acad Sci U S A*, 95(1), pp.346–351.

Hollenstein, K., de Graaf, C., Bortolato, A., Wang, M.-W., Marshall, F.H. and

Stevens, R.C., 2014. Insights into the structure of class B GPCRs. *Trends Pharmacol Sci*, 35(1), pp.12–22.

Hollenstein, K., Kean, J., Bortolato, A., Cheng, R.K.Y., Dore, A.S., Jazayeri, A., Cooke, R.M., Weir, M. and Marshall, F.H., 2013. Structure of class B GPCR corticotropin-releasing factor receptor 1. *Nature*, 499(7459), pp.438–43.

Irannejad, R., Tomshine, J.C., Tomshine, J.R., Chevalier, M., Mahoney, J.P., Steyaert, J., Rasmussen, S.G.F., Sunahara, R.K., El-Samad, H., Huang, B. and Zastrow, von, M., 2013. Conformational biosensors reveal GPCR signalling from endosomes. *Nature*, 495(7442), pp.534–538.

Isberg, V., de Graaf, C., Bortolato, A., Cherezov, V., Katritch, V., Marshall, F.H., Mordalski, S., Pin, J.-P., Stevens, R.C., Vriend, G. and Gloriam, D.E., 2015. Generic GPCR residue numbers - aligning topology maps while minding the gaps. *Trends Pharmacol Sci*, 36(1), pp.22–31.

Isberg, V., Mordalski, S., Munk, C., Rataj, K., Harpsøe, K., Hauser, A.S., Vroling, B., Bojarski, A.J., Vriend, G. and Gloriam, D.E., 2017. GPCRdb: an information system for G protein-coupled receptors. *Nucleic acids research*, 45(5), pp.2936–2936.

Jaakola, V.-P., Griffith, M.T., Hanson, M.A., Cherezov, V., Chien, E.Y.T., Lane, J.R., Ijzerman, A.P. and Stevens, R.C., 2008. The 2.6 angstrom crystal structure of a human A2A adenosine receptor bound to an antagonist. *Science*, 322(5905), pp.1211–1217.

Janssen, P., Rotondo, A., Mulé, F. and Tack, J., 2013. Review article: a comparison of glucagon-like peptides 1 and 2. *Aliment Pharmacol Ther*, 37(1), pp.18–36.

Jarvis, M.F., Schulz, R., Hutchison, A.J., Do, U.H., Sills, M.A. and Williams, M., 1989. [3H]CGS 21680, a selective A2 adenosine receptor agonist directly labels A2 receptors in rat brain. *J Pharmacol Exp Ther*, 251(3), pp.888–893.

Jazayeri, A., Dore, A.S., Lamb, D., Krishnamurthy, H., Southall, S.M., Baig, A.H., Bortolato, A., Koglin, M., Robertson, N.J., Errey, J.C., Andrews, S.P., Teobald, I., Brown, A.J.H., Cooke, R.M., Weir, M. and Marshall, F.H., 2016. Extra-helical binding site of a glucagon receptor antagonist. *Nature*, 533(7602):274-7.

Jazayeri, A., Rappas, M., Brown, A.J.H., Kean, J., Errey, J.C., Robertson, N.J., Fiez-Vandal, C., Andrews, S.P., Congreve, M., Bortolato, A., Mason, J.S., Baig, A.H., Teobald, I., Dore, A.S., Weir, M., Cooke, R.M. and Marshall, F.H., 2017. Corrigendum: Crystal structure of the GLP-1 receptor bound to a peptide agonist. *Nature*, 548(7665), pp.122–122.

Jiang, Y. and Fleet, J.C., 2012. Effect of phorbol 12-myristate 13-acetate activated signaling pathways on 1α , 25 dihydroxyvitamin D3 regulated human 25-hydroxyvitamin D3 24-hydroxylase gene expression in differentiated Caco-2 cells. *J Cell Biochem*, 113(5), pp.1599–1607.

Jiang, Y., Cypess, A.M., Muse, E.D., Wu, C.R., Unson, C.G., Merrifield, R.B. and Sakmar, T.P., 2001. Glucagon receptor activates extracellular signal-regulated protein kinase 1/2 via cAMP-dependent protein kinase. *Proc Natl Acad Sci U S A*, 98(18), pp.10102–10107.

Jones, B.J., Tan, T. and Bloom, S.R., 2012. Minireview: Glucagon in stress and energy homeostasis. *Endocrinology*, 153(3), pp.1049–1054.

Jones, D.T. and Reed, R.R., 1989. Golf: an olfactory neuron specific-G protein involved in odorant signal transduction. *Science (New York, N.Y.)*, 244(4906), pp.790–795.

Kadamur, G. and Ross, E.M., 2013. Mammalian phospholipase C. *Ann Rev Physiol*, 75(1), pp.127–154.

Kenakin, T., 1995. Agonist-receptor efficacy. II. Agonist trafficking of receptor signals. *Trends in pharmacological sciences*, 16(7), pp.232–238.

Kenakin, T., 2003. Predicting therapeutic value in the lead optimization phase of drug discovery. *Nature reviews. Drug discovery*, 2(6), pp.429–438.

Kenakin, T., Watson, C., Muniz-Medina, V., Christopoulos, A. and Novick, S., 2012. A simple method for quantifying functional selectivity and agonist bias. *ACS chemical neuroscience*, 3(3), pp.193–203.

Khan, S.M., Sleno, R., Gora, S., Zylbergold, P., Laverdure, J.-P., Labbé, J.-C., Miller, G.J. and Hébert, T.E., 2013. The expanding roles of G $\beta\gamma$ subunits in G protein-coupled receptor signaling and drug action. *Pharmacol Rev*, 65(2), pp.545–577.

Kim, T.K. and Eberwine, J.H., 2010. Mammalian cell transfection: the present and the future. *Analytical and bioanalytical chemistry*, 397(8), pp.3173–3178.

Kirkpatrick, A., Heo, J., Abrol, R. and Goddard, W.A., 2012. Predicted structure of agonist-bound glucagon-like peptide 1 receptor, a class B G protein-coupled receptor. *Proc Natl Acad Sci U S A*, 109(49), pp.19988–19993.

Kleinau, G., Jaeschke, H., Worth, C.L., Mueller, S., Gonzalez, J., Paschke, R. and Krause, G., 2010. Principles and determinants of G-protein coupling by the rhodopsin-like thyrotropin receptor. *PLoS ONE*, 5(3), p.e9745.

Kobilka, B.K., 2007. G protein coupled receptor structure and activation. *Biochim Biophys Acta*, 1768(4), pp.794–807.

Kolakowski, L.F., 1994. GCRDb: a G-protein-coupled receptor database. *Receptors & channels*, 2(1), pp.1–7.

Koole, C., Savage, E.E., Christopoulos, A., Miller, L.J., Sexton, P.M. and Wootten, D., 2013. Minireview: Signal bias, allosterism, and polymorphic variation at the GLP-1R: implications for drug discovery. *Mol Endocrinol*, 27(8), pp.1234–1244.

Koth, C.M., Murray, J.M., Mukund, S., Madjidi, A., Minn, A., Clarke, H.J., Wong, T., Chiang, V., Luis, E., Estevez, A., Rondon, J., Zhang, Y., Hötzel, I. and Allan, B.B., 2012. Molecular basis for negative regulation of the glucagon receptor. *Proc Natl Acad Sci U S A*, 109(36), pp.14393–14398.

Kozasa, T., Itoh, H., Tsukamoto, T. and Kaziro, Y., 1988. Isolation and characterization of the human Gs alpha gene. *Proc Natl Acad Sci U S A*, 85(7), pp.2081–2085.

Krilov, L., Nguyen, A., Miyazaki, T., Unson, C.G., Williams, R., Lee, N.H., Ceryak, S. and Bouscarel, B., 2011. Dual mode of glucagon receptor internalization: role of PKC α , GRKs and β -arrestins. *Experimental cell research*, 317(20), pp.2981–2994.

Krueger, K.M., Daaka, Y., Pitcher, J.A. and Lefkowitz, R.J., 1997. The role of sequestration in G protein-coupled receptor resensitization. Regulation of beta2-adrenergic receptor dephosphorylation by vesicular acidification. *J Biol Chem*, 272(1), pp.5–8.

Kuhn, H., Hall, S.W. and Wilden, U., 1984. Light-Induced Binding of 48-Kda Protein to Photoreceptor-Membranes Is Highly Enhanced by Phosphorylation of Rhodopsin. *Febs Letters*, 176(2), pp.473–478.

Kumari, P., Srivastava, A., Banerjee, R., Ghosh, E., Gupta, P., Ranjan, R., Chen, X., Gupta, B., Gupta, C., Jaiman, D. and Shukla, A.K., 2016. Functional competence of a partially engaged GPCR- β -arrestin complex. *Nat Commun*, 7, p.13416.

Laporte, S.A., Miller, W.E., Kim, K.-M. and Caron, M.G., 2002. beta-Arrestin/AP-2 interaction in G protein-coupled receptor internalization: identification of a beta-arrestin binding site in beta 2-adaptin. *J Biol Chem*, 277(11), pp.9247–9254.

Lebon, G., Edwards, P.C., Leslie, A.G.W. and Tate, C.G., 2015. Molecular

Determinants of CGS21680 Binding to the Human Adenosine A2A Receptor. *Mol Pharmacol*, 87(6), pp.907–915.

Lebon, G., Warne, T., Edwards, P.C., Bennett, K., Langmead, C.J., Leslie, A.G.W. and Tate, C.G., 2011. Agonist-bound adenosine A2A receptor structures reveal common features of GPCR activation. *Nature*, 474(7352), pp.521–525.

Lefkowitz, R.J. and Shenoy, S.K., 2005. Transduction of receptor signals by beta-arrestins. *Science*, 308(5721), pp.512–517.

Lefkowitz, R.J., 2007. Seven transmembrane receptors: something old, something new. *Acta physiologica*, 190(1), pp.9–19.

Lefkowitz, R.J., Rajagopal, K. and Whalen, E.J., 2006. New roles for beta-arrestins in cell signaling: not just for seven-transmembrane receptors. *Molecular cell*, 24(5), pp.643–652.

Lehmann, D.M., Seneviratne, A.M.P.B. and Smrcka, A.V., 2008. Small molecule disruption of G protein beta gamma subunit signaling inhibits neutrophil chemotaxis and inflammation. *Mol Pharmacol*, 73(2), pp.410–418.

Lenzen, R., Hruby, V.J. and Tavoloni, N., 1990. Mechanism of glucagon choleresis in guinea pigs. *Am J Physiol*, 259(5 Pt 1), pp.G736–44.

Lerea, C.L., Somers, D.E., Hurley, J.B., Klock, I.B. and Buntmilam, A.H., 1986. Identification of Specific Transducin Alpha-Subunits in Retinal Rod and Cone Photoreceptors. *Science*, 234(4772), pp.77–80.

Li, X.C., Carretero, O.A., Shao, Y. and Zhuo, J.L., 2006. Glucagon receptor-mediated extracellular signal-regulated kinase 1/2 phosphorylation in rat mesangial cells: role of protein kinase A and phospholipase C. *Hypertension*, 47(3), pp.580–585.

Liang, Y.-L., Khoshouei, M., Radjainia, M., Zhang, Y., Glukhova, A., Tarrasch, J., Thal, D.M., Furness, S.G.B., Christopoulos, G., Coudrat, T., Danev, R., Baumeister, W., Miller, L.J., Christopoulos, A., Kobilka, B.K., Wootten, D., Skiniotis, G. and Sexton, P.M., 2017. Phase-plate cryo-EM structure of a class B GPCR-G-protein complex. *Nature*, 546(7656), pp.118–123.

Lin, Y.-C., Boone, M., Meuris, L., Lemmens, I., Van Roy, N., Soete, A., Reumers, J., Moisse, M., Plaisance, S., Drmanac, R., Chen, J., Speleman, F., Lambrechts, D., Van de Peer, Y., Tavernier, J. and Callewaert, N., 2014. Genome dynamics of the human embryonic kidney 293 lineage in response to cell biology manipulations. *Nat Commun*, 5, p.4767.

Linscheid, P., Seboek, D., Zulewski, H., Keller, U. and Müller, B., 2005. Autocrine/paracrine role of inflammation-mediated calcitonin gene-related peptide and adrenomedullin expression in human adipose tissue. *Endocrinology*, 146(6), pp.2699–2708.

Liu, J., Chen, M., Deng, C., Bourc'his, D., Nealon, J.G., Erlichman, B., Bestor, T.H. and Weinstein, L.S., 2005. Identification of the control region for tissue-specific imprinting of the stimulatory G protein alpha-subunit. *Proc Natl Acad Sci U S A*, 102(15), pp. 5513–5518.

Liu, W., Chun, E., Thompson, A.A., Chubukov, P., Xu, F., Katritch, V., Han, G.W., Roth, C.B., Heitman, L.H., Ijzerman, A.P., Cherezov, V. and Stevens, R.C., 2012. Structural basis for allosteric regulation of GPCRs by sodium ions. *Science*, 337(6091), pp.232–236.

Lodish, H., Berk, A., Zipursky, S.L., Matsudaira, P., Baltimore, D. and Darnell J., 2002. *Molecular Cell Biology*, 4th Edition.

Lotfy, M., Kalasz, H., Szalai, G., Singh, J. and Adeghate, E., 2014. Recent Progress in the Use of Glucagon and Glucagon Receptor Antagonists in the Treatment of Diabetes Mellitus. *Open Med Chem J*, 8(1), pp.28–35.

Luttrell, L.M. and Gesty-Palmer, D., 2010. Beyond desensitization: physiological relevance of arrestin-dependent signaling. *Pharmacol Rev*, 62(2), pp.305–330.

Luttrell, L.M., Roudabush, F.L., Choy, E.W., Miller, W.E., Field, M.E., Pierce, K.L. and Lefkowitz, R.J., 2001. Activation and targeting of extracellular signal-regulated kinases by beta-arrestin scaffolds. *Proc Natl Acad Sci U S A*, 98(5), pp.2449–2454.

Magalhaes, A.C., Dunn, H. and Ferguson, S.S.G., 2012. Regulation of GPCR activity, trafficking and localization by GPCR-interacting proteins. *Br J Pharmacol*, 165(6), pp.1717–1736.

Maier, T., Güell, M. and Serrano, L., 2009. Correlation of mRNA and protein in complex biological samples. *Febs Letters*, 583(24), pp.3966–3973.

Mancini, A., Bertrand, G., Vivot, K., Carpentier, É., Tremblay, C., Ghislain, J., Bouvier, M. and Poitout, V., 2015. β -arrestin recruitment and biased agonism at free fatty acid receptor 1. *J Biol Chem*, 290(34):21131-40.

Manni, S., Mauban, J.H., Ward, C.W. and Bond, M., 2008. Phosphorylation of the cAMP-dependent protein kinase (PKA) regulatory subunit modulates PKA-AKAP interaction, substrate phosphorylation, and calcium signaling in cardiac cells. *J Biol Chem*, 283(35), pp.24145–24154.

Margeta-Mitrovic, M., Jan, Y.N. and Jan, L.Y., 2000. A trafficking checkpoint controls GABA(B) receptor heterodimerization. *Neuron*, 27(1), pp.97–106.

Marshall, F.H., Jones, K.A., Kaupmann, K. and Bettler, B., 1999. GABAB receptors - the first 7TM heterodimers. *Trends Pharmacol Sci*, 20(10), pp.396–399.

Martínez-Archundia, M. and Correa-Basurto, J., 2013. Molecular dynamics simulations reveal initial structural and dynamic features for the A 2AR as a result of ligand binding. *Molecular Simulation*, 40(13), pp.996–1014.

Mathi, S.K., Chan, Y., Li, X. and Wheeler, M.B., 1997. Scanning of the glucagon-like peptide-1 receptor localizes G protein-activating determinants primarily to the N terminus of the third intracellular loop. *Mol Endocrinol (Baltimore, Md.)*, 11(4), pp.424–432.

McDonald, P.H., Chow, C.W., Miller, W.E., Laporte, S.A., Field, M.E., Lin, F.T., Davis, R.J. and Lefkowitz, R.J., 2000. Beta-arrestin 2: a receptor-regulated MAPK scaffold for the activation of JNK3. *Science*, 290(5496), pp.1574–1577.

McLatchie, L.M., Fraser, N.J., Main, M.J., Wise, A., Brown, J., Thompson, N., Solari, R., Lee, M.G. and Foord, S.M., 1998. RAMPs regulate the transport and ligand specificity of the calcitonin-receptor-like receptor. *Nature*, 393(6683), pp.333–339.

McLaughlin, S.K., McKinnon, P.J. and Margolskee, R.F., 1992. Gustducin Is a Taste-Cell-Specific G-Protein Closely Related to the Transducins. *Nature*, 357(6379), pp.563–569.

McLaughlin, S.K., McKinnon, P.J., Robichon, A., Spickofsky, N. and Margolskee, R.F., 1993. Gustducin and transducin: a tale of two G proteins. *Ciba Foundation symposium*, 179, pp.186–96.

Mederacke, I., Dapito, D.H., Affò, S., Uchinami, H. and Schwabe, R.F., 2015. High-yield and high-purity isolation of hepatic stellate cells from normal and fibrotic mouse livers. *Nature protocols*, 10(2), pp.305–315.

Milligan, G. and Bouvier, M., 2005. Methods to monitor the quaternary structure of G protein-coupled receptors. *The FEBS journal*, 272(12), pp.2914–2925.

Milligan, G., 2004. G protein-coupled receptor dimerization: function and ligand pharmacology. *Mol Pharmacol*, 66(1), pp.1–7.

Milligan, G., 2007. G protein-coupled receptor dimerisation: molecular basis and relevance to function. *Biochim Biophys Acta*, 1768(4), pp.825–835.

Milligan, G., 2009. G protein-coupled receptor hetero-dimerization: contribution to

pharmacology and function. *Br J Pharmacol*, 158(1), pp.5–14.

Milligan, G., 2010. The role of dimerisation in the cellular trafficking of G-protein-coupled receptors. *Current opinion in pharmacology*, 10(1), pp.23–29.

Moore, C.A.C., Milano, S.K. and Benovic, J.L., 2007. Regulation of receptor trafficking by GRKs and arrestins. *Ann Rev Physiol*, 69(1), pp.451–482.

Moore, E.L. and Salvatore, C.A., 2012. Targeting a family B GPCR/RAMP receptor complex: CGRP receptor antagonists and migraine. *Br J Pharmacol*, 166(1), pp.66–78.

Müller, C.E., Schiedel, A.C. and Baqi, Y., 2012. Allosteric modulators of rhodopsin-like G protein-coupled receptors: opportunities in drug development. *Pharmacol Ther*, 135(3), pp.292–315.

Ng, S.Y.L., Lee, L.T.O. and Chow, B.K.C., 2012. Receptor oligomerization: from early evidence to current understanding in class B GPCRs. *Frontiers in endocrinology*, 3, p.175.

Nishimura, A., Kitano, K., Takasaki, J., Taniguchi, M., Mizuno, N., Tago, K., Hakoshima, T. and Itoh, H., 2010. Structural basis for the specific inhibition of heterotrimeric Gq protein by a small molecule. *Proc Natl Acad Sci U S A*, 107(31), pp.13666–13671.

Niswender, C.M. and Conn, P.J., 2010. Metabotropic Glutamate Receptors: Physiology, Pharmacology, and Disease. *Annu Rev Pharmacol Toxicol*, 50(1), pp.295–322.

Nuber, S., Zabel, U., Lorenz, K., Nuber, A., Milligan, G., Tobin, A.B., Lohse, M.J. and Hoffmann, C., 2016. β -Arrestin biosensors reveal a rapid, receptor-dependent activation/deactivation cycle. *Nature*, 531(7596), pp.661–664.

Offermanns, S. and Simon, M.I., 1995. G alpha 15 and G alpha 16 couple a wide variety of receptors to phospholipase C. *J Biol Chem*, 270(25), pp.15175–15180.

Offermanns, S., 2003. G-proteins as transducers in transmembrane signalling. *Progress in biophysics and molecular biology*, 83(2), pp.101–130.

Oh, D.Y., Talukdar, S., Bae, E.J., Imamura, T., Morinaga, H., Fan, W., Li, P., Lu, W.J., Watkins, S.M. and Olefsky, J.M., 2010. GPR120 is an omega-3 fatty acid receptor mediating potent anti-inflammatory and insulin-sensitizing effects. *Cell*, 142(5), pp.687–698.

Okamoto, H., Kim, J., Aglione, J., Lee, J., Cavino, K., Na, E., Rafique, A., Kim, J.H., Harp, J., Valenzuela, D.M., Yancopoulos, G.D., Murphy, A.J. and Gromada, J., 2015. Glucagon Receptor Blockade With a Human Antibody Normalizes Blood Glucose in Diabetic Mice and Monkeys. *Endocrinology*, 156(8), pp.2781–2794.

Okamoto, T. and Okabe, S., 2000. Ultraviolet absorbance at 260 and 280 nm in RNA measurement is dependent on measurement solution. *International journal of molecular medicine*, 5(6), pp.657–659.

Orr, A.G., Hsiao, E.C., Wang, M.M., Ho, K., Kim, D.H., Wang, X., Guo, W., Kang, J., Yu, G.-Q., Adame, A., Devidze, N., Dubal, D.B., Masliah, E., Conklin, B.R. and Mucke, L., 2015. Astrocytic adenosine receptor A2A and Gs-coupled signaling regulate memory. *Nature neuroscience*, 18(3), pp.423–434.

Ostrom, R.S., Gregorian, C. and Insel, P.A., 2000. Cellular release of and response to ATP as key determinants of the set-point of signal transduction pathways. *J Biol Chem*, 275(16), pp.11735–11739.

Pal, K., Melcher, K. and Xu, H.E., 2012. Structure and mechanism for recognition of peptide hormones by Class B G-protein-coupled receptors. *Acta pharmacologica Sinica*, 33(3), pp.300–311.

Palczewski, K., Kumasaka, T., Hori, T., Behnke, C.A., Motoshima, H., Fox, B.A., Le Trong, I., Teller, D.C., Okada, T., Stenkamp, R.E., Yamamoto, M. and Miyano,

M., 2000. Crystal structure of rhodopsin: A G protein-coupled receptor. *Science (New York, N.Y.)*, 289(5480), pp.739–745.

Parthier, C., Kleinschmidt, M., Neumann, P., Rudolph, R., Manhart, S., Schlenzig, D., Fanghänel, J., Rahfeld, J.-U., Demuth, H.-U. and Stubbs, M.T., 2007. Crystal structure of the incretin-bound extracellular domain of a G protein-coupled receptor. *Proc Natl Acad Sci U S A*, 104(35), pp.13942–13947.

Pasolli, H.A., Klemke, M., Kehlenbach, R.H., Wang, Y. and Huttner, W.B., 2000. Characterization of the extra-large G protein alpha-subunit XLalphas. I. Tissue distribution and subcellular localization. *J Biol Chem*, 275(43), pp.33622–33632.

Pierce, K.L., Premont, R.T. and Lefkowitz, R.J., 2002. Seven-transmembrane receptors. *Nat Rev Mol Cell Biol*, 3(9), pp.639–650.

Pin, J.-P., Galvez, T. and Prézeau, L., 2003. Evolution, structure, and activation mechanism of family 3/C G-protein-coupled receptors. *Pharmacol Ther*, 98(3), pp.325–354.

Pitcher, J.A., Touhara, K., Payne, E.S. and Lefkowitz, R.J., 1995. Pleckstrin homology domain-mediated membrane association and activation of the beta-adrenergic receptor kinase requires coordinate interaction with G beta gamma subunits and lipid. *J Biol Chem*, 270(20), pp.11707–11710.

Plagge, A., Gordon, E., Dean, W., Boiani, R., Cinti, S., Peters, J. and Kelsey, G., 2004. The imprinted signaling protein XL alpha s is required for postnatal adaptation to feeding. *Nature genetics*, 36(8), pp.818–826.

Plagge, A., Kelsey, G. and Germain-Lee, E.L., 2008. Physiological functions of the imprinted Gnas locus and its protein variants Galpha(s) and XLalpha(s) in human and mouse. *The Journal of endocrinology*, 196(2), pp.193–214.

Pocai, A., 2012. Unraveling oxyntomodulin, GLP1's enigmatic brother. *J Endocrinol*, 215(3), pp.335–346.

Pocai, A., 2014. Action and therapeutic potential of oxyntomodulin. *Molecular metabolism*, 3(3), pp.241–251.

Pocai, A., Carrington, P.E., Adams, J.R., Wright, M., Eiermann, G., Zhu, L., Du, X., Petrov, A., Lassman, M.E., Jiang, G., Liu, F., Miller, C., Tota, L.M., Zhou, G., Zhang, X., Sountis, M.M., Santoprete, A., Capito, E., Chicchi, G.G., Thornberry, N., Bianchi, E., Pessi, A., Marsh, D.J. and SinhaRoy, R., 2009. Glucagon-like peptide 1/glucagon receptor dual agonism reverses obesity in mice. *Diabetes*, 58(10), pp.2258–2266.

Qi, M. and Elion, E.A., 2005. MAP kinase pathways. *Journal of cell science*, 118(Pt 16), pp.3569–3572.

Qi, T. and Hay, D.L., 2010. Structure-function relationships of the N-terminus of receptor activity-modifying proteins. *Br J Pharmacol*, 159(5), pp.1059–1068.

Qin, J.Y., Zhang, L., Clift, K.L., Huler, I., Xiang, A.P., Ren, B.-Z. and Lahn, B.T., 2010. Systematic comparison of constitutive promoters and the doxycycline-inducible promoter. *PLoS ONE*, 5(5), p.e10611.

Quesada, I., Tuduri, E., Ripoll, C. and Nadal, A., 2008. Physiology of the pancreatic α -cell and glucagon secretion: role in glucose homeostasis and diabetes. *Journal of Endocrinology*, 199(1), pp.5–19.

Quoyer, J., Longuet, C., Broca, C., Linck, N., Costes, S., Varin, E., Bockaert, J., Bertrand, G. and Dalle, S., 2010. GLP-1 mediates antiapoptotic effect by phosphorylating Bad through a beta-arrestin 1-mediated ERK1/2 activation in pancreatic beta-cells. *J Biol Chem*, 285(3), pp.1989–2002.

Rajagopal, S., Ahn, S., Rominger, D.H., Gowen-MacDonald, W., Lam, C.M., Dewire, S.M., Violin, J.D. and Lefkowitz, R.J., 2011. Quantifying ligand bias at seven-transmembrane receptors. *Mol Pharmacol*, 80(3), pp.367–377.

Ran, F.A., Hsu, P.D., Wright, J., Agarwala, V., Scott, D.A. and Zhang, F., 2013. Genome engineering using the CRISPR-Cas9 system. *Nature protocols*, 8(11), pp.2281–2308.

Rang, H.P., 2006. The receptor concept: pharmacology's big idea. *Br J Pharmacol*, 147 Suppl 1(S1), pp.S9–16.

Rasheed, S.A.K., Teo, C.R., Beillard, E.J., Voorhoeve, P.M., Zhou, W., Ghosh, S. and Casey, P.J., 2015. MicroRNA-31 controls G protein alpha-13 (GNA13) expression and cell invasion in breast cancer cells. *Molecular Cancer*, 14(1).

Rasmussen, S.G.F., DeVree, B.T., Zou, Y., Kruse, A.C., Chung, K.Y., Kobilka, T.S., Thian, F.S., Chae, P.S., Pardon, E., Calinski, D., Mathiesen, J.M., Shah, S.T.A., Lyons, J.A., Caffrey, M., Gellman, S.H., Steyaert, J., Skiniotis, G., Weis, W.I., Sunahara, R.K. and Kobilka, B.K., 2011. Crystal structure of the β_2 adrenergic receptor-Gs protein complex. *Nature*, 477(7366), pp.549–555.

Recino, A., Barkan, K., Wong, F.S., Ladds, G., Cooke, A. and Wallberg, M., 2017. Hyperglycaemia does not affect antigen-specific activation and cytolytic killing by CD8(+) T cells in vivo. *Biosci Rep*, 37(4), p.BSR20171079.

Reddy, P.S. and Corley, R.B., 1998. Assembly, sorting, and exit of oligomeric proteins from the endoplasmic reticulum. *BioEssays : news and reviews in molecular, cellular and developmental biology*, 20(7), pp.546–554.

Robinson, P.J., 1992. Differential stimulation of protein kinase C activity by phorbol ester or calcium/phosphatidylserine in vitro and in intact synaptosomes. *J Biol Chem*, 267(30), pp.21637–21644.

Rosenbaum, D.M., Rasmussen, S.G.F. and Kobilka, B.K., 2009. The structure and function of G-protein-coupled receptors. *Nature*, 459(7245), pp.356–363.

Rouillé, Y., Kantengwa, S., Irminger, J.C. and Halban, P.A., 1997. Role of the prohormone convertase PC3 in the processing of proglucagon to glucagon-like peptide 1. *J Biol Chem*, 272(52), pp.32810–32816.

Rovati, G.E., Capra, V. and Neubig, R.R., 2007. The highly conserved DRY motif of class A G protein-coupled receptors: beyond the ground state. *Mol Pharmacol*, 71(4), pp.959–964.

Runge, S., Thøgersen, H., Madsen, K., Lau, J. and Rudolph, R., 2008. Crystal structure of the ligand-bound glucagon-like peptide-1 receptor extracellular domain. *J Biol Chem*, 283(17), pp.11340–11347.

Runge, S., Wulff, B.S., Madsen, K., Bräuner-Osborne, H. and Knudsen, L.B., 2003. Different domains of the glucagon and glucagon-like peptide-1 receptors provide the critical determinants of ligand selectivity. *Br J Pharmacol*, 138(5), pp.787–794.

Sadana, R. and Dessauer, C.W., 2009. Physiological roles for G protein-regulated adenylyl cyclase isoforms: insights from knockout and overexpression studies. *Neuro-Signals*, 17(1), pp.5–22.

Salon, J.A., Lodowski, D.T. and Palczewski, K., 2011. The significance of G protein-coupled receptor crystallography for drug discovery. *Pharmacol Rev*, 63(4), pp.901–937.

Sambrook, J., Fritsch, E.F. and Maniatis, T., 1989. Molecular cloning: a laboratory manual. Cold Spring Harbor, N.Y., Cold Spring Harbor Laboratory.

Sassone-Corsi, P., 2012. The cyclic AMP pathway. *Cold Spring Harbor perspectives in biology*, 4(12), pp.a011148–a011148.

Schelshorn, D., Joly, F., Mutel, S., Hampe, C., Breton, B., Mutel, V. and Lütjens, R., 2012. Lateral allostery in the glucagon receptor family: glucagon-like peptide 1 induces G-protein-coupled receptor heteromer formation. *Mol Pharmacol*, 81(3), pp.309–318.

Schertler, G.F., Villa, C. and Henderson, R., 1993. Projection structure of rhodopsin. *Nature*, 362(6422), pp.770–772.

Schiöth, H.B. and Fredriksson, R., 2005. The GRAFS classification system of G-protein coupled receptors in comparative perspective. *Gen Comp Endocrinol*, 142(1-2), pp.94–101.

Schmidt, D.T., Watson, N., Dent, G., Rühlmann, E., Branscheid, D., Magnussen, H. and Rabe, K.F., 2000. The effect of selective and non-selective phosphodiesterase inhibitors on allergen- and leukotriene C(4)-induced contractions in passively sensitized human airways. *Br J Pharmacol*, 131(8), pp.1607–1618.

Schmitz, A.-L., Schrage, R., Gaffal, E., Charpentier, T.H., Wiest, J., Hiltensperger, G., Morschel, J., Hennen, S., Häußler, D., Horn, V., Wenzel, D., Grundmann, M., Büllsbach, K.M., Schröder, R., Brewitz, H.H., Schmidt, J., Gomeza, J., Gales, C., Fleischmann, B.K., Tüting, T., Imhof, D., Tietze, D., Gütschow, M., Holzgrabe, U., Sondek, J., Harden, T.K., Mohr, K. and Kostenis, E., 2014. A cell-permeable inhibitor to trap Gαq proteins in the empty pocket conformation. *Chem Biol*, 21(7), pp.890–902.

Schrage, R., Schmitz, A.-L., Gaffal, E., Annala, S., Kehraus, S., Wenzel, D., Buellsbach, K.M., Bald, T., Inoue, A., Shinjo, Y., Galandrin, S., Shridhar, N., Hesse, M., Grundmann, M., Merten, N., Charpentier, T.H., Martz, M., Butcher, A.J., Slodczyk, T., Armando, S., Efferm, M., Namkung, Y., Jenkins, L., Horn, V., Stoessel, A., Dargatz, H., Tietze, D., Imhof, D., Gales, C., Drewke, C., Mueller, C.E., Hoelzel, M., Milligan, G., Tobin, A.B., Gomeza, J., Dohlman, H.G., Sondek, J., Harden, T.K., Bouvier, M., Laporte, S.A., Aoki, J., Fleischmann, B.K., Mohr, K., Koenig, G.M., Tüting, T. and Kostenis, E., 2015. The experimental power of FR900359 to study Gq-regulated biological processes. *Nat Commun*, 14;6:10156.

Schulte, G. and Fredholm, B.B., 2000. Human adenosine A(1), A(2A), A(2B), and A(3) receptors expressed in Chinese hamster ovary cells all mediate the phosphorylation of extracellular-regulated kinase 1/2. *Mol Pharmacol*, 58(3), pp.477–482.

Schwede, F., Maronde, E., Genieser, H. and Jastorff, B., 2000. Cyclic nucleotide analogs as biochemical tools and prospective drugs. *Pharmacol Ther*, 87(2-3), pp.199–226.

Seamon, K.B., Padgett, W. and Daly, J.W., 1981. Forskolin: unique diterpene activator of adenylate cyclase in membranes and in intact cells. *Proc Natl Acad Sci U S A*, 78(6), pp.3363–3367.

Sensoy, O. and Weinstein, H., 2015. A mechanistic role of Helix 8 in GPCRs: Computational modeling of the dopamine D2 receptor interaction with the GIPC1-PDZ-domain. *Biochim Biophys Acta*, 1848(4), pp.976–983.

Sexton, P.M. and Wootten, D., 2013. Structural biology: meet the B family. *Nature*, 499(7459), pp.417–418.

Sexton, P.M., Morfis, M., Tilakaratne, N., Hay, D.L., Udawela, M., Christopoulos, G. and Christopoulos, A., 2006. Complexing receptor pharmacology: modulation of family B G protein-coupled receptor function by RAMPs. *Ann N Y Acad Sci*, 1070(1), pp.90–104.

Shen, L., Hillebrand, A., Wang, D.Q.-H. and Liu, M., 2012. Isolation and primary culture of rat hepatic cells. *J Vis Exp*, (64), pp.e3917–e3917.

Shenoy, S.K., McDonald, P.H., Kohout, T.A. and Lefkowitz, R.J., 2001. Regulation of receptor fate by ubiquitination of activated beta(2)-adrenergic receptor and beta-arrestin. *Science*, 294(5545), pp.1307–1313.

Sheth, S., Brito, R., Mukherjea, D., Rybak, L.P. and Ramkumar, V., 2014. Adenosine receptors: expression, function and regulation. *Int J Mol Sci*, 15(2),

pp.2024–2052.

Shukla, A.K., Westfield, G.H., Xiao, K., Reis, R.I., Huang, L.-Y., Tripathi-Shukla, P., Qian, J., Li, S., Blanc, A., Oleskie, A.N., Dosey, A.M., Su, M., Liang, C.-R., Gu, L.-L., Shan, J.-M., Chen, X., Hanna, R., Choi, M., Yao, X.J., Klink, B.U., Kahsai, A.W., Sidhu, S.S., Koide, S., Penczek, P.A., Kossiakoff, A.A., Jr, V.L.W., Kobilka, B.K., Skiniotis, G. and Lefkowitz, R.J., 2014. Visualization of arrestin recruitment by a G-protein-coupled receptor. *Nature*, 512(7513), pp.218–222.

Siehl, S., 2009. Regulation of RhoGEF proteins by G12/13-coupled receptors. *Br J Pharmacol*, 158(1), pp.41–49.

Simon, M.I., Strathmann, M.P. and Gautam, N., 1991. Diversity of G proteins in signal transduction. *Science (New York, N.Y.)*, 252(5007), pp.802–808.

Siu, F.Y., He, M., de Graaf, C., Han, G.W., Yang, D., Zhang, Z., Zhou, C., Xu, Q., Wacker, D., Joseph, J.S., Liu, W., Lau, J., Cherezov, V., Katritch, V., Wang, M.-W. and Stevens, R.C., 2013. Structure of the human glucagon class B G-protein-coupled receptor. *Nature*, 499(7459), pp.444–449.

Smrcka, A.V., 2008. G protein $\beta\gamma$ subunits: central mediators of G protein-coupled receptor signaling. *Cell Mol Life Sci*, 65(14), pp.2191–2214.

So, C.H., Varghese, G., Curley, K.J., Kong, M.M.C., Alijaniam, M., Ji, X., Nguyen, T., O'dowd, B.F. and George, S.R., 2005. D1 and D2 dopamine receptors form heterooligomers and cointernalize after selective activation of either receptor. *Mol Pharmacol*, 68(3), pp.568–578.

Song, G., Yang, D., Wang, Y., de Graaf, C., Zhou, Q., Jiang, S., Liu, K., Cai, X., Dai, A., Lin, G., Liu, D., Wu, F., Wu, Y., Zhao, S., Ye, L., Han, G.W., Lau, J., Wu, B., Hanson, M.A., Liu, Z.-J., Wang, M.-W. and Stevens, R.C., 2017. Human GLP-1 receptor transmembrane domain structure in complex with allosteric modulators. *Nature*.

Spandidos, A., Wang, X., Wang, H. and Seed, B., 2010. PrimerBank: a resource of human and mouse PCR primer pairs for gene expression detection and quantification. *Nucleic Acids Res*, 38(Database issue), pp.D792–9.

Stanasila, L., Perez, J.B., Vogel, H. and Cotecchia, S., 2003. Oligomerization of the alpha 1a- and alpha 1b-adrenergic receptor subtypes. Potential implications in receptor internalization. *J Biol Chem*, 278(41), pp.40239–40251.

Stockinger, S., Reutterer, B., Schaljo, B., Schellack, C., Brunner, S., Materna, T., Yamamoto, M., Akira, S., Taniguchi, T., Murray, P.J., Müller, M. and Decker, T., 2004. IFN regulatory factor 3-dependent induction of type I IFNs by intracellular bacteria is mediated by a TLR- and Nod2-independent mechanism. *J Immunol*, 173(12), pp.7416–7425.

Stott, L.A., Hall, D.A. and Holliday, N.D., 2016. Unravelling intrinsic efficacy and ligand bias at G protein coupled receptors: A practical guide to assessing functional data. *Biochem Pharmacol*, 101, pp.1–12.

Strathmann, M. and Simon, M.I., 1990. G protein diversity: a distinct class of alpha subunits is present in vertebrates and invertebrates. *Proc Natl Acad Sci U S A*, 87(23), pp.9113–9117.

Strudwick, N., Bhogal, N., Evans, N.A., Blaney, F.E. and Findlay, J.B.C., 2004. Evidence to support a spectrum of active states for the glucagon receptor. *Biochem Soc Trans*, 32(Pt 6), pp.1037–1039.

Taborsky, G.J., 2010. The physiology of glucagon. *Journal of diabetes science and technology*, 4(6), pp.1338–1344.

Takasaki, J., Saito, T., Taniguchi, M., Kawasaki, T., Moritani, Y., Hayashi, K. and Kobori, M., 2004. A novel Galphaq/11-selective inhibitor. *J Biol Chem*, 279(46), pp.47438–47445.

Tang, W.J. and Gilman, A.G., 1991. Type-specific regulation of adenylyl cyclase by G protein beta gamma subunits. *Science*, 254(5037), pp.1500–1503.

Terrillon, S. and Bouvier, M., 2004. Roles of G-protein-coupled receptor dimerization. *EMBO reports*, 5(1), pp.30–34.

Thomas, B.E., Wittelsberger, A., Woznica, I., Hsieh, M.-Y., Monaghan, P., Lee, B.K. and Rosenblatt, M., 2007. Cysteine at position 217 in the intracellular loop 1 plays a critical role in human PTH receptor type 1 membrane translocation and function. *J Bone Miner Res*, 22(4), pp.609–616.

Thompson, G.L., Lane, J.R., Coudrat, T., Sexton, P.M., Christopoulos, A. and Canals, M., 2015. Biased Agonism of Endogenous Opioid Peptides at the μ -Opioid Receptor. *Mol Pharmacol*, 88(2), pp.335–346.

Thomsen, A.R.B., Plouffe, B., Cahill, T.J., Shukla, A.K., Tarrasch, J.T., Dosey, A.M., Kahsai, A.W., Strachan, R.T., Pani, B., Mahoney, J.P., Huang, L., Breton, B., Heydenreich, F.M., Sunahara, R.K., Skiniotis, G., Bouvier, M. and Lefkowitz, R.J., 2016. GPCR-G Protein- β -Arrestin Super-Complex Mediates Sustained G Protein Signaling. *Cell*, 11;166(4):907-19.

Tilakaratne, N., Christopoulos, G., Zumpe, E.T., Foord, S.M. and SEXTON, P.M., 2000. Amylin receptor phenotypes derived from human calcitonin receptor/RAMP coexpression exhibit pharmacological differences dependent on receptor isoform and host cell environment. *J Pharmacol Exp Ther*, 294(1), pp.61–72.

Timossi, C., Ortiz-Elizondo, C., Pineda, D.B., Dias, J.A., Conn, P.M. and Ulloa-Aguirre, A., 2004. Functional significance of the BBXXB motif reversed present in the cytoplasmic domains of the human follicle-stimulating hormone receptor. *Mol Cell Endocrinol*, 223(1-2), pp.17–26.

Triggle, D.J., 2000. Pharmacological receptors: a century of discovery--and more. *Pharm Acta Helv*, 74(2-3), pp.79–84.

Trzaskowski, B., Latek, D., Yuan, S., Ghoshdastider, U., Debinski, A. and Filipek, S., 2012. Action of molecular switches in GPCRs--theoretical and experimental studies. *Current medicinal chemistry*, 19(8), pp.1090–1109.

Underwood, C.R., Garibay, P., Knudsen, L.B., Hastrup, S., Peters, G.H., Rudolph, R. and Reedtz-Runge, S., 2010. Crystal structure of glucagon-like peptide-1 in complex with the extracellular domain of the glucagon-like peptide-1 receptor. *J Biol Chem*, 285(1), pp.723–730.

Underwood, C.R., Knudsen, L.B., Garibay, P.W., Peters, G.H. and Reedtz-Runge, S., 2013. Development of a cysteine-deprived and C-terminally truncated GLP-1 receptor. *Peptides*, 49, pp.100–108.

Unson, C.G., Gurzenda, E.M. and Merrifield, R.B., 1989. Biological activities of des-His1[Glu9]glucagon amide, a glucagon antagonist. *Peptides*, 10(6), pp.1171–1177.

Venkatakrishnan, A.J., Deupi, X., Lebon, G., Tate, C.G., Schertler, G.F. and Babu, M.M., 2013. Molecular signatures of G-protein-coupled receptors. *Nature*, 494(7436), pp.185–194.

Vogel, R., Mahalingam, M., Lüdeke, S., Huber, T., Siebert, F. and Sakmar, T.P., 2008. Functional role of the 'ionic lock'--an interhelical hydrogen-bond network in family A heptahelical receptors. *J Mol Biol*, 380(4), pp.648–655.

Vohra, S., Taddese, B., Conner, A.C., Poyner, D.R., Hay, D.L., Barwell, J., Reeves, P.J., Upton, G.J.G. and Reynolds, C.A., 2013. Similarity between class A and class B G-protein-coupled receptors exemplified through calcitonin gene-related peptide receptor modelling and mutagenesis studies. *J R Soc Interface*, 10(79), pp.20120846–20120846.

Wakelam, M.J., Murphy, G.J., Hruby, V.J. and Houslay, M.D., 1986. Activation of

two signal-transduction systems in hepatocytes by glucagon. *Nature*, 323(6083), pp.68–71.

Wang, C., Wu, H., Evron, T., Vardy, E., Han, G.W., Huang, X.-P., Hufeisen, S.J., Mangano, T.J., Urban, D.J., Katritch, V., Cherezov, V., Caron, M.G., Roth, B.L. and Stevens, R.C., 2014. Structural basis for Smoothed receptor modulation and chemoresistance to anticancer drugs. *Nat Commun*, 5, p.4355.

Watkins, H.A., Walker, C.S., Ly, K.N., Bailey, R.J., Barwell, J., Poyner, D.R. and Hay, D.L., 2014. Receptor activity-modifying protein-dependent effects of mutations in the calcitonin receptor-like receptor: implications for adrenomedullin and calcitonin gene-related peptide pharmacology. *Br J Pharmacol*, 171(3), pp.772–788.

Wei, H., Ahn, S., Shenoy, S.K., Karnik, S.S., Hunyady, L., Luttrell, L.M. and Lefkowitz, R.J., 2003. Independent beta-arrestin 2 and G protein-mediated pathways for angiotensin II activation of extracellular signal-regulated kinases 1 and 2. *Proc Natl Acad Sci U S A*, 100(19), pp.10782–10787.

Weston, C., Lu, J., Li, N., Barkan, K., Richards, G.O., Roberts, D.J., Skerry, T.M., Poyner, D., Pardamwar, M., Reynolds, C.A., Dowell, S.J., Willars, G.B. and Ladds, G., 2015. Modulation of Glucagon Receptor Pharmacology by RAMP2. *J Biol Chem*, 18;290(38), pp. 23009-22.

Weston, C., Poyner, D., Patel, V., Dowell, S. and Ladds, G., 2014. Investigating G protein signaling bias at the glucagon-like peptide-1 receptor in yeast. *Br J Pharmacol*, 171(15), pp.3651-65.

Wettschureck, N. and Offermanns, S., 2005. Mammalian G proteins and their cell type specific functions. *Physiol Rev*, 85(4), pp.1159–1204.

Wilke, B.U., Lindner, M., Greifenberg, L., Albus, A., Kronimus, Y., Bünemann, M., Leitner, M.G. and Oliver, D., 2014. Diacylglycerol mediates regulation of TASK potassium channels by Gq-coupled receptors. *Nat Commun*, 5, p.5540.

Wilkie, T.M., Scherle, P.A., Strathmann, M.P., Slepak, V.Z. and Simon, M.I., 1991. Characterization of G-protein alpha subunits in the Gq class: expression in murine tissues and in stromal and hematopoietic cell lines. *Proc Natl Acad Sci U S A*, 88(22), pp.10049–10053.

Willard, F.S., Bueno, A.B. and Sloop, K.W., 2012. Small molecule drug discovery at the glucagon-like peptide-1 receptor. *Experimental diabetes research*, 2012(7329), pp.709893–9.

Wisler, J.W., Xiao, K., Thomsen, A.R.B. and Lefkowitz, R.J., 2014. Recent developments in biased agonism. *Curr Opin Cell Biol*, 27, pp.18–24.

Woehler, A. and Ponimaskin, E.G., 2009. G protein-mediated signaling: same receptor, multiple effectors. *Curr Mol Pharmacol*, 2(3), pp.237–248.

Wong, W. and Scott, J.D., 2004. AKAP signalling complexes: focal points in space and time. *Nat Rev Mol Cell Biol*, 5(12), pp.959–970.

Wootten, D., Lindmark, H., Kadmiel, M., Willcockson, H., Caron, K.M., Barwell, J., Drmota, T. and Poyner, D.R., 2013. Receptor activity modifying proteins (RAMPs) interact with the VPAC2 receptor and CRF1 receptors and modulate their function. *Br J Pharmacol*, 168(4), pp.822–834.

Wootten, D., Reynolds, C.A., Smith, K.J., Mobarec, J.C., Furness, S.G.B., Miller, L.J., Christopoulos, A. and Sexton, P.M., 2016. Key interactions by conserved polar amino acids located at the transmembrane helical boundaries in Class B GPCRs modulate activation, effector specificity and biased signalling in the glucagon-like peptide-1 receptor. *Biochem Pharmacol*, 15;118, pp. 68-87.

Wootten, D., Savage, E.E., Willard, F.S., Bueno, A.B., Sloop, K.W., Christopoulos, A. and Sexton, P.M., 2013b. Differential activation and modulation of the glucagon-like peptide-1 receptor by small molecule ligands. *Mol Pharmacol*,

83(4), pp.822–834.

Wootten, D., Simms, J., Miller, L.J., Christopoulos, A. and Sexton, P.M., 2013c. Polar transmembrane interactions drive formation of ligand-specific and signal pathway-biased family B G protein-coupled receptor conformations. *Proc Natl Acad Sci U S A*, 110(13), pp.5211–5216.

Xiong, X.-F., Zhang, H., Underwood, C.R., Harpsøe, K., Gardella, T.J., Wöldike, M.F., Mannstadt, M., Gloriam, D.E., Bräuner-Osborne, H. and Strømgaard, K., 2016. Total synthesis and structure-activity relationship studies of a series of selective G protein inhibitors. *Nature chemistry*, 8(11), pp.1035–1041.

Xu, Y. and Xie, X., 2009. Glucagon receptor mediates calcium signaling by coupling to G alpha q/11 and G alpha i/o in HEK293 cells. *Journal of receptor and signal transduction research*, 29(6), pp.318–325.

Xue, L., Rovira, X., Scholler, P., Zhao, H., Liu, J., Pin, J.-P. and Rondard, P., 2015. Major ligand-induced rearrangement of the heptahelical domain interface in a GPCR dimer. *Nat Chem Biol*, 11(2), pp.134–140.

Yao, X., Parnot, C., Deupi, X., Ratnala, V.R.P., Swaminath, G., Farrens, D. and Kobilka, B., 2006. Coupling ligand structure to specific conformational switches in the beta2-adrenoceptor. *Nat Chem Biol*, 2(8), pp.417–422.

Zhang, G., Liu, Y., Ruoho, A.E. and Hurley, J.H., 1997. Structure of the adenylyl cyclase catalytic core. *Nature*, 386(6622), pp.247–253.

Zhang, H., Qiao, A., Yang, D., Yang, L., Dai, A., de Graaf, C., Reedtz-Runge, S., Dharmarajan, V., Zhang, H., Han, G.W., Grant, T.D., Sierra, R.G., Weierstall, U., Nelson, G., Liu, W., Wu, Y., Ma, L., Cai, X., Lin, G., Wu, X., Geng, Z., Dong, Y., Song, G., Griffin, P.R., Lau, J., Cherezov, V., Yang, H., Hanson, M.A., Stevens, R.C., Zhao, Q., Jiang, H., Wang, M.-W. and Wu, B., 2017a. Structure of the full-length glucagon class B G-protein-coupled receptor. *Nature*, 25, p.366.

Zhang, Y., Sun, B., Feng, D., Hu, H., Chu, M., Qu, Q., Tarrasch, J.T., Li, S., Sun Kobilka, T., Kobilka, B.K. and Skiniotis, G., 2017b. Cryo-EM structure of the activated GLP-1 receptor in complex with a G protein. *Nature*, 1335, p.29.

Zhou, X.E., Melcher, K. and Xu, H.E., 2012. Structure and activation of rhodopsin. *Acta pharmacologica Sinica*, 33(3), pp.291–299.

Zhuang, X., Belluscio, L. and Hen, R., 2000. G(olf)alpha mediates dopamine D1 receptor signaling. *J Neurosci*, 20(16), p.RC91.

Zigman, J.M., Westermark, G.T., LaMendola, J. and Steiner, D.F., 1994. Expression of cone transducin, Gz alpha, and other G-protein alpha-subunit messenger ribonucleic acids in pancreatic islets. *Endocrinology*, 135(1), pp.31–37.

Zwermann, O., Suttman, Y., Bidlingmaier, M., Beuschlein, F. and Reincke, M., 2009. Screening for membrane hormone receptor expression in primary aldosteronism. *Eur J Endocrinol*, 160(3), pp.443–451.